Application of 1,5-Diaza-3,7-diphosphacyclooctane (P_2N_2) Ligands Towards Ni- and Pd-Catalyzed Cross-Couplings

By: Eric Isbrandt

A thesis submitted in partial fulfillment of the requirements for the
Doctor of Philosophy degree in Chemistry

Faculty of Science
Department of Chemistry and Biomolecular Sciences
University of Ottawa

Thesis Supervisor: Dr. Stephen G. Newman

Abstract

Contemporary challenges in synthetic organic chemistry require innovative solutions. The discovery of highly-effective and readily accessible scaffolds drives the ever expanding scope of catalytic transformations. This dissertation outlines the repurposing of 1,5-Diaza-3,7-diphosphacyclooctanes (P_2N_2) ligands, commonly employed in inorganic or coordination chemistry, towards organic cross-coupling reactions. Despite their prominence in energy-storage applications, P_2N_2 ligands have been underexplored in catalytic C–C bond formation reactions. Chapter 1 provides a detailed introduction to late transition metal catalysis and the history of P_2N_2 ligands. Chapter 2 outlines the discovery of $P^{Cy}{}_2N^{ArCF3}{}_2$ as a powerful P_2N_2 ligand for the Ni-catalyzed reductive cross-coupling of aryl iodides with aldehydes. Chapter 3 details the extrapolation of the Ni/$P^{Cy}{}_2N^{ArCF3}{}_2$ catalyst system to the related, but less established, redox-neutral α-arylation of primary alcohols. Chapter 4 highlights the applicability of P_2N_2 ligands towards Ni- and Pd-catalyzed Mizoroki-Heck reactions. High-throughput experimentation (HTE) indicated a range of hits with P_2N_2 ligands compared to established ligands in Heck-type couplings. We discovered that absolute site selectivity of C–C bond formation could be controlled by simply altering the phosphorus substituent on the P_2N_2 ligand for the coupling of aryl triflates with styrenes. Notably, this degree of selectivity was not observed with conventional ligands. Chapter 5 focuses on the preparation of the P_2N_2 ligands. Finally, chapter 6 offers a perspective on future developments of P_2N_2 ligands and the prospective directions of their application in transition metal-catalyzed transformations.

Acknowledgements

First and foremost I would like to thank my research supervisor, Professor Steve Newman for his guidance, kindness, and for fostering an amazing research group. I overlapped with many amazing people over my times in the Newman lab: Sam, Bharath, Annika, Mads, Niraj, Sara, Claudia, Kendra, Émile, Ashley, Jacob, Rama, Yang, Katie, Jack, Jean-Danick, Casey, Max, Jonathan, Kathleen, Carlos, Laura, Rhiannon, Yeva, Imane, Kaylie, Mohanad, Jeanne, Prakash, Taoufik, Louis, Hadyn, Saeed, Yanlong, Eric, Garrett, Omid, August, Filiz, Hana, Nav, Robynne, Janice, Baha, Kostya, Kian, Fran, Isuru, Shajia, Piyas, Aref, Piers, and Adam. Special thanks to Wanying and Ryan for directly mentoring me as an undergraduate student. Also, a huge thank you to the collaborators across various projects: Jaya, Thomas, Lars, Karen, Amrah, Victoria, Gilian, Zichuan and Aisha – you taught me many new skills and how to do good research.

Thank you to the broader uOttawa community for their kindness and insightful conversations, especially Roxanne, the CCRI, the NMR facility, Patrick, Alex, and Behnaz.

I would also like to thank the University of Ottawa for their admission scholarship, the Ontario government for an OGS scholarship, and NSERC for a CGS-D scholarship.

I am also especially grateful to Professors Baker, Gagosz, Scaiano, and Arndtsen for being on my committee – their expertise and feedback has taught me many valuable lessons about scientific research.

We are very thankful to Professor Apfel (UMSICHT) for the kind donation of several tripodal phosphine ligands to study as analogues of triphos.

We are also incredibly thankful to Solvay (Cytec-Canada Inc) for their generous donation of primary alkyl phosphines. Without these valuable building blocks, the work outlined in this dissertation would not have been possible.

Lastly, I would like to thank my friends and family for all their support throughout my studies. Without my mother and father, this degree would not have been possible. Thank you to my grandparents, aunts, uncles, cousins, Mark, Livia, and Cara for everything. Thank you for everything.

Statement of Contributions

Unless otherwise noted, all work was performed by the author of this dissertation. Chapters 2-5 each have a respective contribution section which fully details portions and experiments which were run by collaborators. The work in Chapter 2 was performed in collaboration with Amrah Nasim (MSc) and Karen Zhao (Hon BSc). Chapter 3 was performed in collaboration with Amrah Nasim (MSc), Karen Zhao (Hon BSc), and Aishabibi Kassymbek (PDF). Chapter 4 was performed in collaboration with Dr. Devon E. Chapple (PhD, Western University), Nguyen Thien Phuc Tu (PhD candidate, Carleton University), Dr. Victoria Dimakos (PDF, University of Ottawa), Anne Marie M. Beardall (PhD candidate, Western University), Dr. Paul D. Boyle (X-ray facility, Western University), Prof. Christopher N. Rowley (Carleton University) and Prof. Johanna M. Blacquiere (Western University). The experiments described in Chapter 5 were performed solely by the author of this dissertation.

The research presented in this dissertation is original and, where indicated, has been incorporated into peer-reviewed publications.

Claims to Original Research

The research presented in Chapter 2, the first half of Chapter 3 (up to, and including Section 3.5), and Chapter 5 (syntheses of $P^{Cy}{}_2N^{ArCF3}{}_2$, $P^{Cy}{}_2N^{ArOMe}{}_2$ and $P^{Ph}{}_2N^{ArCF3}{}_2$) originally appeared in:

1. Isbrandt, E. S.; Nasim, A.; Zhao, K.; Newman, S. G. Catalytic Aldehyde and Alcohol Arylation Reactions Facilitated by a 1,5-Diaza-3,7-diphosphacyclooctane Ligand. *J. Am. Chem. Soc.* **2021**, *143*, 14646–14656. https://doi.org/10.1021/jacs.1c05661.

This work has been partially rewritten and expanded upon for this dissertation.

The research presented in Section 3.6 represents a manuscript in preparation with the following tentative title:

2. Isbrandt, E.S.; Kassymbek, A. Newman, S. G. Mechanistic Study of Well-defined Nickel 1,5-Diaza-3,7-diphosphacyclooctane Complexes in the Reductive Arylation of Aldehydes.

This work has been partially rewritten and expanded upon for this dissertation.

The research presented in Chapter 4 and Chapter 5 (synthesis of $P^{tBu}{}_2N^{ArCF3}{}_2$ and general P_2N_2 synthesis procedure) is currently accepted to a peer-reviewed journal

3. Isbrandt, E.S.; Chapple D. E.; Tu, N. P. T.; Dimakos, V.; Beardall, A. M. M.; Boyle, P. D.; Rowley, C.; Blacquiere, J. M.; Newman, S. G. Controlling Reactivity and Selectivity in the Mizoroki-Heck Reaction: High Throughput Evaluation of 1,5-Diaza-3,7-diphosphacyclooctane Ligands. *J. Am. Chem. Soc.* **2024**, *in press*. Preprint available at: *ChemRxiv* **2023**. DOI: 10.26434/chemrxiv-2023-t9p7j.

This work has been partially rewritten and expanded upon for this dissertation.

Table of Contents

List of Schemes

List of Figures

List of Tables

Abbreviations

ABP – 2-aminobiphenyl

Ac – acetyl group

Ar – generic aromatic ring

^{ArCF3} – 4-(trifluoromethyl)phenyl group

$^{Ar(CF3)2}$ – 3,5-bis(trifluoromethyl)phenyl group

^{ArOMe} – 4-methoxyphenyl group

ATR – attenuated total reflectance

BARF – tetrakis[3,5-bis(trifluoromethyl)phenyl]borate

Bbbpy – 4,4’-di-*tert*-butyl-2,2’-dipyridyl

BHE – β-hydride elimination

BIPHEP – 2,2’-bis(diphenylphosphino)biphenyl

Bn – benzyl group

Boc – *tert*-butyloxycarbonyl group

Bpy – 2,2’-bipyridine

br – branched isomer

Bu – butyl group

Bz – benzoyl group

C(+) – graphite cathode

CAM – cerium ammonium molybdate

Cat – catalyst

CCDC – Cambridge Crystallographic Data Centre

CCRI – Centre for Catalysis Research and Innovation

$CDCl_3$ – deuterated chloroform

CM3 – Core Module 3

CO – carbon monoxide

Cp – cyclopentadienyl

Cp* – 1,2,3,4,5-pentamethylcyclopentadienyl

Cod – 1,5-cyclooctadiene

Cy – cyclohexyl group

Cz – carbazole group

4CzIPN –1,2,3,5-tetrakis(carbazol-9-yl)-4,6-dicyanobenzene, 2,4,5,6-tetrakis(9H-carbazol-9-yl) isophthalonitrile

d – doublet

DABCO – 1,4-diazabicylco[2.2.2]octane

DavePhos – 2-dicyclohexylphosphino-2′-(*N*,*N*-dimethylamino)biphenyl

dba – dibenzylideneacetone

DCC – *N,N*′-dicyclohexylcarbodiimide

DCE – 1,2-dichloroethane

DCM – dichloromethane

Dcpp•2HBF$_4$ – 1,3-bis(dicyclohexylphosphino)propane bis(tetrafluoroborate)

Dcype – 1,2-bis(dicyclohexylphosphino)ethane

DEPT – Distortionless Enhancement by Polarization Transfer

DFT – density-functional theory

DIPEA – *N*,*N*-diisopropylethylamine; also called Hunig's base or *i*Pr$_2$NEt

DIPPE – 1,2-bis(diisopropylphosphino)ethane

DMA – *N*,*N*-dimethylacetamide

DMAP – *N,N*-dimethylpyridin-4-amine

DME – 1,2-dimethoxyethane; also called glyme

DMF – dimethylformamide

^{DMP}DAB – *N,N*′-bis(2,6-dimethylphenyl)-diazabutadiene

DMSO – dimethylsulfoxide

Dnpf – 1,10-bis[di-(1-naphthyl)phosphino]-ferrocene

Dppdpm – 2,2-dimethylpropane-1,3-diylbis(diphenylphosphane),

Dppf – 1,1′-bis(diphenylphosphino)ferrocene

Dppe – 1,2-bis(diphenylphosphino)ethane

Dppm – bis(diphenylphosphino)methane

Dppp – 1,3-bis(diphenylphosphino)propane

dr – diastereomeric ratio

EDG – electron-donating group

ee – enantiomeric excess

Eg. – for example

EI – electron-ionization

EPR – electron paramagnetic resonance

ESI – electron-spray ionization

ES- – electron-spray ionization negative ion mode

ESI+ – electron-spray ionization positive ion mode

ESI-TOF – electrospray ionization time-of-flight

Et – ethyl group

EtOH – ethanol

Equiv – equivalent(s)

EWG – electron-withdrawing group

Fc – ferrocenyl group

FTIR – Fourier-transform infrared spectroscopy

GC-FID – gas chromatography-flame ionization detection

GC-MS – gas chromatography-mass spectrometry

[H] – reductant

$H^{\oplus}$ – unspecified proton source; usually a generic acid quench

HE – Hantzsch ester; 1,4-dihydro-2,6-dimethyl-3,5-pyridinedicarboxylic acid diethyl ester

Hept – heptyl group

HSQC – heteronuclear single quantum coherence

HTE – high-throughput experimentation

HX – generic strong acid

Hz – Hertz

IMES – 1,3-bis(2,4,6-trimethylphenyl)-1,3-dihydro-2H-imidazol-2-ylidene

IMES•HCl – 1,3-dimesitylimidazolium chloride

IPr – 1,3-bis(2,6-diisopropylphenyl)imidazol-2-ylidene

IPr•HCl – 1,3-bis-(2,4,6-tribenzhydrylphenyl)-1H-imidazol-3-ium chloride

^{i}Pr – isopropyl group

IR – infrared spectroscopy

I.S. – internal standard

JohnPhos – (2-biphenyl)di-*tert*-butylphosphine,

L- generic L-type ligand

L_n – generic L-type ligand; unspecified number around metal centre

LED – light-emitting diode

LG – leaving group

lin – linear isomer

M – metal

m – multiplet

mA – constant current

MAH – maleic anhydride

Me – methyl group

MeCN – acetonitrile

MeOH – methanol

MHz – megaHertz

µm – micrometer

µW – microwave irradiation

Ms – mesyl group

Nap – naphthyl group

Neo – neopentyl

NHC – N-heterocyclic Carbene

NHK – Nozaki-Hiyama-Kishi

Ni(-) – nickel anode

nm – nanometer

NMP – N-methyl-2-pyrrolidinone

NMR – nuclear magnetic resonance spectroscopy

o – ortho substituent

[O] – oxidant

OAC – oxidative addition complex

OAc – acetate

OMs – mesylate

ORTEP – Oak Ridge Thermal Ellipsoid Plot

OTf – triflate (trifluoromethane sulfonate)

p – para substituent

P_2N_2 – 1,5-diaza-3,7-diphosphacyclooctane

pent – pentet

PFA – perfluoroalkoxy alkanes

Ph – phenyl group

PyBOX – pyridine bis(oxazoline) ligand

1-PhEtOH – 1-phenyl ethanol (also known as methyl phenyl carbinol)

PhMe – toluene

Piv – pivaloyl

PMP – 1,2,2,6,6-pentamethylpiperidine

Ppm – parts-per-million

Py – pyridine

q – quartet

Q-TOF – quadrupole-time-of-flight

R – generic carbon chain

rac – racemic

rr – regioisomeric ratio

s – singlet

*s*Bu – *sec*-butyl group

SI – Supporting Information

t – triplet

$TBABPh_4$ – tetrabutylammonium tetraphenylborate

^{t}Bu – t*ert*-butyl group

TeCA – 1,1,2,2-tetrachloroethane

TES – triethylsilane

THF – tetrahydrofuran

THPC – tetrakis(hydroxymethyl)phosphonium chloride

TLC – thin-layer chromatography

TMB – 1,3,5-trimethoxybenzene

TMEDA – *N,N,N′,N*′-tetramethylethane-1,2-diamine

TMP – 2,2,6,6-tetramethypiperidine

TMPhATB – trimethylphenylammonium tribromide

TOF – turnover frequency

Tol – tolyl group

Triphos – 1,1,1-tris(diphenylphosphinomethyl)ethane

TS – transition state

UV – ultraviolet

X – generic Cl, Br, I or (pseudo)halide

XantPhos – (9,9-dimethyl-9H-xanthene-4,5-diyl)bis(diphenylphosphane)

Chapter 1 : Transition Metal Catalysis and 1,5-Diaza-3,7-Diphosphacyclooctanes (P_2N_2) Ligands

1.1 Catalysis: A primer

Discovery of novel or improved methods to form carbon-carbon bonds is a key aspect of synthetic organic chemistry that pushes the field forward. Since the late 19th century, catalytic methods have become increasingly common to derivatize organic building blocks into complex scaffolds. The following section discusses how metals, both as stoichiometric additives and as catalysts, can be used to facilitate reactions which would otherwise not occur in their absence at any reasonable rate.

1.1.1 Early 20th century metal-assisted couplings

The Barbier reaction, discovered in 1899, enables the coupling of alkyl halides with carbonyl groups in the presence of a stoichiometric metal such as zinc or magnesium (Scheme 1.1A).[1] While the reactivity of organozinc compounds had been established in the 1800's,[2] Barbier's conditions enabled a one-pot reaction of aryl halide, zinc, and electrophile by generating the nucleophile *in situ* rather than preforming it in a separate synthetic step. Grignard reported that nucleophilic organomagnesium compounds, which were synthesized from the corresponding organohalide and magnesium power, react with many simple carbonyl electrophiles in 1900 (Scheme 1.1B).[3] The Ullmann reaction, first reported in 1901, enabled the homocoupling of aryl halides in the presence of stoichiometric copper (Scheme 1.1C).[4] In 1906, Goldberg disclosed conditions for C-N bond formation between anilines and aryl halides using a copper catalyst at high temperatures (Scheme 1.1D).[5] Goldberg's work represents one of the first examples of intermolecular cross-coupling catalysis, though this class of reactions had not yet been defined. Kharasch & Fields expanded on cross-coupling catalysis in 1941, with the transition metal-catalyzed coupling of Grignard reagents with aryl halides to make biaryls (Scheme 1.1E).[6] The

reactions in Scheme 1.1 represent notable achievements in synthetic chemistry by enabling new reactivity between materials that would not occur otherwise under reasonable reaction conditions.

Scheme 1.1 Metal-promoted and metal-catalyzed coupling reactions from the early 20th century

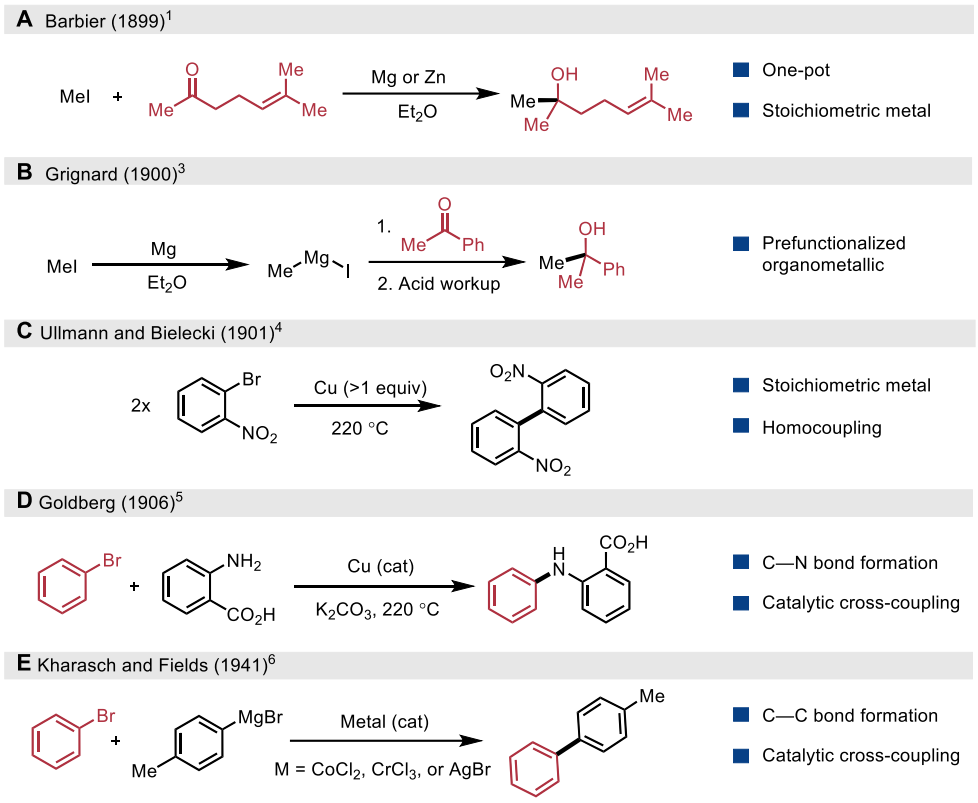

1.1.2 Fundamentals of catalysis

In the simplest definition, catalysts are species which are *theoretically* not consumed or destroyed throughout the course of a reaction but serve to lower the energy of activation. By definition, catalysts are added in substoichiometric quantities to a reaction, generally on the order of 0.1 equivalents or less relative to the limiting reagent. Catalysts allow transformations that would be exceedingly slow otherwise or that cannot occur due to other reaction pathways

being faster. For example, the starting materials may decompose faster than the noncatalyzed pathway can occur.

1.1.3 The cross-coupling renaissance

The early *catalytic* cross-coupling reactions described in Section 1.1.1 failed to achieve notable attention from the scientific community and, thus, extensions of the work were sparsely reported.

Starting from the late 1960's, the rediscovery and expansion of cross-coupling reactions caused a paradigm shift in organic synthesis. Palladium catalysts were found to be highly efficient, reproducible, functional group tolerant, and stable for a large number of transformations.[7] The Mizoroki-Heck (1971),[8] Sonogashira (1975),[9] Negishi (1976),[10] Stille (1978),[11] Suzuki-Miyuara (1979),[12] and Hiyama (1988)[13] cross-couplings were landmark discoveries that drastically changed how synthetic chemists build complex molecules (Scheme 1.2).

A simplified, generic, catalytic cycle for the aforementioned cross-couplings, with the exception of the Heck reaction, is shown in Scheme 1.2**.** Starting from a palladium(0) source, oxidative addition of an organo(pseudo)halide occurs to form the $Ar[Pd]^{II}X$ species – often called an oxidative addition complex (OAC). Transmetallation follows, exchanging the charged X species (commonly X = Cl, Br, I) for an organic group on the oxidative addition complex. As charged ligands are exchanged, this does not change the oxidation state of the Pd(II) complex. Reductive elimination can then occur, forging a new C—C bond and regenerating Pd(0). Pd(0) can participate in a subsequent reaction, thus propagating the catalytic cycle. In Scheme 1.2, the presence of neutral ligands, such as monodentate phosphines, is obviated for simplicity. The

Scheme 1.2 Generic palladium catalytic cycle

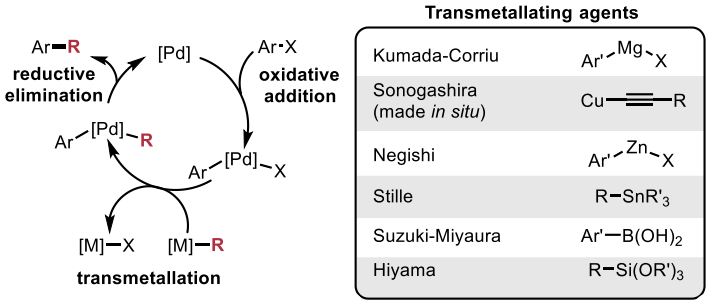

exact number of ligands surrounding the metal centre, the identity of the ligands, and whether the metal exists as a monomer or high-order species can vary depending on the conditions used and, in some cases, is not well-defined. It is generally accepted that for homogenenous catalysis, the metal centre is surrounded by some ancillary ligands which might coordinate to or dissociate from the metal as needed. In recent years, the field of transition metal catalysis has exploded to include increasingly unactivated substrates, milder conditions, and a greater diversity of metals. This is further detailed in Section 1.3.

The Mizoroki-Heck reaction features some unique steps from the other cross-couplings and will be discussed in extended detail in the following section, Section 1.2, as it directly pertains to Chapter 4 of this thesis.

1.2 The Mizoroki-Heck reaction

Around 1970, Mizoroki and Heck independently discovered that disubsituted alkenes could be prepared from a Pd-catalyzed coupling between a monosubsituted alkene and an aryl halide (Scheme 1.3).[8] The traditional Mizoroki-Heck conditions are highly selective for the trans (*E*) geometry of the alkene when a terminal styrene is coupled with an aryl halide. No transmetallating agent is required for the reaction to occur and, as a result, acid (HX) is the only stoichiometric byproduct of the reaction. This directly contrasts with most other early cross-couplings (Section 1.1.1), which feature a transmetallating agent and, therefore, generate stoichiometric metal or metalloid waste products. Base is added to the Heck-type couplings to react with the acid (HX), as otherwise reversible oxidative addition of HX is possible. This serves to bias the equilibrium towards product formation by consuming any strong acids formed.

Scheme 1.3 The Mizoroki-Heck reaction

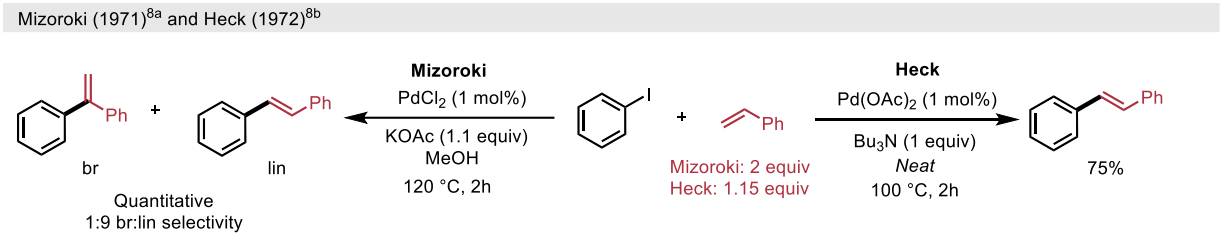

1.2.1 Mechanism of the Mizoroki-Heck coupling

The accepted catalytic cycle for the Mizoroki-Heck reaction features a productive β-hydride elimination to regenerate the unsaturation after π-bond insertion (Scheme 1.4). Ancillary ligands are assumed to be present but the exact number coordinated to any given intermediate can vary based on their identity and reaction mechanism. As a result, the cycle is drawn with a generic [Pd] complex. As show in Scheme 1.4, Pd(0) **1.1** is generated *in situ* and adds across an aryl halide

bond to generate the OAC **1.2**. The alkene is freely able to coordinate reversibly to the metal centre as an L-type ligand forming intermediate **1.3**. π-Bond insertion can then occur creating an alkyl palladium species **1.4a** or **1.4b**, which can readily β-hydride eliminate to form **1.5** and release the substituted alkene product. The β-hydride must be *syn* to the metal centre to allow for proper orbital overlap for the resulting elimination, thus introducing an element of geometrical constraint.[14] Base-induced reductive elimination can regenerate species **1.1**, allowing catalyst turnover by formally deprotonating the metal hydride **1.5**.

As shown in Scheme 1.4, there are two possible sites of Pd insertion on a terminal alkene. Selectivity for the linear (β-substituted) or the branched (α-substituted) products is not always trivial and remains as a contemporary challenge with certain Mizoroki-Heck coupling partners.

Chapter 4 will further detail state-of-the-art regioselective Mizoroki-Heck couplings along with current gaps in the primary literature. It should be noted that disubstituted linear *cis* products are rarely observed in significant quantities under standard Mizoroki-Heck conditions.[15] A recent mechanistic investigation by Xu et al. indicated that a Pd-phosphine catalyst system can quantitatively isomerize *cis* stilbene to *trans* stilbene in the presence of mildly acidic EtOH at 140 °C via a proposed Pd^{II}-H intermediate.[16] This suggests that if the linear *cis* product were to be formed, it can be readily isomerized by Pd to the less hindered *trans* isomer owing to the reversibility of the β-hydride elimination step and that product distribution between the regioisomers is dictated by equilibrium.

Scheme 1.4. Generic Mizoroki-Heck catalytic cycle

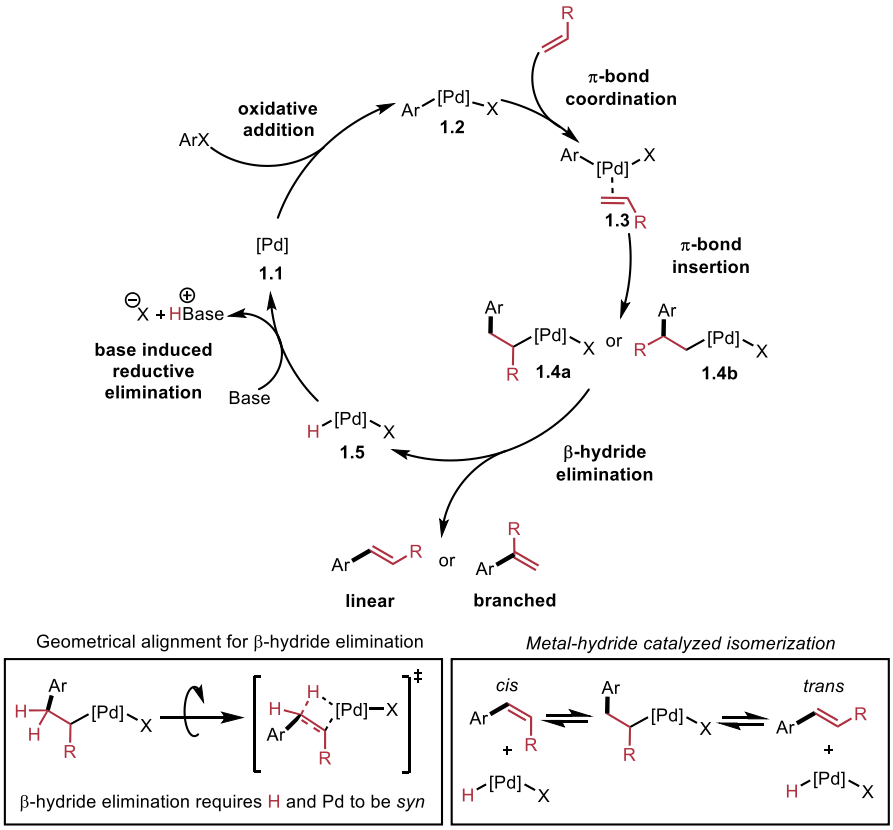

1.2.2 Utility of Mizoroki-Heck couplings beyond academia

The Mizoroki-Heck reaction has enabled the direct functionalization of alkenes from simple, commercially-available building blocks without requiring preactivation of the substrates or generating stoichiometric metallic waste.

The Mizoroki-Heck reaction, although not as widely-used as the Suzuki-Miyaura or Buchwald-Hartwig cross-couplings,[17] still has invaluable industrial applications.[18] The monomer precursor for Dow's Cyclotene™ polymer, which is used in microelectronics, has been manufactured on scale starting from a Mizoroki-Heck reaction (Scheme 1.5A).[19] A small number of pharmaceuticals and agrochemicals have also been manufactured on an industrial multi-ton scale using the Mizoroki-Heck reaction as a key step. Representative examples include

naratriptan– a pharmaceutical for treating migraine from GlaxoSmithKline (Scheme 1.5B)[20], Prosulfuron – an agrochemical from Novartis (Scheme 1.5C),[21] and Singulair – a treatment for asthma from Merck (Scheme 1.5D).[22] The Albemarle Corporation patented and prepared (*S*)-naproxen, a generic anti-inflammatory pharmaceutical that has been available on the market for decades,[23] through a Mizoroki-Heck coupling with ethylene gas (Scheme 1.5E).[24] One notable trend is that the olefins used in Scheme 1.5 are often activated (polarized) such that one regioisomer is preferred. Another observation is the final manufactured products do not contain the substituted alkenes derived from the Mizoroki-Heck coupling and have been subsequently reduced or isomerized to the saturated alkane (Scheme 1.5E).

Scheme 1.5. Selected industrial applications of the Mizoroki-Heck reaction

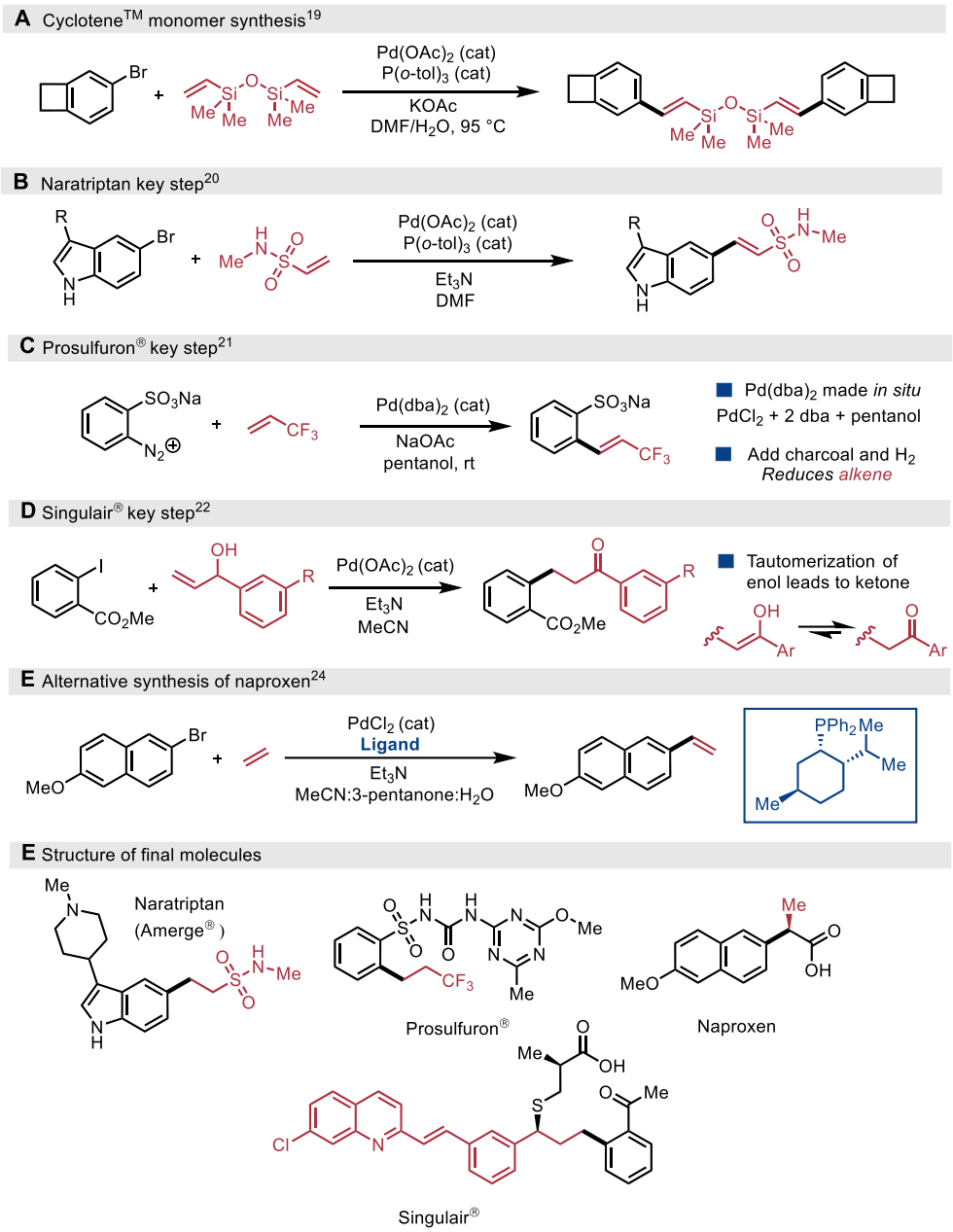

1.2.3 A brief detour: Classical alkene syntheses

There are many alternative methods to make alkenes other than the Mizoroki-Heck reaction. Elimination of a leaving group can occur through either an E_1 (unimolecular elimination) or E_2 (bimolecular elimination) mechanism to produce an alkene (Scheme 1.6A).[25] While this approach is operationally simple, a mixture of isomers is often observed when there are multiple β-protons (Zaitsev vs. Hoffmann product) and the reaction conditions are aggressive. The Wittig olefination enabled the reaction of aldehyde or ketones with phosphonium ylides to make alkenes with stoichiometric phosphine oxide waste (Scheme 1.6B).[26] Modifications have been made to improve regiochemical selectivity[27] and, more recently, to render the phosphine catalytic.[28] Although not strictly classical, the Corey-Winter olefination (Scheme 1.6C)[29], the Shapiro olefination (Scheme 1.6D),[30] the Peterson olefination (Scheme 1.6E)[31], and the Julia olefination (Scheme 1.6F)[32] are examples of alkene syntheses published around the same time as the Mizoroki-Heck reaction. It should be noted that alternative substitution patterns complementary to the linear (*E*) isomer of the classical Mizoroki-Heck reaction can be obtained, depending on how the molecule is prefunctionalized.

In the 1970's, olefin metathesis was discovered as an alternate catalytic method to synthesize substituted alkenes via a π-bond rearrangement through reversible [2+2] cyloadditions (Scheme 1.6G).[33] Using alkene metathesis, simple terminal olefins can be selectively coupled together generating ethylene gas as the byproduct, which also serves as a driving force for the reaction. However, in complex systems, achieving selectivity for the desired product can be problematic.[34] Many of the reactions presented in Scheme 1.6 require substrates that are not broadly commercially available, require harsh reaction conditions, or can suffer from

poor regiocontrol.[35] The Mizoroki-Heck reaction remains an appealing method to prepare substituted alkenes from simple starting materials despite challenges in overcoming regiochemical bias or poor selectivity.[36]

Scheme 1.6 Other synthetic methods to prepare alkenes

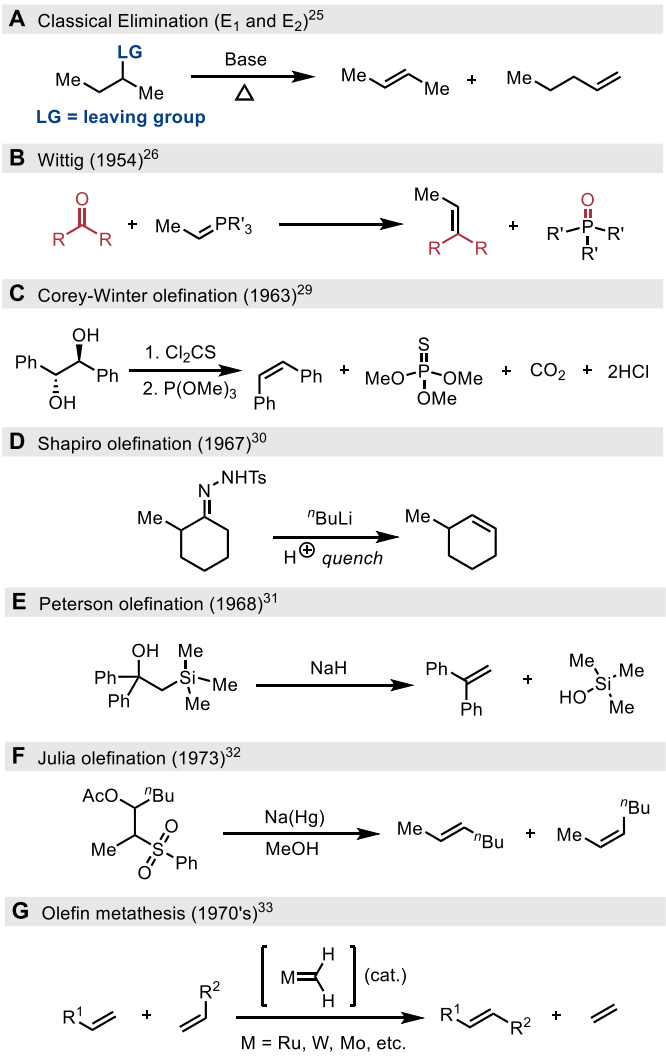

1.3 Nickel catalysis: A comparison to palladium

Palladium was the most common metal catalyst used in the pioneering efforts in cross-coupling described in Section 1.1.3; however, homogeneous catalytic applications for the other stable group 10 transition metals were being studied concurrently. Homogeneous platinum catalysts have a major application to the regioselective hydrosilylation of olefins.[37] On the other hand, nickel catalysis has seen a more diverse range of study and application, owing to its distinct reactivity. A recent perspective by Chernyshev and Ananikov has detailed key similarities between Ni and Pd along with their differences.[38]

1.3.1 Comparing nickel and palladium catalysis

Applications of nickel in catalysis include parallel reactivity to classical Pd-catalyzed transformations,[39] acting as a Lewis acid,[40] unique couplings not afforded by other transition metals, or pairing with a photocatalyst to react with radical species.[41] Nickel is capable of undergoing both radical (single electron) and polar (two electron) reaction mechanisms.[42] Nickel more readily accesses odd oxidation states, +1 and +3, than Pd. However, the 0 and +2 oxidation states commonly observed in palladium chemistry are also fully accessible to nickel as well.

The seminal Kumada-Corriu cross-couplings, using organomagnesium transmetallating agents, were first reported with nickel catalysts.[43] While nickel can perform the same elementary organometallic steps as palladium, there are nuances in its reactivity. Certain catalytic steps are more facile with nickel as opposed to palladium and vice versa. This has huge implications on rational experiment design and mechanistic aspects such as the rate-determining steps of the

associated catalytic cycles. Nickel catalyzed variants of classical palladium cross-couplings have been widely reported in the primary literature – as discussed further in this section.

Nickel has a smaller atomic radius than palladium and is less electronegative. Nickel is, therefore, more easily oxidized than palladium – this is reflected in catalysis as nickel can readily perform oxidative addition of halides and nonconventional pseudohalides (eg. aryl pivalates) under mild conditions.[44] Rather than focus on all cross-couplings, the Suzuki-Miyaura coupling will be used as a representative mini-case study to highlight advances in cross-coupling with less activated partners. The duality between nickel and palladium catalysis will also be discussed.

The first nickel-catalyzed Suzuki-Miyaura was reported in 1995 by Percec et al. – approximately 15 years after the initial report with palladium.[12,45] Aryl triflates work well with Pd-catalyzed Suzuki reactions under conditions disclosed by Snieckus and coworkers (Scheme 1.7A).[46] However, the Percec group noted that aryl mesylates worked poorly (Scheme 1.7B).[45] Owing to its ability to cleave stronger bonds, a simple nickel-catalyzed system was able to couple boronic acids with aryl mesylates (Scheme 1.7B). Notably, it took 13 additional years for the general palladium-catalyzed Suzuki-Miyaura cross-coupling of aryl mesylates to be reported (Scheme 1.7C).[47] The Pd-catalyzed variant required development of a novel Buchwald-inspired ligand to achieve high reactivity. More recently, Suzuki-Miyaura cross-couplings of difficult-to-activate aryl (pseudo)halides such as aryl ethers[48], aryl fluorides[49], and methyl esters[50] have been reported with nickel catalysis (Scheme 1.7D-1.7F). Conversely, the aforementioned reactivity has not been reported to the same extent, or at all, with palladium catalysts – depending on the particular coupling. These examples demonstrate that nickel is not simply a less costly alternative to palladium; Ni can facilitate unique couplings.

Scheme 1.7. Evolution of nickel-catalyzed Suzuki-Miyaura couplings with comparisons to analogous Pd-catalyzed conditions

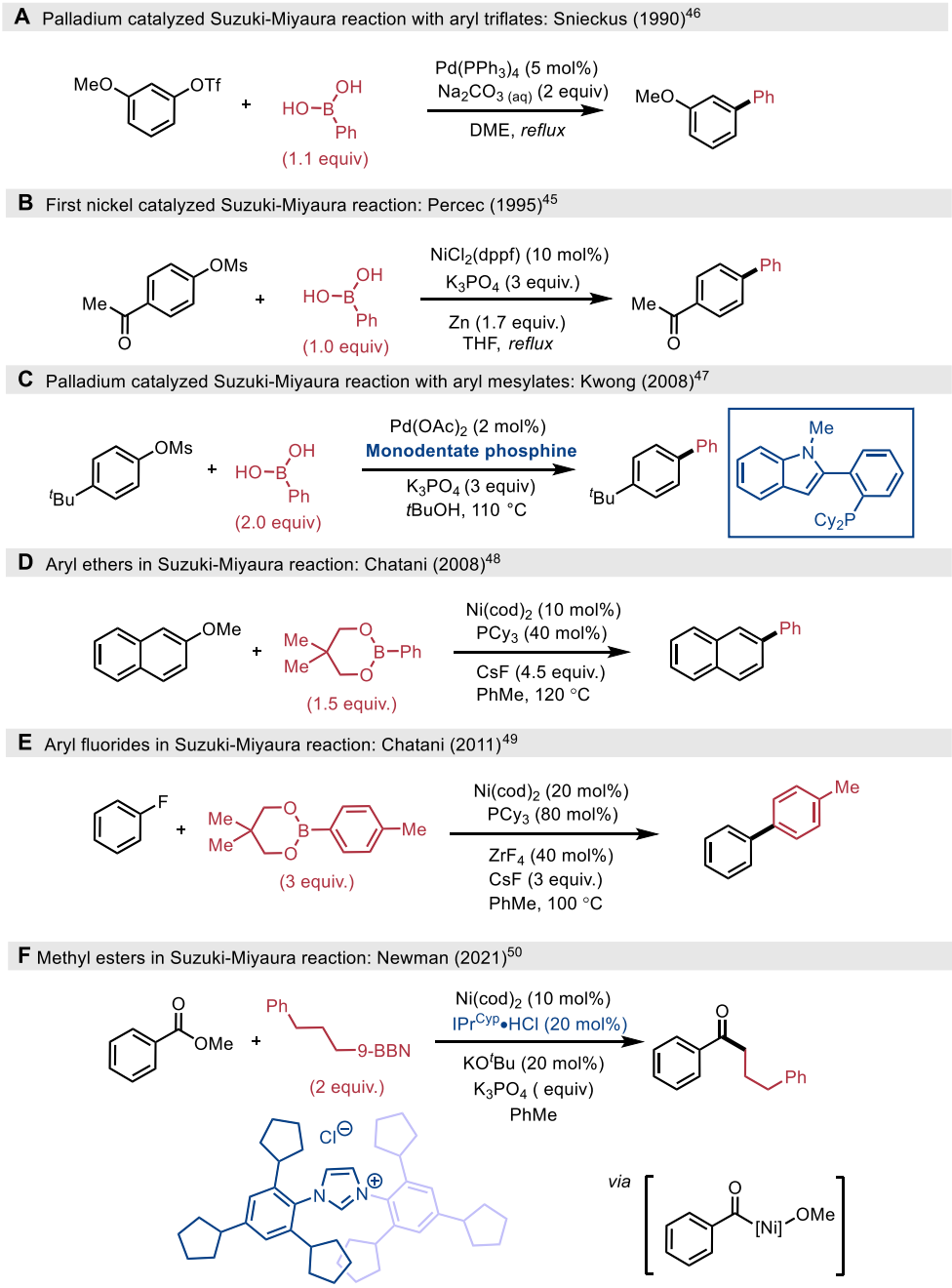

Transmetallation has been proposed as the rate-limiting step in some Ni(0)/Ni(II) catalytic cycles.[51] However, reductive elimination must also be considered for a complete mechanistic picture. Nickel is less prone to reduction and reductive elimination can also be the rate-

determining step in a catalytic cycle.[52] Yamamoto et al. found that the mechanism for reductive elimination can vary between closely related palladium(II) and nickel(II) complexes.[53] They postulated that nickel tends to prefer an *associative* reductive elimination featuring a 5-coordinate Ni(II) species, while palladium(II) tends to prefer a *dissociative* reductive elimination (T-shaped) for C–C bond formation (sp^3-sp^3) and C–O (sp^3-sp^3) bond formation. However, it should be noted that the mechanism of reductive elimination can also change depending on the nature of the organometallic species and the type of bond being formed. A computational study of structurally-related Ni(II) and Pd(II) complexes has also indicated that Ni(II) has a higher energetic barrier for reductive elimination than the corresponding Pd(II) species.[54]

The mechanistic subtleties of single-electron and two-electron nickel reaction pathways are described in greater detail by recent perspectives.[38,55]

1.3.2 Formation of active catalysts: Ni vs. Pd

Pd precatalysts are well-established to form dimers, nanoparticles, or heterogeneous species which can be the active catalyst.[56] These species are often created under "ligandless" reaction conditions – a misnomer because the Pd will find something to bind to in solution such as coordinating solvent or base. Conversely, nickel tends to decompose into catalytically inactive species when forming clusters or heterogeneous species.[38]

While Pd(II) precatalysts can be often be reduced to active Pd(0) in situ without requiring dedicated additives, Ni(II) precatalysts are more challenging to reduce to Ni(0) and may require additives to generate a catalytically active species.[38] To avoid any doubt in catalyst activation, air-sensitive $Ni(cod)_2$ is frequently used as a reliable Ni(0) source that is soluble in many organic

solvents.[57] The 1,5-cyclooctadiene (cod) ligands can be displaced with stronger coordinating ligands such as phosphines, bipyridines, N-heterocyclic carbenes, etc. However, the presence of cod in the reaction mixture can have unanticipated results. For example, Schoenebeck and colleagues observed the formation of a Ni(dppf)(cod) complex as the resting state of their catalytic transformation after detailed mechanistic studies.[58]

Ni(II) precatalysts can also be reduced to a lower oxidation state in situ. Transmetallating agents, such as organomagnesiums, can transmetallate twice to form a bis(organo) Ni(II) species which can reductively eliminate to generate active Ni(0) and an organic byproduct (Scheme 1.8A).[43] Metallic Zn or Mn powder is often added to Ni-catalyzed reactions either as a catalytic or a stoichiometric additive.[45] However, this can create ambiguity in mechanism as reducing metals have been proposed to facilitate the formation of Ni(I) species (Scheme 1.8B).[59]

Nickel is known to comproportionate and disproportionate passively in solution (Scheme 1.8C). Comproportionation can be defined as a metal of oxidation state (n-1) donating an electron to metal of oxidation state (n+1), forming two metal centres of oxidation state (n). For example, a Ni(0) complex can give an electron (eg. through a chlorine radical) to a Ni(II) species which results in the formation of two Ni(I) centres. Disproportionation refers to the opposite reaction, where a Ni(I) centre donates an electron to another Ni(I) centre (eg. through a chlorine radical), thus forming a Ni(II) species and a Ni(0) species. As a result, by simply starting from a Ni(0) source and forming a clean Ni(II) oxidative addition complex, one cannot immediately rule out the possibility of Ni(I) being the active catalyst. Ni(I) can oxidatively add to electrophiles, such as aryl halides, to form Ni(III).[60] Ni(III) can either be reduced down to Ni(II) via a single-electron transfer or can directly reductively eliminate to Ni(I).[61]

A major challenge in the elucidation of nickel-catalyzed transformations is determining which oxidation states the active catalyst is going through. While there are many exceptions, palladium chemistry *usually* proceeds through either a Pd(0)/Pd(II) or, less commonly, a Pd(II)/Pd(IV) catalytic cycle.[62] Palladium has a rich history of mechanistic studies and many key organometallic intermediates have been well-characterized through a variety of methods including NMR, FT-IR, EPR, and single crystal X-ray crystallography.[63] In general, there is less data in the primary literature for nickel-based species. However, over the past decade, there has been a significant increase in detailed mechanistic studies of nickel-catalyzed transformations.[64]

Scheme 1.8. Methods to form Ni(0) from Ni(II)

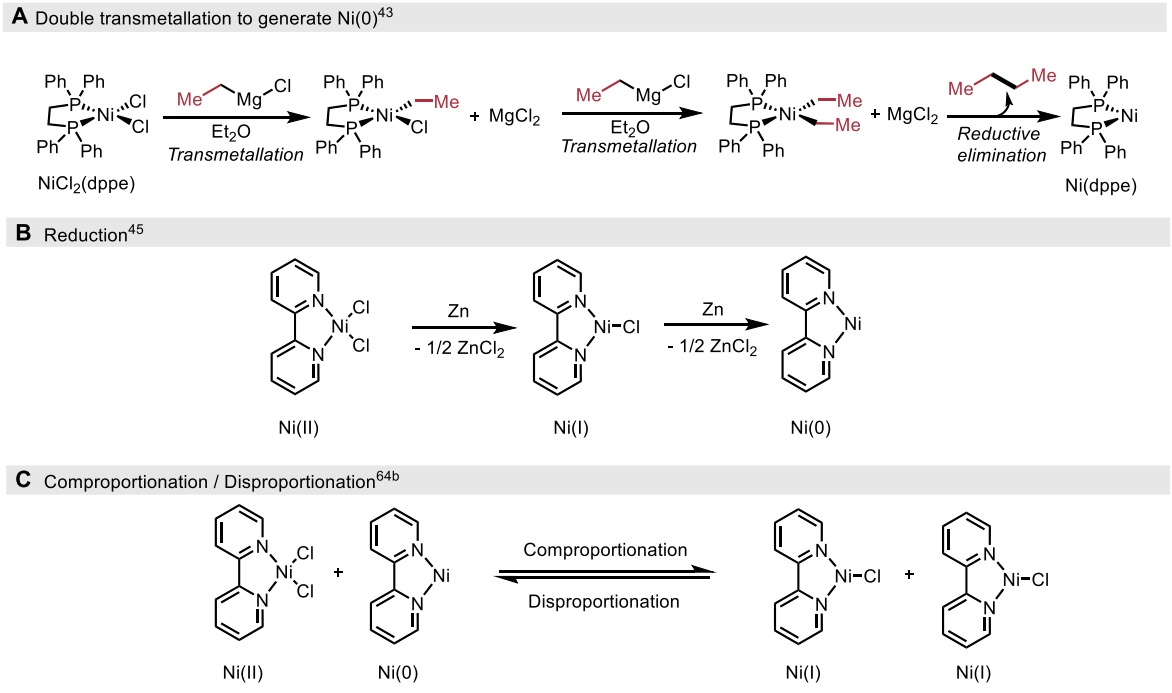

1.3.3 Where are the nickel-catalyzed Mizoroki-Heck reactions?

While nickel has been widely adapted for use in classical palladium-catalyzed cross-couplings, the Mizoroki-Heck reaction is an outlier. Intermolecular nickel catalyzed Heck reactions have been sparsely reported in the primary literature.

The first report of intermolecular Mizoroki-Heck reactivity using stoichiometric nickel was observed in 1973 by Otsuka et al.[65] The first nickel-catalyzed Mizoroki-Heck reaction was reported in 1981 between β-styrenyl halides and potassium 3-butenoate with poor regioselectivity and yield.[66] Throughout the 1980's and 1990's, many independent research groups reported nickel-catalyzed variants with a catch – stoichiometric zinc was required to turn over the catalyst (Scheme 1.11A).[67] While the use of zinc powder enabled product formation, it is an undesirable stoichiometric reductant in contemporary transition metal catalysis – especially for a redox-neutral transformation such as the Mizoroki-Heck reaction. It is wasteful to use a stoichiometric metal to promote the catalytic activity of another metal. This is very relevant considering that simple palladium precatalysts (eg. $[Pd(PPh_3)_4]$ or $Pd(OAc)_2$) can efficiently perform Mizoroki-Heck reactions, generating acid (HX) as the only formal waste product.[8]

In 1994, Sugi *et al.* reported a reductant-free Ni-catalyzed Mizoroki-Heck coupling of aryl halides and acrylic esters (Scheme 1.11B).[68] Their approach enabled low nickel-loading (1 mol%) and excellent selectivity; however, the reaction conditions were harsh, requiring 160 °C. Notably at 180 °C, the authors observed undesired polymerization, indicating that there is a small thermal window where productive chemistry may occur. Noting the rarity of mild nickel-catalyzed Mizoroki-Heck conditions, Walker and Sevov recently discovered an electrocatalytic variant that proceeds at 70 °C (Scheme 1.11C).[69] However, the regioselectivity of their method varied

significantly depending on the type of alkene used. Walker and Sevov proposed that the Ni(II) oxidative addition complex is not readily reduced to Ni(I) under their electrocatalytic conditions. Cyclohexenone was added as an ancillary ligand to coordinate to nickel, forming a redox active Ni(II) centre. The authors postulated that Ni(I) was the active catalyst and that slow catalytic activity of the Ni(II) oxidative addition complex under thermal conditions could be a result of comproportionation to form Ni(I) in situ. This theory could also explain the low catalyst turnover observed under thermal conditions. More broadly, this research may help to explain why zinc powder is prevalent in nickel catalyzed Mizoroki-Heck couplings and why reactivity in its absence is often poor – it could serve as a convenient method to generate Ni(I) from a Ni(0) or Ni(II) precatalyst.

While the aforementioned methods offer little practical advantage to contemporary palladium-catalyzed Mizoroki-Heck couplings, over the past decade nickel has become increasingly prevalent in the regioselective cross-coupling of aryl pseudohalides with alkenes.

Scheme 1.9. Landmark examples highlighting the challenges of nickel-catalyzed Mizoroki-Heck reactions

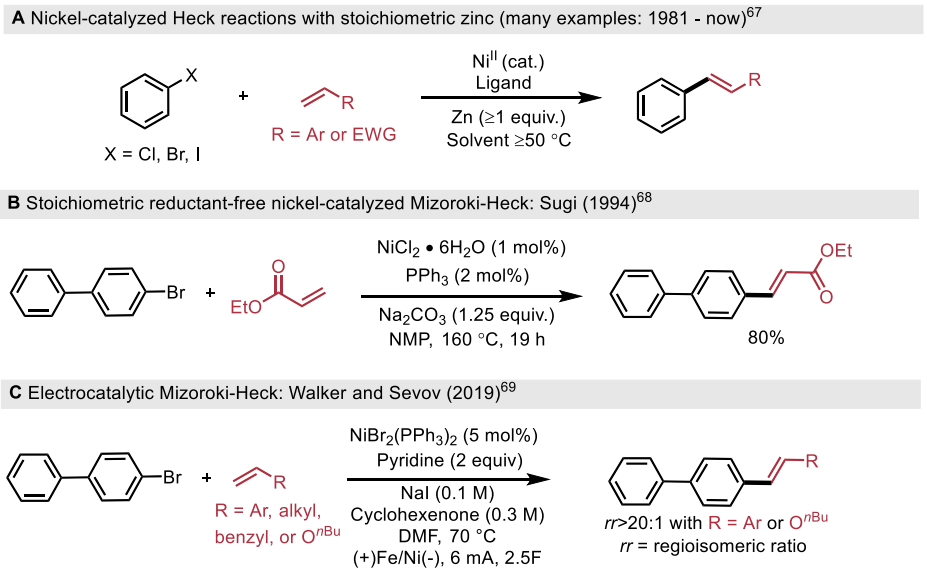

These applications will be discussed further in detail (see: Section 1.4)

In 2004, Guo et al. published a computational study comparing palladium- and nickel-catalyzed Mizoroki-Heck reactions to elucidate why the latter were sparsely reported.[70] Scheme 1.9 demonstrates a theoretical catalytic cycle with the *relative* difficulty of each step indicated relative to palladium. While oxidative addition (**1.6**→**1.7**) and β-migratory insertion (also called 1,2-alkene insertion, **1.8**→**1.9**) is facile, the β-hydride elimination (**1.9**→**1.10**) is proposed to be a challenging step along with the reductive elimination (**1.10**→**1.6**). A more recent DFT study by Cundari et al. comparing the ability of Ni- and Pd-NHC complexes to perform the Mizoroki-Heck reaction came to the same general conclusions as Guo and coworkers.[71] This adds a layer of complexity as the alkyl nickel species (**1.9**) is calculated to be considerably more stable than the palladium analogue and there is no thermodynamic driving force to form the β-hydride elimination product (**1.10**). This suggests that β-hydride elimination is far more reversible under general nickel-catalyzed Mizoroki-Heck conditions than general palladium-catalyzed conditions.

It can be challenging to study discrete catalytic steps when the intermediates are unstable and can't be isolated. As a result, there have been limited experimental mechanistic studies on nickel β-hydride eliminations. Nonetheless, Cámpora et al. reported a stoichiometric study comparing the β-hydride elimination of nickel and palladium methoxide complexes, **1.11**,

Scheme 1.10. Elementary steps of a nickel-catalyzed Mizoroki-Heck mechanism (Guo)[70]

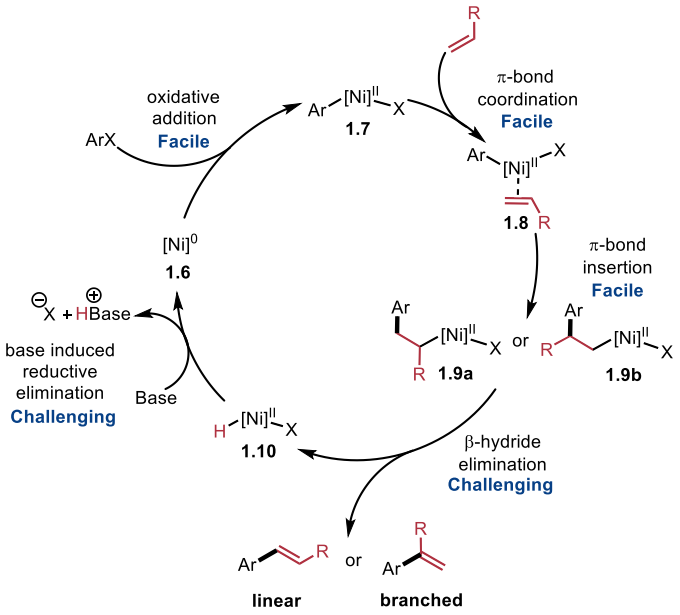

stabilized by pincer ligands (Scheme 1.10).[72] Their detailed mechanistic study corroborated theoretical claims in the primary literature – palladium β-hydride elimination was more kinetically and thermodynamically favourable than the corresponding nickel β-hydride elimination. Scheme 1.10 also reinforces the divergent reactivity between palladium and nickel. The authors proposed multiple pathways for the decomposition of the nickel hydride species **1.12a** to carbonyl complex **1.13a**. Notably, reductive elimination from species **1.12b** to dimer **1.13b** was proposed to occur through a dissociative mechanism that is unfavourable for the corresponding nickel complex **1.12a**.

Although β-hydride elimination and reductive elimination are challenging organometallic steps for nickel, that doesn't preclude Mizoroki-Heck reactivity. However, it does offer an explanation why a limited selection of intermolecular Heck-type reactions have been reported with nickel relative to the abundance of palladium-catalyzed Heck-type reactions. The following sections will highlight advancements and contemporary challenges in nickel Heck-type reactions.

Scheme 1.11. Comparing the β-hydride eliminations of Ni and Pd pincer complexes

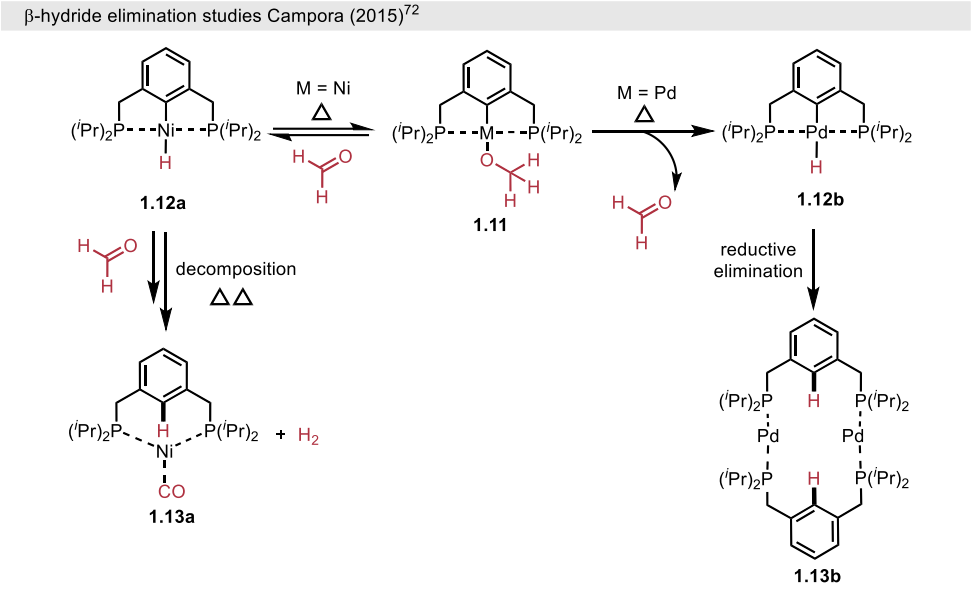

1.4 Nickel-catalyzed Mizoroki-Heck couplings with aryl pseudohalides

A methodology was reported by Jamison and coworkers in 2014 to enable the highly branch-selective (also referred to as α-selective) arylation of terminal alkyl olefins through a Mizoroki-Heck coupling (Scheme 1.12A).[73] In a preceding communication from 2011, the regioselective benzylation of aliphatic olefins was also reported by the Jamison group through a similar mechanism.[74] The authors note that this was the first report of appreciable selectivity with unbiased aliphatic alkenes with regioisomeric ratios *(rr)* > 19:1 for most examples. The reaction is proposed to go through a cationic nickel mechanism, owing to the poorly-coordinating triflate (trifluoromethanesulfonate) counter-ion, which was crucial for obtaining high regioselectivity. Aryl chlorides were used with TESOTf – a species which may induce a halide exchange on the metal centre; however, the corresponding aryl triflate could also be used directly without addition of TESOTf. An unconventional 1,4-bis(dicyclopentylphosphonium)butane bis(tetrafluoroborate) bidentate ligand was used for this transformation. Jamison and coworker's optimal ligand had superior selectivity compared to commonly used ligands for Ni and Pd catalysis. The explanation for this trend was attributed to a mixture of steric and electronic effects – Jamison et al. hypothesized the decreased nickel-carbon bond length amplifies steric effects by bringing the organic component closer to the metal. Although not initially intuitive, regioisomeric ratio (*rr*) appears to be partially affected by the choice of base. To explain this trend, the authors propose that a long-lived nickel-hydride species could erode *rr* over time through reversible olefin insertion followed by β-hydride elimination at a different position (Scheme 1.12A). A palladium-catalyzed variant with high selectivity (*rr* >20:1) remains unreported in the primary literature – although there is one example with moderate selectivity.[75]

Skrydstrup et al. reported the nickel-catalyzed α-selective arylation of vinyl ethers in 2012 (Scheme 1.12B).[76] Noting that the Jamison group had effectively used TESOTf in a nickel catalyzed Heck reaction, the authors opted to try aryl triflates as coupling partners.[70] The reaction between phenyl triflate and *n*-butyl vinyl ether was reported to occur smoothly under mild conditions. While the regioselective reaction of electron-rich olefins with aryl triflates has been established with palladium catalysis,[77] Skrydstrup and coworkers proposed that their conditions are competitive with other variants.

Density-functional theory (DFT) calculations were performed by the Skrydstrup group to support mechanistic hypotheses. The reductive elimination was proposed to be the rate determining step in the catalytic cycle, paralleling the computational studies of nickel-catalyzed Mizoroki-Heck reactions by the Guo and Cundari groups (Section 1.3.3).[61,62] Cationic nickel intermediates, with a non-coordinating triflate anion, were shown to enable the chemistry by having an open coordination site for the olefin to interact with (Scheme 1.12B). Experimentally, stoichiometric halogen salt additives were found to shut down the reaction. The Skrydstrup group proposed that a counter-ion exchange was occurring and coordinating X-type ligands, such as halides, block the ability of the olefin to bind to the metal. This hypothesis was supported with a DFT study contrasting the reaction of an aryl bromide with *n*-butyl vinyl ether to the standard reaction conditions with an aryl triflate. The neutral Ni(II) oxidative addition complex (OAC) was found to be more stable than the corresponding cationic nickel(II) OAC by approximately 16.5 kcal/mol (Scheme 1.12B). The increased stability of the neutral complex increases the barrier of activation for subsequent catalytic steps, shutting down the reaction pathway when coordinating counter-ions are used.

The Watson group developed a *trans* linear-selective (also referred to as β-arylation) Mizoroki-Heck coupling between aryl pivalates and styrenes (Scheme 1.12C).[78] This approach was notable as it involves cleavage of a strong C—O bond and represents the first example of Mizoroki-Heck chemistry with a traditionally unreactive pseudohalide. No stoichiometric reductant was required to achieve reactivity when starting from a Ni(0) precatalyst. Stoichiometric zinc was added when starting from an air-stable Ni(II) salt; however, it was noted that this afforded lower yields than starting directly from $Ni(cod)_2$.

The discussion up to this point has focused on using olefins in Mizoroki-Heck reactions, as they are the conventional substrates. In 2017, the Newman group reported the redox-neutral arylation of aldehydes to ketones (Scheme 1.12D).[79] The reaction mechanism was proposed to proceed via a Heck-type catalytic cycle, using aldehydes as an alkene surrogate (Scheme 1.13). This reaction was proposed based on the plausibility and established precedence of the elementary catalytic steps. Subsequent generations of high-throughput experimentation and one-variable-at-a-time optimization uncovered broadly-applicable conditions.[80] Newman and coworkers proposed that a cationic Ni(II) species was capable of 1,2-insertion into an aldehyde, analogous to the more established 1,2-insertion into olefins. The π-bond insertion step in the Mizoroki-Heck reaction is a traditional example of 1,2-insertion, as the β-hydride elimination of the nickel alkoxide intermediate, **1.17**, generates the desired ketone product, **1.19**, and a nickel hydride species, **1.18**. **1.18** is proposed to react with a base, through a base-induced reductive elimination, to regenerate nickel(0) and turn over the catalytic cycle (Scheme 1.13). 1,1,1-Tris(diphenylphosphinomethyl)ethane, commonly known as triphos, is a tripodal phosphine ligand found to be uniquely effective in the chemistry. The exact reason for triphos' effectiveness

Scheme 1.12. Ni-catalyzed Heck-type couplings with aryl pseudohalides

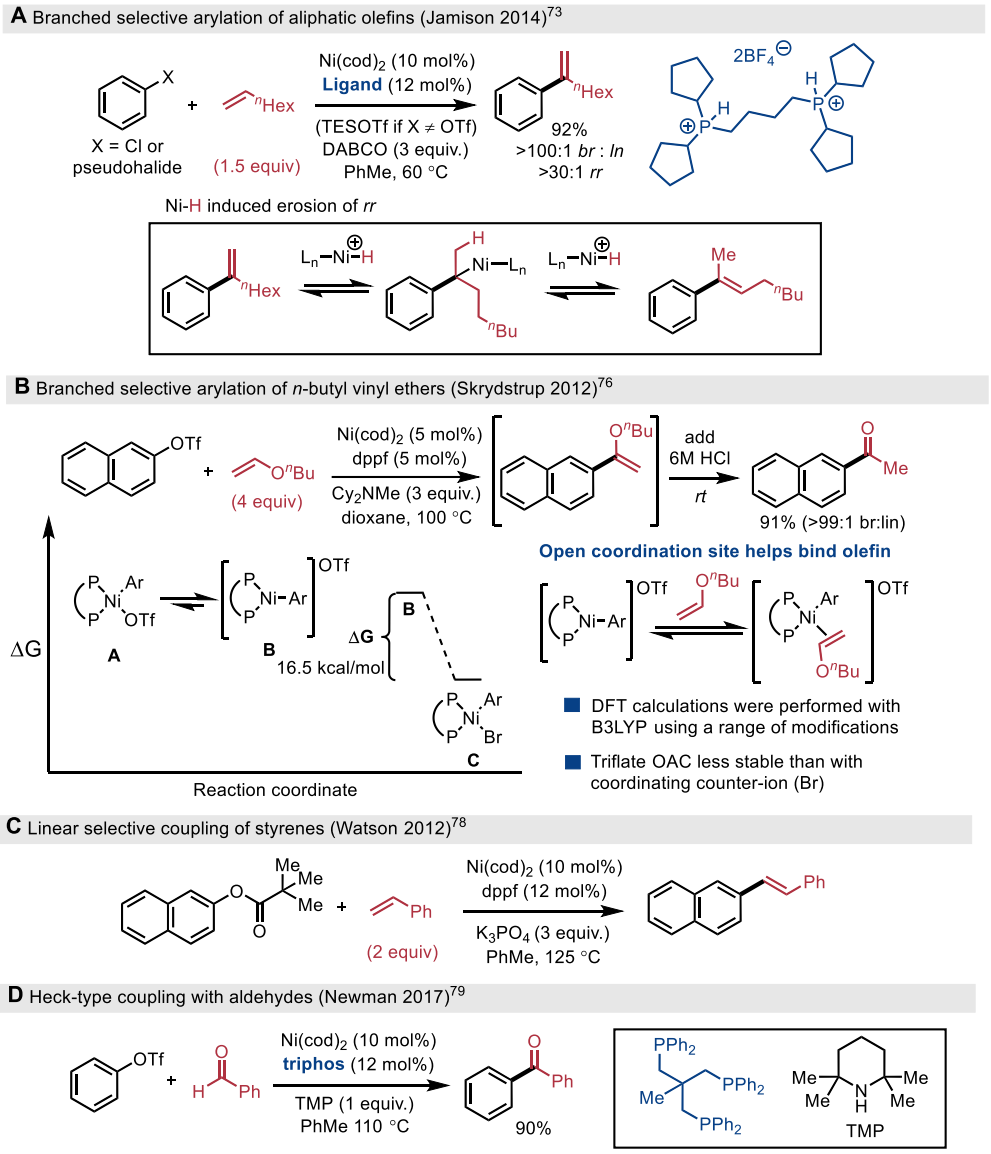

compared to commonly-used bidentate and monodentate phosphine ligands in the carbonyl-Heck reaction has not been established. To test whether a Thorpe-Ingold effect, from the quaternary carbon in the backbone of triphos, was a key feature of the tripodal ligand, the bidentate analogue with a germinal dimethyl backbone was prepared. 2,2-Dimethylpropane-1,3-diylbis(diphenylphosphane), dppdpm, afforded trace coupling under the reaction conditions

compared to triphos (Scheme 1.14A). In a similar vein, triphos analogues were tested indicating that structural changes to triphos did not improve chemistry and, in all cases, resulted in significantly decreased yields compared to the standard yield of 90% (Scheme 1.14B).

Scheme 1.13. Proposed catalytic cycle for the carbonyl-Heck reaction

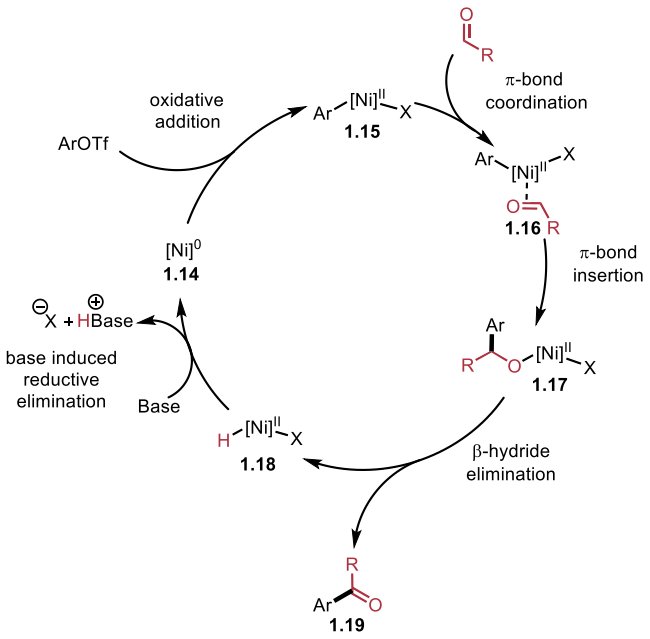

As mechanistic support of a Heck-type reaction, Newman et al. ran two Mizoroki-Heck substrates, in parallel, under the standard carbonyl-Heck conditions (Scheme 1.14C-D). Significant product was obtained with both olefins, despite reaction conditions being unoptimized for them, reinforcing a unified reaction mechanism. Notably the coupling with styrene afforded both the linear *trans* stilbene (β-arylated) and the branched 1,1-diphenylethylene (α-arylated) in roughly equal amounts. Similar selectivity has been observed with dppp when coupling aryl triflates with styrene.[81]

It remains unclear why triphos is an effective ligand for the carbonyl-Heck reaction. One plausible theory is that triphos enforces structural rigidification of the resulting nickel complex

through a κ^3-P,P,P interaction or that the pendant phosphorus arm acts as an intramolecular base to rapidly deprotonate a nickel hydride. Surprisingly, triphos^{Si}, a structural variant that replaces the quaternary carbon atom with a silicon atom, resulted in only trace formation of benzophenone (Scheme 1.14B).

Scheme 1.14. Ligand studies and Mizoroki-Heck under Newman's conditions

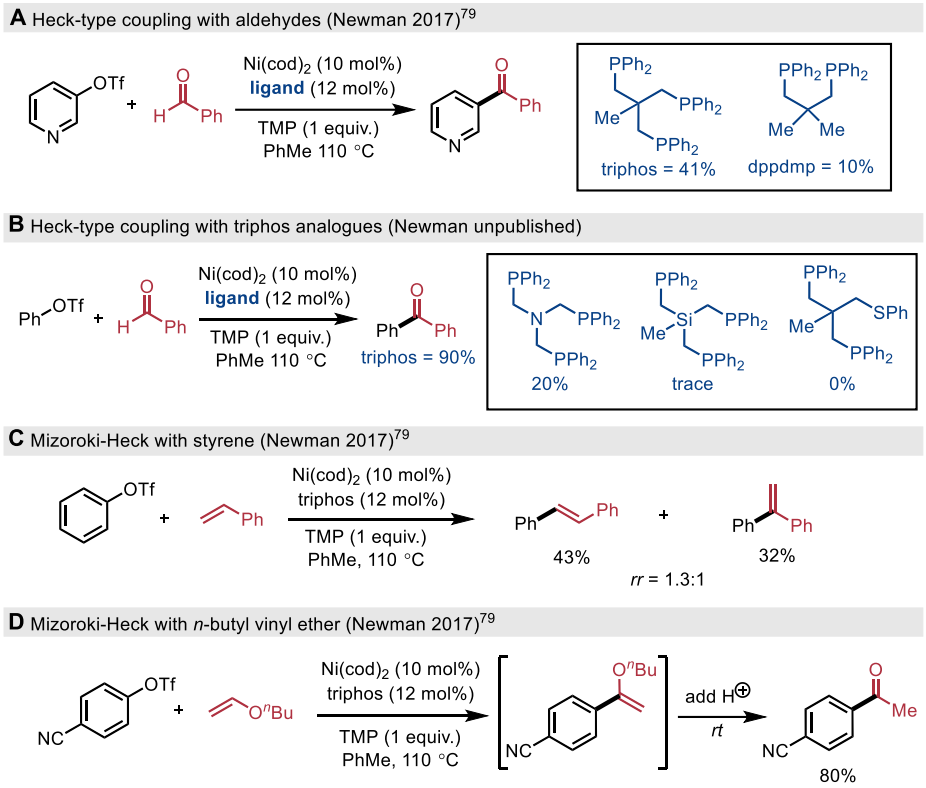

We wished to further study the mechanism of carbonyl-Heck couplings. Preparing a library of catalytically-relevant triphos analogues could provide strong mechanistic information about the nature of triphos as a highly-effective ligand. However, the triphos analogues presented in Scheme 1.14A/B did not provide any obvious trends about beneficial or deleterious ligand features. As some very close structural analogues to triphos or dppp did not provide intuitive data, it was unclear if strong mechanistic evidence could be ascertained. Literature

conditions for the synthesis of triphos derivatives were also diverse, and, as such, a single modular reaction pathway could not be used to prepare a large family of derivatives.

Serendipitously, we became aware of 1,5-diaza-3,7-diphosphacyclooctane (P_2N_2) ligands as unique bidentate phosphine ligands. P_2N_2 ligands feature a pendant amine arm, which is not entirely dissimilar to triphos. As such, we decided to perform a detailed literature search on this class of ligands and their application in organic synthesis. The following section will provide an introduction to P_2N_2 ligands, their synthesis, and the state-of-the-art catalytic transformations reported with them.

Figure 1.1 Comparing the structures of triphos to a P_2N_2 core

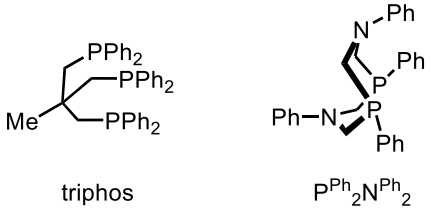

triphos $P^{Ph}{}_2N^{Ph}{}_2$

1.5 1,5-Diaza-3,7-diphosphacyclooctanes (P_2N_2) ligands

In 1980, the synthesis of novel heterocyclic compounds featuring a 1,5-diaza-3,7-diphosphacyclooctane ring was first disclosed by Schoerner and coworkers.[82] **Note**: Today, these species are commonly abbreviated as P_2N_2 ligands. P_2N_2 has also been used in the literature to describe any ligand featuring two phosphorus and two nitrogen atoms.[83] To avoid any confusion, unless otherwise noted, P_2N_2 will refer exclusively to the 1,5-diaza-3,7-diphosphacyclooctane framework throughout this dissertation rather than any ligand featuring two phosphorus atoms and two nitrogen atoms.

Bis(hydroxymethyl)organophosphines were found to undergo condensation reactions in the presence of primary amines resulting in the selective formation of eight-membered rings (Scheme 1.15A). It is conventional to name P_2N_2 compounds $P^R{}_2N^{R'}{}_2$ – in which R and R' refer to the substituents on phosphorus and nitrogen, respectively. This seminal work by Schoerner et al. also studied how a simple P_2N_2 ligand, $P^{Ph}{}_2N^{Ph}{}_2$, interacts with metal complexes (Scheme 1.15B). The aforementioned study reported that $P^{Ph}{}_2N^{Ph}{}_2$ acts as a bidentate ligand via coordination of both phosphorus atoms to form nickel and molybdenum complexes. Of particular note, the hard Lewis basic anilines were not observed to coordinate to the metal centres in either solution (NMR analysis) or solid phase (single X-ray crystals).

Despite the unique features of the P_2N_2 ligands and their modular synthesis, this class of ligands was not investigated in detail by synthetic organic chemists. Nonetheless, a range of novel P_2N_2 variants and their associated coordination complexes were prepared – primarily in the early 2000's.[84] See Section 1.5.3 for a detailed overview of the coordination complexes with P_2N_2 ligands and closely related analogues.

Scheme 1.15 Initial discovery and coordination of P_2N_2 ligands

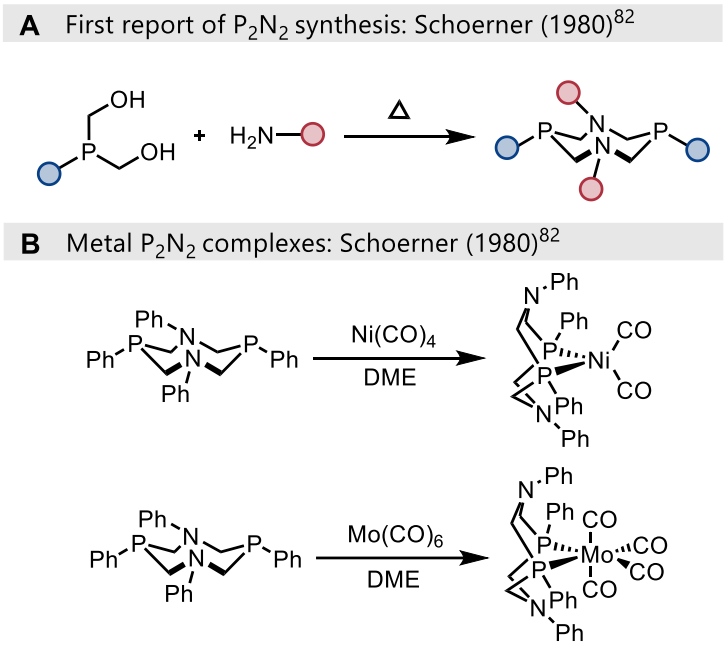

1.5.1 Methods to prepare P_2N_2 ligands and literature review

A recent review by Moissev et al. has extensively detailed the synthetic methods to prepare P_2N_2 ligands amongst a wider range of structurally-related P,N-acetals.[85] A brief summary of the contemporary pathways to prepare the P_2N_2 scaffold along with representative examples of each transformation are presented in Scheme 1.16 with key literature citations. A common feature of all main reaction pathways is the formation of an intermediate bis(hydroxymethyl)organophosphine which has desired organic R substituent on the phosphorus. What differentiates the synthetic pathways is the method of how this intermediate is prepared.

The most common method to prepare bis(hydroxymethyl)organophosphines is from mixing the corresponding primary phosphine (H_2PR) with formaldehyde (Scheme 1.16A). Paraformaldehyde is often used in the place of formaldehyde and depolymerisation occurs in the pot without requiring exogenous acid or base. Scheme 1.16B provides an alternative pathway to

Scheme 1.16 Common methods to prepare P_2N_2 ligands

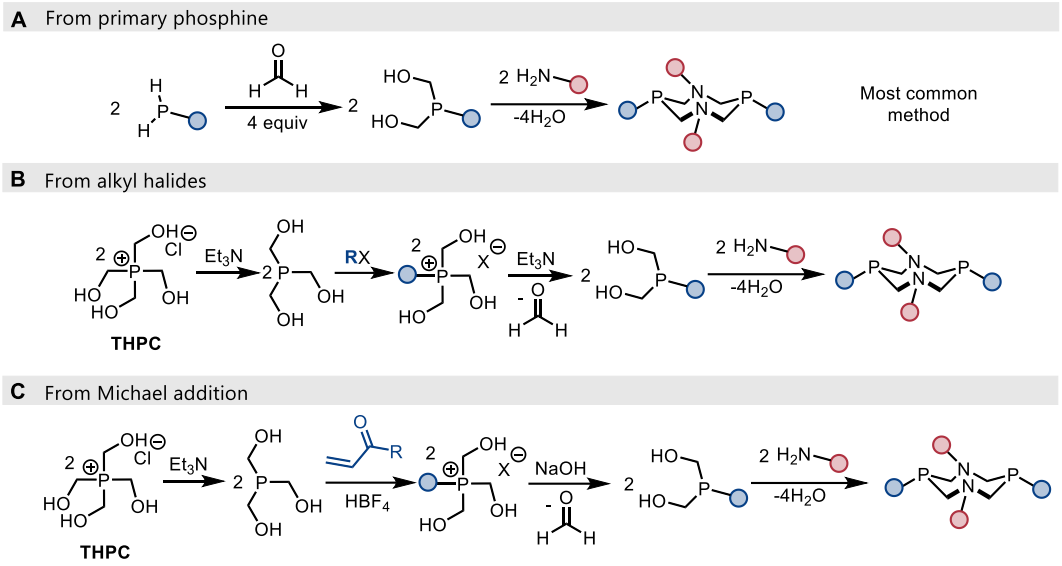

synthesize P_2N_2 ligands – which bypasses the need for primary phosphines. Kubiak and coworkers reported a modification of known organophosphorus chemistry starting from tetrakis(hydroxymethyl)phosphonium chloride (THPC), an air-stable precursor.[86] Under basic conditions, tris(hydroxymethyl)phosphine is formed and this can react directly with an organohalide (RX) to form a phosphonium salt. Under basic conditions, this phosphonium salt can be deprotected to the desired bis(hydroxymethyl)organophosphine. Condensation with a free amine leads to formation of the desired $P^{R}_2N^{R'}_2$ ligand. This method allows preparation of P_2N_2's from which the parent primary phosphine is not readily available. Scheme 1.16C shows a less common but useful pathway to prepare P_2N_2 ligands from Michael acceptors.[87] Tris(hydroxymethyl)phosphine can instead react with an α,β-unsaturated carbonyl via a 1,4-conjugate addition to furnish an alkyl phosphonium salt, which is subsequently deprotected under basic conditions to the desired bis(hydroxymethyl)organophosphine. From this

intermediate, the standard condensation reaction with a primary amine can occur to yield the $P^{R}_{2}N^{R'}_{2}$ ligand.

P_2N_2 ligands have been prepared with a wide range of functionalities on phosphorus. Scheme 1.17 shows a literature survey of reported P_2N_2 ligands highlighting the diversity of phosphorus substituents.[86-99] Many of the primary phosphines presented in Scheme 1.17 are not currently commercially available as of 2023 and, in general, require multistep air-sensitive chemistry to prepare. Primary phosphines are prone to aerobic oxidation and are often pyrophoric when neat.[100] These properties limit the accessibility of primary phosphines, as the synthesis and workup of these compounds must be air-free. Analogously, the intermediates associated with preparing P_2N_2 ligands from alkyl halides (Scheme 1.16B) or Michael acceptors (Scheme 1.16C) are also air-sensitive. Low molecular weight primary phosphines, such as $^{i}PrPH_2$, are gaseous and can be prepared in situ from hydrolysis of the corresponding phosphide.[98]

Scheme 1.17 Variation of P_2N_2 phosphorus substituents

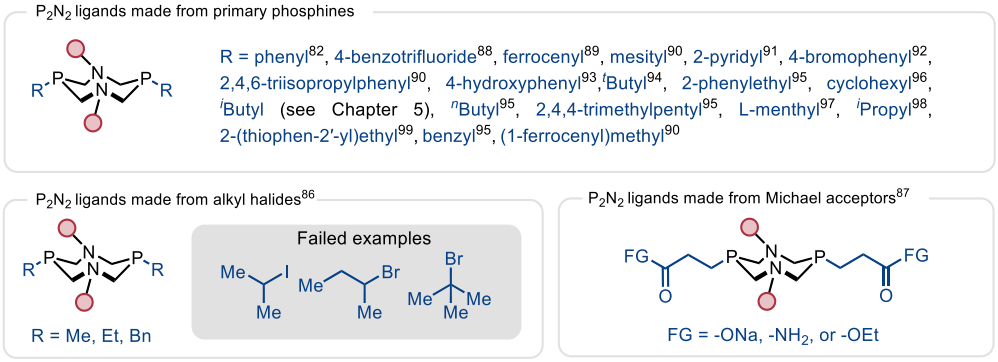

A wide range of primary amines have been used to synthesize P_2N_2 ligands. The particular N-substituent can have a drastic effect on the observed reaction outcome by influencing the secondary coordination sphere of the metal centre (see 1.5.4 for examples of reactions using

Scheme 1.18 A small selection of diverse primary amines used to make P_2N_2 ligands

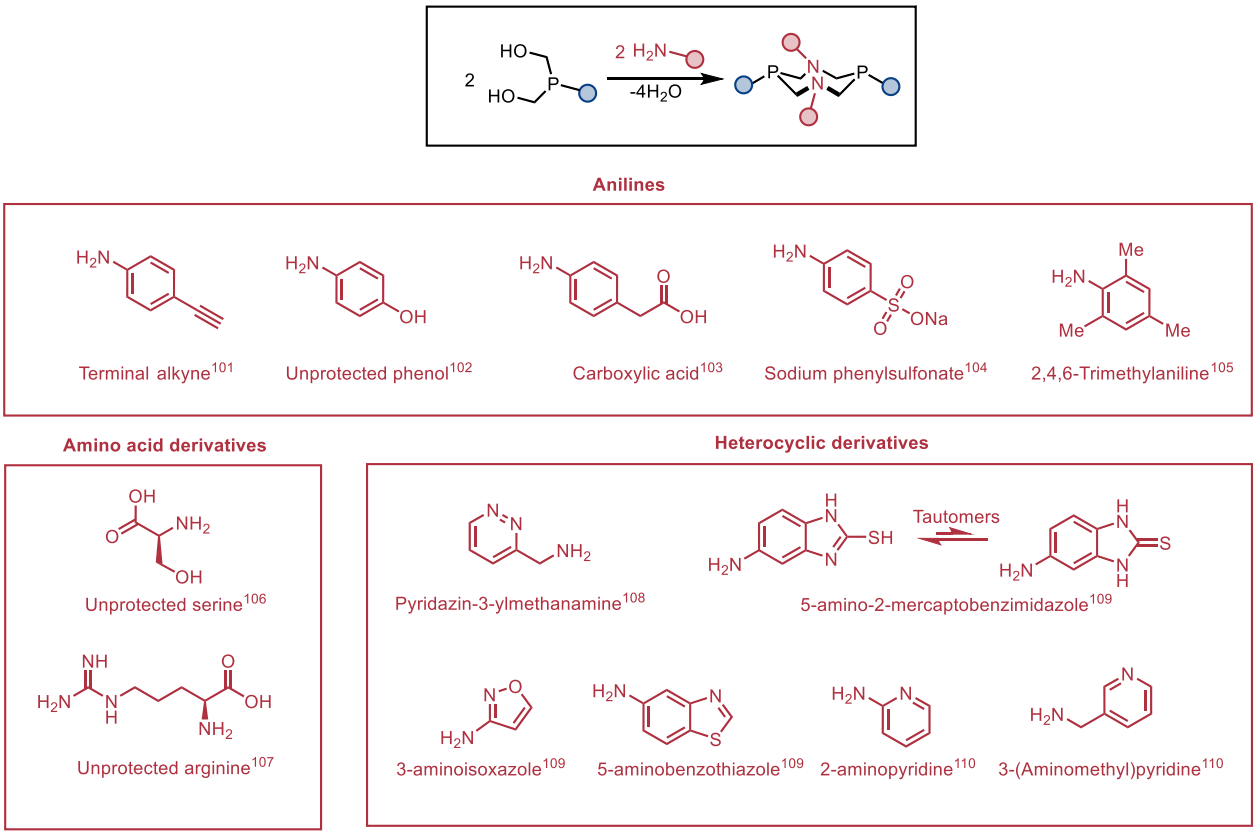

P_2N_2 ligands). Simple amines are generally well-tolerated in the synthesis and have been widely used with the methods from Scheme 1.16– see Moissev et al. for representative examples.[85] Scheme 1.18 highlights a subset of primary amines bearing synthetically diverse functionalities which successfully formed P_2N_2 ligands and, in most cases, have been directly applied to transition metal electrocatalysis. Arenes bearing mildly acidic groups,[101,102] an unprotected carboxylic acid,[103] a polar salt,[104] and a hindered aniline[105] have all been incorporated into P_2N_2 ligands without requiring protecting groups or modified procedures. Unprotected serine, bearing a free alcohol, and unprotected arginine, bearing a guanidino group, successfully formed P_2N_2 ligands without any special modifications to the synthesis.[106,107] Additionally, a range of heterocyclic amines have also been reported.[108-110]

1.5.2 Direct derivatization of P_2N_2 ligands

P_2N_2 ligands are rarely modified after cyclization. All reported modifications involve orthogonal reactions with distal functionalities attached to either the phosphorus or the nitrogen atoms. Schemes 1.19-1.21 detail three unique modifications of P_2N_2 ligands.

In Scheme 1.19, lithium-halogen exchange can be exploited to functionalize an aryl bromide. Of particular note, P_2N_2 ligands derived from either 4-bromophenylphosphine *or* 4-bromoaniline could be functionalized through this method.[92] Kubiak and coworkers quenched the reactive carbanion with a chlorophosphate electrophile, although it is assumed that a variety of electrophiles could react with the aryl lithium species.

Scheme 1.19 Lithium-halogen exchange to modify P_2N_2 ligands after cyclization: Kubiak (2020)[92]

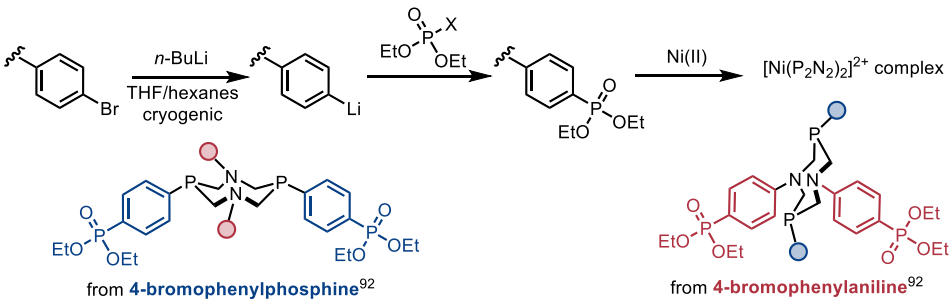

Scheme 1.20 details the applicability of peptide couplings towards P_2N_2 modification.[111] A variety of amino acids can be coupled to increase the complexity and alter the secondary coordination sphere around the metal centre. Notably, a P_2N_2 ligand was appended to a solid phase amino acid resin.[112]

Scheme 1.20 Peptide coupling to modify P_2N_2 ligands after cyclization: Shaw (2011)[111]

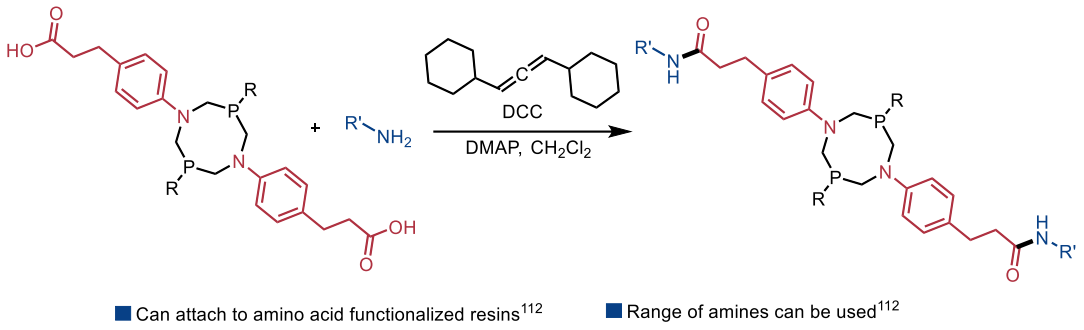

Scheme 1.21 shows that P_2N_2 ligands bearing alkynes can participate in click chemistry. In this case, the Lewis basic phosphorus lone pairs had to be protected with borane. Bullock et al. indicated that this protection step was necessary; otherwise no product was observed and, in some cases, decomposition to an unknown species could be observed via NMR studies.[101] Once the phosphorus atoms were protected, a copper-catalyzed click reaction formed the desired triazole cleanly. This process was performed in order to attach the P_2N_2 ligand to a glassy carbon electrode – a solid surface for electrocatalysis. DABCO, a Lewis-basic saturated heterocycle, could be used to remove the borane protecting groups on the phosphorus atoms.

Scheme 1.21 Click coupling to modify P_2N_2 ligands after cyclization: Bullock (2015)[101]

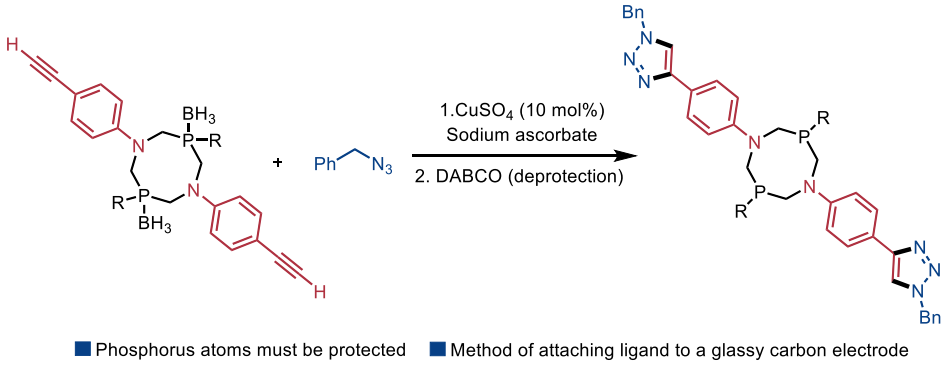

While it is clear from the preceding examples that P_2N_2 ligands can be further modified after synthesis, this is seldom done. In most cases, the desired functionality can be directly installed on the corresponding phosphine or amine prior to synthesis of the ligand. Currently

these derivatization methods are not applicable to commercially available primary phosphines. A method to directly functionalize the phosphorus substituent on P_2N_2 ligands derived from abundant primary phosphines would be highly desirable and useful. Likewise, there are no reported methods to further functionalize the methylene groups of the P_2N_2 core.

1.5.3 Transition metal coordination complexes of P_2N_2 ligands

The preceding sections have focused on the methodologies associated with preparing P_2N_2 ligands. The coordination chemistry of metals bound to P_2N_2 ligands is rich and diverse. Figure 1.2 highlights the *d*-block elements that have at least one well-defined crystal structure and corresponding spectroscopic data for a metal P_2N_2 complex. Most first row transition metals have reported complexes. The nature of the complex, the relevant citation, and the relative abundance of documents for each metal is detailed in Table 1.1. While methods of binding can vary between the elements, all representative transition metal complexes (Table 1.1, entries 1-14) feature P_2N_2s acting as multidentate ligands with the exception of gold (Table 1.1, entry 15).

Figure 1.2 *d*-block elements which have at least one well-defined P_2N_2 complex

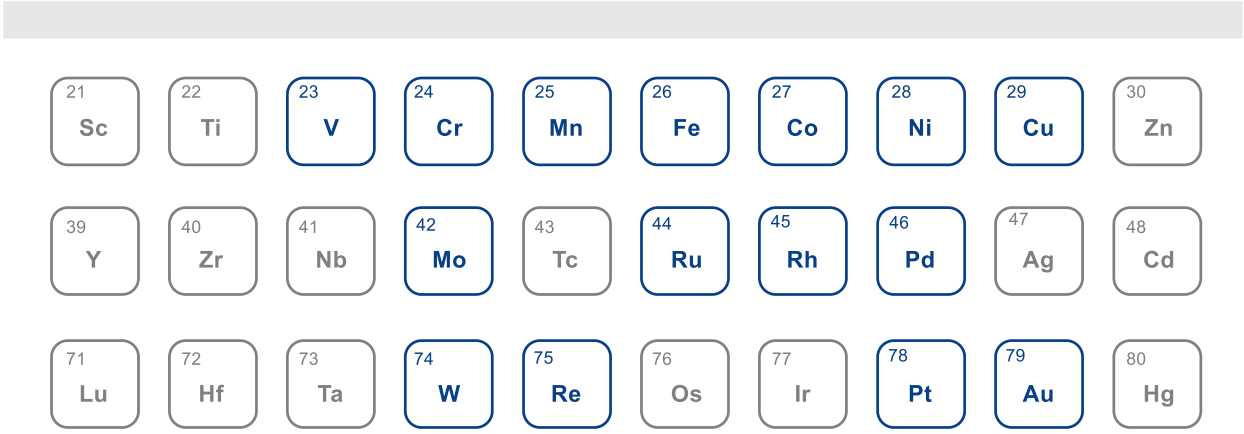

Greyed out elements do not have reported P_2N_2 complexes. Fourth row *d*-block elements were omitted as they are radioactive and not naturally abundant.

Table 1.1 Literature precedence of transition metal P_2N_2 complexes

Entry	Metal	Representative complex	Relative abundance	Citation
1	Vanadium	$CpV(P^{Ph}{}_2N^{Ph}{}_2)I$	1 document	[113]
2	Chromium	$(k^3\text{-}P^{Ph}{}_2N^{Bn}{}_2)CrCl_3$[a]	<5 documents	[114]
3	Manganese	$Mn(P^{Ph}{}_2N^{Bn}{}_2)(dppm)(CO)(H)$[b]	<5 documents	[115]
4	Iron	$CpFe(P^{Ph}{}_2N^{Ph}{}_2)Cl$	>20 documents	[116]
5	Cobalt	$[Co(P^{tBu}{}_2N^{Ph}{}_2)(MeCN)_3](BF_4)_2$	>20 documents	[117]
6	Nickel	$[Ni(P^{tBu}{}_2N^{Bz}{}_2)(MeCN)_2](BF_4)_2$	>20 documents	[117]
7	Copper	$[Cu(P^{2\text{-}py}{}_2N^{p\text{-}tol}{}_2)_2]I$[c]	~10 documents	[118]
8	Molybdenum	$Mo(P^{Ph}{}_2N^{2\text{-}py}{}_2)(CO)_4$	<5 documents	[119]
9	Ruthenium	$[CpRu(P^{Ph}{}_2N^{Ph}{}_2)(MeCN)]PF_6$	~10 documents	[105]
10	Rhodium	$[Rh(P^{Ph}{}_2N^{Ph}{}_2)_2]PF_6$	<5 documents	[120]
11	Palladium	$PdCl_2(P^{Ph}{}_2N^{Bn}{}_2)$	~10 documents	[119]
12	Tungsten	$W(P^{2\text{-}py}{}_2N^{p\text{-}tol}{}_2)(CO)_4$[c]	<5 documents	[121]
13	Rhenium	$Re[(R,R)\text{-}P^{Ph}{}_2N^{\alpha\text{-}MeBn}{}_2]Br(CO)_3$[d]	1 document	[122]
14	Platinum	$Pt(P^{2\text{-}py}{}_2N^{p\text{-}tol}{}_2)Cl_2$[c]	~10 documents	[121]
15	Gold	$Au_2(P^{Ph}{}_2N^{p\text{-}tol}{}_2)Cl_2$	~10 documents	[123]

[a] k^3- P,P,N [b] dppm = diphenylphosphinomethane. [c] P_2N_2 derived from 2-pyridylphosphine and *p*-toluidine [d] P_2N_2 derived from phenylphosphine and (*R*)-α-methylbenzylamine

Generally, P_2N_2 ligands coordinate to metal centres as bidentate ligands through the phosphorus atoms.[113-123] In some cases, such as the indicated chromium complex (Table 1.1,

entry 2), tridentate k^3-(P,P,N) binding can be observed around the metal centre. Gold (Table 1.1; entry 15) is most likely an exception due to the general propensity of Au(I) centres to form linear complexes.[124] Notably, no iridium complexes bearing P_2N_2 ligands (Figure 1.2) have been reported in the primary literature. This is most likely an oversight as opposed to an incompatibility, as iridium is known to ligate bidentate phosphines.[125] Where possible, well-defined complexes bound bidentate to one P_2N_2 ligand were selected as representative examples for Table 1.1. However, certain metals such as Cu (Table 1.1 entry 7) or Rh (Table 1.1 entry 10) have only been isolated and fully characterized as bis(P_2N_2) metal complexes in the primary literature.

Scheme 1.22 provides an overview of P_2N_2 coordination modes that have been reported in the primary literature. It is important to know how the ligand binds the metal in order to propose mechanistic pathways or to understand why P_2N_2 ligands have unique properties compared to other bidentate ligands. Notably, many transition metals, particularly nickel, are able to form mono(κ^2-P_2N_2) metal complexes *or* bis(κ^2- P_2N_2) metal complexes depending on P_2N_2 stoichiometry and lability of ligands already bound to starting metal precursor (Scheme 1.19A).[96] Tridentate κ^3-P,P,N coordination of P_2N_2 ligands has been reported with octahedral[114,] or half sandwich metal complexes[126] – in some cases, an equilibrium between the κ^3-P,P,N form and the κ^3-P,P,agostic form exists in solution (Scheme 1.22B).[127] The agostic bond, formally a 3-centre-2-electron bond, was computationally modelled and the donating C-H bond was found to be *anti* to nitrogen's lone pair. In very simplified terms, partial overlap of nitrogen's lone pair into the σ* (antibonding) orbital of the C-H bond weakens it and giving the hydrogen some "hydride" characteristic. This increase in electron density allows for donation into an empty metal *d*-orbital

as an agostic interaction. It should be noted that equilibrium for this Mn(I) system favored the κ^3-P,P,N form, although the κ^3-P,P,agostic form was still accessible and spectroscopically visible in solution.[127] More recently, κ^3-P,P,Ar bonding of a P_2N_2 ligand to Ru was observed in a half sandwich complex (Scheme 1.22B).[128] Both crystal structure and spectroscopic studies indicated that the phenyl substituent on $P^{Cy}{}_2N^{Ph}{}_2$ was coordinated to the Ru metal centre.

Copper and gold P_2N_2 complexes are well-precedented to form multimetallic clusters (Scheme 1.22C).[129] This is generally controlled by altering metal-to-ligand ratio.[123,129] A Cu bridged dimer complex (Scheme 1.22C) features a P_2N_2 ligand derived from 2-(2'- pyridyl)ethyl-phosphine. The pyridyl ring acts as a ligand forming a bidentate chelate around the Cu centres. This example is particularly unique as 2-(2'-pyridyl)ethylphosphine has rarely been used to make P_2N_2 ligands.[99]

While many different transition metals form well-defined complexes with P_2N_2 ligands through a range of binding modes, most of these complexes were prepared for targeted mechanistic studies or as proof-of-concept coordination complexes rather than for catalytic use. The following sections will discuss the catalytic applications of P_2N_2 ligands.

Scheme 1.22 Modes of P_2N_2 coordination to transition metals

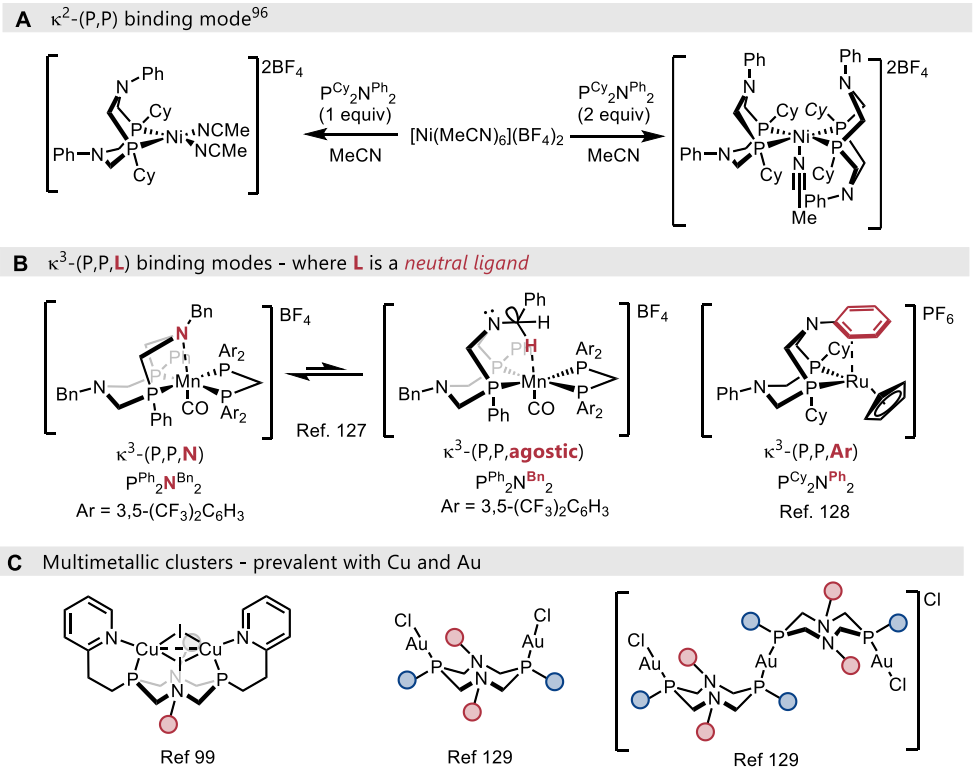

Where applicable, P_2N_2 ligand backbone has been greyed out for clarity.

1.5.4 Electrocatalytic applications of P_2N_2 ligands

1,5-Diaza-3,7-diphosphacyclooctanes (P_2N_2's) are most commonly used as ligands in electrocatalytic reduction or oxidation chemistry. A recent review has extensively detailed the history, contributions, and developments of metal P_2N_2 electrocatalysts; therefore, only a brief overview will be presented here.[130]

Energy can be stored in chemical bonds between two atoms. Electrons can serve as an energy source. The formal reaction of 2 electrons with 2 protons can be used to create hydrogen gas, for storage of energy (Scheme 1.23A). Conversely, one molecule of hydrogen gas can be split into two protons and two electrons to release energy.[130]

Researchers at Pacific Northwest National Laboratories (PNNL) recognized that P_2N_2 ligands have pendant amines which bear structural similarity to the active site of [FeFe]-hydrogenases – a family of metalloenzymes which are responsible for hydrogen splitting in living organisms. The pendant amine in [FeFe]-hydrogenases is proposed to be actively involved in hydrogen splitting.[130]

Metal bis(P_2N_2)-complexes, such as those indicated in Scheme 1.23B and Scheme 1.23C, were found to facilitate hydrogen oxidation or formation of hydrogen with an emphasis on first-row transition metals. $[Ni(P_2N_2)_2]^{2+}$ electrocatalysts react with hydrogen gas in a unique fashion. Oxidative addition to a Ni(IV) dihydride complex was not observed.[130] Instead, the hydrogen gas is split into two protons and two electrons. The two electrons serve to reduce Ni(II) to Ni(0) through a short-lived Ni(I)-hydride species, while the two protons can react with the Brønsted basic pendant amines forming protonated complexes (Scheme 1.23C). [131] Under basic electrochemical conditions, the Ni(0) can be oxidized back to Ni(II) and the base can deprotonate the P_2N_2 ligand allowing for another equivalent of hydrogen to react with the catalyst. This process can also occur in reverse to *form* hydrogen gas from protons and electrons. Mechanistic studies have implicated that the pendant nitrogen arm must be *endo* (boat relationship to nickel centre) in order to split hydrogen.[132]

Computational studies of $[Ni(P_2N_2)_2]^{2+}$ complexes indicated that there are up to seven conformers which are energetically accessible at ambient temperature and the energy of chair-to-boat interconversions were similar in magnitude to those reported for other saturated six-membered rings. [133] It is assumed that interconversion between P_2N_2 conformers occurs dynamically in solution – analogously to cyclohexane.

Scheme 1.23 Energy storage and metal P_2N_2 electrocatalysts

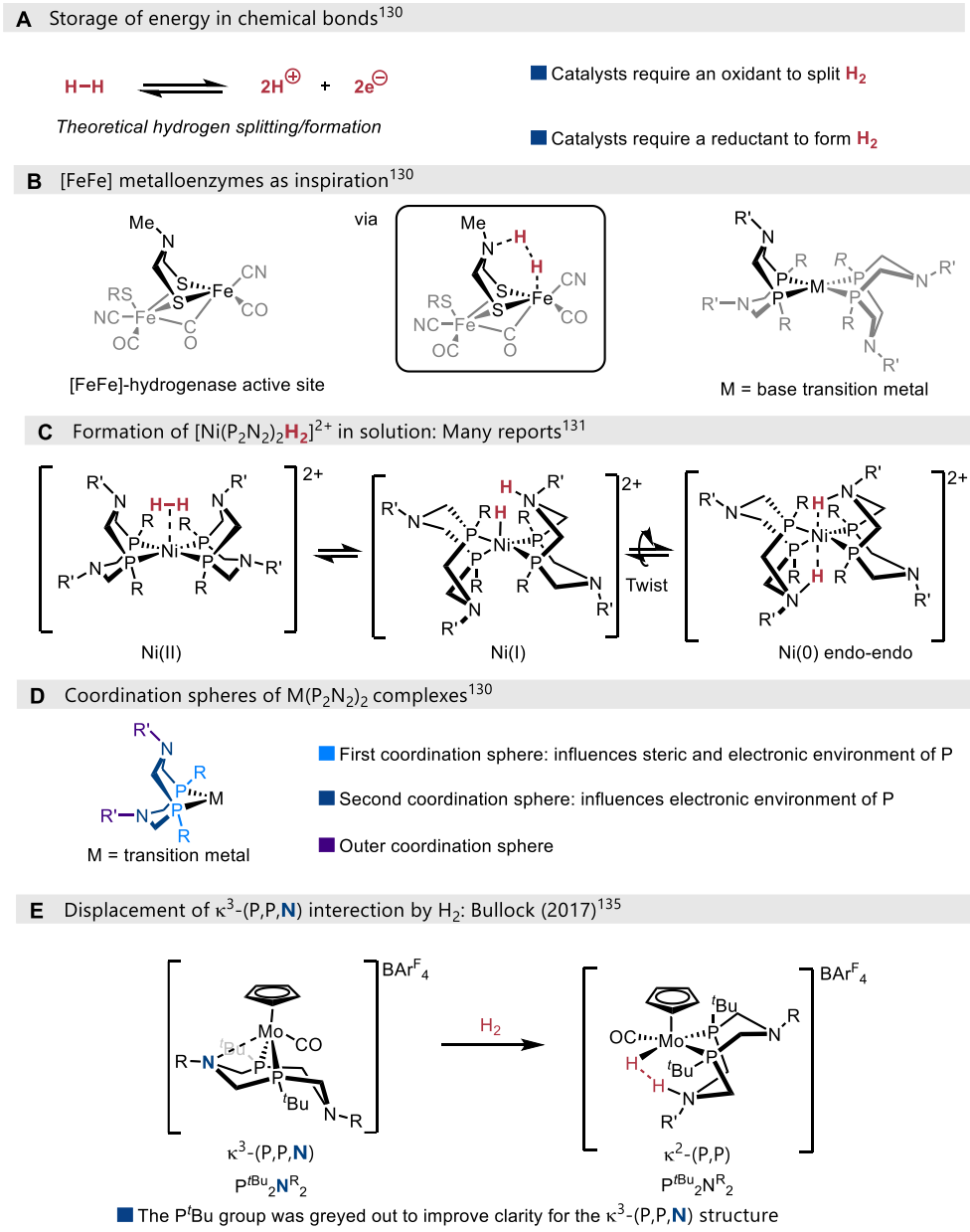

Extensive mechanistic studies uncovered the role of the primary, secondary, and extended coordination spheres around the central metal atom. The first coordination sphere relates to atoms which directly coordinate to the metal centre and their spatial surroundings (Scheme 1.23D). As P_2N_2 ligands share a common backbone, the first coordination sphere is differentiated by the functionality of the R group on phosphorus. This tunes the electronics of

the phosphorus atom but can also impart steric effects to resulting metal complexes. Steric bulk on the phosphorus atom can have an influence on geometry of $[Ni(P_2N_2)_2](BF_4)_2$ complexes and can also affect physical properties such as reduction potential.[86] Electron-withdrawing and/or sterically bulky R groups on phosphorus renders the Ni(II)/Ni(I) reduction more facile.[130,134] Conversely, electron-donating and/or less bulky R groups on phosphorus renders the Ni(II)/Ni(I) reduction less facile.

The second coordination sphere comprises the pendant amine arms of the P_2N_2 ligand. It is generally assumed, for electrocatalysis, that the amines are not directly ligated to the metal centre. While this may appear to contrast the coordination modes of P_2N_2 ligands discussed in Section 1.5.3, κ^3-(P,P,N) binding has not been observed with nickel P_2N_2 complexes. The distance between the Ni and the pendant amine is approximately 3.1-3.4 Å, when in boat conformation, based on reported X-ray crystal structures.[130] In the case of κ^3-(P,P,N) binding, such as with the $[CpMo(CO)(\kappa^3\text{-}P_2N_2)]^+$ complex, the Mo-N bond was found to be particularly weak and could be displaced by hydrogen (Scheme 1.23E).[135] This indicates that κ^3-binding modes of P_2N_2 ligands does not necessarily impede productive hydrogen splitting.

The electronics of the substituent R' on the amine group for the generic ligand $P^R_2N^{R'}_2$ imparts a profound effect on the kinetic rates of electrocatalysis. One may think that the more basic the amine, the faster the reaction – as the proposed mechanism involves protonation of both amines. However, this is not the case. When evaluating a series of P_2N_2 ligands derived from *para* substituted anilines, DuBois et al. found that there was a correlation between enhanced kinetic rates and *decreasing* the electron-density of the aniline derivatives when studying hydrogen formation.[136] These findings indicated that $P^R_2N^{R'}_2$ ligands with electron donating R'

groups (such as *p*-anisole) had a decreased isomerization equilibrium, which is required to form H_2 gas (Scheme 1.24; going from *exo*-*exo* to *endo*-*endo*). In other words, a trend was observed where P_2N_2 ligands made from a series of increasingly electron-deficient anilines resulted in faster production of hydrogen. An exception to the trend, a P_2N_2 ligand derived from *p*-aminobenzotrifluoride, is proposed to be insufficiently basic and, thus, cannot proceed through the protonation mechanism.[115] Therefore, altering the electronic nature of the second coordination sphere can influence reactivity of nickel P_2N_2 complexes.

Computational studies have detailed the intertwined relationship between the first and second coordination spheres.[137] Altering the electronic nature of the substituent on phosphorus (R) or on nitrogen (R') has an effect on the overall physical properties of the corresponding $[Ni(P^R{}_2N^{R'}{}_2)_2]^{2+}$ complex such as the redox potentials (eg. Ni^{II}/Ni^{I}) or the pKa of the corresponding protonated amine. Raugei et al*.* reported equations which require minimal data input to obtain predictive models the properties of $[Ni(P^R{}_2N^{R'}{}_2)_2]^{2+}$ complexes. These equations can be broken down into components related to the phosphorus substituent (experimentally determined Ni^{II}/Ni^{I} and Ni^{I}/Ni^{0} redox potentials for the desired complex) and a component related to the nitrogen subsituent (pKa of the parent aminium ion).[116] To summarize, this work implicates an "electronic communication" between the first and second coordination spheres.[130]

The outer (or third) coordination sphere represents the most distal portion of the P_2N_2 – more specifically, any group that is not part of the 1,5-diaza-3,7-diphosphacyclooctane core functionality (Scheme 1.24). Immobilization of the catalyst system to a solid support, such as in Scheme 1.20 or Scheme 1.21, is often achieved through a linkage in the outer coordination sphere. O'Hagan and coworkers noticed a surprising trend when increasing the length of an alkyl

chain in the outer coordination sphere – the longer the alkyl chain, the faster the rate of hydrogen production.[138] Prior to this discovery, the outer coordination sphere was not implicated in having an effect on catalytic performance and was generally thought as being peripheral.[130] The outer coordination sphere was responsible for controlling the boat-chair equilibrium leading to a protonated species which does not directly result in the production of H_2 (Scheme 1.25). Longer alkyl chains in the outer coordination sphere were found to disrupt the boat-chair equilibrium, thus, increase the rates of hydrogen formation by decreasing the equilibrium population of unreactive species.

Scheme 1.24 Effect of the second coordination sphere on hydrogen production

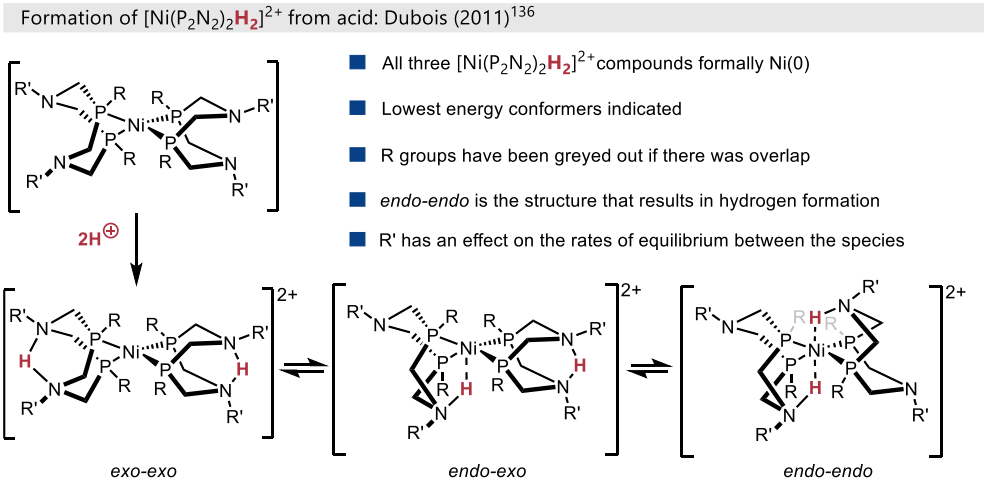

Introduction of a proton relay in the outer coordination sphere has also been shown to facilitate mobility of protons. Mechanistically, the movement of protons to (in the case of hydrogen formation) or from (in the case of hydrogen splitting) the metal centre is a crucial aspect of the electrocatalytic transformation. Introduction of Brønsted basic functionalities in the outer coordination sphere has been observed to shuttle protons, further indicating that distal functionalities can improve catalytic properties.[108]

Scheme 1.25. Effect of outer coordination sphere on productive chemistry

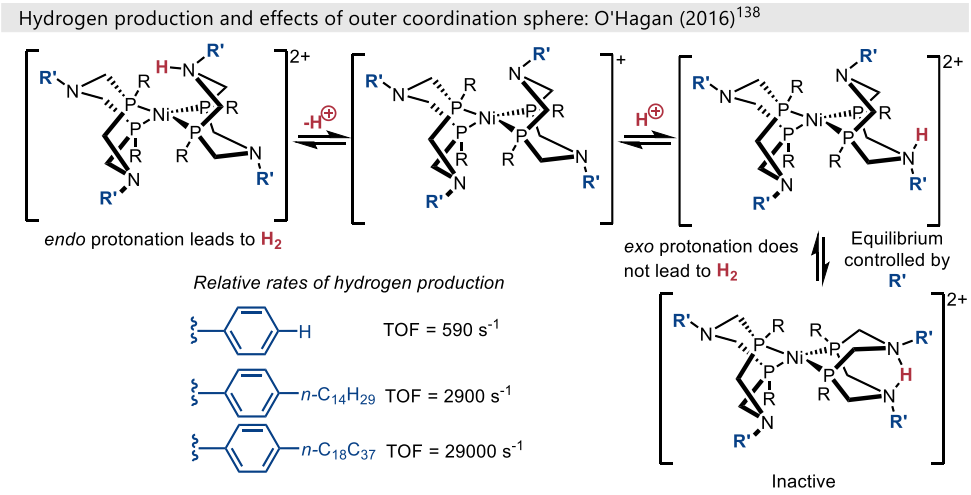

1.5.5 Other applications of P_2N_2 electrocatalysts

The utility of P_2N_2 catalysts is not limited solely to hydrogen-related applications, although electrochemical reactions with hydrogen are the main focus of the primary literature. The formal reduction of oxygen gas with hydrogen gas to form water has been reported, although the exact nature of the mechanism is not known (Scheme 1.26A).[139] A phosphine oxide metal complex was isolated from the reaction mixture; however, this was found to be catalytically inactive suggesting that this could be the aerobic decomposition of an active catalyst.

Formation of carbon dioxide through the oxidation of formate or the reduction of carbon dioxide to formic acid[140] has been reported with first row transition metal catalysts (Scheme 1.26B). The mechanism of the oxidation of formate was originally proposed to involve direct deprotonation of the formyl group by the pendant amine arm.[96] However, upon further study, this mechanism has been revised to involve direct hydride transfer to the nickel centre, (Scheme 1.26B) bypassing the pendant arm.[141] The related hydrogenation of CO_2 to formic acid is also known with $[Rh(P_2N_2)_2]^+$ complexes.[120]

$[Ni(P_2N_2)(MeCN)_2]^{2+}$ complexes can oxidize primary or secondary alcohols under electrocatalytic conditions to the corresponding aldehyde or ketone (Scheme 1.26C).[142] Sterically bulky $P^{tBu}{}_2N^{R'}{}_2$ ligands were used in order to form the monoligated -P_2N_2 nickel(II) complexes. $[Ni(P_2N_2)_2]^{2+}$ complexes were less catalytically active and an induction period was observed, suggesting that dissociation of one bidentate P_2N_2 ligand is required. Subsequent computational studies suggested that the key β-hydride elimination step occurs through a four-coordinate Ni(II) complex.[143] Wiedner et al. reasoned that the alkoxide ligand is a strong donor ligand which supports low-spin, four coordinate complexes in solution, whereas the alcohol ligand is a weak donor ligand prior to deprotonation and thus, the six coordinate octahedral high-spin Ni(II) complex is favored prior to formation of the alkoxide (Scheme 1.26C). Multiple reaction pathways can lead to the low-spin Ni(II) species from the high-spin Ni(II) species, such as competitive deprotonation by the pendant amine versus direct deprotonation by the exogenous base or when the number of coordinated acetonitrile ligands decreases. The authors propose that multiple pathways similar in energy are simultaneously active resulting in the same thermodynamically downhill low-spin, four coordinate nickel species.

Scheme 1.26 Electrocatalytic reactions beyond hydrogen

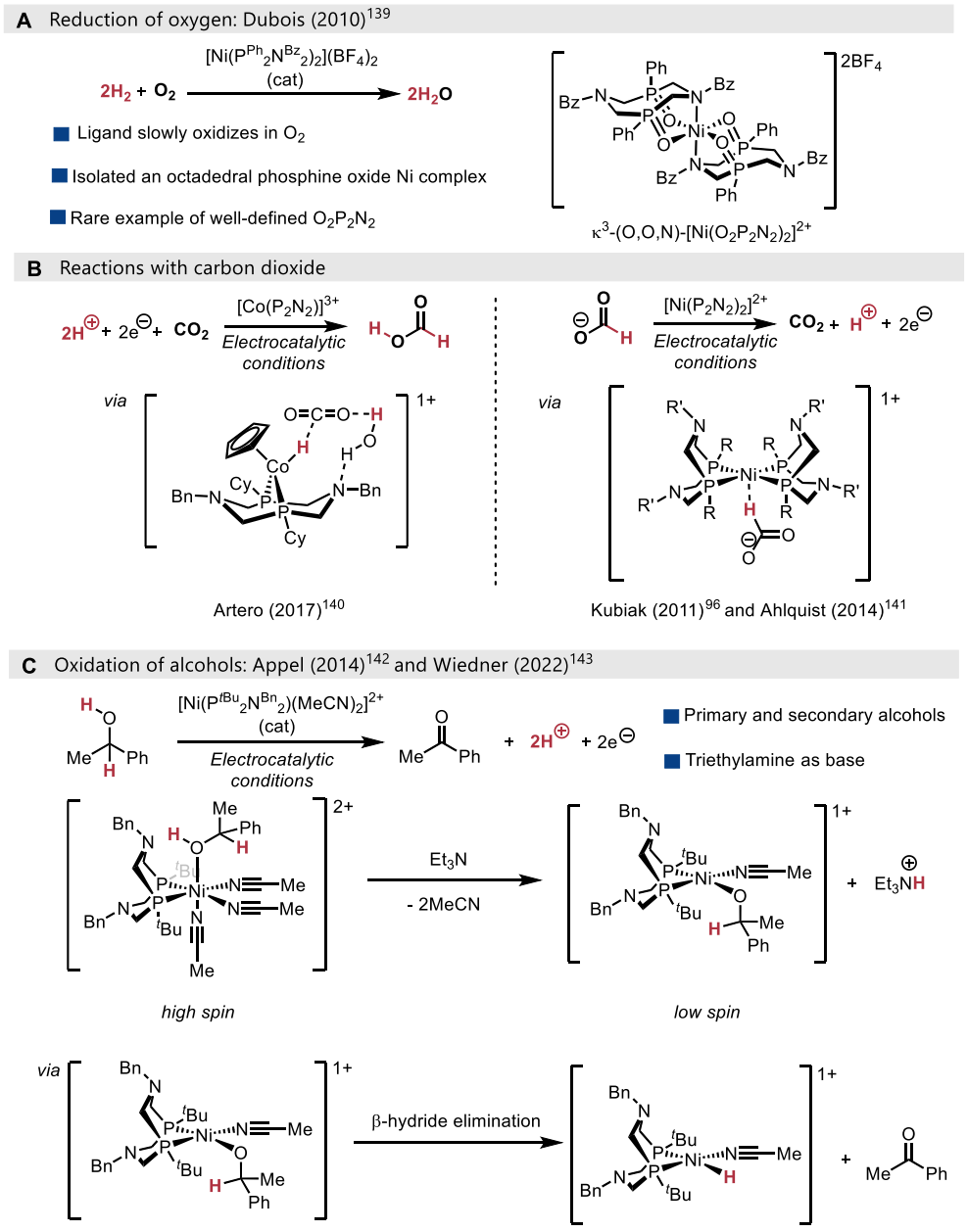

1.5.6 Beyond electrocatalysis: C—C, C—O, and C—N bond formation with P_2N_2 ligands

Despite the prominence of P_2N_2 ligands, there are only a handful of reports from synthetic organic chemistry applications. This is particularly surprising owing to the range of known transition metal complexes (Section 1.5.3) and the utility of P_2N_2 ligands in electrocatalysis (Section 1.5.4). In 2003, Karasik and collaborators disclosed that a Pd/P_2N_2 catalyst system enabled the copolymerization of norbornadiene and carbon monoxide (Scheme 1.27A).[122]

The first cross-coupling reaction with P_2N_2 ligands was discovered by Polshettiwar et al. in 2011 (Scheme 1.27B).[144] A Suzuki-Miyaura coupling using a Pd/P_2N_2 catalyst system was reported in aqueous solvent. Aryl bromides were coupled with boronic acids at low catalyst loading to afford biaryl products. While this catalyst system appears to be particularly efficient with $P^{Cy}{}_2N^{Ph}{}_2$, control experiments, such as whether there was reactivity in the absence of P_2N_2 ligand, were not run. Furthermore, no mechanistic experiments were reported and there was no follow-up work with P_2N_2 ligands published by the Polshettiwar group.

Blacquiere and coworkers have reported a range of Ru or Fe precatalysts that enable intramolecular cyclization of anilines and primary benzyl alcohols onto terminal alkynes forming heterocycles (Scheme 1.27C).[105,128,145] Originally, this work was targeting metal P_2N_2 complexes as catalysts for intermolecular anti-Markovnikov hydration of alkynes to form carbonyls (after tautomerization).[146] The first coordination sphere was assessed, indicating that sterically encumbered $P^{tBu}{}_2N^{Bn}{}_2$ ligand were generally superior to less bulky substituents on phosphorus, except for some deviation at elevated temperatures using ruthenium precatalysts.[145b] The pendant nitrogen arm was implicated as an endogeneous catalytic base – the corresponding conjugate acid is assumed to protodemetallate the resulting vinyl metal species after cyclization,

thus regenerating the base and metal catalyst. When $P^R_2N^{R'}_2$ ligands featuring an R' substituent that was less basic than the substrate alcohol or aniline were prepared, the corresponding [Ru] complexes were less catalytically active than those with R' substituents that were more basic than the corresponding substrate. [105] κ^3-P,P,Ar bonding of a P_2N_2 ligand to Ru was observed in an isolated single crystal as a half sandwich complex (Scheme 1.22B) – this interaction was proposed to stabilize the metal complex. Iron precatalysts were recently found to be applicable to the same transformation.[145c]

Despite the advances in catalytic reactions featuring P_2N_2's, there exists a large amount of chemical space which has not been surveyed with this class of ligands. We hypothesize that diverse libraries of P_2N_2 ligands can be used to solve challenges in catalysis and to discover new reactivity.

Scheme 1.27. C-C, C-O, and C-N bond formation using P_2N_2 ligands in catalysis

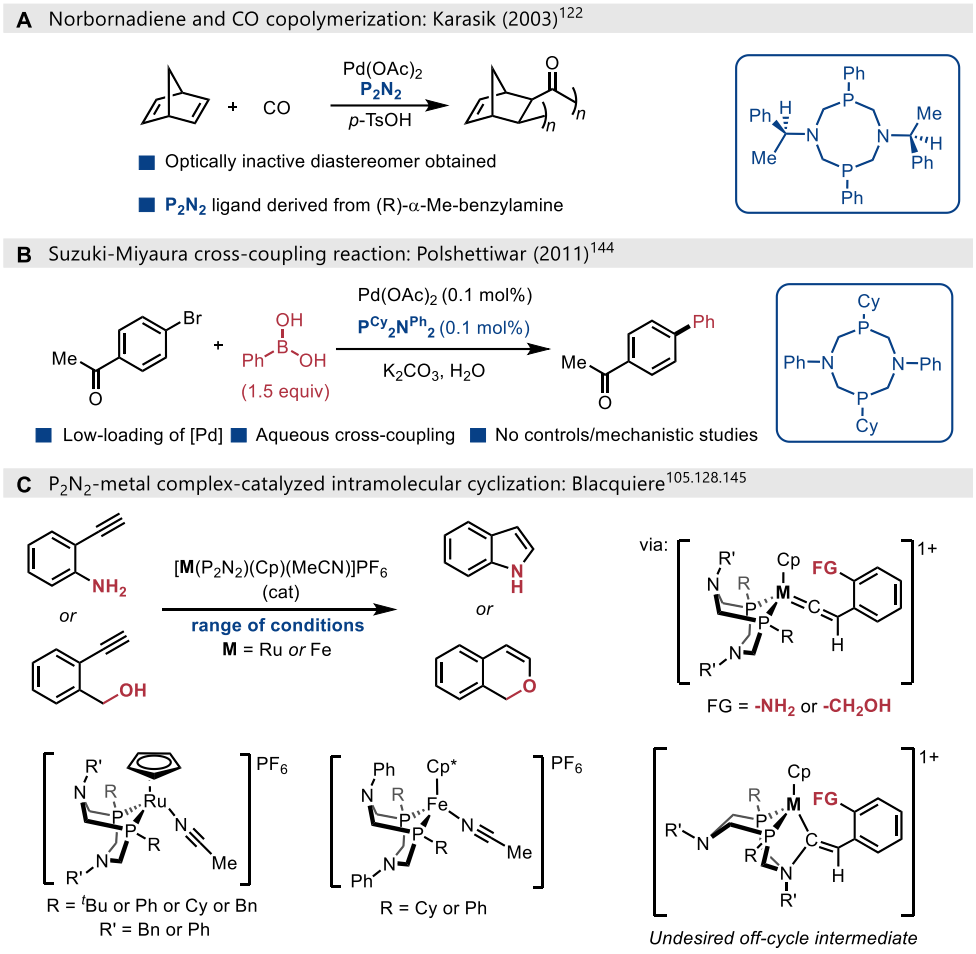

1.6 Research goals

As described in Section 1.4, 1,1,1-tris(diphenylphosphinomethyl)ethane, triphos, was identified as a powerful ligand in the coupling of aryl triflates with aldehydes by our group.[79] It was unintuitive why triphos was the optimal ligand, when similar phosphines failed. We hypothesized that high-throughput evaluation of Mizoroki-Heck couplings and related reactions could enable us to see the 'big picture' trends between ligands. This would allow us to more broadly study whether triphos is a "privileged" ligand for Heck-type couplings. Concurrently, we envisioned deeper mechanistic experiments to probe how variation of the triphos backbone affected the carbonyl-Heck coupling. High-temperature $^{31}P\{^{1}H\}$ NMR studies could uncover whether triphos is acting as a monodentate, bidentate, or tridentate ligand. Isolation of key intermediates and subsequent characterization by single crystal X-ray crystallography could also be used to determine if triphos enforces an atypical geometry. Knowledge about how triphos enables productive catalysis would allow for further development of new methodologies.

Expansion of the carbonyl-Heck coupling beyond aryl triflates was also desirable. Silyl-Heck[147] or boryl-Heck[148] variants of classical Mizoroki-Heck coupling are known in the literature. Modification of the carbonyl-Heck to couple silyl or boryl reactants with aldehydes could enable one-pot synthesis of acylsilanes or acylboranes, respectively (Scheme 1.28A and Scheme 1.28B).

However, we opted to start our study with a reductive variant of the carbonyl-Heck coupling. The catalytic arylation of aldehydes, as shown in Scheme 1.28C, was sparsely reported and had major limitations associated with widespread use (further detailed in Chapter 2). We

hypothesized that small modification of the carbonyl-Heck coupling conditions could achieve a robust and general reductive cross-coupling to form carbinol products.

Scheme 1.28 Extensions of the carbonyl-Heck coupling

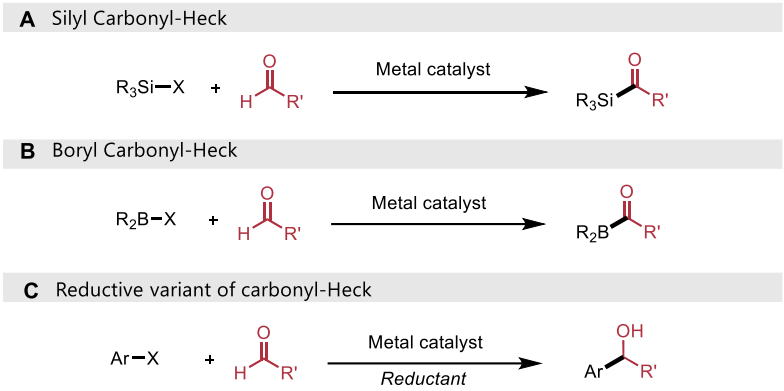

Finally, owing to our interest in having a modular library of ligands to screen in related couplings, we decided to prepare P_2N_2 ligands to screen in cross-coupling reactions. Owing to the limited reports in organic synthesis, we hypothesized that this class of ligands could have important uses in cross-coupling chemistry. We envisioned a high-throughput campaign testing a small, but distinct, subset of P_2N_2 ligands and comparing them to established ligands for late transition metal-catalyzed cross-couplings. We also hypothesized that the pendant arm of P_2N_2 ligands was not entirely dissimilar to the proposed hemilabile pendant arm of triphos and, as a result, P_2N_2 ligands could be used as surrogates to study the mechanism of carbonyl-Heck type chemistry. As P_2N_2 ligands have a rich history of mechanistic studies and isolated coordination complexes with first row transition metals, we believed that this could serve as a valuable guide for our own applications. As 1,5-diaza-3,7-diphosphacyclooctanes (P_2N_2) ligands feature a pendant Lewis basic arm and derivatives can be prepared through a convenient modular synthesis (Section 1.5.1), they could serve as an accessible alternative to the triphos

family of ligands (Section 1.4). Initial results were highly promising and the breadth of the research expanded.

1.7 References

[1] Barbier, P. Synthèse du diéthylhepténol. *C. R. Acad. Sci.* **1899**, *128*, 110-111.

[2] Freund, A. Ueber s. g. sauerstoffhaltige Radicale. *Justus Liebigs Ann. Chem.* **1861**, *118*, 33-43.

[3] Grignard, V. Sur quelques nouvelles combinaisons organométaliques du magnésium et leur application à des synthèses d'alcools et d'hydrocabures. *C. R. Acad. Sci.* **1900**, *130*, 1322-1325.

[4] Ullmann, F.; Bielecki, J. Ueber synthesen in der biphenylreihe. *Ber. Dtsch. Chem. Ges.* **1901**, *34*, 2174-2185.

[5] Goldberg, I. Ueber phenylirungen bei gegenwart von kupfer als katalysator. *Ber. Dtsch. Chem. Ges.* **1906**, *39*, 1691-1692.

[6] Kharasch, M.S.; Fields, E. K. Factors determining the course and mechanisms of Grignard reactions. IV. The effect of metallic halides on the reaction of aryl Grignard reagents and organic halides *J. Am. Chem. Soc*. **1941**, *63*, 2316-2320.

[7] Li, H.; Johansson Seechurn, C. C. C.; Colacot, T. J. Development of preformed Pd catalysts for cross-coupling reactions, beyond the 2010 Nobel prize. *ACS Catal.* **2012**, *2*, 1147–1164.

[8] (a) Mizoroki, T.; Mori, K.; Ozaki, A. Arylation of olefin with aryl iodide catalyzed by palladium. *Bull. Chem. Soc. Jpn.,* **1971**, *44*, 581. (b) Heck, R.F.; Nolley, J. P. Palladium-catalyzed vinylic hydrogen substitution reactions with aryl, benzyl, and styryl halides. *J. Org. Chem.* **1972**, *37,* 2320-2322.

[9] Sonogashira, K.; Tohda, Y.; Hagihara, N. A convenient synthesis of acetylenes: catalytic substitutions of acetylenic hydrogen with bromoalkenes, iodoarenes and bromopyridines. *Tetrahedron Lett.* **1975**, *16*, 4467-4470.

[10] Baba, S.; Negishi, E. A novel stereospecific alkenyl-alkenyl cross-coupling by a palladium- or nickel-catalyzed reaction of alkenylalanes with alkenyl halides. *J. Am. Chem. Soc.* **1976**, *98*, 6729-6731.

[11] Milstein, D.; Stille, J. K. A general, selective, and facile method for ketone synthesis from acid chlorides and organotin compounds catalyzed by palladium. *J. Am. Chem. Soc.* **1978**, *100*, 3636-3638.

[12] Miyaura, N.; Yamada, K.; Suzuki, A. A new stereospecific cross-coupling by the Palladium-catalyzed reaction of 1-alkenylboranes with 1-alkenyl or 1-alkynyl halides. *Tetrahedron Lett.* **1979**, *20*, 3437-3440.

[13] Hatanaka, Y.; Hiyama, T. Cross-coupling of organosilanes with organic halides mediated by a palladium catalyst and tris(diethylamino)sulfonium difluorotrimethylsilicate. *J. Org. Chem.* **1988**, *53*, 918-920.

[14] Knowles, J. P.; Whiting, A. The Heck–Mizoroki cross-coupling reaction: A mechanistic perspective. *Org. Biomol. Chem.* **2007**, *5*, 31-44.

[15] For representative examples of trace *cis* linear products see: (a) Beletskaya, I. P.; Kashin, A. N.; Karlstedt, N. B.; Mitin, A. V.; Cheprakov, A. V.; Kazankov, G. M. NC-palladacycles as highly effective cheap precursors for the phosphine-free Heck reactions. *J. Organomet. Chem.* **2001**, *622*, 89-96. (b) Li, S.; Lin, Y.; Xie, H.; Zhang, S.; Xu, J. Brønsted guanidine acid−base ionic liquids: novel reaction media for the palladium-catalyzed Heck reaction. *Org. Lett.* **2006**, *8*, 391–394. (c) Choi, M.; Lee, D.-H.; Na, K.; Yu, B.-W.; Ryoo, R. High catalytic activity of palladium(II)-exchanged mesoporous sodalite and NaA zeolite for bulky aryl coupling reactions: reusability under aerobic conditions. *Angew. Chem. Int. Ed.* **2009**, *48*, 3673–3676.

[16] Wang, C.; Dong, J.; Xu, D.; Li, T.; Zhao, X. Palladium-catalyzed semihydrogenation of alkynes with EtOH: Highly stereoselective synthesis of E- and Z-alkenes. *Synthesis* **2022**, *54*, 2687–2695.

[17] (a)Roughley, S.D.; Jordan, A. M. The medicinal chemist's toolbox: An analysis of reactions used in the pursuit of drug candidates. *J. Med. Chem.* **2011**, *54*, 3451-3479. (b) Brown, D.G.; Boström, J. Analysis of past and present synthetic methodologies on medicinal chemistry: Where have all the new reactions gone? *J. Med. Chem.* **2016**, *59*, 4443-4458.

[18] Budarin, V. L.; Shuttleworth, P. S.; Clark, H. J.; Luque, R. Industrial applications of C-C coupling reactions. *Curr. Org. Synth*., **2010**, *7*, 614–627.

[19] de Vries, J. G. The Heck reaction in the production of fine chemicals. *Can. J. Chem.* **2001**, *79*, 1086-1092.

[20] Blatcher, P.; Carter, M.; Hornby, R.; Owen, M. R. (Glaxo Group Ltd.). Process for the preparation of N-methyl-3-(1-methyl-4-piperidinyl)-1H-indole-5-ethane sulfonamide. WO/1995/09166, 1995; EP721453, 2002; U.S. Patent 5,659,040, 1997; U.S. Patent 5,786,473, 1998.

[21] Baumeister, P.; Meyer, W.; Oertle, K.; Seifert, G.; Steiner, H. Invention and development of a novel catalytic process for the production of a benzenesulfonic acid-building block *Chimia*, **1997**,*51*, 144-146.

[22] King, A. O.; Corley, E. G.; Anderson, R. K.; Larsen, R. D.; Verhoeven, T. R.; Reider, P. J.; Xiang, Y. B.; Belley, M.; Leblanc, Y. An efficient synthesis of LTD4 antagonist L-699,392. *J. Org. Chem.* **1993**, *58*, 3731–3735.

[23] Harrington, P. J.; Lodewijk, E. Twenty years of naproxen technology. *Org. Process Res. Dev.* **1997**, *1*, 72–76.
[24] Wu, T.-C.; Chockalingham, K. C.; Klobucar, W. D.; Focht, G.D. (Albemarle Corporation). Preparation of olefinic compounds and carboxylic derivatives thereof. U.S. Patent 6,080,888, 2000.
[25] Hughes, E. D.; Ingold, C. K.; Scott, A. D. The mechanism of elimination reactions. Part I. Unimolecular olefin formation from alkyl halides in sulphur dioxide and formic acid. *J. Chem. Soc.* **1937**, *258,* 1271-1277.
[26] Wittig, G.; Schöllkopf, U. Über Triphenyl-phosphin-methylene als olefinbildende reagenzien. *Chem. Ber.* **1954**, *87*, 1318-1330.
[27] (a) Horner, L.; Hoffmann, H. M. R.; Wippel, H. G. Phosphororganische verbindungen, XII. Phosphinoxyde als olefinierungsreagenzien. *Chem. Ber.* **1958**, *91*, 61-63. (b) Wadsworth, W. D.; Emmons, W. D. The utility of phosphonate carbanions in olefin synthesis. *J. Am. Chem. Soc.* **1961**, *83*, 1733-1738.
[28] O'Brien, C. J.; Tellez, J. L.; Nixon, Z. S.; Kang, L, J.; Carter, A. L.; Kunkel, S. R.; Przeworski, K. C.; Chass, G. A. Recycling the waste: the development of a catalytic Wittig reaction. *Angew. Chem. Int. Ed.* **2009**, *48*, 6836-6839.
[29] Corey, E.J. & Winter, R. A. E. A new, stereospecific olefin synthesis from 1,2-diols. *J. Am. Chem. Soc.* **1963**, *85*, 2677-2678.
[30] Shapiro, R. H.; Heath, M. J. Tosylhydrazones. V. Reaction of tosylhydrazones with alkyllithium reagents. A new olefin synthesis. *J. Am. Chem. Soc.* **1967**, *89*, 5734–5735.
[31] Peterson, D. J. Carbonyl olefination reaction using silyl-substituted organometallic compounds. *J. Org. Chem.* **1968**, *33*, 780-784.
[32] Julia, M. & Paris, J.-M. Syntheses a l'aide de sulfones $v^{(+)}$- methode de synthese generale de doubles liaisons. *Tetrahedron*, **1973**, *49*, 4833-4836.
[33] (a) Hérisson, J.-L.; Chauvin, Y. Catalyse de transformation des oléfines par les complexes du tungstène. II. Télomérisation des oléfines cycliques en présence d'oléfines acycliques. *Macromol. Chem. Phys.* **1971**, *141*, 161-176. (b) Grubbs, R. H.; Burk, P. L.; Carr, D. D. Mechanism of the olefin metathesis reaction. *J. Am. Chem. Soc.* **1975**, *97*, 3265-3267. (c) Schrock, R.; Rocklage, S.; Wengrovius, J.; Rupprecht, G.; Fellman, J. Preparation and characterization of active niobium, tantalum and tungsten metathesis catalysts. *J. Mol. Catal.* **1980**, *8*, 73-83.
[34] Shahane, S.; Bruneau, C.; Fischmeister, C. *Z* selectivity: Recent advances in one of the current major challenges of olefin metathesis. *ChemCatChem* **2013**, *5*, 3436–3459.
[35] Vedejs, E.; Peterson, M. J. Stereochemistry and mechanism in the Wittig reaction. *Top. Stereochem*. **1994**, *21*, 1-157.
[36] Ree, N.; Göller, A. H.; Jensen, J. H. What the Heck? – Automated regioselectivity calculations of palladium-catalyzed Heck reactions using quantum chemistry. *ACS Omega* **2022**, *7*, 45617–45623.
[37] Troegel, D.; Stohrer, J. Recent advances and actual challenges in late transition metal catalyzed hydrosilylation of olefins from an industrial point of view. *Coord. Chem. Rev.* **2011**, *255*, 1440-1459.
[38] Chernyshev, V. M.; Ananikov, V. P. Nickel and palladium catalysis: Stronger demand than ever. *ACS Catal.* **2022**, *12*, 1180–1200.
[39] Bumagin, N. A.; Beletskaya, I. P. Key steps in the cross-coupling of organometallic compounds with organic halides, catalysed by nickel and palladium compounds. *Russ. Chem. Rev.* **1990**, *59*, 1174–1184.
[40] Hiroyuki, S.; Akikazu, K.; Masashi, M. Chiral 2,2′-ninaphthyldiimine–nickel(II) complexes as Lewis acid catalysts for enantioselective Diels–Alder reactions. *Bull. Chem. Soc. Jpn.* **2004**, *77*, 561-568.
[41] Zhu, C.; Yue, H.; Chu, L.; Rueping, M. Recent advances in photoredox and nickel dual-catalyzed cascade reactions: pushing the boundaries of complexity. *Chem. Sci.* **2020**, *11*, 4051–4064.
[42] Tasker, S. Z.; Standley, E. A.; Jamison, T. F. Recent advances in homogeneous nickel catalysis. *Nature*, **2014**, *509*, 299-309.
[43] (a) Tamao, K.; Sumitani, K.; Kumada, M. Selective carbon-carbon bond formation by cross-coupling of Grignard reagents with organic halides. Catalysis by nickel-phosphine complexes. *J. Am. Chem. Soc.* **1972**, *94*, 4374-4376. Corriu, R. J. P. & Masse, J. P. Activation of Grignard reagents by transition-metal complexes. A new and simple synthesis of trans-stilbenes and polyphenyls .*J. Chem. Soc.*, *Chem. Commun*. **1972**, 144a.
[44] (a) Bajo, S.; Laidlaw, G.; Kennedy, A. R.; Sproules, S.; Nelson, D. J. Oxidative addition of aryl electrophiles to a prototypical nickel(0) complex: Mechanism and structure/reactivity relationships. *Organometallics*, **2017**, *36,* 1662-1672. (b) Quasdorf, K. W.; Tian, X.; Garg, N. K. Cross-coupling reactions of aryl pivalates with boronic acids. *J. Am. Chem. Soc.* **2008**, *130*, 14422–14423.

[45] Percec, V.; Bae, J.-Y.; Hill, D. H. Aryl mesylates in metal catalyzed homocoupling and cross-coupling reactions. 2. Suzuki-type nickel-catalyzed cross-coupling of aryl arenesulfonates and aryl mesylates with arylboronic acids. *J. Org. Chem.* **1995**, *60*, 1060-1065.
[46] Fu, J.-M.; Snieckus, V. Connections to the directed ortho metalation strategy. Pd(0)-catalyzed cross coupling of aryl boronic acids with aryl triflates. *Tetrahedron Lett.* **1990**, *31*, 1665-1668.
[47] So, C. M.; Lau, C. P.; Kwong, F. Y. A general palladium-catalyzed Suzuki-Miyaura coupling of aryl mesylates. *Angew. Chem. Int. Ed.* **2008**, *47*, 8059–8063.
[48] (a) Tobisu, M.; Shimasaki, T.; Chatani, N. Nickel-catalyzed cross-coupling of aryl methyl ethers with aryl boronic esters. *Angew. Chem. Int. Ed.* **2008**, *47*, 4866-4869. (b) Àlvarez-Bercedo, P. & Martin, R. Ni-catalyzed reduction of inert C-O bonds: a new strategy for using aryl ethers as easily removable directing groups. *J. Am. Chem. Soc.* **2010**, *132*, 17352-17353.
[49] (a) Yoshikai, N.; Mashima, H.; Nakamura, E. Nickel-catalyzed cross-coupling reaction of aryl fluorides and chlorides with Grignard reagents under nickel/magnesium bimetallic cooperation. *J. Am. Chem. Soc.* **2005**, *127*, 17978-17979. (b) Tobisu, M.; Xu, T.; Shimasaki, T.; Chatain, N. Nickel-catalyzed Suzuki-Miyaura reaction of aryl fluorides. *J. Am. Chem. Soc.* **2011**, *133*, 19505-19511.
[50] Zheng, Y.; Xie, P.; Daneshfar, O.; Houk, K. N.; Hong, X.; Newman, S. G. Direct synthesis of ketones from methyl esters by nickel-catalyzed Suzuki–Miyaura coupling. *Angew. Chem. Int. Ed.* **2021**, *60*, 13476–13483.
[51] (a) Jin, L.; Xin, J.; Huang, Z.; He, J.; Lei, A. Transmetalation is the rate-limiting step: Quantitative kinetic investigation of nickel-catalyzed oxidative coupling of arylzinc reagents. *J. Am. Chem. Soc.* **2010**, *132*, 9607–9609. (b) Payard, P.-A.; Perego, L. A.; Ciofini, I.; Grimaud, L. Taming Nickel-catalyzed Suzuki-Miyaura coupling: A mechanistic focus on boron-to-nickel transmetalation. *ACS Catal*. **2018**, *8*, 4812–4823.
[52] Lanni, E.L. & McNeil, A. Mechanistic studies on Ni(dppe)Cl_2-catalyzed chain-growth polymerizations: Evidence for rate-determining reductive elimination. *J. Am. Chem. Soc.* **2009**, *131*, 16573-16579.
[53] (a) Yamamoto, T.; Yamamoto, A.; Ikeda, S. Organo (dipyridyl) nickel complexes. I. Stability and activation of the alkyl-nickel bonds of dialkyl (dipyridyl) nickel by coordination with various substituted olefins. *J. Am. Chem. Soc.* **1971,** *93*, 3350-3359. (b) Yamamoto, A.; Yamamoto, T.; Ozawa, F. Chemistry of organopalladium and nickel complexes relevant to catalysis. *Pure & Appl. Chem.* **1985**, *57*, 1799-1808.
[54] Li, R.; Xu, H.; Zhao, N.; Jin, X.; Dang, Y. Origins of chemoselectivity in the Ni-catalyzed biaryl and Pd-catalyzed acyl Suzuki–Miyaura cross-coupling of N-acetyl-amides. *J. Org. Chem.* **2020**, *85*, 833–840.
[55] Diccianni, J., B.; Diao, T. Mechanisms of nickel-catalyzed cross-coupling reactions. *Trends Chem.* **2019**, *1*, 830-844.
[56] (a) Zalesskiy, S. S.; Ananikov, V. P. $Pd_2(dba)_3$ as a precursor of soluble metal complexes and nanoparticles: determination of palladium active species for catalysis and synthesis. *Organometallics* **2012**, *31*, 2302–2309. (b) Bej, A.; Ghosh, K.; Sarkar, A.; Knight, D. W. Palladium nanoparticles in the catalysis of coupling reactions. *RSC Adv.* **2016**, *6*, 11446–11453. (c) Fricke, C.; Sperger, T.; Mendel, M.; Schoenebeck, F. Catalysis with palladium(I) dimers. *Angew. Chem. Int. Ed.* **2021**, *60*, 3355–3366.
[57] (a) Sicard, A. J.; Baker, R. T. Safe and expeditious preparation of $Ni(cod)_2$ for same-day high-throughput screening. *Org. Process Res. Dev.* **2020**, *24*, 2950–2952. For examples of air-stable Ni(0) precatalysts see:
[58] Yin, G.; Kalvet, I.; Englert, U.; Schoenebeck, F. Fundamental studies and development of nickel-catalyzed trifluoromethylthiolation of aryl chlorides: active catalytic species and key roles of ligand and traceless MeCN additive revealed. *J. Am. Chem. Soc*. **2015**, *137*, 4164–4172.
[59] Anthony, D.; Lin, Q.; Baudet, J.; Diao, T. Nickel-catalyzed asymmetric reductive diarylation of vinylarenes. *Angew. Chem. Int. Ed*. **2019**, *58*, 3198–3202.
[60] Ting, S. I.; Williams, W. L.; Doyle, A. G. Oxidative addition of aryl halides to a Ni(I)-bipyridine complex. *J. Am. Chem. Soc.* **2022**, *144*, 5575–5582.
[61] Bour, J. R.; Camasso, N. M.; Meucci, E. A.; Kampf, J. W.; Canty, A. J.; Sanford, M. S. Carbon–carbon bond-forming reductive elimination from isolated nickel(III) complexes. *J. Am. Chem. Soc*. **2016**, *138*, 16105–16111.
[62] Sehnal, P.; Taylor, R. J. K.; Fairlamb, I. J. S. Emergence of palladium(IV) chemistry in synthesis and catalysis. *Chem. Rev.* **2010**, *110*, 824–889.
[63] For representative examples see: (a) Gavrish, S. P.; Lampeka, Y. D.; Babak, M. V.; Arion, V. B. Palladium complexes of *N,N'*-bis(2-aminoethyl)oxamide (H_2L): Structural ($Pd^{II}L$, $Pd^{II}{}_2L_2$, and $Pd^{IV}LCl_2$), electrochemical, dynamic ^1H NMR, and cytotoxicity. *Inorg. Chem.* **2018**, *57*, 1288–1297. (b) Tran, G. N.; Bouley, B. S.; Mirica, L. M. Isolation and characterization of heteroleptic mononuclear palladium(I) complexes. *J. Am. Chem. Soc*. **2022**, *144*, 20008–20015.

[64] Selected examples include: (a) Borowski, J. E.; Newman-Stonebraker, S. H.; Doyle, A. G. Comparison of monophosphine and bisphosphine precatalysts for Ni-catalyzed Suzuki–Miyaura cross-coupling: Understanding the role of the ligation state in catalysis. *ACS Catal*. **2023**, *13*, 7966–7977. (b) Day, C. S.; Rentería-Gómez, Á.; Ton, S. J.; Gogoi, A. R.; Gutierrez, O.; Martin, R. Elucidating electron-transfer events in polypyridine nickel complexes for reductive coupling reactions. *Nat. Catal.* **2023**, *6*, 244–253.

[65] Otsuka, S.; Nakamura, A.; Yoshida, T.; Naruto, M.; Ataka, K. Chemistry of alkoxycarbonyl, acyl, and alkyl compounds of nickel(II) and palladium(II). *J. Am. Chem. Soc.* **1973**, *95*, 3180-3188.

[66] Chiusoli, G.P.; Salerni, G.; Giroldini, W.; Pallini, L. Transition metal-catalyzed syntheses of organic acids by chelation-promoted regioselective double bond insertion. *J. Organomet. Chem.* **1981**, *219*, C16-C20.

[67] (a) Colon, I. Preparation of substituted olefins. U.S. Patent 4,334,081 January 23rd 1981. (b) Boldrini, G. P.; Savoia, D.; Tagliavini, E.; Trombini, C.; Ronchi, U. A. nickel-catalyzed coupling of activated alkenes with organic halides. *J. Organomet. Chem.* **1986**, *301*, C62-C64. (c) Lebedev, S. A.; Lopatina, V. S.; Petrov, E. S.; Beletskaya, I. P. Condensation of organic bromides with vinyl compounds catalysed by nickel complexes in the presence of zinc. *J. Organomet. Chem.* **1988**, *344*, 253-259. (d) Sustmann, R.; Hopp, P.; Holl, P. Reactions of organic halides with olefins under Ni^0-catalysis. Formal addition of hydrocarbons to CC-double bonds. *Tetrahedron Lett.* **1989**, *30*, 689-692. (e) Kong, K.-C. & Cheng, C.-H. Synthesis of spiro dienones from internal acetylene and cyclic 3-iodo enones in the presence of nickel bromide and zinc powder. *Organometallics* **1992**, *11*, 1972-1975.

[68] Hanaoaka, T.; Kubota, Y.; Sugi, Y. The vinylation of bromobiphenyls using homogeneous nickel catalysts. *Catal. Letters* **1994**, *29*, 69-75.

[69] Walker, B. R.; Sevov, C. S. An electrochemically promoted, nickel-catalyzed Mizoroki–Heck reaction. *ACS Catal.* **2019**, *9*, 7197–7203.

[70] Lin, B.-L.; Lui, L.; Fu, Y.; Luo, S.-W.; Chen, Q.; Guo, Q.-X. Comparing nickel- and palladium-catalyzed Heck reactions *Organometallics* **2004**, *23*, 2114-2123.

[71] Menezes da Silva, V. H.; Braga, A. C. A.; Cundari, T. R. Influence of R−NHC Coupling on the outcome of R−X oxidative addition to Pd/NHC complexes (R = Me, Ph, Vinyl, Ethynyl). *Organometallics*, **2016**, *35*, 3170-3181.

[72] Martínez-Prieto, L. M.; Ávila, E.; Palma, P.; Álvarez, E.; Cámpora, J. β-Hydrogen elimination reactions of nickel and palladium methoxides stabilised by PCP pincer ligands. *Chem. Eur. J.* **2015**, *21*, 9833-9849.

[73] Tasker, S. Z.; Gutierrez, A. C.; Jamison, T. F. Nickel-catalyzed Mizoroki-Heck reaction of aryl sulfonates and chlorides with electronically unbiased terminal olefins: high selectivity for branched products. *Angew. Chem. Int. Ed.* **2014**, *53*, 1858-1861.

[74] Matsubara, R.; Gutierrez, A. C.; Jamison, T. F. Nickel-catalyzed Heck-type reactions of benzyl chlorides and simple olefins. *J. Am. Chem. Soc.* **2011**, *133,* 19020-19023.

[75] Closest Pd example has *rr* > 10:1: Qin, L.; Ren, X.; Lu, Y.; Li, Y.; Zhou, J. S. Intermolecular Mizoroki-Heck reaction of aliphatic olefins with high selectivity for substitution at the internal position. *Angew. Chem. Int. Ed.* **2012**, *51*, 5915–5919.

[76] Gøgsig, T. M.; Kleimark, J.; Lill, S. O. N.; Korsager, S.; Lindhardt, A. T.; Norrby, P.-O.; Skrydstrup, T. Mild and efficient nickel-catalyzed Heck reactions with electron-rich olefins. *J. Am. Chem. Soc*. **2012**, *134*, 443-452.

[77] Selected examples include: (a) Cabri, W.; Candiani, I.; Bedeschi, A.; Santi, R. Palladium-catalyzed arylation of unsymmetrical olefins. Bidentate phosphine ligand controlled regioselectivity. *J. Org. Chem.* **1992**, *57*, 3558-3563. (b) Vallin, K. S. A.; Zhang, Q.; Larhed, M.; Curran, D. P.; Hallberg, A. A new regioselective Heck vinylation with enamides. Synthesis and investigation of fluorous-tagged bidentate ligands for fast separation. *J. Org. Chem.* **2003**, *68*, 6639-6645. (c) Hansen, A. L.; Skrydstrup, T. Fast and regioselective Heck couplings with *N*-Acyl-*N*-vinylamine derivatives. *J. Org. Chem.* **2005**, *70*, 5997-6003.

[78] Ehle, A. R.; Zhou, Q.; Watson, M. P. Nickel(0)-catalyzed Heck cross-coupling via activation of aryl C–OPiv bonds. *Org. Lett*. **2012**, *14*, 1202–1205.

[79] Vandavasi, J. K.; Hua, X.Y.; Ben Halima, H.; Newman, S. G. A nickel-catalyzed carbonyl-Heck reaction. *Angew. Chem. Int. Ed.* **2017**, *56*, 15441-15445.

[80] (a) Hua, X. Y. Expanding the scope of coupling partners in cross-coupling reactions. Masters Thesis (online), University of Ottawa, Ottawa, ON, **2016.** http://dx.doi.org/10.20381/ruor-479 (Accessed May 11th 2020).
(b) Vandavasi, J.K.; Newman, S. G. A high-throughput approach to discovery: Heck-type reactivity with aldehydes. *Synlett*, **2018**, *29*, 2081-2086.

[81] Cabri, W.; Candiani, I.; Bedeshi, A.; Santi, R. Palladium-catalyzed arylation of unsymmetrical olefins. Bidentate phosphine ligand controlled regioselectivity. *J. Org. Chem*. **1992**, *57*, 3558 – 3563.

[82] Märkl, V. G.; Jin, G. Y.; Schoerner, C. 1,5-Diaza-3,7-diphospha-cyclooctane. *Tetrahedron Lett.* **1980**, *21*, 1409−1412.
[83] For an example of a cyclic 12-membered P_2N_2 ligand see: Fryzuk, M. D.; Johnson, S. A.; Rettig, S. J. Synthesis and structure of the tantalum trimethyl complex $[P_2N_2]TaMe_3$ and its Conversion to the tantalum methylidene species $[P_2N_2]Ta{=}CH_2(Me)$ ($[P_2N_2]$ = $PHP(CH_2SiMe_2NSiMe_2CH_2)_2PPh$). *Organometallics* **1999**, *18*, 4059–4067.
[84] (a) Karasik, A. A.; Krashilina,A. V.; Gubaidullin, A. T.; Litvinov, I. A.; Cherkasov, V. K.; Sinyashin, O.G.; Abakumov, G. A. Synthesis, structures, and properties of 3,6-di-tert-butyl-o-benzosemiquinone complexes of copper(0) with 1,5-diaza-3,7-diphosphacyclooctanes. *Russ. Chem. Bull*. **2000**,*49*, 1782-1788. (b) Strelnik, I. D.; Dayanova, I. R.; Krivolapov, D. B.; Litvinov, I.A.; Musina, E. I.; Karasik, A. A.; Sinyashin, O. G. Unpredicted concurrency between P,P-chelate and P,P-bridge coordination modes of 1,5-diR-3,7-di(Pyridine-2-yl)-1,5-diaza-3,7-diphosphacyclooctane ligands in copper(I) complexes. *Polyhedron* **2018**, *139*, 1−6.
[85] Moiseev, D. V.; James, B. R. Phospha-mannich reactions of RPH_2, R_2PH, and R_3P. *Phosphorus Sulfur Silicon Relat. Elem.* **2022**, *197*, 327–391.
[86] Doud, M. D.; Grice, K. A.; Lilio, A. M.; Seu, C. S.; Kubiak, C. P. Versatile synthesis of $P^R{}_2N^{R'}{}_2$ ligands for molecular electrocatalysts with pendant bases in the second coordination sphere. *Organometallics* **2012**, *31*, 779–782.
[87] Doud, M. D. Synthetic advances for P_2N_2 Molecular Electrocatalysts with Pendant bases in the second coordination sphere. PhD dissertation, University of California San Diego, San Diego, CA, 2016. Retrieved from https://escholarship.org/uc/item/19c203gd (accessed 2023-07-07).
[88] Klug, C. M.; Cardenas, A. J. P.; Bullock, R. M.; O'Hagan, M.; Wiedner, E. S. Reversing the tradeoff between rate and overpotential in molecular electrocatalysts for H_2 production. *ACS Catal.* **2018**, *8*, 3286–3296.
[89] Song, L.-C.; Tan, H.; Luo, F.-X.; Wang, Y.-X.; Ma, Z.; Niu, Z. Synthesis, structural characterization, and catalytic H_2 production of ferrocenyl (Fc) group containing complexes $[Ni(P^{Fc}{}_2N^{Ar}{}_2)_2](BF_4)_2$ (Ar = Ph, *p*-BrC_6H_4). *Organometallics* **2014**, *33*, 5246–5253.
[90] Kulikov, D. V.; Balueva, A. S.; Karasik, A. A.; Kozlov, A. V.; Latypov, S. K.; Kataeva, O. N.; Lönnecke, P.; Hey-Hawkins, E.; Sinyashin, O. G. Novel 36- and 38-membered P,N-containing cyclophanes with large hydrophobic cavities. *Phosphorus, Sulfur, and Silicon Relat. Elem.* **2008**, *183*, 667–668.
[91] Musina, E. I.; Khrizanforova, V. V.; Strelnik, I. D.; Valitov, M. I.; Spiridonova, Y. S.; Krivolapov, D. B.; Litvinov, I. A.; Kadirov, M. K.; Lönnecke, P.; Hey-Hawkins, E.; Budnikova, Y. H.; Karasik, A. A.; Sinyashin, O. G. New functional cyclic aminomethylphosphine ligands for the construction of catalysts for electrochemical hydrogen transformations. *Chem. Eur. J*. **2014**, *20*, 3169–3182.
[92] Brunner, F. M.; Neville, M. L.; Kubiak, C. P. Investigation of immobilization effects on $Ni(P_2N_2)_2$ electrocatalysts. *Inorg. Chem.* **2020**, *59*, 16872–16881.
[93] Karasik, A. A.; Heinicke, J. W.; Balueva, A. S.; Thede, G.; Jones, P. G.; Sinyashin, O. G. Pt- and Pd-complexes with acyclic and heterocyclic P -hydroxyaryl-substituted N -phosphanylmethyl amino acids $RP(CH_2NHR')_2$ and $(RPCH_2NR'CH_2)_2$ – Evaluation of (P^O)M chelate formation. *Eur. J. Inorg. Chem.* **2020**, *2020*, 3682–3691.
[94] Weiss, C. J.; Wiedner, E. S.; Roberts, J. A. S.; Appel, A. M. Nickel phosphine catalysts with pendant amines for electrocatalytic oxidation of alcohols. *Chem. Commun.* **2015**, *51*, 6172–6174.
[95] Kilgore, U. J.; Stewart, M. P.; Helm, M. L.; Dougherty, W. G.; Kassel, W. S.; Dubois, M. R.; Dubois, D. L.; Bullock, R. M. Studies of a series of $[Ni(P^R{}_2N^{Ph}{}_2)_2(CH_3CN)]^{2+}$ complexes as electrocatalysts for H_2 production: substituent variation at the phosphorus atom of the P_2N_2 ligand. *Inorg. Chem.* **2011**, *50*, 10908–10918.
[96] Galan, B. R.; Schöffel, J.; Linehan, J. C.; Seu, C.; Appel, A. M.; Roberts, J. A. S.; Helm, M. L.; Kilgore, U. J.; Yang, J. Y.; Dubois, D. L.; Kubiak, C. P. Electrocatalytic oxidation of formate by $[Ni(P^R{}_2N^{R'}{}_2)_2(CH_3CN)]^{2+}$ complexes. *J. Am. Chem. Soc.* **2011**, *133*, 12767–12779.
[97] Ignatieva, S. N.; Balueva, A. S.; Karasik, A. A.; Latypov, S. K.; Nikonova, A. G.; Naumova, O. E.; Lönnecke, P.; Hey-Hawkins, E.; Sinyashin, O. G. First representative of optically active *P*-L-menthyl-substituted (aminomethyl)phosphine and its borane and metal complexes. *Inorg. Chem*. **2010**, *49*, 5407–5412.
[98] Das, P.; Stolley, R. M.; Van Der Eide, E. F.; Helm, M. L. A Ni^{II}–bis(diphosphine)–hydride complex containing proton relays – Structural characterization and electrocatalytic studies. *Eur. J. Inorg. Chem.* **2014**, *2014*, 4611–4618.
[99] Strelnik, I. D.; Dayanova, I.; Gerasimova, T. P.; Katsyuba, S. A.; Kolesnikov, I. E.; Kalinichev, A.; Shmelev, A.; Islamov, D. R.; Lönnecke, P.; Hey-Hawkins, E.; Musina, E. I.; Karasik, A. A. Deep-blue emissive copper(I) complexes based on P-thiophenylethyl-substituted cyclic bisphosphines displaying photoinduced structural transformations of the excited states. *Inorg. Chem*. **2022**, *61*, 16596–16606.

[100] Primary phosphines and their corresponding safety data sheets are available from Strem. Cyclohexylphosphine (822-68-4) min 97% catalogue number: 15-0950 and Phenylphosphine (638-21-1) 99% catalogue number: 15-4400 are both listed as pyrophoric compounds. Accessed 2023-07-09.
[101] Das, A. K.; Engelhard, M. H.; Lense, S.; Roberts, J. A. S.; Bullock, R. M. Covalent attachment of diphosphine ligands to glassy carbon electrodes via Cu-catalyzed alkyne-azide cycloaddition. Metallation with Ni(II). *Dalton Trans.* **2015**, *44*, 12225–12233.
[102] Hoffert, W. A.; Roberts, J. A. S.; Morris Bullock, R.; Helm, M. L. Production of H_2 at fast rates using a nickel electrocatalyst in water–acetonitrile solutions. *Chem. Commun.* **2013**, *49*, 7767.
[103] Das, A. K.; Engelhard, M. H.; Bullock, R. M.; Roberts, J. A. S. A Hydrogen-evolving $Ni(P_2N_2)_2$ electrocatalyst covalently attached to a glassy carbon electrode: Preparation, characterization, and catalysis. Comparisons with the homogeneous analogue. *Inorg. Chem.* **2014**, *53*, 6875–6885.
[104] Zhou, Y.; Yang, S.; Huang, J. Light-driven hydrogen production from aqueous solutions based on a new Dubois-type nickel catalyst. *Phys. Chem. Chem. Phys.* **2017**, *19*, 7471–7475.
[105] Stubbs, J. M.; Chapple, D. E.; Boyle, P. D.; Blacquiere, J. M. Catalyst pendent-base effects on cyclization of alkynyl amines. *ChemCatChem* **2018**, 1*0*, 4001-4009.
[106] Boralugodage, N. P.; Arachchige, R. J.; Dutta, A.; Buchko, G. W.; Shaw, W. J. Evaluating the role of acidic, basic, and polar amino acids and dipeptides on a molecular electrocatalyst for H_2 oxidation. *Catal. Sci. Technol.* **2017**, *7*, 1108–1121.
[107] Dutta, A.; Roberts, J. A. S.; Shaw, W. J. Arginine-Containing Ligands Enhance H_2 Oxidation Catalyst Performance. *Angew. Chem. Int. Ed.* **2014**, *53*, 6487–6491.
[108] Lense, S.; Dutta, A.; Roberts, J. A. S.; Shaw, W. J. A proton channel allows a hydrogen oxidation catalyst to operate at a moderate overpotential with water acting as a base. *Chem. Commun.* **2014**, *50*, 792–795.
[109] Spiridonova, J. S.; Karasik, A. A.; Sinyashin, O. G. The first example of diazadiphosphacyclooctanes with bicyclic substituents. *Phosphorus Sulfur Silicon Relat. Elem.* **2011**, *186*, 764–765.
[110] Spiridonova, Y. S.; Musina, E. I.; Dayanova, I. R.; Naumova, O. E.; Litvinov, I. A.; Karasik, A. A. Synthesis and structure of N-pyridyl-containing cyclic aminomethylphosphines. *Russ. J. Gen. Chem.* **2018**, *88*, 2257–2262.
[111] Jain, A.; Lense, S.; Linehan, J. C.; Raugei, S.; Cho, H.; Dubois, D. L.; Shaw, W. J. Incorporating peptides in the outer-coordination sphere of bioinspired electrocatalysts for hydrogen production. *Inorg. Chem.* **2011**, *50*, 4073–4085.
[112] Jain, A.; Reback, M. L.; Lindstrom, M. L.; Thogerson, C. E.; Helm, M. L.; Appel, A. M.; Shaw, W. J. Investigating the role of the outer-coordination sphere in $[Ni(P^{Ph}_2N^{Ph\text{-}R}_2)_2]^{2+}$ hydrogenase mimics. *Inorg. Chem.* **2012**, *51*, 6592–6602.
[113] Egbert, J. D.; Labios, L. A.; Darmon, J. M.; Piro, N. A.; Scott Kassel, W.; Mock, M. T. Synthesis and structure of vanadium halide complexes containing diphosphine ligands with pendant amines. *Eur. J. Inorg. Chem.* **2016**, *2016*, 1293–1299.
[114] Mock, M. T.; Chen, S.; Rousseau, R.; O'Hagan, M. J.; Dougherty, W. G.; Kassel, W. S.; Dubois, D. L.; Bullock, R. M. A rare terminal dinitrogen complex of chromium. *Chem. Commun.* **2011**, *47*, 12212-12214.
[115] Welch, K. D.; Dougherty, W. G.; Kassel, W. S.; Dubois, D. L.; Bullock, R. M. Synthesis, structures, and reactions of manganese complexes containing diphosphine ligands with pendant amines. *Organometallics* **2010**, *29*, 4532–4540.
[116] Liu, T.; Chen, S.; O'Hagan, M. J.; Rakowski Dubois, M.; Bullock, R. M.; Dubois, D. L. Synthesis, characterization, and reactivity of Fe complexes containing cyclic diazadiphosphine ligands: The role of the pendant base in heterolytic cleavage of H_2. *J. Am. Chem. Soc.* **2012**, *134*, 6257–6272.
[117] Wiedner, E. S.; Yang, J. Y.; Dougherty, W. G.; Kassel, W. S.; Bullock, R. M.; Dubois, M. R.; Dubois, D. L. Comparison of cobalt and nickel complexes with sterically demanding cyclic diphosphine ligands: Electrocatalytic H_2 production by $[Co(P^{tBu}_2N^{Ph}_2)(CH_3CN)_3](BF_4)_2$. *Organometallics* **2010**, *29*, 5390–5401.
[118] Strelnik, I. D.; Dayanova, I. R.; Krivolapov, D. B.; Litvinov, I. A.; Musina, E. I.; Karasik, A. A.; Sinyashin, O. G. Unpredicted concurrency between P,P-chelate and P,P-bridge coordination modes of 1,5-diR-3,7-di(pyridine-2-yl)-1,5-diaza-3,7-diphosphacyclooctane ligands in copper (I) complexes. *Polyhedron*, **2018**, *139*, 1-6.
[119] Kane, J. C.; Wong, E. H.; Yap, G. P.; Rheingold, A. L. Synthesis and structural studies of molybdenum and palladium complexes of 1,5-diaza-3, 7-diphosphacyclooctane ligands. *Polyhedron*, **1999**, *18*, 1183-1188.
[120] Lilio, A. M.; Reineke, M. H.; Moore, C. E.; Rheingold, A. L.; Takase, M. K.; Kubiak, C. P. Incorporation of pendant bases into Rh(diphosphine)$_2$ complexes: Synthesis, thermodynamic studies, and catalytic CO_2 hydrogenation activity of $[Rh(P_2N_2)_2]^+$ complexes. *J. Am. Chem. Soc.* **2015**, *137*, 8251–8260.
[121] Musina, E. I.; Khrizanforova, V. V.; Strelnik, I. D.; Valitov, M. I.; Spiridonova, Y. S.; Krivolapov, D. B.; Litvinov, I. A.; Kadirov, M. K.; Lönnecke, P.; Hey-Hawkins, E.; Budnikova, Y. H.; Karasik, A. A.; Sinyashin, O. G. New Functional Cyclic

Aminomethylphosphine Ligands for the construction of catalysts for electrochemical hydrogen transformations. *Chem. Eur. J.* **2014**, *20*, 3169–3182.
[122] Karasik, A. A.; Naumov, R. N.; Sinyashin, O. G.; Belov, G. P.; Novikova, H. V.; Lönnecke, P.; Hey-Hawkins, E. Novel chiral 1,5-diaza-3,7-diphosphacyclooctane ligands and their transition metal complexes. *Dalton Trans*. **2003**, *11*, 2209–2214.
[123] Spiridonova, Y. S.; Strelnik, I. D.; Musina, E. I.; Hey-Hawkins, E.; Litvinov, I. A.; Karasik, A. A. New gold (I) complexes with 1, 5-diaza-3, 7-diphosphacyclooctanes: Synthesis and structures. *Russ. J. Coord. Chem.* **2020**, *46*, 477-484.
[124] Herrera, R. P.; Gimeno, M. C. Main avenues in gold coordination chemistry. *Chem. Rev.* **2021**, *121*, 8311–8363.
[125] Fernandez, M. J.; Esteruelas, M. A.; Covarrubias, M.; Oro, L. A. Preparation of IrH (diene)L_2 compounds via methoxyiridium complexes: Catalysts for hydrogen transfer reactions. *J. Organomet. Chem.* **1986**, *316*, 343-349.
[126] Bhattacharya, P.; Heiden, Z. M.; Chambers, G. M.; Johnson, S. I.; Bullock, R. M.; Mock, M. T.. Catalytic ammonia oxidation to dinitrogen by hydrogen atom abstraction. *Angew. Chem. Int. Ed.* **2019**, *58*, 11618–11624.
[127] Hulley, E. B.; Helm, M. L.; Bullock, R. M. Heterolytic cleavage of H_2 by bifunctional manganese(I) complexes: Impact of ligand dynamics, electrophilicity, and base positioning. *Chem. Sci.* **2014**, *5*, 4729–4741.
[128] Chapple, D. E.; Boyle, P. D.; Blacquiere, J. M. Origin of stability and inhibition of cooperative alkyne hydrofunctionalization catalysts. *ChemCatChem* **2021**, *13*, 3789–3800.
[129] Strelnik, I.; Musina, E.; Grachova, E.; Karasik, A.; Sinyashin, O. Luminescent copper(I) and gold(I) complexes of 1,5-diaza-3,7-diphosphacyclooctanes. *Phosphorus Sulfur Silicon Relat. Elem.* **2016**, *191*, 1518–1519.
[130] Wiedner, E. S.; Appel, A. M.; Raugei, S.; Shaw, W. J.; Bullock, R. M. Molecular catalysts with diphosphine ligands containing pendant amines. *Chem. Rev.* **2022**, *122*, 12427–12474.
[131] (a) O'Hagan, M.; Shaw, W. J.; Raugei, S.; Chen, S.; Yang, J. Y.; Kilgore, U. J.; Dubois, D. L.; Bullock, R. M. Moving protons with pendant amines: Proton mobility in a nickel catalyst for oxidation of hydrogen. *J. Am. Chem. Soc.* **2011**, *133*, 14301–14312. (b) O'Hagan, M.; Ho, M.-H.; Yang, J. Y.; Appel, A. M.; Dubois, M. R.; Raugei, S.; Shaw, W. J.; Dubois, D. L.; Bullock, R. M. Proton delivery and removal in $[Ni(P^R_2N^{R'}_2)_2]^{2+}$ hydrogen production and oxidation catalysts. *J. Am. Chem. Soc.* **2012**, *134*, 19409–19424.
[132] Franz, J. A.; O'Hagan, M.; Ho, M.-H.; Liu, T.; Helm, M. L.; Lense, S.; Dubois, D. L.; Shaw, W. J.; Appel, A. M.; Raugei, S.; Bullock, R. M. Conformational dynamics and proton relay positioning in nickel catalysts for hydrogen production and oxidation. *Organometallics* **2013**, *32*, 7034–7042.
[133] Raugei, S.; Chen, S.; Ho, M.-H.; Ginovska-Pangovska, B.; Rousseau, R. J.; Dupuis, M.; Dubois, D. L.; Bullock, R. M. The role of pendant amines in the breaking and forming of molecular hydrogen catalyzed by nickel complexes. *Chem. Eur. J.* **2012**, *18*, 6493–6506.
[134] (a) Kilgore, U. J.; Stewart, M. P.; Helm, M. L.; Dougherty, W. G.; Kassel, W. S.; Dubois, M. R.; Dubois, D. L.; Bullock, R. M. Studies of a series of $[Ni(P^R_2N^{Ph}_2)_2(CH_3CN)]^{2+}$ complexes as electrocatalysts for H_2 production: Substituent variation at the phosphorus atom of the P_2N_2. *Inorg. Chem.* **2011**, *50*, 10908–10918. (b) Klug, C. M.; Cardenas, A. J. P.; Bullock, R. M.; O'Hagan, M.; Wiedner, E. S. Reversing the tradeoff between rate and overpotential in molecular electrocatalysts for H_2 production. *ACS Catal.* **2018**, *8*, 3286–3296.
[135] Zhang, S.; Appel, A. M.; Bullock, R. M. Reversible heterolytic cleavage of the H–H bond by molybdenum complexes: Controlling the dynamics of exchange between proton and hydride. *J. Am. Chem. Soc.* **2017**, *139*, 7376–7387.
[136] Kilgore, U. J.; Roberts, J. A. S.; Pool, D. H.; Appel, A. M.; Stewart, M. P.; Dubois, M. R.; Dougherty, W. G.; Kassel, W. S.; Bullock, R. M.; Dubois, D. L. $[Ni(P^{Ph}_2N^{C6H4X}_2)_2]^{2+}$ complexes as electrocatalysts for H_2 production: Effect of substituents, acids, and water on catalytic rates. *J. Am. Chem. Soc.* **2011**, *133*, 5861–5872.
[137] Chen, S.; Ho, M.-H.; Bullock, R. M.; Dubois, D. L.; Dupuis, M.; Rousseau, R.; Raugei, S. Computing free energy landscapes: Application to Ni-based electrocatalysts with pendant amines for H_2 production and oxidation. *ACS Catal.* **2014**, *4*, 229–242.
[138] Cardenas, A. J. P.; Ginovska, B.; Kumar, N.; Hou, J.; Raugei, S.; Helm, M. L.; Appel, A. M.; Bullock, R. M.; O'Hagan, M. Controlling proton delivery through ctalyst structural dynamics. *Angew. Chem. Int. Ed.* **2016**, *55*, 13509–13513.
[139] Yang, J. Y.; Bullock, R. M.; Dougherty, W. G.; Kassel, W. S.; Twamley, B.; Dubois, D. L.; Rakowski Dubois, M. Reduction of oxygen catalyzed by nickel diphosphine complexes with positioned pendant amines. *Dalton Trans.* **2010**, *39*, 3001-3010.
[140] Roy, S.; Sharma, B.; Pécaut, J.; Simon, P.; Fontecave, M.; Tran, P. D.; Derat, E.; Artero, V. Molecular cobalt complexes with pendant amines for selective electrocatalytic reduction of carbon dioxide to formic acid. *J. Am. Chem. Soc*. **2017**, *139*, 3685–3696.

[141] Xue, L.; Ahlquist, M. S. G. A DFT Study: Why do $[Ni(P^{R}_{2}N^{R'}_{2})_{2}]^{2+}$ complexes facilitate the electrocatalytic oxidation of formate? *Inorg. Chem.* **2014**, *53*, 3281–3289.
[142] Weiss, C. J.; Das, P.; Miller, D. L.; Helm, M. L.; Appel, A. M. Catalytic oxidation of alcohol via nickel phosphine complexes with pendant amines. *ACS Catal*. **2014**, *4*, 2951–2958.
[143] Gunasekara, T.; Tong, Y.; Speelman, A. L.; Erickson, J. D.; Appel, A. M.; Hall, M. B.; Wiedner, E. S. Role of high-spin species and pendant amines in electrocatalytic alcohol oxidation by a nickel phosphine complex. *ACS Catal.* **2022**, *12*, 2729–2740.
[144] Fihri, A.; Luart, D.; Len, C.; Solhy, A.; Chevrin, C.; Polshettiwar, V. Suzuki–Miyaura cross-coupling coupling reactions with low catalyst loading: a green and sustainable protocol in pure water. *Dalton Trans*. **2011**, *40*, 3116-3121.
[145] (a) Stubbs, J. M.; Bow, J.-P. J.; Hazlehurst, R. J.; Blacquiere, J. M. Catalytic cyclization and competitive deactivation with $Ru(P^{R}_{2}N^{R'}_{2})$ complexes. *Dalton Trans*. **2016**, *45*, 17100–17103. (b) Stubbs, J. M.; Bridge, B. J.; Blacquiere, J. M. Optimizing ligand structure for low-loading and fast catalysis for alkynyl-alcohol and -amine cyclization. *Dalton Trans.* **2019**, *48*, 7928–7937. (c) Bridge, B. J.; Boyle, P. D.; Blacquiere, J. M. *endo*-selective iron catalysts for intramolecular alkyne hydrofunctionalization. *Organometallics* **2020**, *39*, 2570–2574. (d) Chapple, D. E.; Hoffer, M. A.; Boyle, P. D.; Blacquiere, J. M. Alkyne Hydrofunctionalization mechanism including an off-cycle alkoxycarbene deactivation complex. *Organometallics* **2022**, *41*, 1532–1542.
[146] Bow, J. J.; Boyle, P. D.; Blacquiere, J. M. Substrate-mediated deactivation of a $Ru(P^{tBu}_{2}N^{Bn}_{2})$ cooperative complex. *Eur. J. Inorg. Chem.* **2015**, *2015*, 4162–4166.

[147] Martin, S. E. S.; Watson, D. A. Preparation of vinyl silyl ethers and disiloxanes via the Silyl-Heck reaction of silyl ditriflates. *J. Am. Chem. Soc.* **2013**, *135*, 13330–13333.
[148] Reid, W. B.; Spillane, J. J.; Krause, S. B.; Watson, D. A. Direct synthesis of alkenyl boronic esters from unfunctionalized alkenes: A boryl-Heck reaction. *J. Am. Chem. Soc.* **2016**, *138*, 5539–5542.

Chapter 2 : Catalytic Arylation of Aldehydes Facilitated by 1,5-Diaza-3,7-diphosphacyclooctanes (P_2N_2) Ligands

2.1 Reuse permissions

The data presented was derived from the manuscript "Catalytic Aldehyde and Alcohol Arylation Reactions Facilitated by a 1,5-Diaza-3,7-diphosphacyclooctane Ligand", by Eric S. Isbrandt, Amrah Nasim, Karen A. Zhao, and Stephen G. Newman, published in *J. Am. Chem. Soc.* **2021**, 143, 14646-14656. Copyright 2021 American Chemical Society. The dissertation author is the primary author of this manuscript. To supplement the original publication, additional relevant data has been incorporated into the text (vide infra).

Section 2.3 had some text added (fully describing Yamaguchi's contributions) and Scheme 2.1 was fully reimagined to incorporate more detailed information about prior art. Scheme 2.2 provides a clearer image of a key point from the introduction – it was not present in the original publication. Section 2.4 is new and was added to illustrate some background philosopy about the project. Section 2.5.1 was derived from the main text of the manuscript with additional optimization results from the Supporting Information added in. The entries derived from the Supporting Information have been italicized and the table was reorganized to group related entries together. New text was written to contextualize the added entries in Table 2.1. Table 2.3 was originally found in the Supporting Information. Section 2.5.2 was directly derived from the original publication, although the numbering and order of compounds was changed in Scheme 2.4. Section 2.5.3 was directly derived from the original publication, however, the reference to find Scheme 2.6 in the Supporting Information has been removed and Scheme 2.6 has been reproduced with new compound numbering. Scheme 2.8 was remade from the original manuscript to improve clarity. Section 2.5.4 was fully reproduced from the Supporting Information. Compounds in Scheme 2.9 were renumbered. Section 2.6.1 was directly adapted

from the manuscript. All other sections (2.6.2 and 2.6.3) are original and found exclusively in this thesis. Section 2.7 is directly adapted from the Supporting Information with only renumbering of compounds.

2.2 Contributions

Amrah Nasim (MSc) contributed to the scope table with the isolation of compounds **2.10, 2.17, 2.25-2.27**, **2.31.** Karen Zhao (Hon. BSc) contributed to the scope table with the preparation of starting material 6-iodoquinoline. Karen also performed the experiments described in Scheme 2.6 and the experiment described in Scheme 2.8.

2.3 Organometallic arylation of aldehydes

The reaction of aldehydes with organometallic reagents represents an important synthetic pathway for producing secondary alcohols both industrially and academically. The Grignard reaction, which uses organomagnesium reagents, is particularly common and remains one of the most frequently used methods for forming C–C bonds despite its stoichiometric nature and poor functional group tolerance.[1] Moreover, Grignard reagents are usually prepared from organohalides and magnesium metal, and these highly reactive species often necessitate the use of low temperatures to counter the exothermic nature of their reactions. The direct use of organohalides as starting materials is an appealing alternative. For example, classical Reformatsky and Barbier-type reactions feature stoichiometric metal additives that allow the reactive organometallic nucleophile to be formed *in situ*.[2] Catalytic methods have also been developed. For example, the Nozaki-Hiyama-Kishi (NHK) reaction is a powerful chromium-mediated method for reductively coupling organohalides and aldehydes, generally facilitated by a nickel catalyst (Scheme 2.2A).[3] In the commonly proposed mechanism, Ni serves to activate the carbon–halogen bond and transmetallates with Cr(III) (Scheme 2.2).[4] The resultant organochromium species serves as the reactive nucleophile. While substantial efforts have been made to generalize the NHK reaction and render chromium catalytic,[5] most practical applications use a substantial excess.[6] Although organometallic nucleophiles are still broadly used in carbonyl addition,[7,8] progress toward the development of catalytic carbonyl reductive couplings using non-metallic reductants (H_2, 2-PrOH) and related hydrogen auto-transfer reactions has been made.[9] The reductive arylation of aldehydes with organohalides was first reported by Cheng and co-workers in 2000, who found that Ni/dppe could catalyze this reaction by using stoichiometric Zn

Scheme 2.1 Accessing secondary alcohols from coupling aryl halides with aldehydes

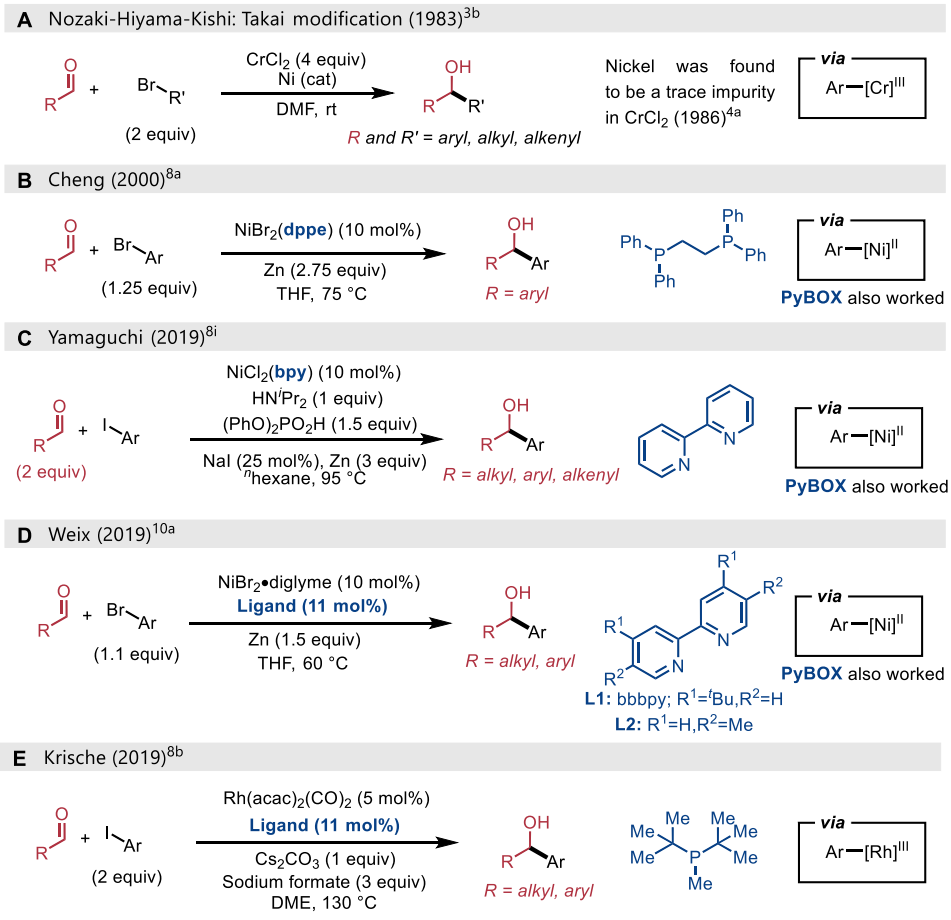

(Scheme 2.2B).[8a] Yamaguchi also reported a similar coupling of aryl iodides with aldehydes using bipyridine as a ligand and stoichiometric zinc as a reductant (Scheme 2.2C).[8i] Two recent breakthroughs were made towards expanding these direct, chromium-free methods. Weix and co-workers reported that nitrogen ligands such as bipyridine and a PyBOX enable Ni-catalyzed reductive coupling of diverse aryl bromides and aldehydes to synthesize predominantly hindered secondary alcohols (Scheme 2.2D).[10a] Like most other reductive couplings, a stoichiometric metal – in this case, zinc – was also needed to facilitate the reaction. Simultaneously, the Krische lab described the first variant of this reaction that exploited a mild organic reducing agent – sodium formate – merging the areas of reductive coupling and transfer hydrogenation (Scheme 2.1E).[10b]

Their conditions featured a Rh(I) catalyst and two equivalents of an aryl iodide coupling partner, which facilitated the arylation of both aryl- and alkyl-substituted aldehydes at high temperatures. Our group previously reported related cross-coupling reactions with both aldehyde and alcohol starting materials, enabling the synthesis of ketones from aryl triflates using a Ni(0)/triphos catalytic system.[11,12] These reactions were proposed to occur through Heck-type pathways, with β-hydride elimination of an intermediate nickel alkoxide providing the ketone product. Efforts to divert this intermediate to produce alcohol products were unsuccessful with the reported catalyst system. Such reductive couplings can be plagued with side reactions, including reduction of the aryl halide to the corresponding homocoupled dimer[13] or hydrodehalogenation product.[14] With the limitations of existing reductive couplings in mind, we sought a new catalyst that might be capable of forming secondary alcohols from the coupling of organohalides without the use of stoichiometric metal reagents while avoiding these side-products. Herein, we describe our discoveries which demonstrate that a Ni catalyst featuring 1,5-diaza-3,7-diphosphacyclooctane (P_2N_2) ligands enables the efficient cross-coupling of aryl iodides with aldehydes to form secondary benzylic alcohols.

Scheme 2.2 Proposed mechanism of the NHK reaction

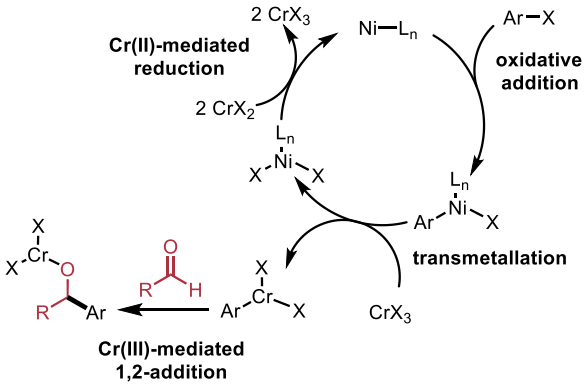

2.4 Research goals

While studying the carbonyl-Heck reaction with high-throughput screenings, we noticed trace amounts of benzhydrol, a reduced side-product (Scheme 2.3A). After a few trial experiments, it was clear that small modifications of the working catalyst system would not simply yield the reduced product. For example, simple addition of a mild reducing agent, such as isopropanol, to the published conditions[12] did not form the carbinol (Scheme 2.3B).

After searching the literature (further elaborated in Section 2.3), we hypothesized that nickel could catalyze reductive coupling of organohalides with aldehydes using a mild reductant. The use of a mild reductant, in contrast to established methods, could enable a broader scope of transformation allowing for incorporation of sensitive functional groups.

Modification of the optimized carbonyl-Heck Ni/triphos catalyst system was not promising, so we turned to more common ligands. After extensively testing many classes of commercially-available ligands, such as monodentate phosphines, bidentate phosphines, NHCs, diamine ligands, etc., robust conditions remained elusive. We became interested in 1,5-diaza-3,7-diphosphacyclooctane (P_2N_2) ligands since they follow a modular synthesis and electrocatalytic applications had noted that structural modification could tune activity. We also noted that P_2N_2 ligands have pendant amine arms, not entirely dissimilar from triphos' pendant phosphino arm. This chapter details our study of P_2N_2 ligands and their application in the reductive Ni-catalyzed cross-coupling of aryl iodide with aldehydes. Our primary research goal was to design a P_2N_2 ligand capable of facilitating the arylation of aldehydes with a (pseudo)halide.

Scheme 2.3 A reductive carbonyl-Heck

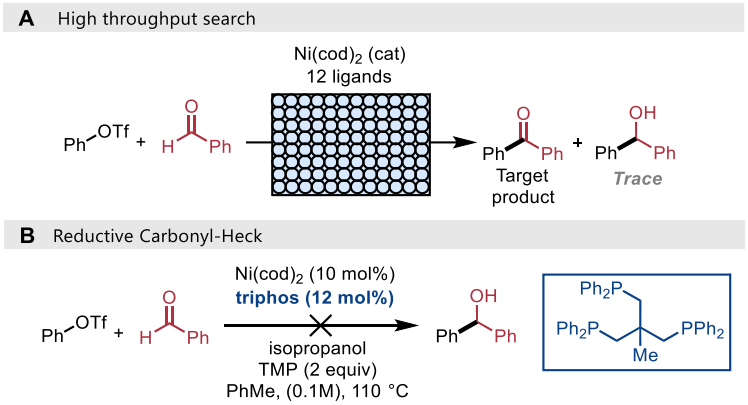

2.5 Results and discussion

2.5.1 Optimization of the reductive arylation of aldehydes

Our study began by the investigation of the coupling of organohalides and aldehydes using inexpensive alcohol additives as mild stoichiometric reducing agents (Table 2.1). Two major by-products plagued most attempts. For instance, in the coupling of 6-iodoquinoline **2.1** and benzaldehyde **2.2**, the desired alcohol was often formed alongside the redox-neutral carbonyl-Heck product **2.3**. An even greater challenge is the need for this net reduction reaction to occur without deleterious reduction of the organohalide to form quinoline **2.4**. Success was finally realized when testing 1,5-diaza-3,7-diphosphacyclooctanes (P_2N_2). These modular ligands are easily synthesized in two steps by condensation between a phosphine, formaldehyde, and an amine (see Section 1.5.1). While they are well established in coordination chemistry,[15] hydrogen splitting or formation,[16] and related organometallic studies,[17,18] they have rarely been reported in cross-coupling.[19] In the optimal conditions identified, a P_2N_2 ligand derived from cyclohexylphosphine and *p*-trifluoromethylaniline, $P^{Cy}{}_2N^{ArCF3}{}_2$, along with 1-phenylethanol as a stoichiometric reducing agent, was found to completely suppress side-product formation to give the desired alcohol **2.5** in 78% yield (entry 1). Both points of derivatization of the P_2N_2 ligands had a significant influence over the reaction outcome. For example, substituting the N(4-F_3C-C_6H_4) group with N(4-MeO-C_6H_4) or N(3,5-F_3C-C_6H_3) group resulted in a catalyst prone to reducing the organohalide (entries 3-4). Trace coupling was observed with the P-*iso*-butyl analogue (entry 5) while no reactivity was observed with the P-*tert*-butyl analogue (entry 6).In contrast, replacing the P-cyclohexyl fragment with P-phenyl gave the desired selectivity but relatively low conversion (entry 7). Common phosphine ligands used in Ni-catalyzed Heck-type and related reactions such

as dppp, dppf, dcype, PCy_3, and IPr all reduced the organohalide (entries 8-12). While $Ni(cod)_2$ could successfully be employed as an alternative nickel source (entry 13), we elected to use $NiBr_2$•diglyme due to its higher stability. In addition to being a mild, organic reducing agent, 1-phenylethanol was also the most selective. Zn and Mn were entirely ineffective as a replacement for the 1-phenylethanol (entries 14-15), despite being common reducing agents for related reactions. Lighter alcohols such as 2-propanol or 2-butanol were more promising but still resulted in significant organohalide reduction (entries 16-17). 1,4-butanediol resulted in a roughly one-to-one mixture of ketone to alcohol (entry 18). Sodium formate, the reductant used by Krische et al., was also found to be ineffective (entry 19).[11b] Similarly, hydrogen gas rapidly reduced the aryl iodide without no trace of reductive arylation (entry 20). As was the case in our previous work on ketone synthesis,[12] the use of 2,2,6,6-tetramethylpiperidine (TMP) as a base was critical.

Table 2.1 Optimization of the reductive 1,2-arylation

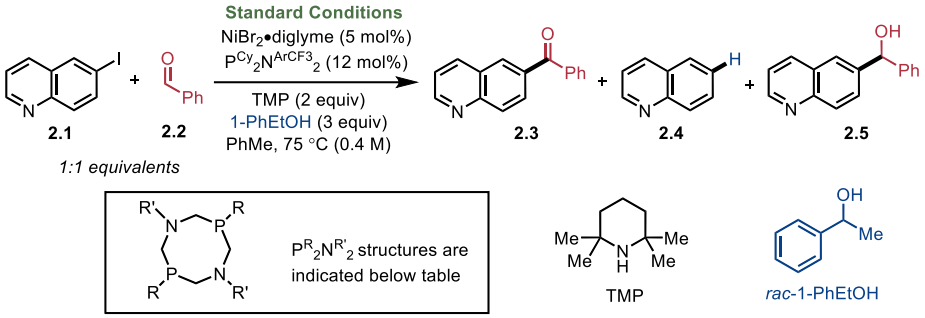

entry	deviation	yield 2.3	yield 2.4	yield 2.5
1	None[a]	Trace	0%	78%
2	*$P^{Cy}{}_2N^{ArCF3}{}_2$ (6 mol%)*	*Trace*	*0%*	*70%*
3	$P^{Cy}{}_2N^{ArOMe}{}_2$as ligand	0%	63%	13%
4	*$P^{Cy}{}_2N^{Ar(CF3)2}{}_2$ as ligand*	*0%*	*80%*	*0%*
5	*$P^{iBu}{}_2N^{ArCF3}{}_2$ as ligand*	*0%*	*59%*	*13%*
6	*$P^{tBu}{}_2N^{ArCF3}{}_2$ as ligand*	*0%*	*91%*	*0%*
7	$P^{Ph}{}_2N^{ArCF3}{}_2$ as ligand	0%	10%	35%
8	Dppp as ligand	0%	53%	5%
9	Dppf as ligand	0%	0%	0%
10	Dcype as ligand	0%	85%	0%
11	PCy_3[b] as ligand	Trace	88%	0%
12	$IPr^{\bullet}HCl$ as ligand	0%	81%	Trace
13	$Ni(cod)_2$ as Ni source	Trace	0%	74%
14	Zn as [H]	14%	58%	0%

Table 2.2 Optimization of the reductive 1,2-arylation (continued)

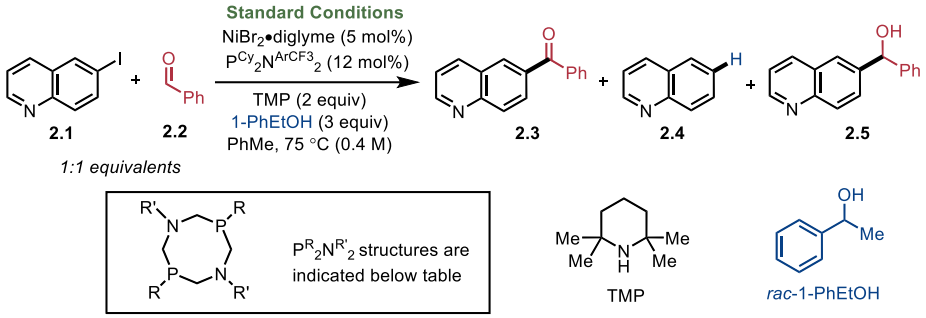

entry	deviation	yield 2.3	yield 2.4	yield 2.5
15	*Mn as [H]*	*0%*	*0%*	*0%*
16	2-PrOH as [H]	34%	Trace	47%
17	*sec*-BuOH as [H]	52%	Trace	46%
18	*1,4-butanediol as [H][c]*	*42%*	*Trace*	*50%*
19	HCO_2Na as [H]	8%	68%	Trace
20	H_2 (1 atm) as [H]	0%	86%	0%
21	Et_3N as base	10%	50%	Trace
22	Pyridine as base	12%	50%	0%
23	K_3PO_4 as base	10%	50%	Trace
24	*PMP[d] as base*	*21%*	*20%*	*37%*
25	*DIPEA as base*	*Trace*	*29%*	*44%*

General conditions: aryl iodide (0.30 mmol), aldehyde (0.30 mmol), TMP (0.6 mmol), 1-phenylethanol (0.90 mmol), $NiBr_2$•diglyme (5 mol%), $P^{Cy}{}_2N^{ArCF3}{}_2$ (12 mol%), PhMe (0.75 mL), 75 °C for 16 h. Crude yields are given as assessed by ^1H NMR using 0.05 mmol 1,3,5-trimethoxybenzene as internal standard. [a]Stoichiometric acetophenone was observed as a byproduct of 1-PhEtOH oxidation. [b]24 mol% ligand since monodentate ligand. [c] 1.5 equivalents were used as 1,4-butanediol can be oxidized twice to γ-butyrolactone. [d] PMP = 1,2,2,6,6-Pentamethylpiperidine. **Entries which were not present in the original publication have been italicized.**

Figure 2.1 Structures of ligands for Table 2.2

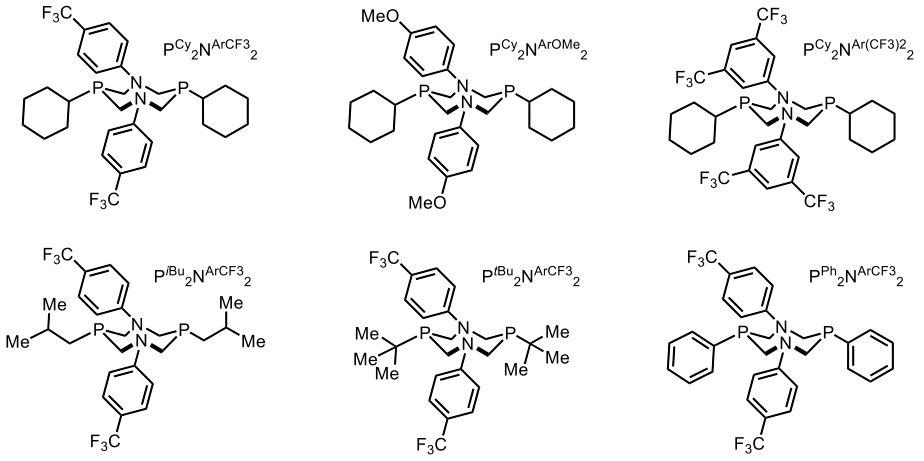

Common amines like triethylamine (entry 21) and pyridine (entry 22) were ineffective, as were inorganic bases such as K_3PO_4 (entry 23). Pentamethylpiperidine (PMP) resulted in a mixture of **2.3**, **2.4**, **2.5** (entry 24), indicating that the N-H bond may play a key role in obtaining desired selectivity for the carbinol product. Diisopropylethylamine (DIPEA), a tertiary amine, gave a significant amount of reduced quinolone, **2.3**, as a side-product (entry 25) but product **2.5** was formed selectively over the ketone **2.3**.

Using the best conditions from Table 2.1, an assessment of different aryl (pseudo)halide coupling partners and solvents was performed at a 0.2 M concentration (Table 2.3). The concentration was reduced from 0.4 M to 0.2 M to dilute the reaction mixture – the free ligand is sparingly soluble in toluene and this created problems with stirring. For convenient availability of organo(pseudo)halides, phenyl derivatives were used for this study. Chlorobenzene, phenyl mesylate, phenyl toslylate, and phenyl triflate did not allow for formation of cross-coupled products in toluene (entries 1-4). Bromobenzene displayed trace, non-zero, product formation in toluene (entry 5), suggesting that a targeted optimization could be possible to bring aryl bromides

into scope. Iodobenzene reacted as expected in toluene, with high product formation and negligible ketone formation, under the conditions optimized for 6-iodoquinoline (entry 6). THF, the solvent of choice by the Cheng and Weix groups for similar couplings,[8a,10a] was found to be equivalent to toluene (entry 7). Dimethoxyethane and N-methyl-2-pyrrolidone (NMP) were viable solvents but gave reduced yields of **2.8** (entries 8-9). Acetonitrile greatly impacted formation of the desired product (entry 10); MeCN is a coordinating solvent and could poison the nickel catalyst by acting as a ligand and disrupting coordination of the aldehyde.

With optimized conditions identified, a formal scope could be evaluated to isolate compounds and determine the extent of substrates this transformation was applicable for.

Table 2.3 Screening of aryl (pseudo)halides and solvents

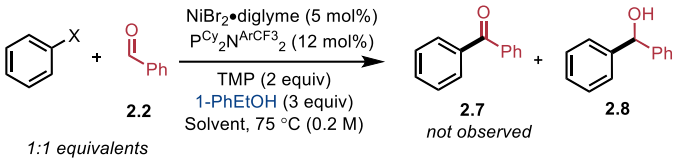

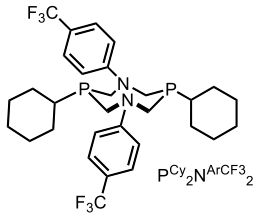

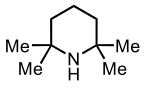

entry	aryl(pseudo)halide	solvent	yield 2.8
1	PhCl	PhMe	0%
2	PhOMs	PhMe	0%
3	PhOTs	PhMe	0%
4	PhOTf	PhMe	0%
5	PhBr	PhMe	4%
6	PhI	PhMe	82%
7	PhI	THF	83%
8	PhI	dimethoxyethane	50%
9	PhI	NMP	61%
10	PhI	MeCN	18%

General reaction conditions: aryl (pseudo)halide (0.30 mmol), aldehyde (0.30 mmol), TMP (0.6 mmol), 1-phenylethanol (0.90 mmol), $NiBr_2$●diglyme (5 mol%), $(P^{Cy},N^{ArCF3})_2$(12 mol%) in toluene, 0.20 M, 75 °C for 16 h. [a]Crude NMR yield determined using 0.05 mmol 1,3,5-trimethoxybenzene as internal standard.

2.5.2 Scope of the reductive arylation of aldehydes

With conditions for the mild, reductive coupling of equimolar organohalide and aldehyde in hand, the scope of this transformation was investigated, particularly focused on the compatibility of this method with heterocyclic scaffolds (Scheme 2.4). Alcohol **2.5**, derived from the coupling of 6-iodoquinoline **2.1** and benzaldehyde **2.2** described in Table 2.1, was isolated in 89% yield. Alternative aldehyde coupling partners were similarly effective. Products derived from an *ortho*-substituted benzaldehyde derivative **2.9**, derived bearing an aryl bromide **2.10** or free O–H **2.11** were all efficiently made. Heterocycle-bearing aldehydes including a pyrimidine **2.12**, thiazole **2.13**, pyrrole **2.14**, chloropyridine **2.15** and 1,3-benzodioxoles **2.16** and **2.17** yielded the desired secondary alcohols in 57-83% yield. A wide range of aryl iodides also participated in the chemistry. Accordingly, pyridine, acetanilide, and methyl ester-containing products **2.18**-**2.20** were prepared in yields from 77-81%. Products containing morpholinyl **2.21**, pyrazolyl **2.22**, and pinacol boranyl **2.23** substituents were also prepared in moderate to good yield. Aldehydes bearing potentially coordinating heterocycles were more problematic. For example, 6-bromo-2-pyridinecarboxaldehyde underwent coupling in just 21% yield **2.24**, suggesting it may chelate with the Ni catalyst.

Next, aliphatic aldehydes were explored. In most cases, these substrates gave a mixture of the (reductive) alcohol product as well the (redox-neutral) ketone product. This selectivity was found to be dependent on the nature of the aryl iodide. For example, iodonaphthalene could be coupled with hexanal **2.25**, cyclopropylcarboxaldehyde **2.26**, and phenylacetaldehyde **2.27** in 50-73% yield with trace formation of ketone. While less selective reactions could be rendered useful by including a sodium borohydride reduction step in the work-up,[20] aliphatic aldehydes are less

abundant and less stable than aliphatic alcohols. As such, we recommend using the redox-neutral α-arylation procedure to access these types of products (Chapter 3).

Lastly, complex bioactive scaffolds were investigated. Highly functionalized 4-[3-chloro-4-(3-fluorobenzyloxy)phenylamino]-6-iodoquinazoline enabled the direct synthesis of **2.28** in moderate yield.[21] Similarly, loratadine analog **2.29** and open-chain mazindol analog[22] **2.30** could both be readily prepared in 66 and 68% yield, respectively. The vasodilator cloridarol **2.31**, derived from benzofuran-2-carboxyaldehyde and 4-chloroiodobenzene, could be directly formed in 85% yield.[23]

Scheme 2.4 Scope of the reductive arylation of aldehydes

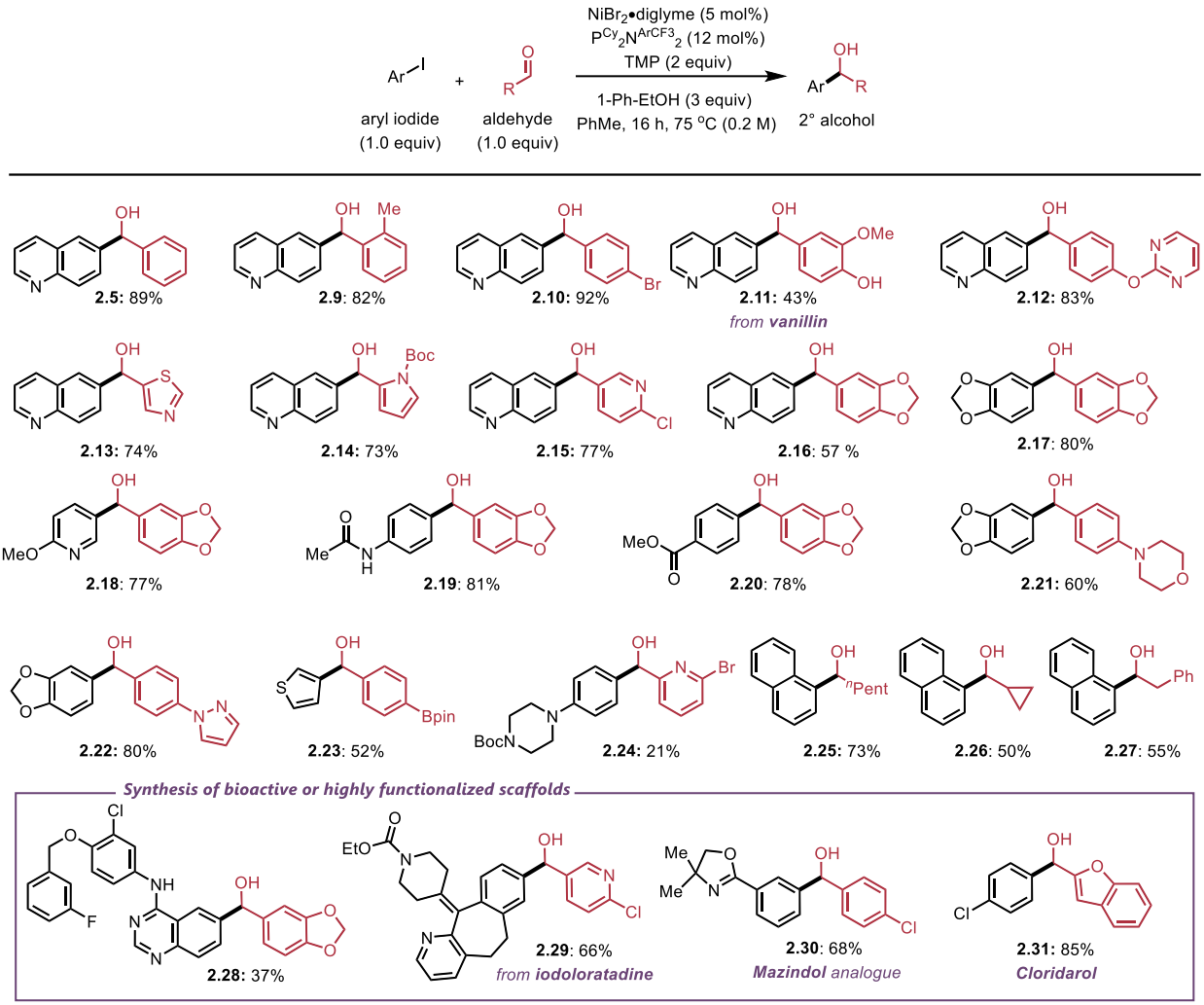

[a]General reaction conditions: aryl iodide (0.30 mmol), aldehyde (0.30 mmol), TMP (0.6 mmol), 1-phenylethanol (0.90 mmol), $NiBr_2$•diglyme (5 mol%), $P^{Cy}{}_2N^{ArCF3}{}_2$ (12 mol%), toluene (0.20 M), 75 °C for 16 h. Isolated yields are reported.

2.5.3 Mechanistic studies

A series of experiments were run with isotopically labeled reactants and reagents to uncover information about the catalytic cycle. 1-PhEtOH-d_1, **2.33**, was prepared to probe whether the hydrogen atom in the product comes from the reducing agent (Scheme 2.5A). We speculated that high deuterium incorporation into product **2.34** would suggest that a Meerwein–Ponndorf–Verley-type equilibrium may be operative. Alcohol **2.34** was formed with minimal deuterium incorporation in the benzylic position, suggesting this proton may originate from the aldehyde. To confirm this, naphthaldehyde-d_1, **2.32-*d*$_1$**, (97% deuterium incorporation) was subjected to the standard reaction conditions, after which **2.34-*d*$_1$** was formed with 94% deuterium in the benzylic position (Scheme 2.5B).

Next, the commercially available oxidative addition complex (TMEDA)Ni(*o*-tolyl)Cl, **2.35**, was combined with $P^{Cy}_2N^{ArCF3}_2$ and treated with 1 equivalent of benzaldehyde, **2.2**, (Scheme 2.5C). The ketone product **2.36** and the alcohol product **2.37** were observed in roughly equal yields, indicating aldehyde insertion is feasible. The observation of ketone **2.36** contrasts the deuterium labeling studies that suggested dehydrogenation of the alcohol does not occur in the catalytic reaction. Under the hypothesis that 1-phenylethanol is required to liberate the alcohol product and serve as a reductant, the stoichiometric arylation experiment was repeated with 1.5 equiv of this additive, leading to 85% yield of alcohol **2.37** with trace formation of ketone **2.36**. The high selectivity for formation of alcohol **2.37** suggests 1-phenylethanol is a better reducing agent for the Ni catalyst than the product is, despite being a doubly benzylic alcohol. This is consistent with observations described in Scheme 2.4, in which coupling with aryl-substituted aldehydes

provided high selectivity for alcohol products, while coupling with alkyl-substituted aldehydes often gave mixtures.

Scheme 2.5 Mechanistic experiments supporting the proposed catalytic cycle

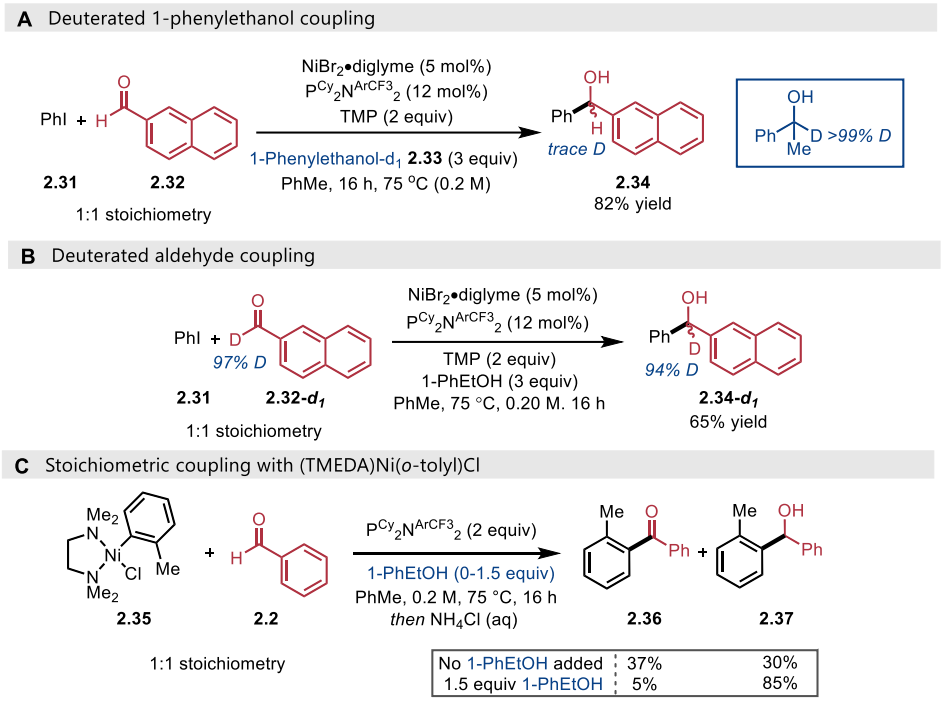

Lastly, the reaction progress of the reductive coupling was monitored over time using $Ni(cod)_2$ (Scheme 2.6). These results were prepared during the optimization and, as a result, the conditions vary slightly from the final optimized conditions. No induction period was observed. Along with stoichiometric experiments noted in Scheme 2.5 and the fact the single electron reductants such as Zn or Mn were ineffective (Table 2.1, entries 14-15), this suggests a catalytic cycle featuring Ni(0) and Ni(II) is likely to be operative versus odd oxidation states.[24]

Scheme 2.6 Reaction conversion over the first 120 minutes

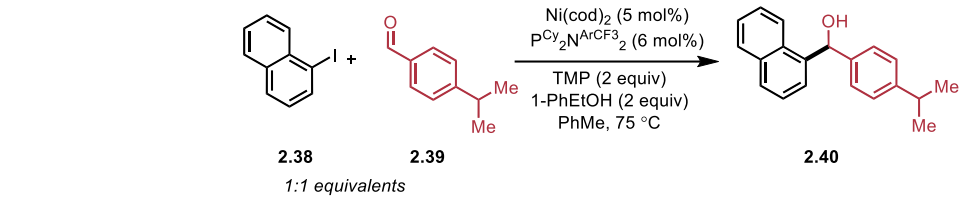

2.38 **2.39** **2.40**

1:1 equivalents

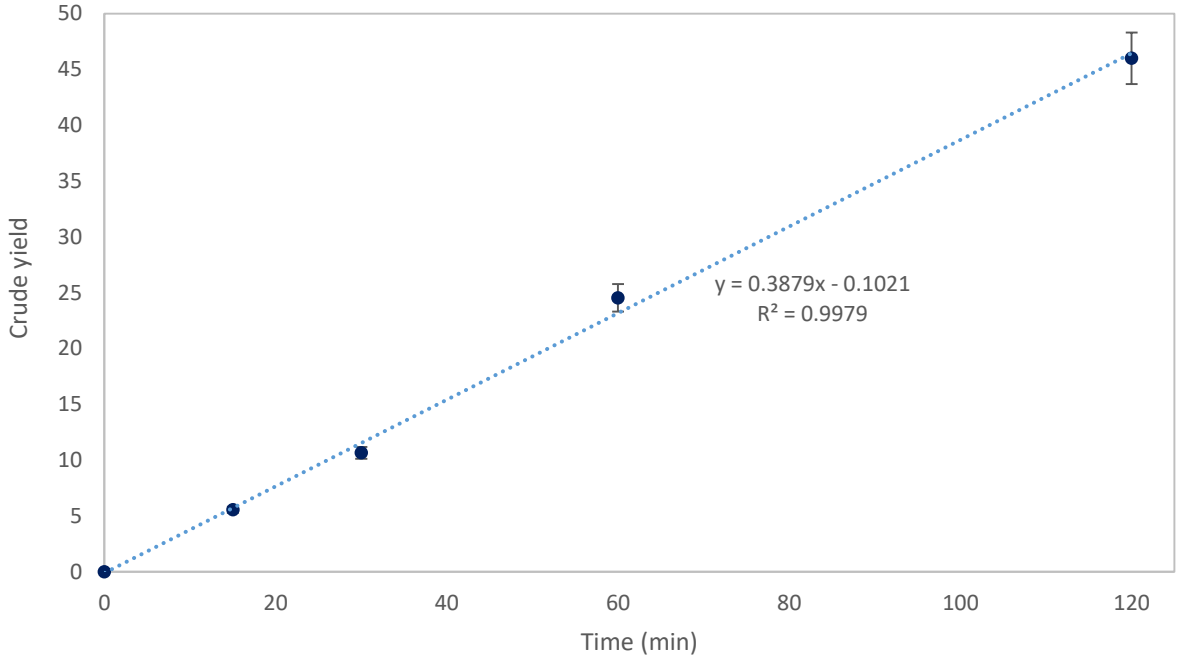

Reaction conditions: aryl iodide (0.30 mmol), aldehyde (0.30 mmol), TMP (0.3 mmol), $Ni(cod)_2$(5 mol%), P_2N_2 (6 mol%), 1-PhEtOH (0.6 mmol) in toluene, 0.45 M, 75 °C for 16 h. The reaction was performed in a glovebox. The vial was opened and aliquots were taken at the specific time points. Sample was filtered through a plug of silica gel with acetonitrile. Analysis was performed by GC-FID after quench.

Based on these mechanistic experiments and analogy to related carbonyl-Heck reactions,[27] a plausible catalytic cycle is proposed in Scheme 2.7. The Ni(II) pre-catalyst **2.A** is first reduced with the sacrificial alcohol reducing agent to make the corresponding oxidized alcohol and a Ni(II) hydride **2.B**, which can undergo reductive elimination to an active Ni(0) catalyst **2.C**. Notably, $Ni(cod)_2$, which was found to be equally effective as $NiBr_2$•diglyme (see Table 2.1**,** entry 13), would avoid the need for the initial reduction and may begin the catalytic cycle with

intermediate **2**.**C**. nickel(II) adduct **2.D**. With most ligands and reducing agents, this species may get reduced to form the dehalogenated arene; however, the optimal conditions appear to block this pathway in favour of productive C–C bond formation. With our identified catalyst system, adduct **2.D** is believed to coordinate with the aldehyde to form intermediate **2.E**. While the nature of these π bond-coordinated intermediates in Pd-catalyzed insertion reactions has been the subject of thorough study,[25] the analogous Ni-catalyzed reactions are less well understood.[26] Intermediate **2.E** may involve binding of the aldehyde in either an η^1 or η^2 fashion,[27] may require temporary dissociation of a phosphine or iodide ligand from nickel(II) adduct **2.D**. Regardless, a π bond insertion may generate the key C–C bond to form Ni(II) alkoxide **2.F**. While this intermediate may be prone to β-hydride elimination, evidenced by the ketone side-products discussed throughout, the lack of deuterium incorporation described in substrate **2.32**, and stoichiometric studies with Ni(II) complex **2.35** suggest this species undergoes exchange of alkoxide groups to form the alcohol products and regenerate Ni(II) intermediate **2.A**. 1-phenylethanol fills this role and serves as a stoichiometric reductant to turn over the catalyst. In addition to the mechanistic experiments presented herein, the key steps proposed are common in the literature. This includes β-hydride elimination of nickel alkoxides (**2.F** to **2.B**),[11b,14b,28] base-mediated reductive elimination of Ni(II) hydrides with subsequent oxidative addition (**2.B** to**2.D**),[29,30] reduction of Ni(II) aryl complexes (**2.D** to **Ar-H**),[14] and carbonyl 1,2 insertion reactions (**2.D** to **2.F**).[7p, 7q] The successful integration of these steps clearly depends on the use of 1,5-diaza-3,7-diphosphacyclooctanes (P_2N_2), though the specific features of these ligands that facilitate the reaction are not yet clear. Coordinatively saturated Ni-P_2N_2 complexes are particularly useful at hydrogen splitting/formation reactions, wherein pendant

Scheme 2.7 Proposed catalytic cycle for the reductive arylation

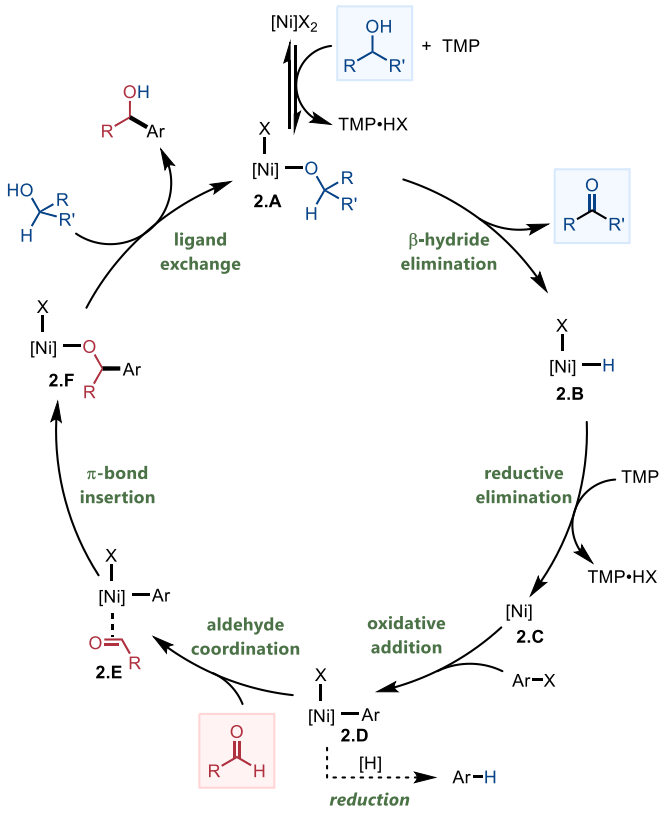

nitrogen atoms exist in close proximity to the metal center and facilitate hydrogen atom transfer.[16] Such steps may be involved in our catalytic cycle, for instance in β-hydride elimination or Ni-hydride reduction steps. However, the optimal ligand in our reaction bears a CF_3-aniline fragment, which is weakly basic and not expected to efficiently promote hydrogen transfer.[16b] Despite being distant from the metal center, the CF_3 group can have profound effect on the Ni, suggesting simple electronic tuning may be occurring.[16a] The pendant nitrogen arm of aniline-derived P_2N_2 ligands has also been found to interact with and stabilize metal centers[31] in a similar manner that Buchwald-type phosphine ligands are known to interact with Pd.[32] Furthermore, the sterically bulky cyclohexylphosphine fragments on our optimal ligand have been shown to result in distortion of square planar Ni(II) complexes in related complexes, which may be important for

reactivity.[16a] While these insights into the behavior of P_2N_2 ligands may be relevant, the reductive and redox-neutral arylation reactions presented herein are unique applications and it is not clear if established or novel aspects of this species are responsible for the reaction's success. Given the precedent for all mechanistic steps in the absence of P_2N_2 ligands, the key to success in our chemistry appears to link to the relative rate of aldehyde coordination/insertion (**2.D** to **2.F**) compared to the rate of Ni-aryl reduction (**2.D** to **Ar-H**). Even with the optimal catalyst, alternative reducing agents such as 2-PrOH and H_2 give substantial amounts of the deleterious reduction side-product (see Table 2.1). We thus speculate that the success of the reaction is a result of the combination of P_2N_2 ligands and 1-phenylethanol reductant promoting aldehyde insertion and/or slowing the reaction of Ni complex **2.D** with the alcohol reductant.

A key step in the mechanism described above is the exchange of alkoxide groups from **2.F** to **2.A** to form the alcohol product and regenerate the catalyst. We hypothesized that omission of alcohols may force metal alkoxide **2.F** to undergo β-hydride elimination, providing a catalytic route to ketones. While we previously described analogous redox-neutral and oxidative carbonyl-Heck reactions, these reactions were exclusively limited to the use of aryl triflate coupling partners at elevated temperatures.[11,12] For instance, coupling of aryl iodide **2.38** with aldehyde **2.41** using previously developed Ni/triphos C–H arylation conditions gave no trace of the corresponding ketone, **2.42** (Scheme 2.8).[12] In contrast, using $P^{Cy}{}_2N^{ArCF3}{}_2$ and the conditions optimized for reductive cross-coupling, the same reaction could be achieved with 86% yield of **2.42** (Scheme 2.8). Not only is this previously undeveloped reaction made possible, it is achieved at a greatly reduced temperature without thorough optimization. We believe this is an important

next step to expanding the breadth of ketone and alcohol arylation chemistry and highlights the previously unrecognized power of P_2N_2 ligands in catalytic coupling chemistry.

Scheme 2.8 Extrapolation of reaction conditions to the carbonyl-Heck coupling

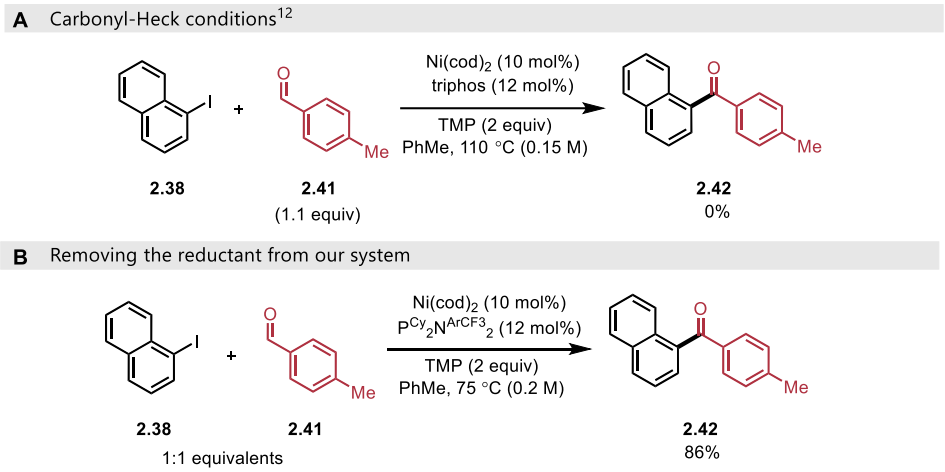

2.5.4 Limitations of the reductive arylation

While evaluating the scope of this transformation, several products could not be obtained in synthetically useful yields using the conditions from the General Procedure. A selection of these is given below (Scheme 2.9). Reactions with highly electron-deficient aryl iodides including 1-Iodo-3,5-bis(trifluoromethyl)benzene, dimethyl 5-iodoisophthalate, and 3-iodopyridine showed, at best, only trace conversion (**2.43-2.45**). We speculate that rendering the aryl nickel (II) species too electron-poor limits its ability to do a 1,2-carbonyl insertion and this stops the productive catalytic cycle. Unreacted aryl iodides were recovered from the reaction mixture of **2.43**-**2.45**, suggesting that direct reduction of the Ni-aryl intermediate is not prominent. Reactions with coordinating functional groups including 4-amino-3-iodobenzonitrile, 2-cyanocarboxaldehyde, 2-nitro-5-fluorobenzaldehyde, 4-iodobenzonitrile, 5-iodouracil 3-formylchromone, and 4-imidazolecarboxaldehyde showed, at best, only trace conversion (**2.46-2.52**). We hypothesize that these functional groups were able to competitively bind to the nickel

centre, reducing the ability of the carbonyl to coordinate. Dipyridyl methanol (**2.53**) could not be separated from 6-bromopyridinemethanol (reduced carboxaldehyde). Similarly, 2-iodothiophene-derived product (**2.54**) could only be obtained in moderate yield. 4-Iodobenzenesulfonamide (**2.55**) gave poor conversion with recovered aryl iodide, suggesting that the acidic sulfonamide could hinder productive chemistry. Highly electron-rich aromatic, 4-morpholinobenzaldehyde, had limited reactivity with standard aryl iodides that performed well in the coupling (**2.56**-**2.57**). It should be noted that product **2.21** successfully incorporated 4-morpholinobenzaldehyde into the scope by pairing it with an electron-rich aryl iodide (Scheme 2.4). This could suggest that a more electron-rich aryl nickel (II) species is required to react with less electrophilic aldehydes. *Ortho*-substituted aryl iodide did not afford product (**2.58**) and was recovered, in contrast with the stoichiometric experiment in Scheme 2.5C. Aliphatic and allylic iodides also did not afford any product (**2.59**-**2.60**). It should be noted that copper inhibitor, a common stabilizer in commercial samples,[33] was not removed and no effort was made to purify cyclohexyl iodide or allyl iodide – they were used as received.

Scheme 2.9 Challenging scope examples of the reductive coupling

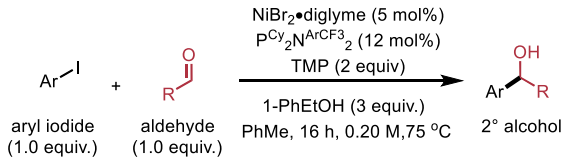

A Highly electron-deficient aryl iodides (trace)

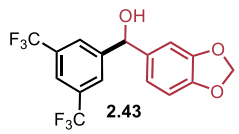
2.43

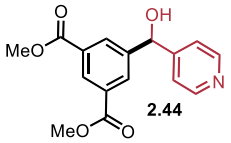
2.44

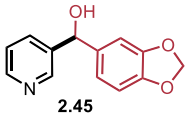
2.45

B Coordinating or chelating functional groups (trace)

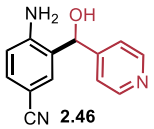
2.46

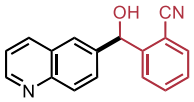
2.47

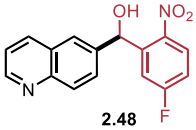
2.48

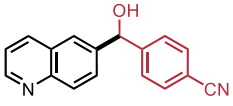
2.49

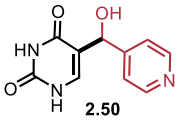
2.50

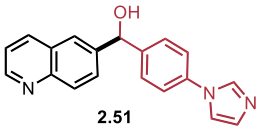
2.51

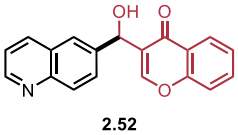
2.52

C Other challenging examples

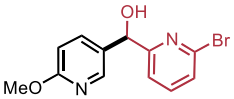
2.53
30-50% yield

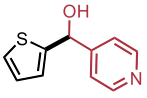
2.54
30-50% yield

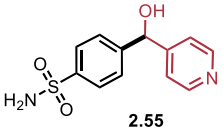
2.55
10-30% yield

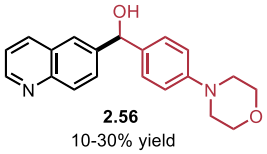
2.56
10-30% yield

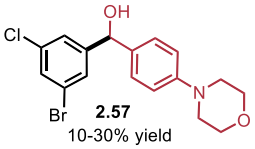
2.57
10-30% yield

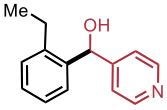
2.58
< 5% yield

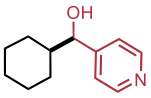
2.59
Trace

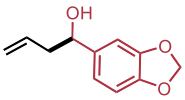
2.60
Trace

2.6 Conclusions, advancement in the field, and future work

2.6.1 Conclusions

The reaction of organometallic nucleophiles with carbonyl groups is among the most important reactions in organic chemistry but suffers numerous inefficiencies. In this work, a catalyst system composed of a Ni(II) salt and a unique 1,5-diaza-3,7-diphosphacyclooctane ligand was found to enable the direct reductive coupling of aryl iodides and aldehydes. A simple alcohol reductant was used in lieu of stoichiometric metal additives. The transformation is proposed to follow a key C–C bond-forming π–bond insertion step and either the sacrificial alcohol or the substrate itself serving to reduce the resulting Ni(II) species into its active Ni(0) form. Extension to ketone-forming reactions is also demonstrated, suggesting that the Ni/P_2N_2 catalyst system has the potential to unlock a variety of challenging reductive, oxidative, and redox-neutral reactions of alcohols and carbonyl compounds.

2.6.2 Advancements in the field

Since the publication of this manuscript, there have been several advancements in the field of reductive cross-coupling of aryl halides with carbonyls (Scheme 2.10). Enantioselective variants were reported featuring chiral bidentate nitrogen-based ligands and stoichiometric zinc (Scheme 2.10A).[34] These catalyst systems are most similar to those of Weix and coworkers.[10a]. Similarly, an asymmetric cobalt-catalyzed variation was recently reported under photocatalytic conditions (Scheme 2.10B).[35] Zhou and coworkers also reported an enantioselective nickel-catalyzed coupling of aryl halides with aldimines, the nitrogen analogue of an aldehyde (Scheme

2.10C).[36] To date, all of the enantioselective procedures to couple aryl halides with carbonyls have featured zinc as a stoichiometric reductant instead of greener variants.

Scheme 2.10 Coupling of aryl halides with aldehydes/aldimines since 2021

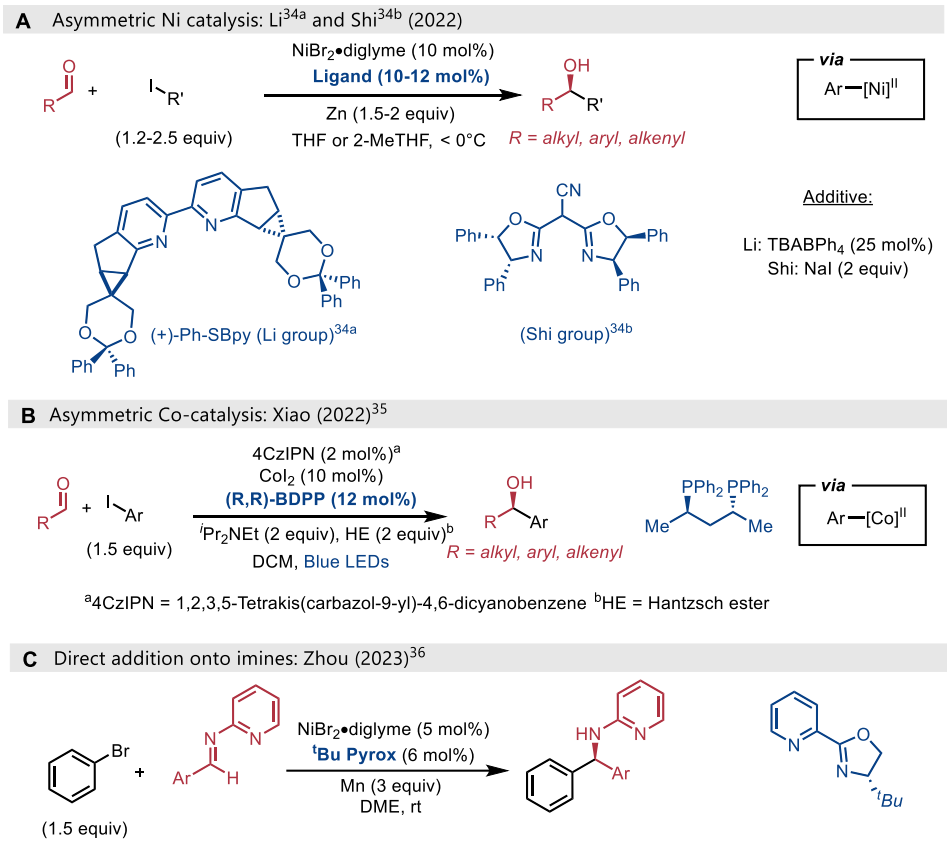

Our group developed modified reaction conditions to bring isatins into the scope of reaction (Scheme 2.11).[37] Of particular note, *sec*-BuOH was found to be a better reductant than 1-phenylethanol for this particular transformation. *sec*-BuOH is an improved reductant over 1-phenylethanol as it is more volatile and lower molecular weight. A crystal structure of $[Ni(P^{Cy}_2N^{ArCF3}_2)_2]$, a catalytically competent Ni(0) complex, was also reported.

Scheme 2.11 Arylation of isatins with aryl iodides

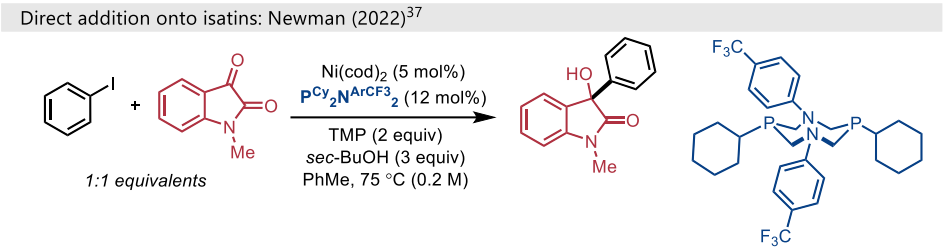

Poater and coworkers performed a computational study to probe the feasibility of our proposed catalytic cycle.[38] They postulate that Ni(0) can be an unstable oxidation state and an alternative mechanism could be operative to avoid it – a previous study of a nickel-catalyzed Suzuki-Miyaura found that formation of Ni(0) can be disfavorable.[39] The Poater group simplified the P_2N_2 ligand for some calculations to be $P^{Me}{}_2N^{Me}{}_2$ in order to lower computational demands. The authors propose that the pendant amine of the P_2N_2 ligand can deprotonate nickel(II) hydride to form an anionic Ni(0) species (Scheme 2.12). Anionic metal complexes have long been proposed as catalytically relevant species in palladium-catalyzed cross-couplings.[40] More recently, anionic species have been implicated in nickel catalysis, indicating that this pathway is theoretically possible.[41] Poater et al. report that the anionic pathway is thermodynamically feasible under our optimized reaction conditions, whereas formation of a neutral $Ni^0(P^{Me}{}_2N^{Me}{}_2)$ complex has a significantly higher energetic barrier of formation at 75 °C.

Scheme 2.12 DFT proposal for anionic Ni(0) (Poater)[38]

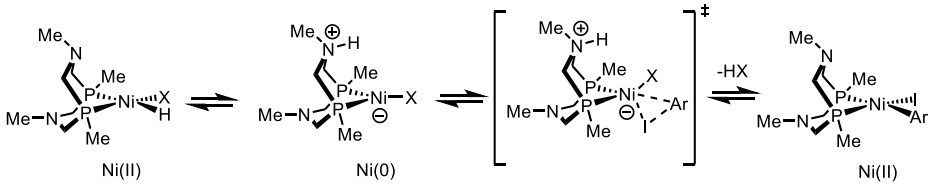

Poater and coworkers also note that iodide has an underappreciated role in the reaction as a ligand. All relevant barriers were lower in energy when considering the halogen ligand to be

iodide rather than bromide. This finding lends support to our observations that aryl bromides afford only trace yields (Table 2.3 entry 4), while aryl iodides participate in the coupling. To further probe this possibility, reactions with aryl chlorides or bromides could be run in the presence of iodide salts (eg. potassium iodide) to see if ligand exchange occurs and if it can bring these coupling partners into scope. Also notable, the Poater group modelled a $P^{Cy}{}_2N^{ArCF3}{}_2$ Ni complex and suggested that the arene can coordinate to the nickel centre via κ^3-P,P,Ar interaction.[42] This noncovalent interaction was observed to influence the relative stability of the computed transition states/intermediates.

While the DFT study reinforces some experimentally observed results, such as why aryl iodides work in our coupling, and also proposes an anionic nickel(0) pathway, which makes use of the P_2N_2 pendant amine arm, there are still many unanswered questions. The role of TMP as a base has not been well-studied. A highly simplified ligand, $P^{Me}{}_2N^{Me}{}_2$, was used to facilitate computations. Based on the trends established in Table 2.1 we would not anticipate $P^{Me}{}_2N^{Me}{}_2$ to be an effective ligand for the reductive cross-coupling. The methyl substituent on phosphorus is known to have different reactivity in electrochemical applications due to lowered steric bulk compared to the cyclohexyl P_2N_2 analogues.[43] During our optimization, the $–ArCF_3$ group was found to be particularly important for catalytic activity. The Poater group also proposes that the $[Ni(P^{Me}{}_2N^{Me}{}_2)_2]$ complex should be highly stable, resistant to losing a $P^{Me}{}_2N^{Me}{}_2$, and thermodynamically downhill from all other species. Recent work published by our group has shown that the corresponding $[Ni(P^{Cy}{}_2N^{NArCF3}{}_2)_2]$ complex is an effective precatalyst for a related reductive coupling (Scheme 2.11).[37]

2.6.3 Future work

It is evident that there is more mechanistic information to uncover and that further improvements of the methodology could be explored. Extension of the work to aryl chlorides and bromides would enable a wider scope of commercially available coupling partners. Likewise, the methodology could be expanded to prepare secondary vinyl alcohols. These species could be derived from either vinyl halides or *α,β*-unsaturated aldehydes, neither of which have been extensively studied. A challenge in catalytic preparation of secondary vinyl alcohols is internal redox isomerization to the corresponding ketone and saturated hydrocarbon (Scheme 2.13).[44]

Scheme 2.13 Coupling of vinyl triflates with aldehydes

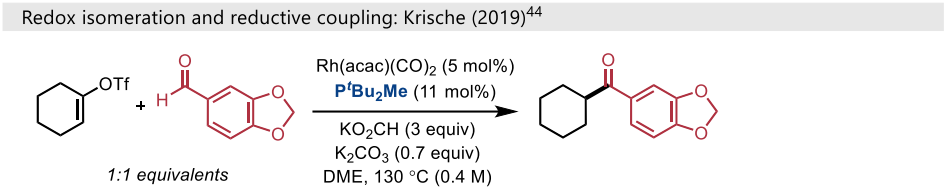

As 1-phenylethanol and acetophenone, the byproduct when 1-PhEtOH is used as a reductant, are high molecular weight and have low volatility, it would be desirable to further optimize conditions with a less wasteful and volatile reductant such as isopropanol.

To further entice chemists to use our method, a convenient, accessible precatalyst such as $[Ni(P^{Cy}{}_2N^{ArCF3}{}_2)]X_2$ (where X is a non-coordinating anionic ligand) could be developed. Currently there is a barrier to access P_2N_2 ligands, as they aren't readily commercially available and many research groups aren't equipped to (or wouldn't want to) handle primary phosphines.

2.7 Experimental

Unless otherwise indicated, reactions were conducted under an atmosphere of nitrogen in 8 mL screw-capped vials that were oven dried (120 °C) or flame dried and shipped into a glovebox. Column chromatography was performed manually using Silicycle F60 40−63 μm silica gel. Analytical thin layer chromatography (TLC) was conducted with aluminum-backed EMD Millipore Silica Gel 60 F_{254} pre-coated plates. Visualization of developed plates was performed under UV light (254 nm). For certain purifications, cerium ammonium molybdate (CAM) or potassium permanganate ($KMnO_4$) stains were used to better visualize the compounds on the TLC plates. The synthesis of P_2N_2 ligands is discussed in Chapter 5. The synthesis of starting materials is fully described and original spectra are available in the freely-available Supporting Information (https://pubs.acs.org/doi/10.1021/jacs.1c05661).

2.7.1 Instrumentation

^{1}H NMR and ^{13}C NMR were recorded on a Bruker AVANCEII 300 MHz spectrometer, a Bruker AVANCEII 400 MHz spectrometer, or a Bruker AVANCEIII 500 MHz spectrometer. ^{1}H NMR spectra were internally referenced to the residual solvent signal (e.g., $CDCl_3$ = 7.27 ppm). ^{13}C NMR spectra were internally referenced to the residual solvent signal (e.g., $CDCl_3$ = 77.00 ppm). Data for ^{1}H NMR are reported as follows: chemical shift (δ ppm), multiplicity (s = singlet, d = doublet, t = triplet, q = quartet, m = multiplet), coupling constant (Hz), integration. NMR yields for optimization studies were obtained by ^{1}H NMR analysis of the crude reaction mixture using 1,3,5-trimethoxybenzene as an internal standard. IR spectra were obtained using a Cary 630 FTIR (Agilent Technologies) and are reported in terms of frequency of absorption (cm^{-1}). Melting point ranges were determined on a Canlab Gallen Kamp Melting Point Apparatus. Accurate mass data

(EI) was obtained from an Agilent 5977A GC/MSD using MassWorks 4.0 from CERNO Bioscience.[45] HRMS data was obtained from a Micromass Q-TOF 2 quadrupole – time-of-flight mass spectrometer with ESI source.

Note: After completion and publication of some of the data described below, it was noticed that the error (in ppm) of several of the Accurate Mass measurements was too large to allow conclusive confirmation of the proposed molecular formula. We regret this mistake. We are still confident in the conclusions made in the data for the following reasons:

1. All molecules previously reported matched the literature.
2. Some functional groups are not amenable to MS accurate analysis and have lower than normal spectral accuracy (aliphatic compounds, boron containing compounds and polyhalogenated groups).
3. The instrument might not have been tuned when the samples were run, or they might have been too dilute for accurate analysis

2.7.2 Optimization Procedure (section 2.5.1)

Inside the glovebox, to a dry 8 mL screw-capped reaction vial equipped with a magnetic stir bar, Ni source (0.05 equiv, 0.015 mmol) and ligand (0.12 equiv, 0.036 mmol) were added and followed by the reaction solvent (1.5 mL). Base (2 equiv, 0.600 mmol), aryl (pseudo)halide (1 equiv, 0.300 mmol), and aldehyde (1 equiv, 0.300 mmol) were added to the stirring solution followed by the reducing agent (3 equiv, 0.900 mmol). The vial was capped, removed from the glovebox, and placed in a stirring (350 rpm) pre-heated mineral oil bath. After stirring for 16 hours, the reaction vial was removed from the oil bath and cooled down to room temperature.

1,3,5-Trimethoxybenzene (0.050 mmol) was added as an internal standard and the mixture was diluted with ethyl acetate. The reaction was filtered through a plug of silica gel with thin layers of sodium sulfate and Celite at the bottom of the frit. For very polar products, a mixture of ethyl acetate and acetone was used to flush the compound off the silica gel. The filtrate was diluted to an appropriate concentration and analyzed by GC-MS. Solvent was removed *in vacuo* and the sample was analyzed with NMR spectroscopy.

2.7.3 General Procedure: The reductive coupling of aryl iodides with aldehydes

Inside the glovebox, to a dry 8 mL screw-capped reaction vial equipped with a magnetic stir bar, $NiBr_2$•diglyme (0.05 equiv, 0.015 mmol, 5.3 mg) and $P^{Cy}{}_2N^{ArCF3}{}_2$ (0.12 equiv, 0.036 mmol, 21.7 mg) were added and followed by toluene (1.5 mL). The solution was stirred as the remaining reagents were added. 2,2,6,6-tetramethyl piperidine (2 equiv, 0.600 mmol, 84.7 mg), aryl iodide (1 equiv, 0.300 mmol), and aldehyde (1 equiv, 0.300 mmol) were added to the stirring solution followed by 1-phenylethanol (3 equiv, 0.900 mmol, 110 mg). The vial was capped, removed from the glove box, and placed in a stirring (350 rpm) mineral oil bath pre-heated to 75 °C. After stirring for 16 hours, the reaction vial was removed from the oil bath and cooled down to room temperature. Two to three small scoops of silica gel were added to the reaction mixture, it was diluted with DCM, dried in vacuo, and purified by flash column chromatography.

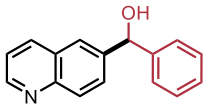

(Phenyl)(6-quinolinyl)methanol (2.5) was prepared according to the general procedure. The product was purified by column chromatography with 5% to 25% acetone in PhMe to afford **2.5** as a white solid (62.6 mg, 89% yield). **^{1}H NMR** ($CDCl_3$, 400 MHz) δ (ppm) 8.73 (d, J = 3.3 Hz, 1H), 8.10 (d, J = 8.2 Hz, 1H), 7.99 (d, J = 8.8 Hz, 1H), 7.88 (br s, 1H), 7.64 (dd, J = 8.8 Hz, 1.64 Hz, 1H). 7.43-7.39 (m, 2H), 7.36-7.30 (m, 4H), 7.29-7.24 (m, 1H), 6.01 (s, 1H), 4.13 (br s, 1H). **^{13}C NMR** ($CDCl_3$, 100 MHz) δ (ppm) 150.0, 147.3, 143.8, 142.7,

136.7, 129.2, 128.9, 128.7, 128.2, 127.9, 126.9, 124.7, 121.3, 75.9. **FT-IR ν (cm^{-1})** 3202, 3025, 2926, 2852, 2643, 1654, 1493, 1451, 1322, 1289, 1241, 1190, 1154, 1117, 1083, 1049, 954, 918, 889, 847, 816, 771, 738, 697. **Melting point** 62 °C. **Accurate Mass (EI)** $H_{13}C_{16}NO$ Theoretical: 235.0992. Found: 235.0874. Spectral Accuracy: 98.9%

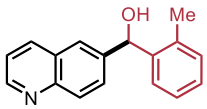

(2-Methylphenyl)(6-quinolinyl)methanol (2.9) was prepared according to the general procedure. The product was purified by column chromatography with 10% to 20% acetone in PhMe to afford **2.9** as a white solid (61.5 mg, 82% yield). **^{1}H NMR** ($(CD_3)_2SO$, 400 MHz) δ (ppm) 8.85 (dd, *J* = 4.2 Hz, 1.7 Hz, 1H), 8.34 (dd, *J* = 8.3 Hz, 0.8 Hz, 1H), 7.94 (d, *J* = 8.8 Hz, 1H), 7.92 (d, *J* = 1.4 Hz, 1H), 7.64 (dd, *J* = 8.7 Hz, 1.9 Hz, 1H), 7.51-7.46 (m, 2H), 7.23-7.10 (m, 3H), 6.05 (d, *J* = 4.2 Hz, 1H), 6.01 (d, *J* = 4.3 Hz, 1H), 2.27 (s, 3H). **^{13}C NMR** ($(CD_3)_2SO$, 100 MHz) δ (ppm) 150.2, 147.0, 142.64, 142.60. 136.0, 134.9, 130.2, 129.0, 128.7, 127.5, 127.0, 126.8, 125.8, 125.1, 121.5, 71.3, 19.1. **FT-IR ν (cm^{-1})** 3331, 2970, 2880, 1460, 1379, 1318, 1158, 1128, 1109, 1042, 951, 891, 854, 816, 783, 731. **Melting point** 144 °C. **Accurate Mass (EI)** $C_{17}H_{15}NO$ Theoretical: 249.1148. Found: 249.1143. Spectral Accuracy: 98.7%

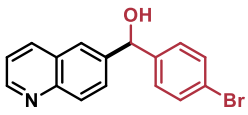

(4-Bromophenyl)(6-quinolinyl)methanol (2.10) was prepared according to the general procedure. The product was purified by column chromatography with 50% acetone in toluene to afford **2.10** as a white solid (87 mg, 92% yield). **^{1}H NMR** ($(CD_3)_2SO$, 400 MHz) δ (ppm) 8.82 (d, *J* = 5.8 Hz, 2.6 Hz, 1H), 8.33 (d, *J* = 7.7 Hz, 1H), 7.96 (broad s, 1H), 7.95 (d, *J* = 8.7 Hz, 1H), 7.65 (dd, *J* = 8.7 Hz, 1.8 Hz, 1H), 7.49-7.46 (m, 3H), 7.35 (d, *J* = 8.4 Hz, 2H), 6.18 (d, *J* = 3.9 Hz, 1H), 5.87 (d, *J* = 3.8 Hz, 1H). **^{13}C NMR** ($(CD_3)_2SO$, 100 MHz) δ (ppm) 150.7, 147.6, 145.1, 143.7, 136.5, 131.6, 129.4, 128.8, 128.1, 124.9, 122.1, 120.4, 73.8. **FT-IR ν (cm^{-1})** 3080, 2924, 1579, 1502, 1323, 1147, 1118, 1069, 1012, 891, 809, 771, 736. **Melting point** 169–171 °C. **Accurate mass (EI):** $H_{12}C_{16}NOBr$ Theoretical: 313.0102. Found: 313.0097. Spectral Accuracy: 98.0%.

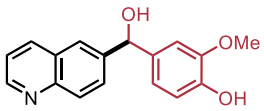

(4-Hydroxy-3-methoxyphenyl)(6-quinolinyl)methanol (2.11) was prepared according to the general procedure. The product was purified by column chromatography with 5% MeOH in DCM to afford **1.11** as a light yellow powder (35.9 mg, 43% yield). **^{1}H NMR** (CD_3OD, 400 MHz) δ (ppm) 8.77 (dd, *J* = 4.3 Hz, 1.6 Hz, 1H),

8.32 (dd, *J* = 8.4 Hz, 0.9 Hz, 1H), 7.97-7.93 (m, 2H), 7.74 (dd, *J* = 8.8 Hz, 1.9 Hz, 1H), 7.49 (dd, *J* = 8.3 Hz, 4.3 Hz, 1H), 6.99 (d, *J* = 1.9 Hz), 6.83 (dd, *J* = 8.2 Hz, 1.9 Hz, 1H), 6.77 (d, *J* = 8.1 Hz), 5.90 (s, 1H), 3.79 (s, 3H). **^{13}C NMR** (CD_3OD, 100 MHz) *δ* (ppm) 150.85, 149.0, 148.1, 147.1, 145.2, 138.4, 136.9, 130.4, 129.6, 128.8, 125.8, 122.6, 120.9, 116.0, 111.6, 76.4, 56.3. **FT-IR ν (cm^{-1})** 3186, 2930, 2854, 1730, 1596, 1577, 1501, 1460, 1426, 1374, 1325, 1268, 1230, 1147, 1117, 1031, 889, 841, 772, 775, 733. **Melting point** 73 °C. **Accurate Mass (EI)** $C_{17}H_{15}NO_3$ Theoretical: 281.1046. Found: 281.1007. Spectral Accuracy: 94.7%

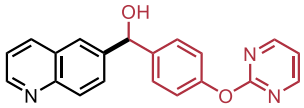

(4-(2-pyrimidinyloxy)phenyl)(6-quinolinyl)methanol (2.12) was prepared according to a modified general procedure. Prior to purification by column chromatography, the crude product in DCM was washed with NH_4Cl (aq). The product was purified by column chromatography with 25% to 50% acetone in PhMe to afford **2.12** as an off-white solid (81.3 mg, 83% yield). **^{1}H NMR** ($(CD_3)_2SO$, 400 MHz) *δ* (ppm) 8.86 (dd, *J* = 4.2 Hz, 1.6 Hz, 1H), 8.60 (d, *J* = 4.8 Hz, 2H), 8.37 (dd, *J* = 8.4 Hz, 1.0 Hz, 1H), 8.06 (d, *J* = 1.4 Hz, 1H), 7.97 (d, *J* = 8.7 Hz, 2H), 7.77 (dd, *J* = 8.8 Hz, 1.8 Hz, 1H), 7.53-7.47 (m, 3H), 7.22 (t, *J* = 8.8 Hz, 1H), 7.16 -7.12 (m, 2H), 6.22 (d, *J* = 3.2 Hz, 1H), 5.97 (d, *J* = 3.6 Hz, 1H). **^{13}C NMR** ($(CD_3)_2SO$, 100 MHz) *δ* (ppm) 164.8, 159.9, 151.6, 150.2, 147.1, 143.7, 142.2, 136.0, 128.9, 128.4, 127.7, 127.6, 124.2, 121.6, 121.4, 116.8, 73.6. **FT-IR ν (cm^{-1})** 3241, 3046, 1568, 1499, 1411, 1399, 1353, 1316, 1288, 1228, 1197, 1152, 1111, 1048, 1020, 992, 923, 902, 865, 809, 787, 749, 729, 662. **Melting point** 167 °C. **Accurate Mass (EI)** $C_{20}H_{15}N_3O_2$ Theoretical: 329.1159. Found: 329.1213. Spectral Accuracy: 97.0%

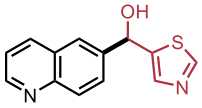

(1,3-thiazol-5-yl)(6-quinolinyl)methanol (2.13) was prepared according to a modified general procedure. Prior to purification by column chromatography, the crude product in DCM was washed with NH_4Cl (aq). The product was purified by column chromatography with 1% to 10% MeOH in DCM to afford **2.13** as a waxy brown semi-solid (54.2 mg, 75% yield). **^{1}H NMR** ($(CD_3)_2SO$, 400 MHz) *δ* (ppm) 8.99 (s, 1H), 8.88 (dd, *J* = 4.1 Hz, 1.5 Hz, 1H), 8.38 (d, *J* = 8.1 Hz, 1H), 8.04 (s, 1H), 8.00 (d, *J* = 8.7 Hz, 1H), 7.81 (s, 1H), 7.77 (d, *J* = 8.7 Hz, 1H), 7.57 (dd, *J* = 8.2 Hz, 4.2 Hz, 1H), 6.66 (d, *J* = 3.7 Hz, 1H), 6.29 (d, *J* = 3.5 Hz, 1H). **^{13}C NMR** ($(CD_3)_2SO$, 100 MHz) *δ* (ppm) 154.1, 150.5, 147.2, 144.6, 142.5, 139.9, 136.2,

129.1, 128.0, 127.6, 124.3, 121.7, 68.2. **FT-IR: ν (cm^{-1})** 3402, 3195, 3078, 2922, 2852, 2255, 2074, 1772, 1719, 1593, 1523, 1499, 1420, 1379, 1325, 1264, 1221, 1146, 1115, 1029, 1005, 883, 825, 771, 697. **Accurate Mass (EI)** $C_{13}H_{10}N_2OS$ Theoretical: 242.0508. Found: 242.0512. Spectral Accuracy: 98.6%

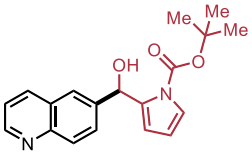

[N-(1,1-Dimethylethoxycarbonyl)pyrrol-2-yl](6-quinolinyl) methanol (2.14) was prepared according to the general procedure. The product was purified by column chromatography with 1% to 10% acetone in PhMe to afford **2.14** as a light brown oil (70.8 mg, 73% yield).**^{1}H NMR** ($CDCl_3$, 400 MHz) *δ* (ppm) 8.91 (s, 1H), 8.18 (d, *J* = 7.6 Hz, 1H), 8.09 (d, *J* = 8.7 Hz, 1H), 7.95 (s, 1H), 7.72 (dd, *J* = 8.8 Hz, 1.9 Hz, 1H), 7.41 (dd, *J* = 8.2 Hz, 4.2 Hz, 1H), 7.22 (dd, *J* = 3.4 Hz, 1.8 Hz, 1H), 6.23 (br s, 1H), 6.06 (t, *J* =3.4 Hz, 1H), 5.73-5.71 (m, 1H), 4.76 (br s, 1H), 1.57 (s, 9H). **^{13}C NMR** ($CDCl_3$, 100 MHz) *δ* (ppm) 150.5, 150.3, 147.9, 140.1, 137.5, 136.5, 129.1, 129.0, 128.4, 128.3, 128.1, 125.3, 122.7, 121.3, 115.0, 110.5, 85.1, 68.8, 28.1. **FT-IR ν (cm^{-1})** 3312, 2977, 1737, 1594, 1571, 1499, 1476, 1409, 1370, 1318, 1257, 1230, 1159, 1113, 1064, 1036, 1003, 889, 839, 772, 723. **HRMS (ESI-TOF**) m/z calc'd for $C_{19}H_{21}N_2O_3$ $[M+H]^+$ Theoretical: 325.1552. Found: 325.1559.

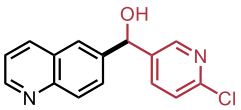

(6-Chloro-3-pyridinyl)(6-quinolinyl)methanol (2.15) was prepared according to the general procedure. The product was purified by column chromatography with 3.5% MeOH in DCM to afford **2.15** as a white solid (62.6 mg, 77% yield). **^{1}H NMR** ($(CD_3)_2SO$, 400 MHz) *δ* (ppm) 8.87 (dd, *J*= 4.2 Hz, 1.7 Hz, 1H), 8.52 (d, *J*= 2.4 Hz, 1H), 8.37 (dd, *J*= 8.4 Hz, 0.9 Hz, 1H), 8.03 (d, *J*= 1.5 Hz, 1H), 7.97 (d, *J*= 8.7 Hz, 1H), 7.83 (dd, *J*= 8.3 Hz, 2.4 Hz, 1H), 7.73 (dd, *J*= 8.7 Hz, 1.9 Hz, 1H), 7.52 (dd, *J*= 8.3 Hz, 4.2 Hz, 1H), 7.46 (d, *J*= 8.3 Hz), 6.42 (d, *J*= 4.1 Hz), 6.03 (d, *J*= 3.8 Hz). **^{13}C NMR** ($(CD_3)_2SO$, 100 MHz) *δ* (ppm) 150.4, 148.9, 148.0, 147.1, 142.5, 140.0, 137.9, 136.0, 129.1, 128.2, 127.6, 124.7, 124.0, 121.6, 71.2. **FT-IR ν (cm^{-1})** 3076, 1581, 1566, 1504, 1458, 1374, 1322, 1281, 1236, 1197, 1141, 1100, 1072, 1042, 1023, 956, 904, 889, 859, 820, 818, 779, 703, 660. **Melting point** 151 °C. **Accurate Mass (EI)** $C_{15}H_{11}ClN_2O$ Theoretical: 270.0554. Found: 270.0649. Spectral Accuracy: 98.0%

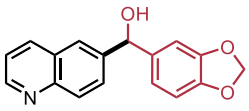

(1,3-Benzodioxol-5-yl)(6-quinolinyl)methanol (2.16) was prepared according to the general procedure. The product was purified by column

chromatography with 10% to 100% EtOAc in hexanes to afford **2.16** as an off-white solid (48.1 mg, 57% yield). **^{1}H NMR** ($(CD_3)_2SO$, 400 MHz) δ (ppm) 8.84 (dd, *J* = 4.2 Hz, 1.7 Hz, 1H), 8.34 (dd, *J* = 8.4 Hz, 0.9Hz, 1H), 7.98 (d, *J* = 1.6 Hz, 1H), 7.93 (d, *J* = 8.8 Hz, 1H), 7.69 (dd, *J* = 8.4 Hz, 1.9Hz, 1H), 7.49 (dd, 8.3 Hz, 4.2 Hz, 1H), 6.95 (d, *J* = 1.6 Hz, 1H), 6.91 (dd, *J* = 8.0 Hz, 1.4 Hz, 1H), 6.84 (d, *J* = 8.0 Hz, 1H), 6.07 (d, *J* = 4.0 Hz, 1H), 5.95 (dd, *J* = 4.4 Hz, 0.9 Hz, 2H), 5.83 (d, *J* = 3.9 Hz, 1H). **^{13}C NMR** ($(CD_3)_2SO$, 100 MHz) δ (ppm) 150.0, 147.1, 146.9, 146.0, 143.8, 139.3, 135.9, 128.6, 128.4, 127.5, 124.1, 121.4, 119.6, 107.8, 106.8, 100.7, 73.6. **Melting point** 133 °C **FT-IR ν (cm^{-1})** 3210, 2904, 2847, 2097, 1592, 1575, 1499, 1488, 1443, 1365, 1323, 1300, 1245, 1227, 1189, 1155, 1118, 1098, 1049, 1035, 986, 926, 891, 868, 844, 794, 788, 772, 751, 703, 665. **Accurate Mass (EI)** $C_{17}H_{13}NO_3$ Theoretical: 279.0890. Found: 279.1016. Spectral Accuracy: 98.7%

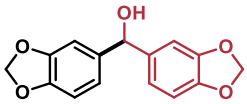

(1,3-benzodioxol-5-yl)-1,3-benzodioxole-5-methanol (2.17) was prepared according to the general procedure. The product was purified by column chromatography with 5% to 10% acetone in PhMe to afford **2.17** as a colorless oil (65.3 mg, 80% yield). **^{1}H NMR** ($CDCl_3$, 400 MHz) δ (ppm) 6.85-6.81 (m, 4H), 6.78-6.75 (m, 2H), 5.94 (s, 4H), 5.68 (s, 1H), 2.15 (br s, 1H). **^{13}C NMR** ($CDCl_3$, 100 MHz) δ (ppm) 147.8, 146.9, 138.0, 119.8, 108.1, 107.0, 101.1, 75.8. Characterization of **2.17** matched a previously reported spectrum.[46]

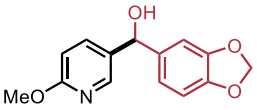

(1,3-Benzodioxol-5-yl)(6-Methoxy-3-pyridinyl)methanol (2.18) was prepared according to the general procedure. The product was purified by column chromatography with 5% to 50% EtOAc in hexanes to afford **2.18** as colourless oil (60.0 mg, 77% yield). **^{1}H NMR** ($CDCl_3$, 400 MHz) δ (ppm) 8.10 (s), 7.54 (d, *J* = 8.4 Hz, 1H), 6.85-6.74 (m, 3 H), 6.70 (d, *J* = 7.8 Hz, 1H), 5.93 (s, 2H), 5.71 (s, 1H), 3.91 (s, 3H), 2.58 (br s, 1H). **^{13}C NMR** ($CDCl_3$, 100 MHz) δ (ppm) 163.8, 148.0, 147.2, 145.0, 137.6, 137.3, 132.3, 119.9, 111.0, 108.2, 107.1, 101.2, 73.7, 53.6. **FT-IR ν (cm^{-1})** 3310, 2949, 2893, 2248, 2034, 1845, 1719, 1607, 1571, 1486, 1439, 1389, 1314, 1284, 1238, 1122, 1094, 1025, 921, 833, 813, 787, 727. **Accurate Mass (EI)** $C_{17}H_{15}NO_3$ Theoretical: 259.0839. Found: 259.0938. Spectral Accuracy: 98.5%

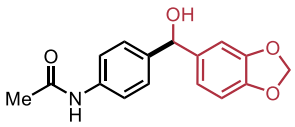

N-[4-[Hydroxy(1,3-Benzodioxol-5-yl)methyl]phenyl]acetamide (2.19) was prepared according to the general procedure. The product was purified by column chromatography with 15% to 75% EtOAc in hexanes to afford **2.19** as a white solid (69.2 mg, 81% yield). **^{1}H NMR** (CD_3OD, 400 MHz) δ (ppm) 7.49 (d, J = 8.5 Hz, 2H), 7.28 (d, J = 8.5 Hz, 2H), 6.84-6.75 (m, 2H), 5.87 (d, J = 1.3 Hz, 1H), 5.65 (s, 1H), 2.09 (s, 3H). **^{13}C NMR** (CD_3OD, 100 MHz) δ (ppm) 171.6, 149.2, 148.3, 139.4, 139.0, 137.5, 128.2, 121.6, 121.0, 108.8, 108.2, 102.3, 85.7, 23.8. **FT-IR ν (cm^{-1})** 3264, 3195, 3124, 3060, 2888, 1664, 1600, 1529, 1501, 1484, 1439, 1405, 1369, 1313, 1234, 1175, 1118, 1091, 1032, 965, 923, 844, 799, 777, 714, 678. **Melting point** 75 °C (dec.) **HRMS (ESI-TOF)** m/z calc'd for $C_{16}H_{15}NO_4Na$ $[M+Na]^+$ Theoretical: 308.0899. Found: 308.1414.

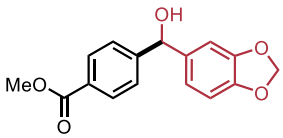

Methyl 4-[hydroxy(1,3-Benzodioxol-5-yl)methyl]benzoate (2.20) was prepared according to the general procedure. The product was purified by column chromatography with 4% to 6% acetone in PhMe to afford **2.20** as a colourless oil (67.2 mg, 78% yield). **^{1}H NMR** ($CDCl_3$, 400 MHz) δ (ppm) 7.99 (d, J = 8.4 Hz, 1H), 7.44 (d, J = 8.2 Hz, 1H), 6.84-6.79 (m, 2H), 6.76 (d, J = 7.9 Hz, 1H), 5.92 (q, J = 1.6 Hz, 1H), 5.78 (s, 1H), 3.90 (s, 3H), 2.52 (br s, 1H). **^{13}C NMR** ($CDCl_3$, 100 MHz) δ (ppm) 167.0, 148.8, 148.1, 147.4, 137.5, 129.9, 129.3, 126.3, 120.4, 108.3, 107.3, 101.2, 75.7, 52.2. **FT-IR ν (cm^{-1})** 3438, 2953, 2890, 2256, 1715, 1609, 1577, 1503, 1486, 1435, 1424, 1310, 1277, 1240, 1187, 1113, 1035, 1016, 921, 861, 800, 753, 727, 705. **Accurate Mass (EI)** $C_{17}H_{15}NO_3$ Theoretical: 286.0836. Found: 286.0882. Spectral Accuracy: 98.7%

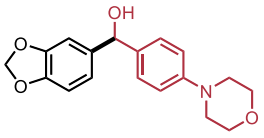

(2H-1,3-benzodioxol-5-yl)(4-(4-Morpholinyl)phenyl)methanol (2.21) was prepared according to the general procedure. The product was purified by column chromatography with 9% to 25% acetone in pentanes to afford **2.21** as a clear oil (56.2 mg, 60% yield).**^{1}H NMR** ($CDCl_3$, 400 MHz) δ (ppm) 7.25 (d, J = 8.6 Hz, 2H), 6.89-6.81 (m, 4H), 6.76 (d, J = 8.6 Hz, 1H), 5.92 (s, 2H), 5.67 (s, 1H), 3.84 (t, J = 4.8 Hz, 2H), 3.12 (t, J = 4.8 Hz, 2H), 2.54 (br s, 1H). **^{13}C NMR** ($CDCl_3$, 100 MHz) δ (ppm) 147.8, 147.1, 142.3, 141.1, 139.3, 138.0, 127.4, 126.9, 120.1, 119.3, 108.1, 107.6, 107.2, 101.1, 75.3. **FT-IR ν (cm^{-1})** 3404, 2962, 2861, 2826, 1708, 1611, 1577, 1486, 1439, 1378, 1331, 1305, 1230, 1176, 1115, 1092, 1033, 921, 830, 805, 781, 734, 701. **Accurate Mass (EI)** $C_{18}H_{19}NO_4$ Theoretical:

313.1309. Found: 313.1191. Spectral Accuracy: 98.1%. **Note: 2.21** was characterized immediately after synthesis as it is prone to decomposition over time.

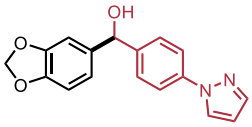

(2H-1,3-benzodioxol-5-yl)(4-(1H-Pyrazol-1-yl)phenyl)methanol (2.22) was prepared according to the general procedure. The product was purified by column chromatography with 10% to 80% EtOAc in hexanes to afford **2.22** as a beige amorphous solid (70.6 mg, 80% yield).**^{1}H NMR** ($CDCl_3$, 400 MHz) δ (ppm) 7.88 (d, *J* = 2.2 Hz, 1H), 7.69 (d, *J* = 1.1 Hz, 1H), 7.60 (d, *J* = 8.5 Hz, 2H), 7.41 (d, *J* = 8.5 Hz, 2H), 6.85-6.81 (m, 2H), 6.77-6.74 (m, 1H), 6.45 (t, *J* = 1.7 Hz, 1H), 5.92 (d, *J* = 1.1 Hz, 2H), 5.74 (s, 1H), 2.93 (br, s, 1H). **^{13}C NMR** ($CDCl_3$, 100 MHz) δ (ppm) 147.8, 147.1, 142.3, 141.1, 139.3, 138.0, 127.4, 126.9, 120.1, 119.3, 108.1, 107.6, 107.2, 101.1, 75.3. **FT-IR ν (cm^{-1})** 3326, 3136, 2886, 2778, 2242, 2052, 1857, 1609, 1523, 1501, 1484, 1439, 1407, 1393, 1331, 1309, 1236, 1195, 1120, 1092, 1031, 934, 919, 874, 848, 803, 781, 749, 727, 656. **Accurate Mass (EI)** $H_{14}C_{17}N_2O_3$ Theoretical: 294.0999. Found: 294.0961. Spectral Accuracy: 98.4%

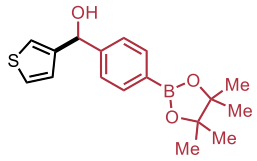

(3-thienyl)[4-(4,4,5,5-tetramethyl-1,3,2-dioxaborolan-2-yl)phenyl]methanol (2.23) was prepared according to the general procedure. The product was purified by column chromatography with 4% to 40% Et_2O in hexanes to afford **2.23** as a clear oil (49.2 mg, 52% yield).**^{1}H NMR** ($CDCl_3$, 400 MHz) δ (ppm) 7.81 (d, *J* = 8.1 Hz, 1H), 7.41 (d, *J* = 7.9 Hz, 1H), 7.28-7.25 (m, 1H), 7.17-7.15 (m, 1H), 6.98 (dd, *J* = 5.0 Hz, 1.2 Hz, 1H), 5.89 (s, 1H), 2.32 (br s, 1H), 1.35 (s, 12H). **^{13}C NMR** ($CDCl_3$, 100 MHz) δ (ppm) 146.3, 145.1, 135.0, 126.3, 126.2, 125.7, 121.7, 83.8, 72.7, 24.8. **FT-IR ν (cm^{-1})** 3374, 2973, 2932, 2175, 1612, 1515, 1465, 1398, 1357, 1320, 1271, 1214, 1163, 1143, 1104, 1087, 1035, 1020, 962, 949, 857, 826, 777, 753, 712, 675, 658. **Accurate Mass (EI)** $C_{17}H_{24}BO_3S$ Theoretical: 315.1335. Found: 315.1383. Spectral Accuracy: 94% **Note**: The boron-bearing carbon atom is not apparent in the ^{13}C spectrum due to the broadening of the signal from boron coupling.[47]

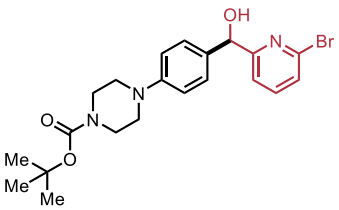

(4-[4-(6-bromopyridin-2-yl-1-hydroxymethyl)phenyl]-1,1-dimethylethyl ester) (2.24) was prepared according to the general procedure. The product was purified by column chromatography with 1.5% to 10% acetone in PhMe to afford **2.24** as an amorphous off-white solid (27.9 mg, 21% yield).**^{1}H NMR** ($CDCl_3$, 400 MHz) δ (ppm) 7.48 (d, J = 7.7 Hz, 1H), 7.40-7.35 (m, 1H), 7.27 (d, J = 8.6 Hz, 2H), 7.14 (d, J = 7.7 Hz, 1H), 6.91 (d, J = 7.7 Hz, 1H), 5.69 (d, J = 2.6 Hz, 1H), 4.32 (d, J = 3.4 Hz, 1H), 3.58 (t, J = 4.4 Hz, 4H), 3.13 (t, J = 4.9 Hz, 4H), 1.48 (s, 9H). **^{13}C NMR** ($CDCl_3$, 100 MHz) δ (ppm) 163.4, 154.7, 150.9, 140.8, 139.1, 128.1, 126.6, 120.0, 116.6, 80.0, 74.6, 49.3, 43.5 (br), 28.4. **FT-IR ν (cm^{-1})** 3396, 2926, 2831, 2162, 1698, 1663, 1641, 1581, 1553, 1512, 1476, 1456, 1422, 1366, 1340, 1273, 1230, 1163, 1120, 1081, 1064, 1021, 986, 919, 859, 794, 759, 731, 694. **HRMS (ESI-TOF)** m/z calc'd for $C_{21}H_{26}N_3O_3NaBr$ $[M+Na]^+$ Theoretical: 470.1055. Found: 470.1047.

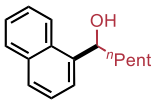

1-(naphthalen-1-yl)hexan-1-ol (2.25) was prepared according to the general procedure. The product was purified by column chromatography with 9% EtOAc in hexanes to afford **2.25** as a colourless oil (40 mg, 85% yield). **^{1}H NMR** ($CDCl_3$, 400 MHz) δ (ppm) 8.10 (d, J = 8.1 Hz, 1H), 7.87 (d, J = 7.7 Hz, 1H), 7.76 (d, J = 8.2 Hz, 1H), 7.63 (d, J = 7.0 Hz, 1H), 7.53-7.44 (m, 3H), 5.45 (dd, J = 8.1 Hz, 3.0 Hz, 1H), 1.99-1.83 (m, 3H), 1.59-1.48 (m, 1H), 1.47-1.39 (m, 1H), 1.35-1.28 (m, 4H), 0.88 (t, J = 6.8 Hz, 3H). **^{13}C NMR** ($CDCl_3$, 100 MHz) δ (ppm) 140.7, 133.9, 130.5, 128.9, 127.9, 125.9, 125.5, 125.4, 123.2, 122.8, 71.4, 38.4, 31.8, 25.9, 22.7, 14.1. Characterization of **2.25** matched a previously reported spectrum.[48]

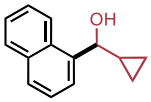

Cyclopropyl(naphthalen-1-yl)methanol (2.26) was prepared according to the general procedure. The product was purified by column chromatography with 10% to 20% EtOAc in hexanes to afford **2.26** as a colorless oil (30 mg, 50% yield). **^{1}H NMR** ($CDCl_3$, 400 MHz) δ (ppm) 8.27 (d, J = 8.2 Hz, 1H), 7.89-7.87 (m, 1H), 7.82 (d, J = 8.2 Hz, 1H), 7.70 (d, J = 7.0 Hz, 1H), 7.56-7.47 (m, 3H), 4.88 (d, J = 7.8 Hz, 1H), 1.61-1.52 (m, 1H), 0.75-0.68 (m, 1H), 0.61-0.49 (m, 2H), 0.43-0.37 (m, 1H). **^{13}C NMR** ($CDCl_3$, 100 MHz) δ (ppm) 138.9, 133.9, 131.1, 128.8, 128.2, 126.0, 125.6, 125.4, 124.0, 123.9, 75.1, 17.7, 3.99, 2.84. Characterization of **2.26** matched a previously reported spectrum.[49]

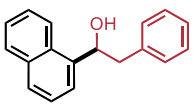

1-(α-naphthyl)-2-phenylethanol (2.27) was prepared according to the general procedure. Title compound was sensitive to acid, so the silica was neutralized with NEt_3 and dried. Compound was dry-loaded with celite. The product was purified by column chromatography with 0% to 15% EtOAc in hexanes to afford **2.27** as a white solid (41.3 mg, 55% yield). **^{1}H NMR** ($CDCl_3$, 400 MHz) δ (ppm) 8.18 (d, J = 6.7 Hz, 1H), 7.91 (d, J = 6.5 Hz, 1H), 7.81 (d, J = 6.8 Hz, 1H), 7.69 (d, J = 5.1 Hz, 1H), 7.59-7.46 (m, 3H), 7.39-7.25 (m, 5H), 5.70 (d, J = 5.9 Hz, 1H), 3.31 (d, J = 12.9 Hz, 1H), 3.08 (t, J = 10.6 Hz, 1H), 1.90 (br s, 1H). **^{13}C NMR** ($CDCl_3$, 100 MHz) δ (ppm) 139.4, 138.5, 133.8, 130.2, 129.5, 129.0, 128.6, 128.1, 126.7, 126.1, 125.5, 125.4, 123.0, 122.9, 72.1, 45.1. Characterization of **2.27** matched a previously reported spectrum.[50]

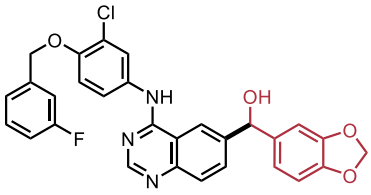

N-[3-Chloro-4-(3-fluorobenzyloxy)phenyl]-6-[Hydroxy(1,3-Benzodioxol-5-yl)methyl]quinazolin-4-amine (2.28) was prepared according to the general procedure. The product was purified by column chromatography with 0.5% to 2.5% of MeOH in 0.5% trimethylamine and DCM to afford a brown solid (containing amine impurities). Compound was further purified with a second column of 50% EtOAc in Hexanes to 100% EtOAc to afford **2.28** as a white solid (60.2 mg, 37% yield). **^{1}H NMR** ($(CD_3)_2SO$, 400 MHz) δ (ppm) 9.85 (s, 1H), 8.60 (d, J = 1.1 Hz, 1H), 8.54 (s, 1H), 8.02 (d, J = 2.6 Hz, 1H), 7.78-7.74 (m, 2H), 7.69 (d, J = 8.6 Hz, 1H), 7.47(td, J = 8.0 Hz, 6.0 Hz, 1H), 7.35-7.30 (m, 2H), 7.27 (d, J = 9.0 Hz, 1H), 7.21-7.15 (m, 1H), 7.00 (d, J = 1.6 Hz, 1H), 6.92 (dd, J = 8.1 Hz, 1.6 Hz, 1H), 6.84 (d, J = 8.0 Hz, 1H), 6.14 (d, J = 3.6 Hz, 1H), 5.96 (dd, J = 5.9 Hz, 0.9 Hz, 2H), 5.81 (J = 3.6 Hz, 1H), 5.26 (s, 2H). **^{13}C NMR** ($(CD_3)_2SO$, 100 MHz) δ (ppm) 162.2 (d, J = 243.6 Hz), 157.6, 154.1, 149.2, 148.8, 147.2, 146.1, 144.0, 139.7 (d, J = 7.4 Hz), 139.4, 133.2, 131.5, 130.5 (d, J = 8.2 Hz), 127.6, 124.2, 123.3 (d, J = 2.7 Hz), 122.4, 121.0, 119.6, 119.2, 114.7 (d, J = 20.9 Hz), 114.6, 114.2, 114.0 (d, J = 21.9 Hz), 107.9, 106.8, 100.8, 74.1, 69.4 (d, J = 1.6 Hz). **^{19}F NMR** ($(CD_3)_2SO$, 325 MHz) δ (ppm) -113.06. **FT-IR ν (cm^{-1})** 3318, 3061, 2886, 2692, 1603, 1571, 1536, 1497, 1424, 1391, 1364, 1331, 1309, 1282, 1252, 1234, 1215, 1145, 1092, 1057, 1040, 1003, 954, 947, 889, 861, 844, 818, 779, 749, 708, 686. **Melting point** 191 °C **HRMS (ESI-TOF)** m/z calc'd for $C_{29}H_{22}N_3O_4ClF$ $[M+H]^+$ Theoretical: 530.1283 Found: 530.1270.

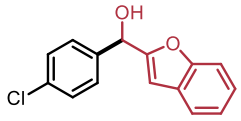

α-(4-Chlorophenyl)-2-benzofuranmethanol (2.29) was prepared according to the general procedure. The product was purified by column chromatography with 9% ether in PhMe to afford **2.29** as a yellow oil (66.0 mg, 85% yield). **^{1}H NMR** ($CDCl_3$, 400 MHz) δ (ppm) 7.51-7.49 (m, 1H), 7.43-7.39 (m, 3H), 7.36-7.33 (m, 2H), 7.28-7.18 (m, 2H), 6.50 (s, 1H), 5.90 (s, 1H), 2.63 (br s, 1H). **^{13}C NMR** ($CDCl_3$, 100 MHz) δ (ppm) 158.0, 155.1, 138.7, 128.8, 128.2, 127.9, 124.6, 122.9 121.3, 111.4, 104.2, 69.9. Characterization of **2.29** matched a previously reported spectrum.[51]

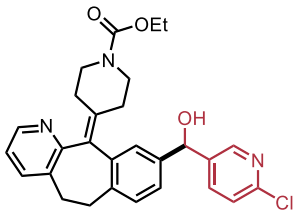

1-(11-(1-(Ethoxycarbonyl)piperidin-4-ylidene)-6,11-dihydro-5H-benzo[5,6]cyclohepta[1,2-b]pyridin-8-yl)(6-Chloro-3-pyridinyl)methanol (2.30) was prepared according to the general procedure. The product was purified by column chromatography with 1% to 40% acetone in DCM to afford **2.30** as a yellow solid (96.5 mg, 66% yield). **^{1}H NMR** ($CDCl_3$, 400 MHz) δ (ppm) 8.32 (d, J = 2.2 Hz, 1H), 8.23 (d, J = 4.1 Hz, 1H), 7.62 (dt, J = 8.2 Hz, 2.5 Hz, 1H), 7.40 (d, J = 7.5 Hz, 1H), 7.21 (d, J = 8.2 Hz, 1H), 7.09 (br s, 1H), 7.06 (br s, 2H), 7.02 (dd, J = 7.6 Hz, 4.9 Hz, 1H), 5.72 (s, 1H), 4.42 (br s, 1H), 4.07 (q, J = 7.1 Hz, 2H), 3.82-3.66 (m, 2H), 3.39-3.25 (m, 2H), 3.13-3.04 (m, 2H), 2.81-2.70 (m, 2H), 2.45-2.37 (m, 1H), 2.32-2.18 (m, 3H), 1.20 (t, J = 7.1 Hz, 3H). **^{13}C NMR** ($CDCl_3$, 100 MHz) (ppm) Rotamers δ 157.3, 155.4, 150.1, 147.9, 146.3, 141.1, 138.7, 138.6, 137.9, 137.4, 137.1, 137.0, 134.5, 133.7, 129.64, 129.60, 128.9, 128.5, 128.3, 128.2, 128.1, 127.3, 127.2, 125.3, 125.2, 124.1, 123.9, 122.2, 72.8, 61.3, 58.0, 44.7, 44.6, 35.3, 31.8, 31.4, 30.6, 30.4, 29.2, 27.5, 14.6. **FT-IR ν (cm^{-1})** 3363, 2970, 2921, 2860, 1676, 1585, 1566, 1437, 1376, 1325, 1277, 1225, 1171, 1100, 1063, 1022, 996, 975, 900, 815, 783, 766, 731. **Melting point** 105 °C. **HRMS (ESI-TOF**) m/z calc'd for $C_{28}H_{29}N_3O_3Cl$ $[M+H]^+$ Theoretical: 490.1897. Found: 490.1905. **Note:** Loratidine analogues are known to be conformationally flexible which complicate the spectral analysis.[52]

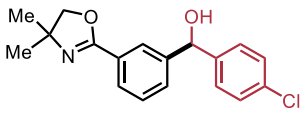

α-(4-Chlorophenyl)-3-(4,5-dihydro-4,4-dimethyl-2-oxazolyl)benzene methanol (2.31) was prepared according to the general procedure and was run on a 0.27 mmol scale rather than the standard 0.3 mmol scale. The product was purified by column chromatography with 10% to 50% EtOAc in hexanes to afford

2.31 as a light yellow oily semi-solid (57.0 mg, 68% yield). **^{1}H NMR** ($CDCl_3$, 400 MHz) δ (ppm) 8.10-8.07 (m, 1H), 7.77 (dt, *J* = 7.6 Hz, 1.3Hz, 1H), 7.41-7.38 (m, 1H), 7.34-7.29 (m, 2H), 7.27-7.24 (m, 2H), 5.80 (s, 1H), 4.37 (br s, 1H), 4.07 (s, 6H), 1.30 (s, 9H). **^{13}C NMR** ($CDCl_3$, 100 MHz) δ (ppm) 162.5, 144.4, 142.6, 133.2, 129.6, 128.65, 128.64, 128.1, 128.0, 127.6, 126.6, 79.3, 74.9, 67.5, 28.3. **FT-IR ν (cm^{-1})** 3192, 3067, 2960, 2865, 2160, 1918, 1735, 1639, 1577, 1482, 1446, 1404, 1357, 1309, 1249, 1172, 1161, 1087, 1048, 1014, 969, 934, 915, 844, 815, 789, 734, 721, 705. **Accurate Mass (EI)** $C_{18}H_{18}ClNO_2$ Theoretical: 315.1021. Found: 315.1023. Spectral Accuracy: 97.5%.

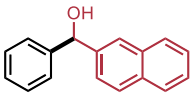

(2-Naphthyl)(phenyl)methanol (2.34) was prepared according to the general procedure with the exception of using 1-PhEtOH-d_1 as the reducing agent. The product was purified by column chromatography with 5% to 15% Et_2O in hexanes to afford **2.34** as a white opaque oil that slowly solidified (57.9 mg, 82% yield).**^{1}H NMR** ($CDCl_3$, 400 MHz) δ (ppm) 7.91 (s, 1H), 7.88-7.80 (m, 3H), 7.54 -7.47 (m, 2H), 7.46-7.42 (m, 3H), 7.39-7.34 (m, 2H), 7.33-7.28 (m, 1H), 6.00 (s, 1H), 2.43 (br s, 1H). **^{13}C NMR** ($CDCl_3$, 100 MHz) δ (ppm) 143.8, 141.2, 133.4, 133.0, 128.7, 128.4, 128.2, 127.79, 127.78, 126.8, 126.3, 126.1, 125.2, 124.9, 76.5. Characterization of **2.34** matched a previously reported spectrum.[53]

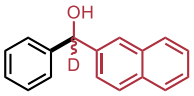

(2-Naphthyl)(phenyl)methan-α-ol-d_1 (2.34-d_1) was prepared according to the general procedure from iodobenzene and 2-naphthaldehyde-formyl-d_1 (prepared with 97% deuterium incorporation). The product was purified by column chromatography with 5% to 15% Et_2O in hexanes to afford **2.34-d_1** as a white opaque oil that slowly solidified (46.1 mg, 65% yield).**^{1}H NMR** ($CDCl_3$, 400 MHz) δ (ppm) 7.92-7.90 (m, 1H), 7.88-7.80 (m, 3H), 7.54 -7.42 (m, 5H), 7.39-7.34 (m, 2H), 7.33-7.28 (m, 1H), 6.01 (s, 0.06H, residual protium signal), 2.41 (br s, 1H). **^{13}C NMR** ($CDCl_3$, 100 MHz) δ (ppm) 143.5, 141.0, 133.2, 132.8, 128.5, 128.3, 128.0, 127.6, 126.6, 126.1, 125.9, 125.0, 124.7, 76.3 (residual peak for protium-

bound carbon), 75.9 (t, J = 22.0 Hz). Characterization of **2.34-d_1** matched a previously reported spectrum.[54]

2.7.4 Procedure for stoichiometric oxidative addition study

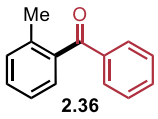

2.36

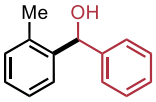

2.37

(2-Methylphenyl)(phenyl)methanone (2.36) and **(2-Methylphenyl)(phenyl)methanol (2.37)**. Inside the glovebox, to a dry 8 mL screw-capped reaction vial equipped with a magnetic stir bar, [(TMEDA)Ni(*o*-tolyl)Cl] (1 equiv, 0.1 mmol, 30.1 mg) and ($P^{Cy}N^{ArCF3}$)$_2$ (2 equiv, 0.2 mmol, 120.5 mg) were added and dissolved in toluene (0.5 mL). Benzaldehyde (1 equiv, 0.1 mmol, 10.6 mg) was then added. 1-phenylethanol was added at this point (1.5 equiv, 0.15 mmol, 18.3 mg) for the second experiment only. The vial was capped, removed from the glove box, and placed in a stirring (350 rpm) mineral oil bath pre-heated to 75 °C. After stirring for 16 hours, the reaction vial was removed from the oil bath and cooled down to room temperature. Internal standard was added (1 mL of 0.05 M solution of 1,3,5-trimethoxybenzene in PhMe). A saturated solution of aqueous ammonium chloride was added followed by EtOAc. A small extraction was performed to remove the organic phase using EtOAc as the organic solvent. The sample was filtered through a long plug of silica with ethyl acetate. Solvent was removed *in vacuo* and $CDCl_3$ was added to enable quantification of **2.36** and **2.37** by crude ^{1}H NMR.

2.7.5 Procedure for synthesis of (4-methylphenyl)(1-naphthyl)methanone (2.42)

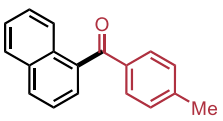

(4-Methylphenyl)(1-naphthyl)methanone (2.42) was prepared with a modified procedure. Inside the glovebox, to a dry 8 mL screw-capped reaction vial equipped with a magnetic stir bar, Ni(cod)$_2$ (0.1 equiv, 0.03 mmol, 8.3 mg) and

$P^{Cy}{}_2N^{ArCF3}{}_2$ (0.12 equiv, 0.036 mmol, 21.7 mg) were added followed by toluene (1.5 mL). 2,2,6,6-tetramethylpiperidine (2 equiv, 0.6 mmol, 85 mg), 1-iodonaphthalene (1 equiv, 0.3 mmol, 76.2 mg) and *p*-tolualdehyde (1 equiv, 0.3 mmol, 36.0 mg) were added to the stirring solution. The vial was capped, removed from the glove box, and placed in a stirring (350 rpm) mineral oil bath pre-heated to 75 °C. After stirring for 16 hours, the reaction vial was removed from the oil bath and cooled down to room temperature. The reaction mixture was diluted with DCM, solvent was removed *in vacuo*, and the crude product was purified by column chromatography with 9% EtOAc in hexanes to afford **2.42** as a white solid (63.7 mg, 86% yield). **^{1}H NMR** ($CDCl_3$, 400 MHz) δ (ppm) 8.11-8.07 (m, 1H), 8.01 (d, *J* = 8.1 Hz, 1H), 7.95-7.92 (m, 1H), 7.80 (d, *J* = 8.2 Hz, 2H), 7.59 (dd, *J* = 7.0 Hz, 1.3Hz, 1H), 7.57-7.48 (m, 3H), 7.27 (d, *J* = 8.0 Hz, 2H), 2.44 (s, 3H). **^{13}C NMR** ($CDCl_3$, 100 MHz) δ (ppm) 197.1, 144.1, 136.7, 135.6, 133.6, 130.8, 130.5, 129.1, 128.3, 127.2, 127.0, 126.3, 125.6, 124.3, 21.6. Characterization of **2.42** matched previously reported spectra.[55]

2.8 References

[1] (a) Grignard, V. C. Sur quelques nouvelles vombinaisons organométalliques du magnésium et leur application à des synthèses d'alcools et d'hydrocarbures. *C. r. hebd. séances Acad. sci*. **1900**, *130*, 1322−1324 (b) Seyferth, D. The Grignard Reagents. *Organometallics* **2009**, *28*, 1598-1605. (c) Krasovskiy, A. and Knochel, P. A LiCl-mediated Br/Mg exchange reaction for the preparation of functionalized aryl- and heteroarylmagnesium compounds from organic bromides. *Angew. Chem. Int. Ed.* **2004**, *43*, 3333-3336. (d) Pedersen, M. J.; Skovby, T.; Mealy, M. J.; Dam-Johansen, K.; Kiil, S. Redesign of a Grignard-based active pharmaceutical ingredient (API) batch synthesis to a flow process for the preparation of Melitracen HCl. *Org. Process Res. Dev.* **2018**, *22*, 228-235.

[2] (a) Reformatsky, S. Neue Synthese zweiatomiger einbasischer säuren aus den ketonen. *Ber. Dtsch. Chem. Ges*. **1887**, *20*, 1210-1211. (b) Barbier, P. Synthèse du diéthylhepténol. *C. r. hebd. séances Acad. sci*. **1899**, *128*, 110-111. (c) Blomberg, C. and Hartog, F.G. The Barbier reaction – A one-step alternative for syntheses via organomagnesium compounds. *Synthesis*, **1977**, *1*, 18-30. (d) Rathke, M. W. The Reformatsky reaction. *Org. Reactions* **2011**, 423−460.

[3] (a) Okude, Y.; Hirano, S.; Hiyama, T.; Nozaki, H. Grignard-type carbonyl addition of allyl halides by means of chromous salt. A chemospecific synthesis of homoallyl alcohols. *J. Am. Chem. Soc.* **1977**, *99*, 3179-3181. (b) Takai, K.; Kimura, K.; Kuroda, T.; Hiyama, T.; Nozaki, H. Selective Grignard-type carbonyl addition of alkenyl halides mediated by chromium(II) chloride *Tetrahedron Lett.* **1983**, *24*, 5281-5284. (c) Jin, H.; Uenishi, J.; Christ, W. J.; Kishi, Y. Catalytic effect of nickel(II) chloride and palladium(II) acetate on chromium(II)-mediated coupling reaction of iodo olefins with aldehydes. *J. Am. Chem. Soc.* **1986**, *108*, 5644-5646.

[4] (a) Takai, T.; Tagashira, M.; Kuroda, T.; Oshima, K.; Utimoto, K.; Nozaki, H. Reactions of alkenylchromium reagents prepared from alkenyl trifluoromethanesulfonates (triflates) with chromium(II) chloride under nickel catalysis. *J. Am. Chem. Soc*. **1986**, *108*, 6048–6050. (b) Namba, K. and Kishi, Y. New catalytic cycle for couplings of aldehydes with organochromium reagents. Org. *Lett.* **2004**, *6*, 5031-5033. (c) Fürstner, A. Carbon−carbon bond formations involving organochromium(III) reagents. *Chem. Rev.* **1999**, *99*, 991-1046.

[5] (a) Fürstner, A. and Shi, N. Nozaki−Hiyama−Kishi reactions catalytic in chromium. *J. Am. Chem. Soc.* **1996**, *118*, 12349-12357. (b) Durandetti, M.; Périchon, J.; Nédélec, J.-Y. Nickel- and chromium-Catalysed electrochemical coupling of aryl halides with arenecarboxaldehydes. *Tetrahedron Lett.* **1999**, *40*, 9009-9013. (c)Harnying, W.; Kaiser, A.; Klein, A.; Berkessel, A. Cr/Ni-catalyzed vinylation of aldehydes: A mechanistic study on the catalytic roles of nickel and chromium. *Chem. Eur. J.* **2011**, *17*, 4765-4773. (e) Gao, Y.; Hill, D.; Hao, W.; McNicholas, B., Vantourout, J.; Hadt, R.; Reisman, S.; Blackmond, D.; Baran, P. Electrochemical Nozaki–Hiyama–Kishi coupling: Scope, applications, and mechanism. *J. Am. Chem. Soc.* **2021**, *143*, 9478-9488.

[6] Gil, A.; Albericio, F.; Álvarez, M. Role of the Nozaki–Hiyama–Takai–Kishi reaction in the synthesis of natural products. *Chem. Rev.* **2017**, *117*, 8420-8446.

[7] For examples of catalytic reactions of aldehydes with mild organometallic nucleophiles: (a) Yamamoto, Y.; Kurihara, K.; Miyaura, N. Me-bipam for enantioselective ruthenium(II)-catalyzed arylation of aldehydes with arylboronic acids. *Angew. Chem. Int. Ed.* **2009,** *48*, 4414-4416. (b) Yamamoto, T.; Iizuki, M.; Takenaka, H.; Ohta, T.; Ito, Y. Addition reaction of arylboronic acids to aldehydes and α,β-unsaturated carbonyl compounds catalyzed by conventional palladium complexes in the presence of chloroform. *J. Organomet. Chem.* **2009**, *694*, 1325-1332. (c) He, P.; Lu, Y.; Hu, Q.-S. Phosphinite- and phosphite-based type I palladacycles as highly active catalysts for addition reactions of arylboronic acids with aldehydes, α,β-unsaturated ketones, α-ketoesters, and aldimines. *Tetrahedron Lett.* **2007**, *48*, 5283-5288. (d) Suzuki, K.; Arao, T.; Ishii, S.; Maeda, Y.; Kondo, K.; Aoyama, T. Use of cheaper metal than Rh, $CHCl_3$-free Pd catalyst, in 1,2-addition of aromatic aldehydes with arylboronic acids. *Tetrahedron Lett.* **2006**, *47*, 5789-5792. (e) Karthikeyan, J.; Jeganmohan, M.; Cheng, C.-H. Cobalt-catalyzed addition reaction of organoboronic acids with aldehydes: Highly enantioselective synthesis of diarylmethanols. *Chem. Eur. J.* **2010***, 16*, 8989-8992. (f) Yu, A.; Cheng, B.; Wu, Y.; Li, J.; Wei, K. Cyclopalladated complexes catalyzed addition of arylboronic acids to aldehydes in neat water. *Tetrahedron Lett.* **2008**, *49*, 5405-5407. (g) Zou, T.; Pi, S.-S.; Li, J.-H.; $FeCl_3$-catalyzed 1,2-addition reactions of aryl aldehydes with arylboronic acids. *Org. Lett.* **2009**, *11*, 453-456. (h) Kuriyama, M.; Shimazawa, R.; Shirai, R. Efficient 1,2-addition of aryl- and alkenylboronic acids to aldehydes catalyzed by the palladium/thioether−imidazolinium chloride system. *J. Org. Chem.* **2008**, *73*, 1597-1600. (i) Trindade, A.F.; Gois, P. M. P.; Veiros, L.F.; André, V.; Duarte, M. T.; Afonso, C. A. M.; Caddick, S.; Cloke, F. G. N. Axial coordination of NHC ligands on dirhodium(II) complexes: Generation of a new family of catalysts. *J. Org. Chem.* **2008**, *73*, 4076-4086. (j) Cleghorn, L. A. T.; Grigg, R.; Savic, V.; Simic, M. Reactive organoallyl species generated from aryl halides and allene:

allylation of α,β-unsaturated aldehydes and cyclic ketones employing Pd/In transmetallation processes. *Tetrahedron,* **2008**, *64*, 8731-8737. (k) Zheng, B. and Srebnik, M. 1,2-Addition of alkyl- and alkenylzirconocene chlorides to aldehydes accelerated by catalytic amounts of $ZnBr_2$ as a method of synthesizing secondary slcohols, secondary allylic alcohols, and in-Situ Oppenauer-type oxidation of the alcohols to ketones. *J. Org. Chem.* **1995**, *60*, 3278-3279. (l) Bouffard, J. and Itami, K. A nickel catalyst for the addition of organoboronate esters to ketones and aldehydes. *Org. Lett.* **2009**, *11*, 4410-4413. (n) Oi, S.; Moro, M.; Inoue, Y. Rhodium-catalysed arylation of aldehydes with arylstannanes. *Chem. Commun.* **1997**, 1621-1622 (o) Sakai, M.; Ueda, M.; Miyaura, N. Rhodium-catalyzed addition of organoboronic acids to aldehydes. *Angew. Chem. Int. Ed.* **1998**, *37*, 3279-3281. (p) Chen, W.; Baghbanzadeh, M.; Kappe, C. O. Microwave-assisted nickel(II) acetylacetonate-catalyzed arylation of aldehydes with arylboronic acids. *Tetrahedron Lett.* **2011**, *52*, 1677-1679. (q) Zhou, L.; Du, X.; He, R.; Ci, Z.; Bao, M. Nickel salt-catalyzed addition reaction of arylboronic acids to aromatic aldehydes. *Tetrahedron Lett.* **2009**, *50*, 406-408. (r) Yang, Y.-X.; Liu, Y.; Zhang, L.; Jia, Y.-E.; Wang, P.; Zhuo, F.-F.; An, X.-T.; Da, C.-S. Aryl bromides as inexpensive starting materials in the catalytic enantioselective arylation of aryl aldehydes: The additive TMEDA enhances the enantioselectivity *J. Org. Chem.* **2014**, *79*, 10696-10702.

[8] For progress in reductive coupling of aldehydes with organohalides, see: (a) Majumdar, K. K. and Cheng, C.-H. Ni(II)/Zn-mediated chemoselective arylation of aromatic aldehydes: Facile synthesis of diaryl carbinols. *Org. Lett.* **2000**, *2*, 2295-2298. (b) Panhani, F.; Bahmani, M.; Iranpoor, N. Nickel-catalyzed reductive benzylation of aldehydes with benzyl halides and pseudohalides. *Adv. Syn. Catal.* **2015**, *357*, 1211-1220. (c) Asachenko, A. F.; Valaeva, V. N.; Kudakina, V. A.; Uborsky, D. V.; Izmer, V. V.; Kononovich, D. S., Vosokoboynikov, A. Z. Coupling of aromatic aldehydes with aryl halides in the presence of nickel catalysts with diazabutadiene ligands. *Russ. Chem. Bull*. **2016**, *65*, 456-463. (d) Yurino, T.; Ueda, Y.; Shimizu, Y.; Tanaka, S.; Nishiyama, H.; Tsurugi, H.; Sato, K.; Mashima, K. Salt-free reduction of nonprecious transition-metal compounds: Generation of amorphous Ni nanoparticles for catalytic C–C bond formation. *Angew. Chem. Int. Ed.* **2015**, *54*, 14437-14441. (e) Viana, H.; Marques, C. S.; Correira, C. A.; Gilmore, K.; Galvão, L.; Viera, L.; Seeberger, P. H.; Burke, A. J. Novel palladium-catalyzed intramolecular addition of aryl bromides to aldehydes as key to the synthesis of 3,3-dimethylchroman-4-ones and 3,3-dimethylchroman-4-ols. *ChemistrySelect*, **2018**, *3*, 11333-11338. (f) Tang, J.; Lv, L.; Dai, X.-J.; Li, C.-C.; Li, L. Li, C.-J. Nickel-catalyzed cross-coupling of aldehydes with aryl halides via hydrazone intermediates. *Chem. Commun.* **2018**, *54*, 1750-1753. (g) Zhou, F. and Li, C.-J. The Barbier–Grignard-type arylation of aldehydes using unactivated aryl iodides in water *Nat. Commun.* **2014**, *5*, 4254. (h) Presset, M.; Paul, J.; Cherif, G. N. Ratnam, N.; Laloi, N.; Léonel, E.; Gosmini, C.; Le Gall, E. Co^{I}-catalyzed Barbier reactions of aromatic halides with aromatic aldehydes and imines. *Chem. Eur. J.* **2019**, *25*, 4491-4495. (i) Ishida, S.; Suzuki, H.; Uechida, S.; Yamaguchi, E.; Itoh, A. Nickel-catalyzed intermolecular carbonyl addition of aryl halide. *Eur. J. Org. Chem.* **2019**, 7483-7487. (j) Cruz, C.L. and Montgomery, J. Nickel-catalyzed reductive coupling of unactivated alkyl bromides and aliphatic aldehydes. *Chem. Sci.* **2021**, *12*, 11995-12000.

[9] (a) Bower, J.F.; Kim, I. S.; Patman, R. L.; Krische, M. J. Catalytic carbonyl addition through transfer hydrogenation: A departure from preformed organometallic reagents. *Angew. Chem. Int. Ed.* **2008**, *48*, 34-46. (b) Santana, C. G. and Krische, M. J. From hydrogenation to transfer hydrogenation to hydrogen auto-transfer in enantioselective metal-catalyzed carbonyl reductive coupling: Past, present, and future. *ACS Catal*. **2021**, *11*, 5572-5585.

[10] (a) Garcia, K. J.; Gilbert, M. M.; Weix, D. J. Nickel-catalyzed addition of aryl bromides to aldehydes to form hindered secondary alcohols. *J. Am. Chem. Soc.* **2019**, *141,* 1823-1827. (b) Swyka, R. A.; Zhang, W.; Richardson, J.; Ruble, J. C.; Krische, M. J. Rhodium-catalyzed aldehyde arylation via formate-mediated transfer hydrogenation: Beyond metallic reductants in Grignard/Nozaki–Hiyami–Kishi-type addition. *J. Am. Chem. Soc.* **2019**, *141*, 1828-1832.

[11] Verheyen, T.; van Turnhout, L.; Vandavasi, J.K.; Isbrandt, E. S.; De Borggraeve, W. M.; Newman, S. G. Ketone synthesis by a Nickel-catalyzed dehydrogenative cross-coupling of primary alcohols. *J. Am. Chem. Soc.* **2019**, *141*, 6869-6874.

[12] Vandavasi, J.K.; Hua, X.Y.; Ben Halima, H.; Newman, S. G. A Nickel-catalyzed carbonyl-Heck reaction. *Angew. Chem. Int. Ed.* **2017**, *56*, 15441-15445.

[13] Zembayashi, M.; Tamao, K.; Yoshida, J.; Kumada, M. Nickel-phosphine complex-catalyzed homo coupling of aryl halides in the presence of zinc powder. *Tetrahedron Lett.* **1977**, *18*, 4089-4091.

[14] Mutsuji, S.; Ming-San, L.; Koji, Y.; Yasuyuki, K.; Ken, S.; Yasumasa, S. Metallic nickel-catalyzed reduction of aryl halides with zinc powder and ethanol *Bull. Chem. Soc. Jpn.* **1992,** *65*, 1739-1740. (b) Desmarets, C.; Kuhl, S.; Schneider, R.; Fort, Y. Nickel(0)/imidazolium chloride catalyzed reduction of aryl halides. *Organometallics* **2002**, *21*, 1554-1559.

[15] (a) Seu, C. S.; Ung, D.; Doud, M. D.; Moore, C. E.; Rheingold, A. L.; Kubiak, C. P. Synthesis, structural, and electrocatalytic reduction studies of $[Pd(P_2N_2)_2]^{2+}$ complexes. *Organometallics*, **2013**, *32*, 4556-4563. (b) Strelnik, I.; Dayanova, I.; Musina, E.; Karasik, A.; Sinyashin, O. Novel functionalized 1,5-diaza-3,7-diphosphacyclooctanes. *Phosphorus Sulfur Silicon Relat. Elem.* **2016**, *191*, 1515-1517. (c) Spiridonova, Y. S.; Strelnik, I. D.; Musina, E. I.; Hey-Hawkins, E.; Litvinov, I. A.; Karasik, A. A. New gold(I) complexes with 1,5-diaza-3,7-diphosphacyclooctanes: Synthesis and structures. *Russ. J. Coord. Chem.* **2020**, *46*, 477-484. (d) Spiridonova, Y. S.; Nikolaeva, Y. A.; Balueva, A. S.; Musina, E. I.; Litvinov, I. A.; Strelnik, I. D.; Khrizanforova, V. V.; Budnikova, Y. G.; Karasik, A. A. Synthesis and structure of iron (II) complexes of functionalized 1,5-diaza-3,7-diphosphacyclooctanes. *Molecules* **2020**, *25*, 3775. (e) Karasik, A. A. Naumov, R. N.; Sinyashin, O. G.; Belov, G. P.; Novikova, H. V.; Lönnecke, P.; Hey-Hawkins, E. Novel chiral 1,5-diaza-3,7-diphosphacyclooctane ligands and their transition metal complexes. *Dalton Trans.* **2003**, 2209-2214.

[16] (a) Yang, J. Y.; Chen, S.; Dougherty, W. G.; Kassel, W. S.; Bullock, R. M.; DuBois, D. L.; Raugei, S.; Rousseau, R.; Dupuis, M.; DuBois, M. R. Hydrogenoxidation catalysis by a nickel diphosphine complex with pendant *tert*-butyl amines. *Chem. Commun.* **2010**, *46*, 8618-8620. (b) DuBois, D. L. and Bullock, R. M. Molecular electrocatalysts for the oxidation of hydrogen and the production of hydrogen – The role of pendant amines as proton relays. *Eur. J. Inorg. Chem.* **2011**, 1017-1027. (c) Kilgore U. J.; Stewart, M. P.; Helm, M. L.; Dougherty, W. G.; Kassel, W. S.; DuBois, M.R.; DuBois, D. L.; Bullock, R. M. Studies of a series of $[Ni(P^R_2N^{Ph}_2)_2(CH_3CN)]^{2+}$ complexes as electrocatalysts for H_2 production: Substituent variation at the phosphorus atom of the P_2N_2 ligand. *Inorg. Chem.* **2011**, *50*, 10908-10918. (d) Liu, T.; DuBois, D. L.; Bullock, M. R. An iron complex with pendent amines as a molecular electrocatalyst for oxidation of hydrogen. *Nat. Chem.* **2013**, *5*, 228-233. (e) Das, A. K.; Engelhard, M. H.; Bullock, M. R.; Roberts, J. A. S. A Hydrogen-evolving $Ni(P_2N_2)_2$ electrocatalyst covalently attached to a glassy carbon electrode: Preparation, characterization, and catalysis. Comparisons with the homogeneous analogue. *Inorg. Chem.* **2014**, *53*, 6875-6885. (f) Bullock, R. M. and Helm, M. L. Molecular electrocatalysts for oxidation of hydrogen using earth-abundant metals: Shoving protons around with proton relays. *Acc. Chem. Res.* **2015**, *48*, 2017-2026. (g) Galan, B.R.; Schöffel, J.; Linehan, J. C.; Seu, C.; Appel, A. M.; Roberts, J. A. S.; Helm, M. L.; Kilgore, U. J.; Yang, J. Y.; DuBois, D. L.; Kubiak, C. P. Electrocatalytic oxidation of formate by $[Ni(P^R_2N^{R'}_2)_2(CH_3CN)]^{2+}$ complexes. *J. Am. Chem. Soc.* **2011**, *133*, 12767-127779. (h) Kilgore, U. H.; Roberts, J. A. S.; Pool, D. H.; Appel, A. M.; Stewart, M. P.; DuBois, M. R.; Dougherty, W. M.; Kassel, W. S.; Bullock, R. M.; DuBois, D. L. $[Ni(P^{Ph}_2N^{C6H4X}_2)_2]^{2+}$ complexes as electrocatalysts for H_2 production: Effect of substituents, acids, and water on catalytic rates. *J. Am. Chem. Soc.* **2011**, *133*, 5861-5872. (i) Appel, A. M.; Pool, D. H.; O'Hagan, M.; Shaw, W. J.; Yang, J. Y.; DuBois, M. R.; DuBois, D. L.; Bullock, M. R. $[Ni(P^{Ph}_2N^{Bn}_2)_2(CH_3CN)]^{2+}$ as an electrocatalyst for H_2 production: Dependence on acid strength and isomer distribution. *ACS Catal.* **2011,** *1*, 777-785. (j) Seu, C. S.; Appel, A. M.; Doud, M. D.; DuBois, D. L.; Kubiak, C. P. Formate oxidation via β-deprotonation in $[Ni(P^R_2N^{R'}_2)_2(CH_3CN)]^{2+}$ complexes. *Energy Environ. Sci.* **2012**, *5*, 6480-6490. (k) Yang, J. Y.; Chen, S.; Dougherty, W. G.; Kassel, W. S.; Bullock, R.M.; DuBois, D. L.; Raugei, S.; Rousseau, R.; Dupuis, M.; DuBois, M. R. Hydrogen oxidation catalysis by a nickel diphosphine complex with pendant *tert*-butyl amines. *Chem. Commun.* **2010**, *46*, 8618-8620.

[17] (a) Bridge, B. J.; Boyle, P. D.; Blacquiere, J. M. *endo*-Selective iron catalysts for intramolecular alkyne hydrofunctionalization. *Organometallics* **2020**, *39*, 2570-2574. (b) Stubbs, J.M.; Bridge, B. J.; Blacquiere, J. M. Optimizing ligand structure For low-loading and fast catalysis for alkynyl-alcohol and -amine cyclization. *Dalton Trans.* **2019**, *48*, 7928-7937. (c) Stubbs, J. M.; Chapple, D. E.; Boyle, P. D.; Blacquiere, J. M. Catalyst pendent-base effects on cyclization of alkynyl amines. *ChemCatChem* **2018**, *10*, 4001-4009. (d) Stubbs, J. M.; Bow, J.-P. J.; Hazlehurst, R. J.; Blacquiere, J. M. Catalytic cyclization and competitive deactivation with $Ru(P^R_2N^{R'}_2)$ complexes. *Dalton Trans.* **2016**, *45*, 17100-17103. (f) Bow, J.-P. P.; Boyle, P. D.; Blacquiere, J. M. Substrate-mediated deactivation of a $Ru(P^{tBu}_2N^{Bn}_2)$ cooperative complex. *Eur. J. Inorg. Chem.* **2015**, 4162-4166.

[18] Stubbs, J. M.; Hazlehurst, R. J.; Boyle, P. D.; Blacquiere, J. M. Catalytic acceptorless dehydrogenation of amines with $Ru(P^R_2N^{R'}_2)$ and Ru(dppp) complexes. *Organometallics* **2017**, *36*, 1692-1698.

[19] Fihri, A.; Luart, D.; Len, C.; Solhy, A.; Chevrin, C.; Polshettiwar, V. Suzuki–Miyaura cross-coupling coupling reactions with low catalyst loading: a green and sustainable protocol in pure water. *Dalton Trans*. **2011**, *40*, 3116-3121.

[20] Twilton, J.; Christensen, M.; DiRocco, D. A.; Ruck, R. T.; Davies, I.W.; MacMillan, D. W. C. Selective hydrogen atom abstraction through induced bond polarization: Direct α-arylation of alcohols through photoredox, HAT, and nickel catalysis. *Angew. Chem. Int. Ed*. **2018**, *57*, 5369-5373.

[21] For a biological study involving the parent compound see: Simard, J. R.; Grütter, C.; Pawar, V.; Aust, B.; Wolf, A.; Rabiller, M.; Wulfert, S.; Robubi, A.; Klüter, S.; Ottmann, C.; Rauh, D. High-throughput screening to identify inhibitors which stabilize inactive kinase conformations in p38α. *J. Am. Chem. Soc.* **2009**, *131*, 18478-18488.

[22] For a study of **2.30** and related open chain Mazindol analogues, see: Kulkarni, S. S.; Newman, A. H.; Houlihan, W. J. Three-dimensional quantitative structure-activity relationships of Mazindol analogues at the dopamine transporter. *J. Med. Chem.* **2002**, *45*, 4119-4127.

[23] Bernini, F.; Musanti, R.; Trezzi, E.; Corsini, A.; Fumagalli, R.; Meldolesi, J.; Catapano, A. L. Experimental studies on the hypolipidemic sctivity of chloridarol. *Pharmacol. Res. Commun*. **1983**, *15*, 201-215.

[24] For some examples of proposed single-electron reductions of Ni by stoichiometric Zn or Mn see: (a) Heinz, C.; Lutz, J. P.; Simmons, E. M.; Miller, M. M.; Ewing, W. R.; Doyle, A. G. Ni-catalyzed carbon–carbon bond-forming reductive amination. *J. Am. Chem. Soc.* **2018**, *140*, 2292-2300. (b) Lyu, H.; Kevlishvili, I.; Yu, X.; Liu, P.; Dong, G. Boron insertion into alkyl ether bonds via zinc/nickel tandem catalysis. *Science* **2021**, *372*, 175-182. (c) Liao, J.; Basch, C. H.; Hoerrner, M. E. ; Talley, M. R.; Boscoe, B .P.; Tucker, J, W.; Garnsey, M. R.; Watson, M. P. Deaminative reductive cross-electrophile couplings of alkylpyridinium salts and aryl bromides *Org Lett.* **2019**, *21*, 2941-2946.

[25] (a) Cabri, W. and Candiani, I. Recent developments and new perspectives in the Heck reaction. *Acc. Chem. Res.* **1995**, *28*, 2-7. (b) Juttand, A. Mechanisms of the Mizoroki–Heck reaction. In *The Mizoroki–Heck Reaction*; Oestreich, M., Ed.; Wiley, Chichester, **2009**; 1-50.

[26] Gøgsig, T. M.; Kleimark, J.; Lill, S. O. N.; Korsager, S.; Lindhardt, A. T.; Norrby, P.-O.; Skrydstrup. Mild and efficient nickel-catalyzed Heck reactions with electron-rich olefins. *J. Am. Chem. Soc.* **2012**, *134*, 443-452.

[27] (a) Delbecq, F. and Sautet, P. η_2 versus η_1 Coordination of aldehydes and ketones in organometallic vomplexes. A semiempirical theoretical study. *J. Am. Chem. Soc.* **1992**, *114*, 2446-2455. (b) Hoshimoto, Y.; Ohashi, M.; Ogoshi, S. Catalytic Transformation of aldehydes with nickel complexes through η_2 coordination and oxidative cyclization. *Acc. Chem. Res.* **2015**, *48*, 1746-1755.

[28] Cai, Y.; Shi, S.-L. Enantioconvergent arylation of racemic secondary alcohols to chiral tertiary alcohols enabled by nickel/N-Heterocyclic carbene catalysis. *J. Am. Chem. Soc.* **2021**, *143*, 11963-11968.

[29] Bian, J.-H.; Tong, W.-Y.; Pitsch, C. E.; Wu, Y.-B.; Wang X. Mechanism of nickel-catalyzed direct carbonyl-Heck coupling reaction: The crucial role of second-sphere interactions. *Dalton Trans.* **2021**, *50*, 2654-2662.

[30] (a) Ma, S.; Wang, H.; Gao, K.; Zhao, F. Nickel complexes catalyzed Heck reaction of iodobenzene and methyl acrylate. *J. Mol. Catal. A Chem*. **2006**, *248*, 17-20. (b) Matsubara, R.; Gutierrez, A. C.; Jamison, T. F. Nickel-catalyzed Heck-type reactions of benzyl chlorides and simple olefins. *J. Am. Chem. Soc.* **2011**, *133*, 19020-19023. (b) Ehle, A. R.; Zhou, Q.; Watson, M. P. Nickel(0)-catalyzed Heck cross-coupling via activation of aryl C–OPiv bonds. *Org. Lett.* **2012**, *14*, 1202-1205.

[31] Chapple, D. E.; Boyle, P. D.; Blacquiere, J. M. Origin of stability and inhibition of cooperative alkyne hydrofunctionalization catalysts. *ChemCatChem* **2021**, *13*, 3789–3800.

[32] (a) Barder, T. E.; Biscoe, M. R.; Buchwald, S. L. Structural insights into active catalyst structures and oxidative addition to (biaryl)phosphine−palladium complexes via density functional theory and experimental studies. *Organometallics* **2007**, *26*, 2183-2192. (b) Martin, R. & Buchwald, S. L. Palladium-catalyzed Suzuki−Miyaura cross-coupling reactions employing dialkylbiaryl phosphine ligands. *Acc. Chem. Res.* **2008,** *41*, 1461-1473.

[33] For example; Sigma-Aldrich sells allyl iodide (98%) PN: 238325 and cyclohexyl iodide(98%) PN: 238244 with copper stabilizer. (Accessed August 3rd 2023).

[34] (a) Zhang, S.; Perveen, S.; Ouyang, Y.; Xu, L.; Yu, T.; Zhao, M.; Wang, L.; Song, P.; Li, P. Design and synthesis of tunable chiral 2,2'-bipyridine ligands: Application to the enantioselective nickel-catalyzed reductive arylation of aldehydes. *Angew. Chem. Int. Ed.* **2022**, *61*, e202117843. (b) Zhu, Z.; Xiao, J.; Li, M.; Shi, Z. Nickel-catalyzed intermolecular asymmetric addition of aryl iodides across aldehydes. *Angew. Chem. Int. Ed.* **2022**, *61*, e202201370.

[35] Jiang, X.; Jiang, H.; Yang, Q.; Cheng, Y.; Lu, L.-Q.; Tunge, J. A.; Xiao, W.-J. Photoassisted cobalt-catalyzed asymmetric reductive Grignard-type addition of aryl iodides. *J. Am. Chem. Soc.* **2022**, *144*, 8347–8354.

[36] Zhang, L.; Wang, X.; Pu, M.; Chen, C.; Yang, P.; Wu, Y.-D.; Chi, Y. R.; Zhou, J. S. Nickel-catalyzed enantioselective reductive arylation and heteroarylation of aldimines via an elementary 1,4-addition. *J. Am Chem. Soc.* **2023**, *145*, 8498-8509.

[37] Nasim, A.; Thomas, G. T.; Ovens, J. S.; Newman, S. G. Reductive 1,2-arylation of isatins. *Org. Lett.* **2022**, *24*, 7232–7236.

[38] Heitkämper, J.; Posada-Pérez, S.; Escayola, S.; Solà, M.; Kästner, J.; Poater, A. A non expected alternative Ni(0) species in the Ni-catalytic aldehyde and alcohol arylation reactions facilitated by a 1,5-diaza-3,7-diphosphacyclooctane Ligand. *Chem. Eur. J.*, **2023**, *29*, e2023001.

[39] Meconi, G. M.; Vummaleti, S. V. C.; Luque-Urrutia, J. A.; Belanzoni, P.; Nolan, S. P.; Jacobsen, H.; Cavallo, L.; Solà, M.; Poater, A. Mechanism of the Suzuki–Miyaura cross-coupling reaction mediated by [Pd(NHC)(Allyl)Cl] precatalysts. *Organometallics* **2017**, *36*, 2088–2095
[40] Amatore, C.; Jutand, A. Anionic Pd(0) and Pd(II) intermediates in palladium-catalyzed Heck and cross-coupling reactions. *Acc. Chem. Res.* **2000**, *33*, 314–321.
[41] Borys, A. M.; Hevia, E. The anionic pathway in the Nickel-catalysed cross-coupling of aryl ethers. *Angew. Chem. Int. Ed.* **2021**, *60*, 24659–24667.
[42] Chapple, D. E.; Boyle, P. D.; Blacquiere, J. M. Origin of stability and inhibition of cooperative alkyne hydrofunctionalization catalysts. *ChemCatChem* **2021**, *13*, 3789–3800.
[43] Doud, M. D.; Grice, K. A.; Lilio, A. M.; Seu, C. S.; Kubiak, C. P. Versatile synthesis of $P^{R}{}_2N^{R'}{}_2$ Ligands for molecular electrocatalysts with pendant bases in the second coordination sphere. *Organometallics* **2012**, *31*, 779–782.
[44] Shuler, W. G.; Swyka, R. A.; Schempp, T. T.; Spinello, B. J.; Krische, M. J. Vinyl triflate–aldehyde reductive coupling–redox isomerization mediated by formate: Rhodium-catalyzed ketone synthesis in the absence of stoichiometric metals. *Chem. Eur. J.* **2019**, *25*, 12517-12520.
[45] Wang, Y. & Gu, M. The concept of spectral accuracy for MS. *Anal. Chem*. **2010**, *82*, 7055–7062.
[46] Betschmann, P.; Sahli, S.; Diederich, F.; Obst, U.; Gramlich, V. Structure-based design of nonpeptidic thrombin inhibitors: exploring the D-pocket and the oxyanion hole. *Helv. Chim. Acta* **2002**, *85*, 1210-1245.
[47] Asakawa, H.; Lee K.-H.; Lin, Z.; Yamashita, M. Facile scission of isonitrile carbon–nitrogen triple bond using a diborane(4) reagent. *Nat. Commun* **2014**, *5*, 4245.
[48] Tanaka, K.; Thomihama, M.; Yamamoto, K.; Matsubara, N.; Harada, T. Method for catalytic enantioselective alkylation of aldehydes using Grignard reagents as alkyl sources. *J. Org. Chem.* **2018**, *83*, 6127-6132.
[49] Shibata, T.; Tabira, H.; Soai, K. A catalytic and enantioselective cyclopropylation of aldehydes using dicyclopropylzinc. *J. Org. Chem.* **2018**, *83,* 6127-6132.
[50] Kišić, A.; Michel, S.; Mohar, B. Asymmetric transfer hydrogenation of 1-naphthyl ketones by an *ansa*-Ru(II) complex of a DPEN-SO_2N(Me)-$(CH_2)_2$(η^6-*p*-Tol) combined ligand. *Org. Lett.* **2013**, *15*, 1614-1617.
[51] Mongin, F.; Bucher, A.; Bazureau, J. P.; Bayh, O.; Awad, H.; Trécourt, F. Deprotonation of furans using lithium magnesates. *Tetrahedron Lett.* **2005**, *46*, 7989-7992.
[52] Stone, E. A.; Cutrona, K. J.; Miller, S. J. Asymmetric catalysis upon helically chiral Loratadine analogues unveils enantiomer-dependent antihistamine activity. *J. Am. Soc. Chem.* **2020**, *142*, 12690-12698. (b) Cole, J. P.; Chen, D.-F.; Kudisch, M.; Pearson, R. M.; Lim, C.-H.; Miyake, G. M. Organocatalyzed Birch reduction driven by visible light. *J. Am. Chem. Soc.* **2020**, *142*, 13573-13581.
[53] Ishida, S.; Suzuki, H.; Uechida, S.; Yamaguchi, E.; Itoh, A. Nickel catalyzed intermolecular carbonyl addition of aryl halide. *Eur. J. Org. Chem.* **2019**, 7483-7487
[54] Zhu, N.; Su, M.; Wan, W.-M.; Li, Y.; Bao, H. Practical method for reductive deuteration of ketones with magnesium and D_2O. *Org. Lett.* **2020**, *22*, 991-996.
[55] Wang, H.; Wang, Z.; Huang, H.; Tan, J.; Xu, K. KO^{t}Bu-promoted oxidation of (hetero)benzylic C_{sp3}–H to ketones with molecular oxygen. *Org. Lett.* **2016**, *18*, 5680–5683.

Chapter 3 : Catalytic Arylation of Primary Alcohols Facilitated by 1,5-Diaza-3,7-diphosphacyclooctanes (P_2N_2) Ligands

3.1 Research goals

As explored in Chapter 2, the coupling of aryl halides with aldehydes represents a major synthetic pathway to access secondary alcohols. In our work, we found that aliphatic carboxaldehydes were less viable coupling partners than aryl aldehydes (Section 2.5.2 Scope of the reductive arylation of aldehydes). This trend was also observed, to varying extents, in other contemporary catalytic works.[1] Recently, alcohols have been used as convenient and stable surrogates for aldehydes.[2] With the development of a Ni/P_2N_2 catalyst system for the reductive arylation of aldehydes, we hypothesized that a redox-neutral variant of this reaction could be possible (Scheme 3.1). A primary alcohol could be oxidized in situ to the corresponding aldehyde and, then, reductively arylated with an aryl halide. 1,5-Diaza-3,7-diphosphacyclooctanes (P_2N_2) ligands will be a focus as they were crucial in establishing mild reductive cross-coupling conditions (Chapter 2). We hypothesized that adding a co-catalyst could help promote this transformation.[3] Alternatively, a single nickel catalyst may be capable of both oxidation[4] and reduction. Additives (eg. fixed amounts of acetone/ispropanol) may be required to facilitate redox steps.

Scheme 3.1 A redox-neutral method to prepare secondary alcohols from primary alcohols

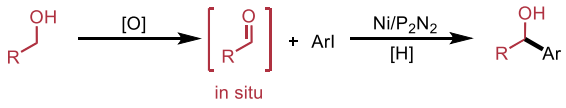

3.2 Reuse permissions

Section 3.4 is original and serves to better contextualize the redox-neutral α-arylation. The data presented in Section 3.5 was derived from the manuscript "Catalytic Aldehyde and Alcohol Arylation Reactions Facilitated by a 1,5-Diaza-3,7-diphosphacyclooctane Ligand", by Eric S. Isbrandt, Amrah Nasim, Karen A. Zhao, and Stephen G. Newman, published in *J. Am. Chem. Soc.* **2021**, 143, 14646-14656. Copyright 2021 American Chemical Society. The dissertation author is the primary author of this manuscript. To supplement the original publication, additional relevant data has been incorporated into the text. Section 3.5.1 was partially derived from the main text of the manuscript. Table 3.1 had additional optimization results from the Supporting Information added in – new additions have been italicized. The entries derived from the SI have been italicized and the table was reorganized to group related entries together. New text was written to contextualize the added entries in Table 3.1. Table 3.2 and Table 3.3 were fully derived from the SI and text was added to describe the results, as they are relevant to the optimization. Section 3.5.4 contains material derived from the original publication (Scheme 3.6) and materials that were found in the Supporting Information (Scheme 3.7). Scheme 3.8 was remade to only include details from the redox-neutral cross-coupling. Scheme 3.9 was remade from the original manuscript to improve clarity. Sections 3.5.5 and 3.5.6 were originally found in the Supporting Information of our publication. They have been directly added as they help contextualize the limitations and extensions of our work.

Sections 3.6 and 3.9 are unpublished mechanistic works that may be incorporated into a future publication.

Section 3.8 is derived exclusively from the Supporting Information of "Catalytic Aldehyde and Alcohol Arylation Reactions Facilitated by a 1,5-Diaza-3,7-diphosphacyclooctane Ligand", by Eric S. Isbrandt, Amrah Nasim, Karen A. Zhao, and Stephen G. Newman, published in *J. Am. Chem. Soc.* **2021**, 143, 14646-14656. It is available free of charge at: 10.1021/jacs.1c05661. Exceptionally, Section 3.8.5 only appears in this dissertation.

3.3 Contributions

For Section 3.5: Amrah Nasim (MSc) assisted with optimization of the redox-neutral coupling of aliphatic alcohols with aryl halides. Amrah contributed to the scope table with the synthesis and isolation of compounds **3.14**, **3.24, 3.25, 3.26, 3.27, 3.28, 3.29, 3.30, 3.31, 3.33, 3.34, 3.35, 3.36**. Karen Zhao (Hon BSc) performed the experiment described in Scheme 3.9 and prepared 4-(4-iodophenyl)-3-morpholinone, the starting material for compound **3.20**. Section 3.5.5 was written with experimental contributions from all authors.

For Section 3.6 and Section 3.9, Dr. Aishabibi Kassymbek (PDF) contributed to this work by running all single X-ray crystallography experiments and solving all X-ray crystal structures. These experiments have been fully detailed in Section 3.9.3.

3.4 Background: α-Arylation of alcohols

3.4.1 Metal-catalyzed oxidation of alcohols and related transformations

Aerobic oxidation of aldehydes to carboxylic acids passively occurs at room temperature without the need for initiators or catalysts, although additives can speed up the rate of the transformation.[5] Recently, kinetic analysis of the aerobic oxidation found that certain aliphatic aldehydes, such as cyclohexanecarboxaldehyde, had greater than an order of magnitude increased rate of aerobic oxidation compared to benzaldehyde.[6] The concentration of atmospheric oxygen is sufficient to passively oxidize aldehydes and, as a result, commercial samples become contaminated with the corresponding carboxylic acid over time. This is particularly relevant for catalysis, as small amounts of impurities could inhibit or fully deactivate the catalyst. Trimerization of alkyl aldehydes can occur in the presence of an acid or base catalyst.[7] As many alkyl aldehydes feature enolizable α-protons, mild self-aldol condensation reactions are also possible, lowering the amount of aldehyde present during a reaction.[8]

There are many classical methods to prepare aldehydes including (but not limited to) ozonolysis,[9] hydroformylation,[10] partial reduction of esters with DIBAL-H,[11] or partial oxidation of primary alcohols with sodium dichromate.[12] The reduction of esters can be especially challenging as aldehydes are more electrophilic and prone to reduction than an ester – recently, continuous flow chemistry has been used to overcome issues with overreduction.[11] Analogously, the oxidation of primary alcohols can also be problematic as aldehydes can be further oxidized to carboxylic acids. The overoxidation is especially favored if there are traces of moisture present

as this forms a hydrate which can easily be oxidized to the carboxylic acid through formal loss of hydride.[12]

A particularly appealing method of preparing carbonyls from alcohols is to use a mild oxidant. The Oppenauer oxidation uses a significant excess of a feedstock ketone such as acetone in solvent quantities, alongside a stoichiometric or catalytic Lewis acid to exploit equilibrium dynamics (Scheme 3.3A).[13] Through a proposed 6-membered, chair-like transition state, the metal facilitates the formal transfer of a hydride from the alcohol to the accepting ketone. It should be noted that the reverse pathway, commonly known as the Meerwein-Ponndorf-Verley (MPV) reduction, can be favored by simply adding a large excess of an alcohol reductant to the desired carbonyl in the presence of a stoichiometric or catalytic Lewis acid.[14] While aluminum alkoxides were commonly applied to Oppenauer or MPV reactions, they were traditionally stoichiometric additives. Over the past three decades, alteration of reaction conditions along with development of new ligands have enabled aluminum to be catalytically active.[15] Nonetheless, a wide range of base metals, transition metals, and lanthanides have also been reported as catalysts for MPV or Oppenauer transformations.[14]

Scheme 3.2 Using equilibrium to control redox state

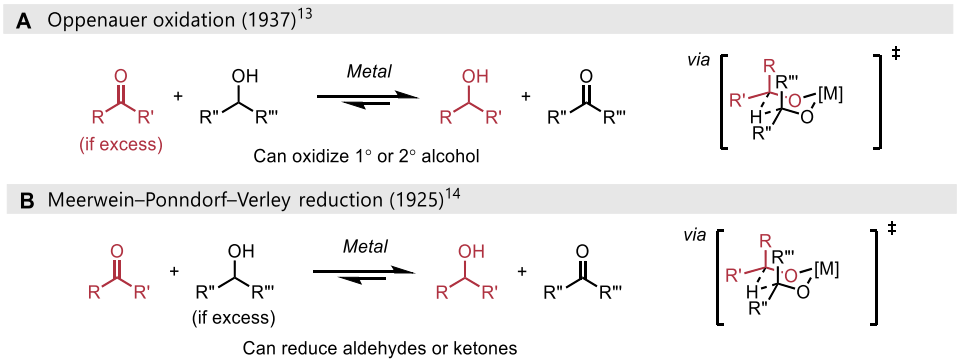

Scheme 3.3 Metal catalyzed oxidation of alcohols and related transformations

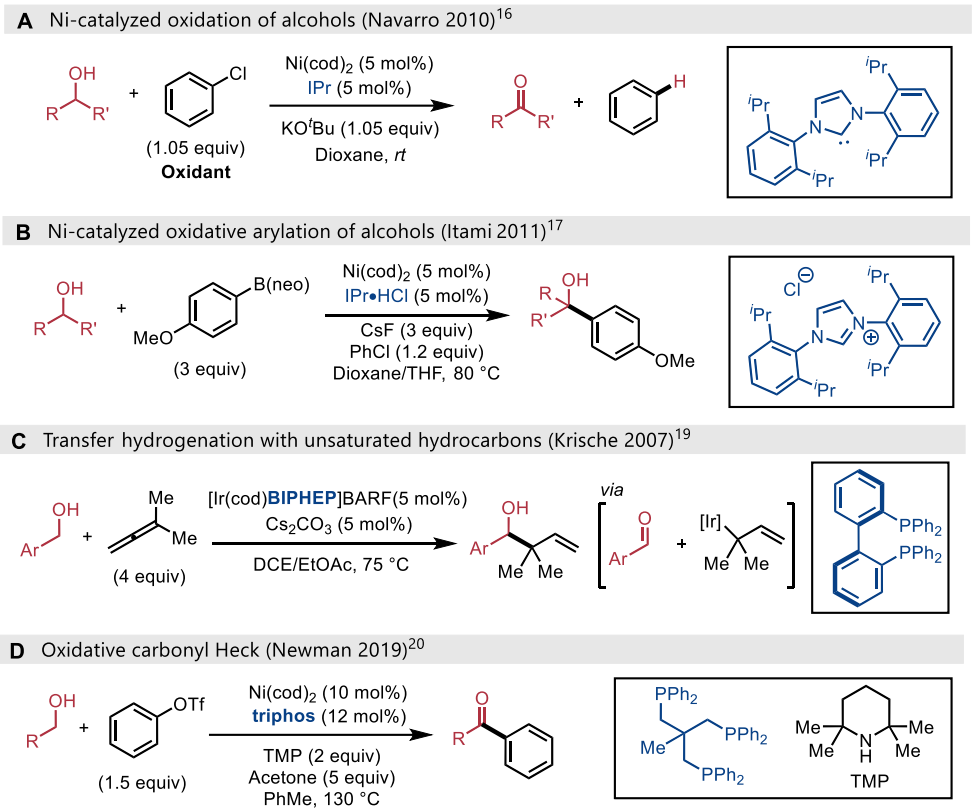

In summary, MPV or Oppenauer reactions operate through a metal-mediated redox transfer of a masked "hydride" from an alcohol to a carbonyl, as governed by equilibrium.

Similarly, direct β-hydride elimination from a metal alkoxide can serve to oxidize an alcohol to the corresponding carbonyl – if there is a stoichiometric oxidant present, this process can be rendered catalytic. Scheme 3.3A shows a Ni-catalyzed coupling that uses an aryl halide as the stoichiometric sacrificial oxidant.[16] Itami and coworkers reported a variation on this oxidation by using an aryl boronate ester to enable 1,2-arylation of the carbonyl (Scheme 3.3B).[17] Starting from a primary alcohol, Itami et al. were able to prepare tertiary carbinol products through a one-

pot multistep synthesis. This approach uses an aryl chloride as a stiochiometric oxidant and this is particularly notable as undesired Suzuki-Miyaura cross-coupling was largely avoided.

The catalytic coupling of primary alcohols with unsaturated hydrocarbons through transfer hydrogenation is well precedented with Ru, Ir, and Rh precatalysts.[18] Chiral bidentate phosphines are often used in this chemistry to achieve enantioselectivity. The reaction is proposed to operate through a β-hydride elimination mechanism; however, the resulting metal hydride reacts with a π-system (alkene, alkyne, or allene) to generate a nucleophilic organometallic species in situ. This organometallic nucleophile can do a 1,2-addition on the newly formed carbonyl. A representative example of transfer hydrogenation from the Krische group is shown in Scheme 3.3C.[19] This approach is highly atom economical and does not require prefunctionalized organometallics.

When assessing the scope of the carbonyl Heck reaction (Section 1.4), our group found that aliphatic aldehydes gave reduced yields and formed byproducts.[1a] The reaction was modified to oxidatively cross-couple aryl triflates with primary alcohols (Scheme 3.3D).[20] The optimized conditions featured acetone as a low molecular weight and benign sacrificial oxidant. By slowly generating the desired aliphatic aldehydes in situ, higher yields and fewer byproducts were observed, resulting in an improved methodology to prepare ketones.

3.4.2 Redox-neutral α-arylation of primary alcohols

While assessing the scope of the reductive cross-coupling of aryl iodides with aldehydes, we also found that aliphatic aldehydes gave decreased yields (Scheme 2.3). Based on the literature examples presented in Section 3.4.1, we hypothesized that redox-neutral α-arylation of

primary alcohols with aryl halides could expand the scope of the transformation by generating the corresponding aldehyde in situ. Aliphatic primary alcohols are more abundant and stable starting materials than the corresponding aldehydes. The classical method for accessing a secondary carbinol would be to first oxidize the primary alcohol to the aldehyde and then use a stoichiometric organometallic reagent to reductively form the C–C bond (Scheme 3.4A). In 2018, the MacMillan group reported that direct α-arylation of primary aliphatic alcohols with aryl halides was possible with tandem Ir and Ni catalysis (Scheme 3.4B).[21] This approach was facilitated by the formation of a zinc alkoxide in situ, which is proposed to be the species which undergoes the hydrogen atom transfer rather than the free alcohol. Efforts were made to render the zinc additive catalytic, however, this was not possible. MacMillan's methodology was a landmark powerful way to prepare functionalized secondary alcohols, although there were some limitations. An unspecified distribution of the two oxidation states (ketone-to-secondary alcohol) was commonly observed, therefore, a sodium borohydride reduction was incorporated into the workup to only obtain the desired alcohol product. Likewise, only aliphatic primary alcohols were amenable to this method. Further development of MacMillan's method was achieved by Wu and coworkers (Scheme 3.4C).[22] An organic photocatalyst was able to catalyze the coupling of primary alcohols with highly electron-deficient polyfluorinated aromatic rings, through a site-selective defluorination.

An electrocatalytic method by Findlater and coworkers achieved the direct α-arylation of benzylic alcohols using benzonitriles with an electron-withdrawing group in the *para* position (Scheme 3.4D).[23] Notably, the reductive arylation of aldehydes and ketones was also possible with

this procedure. While the redox-neutral scope was predominantly focused on forming secondary alcohols, direct α-arylation of secondary alcohols was also possible. By using a graphite anode, C(+) and a nickel cathode, Ni(-), in an undivided cell, a range of benzylic alcohols could be arylated efficiently. However, the use of 4-(EWG)benzonitriles as coupling partners presents a limitation in the utility of the method as only highly electron-deficient coupling partners were tolerated. Aliphatic primary alcohols were not within scope for this transformation, in contrast to the preceding methodologies.

While the synthetic pathways presented in Scheme 3.4B-D represent achievements in direct α-arylation of primary alcohols, a general method to couple benzyl and aliphatic alcohols has remained elusive. We hypothesized that a thermal pathway, through β-hydride elimination to form the corresponding aldehyde in situ, could enable complementary reactivity between aryl halides and primary alcohols.

Scheme 3.4 Redox-neutral α-arylation of primary alcohols

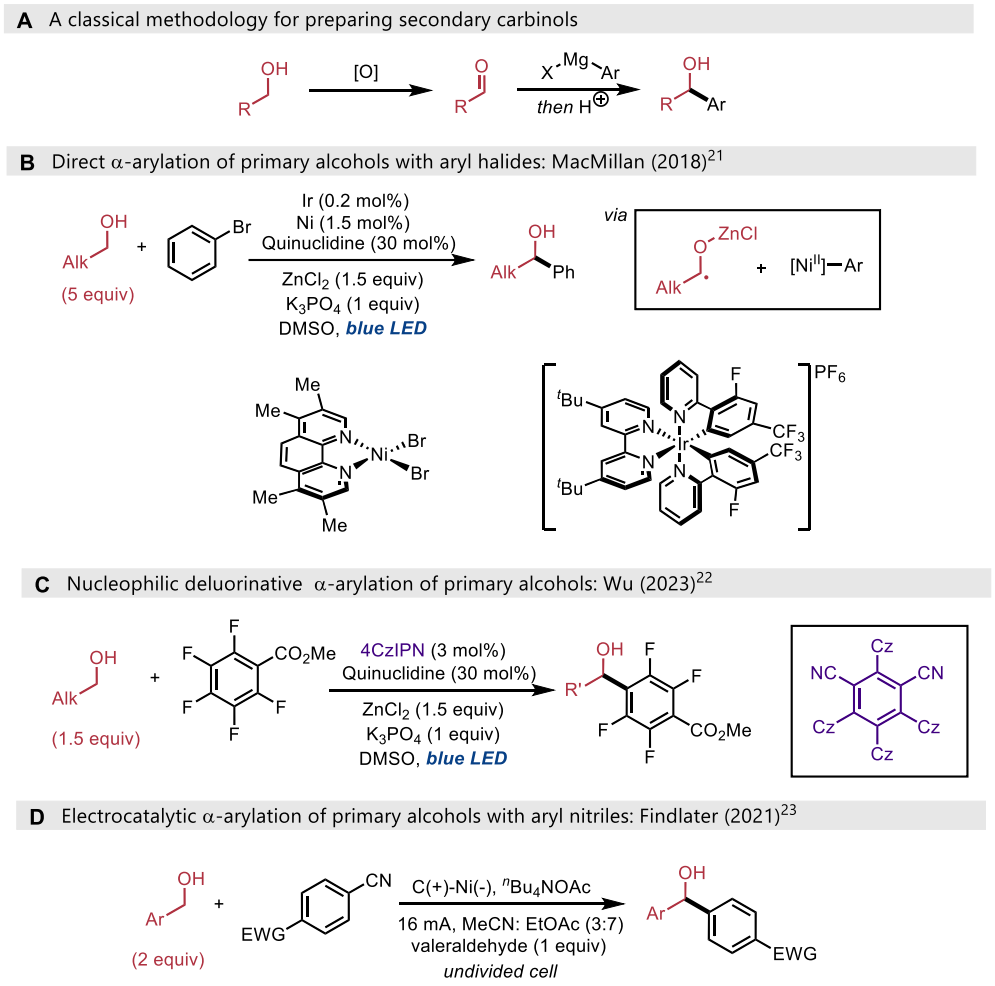

3.5 α-Arylation: Results and discussion

3.5.1 Optimization of the redox-neutral α-arylation of alcohols

With the limitations of existing reductive arylation and alcohol α-arylation reactions in mind, we sought systems that might be capable of directly α-arylating alcohols. Our optimization started from the conditions established in Chapter 2 and investigated the coupling of 5-iodo-1,3-benzodioxole **3.1** with benzyl alcohol **3.2** (Table 3.1). A general set of reaction conditions was identified by increasing the catalyst loading, adjusting the metal-to-ligand ratio, increasing the equivalents of the alcohol coupling partner, and omitting 1-phenylethanol from the reaction mixture (Table 3.1). With these conditions, α-arylation product **3.3** could be formed in 75% yield (entry 1). For this particular reaction, use of equimolar alcohol worked similarly well, albeit with some oxidative coupling product **3.4** formed as a by-product (entry 2). This selectivity issue is exacerbated if aryl iodide is used as the limiting reagent, which may be due to the aryl halide acting as a sacrificial oxidant (entry 3).[16] Later studies on the use of 1:1 stoichiometry showed some scope limitations, so the use excess of alcohol was ultimately found to be most general (vide infra; Table 3.4 and Table 3.5). Use of 10 mol% catalyst loading was not critical but enabled a slightly higher conversion – 5 mol% Ni and 15 mol% ligand gave 61% yield (entry 4). Decreasing the loading of $P^{Cy}{}_2N^{ArCF3}{}_2$ from 30 mol% to 12 mol% while keeping $NiBr_2$•diglyme at 10 mol% loading resulted in trace coupling (entry 5), indicating that an excess of ligand relative to the metal centre is required. Consistent with the reductive arylation procedure (Chapter 2), the nitrogen substituent on the ligand was important with *p*-anisidine-derived $P^{Cy}{}_2$ $N^{ArOMe}{}_2$ giving a reduced yield (entry 6), indicating that the electronics of this group are important for catalysis

despite precedent that 1,5-diaza-3,7-diphosphacyclooctanes are primarily bidentate ligands that bind to Ni through the two phosphorus atoms.[24] $P^{Ph}{}_2N^{ArCF3}{}_2$, $P^{tBu}{}_2N^{ArCF3}{}_2$, and dcpp•2HBF$_4$ were ineffective ligands (entries 7-9). In contrast, $P^{Ph}{}_2N^{ArCF3}{}_2$ was somewhat effective for the reductive variant (Table 2.1). Dppp gave moderate yield but poor selectivity between oxidation states (entry 10). Unlike the reductive arylation procedure (Table 2.1), other bases beyond TMP were somewhat effective. Triethylamine (entry 11) and postassium phosphate tribasic (entry 12) gave 58% and 33% yield, respectively, while pyridine gave no product (entry 13). Piperidine (entry 14) gave equivalent results to 2,2,6,6-tetramethylpiperidine, in sharp contrast to the reductive variant (Table 2.1) Notably, the more precedented O-arylation product **3.5** from coupling of the aryl iodide with the alcohol oxygen atom was not observed throughout the optimization.[25] Likewise, the dehydroxylative coupling product, recently reported with nickel-catalyzed systems, was not observed.[26]

Table 3.1 Optimization of the redox-neutral 1,2-arylation

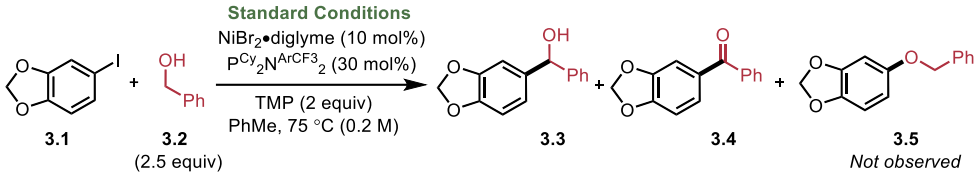

entry	deviation	yield 3.3	yield 3.4
1	None	75%	Trace
2	1.0 equivalent of **3.2**	74%	10%
3	2.0 equivalents of **3.1**[a]	61%	25%
4	5 mol% $NiBr_2$•diglyme; 15 mol% $P^{Cy}{}_2N^{ArCF3}{}_2$	64%	Trace
5	*12 mol% $P^{Cy}{}_2N^{ArCF3}{}_2$ instead of 30 mol%*	*8%*	*Trace*
6	*$P^{Cy}{}_2N^{ArOMe}{}_2$ as ligand*	*30%*	*Trace*
7	*$P^{tBu}{}_2N^{ArCF3}{}_2$ instead of $P^{Cy}{}_2N^{ArCF3}{}_2$*	*0%*	*0%*
8	*$P^{Ph}{}_2N^{ArCF3}{}_2$ instead of $P^{Cy}{}_2N^{ArCF3}{}_2$*	*Trace*	*0%*
9	*Dcpp•2HBF$_4$[b] instead of $P^{Cy}{}_2N^{ArCF3}{}_2$*	*Trace*	*Trace*
10	*Dppp instead of $P^{Cy}{}_2N^{ArCF3}{}_2$*	*34%*	*12%*
11	NEt_3 as base	58%	Trace
12	K_3PO_4 as base	33%	11%
13	Pyridine as base	0%	0%
14	*Piperidine as base*	*74%*	*Trace*

General conditions: aryl iodide **3.1** (0.30 mmol), alcohol **3.2** (0.75 mmol), TMP (0.6 mmol), $NiBr_2$•diglyme (10 mol%), $P^{Cy}{}_2N^{ArCF3}{}_2$ (30 mol%), toluene (1.5 mL), 75 °C for 16 h. Crude NMR yield determined using 0.05 mmol 1,3,5-trimethoxybenzene as internal standard. [a]Aryl iodide **3.1** (0.6 mmol), alcohol **3.2** (0.3 mmol) [b]1,3-Bis(dicyclohexylphosphino)propane bis(tetrafluoroborate). **Entries which were not present in the original publication have been italicized.**

Figure 3.1 P_2N_2 ligands from Table 3.1

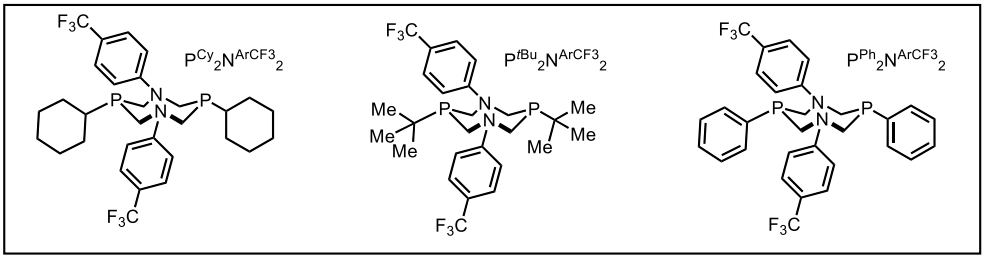

In the discovery phase of the project, nickel precatalysts were screened (Table 3.2). $Ni(cod)_2$ was moderately reactive (entry 1), however, this Ni(0) source was less effective than nickel (II) precatalysts (entries 2-4). $NiBr_2$•diglyme gave the highest yield for desired product **3.7**, so this was selected as the optimal precatalyst. One of the first steps on the proposed catalytic cycle (Scheme 3.8) involves oxidation of the primary alcohol coupled with reduction of Ni(II) to Ni(0). As further discussed in Section 3.5.4, mechanistically, it seems intuitive that Ni(II) precatalysts are more effective than a Ni(0) source.

Table 3.2 Screening nickel precatalysts

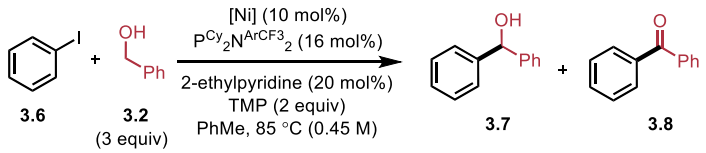

entry	Nickel precatalyst	yield 3.7	3.8
1	$Ni(cod)_2$	58%	Trace
2	$NiBr_2$(2-Ethylpyridine)$_2$	68%	Trace
3	$NiCl_2$•glyme	76%	Trace
4	$NiBr_2$•diglyme	82%	Trace

General reaction conditions: iodobenzene (0.15 mmol), alcohol (0.45 mmol), TMP (0.3 mmol), Ni source (10 mol%), $P^{Cy}{}_2N^{ArCF3}{}_2$ (16 mol%), 2-ethylpyridine (20 mol%), in toluene, 0.45 M, 85 °C for 16 h. [a]Crude NMR yield determined using 0.05 mmol 1,3,5-trimethoxybenzene as internal standard.

A ligand screen was also performed (Table 3.2), showing some divergence from the trends observed for the reductive arylation (Table 2.2). $P^{iBu}{}_2N^{ArCF3}{}_2$ gave moderate yield with high selectivity for desired product 3.10 (entry 1), while $P^{tBu}{}_2N^{ArCF3}{}_2$ was less effective (entry 2). $P^{Ph}{}_2N^{ArCF3}{}_2$ and $P^{Cy}{}_2N^{ArOMe}{}_2$ were ineffective to synthesize 3.10 (entries 3-4). $P^{Cy}{}_2N^{ArCF3}{}_2$ was the optimal ligand for the transformation (entry 5).

Table 3.3 Expanded ligand screen

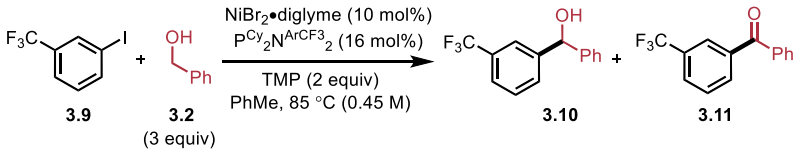

3.9 3.2 (3 equiv) 3.10 3.11

entry	P_2N_2	yield 3.10	yield 3.11
1	$P^{iBu}{}_2N^{ArCF3}{}_2$	47%	Trace
2	$P^{tBu}{}_2N^{ArCF3}{}_2$	10%	Trace
3	$P^{Ph}{}_2N^{ArCF3}{}_2$	Trace	0%
4	$P^{Cy}{}_2N^{ArOMe}{}_2$	0%	Trace
5	$P^{Cy}{}_2N^{ArCF3}{}_2$	64%	Trace

General reaction conditions: aryl iodide (0.15 mmol), alcohol (0.45 mmol), TMP (0.3 mmol), $NiBr_2$•diglyme (10 mol%), P_2N_2 (16 mol%), in toluene (0.45 M), 85 °C for 16 h. [a]Crude NMR yield determined using 0.05 mmol 1,3,5-trimethoxybenzene as internal standard.

Figure 3.2 P_2N_2 ligands from Table 3.1

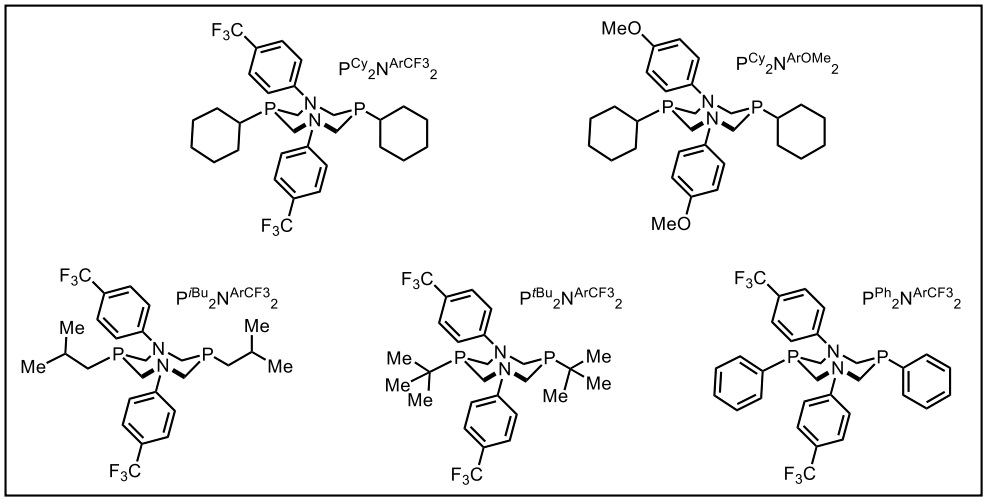

3.5.2 Equivalency of alcohol

While performing optimization, an excess of alcohol improved reaction selectivity for the redox-neutral product. Benzyl (Table 3.4) and aliphatic alcohols (Table 3.5) was gave improved yields with an increased excess of alcohol (**3.2**), so we opted to run the entire scope with 3 equivalents of primary alcohols to avoid any issues with selectivity.

Table 3.4 Alcohol equivalency screen for the redox-neutral α-arylation of benzyl alcohols

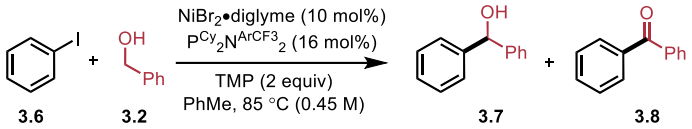

3.6 3.2 3.7 3.8

entry	equiv of 3.2	yield 3.7[a]	yield 3.8[a]
1	1.5	69%	5%
2	3.0	82%	Trace

General reaction conditions: iodobenzene (0.15 mmol), benzyl alcohol (0.225-0.45 mmol), TMP (0.3 mmol), $NiBr_2$•diglyme (10 mol%), $P^{Cy}{}_2N^{ArCF3}{}_2$(16 mol%) in toluene (0.45 M), 85 °C for 16 h. [a]Crude NMR yield determined using 0.05 mmol 1,3,5-trimethoxybenzene as internal standard.

Table 3.5 Alcohol equivalency screen for the redox-neutral α-arylation of aliphatic alcohols

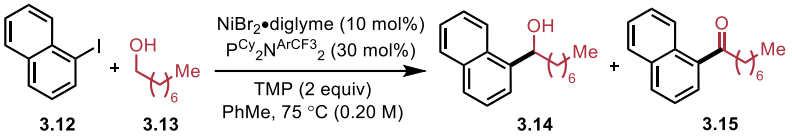

3.12 3.13 3.14 3.15

entry	equiv of 3.13	yield 3.14[a]	yield 3.15[a]
1	1.5	61%	20%
2	2.5	70%	6%

General reaction conditions: 1-iodonaphthalene (0.3 mmol), *n*-octanol (0.4-0.75 mmol), TMP (0.6 mmol), $NiBr_2$•diglyme (10 mol%), $P^{Cy}{}_2N^{ArCF3}{}_2$ (30 mol%) in toluene (0.20 M), 75 °C for 16 h. [a]Crude NMR yield determined using 0.05 mmol 1,3,5-trimethoxybenzene as internal standard.

3.5.3 Scope of the redox-neutral α-arylation of primary alcohols

The scope of the redox-neutral formal C–H bond arylation reaction was found to be broad, encompassing both benzyl and alkyl-substituted alcohols. (Scheme 3.5). 5-Iodo-1,3-benzodioxole was first coupled with a range of benzyl alcohols with varied sterics and electronics. Simple benzyl alcohol and 4-(1H-pyrazol-1-yl)phenyl)methanol cleanly coupled with 5-iodo-1,3-benzodioxole to form **3.3** and **3.16,** respectively, in moderate yields. Product **3.16** was also synthesized in the reductive arylation procedure (**2.20** in Scheme 2.4) and highlights the parallel nature between the methods. Sterically hindered benzo[1,3]dioxol-4-yl-methanol was well-tolerated forming **3.17** in 77% yield. 3-(Dimethylamino)benzyl alcohol formed product **3.18** in 74% yield. Next, 2-fluoro-4-chlorobenzyl alcohol was coupled with a diverse range of aryl iodides. Reaction with 5-iodo-1,3-benzodioxole afforded **3.19** without any evidence of hydrodehalogenation (reduction of the C-Cl bond). Secondary alcohols bearing a morpholinone (**3.20**) and trifluoromethoxy group (**3.21**) were formed in 74% and 71% yield, respectively. A reaction with 4- iodoacetophenone

provided the coupled product **3.22** in 89% yield, indicating excellent tolerance of ketones towards both 1,2 addition and reduction. 5-Iodo-2-methoxypyridine coupled to form product **3.23** in 66% yield. Coupling between 5-iodo-1,3-benzodioxole and *n*-octanol gave good conversion, but the α-arylation product was contaminated with the corresponding ketone in a 3:1 ratio.[1a,20] Work-up with $NaBH_4$ provided a useful 75% yield of **3.24**. In contrast, when electron-neutral or electron-deficient aryl iodides were used with aliphatic primary alcohols, high selectivity for the secondary alcohol is observed. For example, 1-iodonaphthalene was coupled with *n*-octanol and anhydrous reagent alcohol to give **3.14** and **3.25**, respectively, without any need for a reductive workup. Deuterated analog **3.25-*d*$_4$** could also be prepared in 40% yield by using ethanol-d_6. 1-Iodonaphthalene was also coupled with cyclohexylmethanol to give **3.26** in 78% yield. Olefin-containing alcohol **3.27** was formed in a modest 40% yield as an inseparable mixture of diastereomers, albeit with no evidence of competitive Heck-type processes or olefin isomerization. A 2-phenylethanol derivative and a *tert*-butyl carbamate-protected azetidinyl methanol gave **3.28** and **3.29** cleanly in high yields. Reactions of a diverse range of aryl iodides with cyclobutanemethanol were similarly efficient, giving **3.30**-**3.34** in 70-95% yield. Lastly, loratadine derivative **3.35** and tryptophol derivative **3.36** were prepared in 50 and 89% yields respectively, demonstrating the viability of this reaction on the functionalization of bioactive molecules.

Scheme 3.5 Scope of the redox-neutral α-arylation of primary alcohols

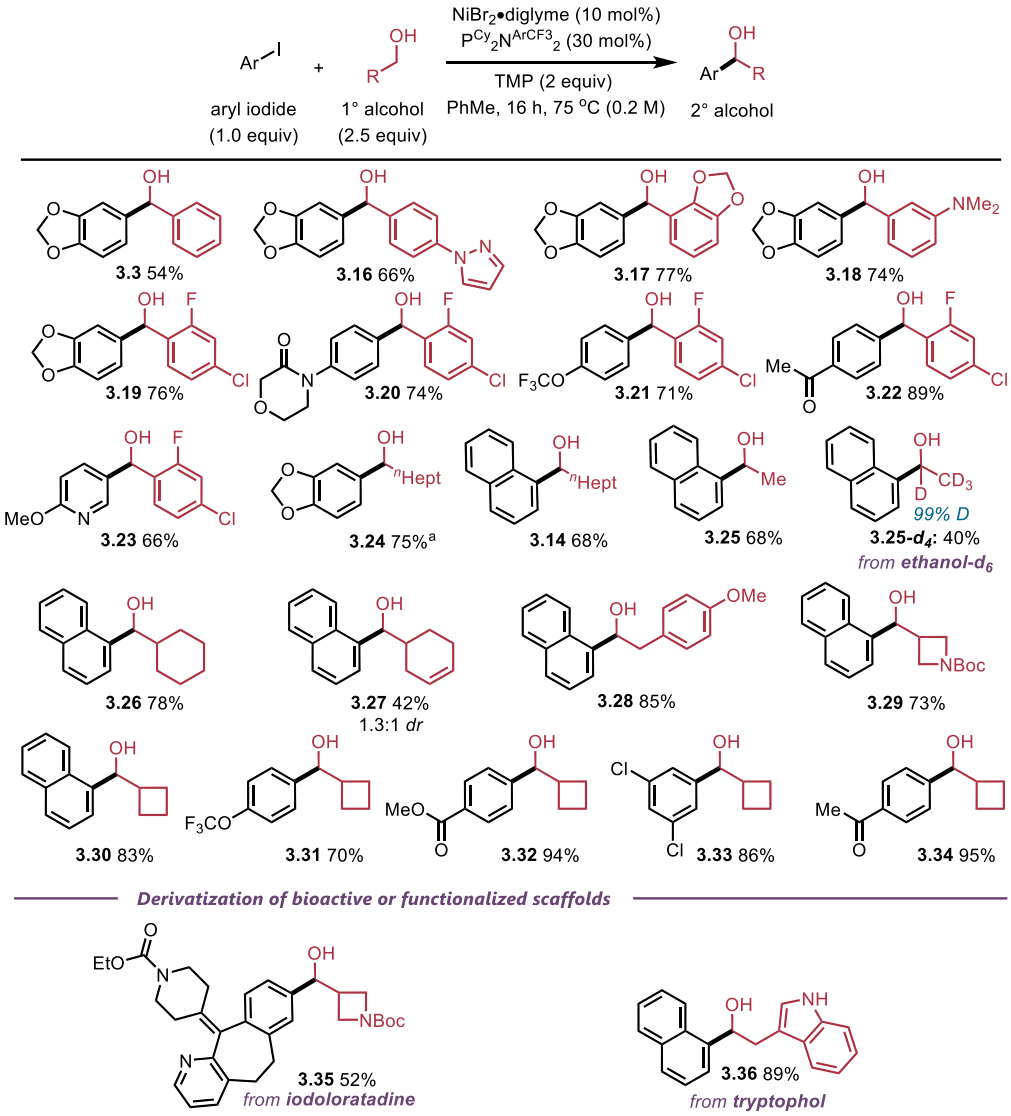

General reaction conditions: aryl iodide (0.30 mmol), alcohol (0.75 mmol), TMP (0.6 mmol), $NiBr_2$•diglyme (10 mol%), $P^{Cy}{}_2N^{ArCF3}{}_2$(30 mol%), toluene (0.20 M), 75 °C for 16 h. Isolated yields are reported. [a]Crude reaction mixture worked up with sodium borohydride

3.5.4 Mechanistic studies

Mono-deuterated 2-naphthalenemethanol **3.37-*d*$_1$** was prepared to investigate the redox-neutral α-arylation. Coupling with iodobenzene, **3.6**, gave **3.38** as the major product with 70% deuterium incorporation at the benzylic position, indicating that C–H bond cleavage is favoured over C–D bond cleavage giving a kinetic isotope effect (KIE) of 2.3 (Scheme 3.7A).

To confirm that the free alcohol group is necessary for the transformation, methyl ether **3.39** was subjected to the reaction conditions (Scheme 3.7B). Quantitative recovery of the starting material was observed, suggesting that hydrogen atom transfer at the α-position to form a stabilized radical is not observed.

To probe the ability of $NiBr_2$•diglyme to oxidize alcohols and insert into the resulting aldehydes, stoichiometric studies were carried out. Treatment of Ni(II) with 2 equiv $P^{Cy}{}_2N^{ArCF3}{}_2$ and 1 equiv of (2-naphthyl)methanol **3.37** resulted in formation of the 2-naphthaldehyde **3.40** in 56% yield with recovery of the alcohol providing the remainder of the mass balance (Scheme 3.7C). Increasing the equivalency of alcohol allowed for full conversion of the Ni(II) to give a 94% yield of aldehyde, suggesting the oxidation may be governed by equilibrium. The oxidation reaction did not occur in the absence of base. The presence of base could facilitate the formation of a nickel alkoxide species, which is able to β-hydride eliminate to form the aldehyde.

The identities of nickel precatalyst, ligand, temperature of reaction, concentration of reaction, and aryl iodide coupling partner were kept consistent between redox-neutral and reductive cross-couplings. Owing to the similarities of the optimized redox-neutral coupling

conditions to the reductive cross-coupling conditions presented in Chapter 2, we hypothesize that both reactions occur through a similar mechanism (Section 2.2).

Scheme 3.6 Mechanistic studies of the redox-neutral α-arylation

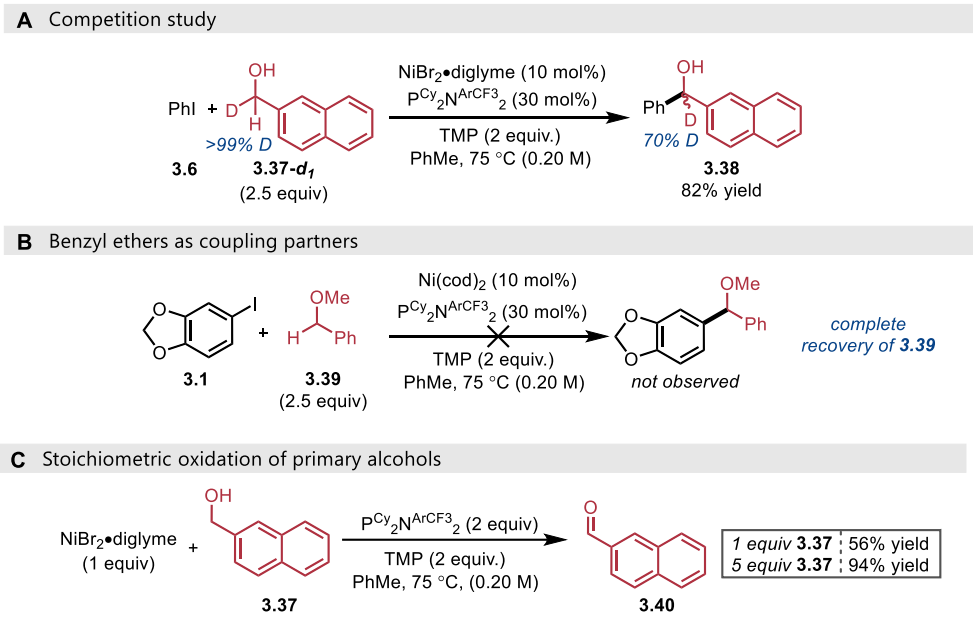

A competition study comparing the reactivity of primary aliphatic alcohols to primary benzyl alcohols was performed. Alcohols are commonly encountered in organic synthesis and the ability to selectively couple one alcohol while leaving the other alcohol untouched is especially desirable. We hypothesized that benzyl alcohols would be more prone to oxidation than primary alkyl alcohols and that high selectivity for the benzhydrol product could be observed (Scheme 3.7A). Unfortunately, 4-(hydroxymethyl)-benzeneethanol (**3.41**) was not amenable to our standard coupling conditions (general procedure), affording benzhydrol derivative **3.42** in low yield with no trace of any other product and recovery of **3.41**.

An intermolecular competition was also performed with 5-iodo-1,3-benzodioxole (**3.1**) and two primary alcohols: benzyl alcohol (**3.2**) and *n*-octanol (**3.13**) (Scheme 3.7B). Yields are were derived

from ^{1}H NMR spectra of the crude reaction mixtures. Moderate selectivity (~6:1) for benzyl alcohol (**3.3**) α-arylation was observed over coupling with primary aliphatic alcohol (**3.43**+**3.44**). While selectivity was observed, it was not high enough to be synthetically useful. We anticipate that further optimization of the general procedure could result in improved yields and selectivities.

Scheme 3.7 Intramolecular competition between an aliphatic and a benzyl alcohol

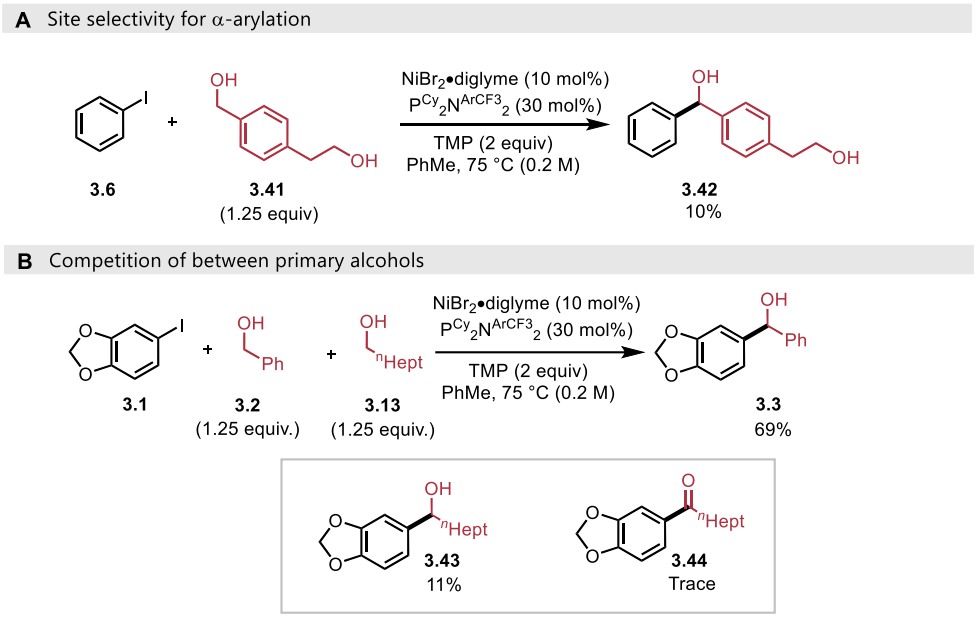

A key difference between the proposed catalytic cycles is the omission of a sacrificial reductant in the direct α-arylation of alcohols (Scheme 3.8). The Ni(II) precatalyst **3.A** may first be reduced by the primary alcohol substrate to make the corresponding aldehyde and a Ni(II) hydride **3.B**, which can undergo reductive elimination to active Ni(0) catalyst **3.C**. The aldehyde produced in this step was never observed in large quantities, indicating that it is consumed as quickly as it is formed. This suggests that the high selectivity for C–H bond cleavage observed in the reaction of **3.38** (Scheme 3.6) may originate from this β-hydride elimination step. Notably,

$Ni(cod)_2$, which was found to be less effective than $NiBr_2$•diglyme (see Table 3.2, entry 1), is unable to directly oxidize the primary alcohol, as it is in the wrong oxidation state, and likely would be required to reduce the aryl halide to generate aldehyde for the first catalytic cycle – from there the reaction could proceed as indicated. Subsequent cycles, after formation of active catalyst, could follow the proposed catalytic cycle. Oxidative addition of the aryl iodide leads to nickel(II) adduct **3.D**. With our identified catalyst system, adduct **3.D** is believed to coordinate with the aldehyde to form intermediate **3.E**. Regardless, a π-bond insertion may generate the key C–C bond to form Ni(II) alkoxide **3.F**. While this intermediate may be prone to β-hydride elimination, evidenced by the ketone side-products discussed throughout, exchange of an alkoxide ligand releases the secondary alcohol product and regenerates Ni(II) intermediate **3.A**. A key step in the mechanism described above is the β-hydride elimination of an alkoxide group from **3.A** to **3.B** to form an aldehyde.

We hypothesized that addition of a stoichiometric oxidant may force metal alkoxide **3.F** to undergo β-hydride elimination, providing a catalytic route to ketones. While we previously described analogous redox-neutral and oxidative carbonyl-Heck reactions, these reactions were exclusively limited to the use of aryl triflate coupling partners at elevated-temperatures.[1a,20] For instance, coupling of aryl iodide **3.45** with benzyl alcohol **3.2** using previously developed Ni/triphos oxidative arylation conditions gave no trace of the corresponding ketone, **3.46** (Scheme 3.9).[20] In contrast, using $P^{Cy}{}_2N^{ArCF3}{}_2$ and slightly modified conditions from the redox-neutral arylation cross-coupling, the same reaction could be achieved with 92% isolated yield of **3.46**. Not only was this previously undeveloped reaction made possible, it is achieved at a greatly

reduced temperature than our previous report without thorough optimization. We believe this is an important next step to expanding the breadth of ketone and alcohol arylation chemistry and highlights the previously unrecognized power of P_2N_2 ligands in catalytic coupling chemistry.

Scheme 3.8 Proposed catalytic cycle for redox-neutral coupling

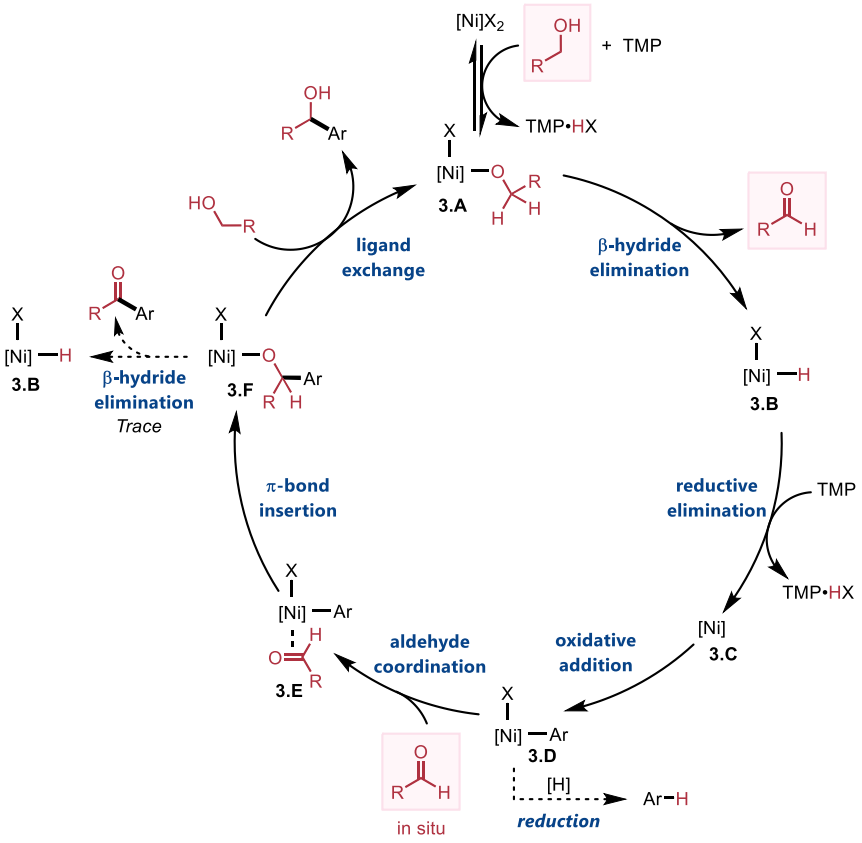

Scheme 3.9 Extrapolation of reaction conditions to oxidative arylation of benzyl alcohols

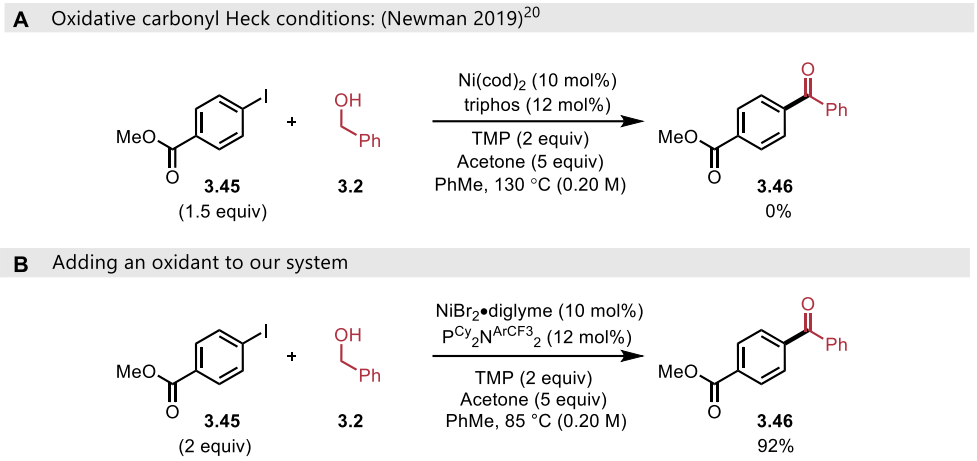

3.5.5 Limitations of the redox-neutral arylation

While evaluating the scope of this transformation, several products could not be obtained in synthetically useful yields using the conditions from the General Procedure. A selection of these is given below (Scheme 3.10). Reactions with highly electron-deficient aryl iodides including 3-iodopyridine, 1-iodo-3,5-bis(trifluoromethyl)benzene, 4-iodo-1-methyl-1H-pyrazole, and 6-iodoquinoline showed, at best, trace conversion (Scheme 3.10A: **3.47-3.50**). Most of these examples are consistent with the reductive arylation and could be due to the generation of poorly nucleophilic aryl nickel(II) complexes. However, 6-iodoquinoline, a model heterocyclic aryl iodide in the reductive arylation scope (Scheme 2.4), was unreactive in the redox-neutral variant (**3.50**). We hypothesize that the quinoline may be a better ligand for nickel than a simple primary alcohol and that this binding impedes the formation of a metal alkoxide. A robustness screen was not performed; however, such a study could uncover whether oxidation to the aldehyde does not occur in the presence of quinoline. A strong base, such as NaH, could be added to make a more reactive alkoxide which can directly substitute an X-type ligand.

Reactions with chelating or coordinating functional groups showed, at best, only trace conversion (Scheme 3.10B: **3.51-3.59**). Some of these functional groups (**3.51**-**3.54**) feature acidic X-H bonds which may poison the catalyst activity – this contrasts the reductive arylation scope, which was more tolerant of Brønsted acidic functionalities (Scheme 2.4). When assessing the aliphatic alcohol scope, it was found that β, γ, or *δ* heteroatoms were not tolerated. Chelation of the alcohol and the proximal heteroatom by the catalyst could form a stable nickelacycle (**3.55-3.59**). Notably, acyclovir derived product **3.59** was possibly observed by ESI-MS as a salt adduct but the crude NMR data were not conclusive to support or refute the formation of the desired product.

The α-arylation of primary alcohols did not work with substrates that are challenging to oxidize such as methanol and a variety of alcohols with electron-withdrawing fluorinated chains (Scheme 3.10C: **3.60-3.63**). We hypothesize that these alcohols are more challenging to oxidize through a β-hydride elimination.

5-decyn-1-ol afforded only the desired product (**3.64**) in 30% crude yield with no trace of side-product formation. The alkyne may have served to poison the catalyst by competitively binding to the metal. 2-chloroethanol gave only limited amounts of desired product (**3.65**) – when this substrate was added to the reaction vial a white smoke was immediately observed at room temperature. We suspect that 2,2,6,6-tetramethylpiperidine could react with the alkyl chloride through either a direct nucleophilic substitution or base induced elimination to degrade the starting material to the alkene. A protected sugar derivative demonstrated promising reactivity, despite the presence of many coordination sites and the possibility of the nickel

catalyst to form bidentate chelates (**3.65**). Finally, 1-adamantyl methanol, a primary alcohol adjacent to a quaternary center did not afford product (**3.66**). This result suggests that large steric bulk surrounding the primary alcohol can hinder the coupling reaction.

Scheme 3.10 Challenging scope examples of the redox-neutral α-arylation of primary alcohols

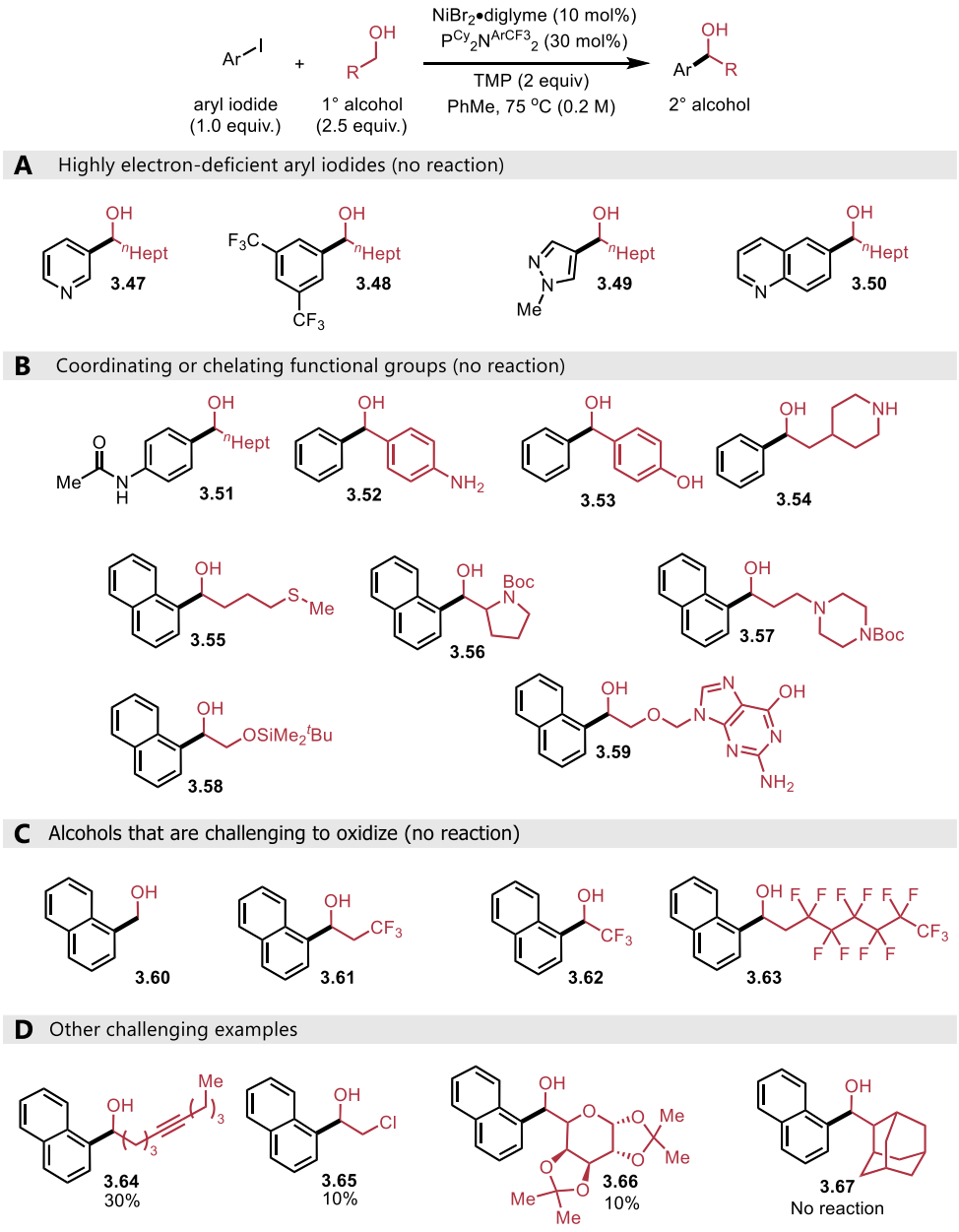

3.5.6 Redox-neutral couplings with aryl bromides

While aryl iodides generally provided higher yields and more consistent results throughout the project, aryl bromides gave appreciable yields of product with modified reaction conditions. These partially optimized conditions are provided below for redox-neutral coupling with both aldehydes and alcohols (Table 3.6). When coupling with benzyl alcohol, **3.2**, under redox-neutral conditions, the desired secondary alcohol was obtained in moderate yield with a small amount of ketone side-product (entry 1). Conversely, when coupling with benzaldehyde, **3.68**, under redox-neutral conditions, the desired ketone was obtained in moderate yield with approximately 10% reduced product – this is particularly notable as the equivalency of the nickel precatalyst was 0.10 equiv, suggesting that it could be a stoichiometric terminal reductant (entry 2). The corresponding reactions with aryl iodides proceeds smoothly with high conversion and minimal redox side-products, Scheme 2.4 and Scheme 3.9, however, the hits presented in Table 3.6 are valuable indications that aryl bromides could be optimized as coupling partners.

Table 3.6 Redo-neutral couplings with aryl bromides

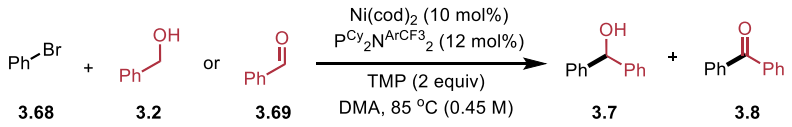

3.68 3.2 3.69 3.7 3.8

entry	electrophile	equiv of electrophile	yield 3.7[a]	yield 3.8[a]
1	**3.2**	2.5	40%	5%
2	**3.68**	1.0	9%	52%

Reaction conditions: bromobenzene (0.15 mmol), alcohol **3.2** (0.225 mmol) or aldehyde **3.68** (0.15 mmol), TMP (0.3 mmol), $Ni(cod)_2$ (10 mol%), $P^{Cy}{}_2N^{ArCF3}{}_2$ (12 mol%) in DMA[b] (0.45 M), 85 °C for 16 h. [a] Crude ^1H NMR yield determined using 0.05 mmol 1,3,5-trimethoxybenzene as internal standard. [b] DMA = *N,N*-Dimethylacetamide

3.5.7 Ligand decomposition: A possible reason for increased ligand equivalency?

Three equivalents of $P^{Cy}_2N^{ArCF3}_2$ relative to the loading of nickel was optimal for the redox-neutral coupling (see Section 3.5.1). A 1:3 metal-to-ligand stoichiometry is quite uncommon using late transition metals as the metal centre won't simultaneously coordinate three bidentate ligands. In crude GC-MS analysis of reaction mixtures with P_2N_2 ligands, we ocassionally observed a side-product derived from 4-aminobenzotrifluoride, suggesting that the P,N-acetal may fragment under our reaction conditions (Scheme 3.11). The imine side-product was more prevalent when higher reaction temperatures were employed (> 100 °C); noting that under standard redox-neutral coupling the formation of an aldehyde is proposed as a key mechanistic step (see Section 3.5.4). Further stability studies, including simply heating a P_2N_2 in organic solvent and characterizing the reaction mixture after cooling, could help understand whether the heterocyclic P,N-acetal core is robust.

Scheme 3.11 Possible decomposition pathway of $P^{Cy}_2N^{ArCF3}_2$ in the presence of aldehydes

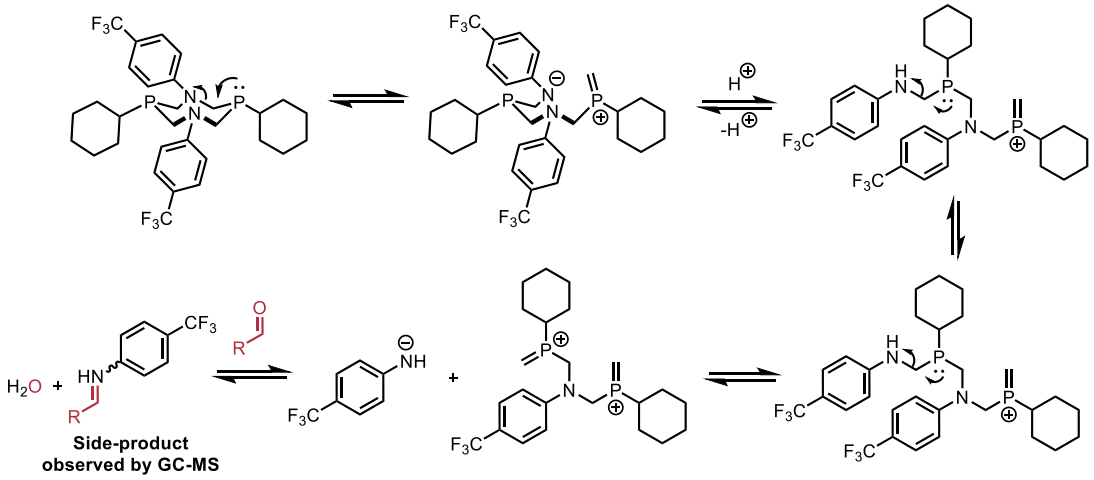

3.6 Isolation and mechanistic study of Ni(P_2N_2) complexes

To further study the application of P_2N_2 ligands in nickel catalysis, a deeper mechanistic understanding for the arylation of aldehydes is required. As further detailed in this section, direct arylation of unactivated ketones is possible with a Ni/$P^{Cy}{}_2N^{ArCF3}{}_2$ catalyst system; however, this chemistry provided, at best, moderate yields and limited scope. We hypothesize that study of the mechanistically related arylation of aldehydes, either starting directly from the aldehyde or preparing it in situ, could enable rational design of a robust catalyst system with wider scope.

3.6.1 The need for a more robust catalyst

Extension of the work presented in Chapter 2 and Section 3.5 was considered to bring ketones into scope for a reductive arylation. The redox-neutral α-arylation of secondary alcohols, through a ketone generated in situ, was also considered. While our research group reported the reductive arylation of isatins, these compounds are electronically-biased and more electrophilic than most ketones.[27] Identification of general conditions to cross-couple organo(pseudo)halides with unactivated ketones remains elusive.[28] Strategies to access tertiary alcohols from coupling of boronic acids with ketones or secondary alcohols are known; however, these processes are proposed to be mechanistically different and feature oxanickelacyclopropane intermediates, derived from oxidative cyclization of the ketone with Ni(0).[17,29,30] Likewise, related Ir-catalyzed reductive coupling of dienes with ketones was recently disclosed.[31] Exploratory high-throughput experimentation and subsequent one-variable-at-a-time optimization revealed an entry point to the reductive arylation of ketones after extensive research (Scheme 3.12A). Interestingly, $P^{Cy}{}_2N^{ArCF3}{}_2$ was once again identified as the ligand of choice and isopropanol was the optimal

reductant screened. While this result appears to be highly promising, the transformation presented in Scheme 3.12A was very limited in scope and suffered from reproducibility issues. A further round of optimization on 4-phenyl-2-butanone, a low yielding substrate, found slightly improved conditions by changing the base to diispropylethylamine and altering stoichiometry of reagents (Scheme 3.12B). While the conditions disclosed in Scheme 3.12B did serve to improve the transformation, a significant amount of reduced triflate, **3.75**, was observed and most ketones still gave <25% crude yield. While these results are a good starting point, it is clear that further optimization is required to improve the transformation. Detailed mechanistic experiments, especially those targeting why P_2N_2 ligands perform better than conventional ligands, could enable the rational design of new ligands to overcome current limitations. It makes the most logical sense to first run mechanistic experiments on the working redox-neutral α-arylation of primary alcohols and reductive arylation of aldehydes before extrapolating to systems involving secondary alcohols or ketones.

Scheme 3.12 Conditions developed for ketone addition

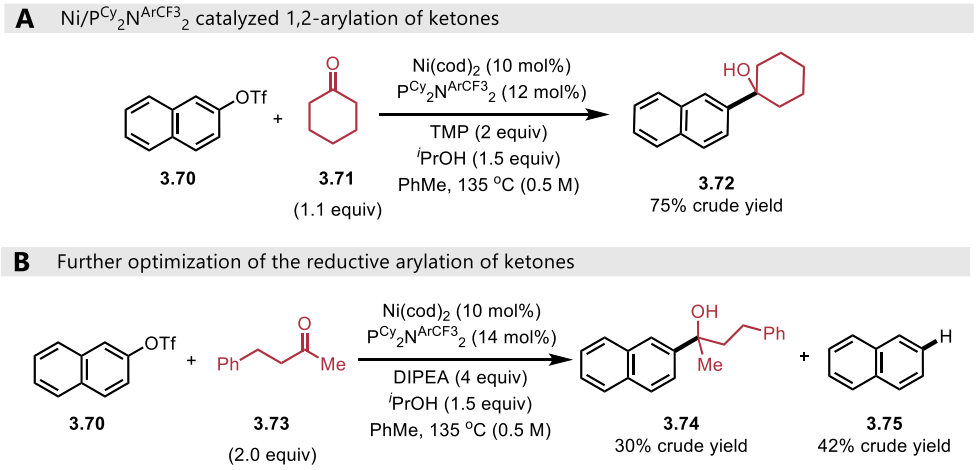

Crude ^{1}H NMR yield determined using 0.05 mmol 1,3,5-trimethoxybenzene as internal standard.

3.6.2 Synthesis and isolation of well-defined Ni(P_2N_2) complexes

While running stoichiometric experiments, we serendipitously found a convenient method to prepare [Ni($P^{Cy}_2N^{ArCF3}_2$)(cod)] (**3.76**), a Ni(0) complex with one equivalent of P_2N_2 ligand bound (Scheme 3.13). Our group had previously reported [Ni($P^{Cy}_2N^{ArCF3}_2$)$_2$], the analogous Ni(0) species with two equivalents of P_2N_2 ligand, however, the cod complex had remained elusive.[27] X-ray crystallography confirmed the structure of **3.76** – it had the expected connectivity with no evidence of κ^3-bonding through either the nitrogen atom or the arene (see Section 1.5.3).

Scheme 3.13 Synthesis of [Ni($P^{Cy}_2N^{ArCF3}_2$)(cod)]

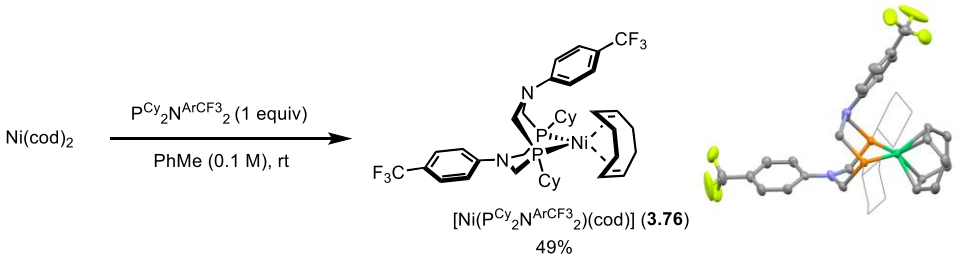

Reaction conditions: Ni(cod)$_2$ (0.30 mmol), $P^{Cy}_2N^{ArCF3}_2$ (0.30 mmol), toluene (0.10 M), rt for 15 min. Isolated yield is reported. Thermal displacement plot is shown with ellipsoids at 50% probability and the cyclohexyl phosphorus substituents are depicted as wireframe. For clarity, hydrogen atoms were removed. Depictions with atom labels along with tables of selected bond lengths and angles are provided in Section 3.9.3 Crystallographic details.

We next turned our attention to isolating species on the proposed catalytic cycle (Section 3.5.4. The oxidative addition complex (OAC), (Scheme 3.8; compound **3.D**), was selected as the target for characterization and isolation. The isolation of nickel OACs is established and they are predominantly accessed through either direct oxidative addition of Ni(0) with an aryl halide[32] or transmetallation of an aryl group to a NiX_2 precursor (where X = Cl, Br, or I).[33] We opted to first try the direct oxidative addition route, starting from Ni(cod)$_2$. Gratifyingly, evidence of oxidative addition was observed at room temperature, through the formation of two new doublets by

$^{31}P\{^{1}H\}$ (see Section 3.9.4 for crude spectra). Equimolar quantities of $Ni(cod)_2$, $P^{Cy}{}_2N^{ArCF3}{}_2$, and 1-naphthyl iodide were combined in d_6-benzene (Scheme 3.14).

Scheme 3.14 Oxidative addition of Ni(0) with $P^{Cy}{}_2N^{ArCF3}{}_2$

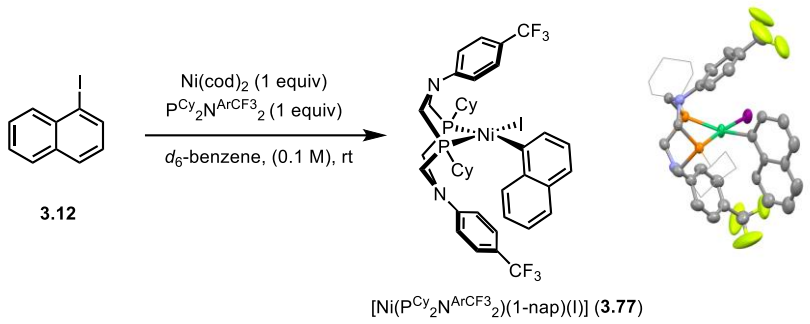

3.12

[Ni($P^{Cy}{}_2N^{ArCF3}{}_2$)(1-nap)(I)] (**3.77**)

Reaction conditions: $Ni(cod)_2$ (0.10 mmol), $P^{Cy}{}_2N^{ArCF3}{}_2$ (0.10 mmol), d_6-benzene (0.10 M), rt for 15 min. Thermal displacement plot is shown with ellipsoids at 50% probability and the cyclohexyl phosphorus substituents are depicted as wireframe. For clarity, hydrogen atoms were removed. Depictions with atom labels along with tables of selected bond lengths and angles are provided in Section 3.9.3 Crystallographic details.

The experiment described in Scheme 3.14 was repeated in toluene and X-ray quality crystals were obtained by cooling the solution to -20°C. However, the species which crystallized was the previously reported [Ni($P^{Cy}{}_2N^{ArCF3}{}_2$)$_2$] complex, rather than the desired OAC (**3.77**). NMR analysis confirmed that the main species in solution was, in fact, the aforementioned Ni(0) complex. Further NMR studies in d_6-benzene indicated that compound **3.77** decomposes over time forming [Ni($P^{Cy}{}_2N^{ArCF3}{}_2$)$_2$] in solution and a dark precipitate which is poorly soluble in organic solvents. We believe a Schlenk-type equilibrium is operative (Scheme 3.15). Two equivalents of **3.77** can exchange ligands (disproportionate) to form [Ni($P^{Cy}{}_2N^{ArCF3}{}_2$)(I)$_2$] (**3.78**) and [Ni($P^{Cy}{}_2N^{ArCF3}{}_2$)(1-nap)$_2$] (**3.79**). [Ni($P^{Cy}{}_2N^{ArCF3}{}_2$)(I)$_2$], **3.78**, has been isolated from a failed experiment between the OAC (**3.77**), prepared in situ, and a ketone (described further in Section 3.9.2.1), giving additional support for a Schlenk equilibrium mechanism. Complex **3.79** has never

been directly observed, however, it can reductively eliminate to form 1,1'-binaphthyl (**3.81**) and a Ni(0) species (**3.82**). Crude GC-MS analysis after NMR experiments has qualitatively indicated that compound **3.81** is formed during the experiment described in Scheme 3.14. We suspect that nickel(II) iodide (**3.80**) precipitates out of the reaction mixture as a non-P_2N_2 ligated salt and that [Ni($P^{Cy}_2N^{ArCF3}_2$)$_2$], **3.82**, preferentially exists in solution. As further mechanistic support, Schlenk equilibrium has been observed in studies of related stoichiometric Ni(II) complexes.[34] While this phenomenon is particularly relevant to our stoichiometric study of Ni(P_2N_2) complexes, we never

Scheme 3.15 Schlenk-type equilibrium of OAC

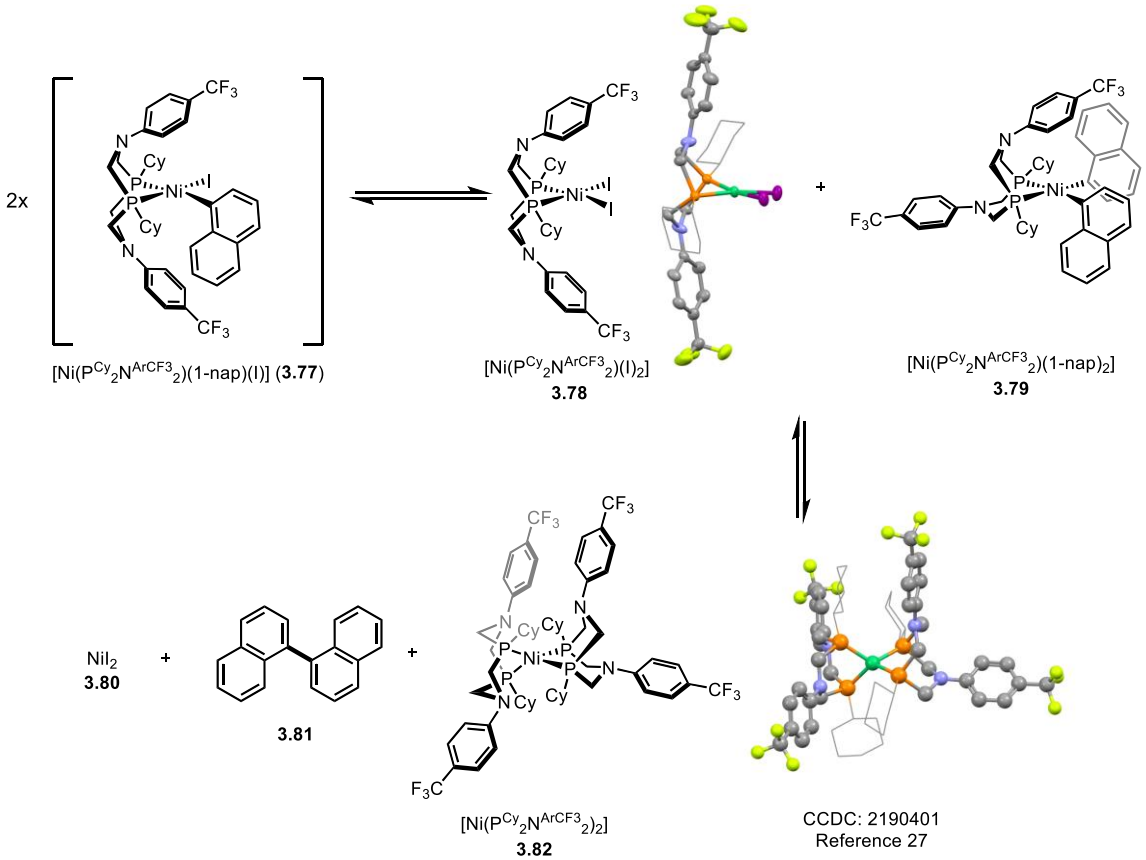

Thermal displacement plot is shown with ellipsoids at 50% probability and the cyclohexyl phosphorus substituents are depicted as wireframe. For clarity, hydrogen atoms were removed. Depictions with atom labels along with tables of selected bond lengths and angles for **3.78** are provided in Section 3.9.3. Crystallographic data for **3.82** can be found in the original publication.[27]

observed homocoupling of the aryl iodide in catalytic experiments with P_2N_2 ligands. We postulate that the relative concentration of OAC in a catalytic experiment is significantly diluted compared to a stoichiometric reaction. Nonetheless, clean isolation of **3.77** was challenging as Schlenk-type equilbria were observed with a range of solvents, resulting in impurities (see Section 3.9.4). Nonetheless, we were able to isolate a small quantity of **3.77** and obtain a crystal structure.

While the crystal structure of **3.77** unambigiously confirmed that the oxidative addition complex looks as expected: κ^2-P,P ligation of a square planar Ni(II) complex, we wanted to be able to isolate larger quantities of clean material for further mechanistic studies. We hypothesized that the identity of the P_2N_2 ligand could affect the Schlenk equilibrium. We found that simply changing the ligand from $P^{Cy}{}_2N^{ArCF3}{}_2$ to $P^{Cy}{}_2N^{Ph}{}_2$ allowed for surprisingly smooth isolation of [Ni($P^{Cy}{}_2N^{Ph}{}_2$)(1-nap)(I)],**3.83** (Scheme 3.16). It remains unclear exactly why such a subtle change allows for a stable OAC, but it could be relevant to our studies on why $P^{Cy}{}_2N^{ArCF3}{}_2$ was the optimal ligand throughout Chapters 2 and 3. Compound **3.83** is considerably less soluble in toluene than compound **3.77** and it rapidly precipitates at room temperature. However, dissolving **3.83** in THF did *not* result in any new peaks by $^{31}P\{^1H\}$ over the course of 72 hours at room temperature, suggesting that **3.83** is also resistant to Schlenk equilibrium in solution. We were able to obtain a crystal structure for complex **3.83** - this structure allows us to confirm that the connectivity of **3.83** is analogous to **3.77**.

Scheme 3.16 Oxidative addition of Ni(0) with $P^{Cy}{}_2N^{Ph}{}_2$

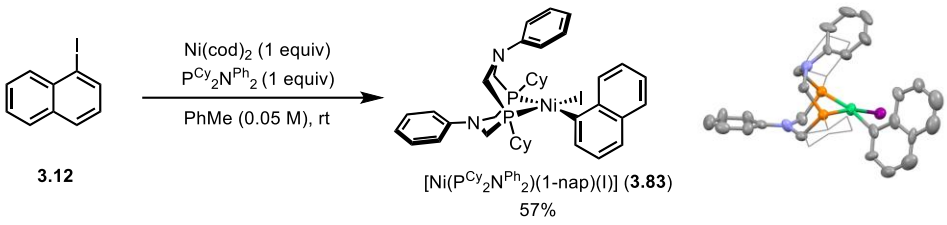

Thermal displacement plot is shown with ellipsoids at 50% probability and the cyclohexyl phosphorus substituents are depicted as wireframe. For clarity, hydrogen atoms were removed. Depictions with atom labels along with tables of selected bond lengths and angles for 3.83 are provided in Section 3.9.3 Crystal structure was of poor resolution but does confirm absolute connectivity.

3.6.3 Catalytic experiments with $P^{Cy}{}_2N^{Ph}{}_2$ as a ligand

At this stage, it was important to establish whether $P^{Cy}{}_2N^{Ph}{}_2$ is an appropriate surrogate for $P^{Cy}{}_2N^{ArCF3}{}_2$. Even if it isn't the optimal ligand, as long as some catalytic activity is observed with this ligand, we believe that subsequent studies with [Ni($P^{Cy}{}_2N^{Ph}{}_2$)(1-nap)(I)] (**3.83**) will be representative of the mechanism with $P^{Cy}{}_2N^{ArCF3}{}_2$.

Table 3.7 indicates that $P^{Cy}{}_2N^{Ph}{}_2$ is a superior ligand to $P^{Cy}{}_2N^{ArCF3}{}_2$ in a coupling between 1-iodonapthalene (**3.12**) and 3-oxetanone (**3.84**), with conditions derived from our group's work on 1,2-addition to isatins.[27] The combined results suggest that reductive hydrodehalogenation to form naphthalene (**3.85**) is less prevalent with $P^{Cy}{}_2N^{Ph}{}_2$ and that the crude yield of desired product **3.86** is higher with $P^{Cy}{}_2N^{Ph}{}_2$. While these conditions are still unoptimized, they do indicate that $P^{Cy}{}_2N^{Ph}{}_2$ is an appropriate model for mechanistic studies of nickel-catalyzed arylation of carbonyls.

Table 3.7 Comparing $P^{Cy}{}_2N^{Ph}{}_2$ and $P^{Cy}{}_2N^{ArCF3}{}_2$

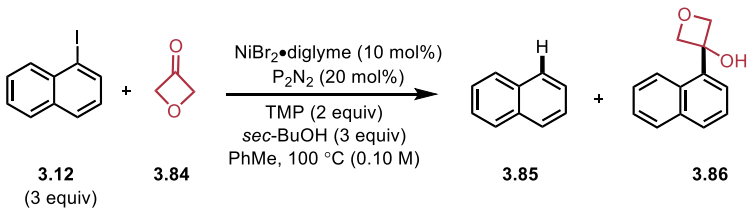

3.12 (3 equiv) **3.84** **3.85** **3.86**

entry	P_2N_2	3.12 (GC-FID)[a]	3.85 (GC-FID)[a]	3.86 (GC-FID)[a]	yield 3.86 (%)[b]
1	$P^{Cy}{}_2N^{ArCF3}{}_2$	1.29	1.09	0.39	30
2	$P^{Cy}{}_2N^{Ph}{}_2$	2.23	0.26	0.58	42

General reaction conditions: 1-iodonaphthalene (0.15 mmol), 3-oxetanone (0.05 mmol), TMP (0.1 mmol), *sec*-BuOH (0.15 mmol), $NiBr_2$•diglyme (10 mol%), P_2N_2 (20 mol%) in toluene (0.10 M), 100 °C for 16 h. 0.05 mmol 1,3,5-trimethoxybenzene as internal standard.[a] Crude GC-FID product/I.S. ratios are presented. [b] Crude NMR yield determined using 0.05 mmol 1,3,5-trimethoxybenzene as internal standard.

A high-temperature NMR study of the reaction presented in Table 3.7 (entry 2) was performed to see if key catalytic intermediates could be observed and, more generally, if the reaction would proceed in an NMR tube without stirring. The reaction temperature was lowered to 75 °C (Scheme 3.17) and the reaction was run in d_8-PhMe. The crude results are summarized in Section 3.9.5. No reaction was observed at room temperature. Upon reaching 75 °C, the oxidative addition complex (**3.83**) was formed, with free ligand also observed in solution. This makes sense, as it is assumed that **3.83**, a square planar 16 electron Ni(II) complex, cannot accommodate a second equivalent of bidentate ligand around the metal centre. After five hours of reaction at 75 °C, only a trace amount of product was observed but it was slowly increasing with each time interval. The NMR tube was removed from the spectrometer and heated in an oil bath at 100 °C overnight. The NMR tube was cooled to room temperature around 12 hours later and directly analyzed by NMR without exposing the solution to air. The solution was diamagnetic

and it appeared that the only phosphorus containing species dissolved was free ligand and a species which has tentatively been assigned as [Ni($P^{Cy}_2N^{Ph}_2$)$_2$] by analogy to **3.82**. Notably, we did not observe formation of a nickel alkoxide (**3.87**) nor a nickel hydride intermediate (**3.88**) throughout the course of the reaction. It could be that these species are short-lived or in low concentration at any given point to not be seen with NMR in the reaction of intermediate **3.83** with ketone **3.84**.

Scheme 3.17 High temperature NMR study

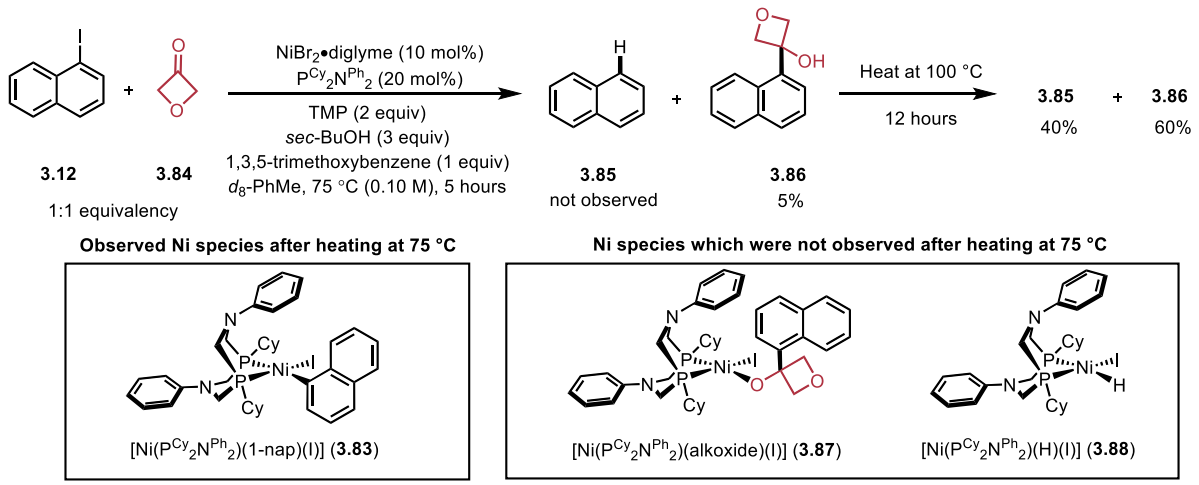

General reaction conditions: 1-iodonaphthalene (0.05 mmol), 3-oxetanone (0.05 mmol), TMP (0.10 mmol), *sec*-BuOH (0.15 mmol), $NiBr_2$•diglyme (10 mol%), $P^{Cy}_2N^{Ph}_2$ (20 mol%) in toluene (0.10 M), 100 °C for 16 h. 0.05 mmol 1,3,5-trimethoxybenzene added as internal standard. Crude NMR yields reported.

3.6.4 Catalytic experiment with [Ni($P^{Cy}_2N^{Ph}_2$)(1-nap)(I)]

As $P^{Cy}_2N^{Ph}_2$ appears to be an effective ligand for 1,2-carbonyl addition, the oxidative addition complex [Ni($P^{Cy}_2N^{Ph}_2$)(1-nap)(I)] **3.83** was next studied as a precatalyst for the reductive coupling of aldehydes with aryl iodides (Scheme 3.18). Carbinol product **3.90** was obtained in 52% crude yield with minimal hydrodehalogenation (**3.85**). This result is highly representative of the coupling presented in Chapter 2 and roughly ten catalytic turnovers were achieved.

Based on the reactivity of the OAC (Scheme 3.18), we can conclude that it is an effective precatalyst. From a mechanistic viewpoint, this unambiguously means that **3.83** is able to form a catalytically active species. **3.83** could be a direct intermediate on our catalytic cycle (as proposed in Scheme 2.7 and Scheme 3.8) or it could be further transformed to be on-cycle (Eg. two equivalents of **3.83** disproportionate to Ni(I) and Ni(III), respectively). Further detailed mechanistic experiments with **3.83** may unravel additional information about the arylation of aldehydes and primary alcohols.

Scheme 3.18 Testing **3.83** as a precatalyst

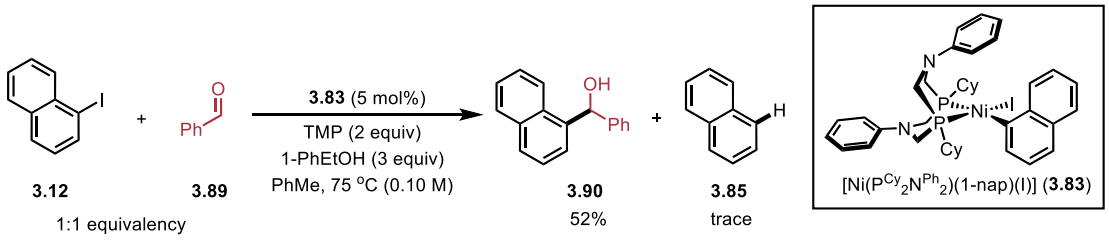

Reaction conditions: 1-iodonaphthalene (0.10 mmol, 1 equiv, 14.6 µL), benzaldehyde (0.10 mmol, 1 equiv, 10.6 µL), TMP (0.2 mmol, 2 equiv, 43.0 µL), [Ni($P^{Cy}_2N^{Ph}_2$)(1-nap)(I)] (0.005 mmol, 5 mol%, 3.9 mg), toluene (0.10 M, 1 mL), 75 °C for 16 h. Yields determined by crude ^{1}H NMR using 0.05 mmol 1,3,5, trimethoxybenzene as internal standard.

3.6.5 η^2-Carbonyl coordination complexes

Another angle to study nickel P_2N_2 complexes would be to prepare η^2-carbonyl complexes and test their reactivity. Recently, the characterization and isolation of well-defined η^2-aldehyde nickel complexes with a range of monodentate phosphines was reported by Doyle and coworkers.[35] Inspired by this work, we attempted to prepare the analogous Ni(P_2N_2) species (Scheme 3.19). We also prepared a nickel dcype η^2-aldehyde complex in situ from Ni(cod)$_2$ (Scheme 3.19A) as a control. While complex **3.92** has limited literature reports,[36] the crude $^{31}P\{^1H\}$ peaks are in agreement with a closely-related [Ni(dippe)(η^2-benzaldehyde)] complex, where dippe = 1,2-bis(diisopropylphosphino)ethane.[37] We found that, in contrast to dcype, $P^{Cy}_2N^{ArCF3}_2$ did not afford the η^2-benzaldehyde complex with 1.5 equivalent of piperonal and the main species in solution was [Ni($P^{Cy}_2N^{ArCF3}_2$)(cod)] (**3.76**). Using solvent quantities of benzaldehyde, a liquid aldehyde, afforded a range of new peaks by $^{31}P\{^1H\}$ (see Section 3.9.6), suggesting that addition of large quantities of the aldehyde creates a variety of new species.

So far, we have been unable to isolate a well-defined Ni(P_2N_2)(η^2-carbonyl) complex. This result could shed some light into the properties of nickel $P^{Cy}_2N^{ArCF3}_2$ complexes. When dcype was used as a ligand, aldehyde binding appears to be nearly quantitative with 1.5 equivalents of benzaldehyde (Scheme 3.19A). Aldehydes and ketones have been proposed to be catalyst poisons in some related cross-couplings.[38] The reluctance of [Ni($P^{Cy}_2N^{ArCF3}_2$)(cod)] (**3.76**) to bind carbonyls (Scheme 3.19B and Scheme 3.19C) could allow for other species, namely an aryl iodide, to bind and react with nickel. As new peaks were observed when solvent quantities of aldehyde were employed (Scheme 3.19C), this doesn't preclude productive π-bond insertion as a

reasonable step in the catalytic cycle, but it should be noted that non trivial amounts of **3.76** were still present in solution.

Scheme 3.19 Qualitative results for η²-benzaldehyde coordination complexes

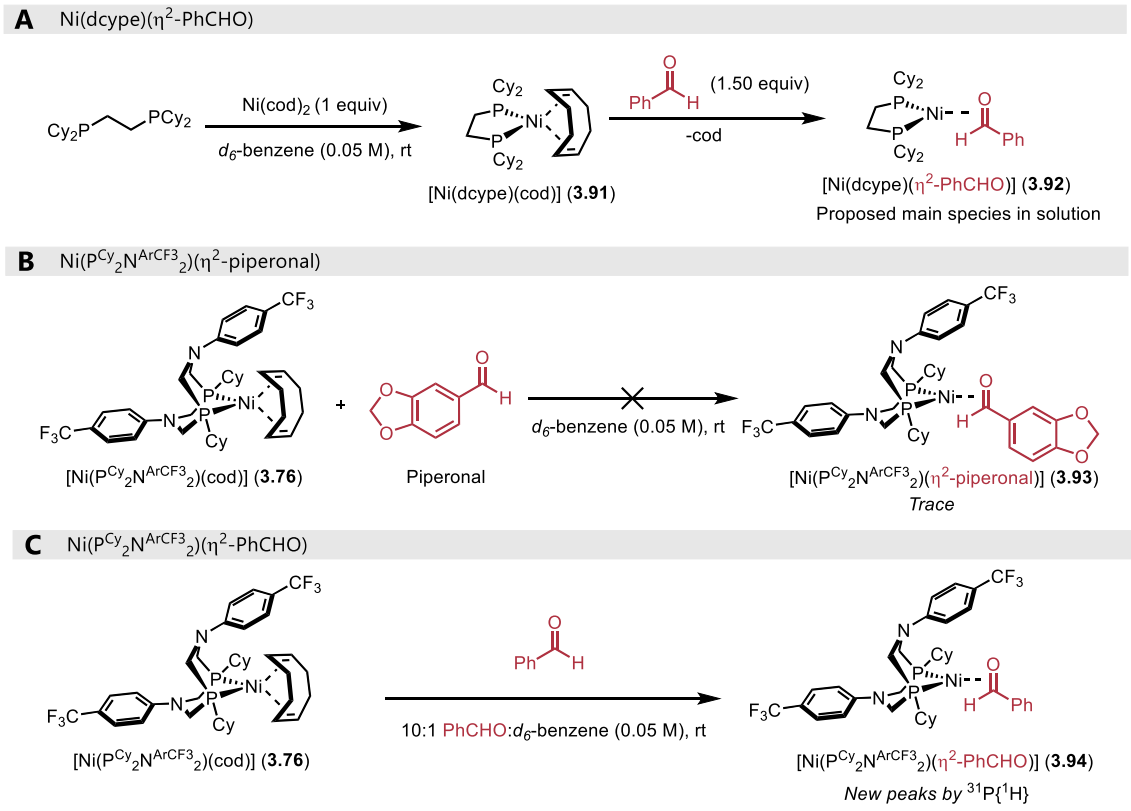

3.7 Conclusions, advancement in the field, and future work

Since the publication of our work, the direct α-arylation of primary alcohols with aryl halides has not seen any major advancements yet. While our conditions are robust and enabled general synthesis of a wide range of secondary alcohols, the optimized catalyst system does require a significantly large excess of $P^{Cy}{}_2N^{ArCF3}{}_2$ (30 mol%; 3 equiv relative to Ni centre) and primary alcohol (2.5 equivalents). Ideally, future research into this area will find more efficient conditions which allow for lowered catalyst loading or decreased equivalency of primary alcohol. While we reported a broad substrate scope, the redox-neutral α-arylation of primary alcohols is more limited in scope than the related reductive arylation of aldehydes (Chapter 2). We hypothesize that coordinating functional groups are more problematic for the redox-neutral α-arylation as the primary alcohol is presumed to be less coordinating than an aldehyde. Nonetheless, despite these shortcomings, we believe that our direct α-arylation of primary alcohols represents a powerful transformation that highlights our ability to control oxidation states with Ni/P_2N_2 catalyst system.

While some mechanistic aspects of the P_2N_2 ligands have been uncovered, there is still more work to be done to get a cohesive picture. By learning more about the reactions described in Chapters 2 and 3, broad extension of the work to ketones may be possible.

3.7.1 Future mechanistic work: Kinetics of hydrodehalogenation vs. carbonyl insertion

With the discovery of a stable oxidative addition complex, kinetic experiments can be run to compare the rate of direct reduction of an aryl iodide with the rate of aldehyde insertion

(Scheme 3.20). Ideally, this data would support that the rate of direct reduction of the oxidative addition complex is kinetically slower than arylation of the aldehyde. We assume that this will be the case, as our optimized ligand $P^{Cy}_2N^{ArCF3}_2$ appeared to suppress the direct reduction of aryl iodide in both the reductive and redox-neutral couplings. However, having experimentally-derived rates would provide deeper insight into how the pathways depicted in Scheme 3.20 differ energetically. THF was selected as the solvent for this hypothetical reaction, as THF performed similarly to PhMe (see Table 2.3) and **3.83** has increased solubility in THF.

Scheme 3.20 Stoichiometric kinetic experiments with OAC

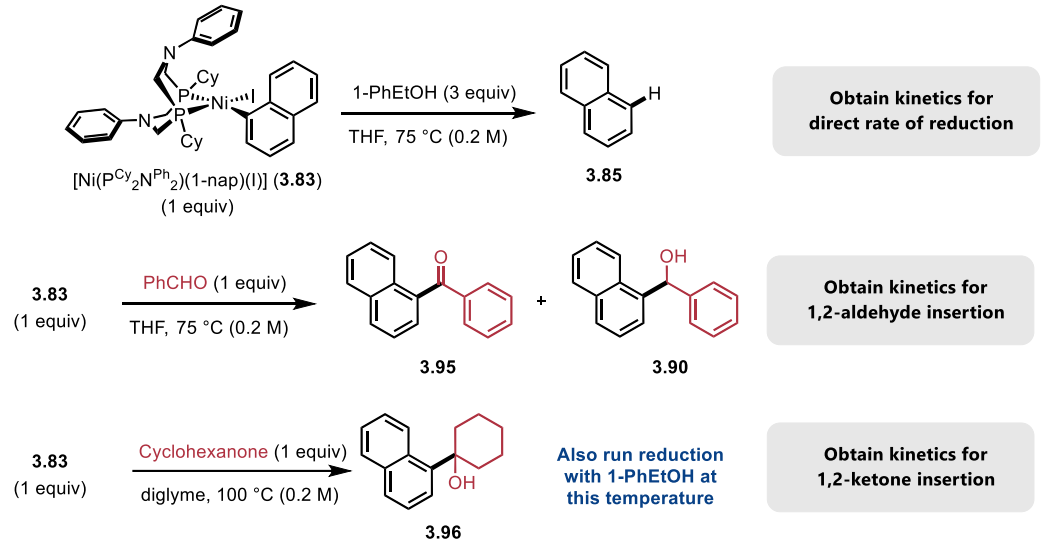

We anticipate that reaction with benzaldehyde could result in a mixture of redox-neutral (**3.95**) and reduced (**3.90**) products. As a result, each product would be analyzed independently. Finally, to learn more about 1,2-ketone addition, the relative rate of 1,2-addition could be studied and compared to the rate of direct reduction at an increased temperature. The results from this experiment may indicate why ketones are less effective coupling partners than aldehydes.

3.7.2 Preparation of a well-defined Ni(I) P_2N_2 precatalyst

Doyle and colleagues have recently reported a convenient method to directly prepare Ni(I) complexes from $Ni(cod)_2$ (Scheme 3.21).[39] Their protocol allows for isolation of [Ni(dppf)Br] – in theory, we could access [Ni(P_2N_2)Br] complexes through this method. However, there is no guarantee that the corresponding Ni(I) complexes will be stable or isolable. If they could be cleanly isolated and fully characterized, their catalytic ability could be assessed. The initial rates of reaction between a nickel(0) and nickel(I) precatalyst could be compared to see if there is any variance. Evidence of an induction period with one precatalyst and absence of an induction period with the other precatalyst could provide further insight into the oxidation state of our on-cycle nickel species. To the best of our knowledge, no P_2N_2 complexes of Ni(I) have been reported.

Scheme 3.21 Preparation of Ni(I) complexes

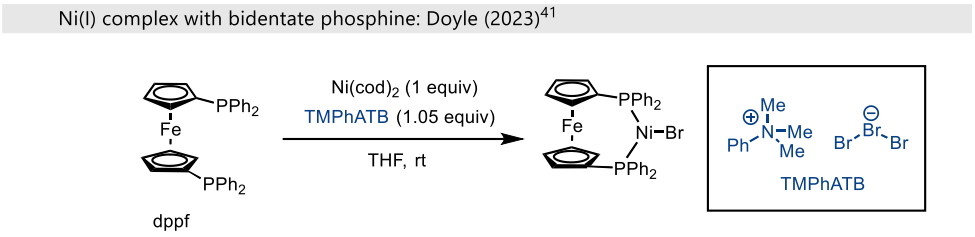

3.7.3 Isolation and characterization of well-defined Ni-hydride or Ni-alkoxide species

While we have managed to isolate and characterize some Ni(P_2N_2) complexes, we have yet to isolate, let alone observe, a nickel alkoxide or a nickel hydride species bound to a P_2N_2 ligand. These intermediates are proposed to be part of our catalytic cycle (Scheme 3.8) and a method to cleanly isolate them for further stoichiometric or catalytic studies would be highly desirable. One possibility is that these species are very short-lived or unstable.

A recent review has showcased synthetic methods and approaches to preparing nickel hydride species.[40] Notably, a $[HNi(P_2N_2)_2]^{2+}$ complex has been isolated and fully characterized.[41] This indicates that we may be able to make an analogous compound for mechanistic study. Isolation of $[HNi(P^{Cy}_2N^{ArCF3}_2)_2]^{2+}$ or the corresponding complex with a closely-related P_2N_2 ligand could be a worthwhile entry-point into accessing Ni-H species. In theory, $[HNi(P_2N_2)_2]^{2+}$should be a competent precatalyst – we would assume that one P_2N_2 ligand would be displaced in solution and that nickel would be reduced in situ to Ni(0) to form an active catalyst. This process could be monitored by $^{31}P\{^1H\}$ NMR to see key events such as loss of a ligand, formation of Ni(0) and subsequent oxidative addition to Ni(II).

To the best of our knowledge, there are no reports of Ni(P_2N_2) alkoxide complexes. β-hydride elimination of a nickel alkoxide could be problematic, assuming the compound has β-hydrogens. However, this could also be another entry point to accessing Ni-H compounds. Alternatively, alkoxides derived from tertiary alcohols could be used to isolate less reactive Ni-alkoxides, as they lack β-hydrogens. Some attempts to isolate Ni(II) alkoxide complexes have been performed thus far with no strong evidence of formation; however, this is an active area of research.

The exact mechanism for how the nickel inserts into a carbonyl remains as a blind spot in our catalytic cycle. We have identified that an oxidative addition complex, $[Ni(P^{Cy}_2N^{Ph}_2)(1\text{-nap})(I)]$ (**3.83**), is an effective precatalyst for the arylation of an aldehyde. However, we have been unable to observe any further intermediates on the catalytic cycle by NMR spectroscopy. We hope that

by targeted synthesis of Ni(P_2N_2) complexes, we will be able to get a better picture for our transformation and why $P^{Cy}{}_2N^R{}_2$ ligands perform better than other ligands.

3.8 α-Arylation: Experimental

Unless otherwise indicated, reactions were conducted under an atmosphere of nitrogen in 8 mL screw-capped vials that were oven-dried (120 °C) or flame-dried and shipped into a glovebox. Column chromatography was performed manually using Silicycle F60 40−63 μm silica gel. Analytical thin layer chromatography (TLC) was conducted with aluminum-backed EMD Millipore Silica Gel 60 F_{254} pre-coated plates. Visualization of developed plates was performed under UV light (254 nm). For certain purifications, cerium ammonium molybdate (CAM) or potassium permanganate ($KMnO_4$) stains were used to better visualize the compounds on the TLC plates. The synthesis of P_2N_2 ligands is discussed in Chapter 5. The synthesis of starting materials is fully described in the freely available Supporting Information. (https://pubs.acs.org/doi/10.1021/jacs.1c05661).

3.8.1 Instrumentation

^{1}H NMR and ^{13}C NMR were recorded on a Bruker AVANCEII 300 MHz spectrometer, a Bruker AVANCEII 400 MHz spectrometer, or a Bruker AVANCEIII 500 MHz spectrometer. ^{1}H NMR spectra were internally referenced to the residual solvent signal (e.g., $CDCl_3$ = 7.27 ppm). ^{13}C NMR spectra were internally referenced to the residual solvent signal (e.g., $CDCl_3$ = 77.00 ppm). Data for ^{1}H NMR are reported as follows: chemical shift (δ ppm), multiplicity (s = singlet, d = doublet, t = triplet, q = quartet, m = multiplet), coupling constant (Hz), integration. NMR yields for optimization studies were obtained by ^{1}H NMR analysis of the crude reaction mixture using 1,3,5-trimethoxybenzene as an internal standard. IR spectra were obtained using a Cary 630 FTIR (Agilent Technologies) and are reported in terms of frequency of absorption (cm^{-1}). Melting point

ranges were determined on a Canlab Gallen Kamp Melting Point Apparatus. Accurate mass data (EI) were obtained from an Agilent 5977A GC/MSD using MassWorks 4.0 from CERNO Bioscience.[42] HRMS data were obtained from a Micromass Q-TOF 2 quadrupole – time-of-flight mass spectrometer with ESI source.

Note: After completion and publication of some of the data described below, it was noticed that the error (in ppm) of several of the Accurate Mass measurements was too large to allow conclusive confirmation of the proposed molecular formula. We regret this mistake. We are still confident in the conclusions made in the data for the following reasons:

1. All molecules previously reported matched the literature.
2. Some functional groups are not amenable to MS accurate analysis and have lower than normal spectral accuracy (aliphatic compounds, boron-containing compounds and polyhalogenated groups).
3. The instrument might not have been tuned when the samples were run, or they might have been too dilute for accurate analysis

3.8.2 Optimization Procedure (Section 3.5.1)

Inside the glovebox, to a dry 8 mL screw-capped reaction vial equipped with a magnetic stir bar, $NiBr_2$•diglyme (0.10 equiv, 0.03 mmol, 10.6 mg) and ligand (0.30 equiv, 0.09 mmol) were added and dissolved in toluene (1.5 mL). Base (2 equiv, 0.6 mmol) and aryl iodide (1 equiv, 0.3 mmol) were added to the stirring solution followed by the alcohol (2.5 equiv, 0.75 mmol). The vial was capped, removed from the glovebox, and placed in a stirring (350 rpm) mineral oil bath

pre-heated to 75 °C. After stirring for 16 hours, the reaction vial was removed from the oil bath and cooled to room temperature. 1,3,5-trimethoxybenzene (0.05 mmol) was added as an internal standard and diluted with ethyl acetate. The reaction was filtered through a plug of silica gel with thin layers of sodium sulfate and Celite at the bottom of the frit. For very polar products, a mixture of ethyl acetate and acetone was used to flush the compound off the silica gel. The filtrate was diluted to an appropriate concentration and analyzed by GC-MS. Solvent was removed *in vacuo* and the sample was analyzed by NMR spectroscopy.

3.8.3 General Procedure: The redox-neutral α-arylation of primary alcohols

Inside the glovebox, to a dry 8 mL screw-capped reaction vial equipped with a magnetic stir bar, $NiBr_2$•diglyme (0.10 equiv, 0.03 mmol, 10.6 mg) and $P^{Cy}{}_2N^{ArCF3}{}_2$ (0.30 equiv, 0.09 mmol, 54.2 mg) were added and dissolved in toluene (1.5 mL). Solution was stirred. 2,2,6,6-tetramethyl piperidine (2 equiv, 0.6 mmol, 84.7 mg) and aryl iodide (1 equiv, 0.3 mmol) were added to the vial followed by primary alcohol (2.5 equiv, 0.75 mmol). The vial was capped, removed from the glove box, and placed in a stirring (350 rpm) mineral oil bath pre-heated to 75°C. After stirring for 16 hours, the reaction vial was removed from the oil bath and cooled down to room temperature. An aliquot was filtered through silica and analyzed by GC-MS to assess crude alcohol:ketone ratio. The reaction was diluted with DCM, dried *in vacuo*, and purified by column chromatography.

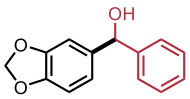

(1,3-Benzodioxol-5-yl)(phenyl)methanol (3.3) was prepared according to the general procedure. The product was purified by column chromatography with 5% to 25% Et_2O in hexanes to afford **3.3** as a colourless oil (37.0 mg, 54%).**^{1}H NMR** ($CDCl_3$, 400 MHz) δ (ppm) 7.40-7.32 (m, 4H), 7.30-7.25 (m, 2H), 6.87-6.84 (m, 2H), 6.79-6.76 (m, 1H), 5.94 (q, J = 1.3 Hz, 2H), 5.77 (s, 1H), 2.21 (br, s, 1H). **^{13}C NMR** ($CDCl_3$, 100 MHz) δ (ppm) 147.8, 147.0, 143.8, 138.0, 128.4, 127.5, 126.3, 120.0, 108.0, 107.2, 101.0, 76.0. Characterization of **3.3** matched previously reported spectra.[43]

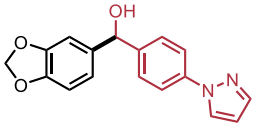

2H-1,3-benzodioxol-5-yl(4-(1H-Pyrazol-1-yl)phenyl)methanol (3.16) was prepared according to the general procedure. The product was purified by column chromatography with 5% to 7.5% acetone in PhMe to afford **3.16** as a clear oil (57.9 mg, 66% yield).**^{1}H NMR** ($CDCl_3$, 400 MHz) δ (ppm) 7.88 (d, J = 2.4 Hz, 1H), 7.70 (d, J = 1.6 Hz, 1H), 7.61 (d, J = 8.4 Hz, 2H), 7.40 (d, J = 8.6 Hz, 2H), 6.85-6.81 (m, 2H), 6.77-6.74 (m, 1H), 6.45 (t, J = 2.1 Hz, 1H), 5.92 (q, J = 1.3 Hz, 2H), 5.76 (s, 1H), 2.91 (br, s, 1H). **^{13}C NMR** ($CDCl_3$, 100 MHz) δ (ppm) 147.8, 147.0, 142.2, 141.0, 139.3, 137.8, 127.4, 126.8, 120.0, 119.2, 108.1, 107.5, 107.1, 101.0, 75.3. **FT-IR ν (cm^{-1})** 3344, 2893, 1607, 1500, 1473, 1413, 1329, 1228, 1204, 1150, 1105, 1072, 1031, 930, 854, 828, 775, 688. **Accurate mass (EI)**: $H_{14}C_{17}N_2O_3$ Theoretical: 294.0999. Found: 294.0961. Spectral Accuracy: 98.4%.

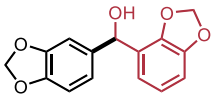

α-1,3-benzodioxol-5-yl-1,3-Benzodioxole-4-methanol (3.17) was prepared according to the general procedure. The product was purified by column chromatography with 30% to 45% EtOAc in Hexanes to afford **3.17** as an opaque oil (63.9 mg, 78% yield).**^{1}H NMR** ($CDCl_3$, 400 MHz) δ (ppm) 6.93 (d, J = 1.6 Hz, 1H), 6.90-6.86 (m, 2H), 6.83 (t, J = 7.7 Hz, 1H), 6.78-6.75 (m, 2H), 5.96-5.93 (m, 4H), 5.87 (s, 1H), 2.52 (br s, 1H). **^{13}C NMR** ($CDCl_3$, 100 MHz) δ (ppm) 147.9, 147.5, 147.2, 136.9, 125.7, 121.9, 119.9, 119.5, 108.2, 108.0, 107.2, 101.14, 101.11, 71.6. **FT-IR ν (cm^{-1})** 3408, 2886, 2779, 2036, 1672, 1601, 1501, 1486, 1456, 1441, 1355, 1236, 1167, 1124, 1096, 1033, 973, 930, 867, 837, 761, 727. **Accurate mass (EI)** $H_{15}C_{12}O_5$ Theoretical: 272.0798. Found: 272.0679. Spectral Accuracy: 98.9%

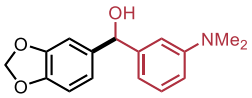

(1,3-Benzodioxol-5-yl)[3-(Dimethylamino)phenyl]methanol (3.18) was prepared according to the general procedure. The product was purified by column chromatography with 1.5% to 10% acetone in PhMe to afford **3.18** as a yellow oil (60.5 mg, 74% yield).**^{1}H NMR** ($CDCl_3$, 400 MHz) δ (ppm) 7.22 (t, J = 7.9 Hz, 1H), 6.90-6.86 (m, 2H), 6.81-6.79 (m, 1H), 6.77 (d, J = 7.9 Hz, 1H), 6.71 (d, J = 7.6 Hz, 1H), 6.67 (dd, J = 2.4 Hz, 8.3 Hz, 1H), 5.92 (q, J = 0.7 Hz, 2H), 5.69 (s, 1H), 2.95 (s, 6H), 2.40 (br s, 1H). **^{13}C NMR** ($CDCl_3$, 100 MHz) δ (ppm) 150.7, 147.6, 146.7, 144.8, 138.2, 129.1, 119.9, 114.7, 111.8, 110.4, 107.9, 107.2, 100.9, 76.3, 40.6. **FT-IR ν (cm^{-1})** 3378, 2882, 2804, 1600, 1579, 1499, 1484, 1437, 1353, 1232, 1124, 1092, 1035, 993, 982, 925, 861, 809, 768, 744, 734, 716, 697. **Accurate mass (EI):** $H_{17}C_{16}NO_3$ Theoretical: 271.1266. Found: 271.1203. Spectral Accuracy: 98.9%

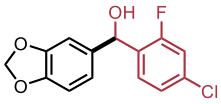

α-(4-chloro-2-fluorophenyl)-1,3-Benzodioxole-5-methanol (3.19) was prepared according to the general procedure. The product was purified by column chromatography with 1.5% acetone in PhMe to afford **3.19** as a yellow oil (64.1 mg, 76% yield).**^{1}H NMR** ($CDCl_3$, 400 MHz) δ (ppm) 7.48 (t, J = 8.2 Hz, 1H), 7.15 (dd, J = 1.9 Hz, 8.3 Hz, 1H), 7.04 (dd, J = 2.0 Hz, 10.0 Hz, 1H), 6.85-6.82 (m, 2H), 6.77-6.74(m, 1H), 5.97 (s, 1H), 5.93 (q, J = 1.5 Hz, 2H), 2.46 (br, s, 1H). **^{13}C NMR** ($CDCl_3$, 100 MHz) δ (ppm) 159.4 (d, J = 250.0 Hz). 147.8, 147.2, 136.3, 133.9 (J = 10.3 Hz), 129.7 (J = 13.1 Hz), 128.1 (d, J = 5.0 Hz), 124.6 (d, J = 3.5 Hz), 119.9 (d, J = 0.5 Hz), 116.1 (d, J = 25.1 Hz), 108.2, 106.9, 101.1, 69.4 (d, J = 2.9 Hz). **FT-IR ν (cm^{-1})** 3294, 2899, 1609, 1579, 1503, 1482, 1443, 1404, 1320, 1240, 1223, 1184, 1120, 1094, 1072, 1036, 1020, 925, 893, 857, 815, 796, 779. **Accurate mass (EI)**: $H_{10}C_{14}ClFO_3$ Theoretical: 280.0323. Found: 280.0297. Spectral Accuracy: 98.9%

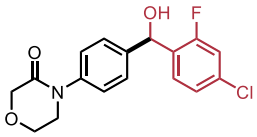

4-[4-(hydroxymethyl(α-(4-chloro-2-fluorophenyl))phenyl]-3-Morpholinone (3.20) was prepared according to the general procedure. The product was purified by column chromatography with 20% acetone in PhMe to afford an orange oil. A second column was run with 50% to 100% EtOAc in Hexanes to afford **3.20** as a colourless oil (74.5 mg, 74% yield).**^{1}H NMR** ($CDCl_3$, 400 MHz) δ (ppm) 7.45 (t, J = 8.2 Hz, 1H), 7.38 (d, J = 8.5 Hz, 2H), 7.26 (d, J = 8.5 Hz, 2H), 7.13 (dd, J = 1.8 Hz,

8.5 Hz, 1H), 7.04 (dd, *J* = 2.0 Hz, 10.0 Hz, 1H), 5.99 (s, 1H), 4.28 (s, 2H), 4.01-3.97 (m, 2H), 3.73-3.69 (m, 2H), 3.22 (br, s, 1H). **^{13}C NMR** ($CDCl_3$, 100 MHz) *δ* (ppm) 166.8, 159.3 (d, *J* = 250.0 Hz), 141.5, 140.5, 133.9 (d, *J* = 10.3 Hz), 129.6 (d, *J* = 13.4 Hz), 128.4 (d, *J* = 5.0 Hz), 127.2, 125.4, 124.7 (d, *J* = 3.5 Hz), 166.0 (d, *J* = 25.2 Hz), 68.7 (d, *J* = 2.8 Hz), 68.4, 64.0, 49.5. **^{19}F NMR** ($CDCl_3$, 100 MHz) *δ* (ppm) -115.9. **FT-IR ν (cm^{-1})** 3370, 2869, 2246, 1646, 1607, 1579, 1508, 1482, 1409, 1325, 1237, 1219, 1178, 1124, 1070, 1040, 1016, 995, 921, 897, 856, 820, 794, 727, 680. **Accurate mass (EI)** $H_{15}C_{17}ClFNO_3$ Theoretical: 335.0719. Found: 335.0690. Spectral Accuracy: 96.7%.

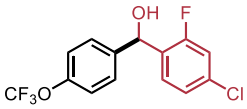

4-chloro-2-fluoro-α-[4-(trifluoromethoxy)phenyl]-Benzenemethanol (3.21) was prepared according to the general procedure. The product was purified by column chromatography with 0.5% to 2.5% acetone in PhMe to afford **3.21** as a colourless oil (68.2 mg, 71% yield).**^{1}H NMR** ($CDCl_3$, 400 MHz) *δ* (ppm) 7.44 (t, *J* = 8.2 Hz, 1H), 7.40 (d, *J* = 8.2 Hz, 2H), 7.22-7.15 (m, 3H), 7.07(dd, *J* = 2.0 Hz, 10.0 Hz), 6.08 (s, 1H), 2.53 (br, s, 1H). **^{13}C NMR** ($CDCl_3$, 100 MHz) *δ* (ppm) 159.4 (d, *J* = 249.9 Hz), 148.8 (d, *J* = 1.7 Hz), 140.9, 134.4 (d, *J* = 10.4 Hz), 129.3 (d, *J* = 13.3 Hz), 128.3 (d, *J* = 4.9 Hz), 127.8, 124.9 (d, *J* = 3.5 Hz), 121.0, 120.4 (d, *J* = 257.3 Hz), 116.3 (d, *J* = 25.0 Hz), 68.9 (d, *J* = 2.9 Hz) **^{19}F NMR** *δ* (ppm) -57.8, -115.9. **FT-IR ν (cm^{-1})** 3335, 1611, 1579, 1508, 1484, 1411, 1253, 1210, 1154, 1076, 1033, 1016, 898, 859, 817, 790, 677. **Accurate mass (EI)** $H_9C_{14}ClF_4O_2$ Theoretical: 320.0222. Found: 320.0239. Spectral Accuracy: 98.2%

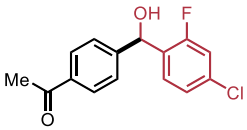

1-[4-[(2-Fluoro-4-Chlorophenyl)hydroxymethyl]phenyl]ethanone (3.22) was prepared according to the general procedure. The product was purified by column chromatography with 2.5% acetone in PhMe to afford **3.22** as a yellow viscous oil (74.0 mg, 89% yield). **^{1}H NMR** ($CDCl_3$, 400 MHz) *δ* (ppm) 7.91 (d, *J* = 8.3 Hz, 2H), 7.48 (d, *J* = 8.2 Hz, 2H), 7.44 (t, *J* = 8.1 Hz, 1H), 7.15 (d, *J* = 8.3 Hz, 1H), 7.06 (dd, *J* = 1.8 Hz, 10.0 Hz, 1H), 6.15 (s, 1H), 2.57 (s, 3H). **^{13}C NMR** ($CDCl_3$, 100 MHz) *δ* (ppm) 197.8, 159.4 (d, *J* = 250.0 Hz), 147.5, 136.5, 134.4 (d, *J* = 10.3 Hz), 129.1 (d, *J* = 13.4 Hz), 128.7, 128.5 (d, *J* = 4.8 Hz), 126.3, 124.9 (d, *J* = 3.5 Hz), 116.2 (d, *J* = 25.1 Hz), 69.1 (d, *J* = 2.8 Hz), 26.6. **^{19}F NMR** *δ* (ppm) -115.9. **FT-IR ν (cm^{-1})** 3363, 1663, 1605, 1577, 1478, 1406, 1359, 1309, 1269, 1228, 1189, 1171,

1126, 1074, 1057, 1016, 956, 893, 856, 824, 790, 745, 695. **Accurate mass (EI)** $H_{12}C_{15}ClFO_2$ Theoretical: 278.0504. Found: 278.0578. Spectral Accuracy: 97.2%

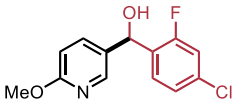

α-(4-chloro-2-fluorophenyl)-6-methoxy-3-Pyridinemethanol (3.23) was prepared according to the general procedure. The product was purified by column chromatography with 2.5% to 8.5% acetone in PhMe to afford **3.23** as a dark oil (52.7 mg, 66% yield).**^{1}H NMR** ($CDCl_3$, 400 MHz) δ (ppm) 8.13 (d, *J* = 1.9 Hz, 1 H), 7.57-7.49 (m, 2H), 7.17 (dd, *J* = 1.4 Hz, 8.3 Hz, 1H), 7.05 (dd, *J* = 2.0 Hz, 10.0 Hz, 1H), 6.71 (d, *J* = 8.6 Hz, 1H), 6.04 (s, 1H), 3.91 (s, 3H), 2.60 (br, s, 1H). **^{13}C NMR** ($CDCl_3$, 100 MHz) δ (ppm) 163.8, 159.3 (d, *J* = 250.0 Hz), 145.0, 137.2, 134.2 (d, *J* = 10.4 Hz), 130.7, 129.2 (d, *J* = 13.1 Hz), 128.0 (d, *J* = 4.8 Hz), 124.8 (d, *J* = 3.6 Hz), 116.2 (d, *J* = 24.9 Hz), 111.0, 67.3 (d, *J* = 3.0 Hz), 53.6. **^{19}F NMR** δ (ppm) -115.8. **FT-IR v (cm^{-1})** 3335, 2947, 2037, 1708, 1607, 1579, 1484, 1393, 1316, 1281, 1221, 1126, 1074, 1022, 897, 857, 824, 805, 785, 733, 675. **Accurate mass (EI)** $H_{11}C_{13}ClFNO_2$ Theoretical: 267.0457. Found: 267.0437. Spectral Accuracy: 98.8%

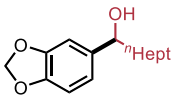

1-benzo[1,3]dioxol-5-yl-octan-1-ol (3.24) was prepared according a modified procedure. The crude reaction mixture was reduced with $NaBH_4$ and worked up as described in the literature.[21] The mixture was purified using column chromatography and the fractions were collected using a solvent system of 15% EtOAc in Hexanes to afford **3.24** as a colourless oil (56.3 mg, 75% yield). **^{1}H NMR** (($CDCl_3$, 400 MHz) δ (ppm) 6.86 (s, 1H), 6.79-6.74 (m, 2H), 4.57 (t, *J* = 7.0 Hz, 1H), 1.94 (br s, 1H), 1.82-1.73 (m, 1H), 1.69-1.62 (m, 1H), 1.42-1.19 (m, 10H), 0.89 (t, *J* = 7.1 Hz, 3H). **^{13}C NMR** ($CDCl_3$, 100 MHz) δ (ppm) 147.8, 146.8, 139.1, 119.3, 108.0, 106.4, 100.9, 74.6, 39.1, 31.8, 29.5, 29.2, 25.9, 22.6, 14.1. **FT-IR**: v (cm^{-1}) 3351, 2924, 2854, 1486, 1441, 1241, 1039, 936, 862, 809, 726, 635.**Accurate mass (EI):** $H_{15}C_{22}O_3$ Theoretical: 250.1563. Found: 250.1561. Spectral Accuracy: 95.0%.

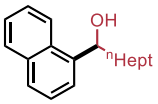

1-(naphthalen-5-yl)octan-1-ol (3.14) was prepared according to the general procedure. The product was purified by column chromatography with 10% EtOAc in hexanes to afford **3.14** as a colourless oil (52.3 mg, 68% yield). **^{1}H NMR** ($CDCl_3$, 400

MHz) δ (ppm) 8.14 (m, 1H), 7.89 (m, 1H), 7.79 (m, 1H), 7.65 (m, 1H), 7.56-7.47 (m, 3H), 5.46 (dd, J = 7.9, 3.0 Hz, 1H), 2.07 (br s, 1H), 1.99-1.86 (m, 2H), 1.62-1.45 (m, 1H), 1.49-1.41 (m, 1H), 1.39-1.24 (m, 1H), 1.39-1.24 (m, 1H), 0.90 (t, J = 6.9 Hz, 3H). **^{13}C NMR** ($CDCl_3$, 100 MHz) δ (ppm) 140.7, 133.9, 130.5, 128.9, 127.9, 125.9, 125.5, 125.4, 123.2, 122.8, 71.4, 38.4, 31.9, 29.6, 29.3, 26.3, 22.7, 14.1. Characterization of **3.14** matched previously reported spectra.[44]

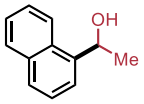

1-(naphthalen-1-yl)ethan-1-ol (3.25) was prepared according to the general procedure. The product was purified by column chromatography with 10% to 20% EtOAc in Hexanes to afford **3.25** as a colourless oil (35.1 mg, 68% yield). **^{1}H NMR** ($CDCl_3$, 400 MHz) δ (ppm) 8.14 (d, J = 7.6 Hz, 1H), 7.89 (m, 1H), 7.79 (d, J = 7.6 Hz, 1H), 7.69 (d, J = 6.9 Hz, 1H), 7.56-7.47 (m, 3H), 5.68 (q, J = 13.1, 6.6 Hz, 1H), 1.99 (br s, 1H), 1.68 (d, J = 6.6 Hz, 3H). **^{13}C NMR** ($CDCl_3$, 100 MHz) δ (ppm) 141.4, 133.8, 130.3, 128.9, 128.0, 126.1, 125.6, 125.5, 123.2, 122.0, 67.1, 24.4. Characterization of **3.25** matched previously reported spectra.[45]

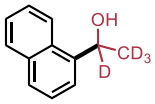

1-(naphthalen-1-yl)-d$_3$-ethan-1-d-ol (3.25-d$_4$) was prepared according to the general procedure E. The product was purified by column chromatography with 10% to 17% EtOAc in hexanes to afford **3.25-d$_4$** as a colourless oil (20.9 mg, 39% yield). **^{1}H NMR** ($CDCl_3$, 400 MHz) δ (ppm) 8.16-8.12 (m, 1H) , 7.91-7.87 (m, 1H), 7.80 (d, J = 8.2 Hz, 1H), 7.79 (dd, J = 7.2, 1.2 Hz, 1H), 7.57-7.47 (m, 3H), 1.88 (br s, 1H). **^{13}C NMR** ($CDCl_3$, 100 MHz) δ (ppm) 141.3, 133.8, 130.3, 128.9, 128.0, 126.1, 125.6, 125.5, 123.2, 122.0. **Accurate mass (EI):** $C_{12}H_8D_4O$ Theoretical: 176.1275. Found: 176.1134. Spectral Accuracy: 98.8%.

Note: C-D bound protons exhibit slow relaxation. Overnight experiments and setting interscan delay (D1) to 5 minutes did not show the "missing" aliphatic carbons. In the corresponding ^{13}C spectrum (*vide infra*) small multiplets (from C-D coupling) are observed at 66.7 and 23.5 ppm, which match the aliphatic peaks of compound **3.25**.

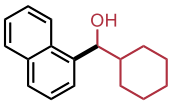

Cyclohexyl(naphthalen-1-yl)methanol (3.26) was prepared according to the general procedure. The product was purified by column chromatography with 10% EtOAc in hexanes to afford **3.26** as a colourless oil (56.2 mg, 78% yield). **^{1}H NMR** ($CDCl_3$,

400 MHz) δ (ppm) 8.16 (d, J = 7.4 Hz, 1H), 7.89 (d, J = 7.2 Hz, 1H), 7.79 (d, J = 8.1 Hz, 1H), 7.55-7.46 (m, 3H), 5.20 (d, J = 6.4 Hz, 1H), 2.01-1.89 (m, 3H), 1.78-1.64 (m, 3H), 1.44 (br s, 1H), 1.29-1.15 (m, 5H). **^{13}C NMR** ($CDCl_3$, 100 MHz) δ (ppm) 139.5, 133.9, 130.9, 128.9, 127.8, 125.8, 125.4, 125.3, 124.2, 123.7, 76.1, 44.4, 30.3, 28.3, 26.5, 26.3, 26.1. Characterization of **3.26** matched previously reported spectra.[46]

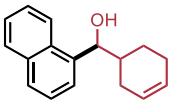

Cyclohex-3-en-1-yl(naphthalen-1-yl)methanol (3.27) was prepared according to the general procedure. The product was purified by column chromatography with 10% to 20% EtOAc in hexanes to afford **3.27** as a colourless oil (30.0 mg, 42% yield). **^{1}H NMR** ($CDCl_3$, 400 MHz) δ (ppm) (1.2:1 mixture of diastereomers): 8.19-8.14 (m, 1H), 7.86 (d, J = 8.2 Hz, 1H), 7.78 (d, J = 8.1 Hz, 1H), 7.61-7.57 (m, 1H), 7.51-7.44 (m, 3H), 5.66-5.53 (m, 2H), 5.29 (minor diastereomer, d, J = 6.4 Hz, 0.42 H), 5.22 (major diastereomer, d, J = 6.5 Hz, 0.53 H), 2.23 – 1.40 (m, 8H). **^{13}C NMR** ($CDCl_3$, 100 MHz) δ (ppm) 139.3, 133.9, 130.9, 130.8, 128.9, 128.1, 127.9, 127.2, 126.7, 126.4, 126.1, 125.9, 125.5, 125.4, 125.3, 124.4, 124.1, 123.7, 123.6, 75.7, 75.2, 40.32, 40.29, 28.8, 27.2, 26.2, 25.4, 25.0, 24.2. **FT-IR**: ν (cm^{-1}) 3405, 3020, 2913, 1702, 1596, 1509, 1435, 1208, 1043, 910, 777, 730. **Accurate mass (EI):** $H_{18}C_{17}O$ Theoretical: 238.1352. Found: 238.1424. Spectral Accuracy: 98.0%.

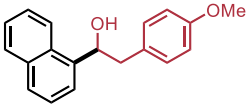

2-(4'-methoxyphenyl)-1-naphthalen-1-yl ethanol (3.28) was prepared according to the general procedure. The product was purified by column chromatography with 10% EtOAc in hexanes to afford **3.28** as a yellow semi-solid (70.9 mg, 85% yield). **^{1}H NMR** ($CDCl_3$, 400 MHz) δ (ppm) 8.15 (d, J = 8.3 Hz, 1H), 7.89 (d, J = 7.7 Hz, 1H), 7.79 (d, J = 8.2 Hz, 1H), 7.65 (d, J = 7.1 Hz, 1H), 7.57-7.46 (m, 3H), 7.19 (d, J = 8.5 Hz, 2H), 6.87 (d, J = 8.5 Hz, 2H), 5.62 (dd, J = 9.0 Hz, 3.5 Hz, 1H), 3.79 (s, 3H) 3.23 (dd, J = 14.1 Hz, 3.5 Hz, 1H), 3.00 (dd, J = 14.1 Hz, 9.0 Hz, 1H), 2.24 (br s, 1H). **^{13}C NMR** ($CDCl_3$, 100 MHz) δ (ppm) 158.5, 139.6, 133.9, 130.5, 130.4, 130.3, 129.0, 128.0, 126.1, 125.5, 123.1, 123.0, 114.1, 114.0, 72.2, 55.3, 44.2. **FT-IR**: ν (cm^{-1}) 3310, 2920, 1610, 1510, 1301, 1241, 1178, 1074, 1039, 985, 803, 783, 769, 734. **Accurate mass (ESI^{+}):** m/z calc'd for [$H_{18}C_{19}O_2$+ Na^{+}] Theoretical: 301.1205. Found: 301.1816.

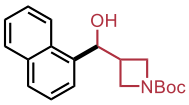

3-(hydroxy-1-naphthalenylmethyl)-1,1-dimethylethyl ester-1-Azetidinecarboxylic acid (3.29) was prepared according to the general procedure. The product was purified by column chromatography with 50% EtOAc in hexanes to afford **3.29** as a colourless oil (68.5 mg, 73% yield). **^{1}H NMR** ($CDCl_3$, 400 MHz) δ (ppm) 8.17 (d, *J* = 8.2 Hz, 1H), 7.88 (dd, *J* = 7.6 Hz, 1.7 Hz, 1H), 7.80 (d, *J* = 8.1 Hz, 1H), 7.56 -7.26 (m, 4H), 5.21 (d, *J* = 7.0 Hz, 1H), 4.10 (dd, *J* = 8.7 Hz, 5.5 Hz, 1H), 3.96 (t, *J* = 8.7 Hz, 1H), 3.87 (t, *J* = 8.6 Hz, 1H), 3.72 (dd, *J* = 8.7 Hz, 5.7 Hz, 1H), 3.19 – 3.10 (m, 1H), 2.65 (br s, 1H), 1.43 (s, 9H). **^{13}C NMR** ($CDCl_3$, 100 MHz) δ (ppm) 156.5, 137.3, 134.0, 130.7, 128.9, 128.7, 126.3, 125.8, 125.3, 123.5, 123.3, 79.4, 72.0, 51.2, 34.3, 28.4. **FT-IR**: ν (cm^{-1}) 3450, 2969, 2888, 1738, 1698, 1479, 1249, 1134, 1069, 804, 771. **Accurate mass (EI):** $H_{23}C_{19}NO_3$ Theoretical: 313.3970. Found: 313.1672. Spectral Accuracy: 96.1%.

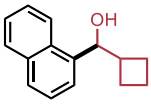

Cyclobutyl(naphthalen-1-yl)methanol (3.30) was prepared according to the general procedure. The product was purified by column chromatography with 10% EtOAc in hexanes to afford **3.30** as a colourless oil (52.9 mg, 83% yield). **^{1}H NMR** (CDl_3, 400 MHz) δ (ppm) 8.24 (d, *J* = 8.3 Hz, 1H), 7.88 (d, *J* = 7.7 Hz, 1H), 7.79 (d, *J* = 8.1 Hz, 1H), 7.56-7.47 (m, 4H), 5.37 (d, *J* = 7.15 Hz, 1H), 3.04-2.94 (m, 1H), 2.19-2.02 (m, 2H), 2.00 (br s, 1H), 1.94-1.83 (m, 4H). **^{13}C NMR** ($CDCl_3$, 100 MHz) δ (ppm) 138.5, 133.9, 131.1, 128.8, 128.1, 126.4, 125.9, 125.5, 125.3, 123.7, 123.5, 74.3, 41.3, 24.6, 24.5, 17.8. **FT-IR**: ν (cm^{-1}) 3396, 2935, 1723, 1510, 1373, 1240, 1044, 988, 775, 619. **Accurate mass (EI):** $H_{15}C_{16}O$ Theoretical: 212.1196. Found: 212.1319. Spectral Accuracy: 98.4%.

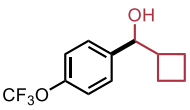

Cyclobutyl-[4-(trifluoromethoxy)phenyl]methanol (3.31) was prepared according to the general procedure E. The product was purified by column chromatography with 12.5% to 16.5% EtOAc in hexanes to afford **3.31** as a colourless oil (51.7 mg, 70% yield). **^{1}H NMR** ($CDCl_3$, 400 MHz) δ (ppm) 7.34 (d, *J* = 8.6 Hz, 2H), 7.18 (d, *J* = 8.0 Hz, 2H), 4.58 (d, *J* = 7.9 Hz, 1H), 2.64-2.54 (m, 1H), 2.12-1.77 (m, 7H). **^{13}C NMR** ($CDCl_3$, 100 MHz) δ (ppm) 148.5, 141.8, 127.5, 123.0 (q, *J* = 257.0 Hz), 120.8, 77.6, 42.5, 24.6, 24.3, 17.7. **^{19}F NMR** δ (ppm) -57.9. **FT-IR**: ν (cm^{-1}) 3416, 2939, 1725, 1508, 1375, 1253, 1156, 1045, 1011,

840, 678. **Accurate mass (EI):** $H_{13}C_{12}F_3O_2$ Theoretical: 246.0774. Found: 246.0862. Spectral Accuracy: 98.3%.

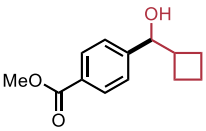

4-(cyclobutylhydroxymethyl)-benzoic acid methyl ester (3.32) was prepared according to the general procedure E. The product was purified by column chromatography with 2.5% to 10% acetone in PhMe to afford **3.32** as a yellow oil (62 mg, 94% yield).**^{1}H NMR** ($CDCl_3$, 400 MHz) δ (ppm) 7.98 (d, *J* = 8.3 Hz, 2H), 7.37 (d, *J* = 8.3 Hz, 2H), 4.62 (d, *J* = 7.7 Hz, 1H), 3.90 (s, 3H), 2.63-2.53 (m, 1H), 2.18 (br, s, 1H), 2.07-1.97 (m, 2H), 1.89-1.74 (m, 4H). **^{13}C NMR** ($CDCl_3$, 100 MHz) δ (ppm) 167.0, 148.3, 129.6, 129.2, 126.0, 77.7, 52.0, 42.4, 24.5, 24.2, 17.7. **FT-IR ν (cm^{-1})** 3510, 2930, 2852, 1696, 1607, 1573, 1430, 1309, 1277, 1191, 1174, 1117, 1094, 1012, 960, 917, 852, 809, 766, 705. **Accurate mass (EI):** $H_{16}C_{13}O_3$ Theoretical: 220.1094. Found: 220.1165. Spectral Accuracy: 98%

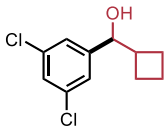

Cyclobutyl-(3,5-dichlorophenyl)methanol (3.33) was prepared according to the general procedure. The product was purified by column chromatography with 10% EtOAc in hexanes to afford **3.33** as a pale yellow semi-solid (59 mg, 86% yield). **^{1}H NMR** ($CDCl_3$, 400 MHz) δ (ppm) 7.25 (t, *J* = 1.9 Hz, 1H), 7.20 (d, *J* = 1.9 Hz, 2H), 4.50 (d, *J* = 7.7 Hz, 1H), 2.60-2.50 (m, 1H), 2.08-1.79 (m, 7H). **^{13}C NMR** ($CDCl_3$, 100 MHz) δ (ppm) 146.6, 134.9, 127.5, 124.6, 77.2, 42.3, 24.4, 24.2, 17.7. **FT-IR**: ν (cm^{-1}) 3214, 2919, 2854, 1620, 1567, 1427, 1383, 1318, 1204, 1096, 1059, 1018, 856, 795, 685. **Accurate mass (EI):** $H_{12}C_{11}Cl_2O$ Theoretical: 230.0265. Found: 230.0260. Spectral Accuracy: 98.3%**.**

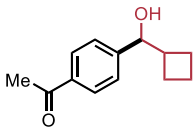

1-[4-[cyclobutyl(hydroxy)methyl]phenyl]ethanone (3.34) was prepared according to the general procedure. The product was purified by column chromatography with 10% EtOAc in hexanes to afford **3.34** as a yellow oil (58 mg, 95% yield). **^{1}H NMR** ($CDCl_3$, 400 MHz) δ (ppm) 7.88 (d, *J* = 8.3 Hz, 2H), 7.37 (d, *J* = 8.2 Hz, 2H), 4.61 (d, *J* = 7.7 Hz, 1H), 2.55 (s, 3H), 2.17 (br s, 1H), 2.02-1.96 (m, 2H), 1.85-1.76 (m, 4H). **^{13}C NMR** ($CDCl_3$, 100 MHz) δ (ppm) 197.9, 148.6, 136.3, 128.4, 126.2, 77.7, 42.5, 26.6, 24.5, 24.3, 17.7. **FT-IR**: ν (cm^{-1}) 3420, 2937, 2861, 1664, 1605, 1568, 1408, 1364, 1274, 1195, 1014, 961, 832, 715. **Accurate mass (EI):** $H_{16}C_{13}O_2$ Theoretical: 204.1115. Found: 204.1145. Spectral Accuracy: 97.1%.

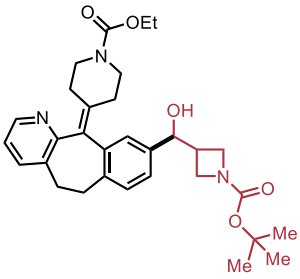

3-(hydroxy-[1-(11-(1-(Ethoxycarbonyl)piperidin-4-ylidene)-6,11-dihydro-5H-benzo[5,6]cyclohepta[1,2-b]pyridin-8-yl])-1,1-dimethylethyl ester-1-Azetidinecarboxylic acid (3.35) was prepared according to the general procedure. The product was purified by column chromatography with 20% to 40% acetone in DCM to afford **3.35** as a purple solid (83.4 mg, 52% yield). **^{1}H NMR** ($CDCl_3$, 400 MHz) δ (ppm) 8.35 (d, J = 4.4 Hz, 1H), 7.47 (d, J = 7.5 Hz, 1H), 7.15-7.08 (m, 4H), 4.70 (d, J = 6.6 Hz, 1H), 4.11 (q, J = 7.1 Hz, 2H), 4.00-3.93 (m, 2H), 3.81-3.77 (m, 3H), 3.64-3.62 (m, 1H), 3.44-3.32 (m, 2H), 3.15-3.09 (m, 2H), 2.87-2.76 (m, 4H), 2.49-2.14 (m, 1H), 2.39-2.24 (m, 3H), 1.41 (s, 9H), 1.23 (t, J = 7.1 Hz, 3H). **^{13}C NMR** ($CDCl_3$, 100 MHz) δ (ppm) 157.1, 156.4, 155.5, 146.0, 141.5, 138.7, 138.0, 137.9, 137.5, 134.2, 134.0, 129.7, 127.1, 127.0, 124.0, 122.4, 79.4, 75.6, 75.5, 61.3, 58.5, 51.6, 44.8, 44.7, 35.4, 31.9, 31.6, 29.7, 28.4, 27.5, 14.6. **Melting point** Decomposition upon heating **FT-IR**: ν (cm^{-1}) 3350, 2972, 1691, 1421, 1365, 1326, 1225, 1112, 995, 767, 728.**Accurate mass (ESI$^+$):** m/z calc'd for [$H_{39}C_{31}N_3O_5$] Theoretical: 556.2787. Found: 556.3256.

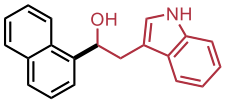

2-(1H-indol-3-yl)-1-(naphthalen-1-yl)ethanol (3.36), was prepared according to the general procedure The fractions were collected using a gradient solvent system of 1% to 4% acetone in DCM to afford **3.36** as a white solid (77.0 mg, 89% yield). **^{1}H NMR** ($CDCl_3$, 400 MHz) δ (ppm) 8.26 (d, J = 8.5 Hz, 1H), 8.10 (br s, 1H), 7.94-7.92 (m, 1H), 7.83 (d, J = 8.2 Hz, 1H), 7.75 (d, J = 7.1 Hz, 1H), 7.69 (d, J = 7.8 Hz, 1H), 7.61-7.49 (m, 3H), 7.40 (d, J = 8.1 Hz, 1H), 7.26 (dt, J = 8.0 Hz, 1.1 Hz, 1H), 7.19 (dt, J = 7.9 Hz, 1.1 Hz, 1H), 7.11 (br s, 1H),), 5.78 (dd, J = 9.0 Hz, 3.6 Hz, 1H), 3.51 (dd, J = 14.7 Hz, 3.5 Hz, 1H), 3.24 (dd, J = 14.8 Hz, 9.0 Hz, 1H), 1.61 (br s, 1H). **^{13}C NMR** ($CDCl_3$, 100 MHz) δ (ppm) 139.8, 136.4, 133.9, 130.5, 129.0, 127.9, 127.6, 126.1, 125.6, 125.5, 123.2, 123.0, 122.3, 119.7, 119.0, 112.4, 111.4, 70.7, 35.0. Characterization of **3.36** matched previously reported spectra.[47]

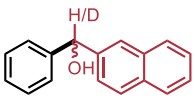

(2-Naphthyl)(phenyl)methan-α-ol-d_1/(2-Naphthyl)(phenyl)methanol (3.38) was prepared according to the general procedure from iodobenzene, **3.2**, and 2-Naphthalenemethanol-d_1, **3.37**, (>99% D) to determine an internal kinetic isotope effect.

The product was purified by column chromatography with 5% to 15% EtOAc in hexanes to afford **3.38** as a white opaque oil that slowly solidified (57.6 mg, 82% yield).**^{1}H NMR** ($CDCl_3$, 400 MHz) δ (ppm) 7.91(s, 1H), 7.88-7.80 (m, 3H), 7.54-7.28 (m, 9H), 6.01 (s, 0.29H, residual protium signal), 2.48 (br s, 1H). **^{13}C NMR** ($CDCl_3$, 100 MHz) δ (ppm) 143.6, 143.5, 141.1, 141.0, 133.2, 132.8, 128.5, 128.3, 128.0, 127.62, 127.61, 126.6, 126.1, 125.9, 125.0, 124.7, 76.3, 75.9 (t, J = 22.1 Hz). **Note:** Some carbons in the ^{13}C spectrum have slightly different chemical shifts between the deuterated and non-deuterated analogue

3.8.4 Procedure for synthesis of methyl 4-benzoylbenzoate (3.46)

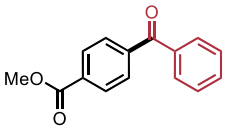

Methyl 4-benzoylbenzoate (3.46) was prepared with a modified procedure. Inside the glovebox, to a dry 8 mL screw-capped reaction vial equipped with a magnetic stir bar, $NiBr_2$•diglyme (0.1 equiv, 0.03 mmol, 10.6 mg) and $P^{Cy}{}_2N^{ArCF3}{}_2$ (0.12 equiv, 0.036 mmol, 21.7 mg) were added and dissolved in toluene (1.5 mL). 2,2,6,6-tetramethylpiperidine (2 equiv, 0.6 mmol, 85 mg), 4-iodomethylbenzoate (2 equiv, 0.3 mmol, 157.2 mg) followed by benzyl alcohol (1 equiv, 0.3 mmol, 32.4 mg) were added to the stirring solution. Finally, acetone (5 equiv, 1.5 mmol, 87.1 mg) was added. The vial was capped, removed from the glovebox, and placed in a stirring (350 rpm) mineral oil bath pre-heated to 85 °C. After stirring for 16 hours, the reaction vial was removed from the oil bath and cooled down to room temperature. The reaction mixture was diluted with DCM, solvent was removed in vacuo, and the crude product was purified by column chromatography with 9% EtOAc in hexanes to afford **3.46** as a white solid (132.7 mg, 92% yield). **^{1}H NMR** ($CDCl_3$, 400 MHz) δ (ppm) 8.14 (d, J = 8.3 Hz, 1H), 7.86-7.77 (m, 4H), 7.64-7.58 (m, 1H), 7.53-7.47 (m, 2H), 3.96 (s, 3H). **^{13}C NMR** ($CDCl_3$, 100 MHz) δ (ppm) 195.9, 166.2, 141.2, 136.9, 133.1, 132.9, 130.0, 129.7, 129.4, 128.4, 52.3. Characterization of **3.46** matched previously reported spectra.[48]

3.8.5 Extension to primary thiols

Late transition metals are not known to make thioaldehydes from thiols through β-hydride elimination. It is presumed that the barrier to β-hydride elimination is too high and that side reactions could dominate. Nonetheless, we opted to try primary thiols as a coupling partner since α-arylated thiols are an interesting class of molecules that are less accessible.[49] Unfortunately, when tested under the conditions optimized for the redox-neutral α-arylation of primary alcohols, carbon-sulfur bond formation (**3.99**) was observed instead (Scheme 3.22). Efficient coupling of aryl (pseudo)halides with alkyl thiols is known with nickel precatalysts.[50]

Scheme 3.22 Extension of work to primary thiols

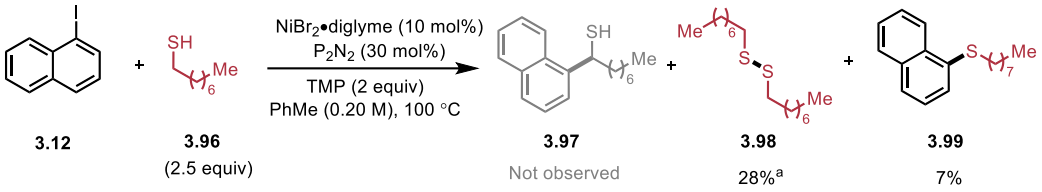

Reaction conditions: 1-iodonaphthalene (0.20 mmol, 1 equiv, 29.2 µL), 1-octanethiol (0.45 mmol, 2.5 equiv, 87.0 µL), TMP (0.4 mmol, 2 equiv, 65.7 µL), $NiBr_2$•diglyme (10 mol%), $P^{Cy}{}_2N^{ArCF3}{}_2$(30 mol%), toluene (0.20 M, 1 mL), 100 °C for 16 h. Crude ^1H yields are reported. [a] Yield based on equivalency of 1-octanethiol.

3.9 [Ni(P_2N_2)] complexes: Experimental

3.9.1 Instrumentation

^{1}H NMR and ^{13}C NMR were recorded on a Bruker AVANCEII 300 MHz spectrometer, a Bruker AVANCEII 400 MHz spectrometer, or a Bruker AVANCEIII 500 MHz spectrometer. ^{1}H NMR spectra were internally referenced to the residual solvent signal (e.g., $CDCl_3$ = 7.27 ppm). ^{13}C NMR spectra were internally referenced to the residual solvent signal (e.g., $CDCl_3$ = 77.00 ppm). Data for ^{1}H NMR are reported as follows: chemical shift (δ ppm), multiplicity (s = singlet, d = doublet, t = triplet, q = quartet, m = multiplet), coupling constant (Hz), integration. NMR yields for optimization studies were obtained by ^{1}H NMR analysis of the crude reaction mixture using 1,3,5-trimethoxybenzene as an internal standard.

3.9.2 Synthesis and characterization of Ni(P_2N_2) complexes

3.9.2.1 [Ni($P^{Cy}_2N^{ArCF3}_2$)(cod)] (3.76)

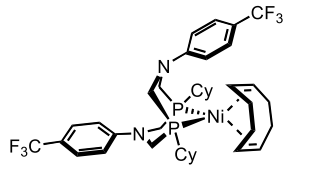

[Ni($P^{Cy}_2N^{ArCF3}_2$)(cod)] (**3.76**)
49%

Inside the glovebox, to a dry 25 mL round-bottom flask equipped with a magnetic stir bar, $Ni(cod)_2$ (1.00 equiv, 0.30 mmol, 82.5 mg) along with $P^{Cy}_2N^{ArCF3}_2$ (1.00 equiv, 0.30 mmol, 180.8 mg) were added to the flask and dissolved in toluene (3.0 mL). The initially homogeneous solution was stirred at room temperature for 15 minutes. The formation of a precipitate was observed within minutes. The flask was capped and placed in a -20 °C freezer overnight. The following day, the solution was filtered in the glovebox. The precipitate was washed with cold (-20 °C) toluene followed by pentanes. Residual solvent was removed in vacuo and **3.76** was obtained as a yellow powder (116.7 mg, 49%). **X-ray quality crystals** were obtained serendipitously from a failed NMR experiment in d_6-benzene (vide infra; Scheme 3.23 and Figure 3.16).

Scheme 3.23 Reaction conditions to obtain X-ray quality crystals of 3.76

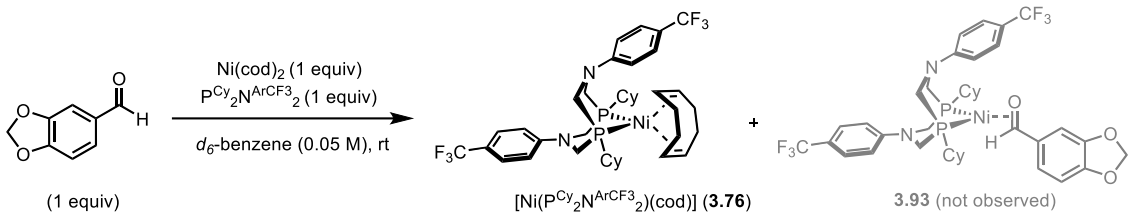

(1 equiv) [Ni($P^{Cy}_2N^{ArCF3}_2$)(cod)] (**3.76**) **3.93** (not observed)

Reaction conditions: $Ni(cod)_2$ (1.00 equiv, 0.05 mmol, 13.7 mg), $P^{Cy}_2N^{ArCF3}_2$ (1.00 equiv, 0.05 mmol, 30.1 mg), and piperonal (1.00 equiv, 0.05 mmol, 7.5 mg) were dissolved in d_6-benzene (0.05 M, 1mL). While attempting to observe an η^2-aldehyde complex **3.93**, fine yellow crystals were observed in the NMR tube. X-ray diffraction of these crystals confirmed the structure of **3.76**.

3.9.2.3 [Ni($P^{Cy}_2N^{ArCF3}_2$)(1-nap)(I)] (3.77)

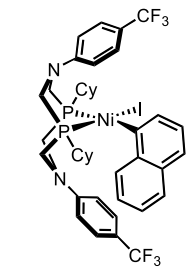

[Ni($P^{Cy}_2N^{ArCF3}_2$)(1-nap)(I)]
3.77

Inside the glovebox, To a dry 8 mL reaction vial equipped with a magnetic stir bar, $Ni(cod)_2$ (1.00 equiv, 0.10 mmol, 27.5 mg) along with $P^{Cy}_2N^{ArCF3}_2$ (1.00 equiv, 0.10 mmol, 60.3 mg) were added to the flask and dissolved in toluene (1.0 mL). The solution was stirred at 100 °C until homogeneous. 2.0 mL of pentanes was quickly added to the solution. The formation of a few X-ray quality red crystals was observed immediately. The vial was capped and placed in a -20 °C freezer overnight. Further precipitation occurred, however, we believe this was decomposition of the oxidative addition complex rather than the OAC. Despite the formation of a slurry, the red crystals remained intact and were used for X-ray characterization. **3.77** is unstable in solution (see Section 3.6.2) and decomposition was observed in a range of common deuterated solvents. This experiment is shown in Scheme 3.24.

Scheme 3.24 Reaction conditions to obtain X-ray quality crystals of **3.77**

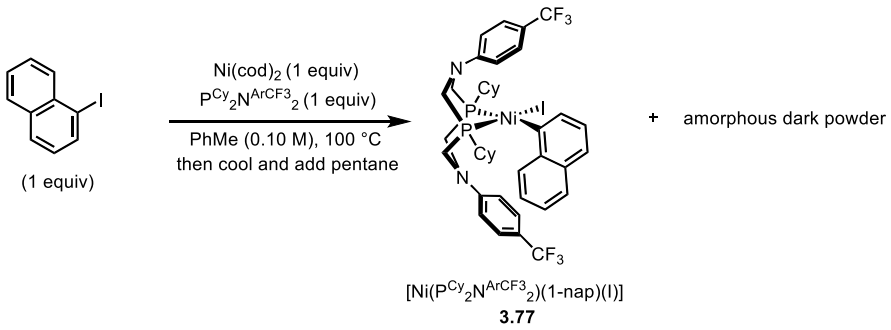

[Ni($P^{Cy}_2N^{ArCF3}_2$)(1-nap)(I)]
3.77

3.9.2.3 [Ni($P^{Cy}_2N^{ArCF3}_2$)$(I)_2$] (3.78)

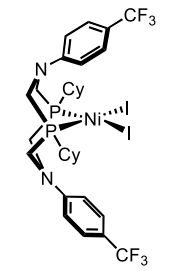

[Ni($P^{Cy}_2N^{ArCF3}_2$)$(I)_2$]
3.78

Inside the glovebox, the experiment described in Scheme 3.25 was set up in a screw-cap NMR tube and analyzed. X-ray quality crystals of **3.78** precipitated from the reaction mixture after heating the NMR tube overnight at 100 °C. **3.78** had limited solubility in organic solvents.

Scheme 3.25 Reaction conditions to obtain X-ray quality crystals of 3.78

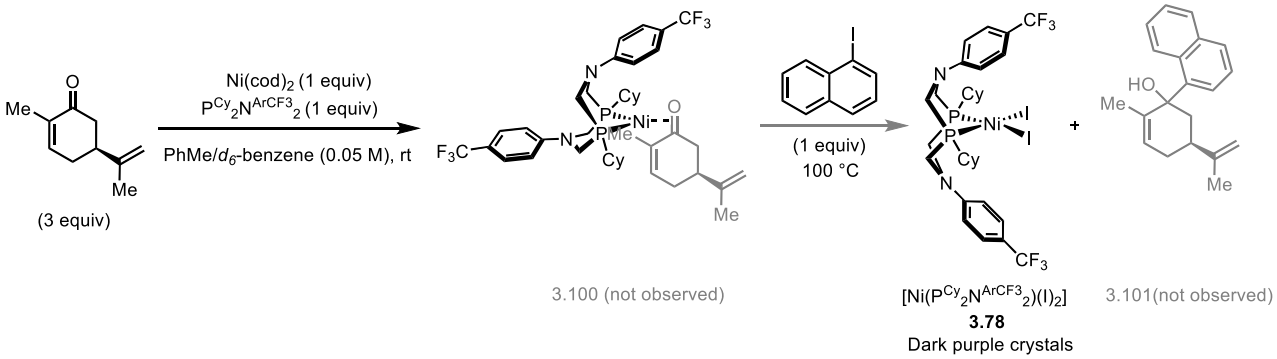

Reaction conditions: $Ni(cod)_2$ (1.00 equiv, 0.05 mmol, 13.7 mg), $P^{Cy}_2N^{ArCF3}_2$ (1.00 equiv, 0.05 mmol, 30.1 mg), and carvone (3 equiv, 0.15 mmol, 23.5 µL) were dissolved in 4:1 PhMe:d_6-benzene (0.05 M). While attempting to obtain ketone complex **3.96**, followed by carbonyl insertion product **3.97**, we observed **3.78** form.

3.9.2.4 [Ni($P^{Cy}_2N^{Ph}_2$)(1-nap)(I)] (3.83)

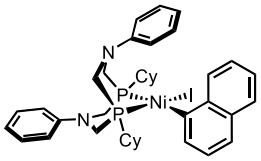

[Ni($P^{Cy}_2N^{Ph}_2$)(1-nap)(I)] (**3.83**)

Inside the glovebox, to a dry 25 mL round-bottom flask equipped with a magnetic stir bar, $Ni(cod)_2$ (1.00 equiv, 0.30 mmol, 82.5 mg) along with $P^{Cy}_2N^{Ph}_2$ (1.00 equiv, 0.30 mmol, 140.0 mg) were added to the flask and dissolved in toluene (6.0 mL). The initially homogeneous solution was stirred at room temperature for 15 minutes. The formation of a precipitate was observed within minutes. The flask was capped and placed in a -20 °C freezer overnight. The following day, the solution was filtered in the glovebox. The precipitate was washed with cold (-20 °C) toluene followed by pentanes. Residual solvent was removed in vacuo and **3.83** was obtained as a reddish brown powder (133.6 mg, 57%).**^{1}H NMR** (d_5-pyridine, 600 MHz) δ (ppm) 9.55 (d, *J* = 8.2 Hz, 1H), 8.52 (t, *J* = 6.1 Hz, 1H), 7.72 (d, *J* = 8.0 Hz, 1H), 7.65-7.60 (m, 5H), 7.55-7.50 (m, 3H), 7.46 (d, *J* = 7.9 Hz, 1H), 7.40 (*J* = 7.3 Hz, 1H), 7.31 (*J* = 7.4 Hz, 1H), 7.27-7.23 (m, 1H), 5.18-5.10 (m, 2H), 4.77 (d, *J* = 13.9 Hz, 1H), 4.50 (d, *J* = 13.9 Hz, 1H), 4.15-4.03 (m, 3H), 3.98 (dd, *J* = 13.9 Hz, 6.1 Hz, 1H), 2.02-1.92 (m, 2H), 1.81 (d, *J* = 11.7 Hz, 1H), 1.56 (d, *J* = 11.7 Hz, 1H), 1.53-148 (m, 1H), 1.47-1.34 (m, 3H), 1.30-1.23 (m, 2H), 1.21-1.14 (m, 5H), 1.05-0.97 (m, 1H), 0.95-0.86 (m, 3H), 0.77-0.66 (m, 2H), 0.58-0.49 (m, 1H), 0.37-0.28 (m, 1H). Note: the residual water signal in d_5-pyridine is observed at ~ 5.00 ppm. **^{31}P{^{1}H} NMR** (d_5-pyridine, 121 MHz) δ (ppm) 13.5 (d, *J* = 66 Hz), -7.43 (d, *J* = 66 Hz). **X-ray quality crystals** were obtained from a smaller (0.05 mmol) scale reaction of the procedure above. Reddish brown crystals were obtained by placing the reaction mixture in the freezer after becoming homogeneous. Note: **3.83** was found to be unstable in halogenated solvents ($CDCl_3$ and d_2-TeCA) and decomposed to poorly defined species. $P^{Cy}_2N^{Ph}_2$ is partially displaced from **3.83** when dissolved in d_6-DMSO – it is assumed that DMSO can coordinate to the Ni centre. **3.83** has poor solubility in d_6-benzene or d_8-PhMe at room temperature.

[Ni($P^{Cy}_2N^{Ph}_2$)(1-nap)(I)] (3.83), d_5-pyridine, ^{1}H (600 MHz)

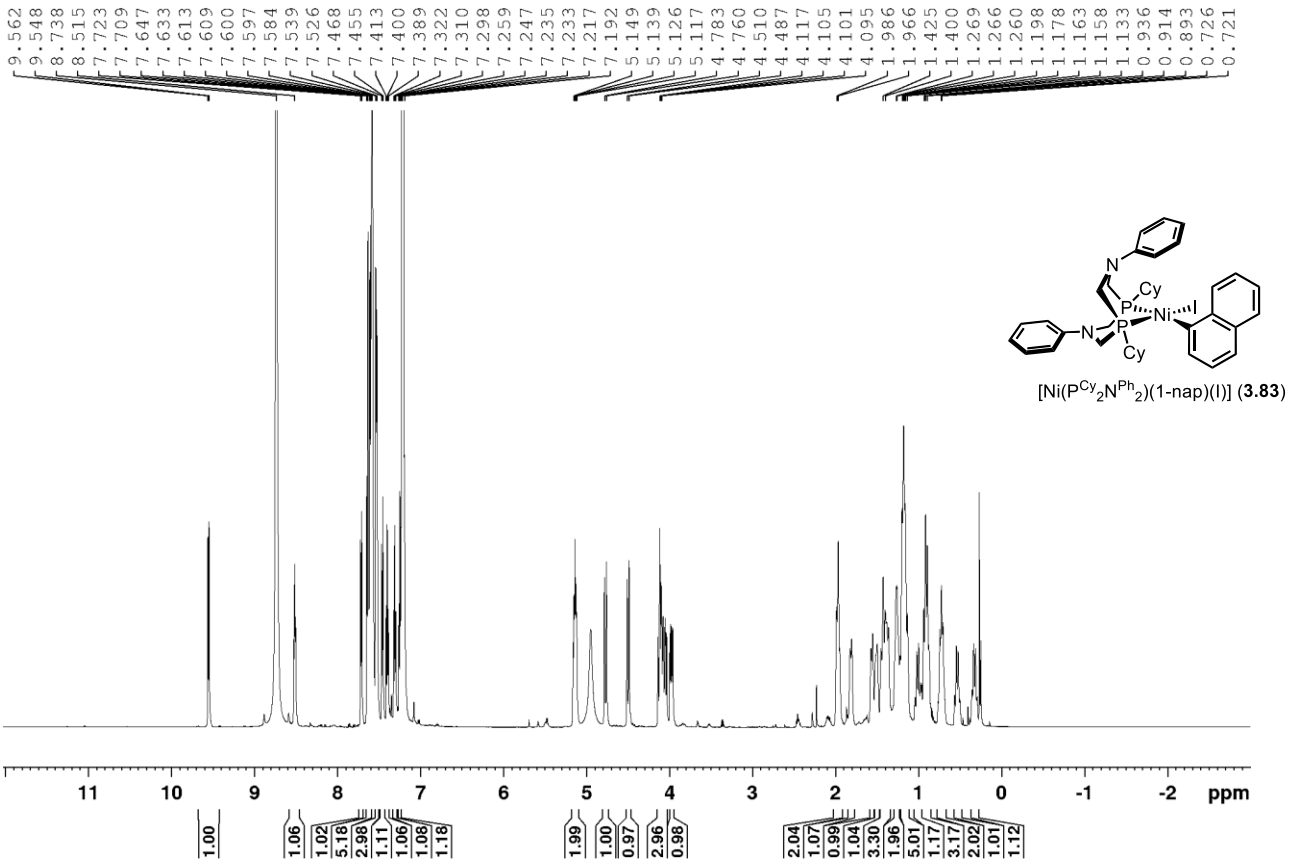

[Ni($P^{Cy}_2N^{Ph}_2$)(1-nap)(I)] (3.83), d_5-pyridine , $^{31}P\{^1H\}$ (121 MHz)

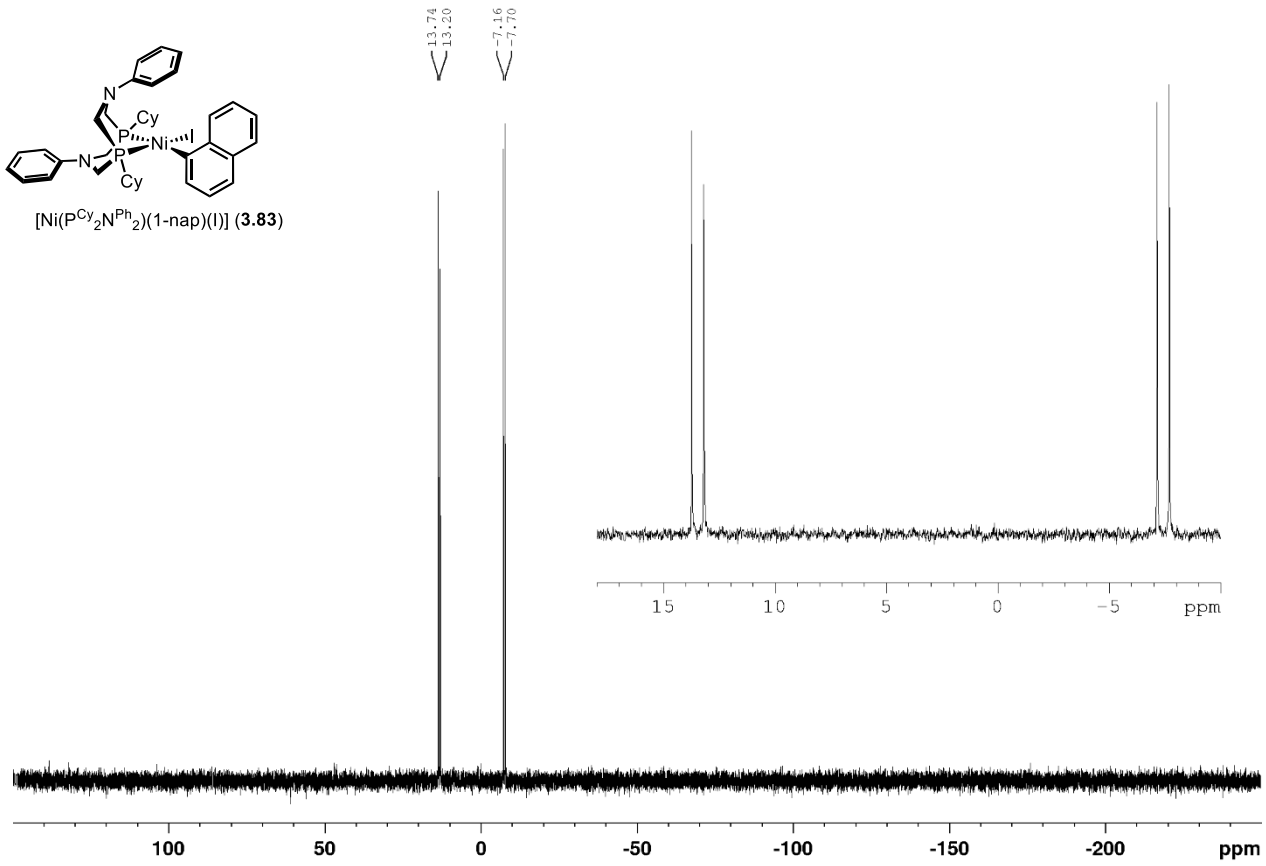

3.9.3 Crystallographic details

Data Collection and Processing. Crystallographic data for Ni($P^{Cy}_2N^{ArCF3}_2$)cod (**3.76**), Ni($P^{Cy}_2N^{ArCF3}_2$)(1-nap)(I)*toluene **(3.77),** Ni($P^{Cy}_2N^{ArCF3}_2$)I_2 **(3.78)**, Ni($P^{Cy}_2N^{Ph}_2$)(1-nap)(I) **(3.83)**.were collected from a single crystal mounted on a MiTeGen MicroMount using parabar oil. Data were collected on a Bruker Kappa ApexII single crystal diffractometer equipped with a sealed tube Mo Kα source (λ= 0.71073 Å), a graphite monochromator, and an ApexII CCD detector. The crystal was held at 200 K using a dry compressed air cooling system. Raw data collection and processing were performed with the Apex3 software package from Bruker.[51] Initial unit cell parameters were determined from 36 data frames from select ω scans. Semi-empirical absorption corrections based on equivalent reflections were applied.[52] Systematic absences in the diffraction data-set and unit-cell parameters were consistent with the assigned space group. All structures were solved via Olex2 program.[53] The initial structural solutions were determined using ShelxT direct methods,[54], and refined with full-matrix least-squares procedures based on F2 using ShelXL.[55] Hydrogen atoms were placed geometrically and refined using a riding model.

Table 3.8 Summary of crystal data for $P^{R}{}_2N^{R'}{}_2$ Ni complexes.

Compound	**Ni($P^{Cy}{}_2N^{ArCF3}{}_2$)cod (3.76)**	**Ni($P^{Cy}{}_2N^{ArCF3}{}_2$)(1-nap)(I)*toluene (3.77)**	**Ni($P^{Cy}{}_2N^{ArCF3}{}_2$)I_2 (3.78)**	**Ni($P^{Cy}{}_2N^{Ph}{}_2$)(1-nap)(I) (3.83)**
Formula	$C_{38}H_{50}F_6N_2NiP_2$	$C_{40}H_{45}F_6N_2NiP_2$, C_7H_8	$C_{30}H_{38}F_6I_2N_2NiP_2$	$C_{38}H_{47}IN_2NiP_2$
Formula Weight (*g/mol*)	769.43	1007.47	915.09	779.32
Crystal Dimensions (*mm*)	0.358 × 0.235 × 0.134	0.230 × 0.131 × 0.118	0.274 × 0.123 × 0.052	0.107 × 0.093 × 0.036
Crystal Colour and Habit	yellow block	orange, block	Violet, plate	Red, block
Crystal System	triclinic	monoclinic	triclinic	monoclinic
Space Group	P-1	$P2_1/n$	P-1	P-1
Temp, K	200	200	200	200
a, Å	9.5339(6)	14.1048(8)	14.6522(11)	10.5127(8)
b, Å	13.3898(9)	21.6621(14)	15.0104(12)	13.3512(10)
c, Å	15.3157(10)	16.2528(10)	16.9076(13)	14.5879(11)
α,°	105.848(1)	90	90.100(2)	72.159(2)
β,°	93.473(9)	113.712(2)	108.720(2)	77.623(2)
γ,°	103.758(1)	90	105.750(2)	76.273(2)
V, $Å^3$	1810.2(2)	4546.6(5)	3373.5(5)	1871.0(2)
Number of reflections to determine final unit cell	9810	9899	9642	6588

Min and Max theta for cell determination, °	2.45, 30.67	2.33, 24.50	2.39, 29.17	2.31, 21.88
Z	2	4	4	2
F(000)	808.0	1964	1872	800
r (*g/cm*)	1.412	1.403	1.861	1.383
l, Å, (MoKa)	0.71073	0.71073	0.71073	0.71073
μ, (cm^{-1})	0.686	1.231	2.560	601.456
Diffractometer Type	Bruker Kappa Axis Apex2	Bruker Kappa Axis Apex2	Bruker Kappa Axis Apex2	Bruker Kappa Axis Apex2
Scan Type(s)	f and w scans	f and w scans	f and w scans	f and w scans
Max theta for data collection, °	25.242	24.554	25.242	22.035
Measured fraction of data	0.996	0.998	0.997	0.991
Number of reflections measured	58573	78903	149963	23773
Unique reflections measured	7474	5139	12455	2699
R_{merge}	0.0645	0.0715	0.0810	0.1175
Number of reflections	7474	5139	12455	2699

included in refinement				
Cut off Threshold Expression	I > 2s(I)	I > 2s(I)	I > 2s(I)	I > 2s(I)
Structure refined using	full matrix least-squares using F^2	full matrix least-squares using F^2	full matrix least-squares using F^2	full matrix least-squares using F^2
Weighting Scheme	$w=1/[s^2(Fo^2)+(0.0471P)^2+1.1270P]$ where $P=(Fo^2+2Fc^2)/3$	$w=1/[s^2(Fo^2)+(0.0303P)^2+7.870P]$ where $P=(Fo^2+2Fc^2)/3$	$w=1/[s^2(Fo^2)+(0.0250P)^2+3.2012P]$ where $P=(Fo^2+2Fc^2)/3$	$w=1/[s^2(Fo^2)+(0.0625P)^2]$ where $P=(Fo^2+2Fc^2)/3$
Number of parameters in least-squares	470	564	775	397
R_1	0.0469	0.0412	0.0396	0.0629
wR_2	0.0992	0.0780	0.0651	0.1136
R_1 (all data)	0.0892	0.0814	0.0894	0.1271
wR_2 (all data)	0.1168	0.0922	0.0790	0.1358
GOF	1.061	1.005	1.065	1.050
Maximum shift/error	0.001	0.001	0.002	0.000
Min & Max peak heights on final DF Map (e^-/Å)	-0.508, 0.710	-0.523, 0.603	-0.764 0.833	-0.667, 0.671

Where:

$R_1 = \Sigma(|F_o| - |F_c|) / \Sigma F_o$

$wR_2 = [\ \Sigma (w(F_o^2 - F_c^2)^2) / \Sigma (w F_o^4)\ ]^{½}$

GOF = $[\ \Sigma (w(F_o^2 - F_c^2)^2) / (\text{No. of reflns.} - \text{No. of params}$

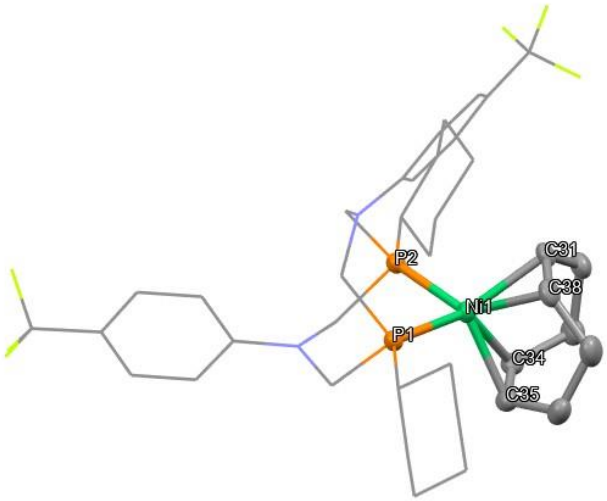

Table 3.9 Selected structural parameters for [Ni($P^{Cy}_2N^{ArCF3}_2$)(cod)] **(3.76)**

Structural Parameter	[Ni($P^{Cy}_2N^{ArCF3}_2$)(cod)] **(3.76)**
Bond Lengths (Å)	
Ni(1)-P(1)	2.1465(5)
Ni(1)-P(2)	2.1485(6)
Ni(1)-C(31)	2.094(2)
Ni(1)-C(38)	2.105(2)
Ni(1)-C(34)	2.115(2)
Ni(1)-C(35)	2.109(2)
C(34)-C(35)	1.379(3)
C(31)-C(38)	1.378(4)
Bond Angle (˚)	
P(1)-Ni(1)-P(2)	87.31(2)

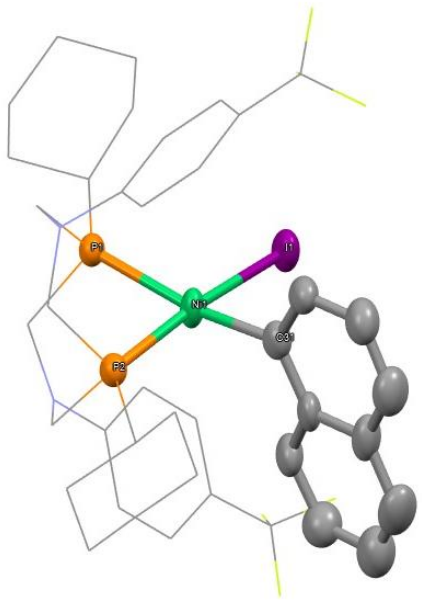

Table 3.10 Selected structural parameters for [Ni($P^{Cy}_2N^{ArCF3}_2$)(1-nap)(I)] **(3.77)**

Structural Parameter	[Ni($P^{Cy}_2N^{ArCF3}_2$)(1-nap)(I)] (**3.77**)
Bond Lengths (Å)	
Ni(1)-P(1)	2.241(1)
Ni(1)-P(2)	2.162(1)
Ni(1)-I(1)	2.5037(6)
Ni(1)-C(31)	1.960(8)
Bond Angle (˚)	
P(1)-Ni(1)-P(2)	85.77(5)
I(1)-Ni(1)-C(31)	87.2(2)

Co-crystallized toluene removed for clarity.

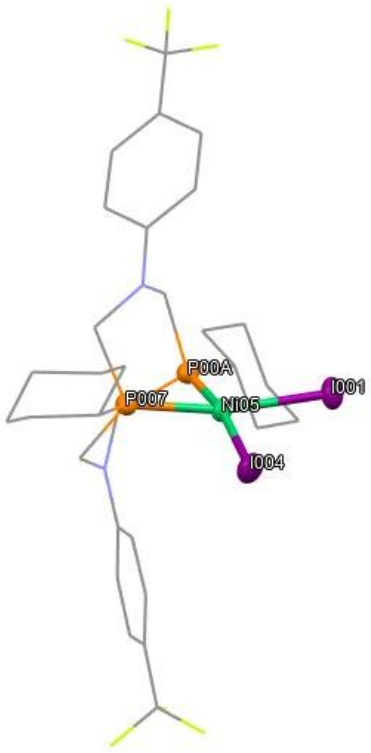

Table 3.11 Selected structural parameters for [Ni($P^{Cy}_2N^{ArCF3}_2$)$(I)_2$] (**3.78**)

Structural Parameter	[Ni($P^{Cy}_2N^{ArCF3}_2$)$(I)_2$] (**3.78**)
Bond Lengths (Å)	
Ni(05)-P(007)	2.175(1)
Ni(05)-P(00A)	2.177(1)
Ni(05)-I(001)	2.5348(6)
Ni(05)-I(004)	2.5291(6)
Bond Angle (˚)	
P(007)-Ni(05)-P(00A)	83.30(4)
I(001)-Ni(05)-I(004)	93.08(2)

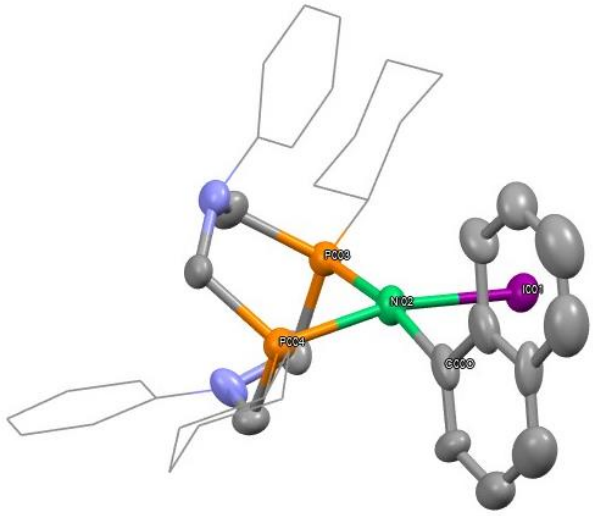

Table 3.12 Selected structural parameters for [Ni($P^{Cy}_2N^{ArCF3}_2$)(1-nap)(I)] (**3.83**)

Structural Parameter	[Ni($P^{Cy}_2N^{ArCF3}_2$)(1-nap)(I)] (**3.83**)
Bond Lengths (Å)	
Ni(02)-P(003)	2.225(3)
Ni(02)-P(004)	2.150(2)
Ni(02)-I(001)	2.524(1)
Ni(05)-C(00O)	1.95(1)
Bond Angle (˚)	
P(003)-Ni(05)-P(004)	86.7(1)
I(001)-Ni(05)-C(00O)	86.7(3)

Note: the resolution for the crystal structure (**3.83**) was poor so the bond lengths are not highly accurate. However, this confirms that 3.83 has similar connectivity to complex **3.77**. Notably, the conformation of the P_2N_2 ligand which crystallized was different between **3.77** and **3.83**. We anticipate that this is solely due to one conformer being more crystalline than the other and does not impact any information about absolute reactivity.

3.9.4 Formation of [Ni($P^{Cy}_2N^{ArCF3}_2$)(1-nap)(I)] (3.77)

Figure 3.3 shows the crude $^{31}P\{^1H\}$ NMR of [Ni($P^{Cy}_2N^{ArCF3}_2$)(1-nap)(I)] (**3.77**), which was formed in situ from Ni(cod)$_2$ (1.00 equiv, 0.05 mmol, 13.7 mg) and $P^{Cy}_2N^{ArCF3}_2$ (1.00 equiv, 0.05 mmol, 30.1 mg). The main peaks, doublets at δ (ppm) = 17.47 (d, *J* = 66 Hz) and -6.40 (d, *J* = 66 Hz), are indicative of oxidative addition as the phosphorus atoms are non-equivalent electronic space and are coupling with each other. It should be noted that [Ni($P^{Cy}_2N^{ArCF3}_2$)$_2$] (**3.82**) was also observed. We initially attributed the presence of **3.82** as unreacted Ni^0 and a trace impurity. However, a further study indicated that **3.77** decomposes in solution over time to form **3.82**. This is evidenced in a subsequent NMR study shown in Figure 3.4.

Figure 3.3 Crude $^{31}P\{^{1}H\}$ of [Ni($P^{Cy}_2N^{ArCF3}_2$)(1-nap)(I)] (**3.77**), C_6D_6, (121 MHz)

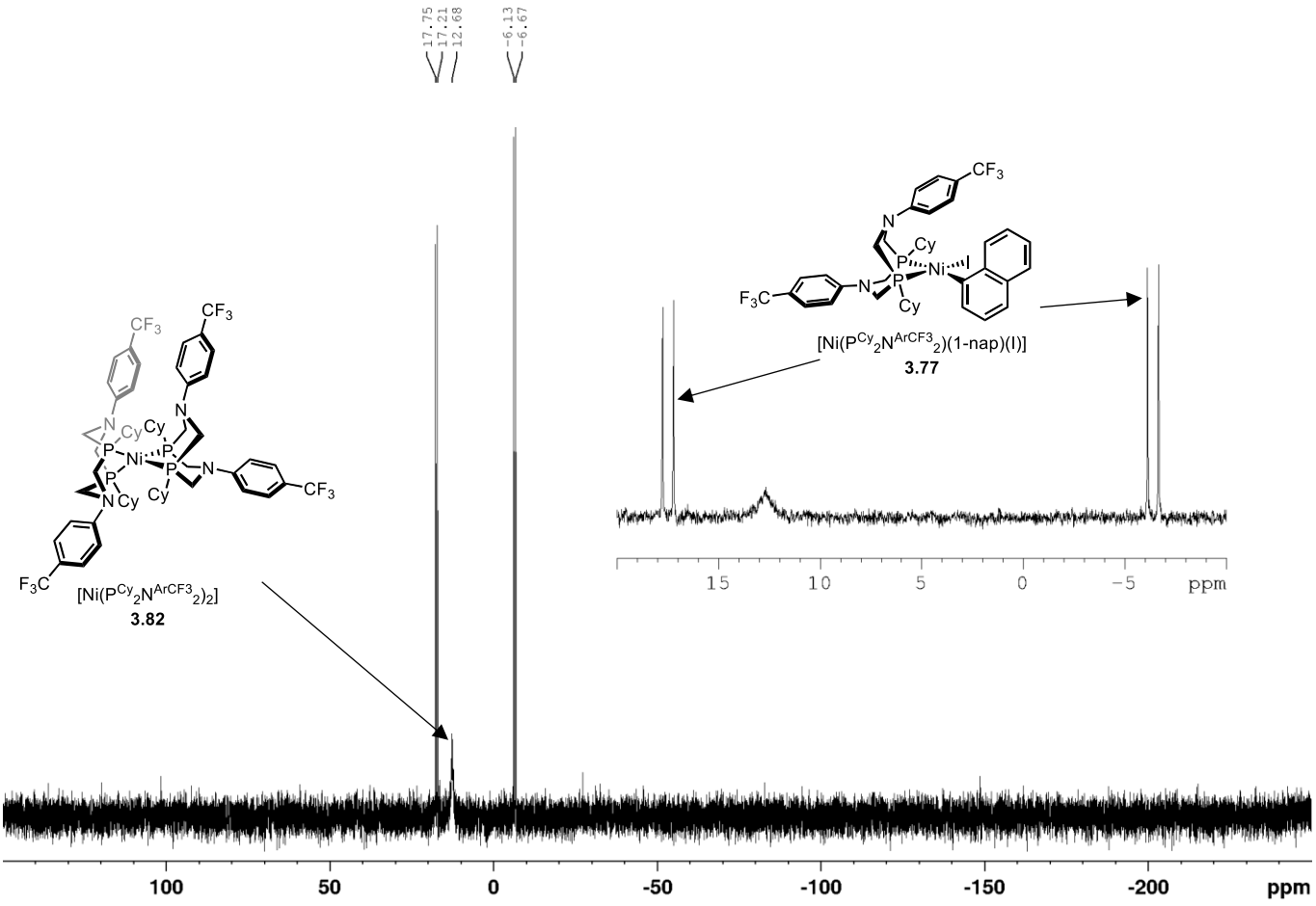

Figure 3.4 Crude $^{31}P\{^{1}H\}$ of [Ni($P^{Cy}_2N^{ArCF3}_2$)(1-nap)(I)] (**3.77**) after sitting at room temp, PhMe with C_6D_6 (trace), (121 MHz)

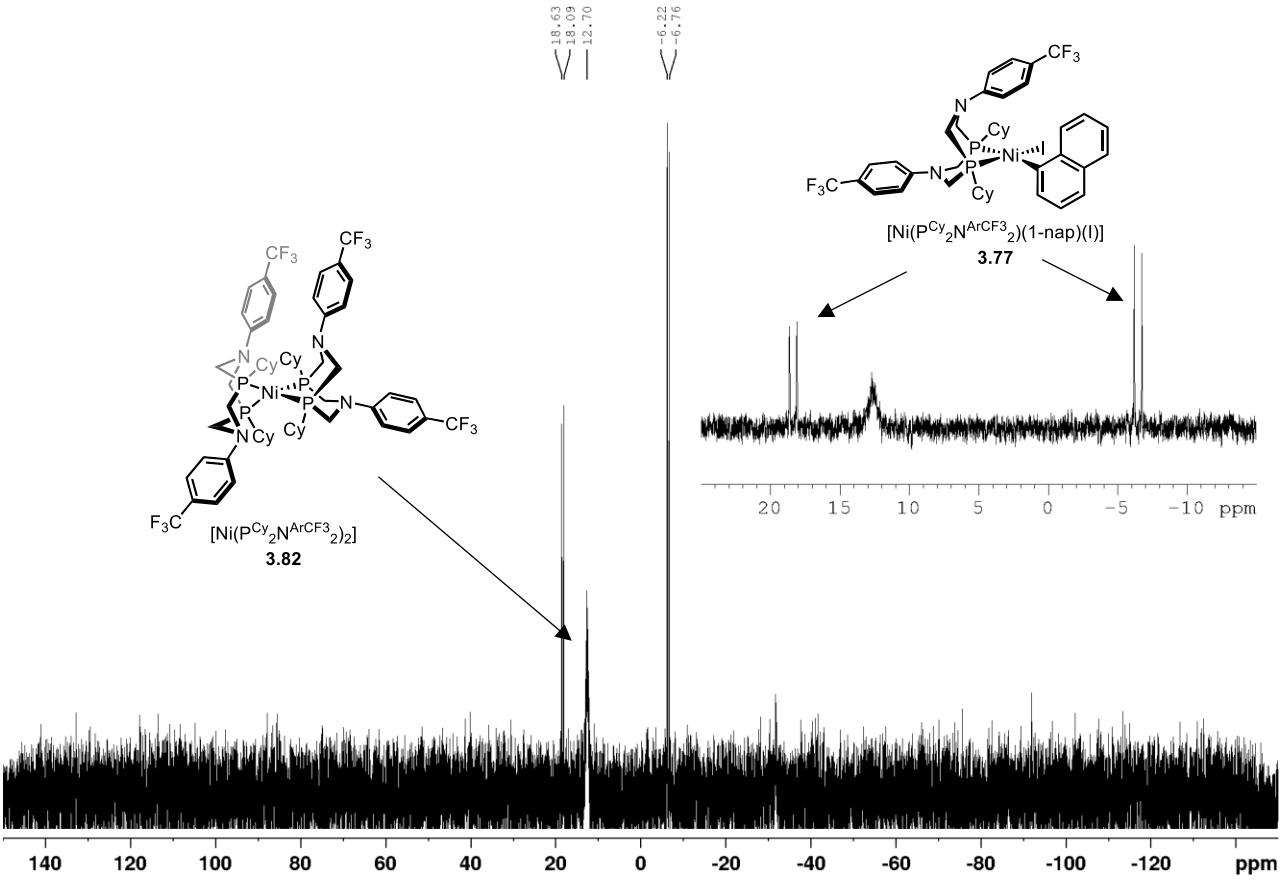

3.9.5 High-Temperature NMR Study (Scheme 3.17): Details

The reaction described in Scheme 3.17 was run at 75 °C in a heated Bruker Avance III HD 500 spectrometer. $^{31}P\{^{1}H\}$ spectra were taken 30 minutes apart. Oxidative addition complex and free ligand were clearly observed as the main phosphorus species in solution for the first 5 hours. At this time, approximately 5% coupling product was observed. The reaction was then placed in an oil bath at 100 °C for approximately 12 hours. Reaction proceeded to full completion after heating at 100 °C.

Figure 3.5 shows stacked $^{31}P\{^{1}H\}$ indicating reaction progress over time. The spectra are ordered in *decreasing* time. It is evident from the spectra that new species are observed as the reaction progresses.

Figure 3.6 shows the $^{31}P\{^{1}H\}$ obtained at room temperature before the NMR spectrometer was heated to 75 °C. We assume that the singlet at δ = 12 ppm is the $[NiBr_2(P^{Cy}{}_2N^{Ph}{}_2)]$ (**3.102**) complex as we don't anticipate that Ni(II) will reduce to Ni(0) quickly at room temperature. Free ligand was not observed – it is poorly soluble in aromatic solvents.

Figure 3.7 is a zoomed-in full page spectrum of the reaction mixture at 75 °C. Free ligand is now also observed in the $^{31}P\{^{1}H\}$ spectrum indicating increased solubility in d_8-PhMe at elevated temperature.

Figure 3.8-3.10 shows reaction progress after 5 hours (300 minutes) of heating in a spectrometer at 75 °C. The $^{31}P\{^{1}H\}$ spectrum shows two species in solution, the oxidative addition complex **3.83** and free ligand. Figure 3.9-Figure 3.10 show the ^{1}H of the reaction. Key peaks have

been integrated. Product formation was observed at 75 °C, however, the reaction was sluggish. We opted to further heat this reaction mixture in an oil bath at 100 °C for an additional 12 hours.

Figure 3.11 indicates that after heating at 100 °C overnight, oxidative addition complex was fully consumed by $^{31}P\{^{1}H\}$ NMR spectrosopy. The reaction mixture appears to contain free ligand (conformers) and peak at δ = 12 ppm. We hypothesize that this species could be a $[Ni(P^{Cy}{}_2N^{Ph}{}_2)_2]$ complex or a $[NiX_2(P^{Cy}{}_2N^{Ph}{}_2)]$ complex. Figure 3.12, the ^{1}H spectrum, shows complete conversion of the starting aryl iodide to either naphthalene (**3.85**) or 3-naphthalen-1-yl)oxetan-3-ol (**3.86**).

Figure 3.5 Reaction progress over time monitored by $^{31}P\{^{1}H\}$ d_8-PhMe, 202 MHz

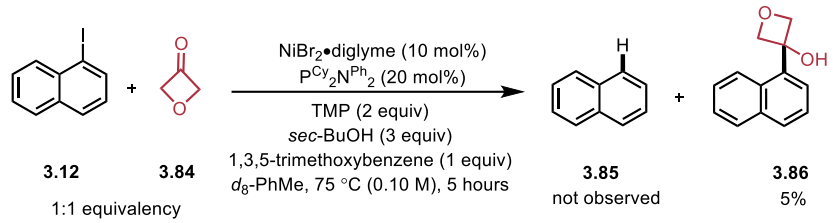

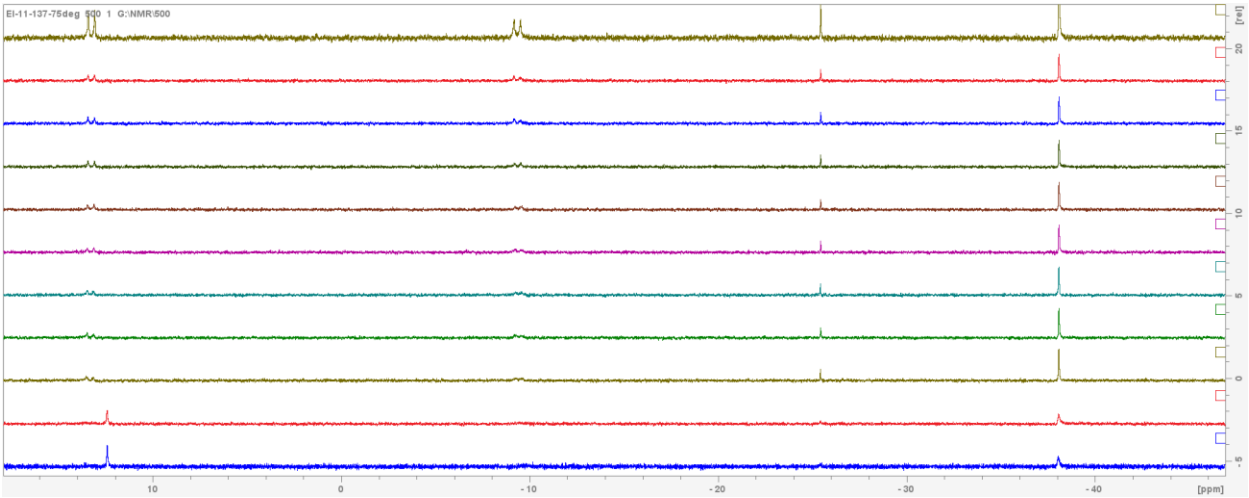

The top stacked spectrum represents the last time point and all spectra are ordered decreasing by 30 minute intervals. As such, the bottom stack spectrum represents as soon as the spectrometer warmed to 75 °C. Key findings will be detailed further in the following pages as full page spectra.

Figure 3.6 $^{31}P\{^{1}H\}$ spectrum taken at room temperature prior to heating, d_8-PhMe, 202 MHz

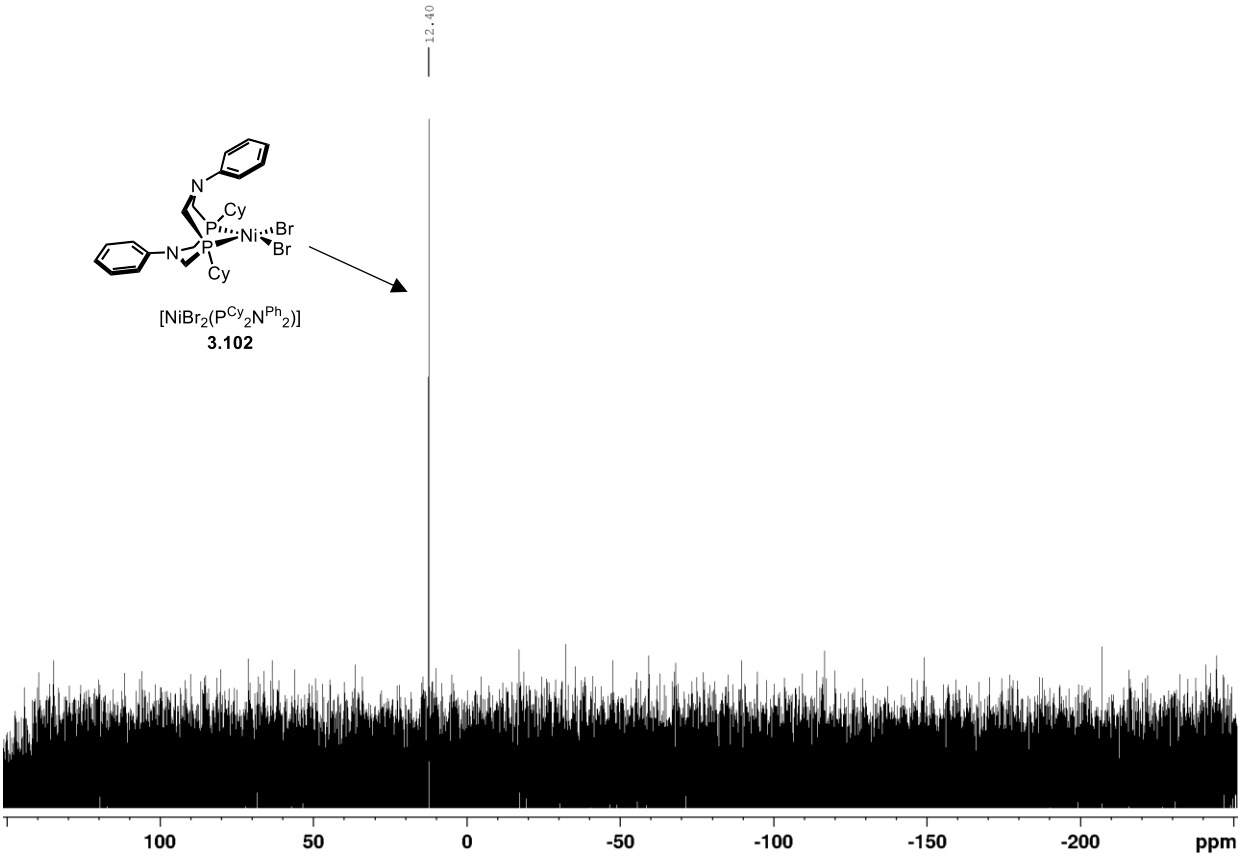

Figure 3.7 $^{31}P\{^{1}H\}$ spectrum taken at time = 0 min (as soon as spectrometer hit 75 °C), d_8-PhMe, 202 MHz

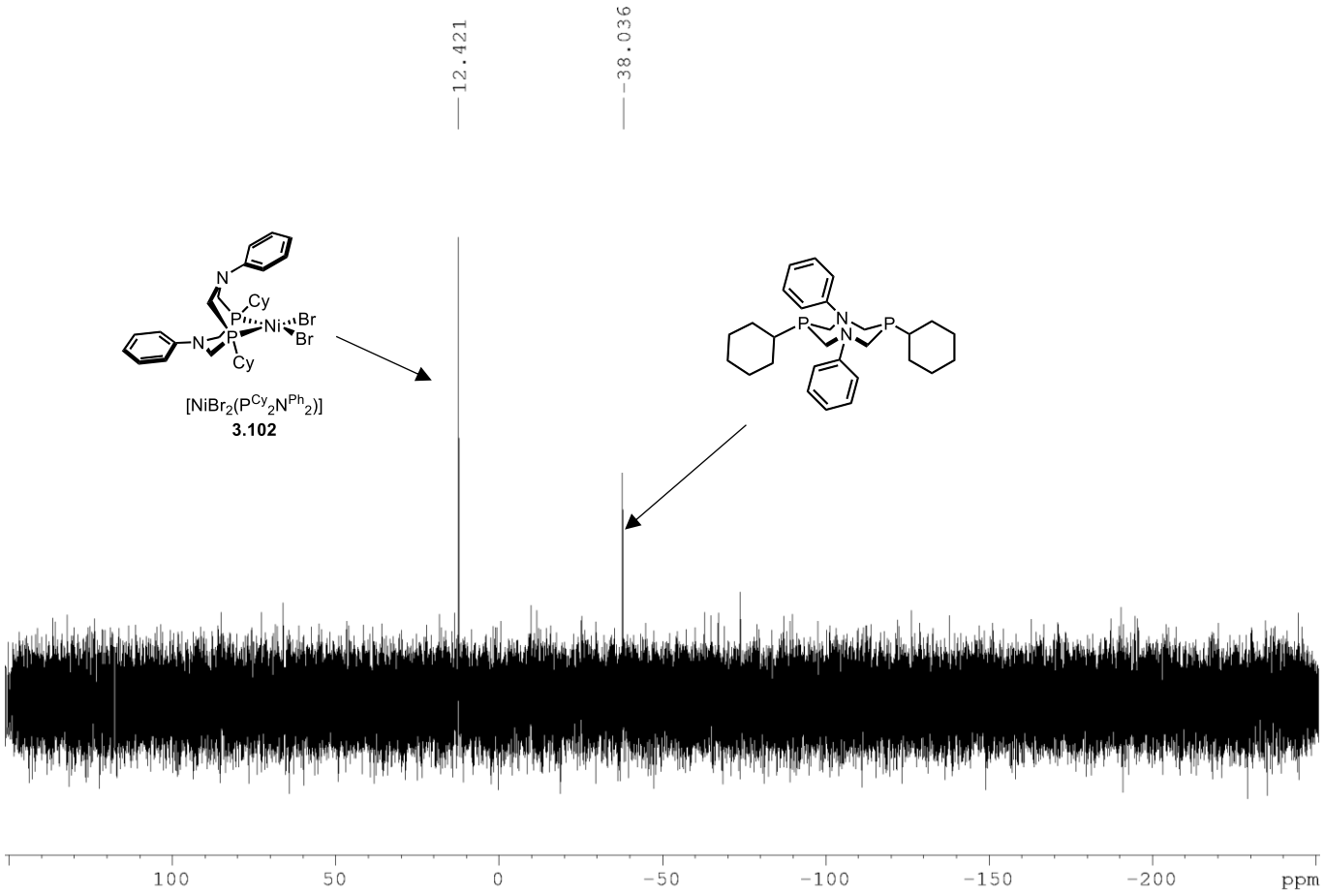

Figure 3.8 $^{31}P\{^{1}H\}$ spectrum taken at time = 300 min at 75 °C, d_8-PhMe, 202 MHz

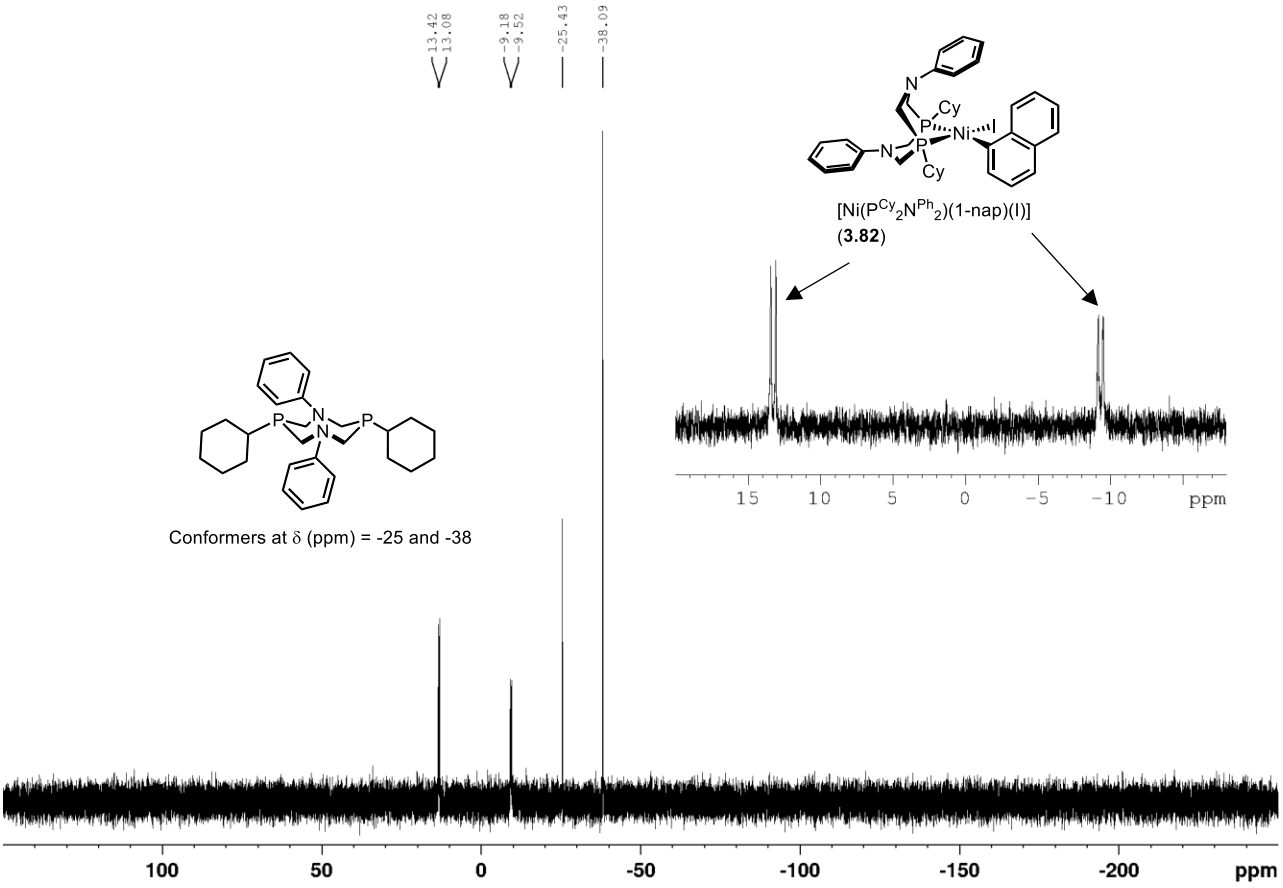

Figure 3.9 ^{1}H spectrum taken at time = 300 min at 75 °C, d_8-PhMe, 500 MHz with key peaks integrated

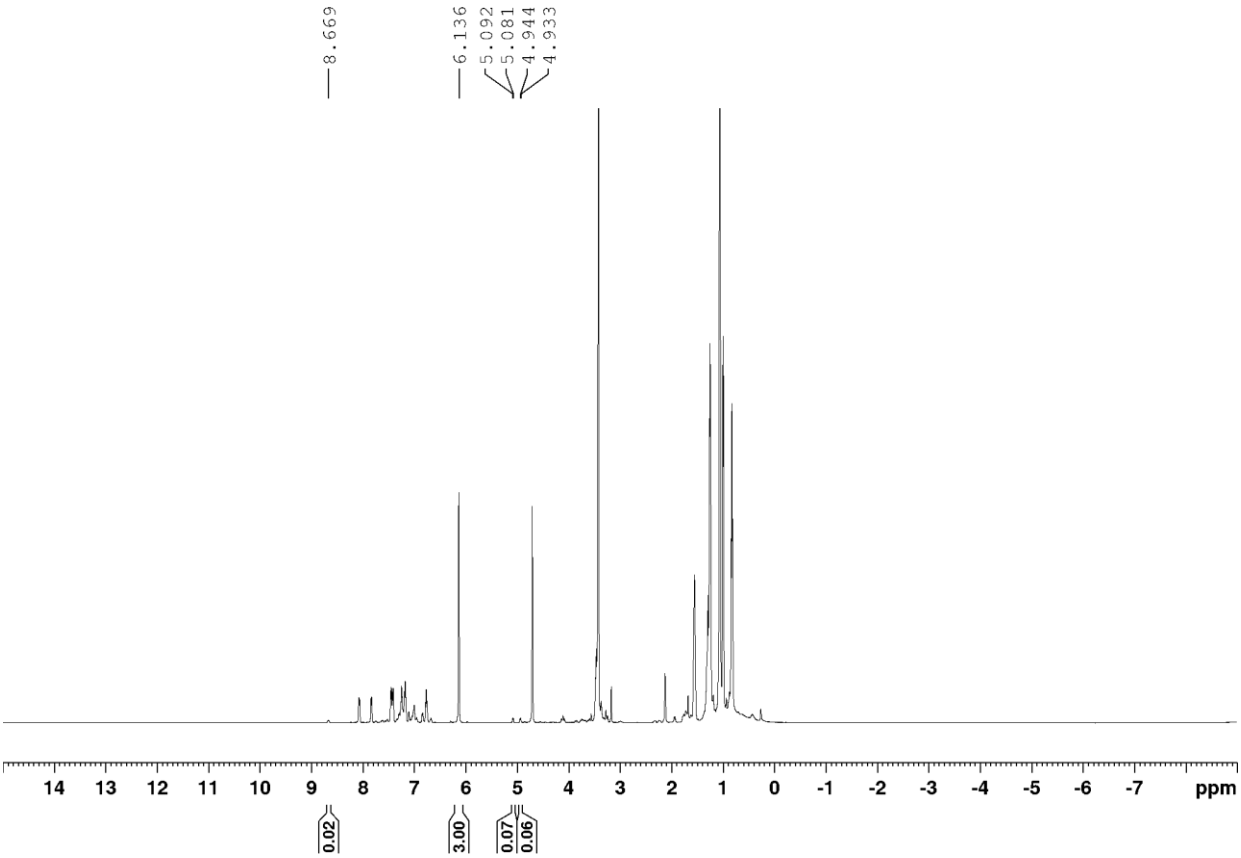

Figure 3.10 ^{1}H spectrum taken at time = 300 min at 75 °C, d_8-PhMe, 500 MHz (zoomed in)

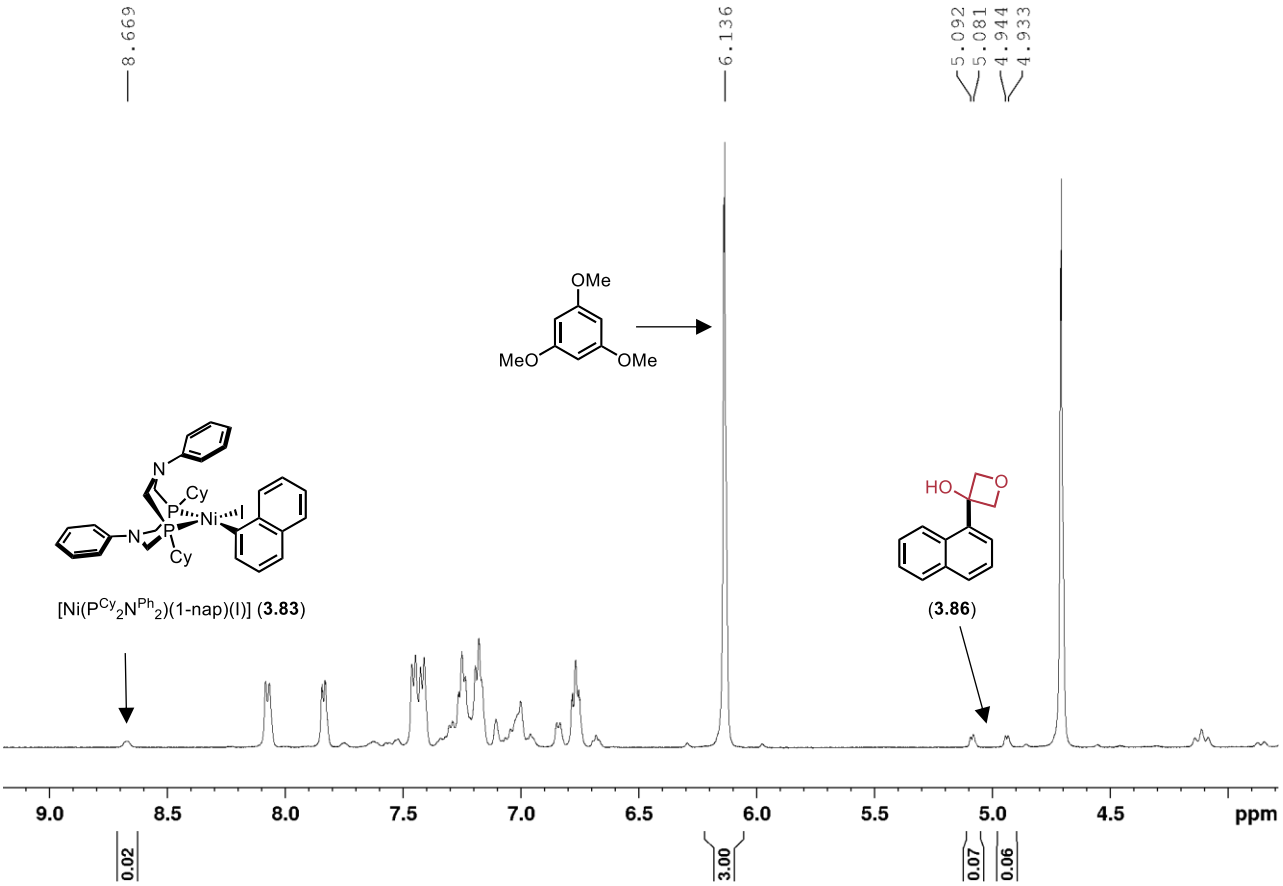

Figure 3.11 $^{31}P\{^{1}H\}$ spectrum taken after heating for ~12 hours at 100 °C, d_8-PhMe, 121 MHz

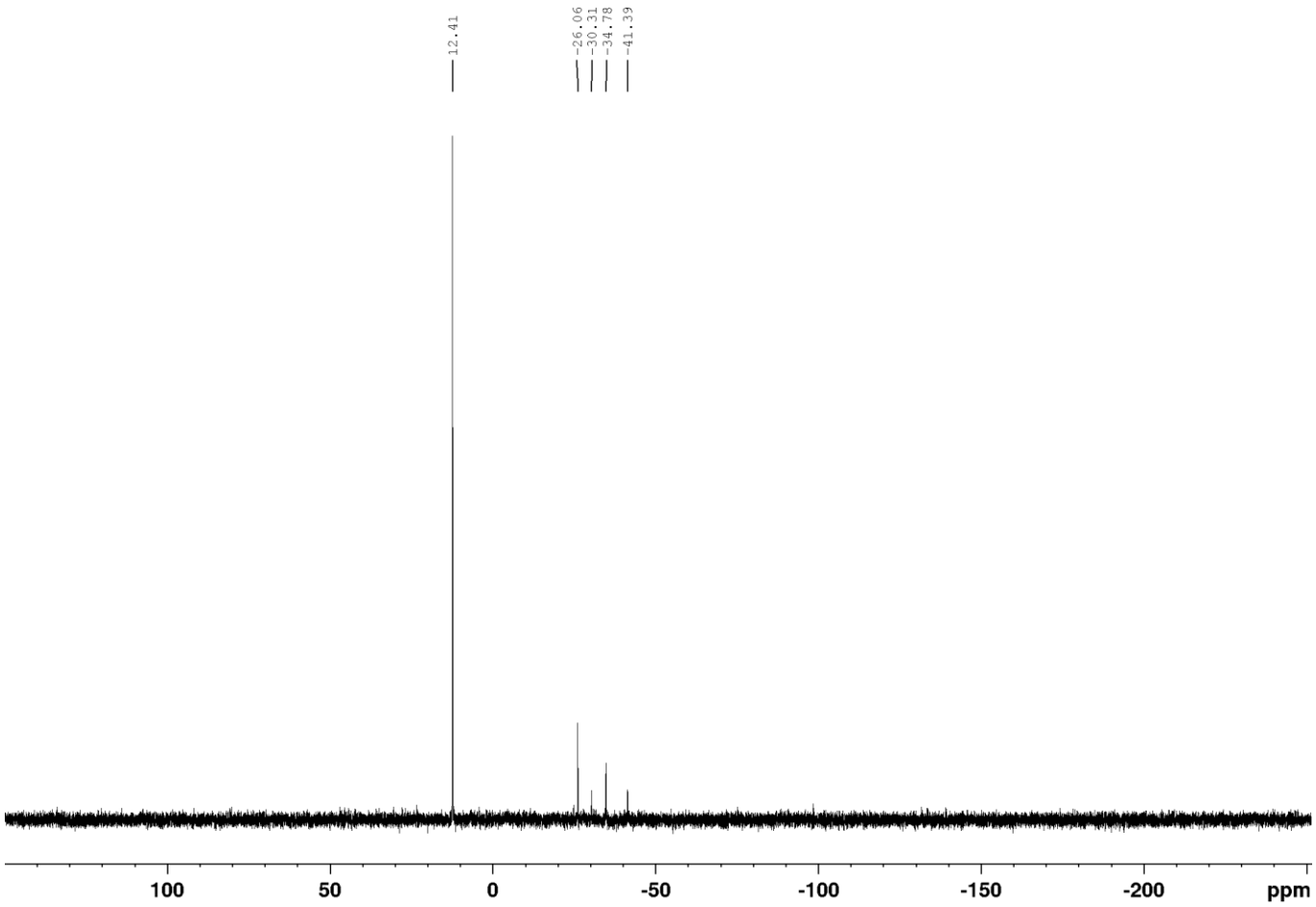

Figure 3.12 ^{1}H spectrum taken after heating for ~12 hours at 100 °C, d_8-PhMe, 300 MHz

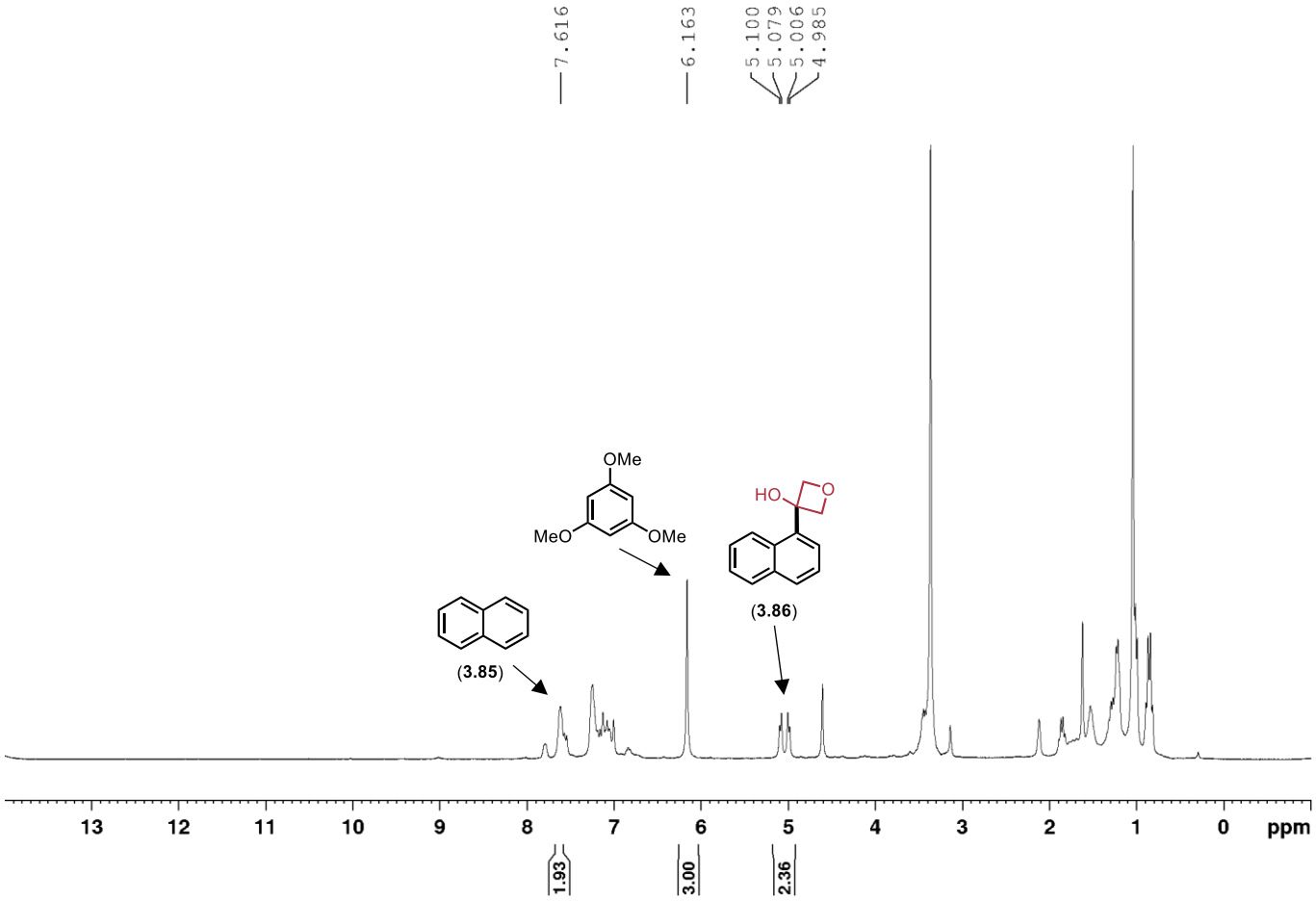

3.9.6 NMR spectra η^2-Carbonyl coordination complexes

Figure 3.13 shows the crude $^{31}P\{^1H\}$ NMR of [Ni(dcype)(cod)] (**3.88**), which was from mixing $Ni(cod)_2$ (1.00 equiv, 0.05 mmol, 13.7 mg) and dcype (1.00 equiv, 0.05 mmol, 21.3 mg) in 1 mL of d_6-benzene. The main peak, a singlet at δ = 57.0 (ppm), matches a previous literature report for compound **3.88**.[56] Figure 3.14 shows the crude $^{31}P\{^1H\}$ NMR of [Ni(dcype)(η^2-PhCHO)] (**3.89**), which was formed in situ by adding benzaldehyde (1.5 equiv, 0.075 mmol, 7.6 µL) to the solution of **3.88.** Two new doublets were observed as the main species in solution. The peaks δ (ppm) = 60.9 (d, *J* = 67 Hz) and 58.4 (d, *J* = 67 Hz) are in accordance with a known literature report of with the closely-related [Ni(dippe)(η^2-PhCHO)],[37] where dippe is 1,2-bis(diispropylphosphino)ethane.

Figure 3.15 shows the crude $^{31}P\{^1H\}$ NMR spectrum obtained after mixing $Ni(cod)_2$ (1.00 equiv, 0.05 mmol, 13.7 mg) and $P^{Cy}{}_2N^{ArCF3}{}_2$ (1.00 equiv, 0.05 mmol, 30.1 mg) in C_6D_6 (0.5 mL). The spectrum indicates the presence of free $P^{Cy}{}_2N^{ArCF3}{}_2$ along with [Ni($P^{Cy}{}_2N^{ArCF3}{}_2$)$_2$] (**3.83**). However, since [Ni($P^{Cy}{}_2N^{ArCF3}{}_2$)(cod)] (**3.78**) is poorly soluble in d_6-benzene the distribution of species in solution is reflective of the equilibrium between species (Scheme 3.25). 1 equivalent of piperonal (1.00 equiv, 0.05 mmol, 7.5 mg) was added to the mixture. Figure 3.16 shows the crude $^{31}P\{^1H\}$ NMR spectrum after addition of piperonal. No new significant peaks were observed.

Figure 3.17 shows the crude $^{31}P\{^1H\}$ NMR spectrum obtained after mixing $Ni(cod)_2$ (1.00 equiv, 0.05 mmol, 13.7 mg) and $P^{Cy}{}_2N^{ArCF3}{}_2$ (1.00 equiv, 0.05 mmol, 30.1 mg) in PhCHO (1 mL) with a trace amount of C_6D_6 added for lock (0.1 mL). Large new, unidentified, peaks were

observed in the $^{31}P\{^{1}H\}$ spectrum, however, no new doublets were observed. We were unable to crystallize or identify any new compounds from this mixture.

Scheme 3.26 Equilibrium between $Ni(P_2N_2)$ complexes

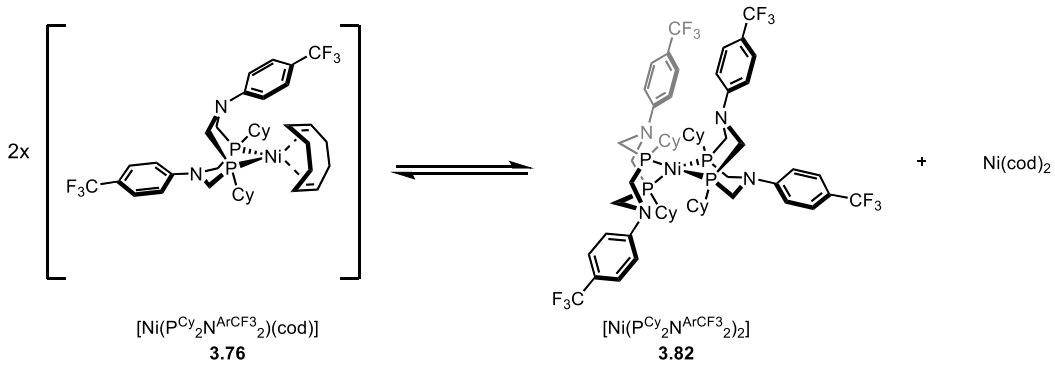

Figure 3.18 shows the crude $^{31}P\{^{1}H\}$ NMR spectrum obtained after mixing $Ni(cod)_2$ (1.00 equiv, 0.05 mmol, 13.7 mg), $P^{tBu}{}_2N^{ArCF3}{}_2$ (1.00 equiv, 0.05 mmol, 27.5 mg), and PhCHO (1.5 equiv, 0.075 mmol, 7.6 µL) in PhMe (1 mL) with a trace amount of C_6D_6 added for lock (0.1 mL). The peaks at δ (ppm) = 41.2 (d, *J* = 26 Hz) and 27.4 (d, *J* = 26 Hz) indicate formation of the η^2-aldhyde complex with this ligand (**3.105**). It should be noted that this ligand was not effective in the catalytic transformations presented in Chapters 2 and 3. The singlets at δ (ppm) = 18.9 and 27.9 are assumed to be $[Ni(P^{tBu}{}_2N^{ArCF3}{}_2)(cod)]$ and $[Ni(P^{tBu}{}_2N^{ArCF3}{}_2)_2]$, respectively.

Figure 3.19 shows the crude $^{31}P\{^{1}H\}$ NMR spectrum obtained after mixing $Ni(cod)_2$ (1.00 equiv, 0.05 mmol, 13.7 mg), $P^{Ph}{}_2N^{ArCF3}{}_2$ (1.00 equiv, 0.05 mmol, 29.5 mg), and PhCHO (1.5 equiv, 0.075 mmol, 7.6 µL) in PhMe (1 mL) with a trace amount of C_6D_6 added for lock (0.1 mL). The chemical shift for $[Ni(P^{Ph}{}_2N^{ArCF3}{}_2)_2]$ (**3.107**), δ (ppm) = 8.5, matches a previous literature report.[27] No aldehyde binding was observed. This ligand was somewhat effective in catalysis (see: Table 2.1, entry 7).

Figure 3.20 shows the crude $^{31}P\{^{1}H\}$ NMR spectrum obtained after mixing $Ni(cod)_2$ (1.00 equiv, 0.05 mmol, 13.7 mg), $P^{Cy}{}_2N^{ArOMe}{}_2$ (1.00 equiv, 0.05 mmol, 26.3 mg), and PhCHO (1.5 equiv, 0.075 mmol, 7.6 µL) in PhMe (1 mL) with a trace amount of C_6D_6 added for lock (0.1 mL). The peaks at δ (ppm) = 20.5 (d, *J* = 48 Hz) and -5.6 (d, *J* = 48 Hz) indicate formation of trace η^2-aldehyde complex with this ligand (**3.110**). This ligand was not effective in catalysis.

Figure 3.13 Crude $^{31}P\{^{1}H\}$ of [Ni(dcype)(cod)] (3.88), C_6D_6, (121 MHz)

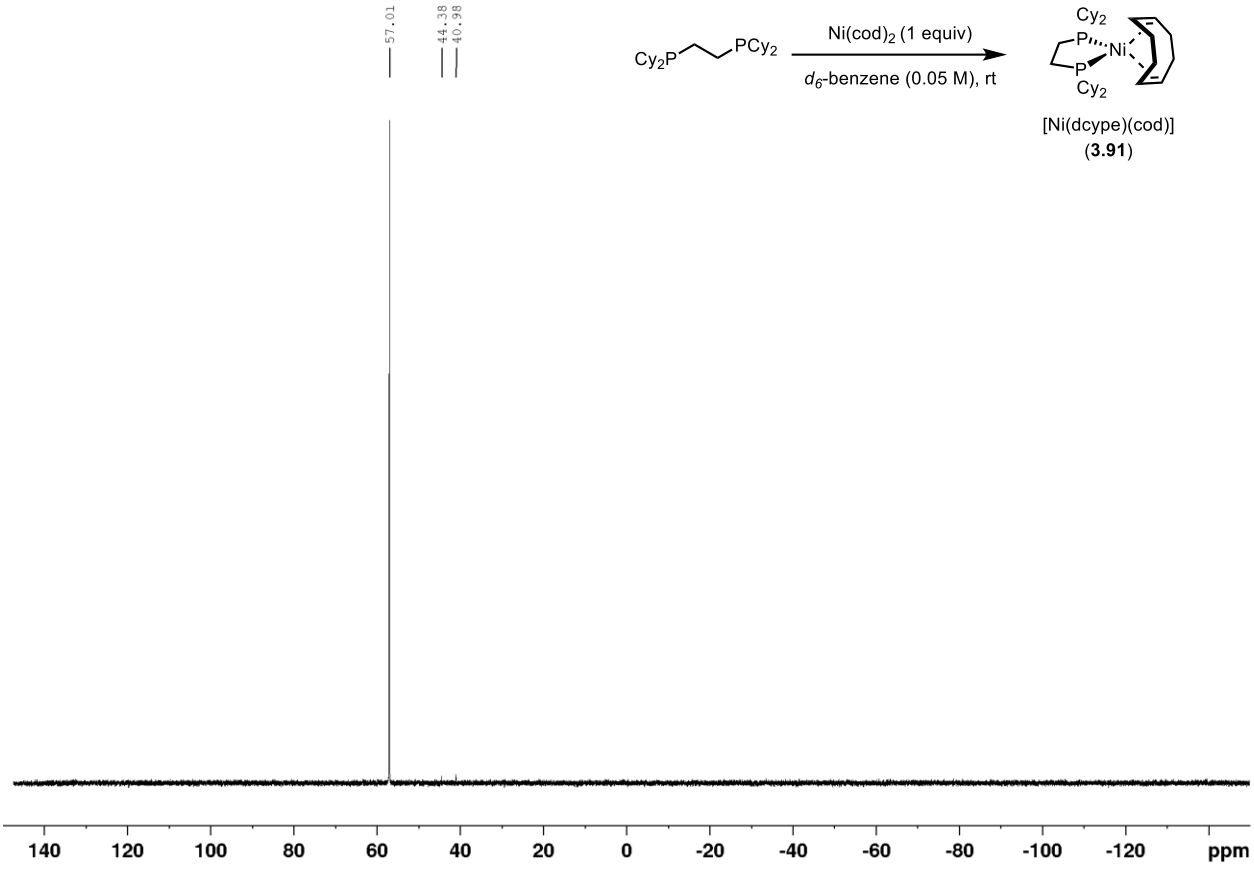

Figure 3.14 Crude $^{31}P\{^{1}H\}$ of [Ni(dcype)(η^2-PhCHO)] (**3.89**), C_6D_6, (121 MHz)

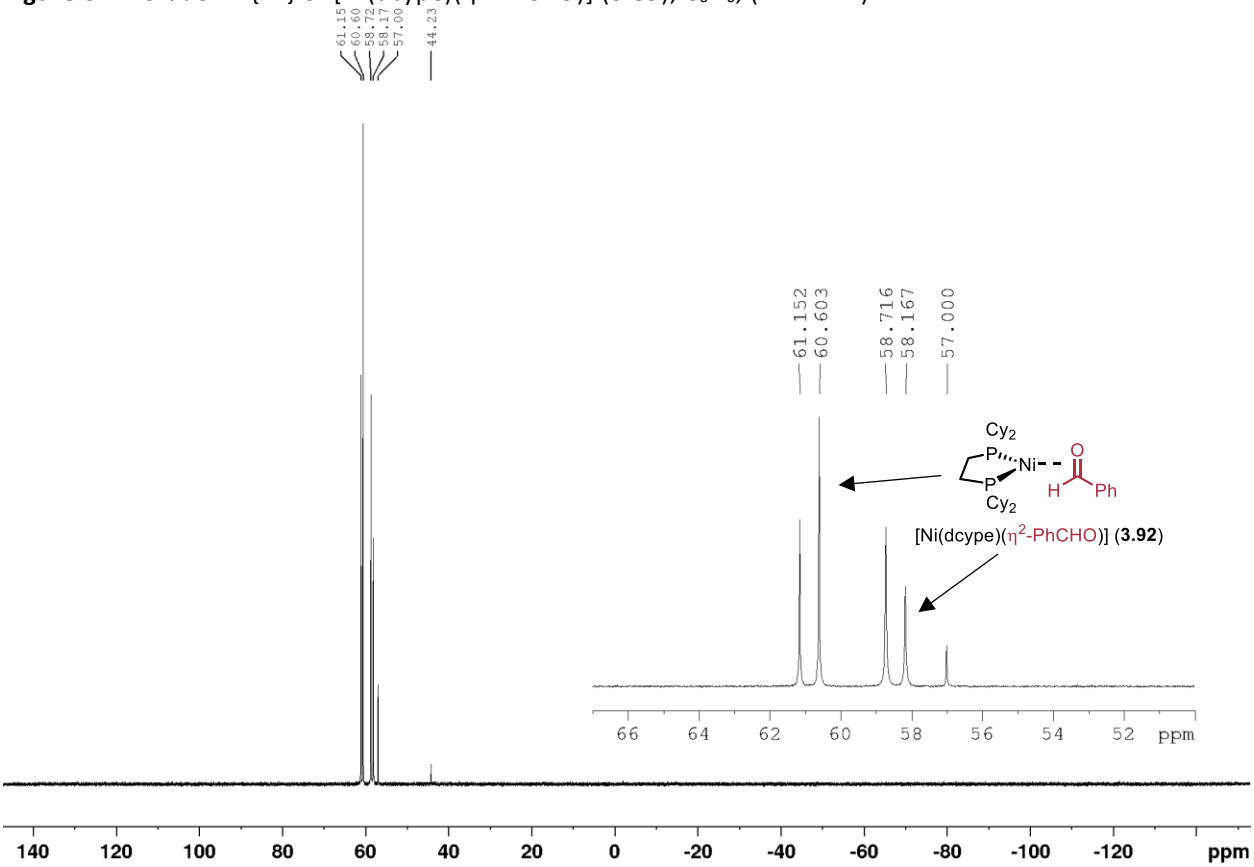

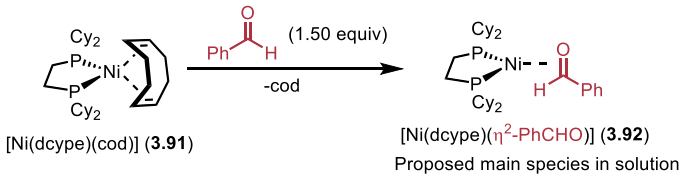

Figure 3.15 Crude $^{31}P\{^{1}H\}$ of [Ni($P^{Cy}_2N^{ArCF3}_2$)(cod)] (**3.89**), C_6D_6, (121 MHz)

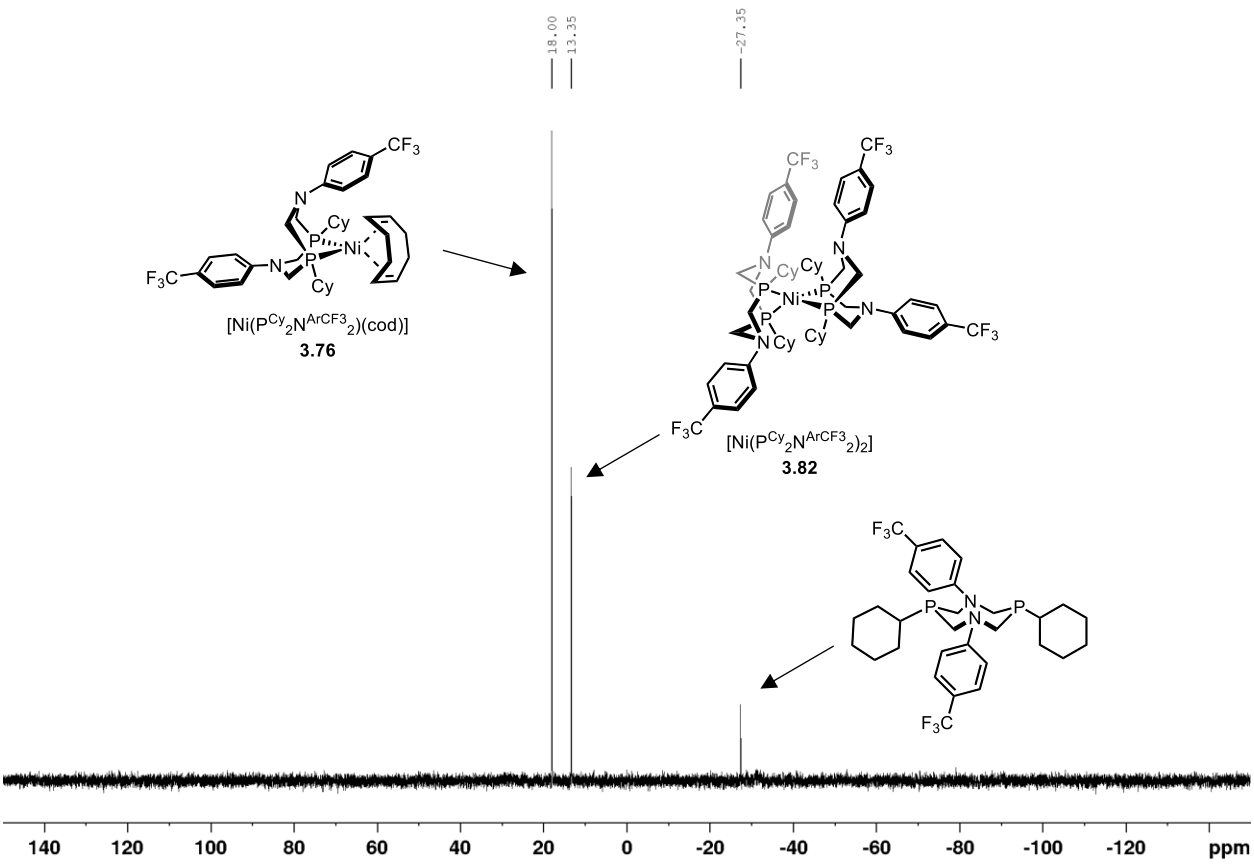

Figure 3.16 Crude $^{31}P\{^{1}H\}$ after addition of piperonal to **3.89**, C_6D_6, (121 MHz)

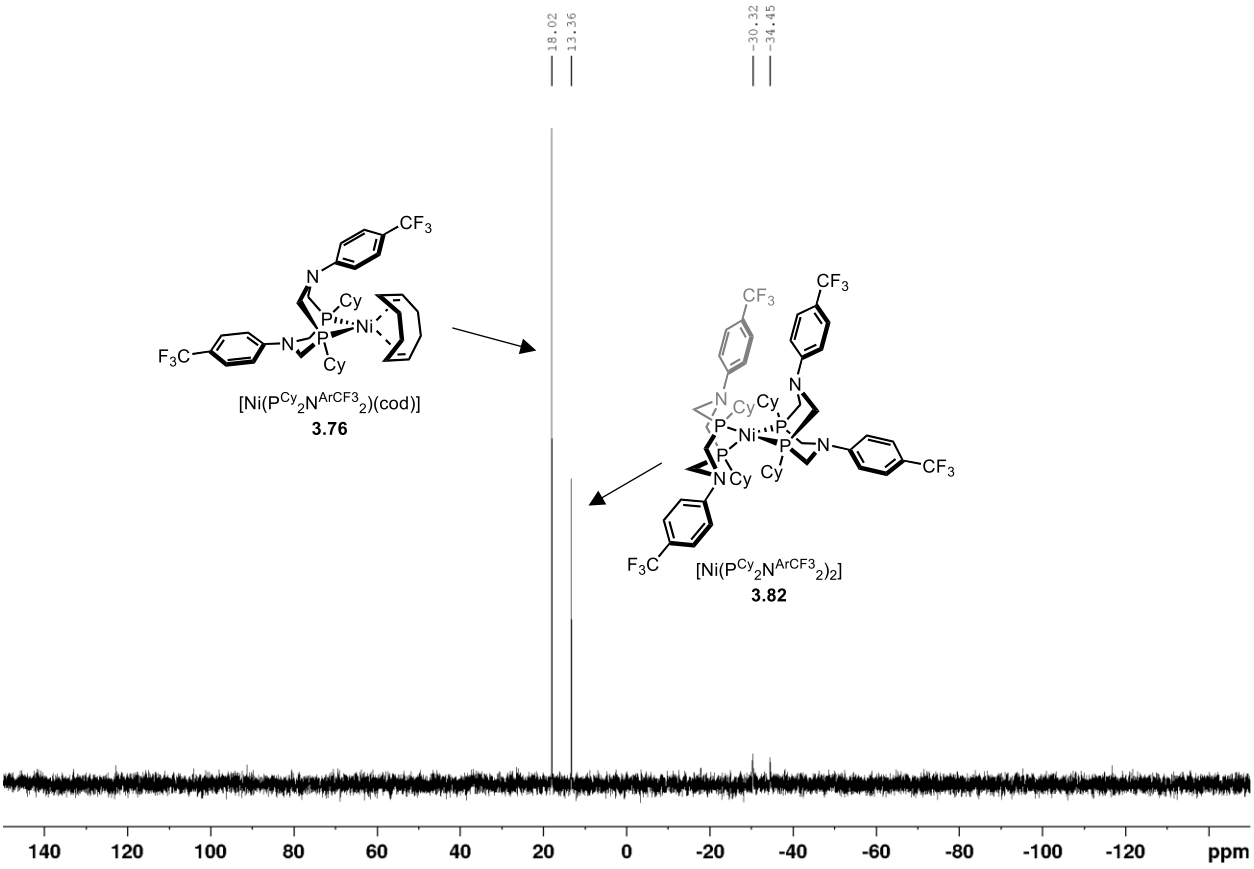

Figure 3.17 Crude $^{31}P\{^{1}H\}$ after mixing $P^{Cy}{}_2N^{ArCF3}{}_2$ and $Ni(cod)_2$ in PhCHO as solvent, C_6D_6 (for lock), (121 MHz)

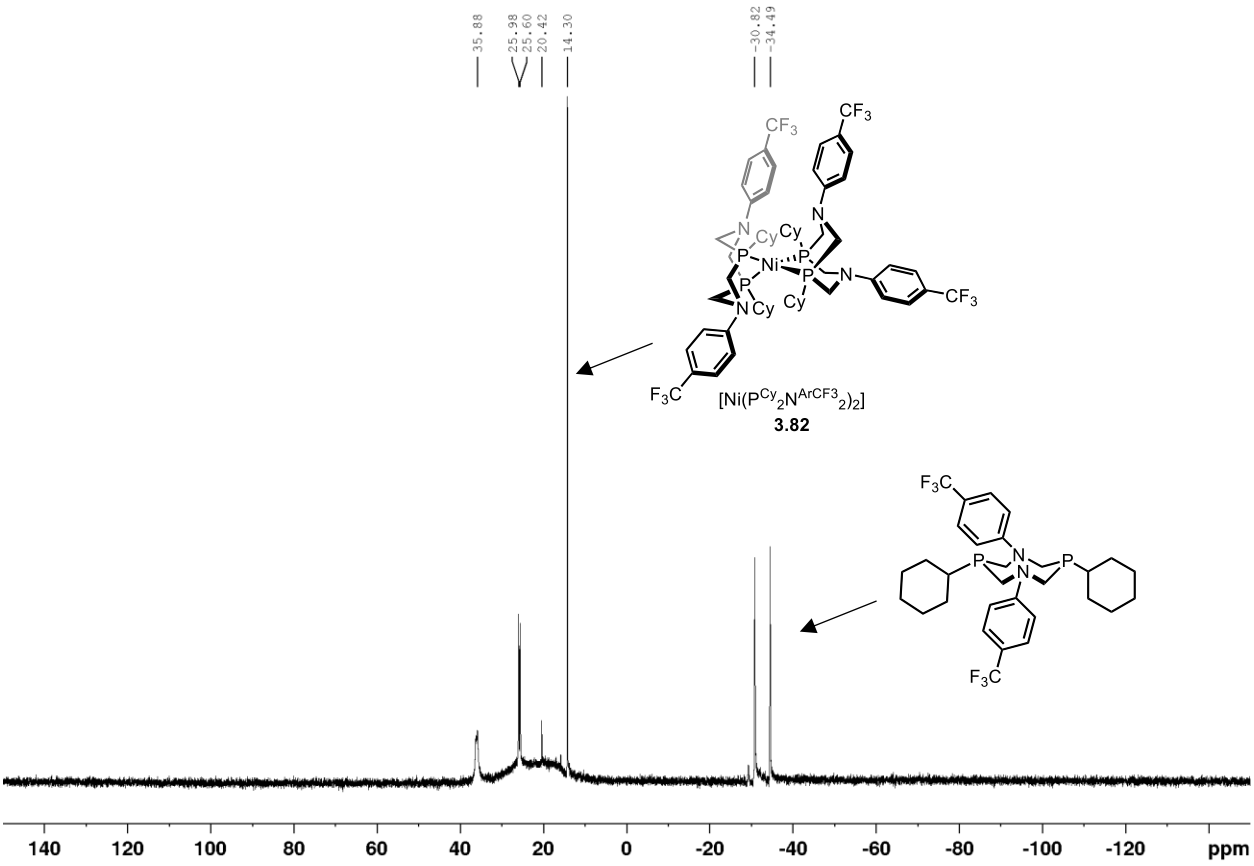

Figure 3.18 Crude $^{31}P\{^{1}H\}$ after mixing $P^{tBu}{}_2N^{ArCF3}{}_2$, $Ni(cod)_2$, and PhCHO, C_6D_6 (for lock), (121 MHz)

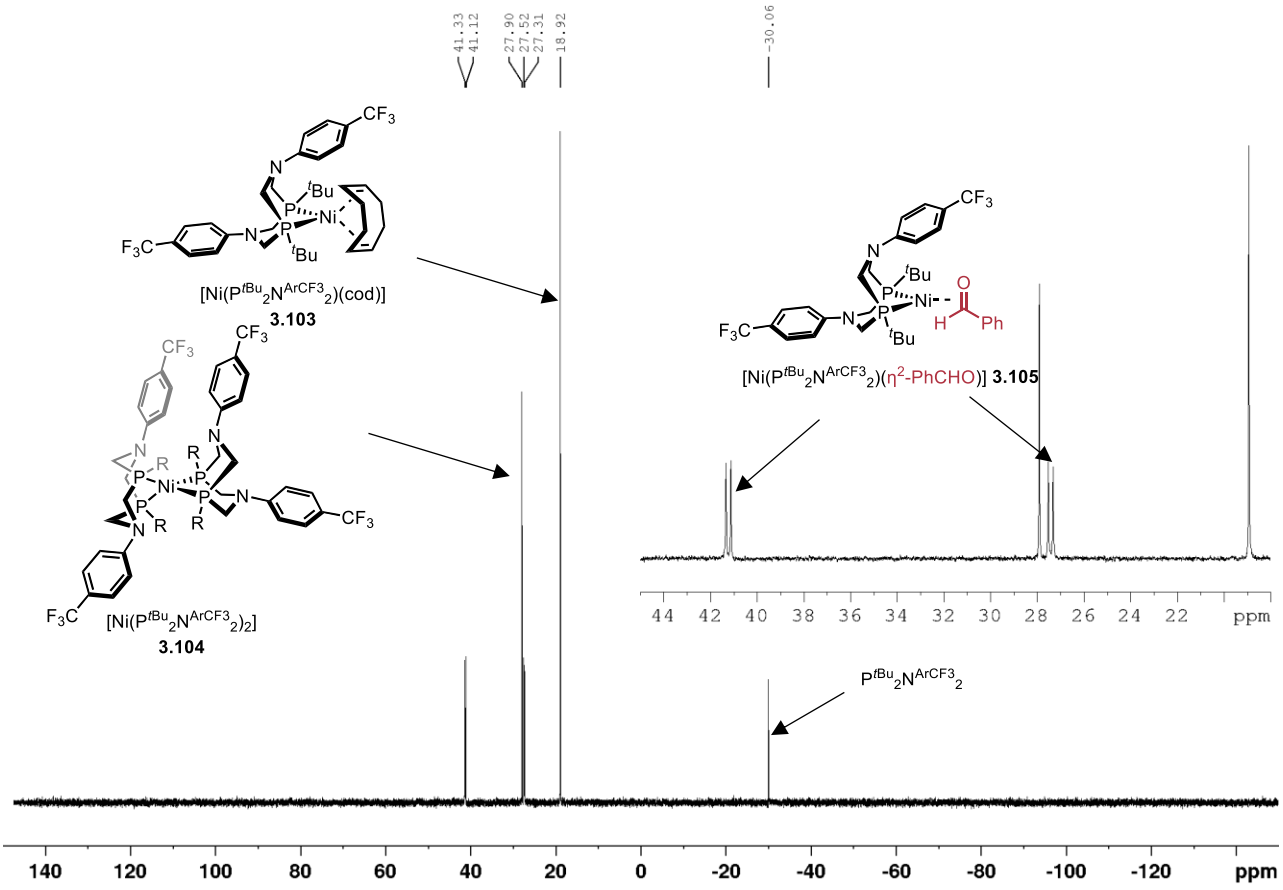

Figure 3.19 Crude $^{31}P\{^{1}H\}$ after mixing $P^{Ph}{}_2N^{ArCF3}{}_2$ and $Ni(cod)_2$, C_6D_6 (for lock), (121 MHz)

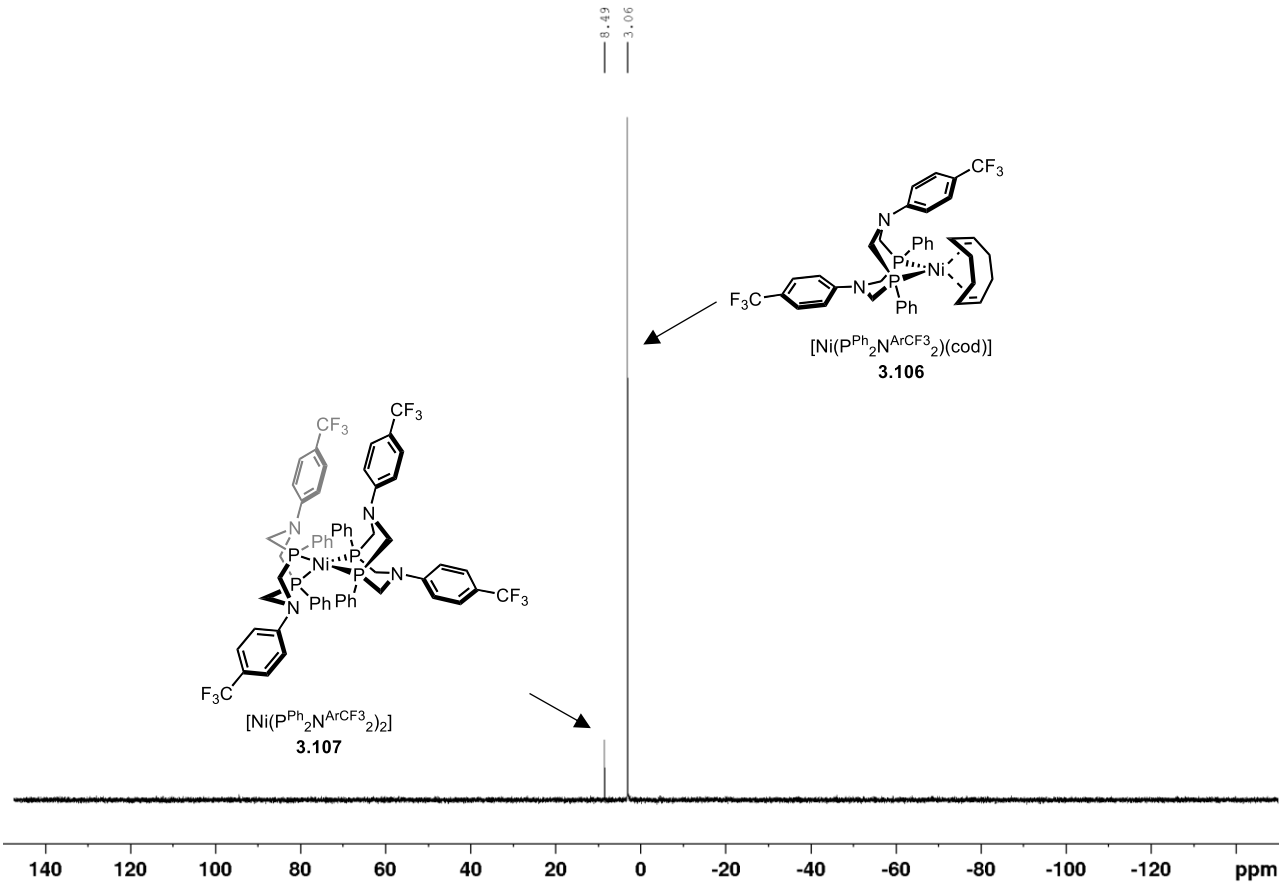

Figure 3.20 Crude $^{31}P\{^{1}H\}$ after mixing $P^{Cy}{}_2N^{ArOMe}{}_2$, PhCHO, and $Ni(cod)_2$, C_6D_6 (for lock), (121 MHz)

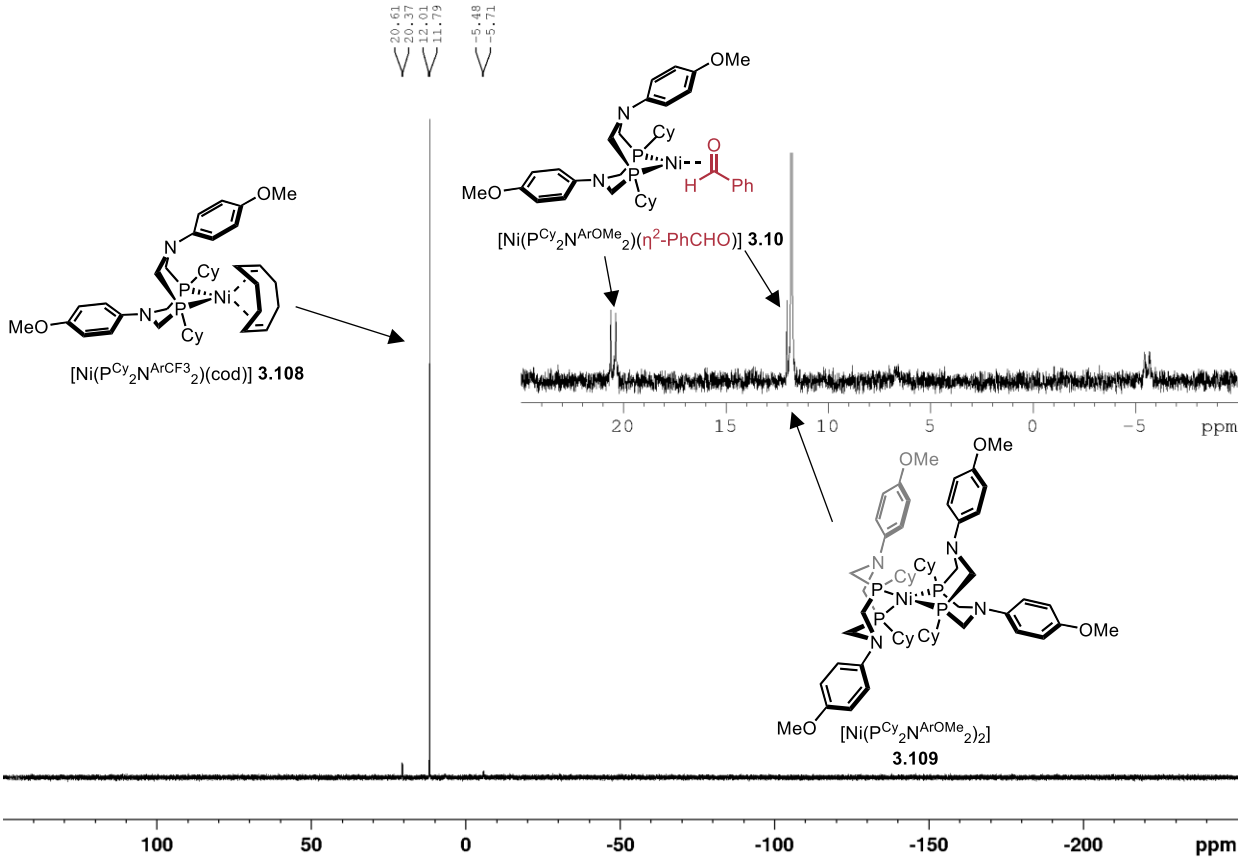

3.10 References

[1] Representative examples include: (a) Vandavasi, J.K.; Hua, X.Y.; Ben Halima, H.; Newman, S. G. A nickel-vatalyzed carbonyl-Heck reaction. *Angew. Chem. Int. Ed.* **2017**, *56*, 15441-15445. (b) Garcia, K. J.; Gilbert, M. M.; Weix, D. J. Nickel-catalyzed addition of aryl bromides to aldehydes to form hindered secondary alcohols. *J. Am. Chem. Soc.* **2019**, *141,* 1823-1827. (c) Swyka, R. A.; Zhang, W.; Richardson, J.; Ruble, J. C.; Krische, M. J. Rhodium-catalyzed aldehyde arylation via formate-mediated transfer hydrogenation: Beyond metallic reductants in Grignard/Nozaki–Hiyami–Kishi-type addition. *J. Am. Chem. Soc.* **2019**, *141*, 1828-1832. (d) Ishida, S.; Suzuki, H.; Uechida, S.; Yamaguchi, E.; Itoh, A. Nickel catalyzed intermolecular carbonyl addition of aryl halide. *Eur. J. Org. Chem.* **2019**, 7483-7487.

[2] For a respresentative example see: Li, C.-C.; Wang, H.; Sim, M. M.; Qiu, Z.; Chen, Z.-P.; Khaliullin, R. Z.; Li, C.-J.. Empowering alcohols as carbonyl surrogates for Grignard-type reactions. *Nat. Commun.* **2020**, *11*, 6022.

[3] Lainer, B.; Das, K.; Dydio, P. Variable structure diversification by multicatalysis: The case of alcohols. *Chem. Commun*. **2023**, *59*, 4716–4725.

[4] Ye, D.; Liu, Z.; Sessler, J. L.; Lei, C. Base-free oxidation of alcohols enabled by nickel(II)-catalyzed transfer dehydrogenation. *Chem. Commun*. **2020**, *56*, 11811–11814.

[5] (a) Shapiro, N.; Vigalok, A. Highly efficient organic reactions "on water", "in water", and both. *Angew. Chem. Int. Ed.* **2008**, *47*, 2849–2852. (b) Vanoye, L.; Aloui, A.; Pablos, M.; Philippe, R.; Percheron, A.; Favre-Réguillon, A.; De Bellefon, C. A safe and efficient flow oxidation of aldehydes with O_2. *Org. Lett*. **2013**, *15*, 5978–5981. (c) Vanoye, L.; Favre-Réguillon, A. Mechanistic insights into the aerobic oxidation of aldehydes: evidence of multiple reaction pathways during the liquid phase oxidation of 2-ethylhexanal. *Org. Process Res. Dev.* **2022**, *26*, 335–346.

[6] Vanoye, L.; Favre-Réguillon, A.; Aloui, A.; Philippe, R.; de Bellefon, C. Insights in the aerobic oxidation of aldehydes. *RSC Advances* **2013**, *3*, 18931-18937.

[7] Grammer,G. N. The trimerization of aldehydes. LSU Historical Dissertations and Theses, Louisiana State University and Agricultural & Mechanical College, 1958.

[8] Watanabe, Y.; Sawada, K.; Hayashi, M. A green method for the self-aldol condensation of aldehydes using lysine. *Green Chem.* **2010**, *12*, 384-386.

[9] Henne, A. L.; Hill, P. The preparation of aldehydes, ketones, and acids by ozone oxidation. *J. Am. Chem. Soc* **1943**, *65*, 752–754.

[10] Franke, R.; Selent, D.; Börner, A. Applied hydroformylation. *Chem. Rev*. **2012**, *112*, 5675–5732.

[11] Yoshida, M.; Otaka, H.; Doi, T. An efficient partial reduction of α,β-unsaturated estersu DIBAL-H in flow. *Eur. J. Org. Chem.2014*, **2014**, 6010–6016.

[12] Lee, D. G.; Spitzer, U. A. Aqueous dichromate oxidation of primary alcohols. *J. Org. Chem.* **1970**, *35*, 3589–3590.

[13] (a) Oppenauer, R. V. Eine methode der dehydrierung von sekundären alkoholen zu ketonen. I. Zur herstellung von sterinketonen und sexualhormonen. *Recl. Trav. Chim. Pays-Bas* **1937**, *56*, 137–144. (b) Djerassi, C. The Oppenauer oxidation. *Org.React.* **1951**, *6*, 207−272.

[14] de Graauw, C. F.; Peters, J. A.; van Bekkum, H.; Huskens, J. Meerwein-Ponndorf-Verley reduction and Oppenauer oxidations: An integrated approach. *Synthesis* **1994**, *1994*, 1007−1017.

[15] For a representative example see: Zheng, L.; Yin, X.; Mohammadlou, A.; Sullivan, R. P.; Guan, Y.; Staples, R.; Wulff, W. D. Asymmetric catalytic Meerwein–Ponndorf–Verley reduction of ketones with aluminum(III)-VANOL catalysts. *ACS Catal.* **2020**, *10*, 7188–7194.

[16] Berini, C.;Winkelmann, O. H.; Otten, J.; Vicic, D. A.; Navarro, O. Rapid and selective catalytic oxidation of secondary alcohols at room temperature by using (N-heterocyclic carbene)-Ni-0 systems. *Chem. Eur. J*. **2010**, *16*, 6857−6860

[17] Maekawa, T.; Sekizawa, H.; Itami, K. Controlled alcohol-carbonyl interconversion by nickel catalysis. *Angew. Chem. Int. Ed.* **2011**, *50*, 7022–7026.

[18] For reviews highlighting transfer hydrogenation, see: Bower, J.F.; Kim, I. S.; Patman, R. L.; Krische, M. J. Catalytic carbonyl addition through transfer hydrogenation: A departure from preformed organometallic reagents. *Angew. Chem. Int. Ed.* **2008**, *48*, 34-46. (b) Santana, C. G. and Krische, M. J. From hydrogenation to transfer hydrogenation to hydrogen auto-transfer in enantioselective metal-catalyzed carbonyl reductive coupling: Past, present, and future. *ACS Catal*. **2021**, *11*, 5572-5585.

[19] Bower, J. F.; Skucas, E.; Patman, R. L.; Krische, M. J. Catalytic C−C coupling via transfer hydrogenation: Reverse prenylation, crotylation, and allylation from the alcohol or aldehyde oxidation level. *J. Am. Chem. Soc.* **2007**, *129*, 15134–15135.
[20] Verheyen, T.; van Turnhout, L.; Vandavasi, J.K.; Isbrandt, E. S.; De Borggraeve, W. M.; Newman, S. G. Ketone synthesis by a nickel-catalyzed dehydrogenative cross-coupling of primary alcohols. *J. Am. Chem. Soc.* **2019**, *141*, 6869-6874.
[21] Twilton, J.; Christensen, M.; DiRocco, D. A.; Ruck, R. T.; Davies, I.W.; MacMillan, D. W. C. Selective hydrogen atom abstraction through induced bond polarization: Direct α-arylation of alcohols through photoredox, HAT, and nickel catalysis. *Angew. Chem. Int. Ed*. **2018**, *57*, 5369-5373.
[22] Xu, W.; Shao, Q.; Xia, C.; Zhang, Q.; Xu, Y.; Liu, Y.; Wu, M.. Visible-light-induced selective defluoroalkylations of polyfluoroarenes with alcohols. *Chem. Sci.* **2023**, *14*, 916–922.
[23] Zhang, S.; Li, L.; Li, J.; Shi, J.; Xu, K.; Gao, W.; Zong, L.; Li, G.; Findlater, M. Electrochemical arylation of aldehydes, ketones, and alcohols: From cathodic reduction to convergent paired electrolysis. *Angew. Chem. Int. Ed.* **2021**, *60*, 7275–7282.
[24] (a) Galan, B.R.; Schöffel, J.; Linehan, J. C.; Seu, C.; Appel, A. M.; Roberts, J. A. S.; Helm, M. L.; Kilgore, U. J.; Yang, J. Y.; DuBois, D. L.; Kubiak, C. P. Electrocatalytic oxidation of formate by $[Ni(P^{R}_2N^{R'}_2)_2(CH_3CN)]^{2+}$ complexes. *J. Am. Chem. Soc.* **2011**, *133*, 12767-127779. (b) Kilgore, U. H.; Roberts, J. A. S.; Pool, D. H.; Appel, A. M.; Stewart, M. P.; DuBois, M. R.; Dougherty, W. M.; Kassel, W. S.; Bullock, R. M.; DuBois, D. L. $[Ni(P^{Ph}_2N^{C6H4X}_2)_2]^{2+}$ complexes as electrocatalysts for H_2 production: Effect of substituents, acids, and water on catalytic rates. *J. Am. Chem. Soc.* **2011**, *133*, 5861-5872. (c) Appel, A. M.; Pool, D. H.; O'Hagan, M.; Shaw, W. J.; Yang, J. Y.; DuBois, M. R.; DuBois, D. L.; Bullock, M. R. $[Ni(P^{Ph}_2N^{Bn}_2)_2(CH_3CN)]^{2+}$ as an electrocatalyst for H_2 production: Dependence on acid strength and isomer distribution *ACS Catal.* **2011,** *1*, 777-785. (d) Seu, C. S.; Appel, A. M.; Doud, M. D.; DuBois, D. L.; Kubiak, C. P. Formate oxidation via β-deprotonation in $[Ni(P^{R}_2N^{R'}_2)_2(CH_3CN)]^{2+}$ complexes. *Energy Environ. Sci.* **2012**, *5*, 6480-6490.
[25] MacQueen, P. M.; Tassone, J. P.; Diaz, C.; Stradiotto, M. Exploiting ancillary ligation to enable nickel-catalyzed C–O cross-couplings of aryl electrophiles with aliphatic alcohols. *J. Am. Chem. Soc*. **2018**, *140*, 5023-5027.
[26] (a) Guo, P.; Wang, K.; Jin, W.-J.; Xie, H.; Qi, L.; Liu, X.-Y.; Shu, X.-Z. Dynamic kinetic cross-electrophile arylation of benzyl alcohols by nickel catalysis. *J. Am. Chem. Soc.* **2021**, *143*, 513-523. (b) Li, J.; Sun, W.; Wang, X.; Li, L.; Zhang, Y.; Li, C. Electrochemically enabled, nickel-catalyzed dehydroxylative cross- coupling of alcohols with aryl halides. *J. Am. Chem. Soc.* **2021**, *143*, 3536-3543. (c) Chen, Y.; Wang, X.; He, X.; An, Q.; Zuo, Z. Photocatalytic dehydroxymethylative arylation by synergistic cerium and nickel catalysis. *J. Am. Chem. Soc. 2021*, *143*, 4896–4902.
[27] Nasim, A.; Thomas, G. T.; Ovens, J. S.; Newman, S. G. Reductive 1,2-arylation of isatins. *Org. Lett.* **2022**, *24*, 7232–7236.
[28] Barbier (stoichiometric magnesium) conditions featuring a catalyst are known, see : Wen, Y.; Chen, G.; Huang, S.; Tang, Y.; Yang, J.; Zhang, Y.. The Barbier-Grignard-type arylation of ketones and unexpected cross-coupling of phenolic ketones using unactivated aryl bromides. *Adv. Synth. Catal*. **2016**, *358*, 947–957
[29] Berini, C.; Navarro, O. Ni-catalysed, domino synthesis of tertiary alcohols from secondary alcohols. *Chem. Commun.* **2012**, *48*, 1538–1540.
[30] For an example of coupling and formal elimination of water see: Lei, C.; Yip, Y. J.; Zhou, J. S. Nickel-catalyzed direct synthesis of aryl olefins from ketones and organoboron reagents under neutral conditions. *J. Am. Chem. Soc.* **2017**, *139*, 6086–6089.
[31] Meyer, C. C.; Dubey, Z. J.; Krische, M. J. Enantioselective iridium-catalyzed reductive coupling of dienes with oxetanones and N-acyl-azetidinones mediated by 2-propanol. *Angew. Chem. Int. Ed.* **2022**, *61*, e202115959.
[32] Newman-Stonebraker, S. H.; Wang, J. Y.; Jeffrey, P. D.; Doyle, A. G. Structure–reactivity relationships of Buchwald-type phosphines in nickel-catalyzed cross-couplings. *J. Am. Chem. Soc.* **2022**, *144*, 19635–19648.
[33] Standley, E. A.; Smith, S. J.; Müller, P.; Jamison, T. F. A broadly applicable strategy for entry into homogeneous nickel(0) catalysts from air-stable nickel(II) complexes. *Organometallics* **2014**, *33*, 2012–2018.
[34] Quisenberry, K. T.; Smith, J. D.; Voehler, M.; Stec, D. F.; Hanusa, T. P.; Brennessel, W. W. Trimethylsilylated allyl complexes of nickel. The stabilized bis(π-allyl)nickel complex $[\eta^3\text{-}1,3\text{-}(SiMe_3)_2C_3H_3]_2Ni$ and its mono(π-allyl)NiX (X = Br, I) derivatives. *J. Am. Chem. Soc*. **2005**, *127*, 4376–4387.

[35] Newman-Stonebraker, S. H.; Wang, J. Y.; Jeffrey, P. D.; Doyle, A. G. Structure–reactivity relationships of Buchwald-type phosphines in nickel-catalyzed cross-couplings. *J. Am. Chem. Soc.* **2022**, *144*, 19635–19648.
[36] Bennett, M. A. The stabilization and reactivity of strained cyclic alkynes on transition metal centres. *Pure Appl. Chem.* **1989**, *61*, 1695-1700.
[37] Matas, I.; Cámpora, J.; Palma, P.; Álvarez, E. Decomposition of methylnickel(II) amido, alkoxo, and alkyl complexes by β-Hydrogen elimination: A comparative study. *Organometallics* **2009**, *28*, 6515–6523.
[38] Cooper, A. K.; Leonard, D. K.; Bajo, S.; Burton, P. M.; Nelson, D. J. Aldehydes and ketones influence reactivity and selectivity in Nickel-catalysed Suzuki–Miyaura reactions. *Chem. Sci.* **2020**, *11*, 1905–1911.
[39] Newman-Stonebraker, S. H.; Raab, T. J.; Roshandel, H.; Doyle, A. G. Synthesis of nickel(I)–bromide complexes via oxidation and ligand displacement: Evaluation of ligand effects on speciation and reactivity. *J. Am. Chem. Soc.* **2023**, *145*, 19368–19377.
[40] Eberhardt, N. A.; Guan, H. Nickel hydride complexes. Chem. Rev. **2016**, *116*, 8373–8426.
[41] Das, P.; Stolley, R. M.; van der Eide, E. F.; Helm, M. L. A Ni^{II}–bis(diphosphine)–hydride complex containing proton relays–structural characterization and electrocatalytic studies. *Eur. J. Inorg.Chem*. **2014**, *2014*, 4611–4618.
[42] Wang, Y. & Gu, M. The concept of spectral accuracy for MS. *Anal. Chem*. **2010**, *82*, 7055–7062.
[43] Yang, S.; Tang, W.; Yang, Z.; Xu, J. Iridium-catalyzed highly efficient and site-selective deoxygenation of alcohols. *ACS Catal.* **2018**, *8*, 9320-9326.
[44] Da, C.-S.; Wang, J.-R.; Ying, X.-G.; Fan, X.-Y.; Liu, Y.; Yu, S.-L. Highly catalytic asymmetric addition of deactivated alkyl Grignard reagents to aldehydes. *Org. Lett.* **2009**, *11*, 5578-5581.
[45] Balakrishnan, V.; Murugesan, V.; Chindan, B.; Rasappan, R. Nickel-mediated enantiospecific silylation via benzylic C–OMe bond cleavage. *Org. Lett.* **2021**, *23*, 1333-1338.
[46] Swyka, R. A.; Zhang, W.; Richardson, J.; Ruble, J. C.; Krische, M. J. Rhodium-catalyzed aldehyde arylation via formate-mediated transfer hydrogenation: Beyond metallic reductants in Grignard/Nozaki–Hiyami–Kishi-type addition. *J. Am. Chem. Soc.* **2019**, *141*, 1828-1832.
[47] Wang, P.; Zhao, J.-Z.; Li, H.-F.; Liang, X.-M.; Zhang, Y.-L.; Da, C.-S. Acid-catalyzed highly diastereoselective and effective synthesis of 1,3-disubstituted tetrahydropyrano[3,4-b]indoles. *Tetrahedron Lett.* **2017**, *58*, 129-133.
[48] Zhu, N.; Su, M.; Wan, W.-M.; Li, Y.; Bao, H. Practical method for reductive deuteration of ketones with magnesium and D_2O. *Org. Lett.* **2020**, *22*, 991-996.
[49] For recent progress making substituted benzyl thiols see: (a) Xiao, Q.; Zhang, H.; Li, J.-H.; Jian, J.-X.; Tong, Q.-X.; Zhong, J.-J. Directing-group-assisted Markovnikov-selective hydrothiolation of styrenes with thiols by photoredox/cobalt catalysis. *Org. Lett.* **2021**, *23*, 3604–3609. (b) Taniguchi, N. Brønsted acid-assisted zinc-catalyzed Markovnikov-type hydrothiolation of alkenes Using thiols. *J. Org. Chem.* **2020**, *85*, 6528–6534.
[50] (a) Yu, T.; Pang, H.; Cao, Y.; Gallou, F.; Lipshutz, B. H. Safe, scalable, inexpensive, and mild nickel-catalyzed migita-like C–S cross-couplings in recyclable water. *Angew. Chem. Int. Ed.* **2021**, *60*, 3708–3713. (b) Oechsner, R. M.; Wagner, J. P.; Fleischer, I. Acetate facilitated nickel catalyzed coupling of aryl chlorides and alkyl thiols. *ACS Catal*. **2022**, *12*, 2233–2243. (c) Oechsner, R. M.; Lindenmaier, I. H.; Fleischer, I. Nickel catalyzed cross-coupling of aryl and alkenyl triflates with alkyl thiols. *Org. Lett.* **2023**, *25*, 1655–1660.
[51] APEX Softward Suite v 2010 Bruker AXS Inc. Madison Wisconsin USA, 2010.
[52] Blessing R. H., *Acta Crystallogr. Sect. A* **1995**, 33–38.
[53] Dolomanov, O.V.; Bourhis, L.J.; Gildea, R.J.; Howard, J.A.K.; Puschmann, H., OLEX2: A complete structure solution, refinement and analysis program *J. Appl. Cryst*. **2009**, *42*, 339-341.

[54] Sheldrick, G. M. SHELXT-Integrated Space-Group and Crystal-Structure Determination. *Acta Cryst.* **2015**, *A7*1, 3–8.
[55] Sheldrick, G. M. Crystal Structure Refinement with SHELXL. *Acta Cryst.* **2015**, *C71*, 3–8.

[56] Delcaillau, T.; Bismuto, A.; Lian, Z.; Morandi, B. Nickel-catalyzed inter- and intramolecular aryl thioether metathesis by reversible arylation. *Angew. Chem. Int. Ed.* **2020**, *59*, 2110–2114.

Chapter 4 : Controlling Reactivity and Selectivity in the Mizoroki-Heck Reaction: High Throughput Evaluation of 1,5-Diaza-3,7-diphosphacyclooctane Ligands

4.1 Introduction: Research goals

Chapters 2 and 3 focused on the application of 1,5-diaza-3,7-diphosphacyclooctane (P_2N_2) ligands in nickel-catalyzed 1,2-carbonyl additions. While this remains an area of interest, we hypothesized that P_2N_2 ligands have broader utility in transition metal-catalyzed cross-couplings. We wished to study a more conventional cross-coupling to see how P_2N_2 ligands performed relative to established ligands and to see if any longstanding issues in catalysis could be addressed. High-throughput experimentation (HTE) can be used to compare a wide range of ligands in parallel. We selected the Mizoroki-Heck reaction as a starting point, as it is an underutilized cross-coupling that has many unsolved challenges (see Section 4.4). We hypothesized that P_2N_2 ligands could solve some of the challenges with Mizoroki-Heck couplings.

4.2 Reuse permissions

Sections 4.4, 4.5 and 4.6.3 were adapted from the manuscript “Controlling Reactivity and Selectivity in the Mizoroki-Heck Reaction: High Throughput Evaluation of 1,5-Diaza-3,7-diphosphacyclooctane Ligands”, by Eric S. Isbrandt, Devon E. Chapple, Phuc Tu, Victoria Dimakos, Anne Marie M. Beardall, Paul D. Boyle, Christopher N. Rowley, Johanna M. Blacquiere, and Stephen G. Newman. *J. Am. Chem. Soc.* **2024**, *in press*. Preprint available at: *ChemRxiv* **2023**. DOI: 10.26434/chemrxiv-2023-t9p7j. The dissertation author is the primary author of this manuscript. Scheme 4.1 was edited from the original manuscript in order to make the narrative of the chapter flow better. Otherwise, all other schemes, figures, and tables were directly incorporated with minor modifications (e.g. compound numbering). Exceptionally Sections 4.5.4, 4.5.3, and 4.5.7 were adapted from the Supporting Information (SI) of the above-mentioned manuscript – these results have been contextualized to the main body of the work. The entirety of Section 4.7 was directly reproduced from the Supporting Information. Sections 4.6.1 and 4.6.2 do not appear in the original manuscript or SI. They have been specifically written for this dissertation.

4.3 Contributions

The initial synthesis and the following optimization of the P_2N_2 Pd G3 precatalyst synthesis was performed by Dr. Victoria Dimakos (Scheme 4.3 and Section 4.7).

Dr. Devon Chapple and Anne Marie Beardall (PhD candidate) from the Blacquiere research group at Western University synthesized and fully characterized the Pd-P_2N_2-MAH complexes, prepared crystals suitable for X-ray diffraction of all four Pd P_2N_2 complexes (Scheme 4.3) and ran some catalytic experiments with them (Table 4.1). Dr. Paul Boyle, also from Western University, was the crystallographer who solved all crystal structures (Scheme 4.3 and Section 4.7.14).

Phuc Tu (PhD candidate) and Professor Chris Rowley, from the Rowley group at Carleton University, performed computational DFT studies to support our experimental work (Section 4.5.8).

4.4 Regioselective Mizoroki-Heck couplings

Transition metal-catalyzed cross-couplings are a cornerstone family of reactions in synthetic organic chemistry. The growth of this field is closely tied to the development of new ligands that enable reactions with novel coupling partners, expanded scope, milder conditions, lowered catalyst loading, and improved selectivity. The search for readily available and powerful ligands continues today, seeking to overcome the many unsolved challenges in catalysis. The Mizoroki-Heck reaction is among the most influencial and fundamental coupling reactions.[1,2] However, despite its prominence in textbooks, Heck-type reactions are rarely used in routine organic synthesis. In one survey of the medicinal chemistry literature, 0.4% of C–C bond-forming experiments were reported to be Mizoroki-Heck reactions, compared to 40.2% that were Suzuki-Miyaura reactions.[3] Given the broad commercial availability of olefins and the value of substituted alkenes in medicinal chemistry, this contrast may seem surprising. One explanation is that, despite decades of research, the intermolecular Mizoroki-Heck reactions remain challenging compared to traditional biaryl-forming cross-coupling. Often reaction conditions are highly optimized for a specific class of substrates and aren't easily applicable to a broader range of coupling partners. Likewise, achieving high selectivity for a particular regioisomer can require very specific ligands or reactants. While issues with selectivity or reactivity are common, many landmark reports have demonstrated that high-yielding, regioselective, intermolecular Mizoroki-Heck reactions are indeed possible (Scheme 4.1A). For example, couplings with aliphatic alkenes,[4] vinyl ethers,[5] and styrenes[6] have been achieved to selectively obtain either the branched or linear products by careful choice of catalyst, reaction conditions, and (pseudo)halide. Progress has also been made with other electron-deficient[7] and electron-rich alkenes[8] among other reaction

partners.[9] Despite the many successes in the regioselective Mizoroki-Heck reaction, navigating the diverse set of available reactions is challenging, and identifying effective conditions for coupling a particular aryl(pseudo)halide and alkene can be arduous or even impossible if the reactant combination of interest has not yet been reported to provide access to the desired alkene regioisomer. Filling these holes and identifying more general catalysts are two important goals when developing site-selective methodologies. Methods which enable the synthesis of multiple regioisomers with general reaction conditions remain sparsely reported, though a recent report by Chen and co-workers on the coupling of dienes demonstrated regiocontrol (Scheme 4.1B).[10] In this case, achieving a switch in regiochemistry involved modifying the ligand, base, solvent, and (pseudo)halide.

4.4.1 Research proposal: P_2N_2s as versatile ligands in Mizoroki-Heck couplings

We hypothesized that many unresolved challenges in Mizoroki-Heck couplings could be solved by identifying more universal ligands and/or reaction conditions. One ligand family we sought to explore was the 1,5-diaza-3,7-diphosphacyclooctanes, abbreviated as P_2N_2 ligands. These are modular and readily accessible from the corresponding phosphine and amine via condensation with formaldehyde.[11] However, their use in organic synthesis has been sparsely reported.[12,13] Herein we report an evaluation of diverse Mizoroki-Heck reactions, using high-throughput experimentation, that reveals that P_2N_2 ligands provide both high reactivity and selectivity with a range of substrates (Scheme 4.1C). The broadness of reactivity between the studied couplings was not afforded by any other ligand class.

Scheme 4.1 Regioselectivity in the Mizoroki-Heck reaction

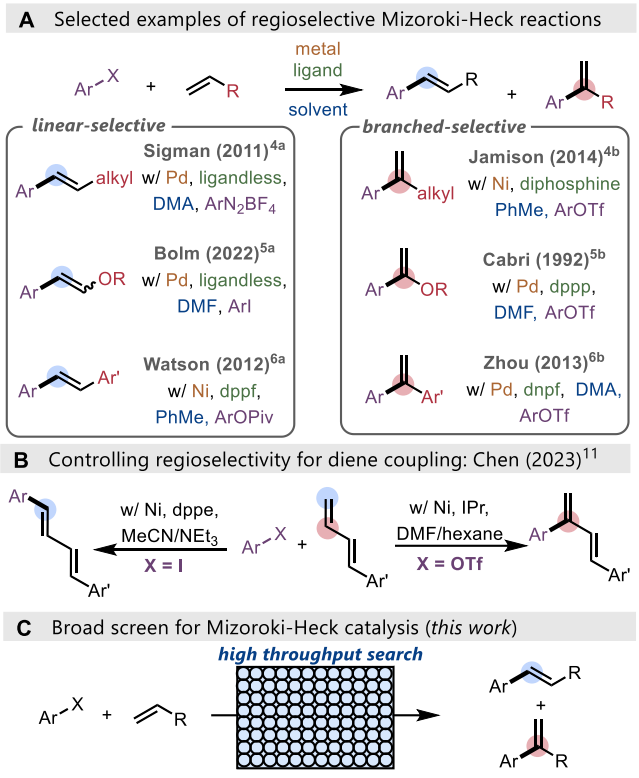

4.5 Results and discussion

4.5.1 High-throughput experimentation: Selection of key parameters and results

To assess if P_2N_2 ligands have any unique utility for Mizoroki-Heck reactions, a high-throughput screening campaign was carried out to compare them with well-established commercial ligands (Scheme 4.2A).[14] Coupling with both Ni and Pd was explored using iodobenzene and phenyl triflate as differing classes of coupling partners.[15,16] A model substrate was chosen from four commonly-used classes of olefins. Similarly, a common polar (DMF) and non-polar (toluene) solvent were chosen for study. According to Sherwood et al., Heck reactions in polar aprotic solvents are favored with aryl iodides but reactions with aryl triflates can be preferred in non-polar solvents.[17] To keep the number of experiments reasonable, we elected to screen all reactions with triethylamine as a common base. Three P_2N_2 ligands derived from benzotrifluoroaniline with differing phosphine substituents (P^{Ph}, P^{Cy}, and P^{tBu}) were explored as $P^{Cy}N^{ArCF3}{}_2$ was previously found to be highly effective in nickel-catalyzed cross couplings.[14h,j] 9 'gold standard' commercially available phosphine ligands shown to be optimal in related methodologies were selected: dppp,[5b, 18] dppf,[6a,18, 19] JohnPhos, [20] P^tBu_3,[5f] PPh_3,[1g] IMes, [21] DavePhos,[22] 1,10-phenanthroline,[23] and XantPhos.[24]

A comprehensive screen of all conditions was carried out representing 384 distinct experiments; the results of which are provided in Section 4.7.11 and can be downloaded in machine-readable format through the Open Reaction Database.[25] As discussed, Mizoroki-Heck reactions can have challenges in both reactivity and regioselectivity, with each combination of aryl (pseudo)halide and olefin coupling partner having unique challenges and solutions. To identify the best hits, a threshold of both >15% assay yield and >10:1 regioselectivity was chosen

for visualization (Scheme 4.2B). Within these parameters, P_2N_2 ligands were the only of those screened that provided hits with each different substrate class, with $P^{tBu}{}_2N^{ArCF3}{}_2$ (L3) in particular proving to be the most broadly effective choice. Interestingly, promising results were observed with P_2N_2 ligands with both Pd and Ni as metals, both toluene and DMF as solvents, and both iodide and triflate substrates, further highlighting the generality of this ligand scaffold. Selected hits were chosen for replication to confirm the yield and regioselectivity (Scheme 4.2C). Each different product class could be accessed in 15-85% yield with regioisomeric ratios of the substituted product ranging from 12:1 to >20:1, demonstrating that synthetically viable quantities of material could be directly accessed without targeted optimization. Of particular note is the coupling with styrene. When using $P^{Ph}{}_2N^{ArCF3}{}_2$ as a ligand, the linear (i.e. stilbene) isomer was found to be the major product in all cases. In contrast, for all styrene hits identified with $P^{tBu}{}_2N^{ArCF3}{}_2$ as a ligand, the branched 1,1-diphenylethylene was found to be the major isomer. This ligand-controlled regioselectivity was apparent with both Ni and Pd catalysts, including several experiments below the 15% yield threshold, demonstrating that the observed selectivity is general. To our knowledge, this level of regiocontrol has not been reported without drastic modification of the catalyst and reaction conditions.[26] Accordingly, we selected this transformation for further study.

The finer details of Scheme 4.2 are further elaborated in the following sections: HTE setup (Section 4.7.3), workup (Section 4.7.4), and reproduction of hits (Section 4.7.8).

Scheme 4.2 High-throughput experimentation to probe general conditions for Ni- and Pd-catalyzed Mizoroki-Heck reaction

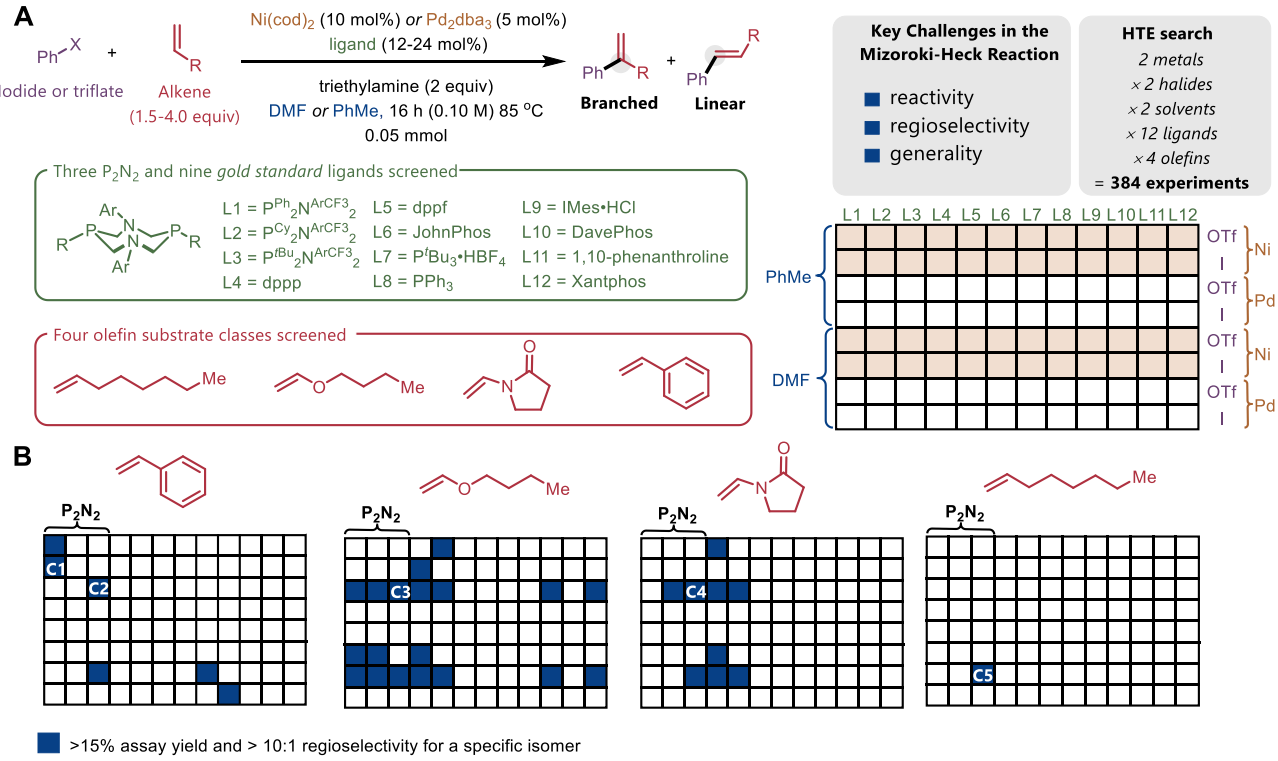

[a]Replication of HTE reactions on 0.2 mmol scale. Regioisomeric ratios given were assessed by GC-FID of the crude reaction mixture. Unless otherwise indicated, isolated yields are reported. [b]With 1 equivalent of styrene. [c]NMR yield after hydrolysis to acetophenone. [d]NMR yield

4.5.2 Synthesis of well-defined Pd P_2N_2 complexes to probe regioselectivity

While it is clear that a drastic change in selectivity can be achieved when switching the ligand from $P^{Ph}{}_2N^{ArCF3}{}_2$ to $P^{tBu}{}_2N^{ArCF3}{}_2$, the mechanistic origin of the regiodivergent reactivity is unclear. One possible explanation is that the different P_2N_2 ligands can have different modes of binding. For example, while they are most commonly observed to be bidentate ligands,[11a] dinuclear complexes bridged by P_2N_2 ligands in a μ-(κ^1-P, κ^1-P') binding mode as well as multimetallic clusters have also been observed.[27] The arene ring on aniline-derived P_2N_2 ligands has also been shown to coordinate to transition metals,[12g] while in other complexes, the nitrogen atom has been observed to directly coordinate.[28] Additionally, agostic bonding of pendant C-H bonds in P_2N_2 metal complexes has been reported.[28b,29] To probe if the differing regioselectivity originated from differing binding of the ligands, we set out to prepare and characterize some well-defined metal complexes.

While initial hits showed both Ni and Pd catalysis was promising, we elected to pursue Pd complexes because of the abundance of methods of accessing stable complexes with multidentate phosphine ligands (Scheme 4.3). In particular, Pd(0) and Pd(II) complexes were targeted since these are the likely operative oxidation states in the Mizoroki-Heck mechanism. Ligand exchange with the Pd(0) species ^{DMP}DAB-Pd-MAH (^{DMP}DAB = *N,N'*-bis(2,6-dimethylphenyl)-diazabutadiene; MAH = maleic anhydride)[30] afforded $P^{tBu}{}_2N^{ArCF3}{}_2$-Pd-MAH (**4.1**) and $P^{Ph}{}_2N^{ArCF3}{}_2$-Pd-MAH (**4.2**) in 85 and 89% yields, respectively. Similarly, the Pd(II) precursor $[Pd(ABP)(\mu\text{-}OMs)]_2$ (ABP = 2-aminobiphenyl; OMs = mesylate)[31] was treated with the P_2N_2 ligands to afford $P^{tBu}{}_2N^{ArCF3}{}_2$ Pd G3 (**4.3**) and $P^{Ph}{}_2N^{ArCF3}{}_2$ Pd G3 (**4.4**) in 87 and 76% yields, respectively. Single crystals were obtained for all four complexes and the structures confirmed a 1:1 ligand to Pd

stoichiometry, and a conventional κ^2-P,P coordination mode of the P_2N_2 ligands. The Pd to ligand bond distances and angles are consistent with related diphosphine complexes.[30,31] However, $P^{tBu}{}_2N^{ArCF3}{}_2$ Pd G3 (**4.3**) has slightly longer Pd-P bond lengths than the phenyl derivative (**4.4**) by ca. 0.02 Å (Table 4.16). The $P^{tBu}{}_2N^{ArCF3}{}_2$ Pd G3 complex (**4.3**) exhibits a significantly distorted square planar geometry with a τ_4 value of 0.21 (τ_4 = 0 for perfect square planar geometry).[32] Conversely, the phenyl derivative (**4.4**) is almost perfectly square planar as evidenced by a τ_4 value of 0.06. The longer Pd—P bond lengths and geometry distortion for the ^{t}Bu derivative (**4.3**) likely occurs to relieve some steric clash with the ABP moiety. The solid-state structures of the four complexes reveals that one or both of the -$ArCF_3$ pendent amine substituents are positioned over the palladium atom (*i.e.*, a boat metallocycle conformation), potentially blocking the axial metal site. However, neither a Pd-N nor a Pd-C_{Arene} π-interaction was observed in any of the complexes. The closest contact was the Pd-C_{ipso} distance that was >3 Å in all complexes, and this is significantly longer than Pd-C_{Arene} interactions (ca. 2.3-2.9 Å) observed for Pd(0) biaryl monophosphine complexes,[33] or a $P^{Cy}{}_2N^{Ph}{}_2$ Ru(II) complex.[12g] Additionally, π-coordination to the aryl group would cause an upfield shift of the ^{13}C resonances, and no such shift was observed for any of the complexes. The barriers for the boat/chair conformational change of nickel P_2N_2 metallocycles were previously calculated to be ca. 4–10 kcal/mol.[34] Therefore, in solution under catalytic conditions the interchange between conformers is likely facile, and the axial positions are likely not completely blocked by these ligands. The catalytic activity of these Pd complexes was also assessed and gave consistent trends as in situ formed catalysts, with complexes bearing the $P^{Ph}{}_2N^{ArCF3}{}_2$ ligand being selective for the linear Mizoroki-Heck product and complexes bearing the $P^{tBu}{}_2N^{ArCF3}{}_2$ ligand being branched selective. Taken together, the structures and activity of

these Pd-P_2N_2 complexes strongly suggests that the difference in regioselectivity is not due to catalyst nuclearity (*i.e.,* monometallic vs. bimetallic) or ligation stoichiometry (*i.e.*, Pd : P_2N_2 = 1:1 vs 1:2). While we cannot discount that an in situ change in P_2N_2 coordination mode alters selectivity, these studies do not provide any positive evidence for this hypothesis. The key insight provided by these Pd(II) spcies relates shows that the ^{t}Bu derivatives experiences significant steric clash within the square planar geometry, whereas the PPh derivatives do not show this distortion, which may play a role in the selectivity-determining step of the catalytic cycle.

Scheme 4.3 Synthesis and isolation of novel P_2N_2 Pd complexes for use in catalytic reactions

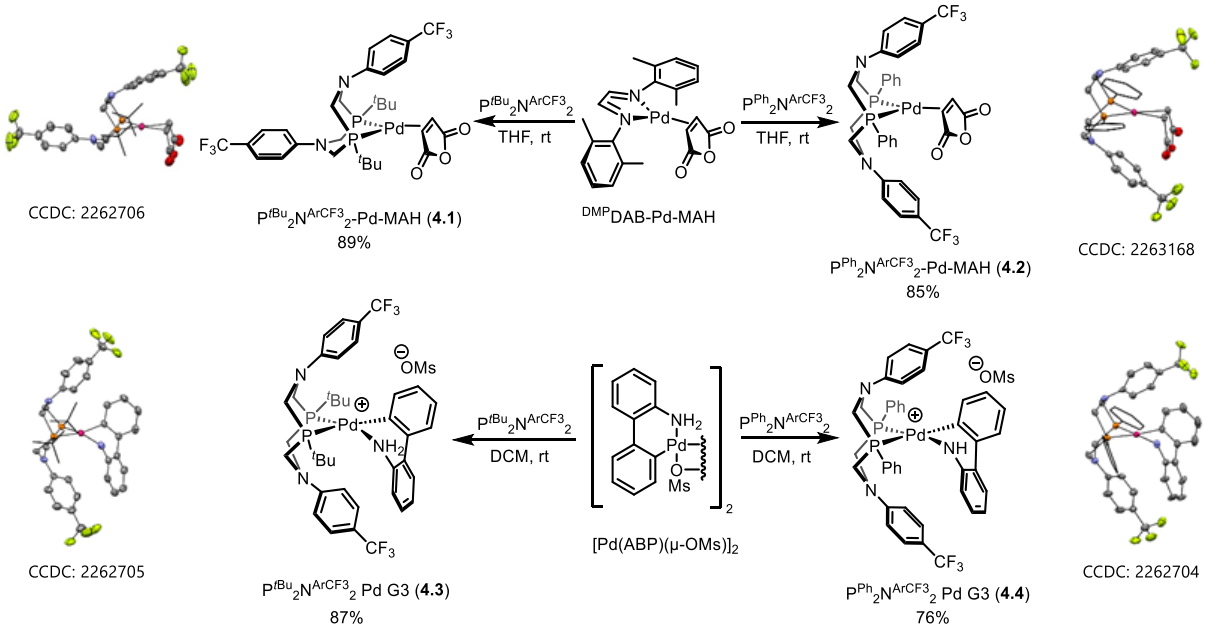

Isolated yields are reported. Thermal displacement plots are shown with ellipsoids at 50% probability. For clarity, hydrogen atoms and mesylate counterions (where relevant) were removed, and the Ph and ^{t}Bu phosphorus substituents are depicted as wireframe. Depictions with atom labels along with tables of selected bond lengths and angles are provided in Section 4.7.14

4.5.3 Catalytic studies with P_2N_2 Pd complexes

With well-defined P_2N_2 Pd complexes in hand, we studied whether they would be effective precatalysts in the Mizoroki-Heck coupling between phenyl triflate and styrene. Initial results, at 1 mol% [P_2N_2 Pd] loading, indicated that catalytic turnover was possible (Table 4.1). $P^{tBu}{}_2N^{ArCF3}{}_2$-Pd-MAH (**4.1**) had limited catalytic activity (entry 1), although the major regioisomer obtained, **4.7-br**, was consistent with our HTE result (Scheme 4.2). $P^{Ph}{}_2N^{ArCF3}{}_2$-Pd-MAH (**4.2**) also resulted in limited amounts of the linear product: **4.7-lin** (entry 2). The P_2N_2 Pd G3 complexes (**4.3** and **4.4**) were both catalytically active (entries 3 and 4), and had the same selectivity trends as the corresponding P_2N_2-Pd-MAH complexes (entries 1 and 2, respectively). Interested in the observed change in site selectivity, but noting that the overall yields in Table 4.1 were low, we decided to study these precatalysts in greater detail.

Table 4.2 highlights a study comparing the Pd complexes at 1 mol% [P_2N_2 Pd] loading. $P^{tBu}{}_2N^{ArCF3}{}_2$-Pd-MAH, **4.1**, (entry 1) was not catalytically active and only a trace amount of **4.7-br** formed. Analogously, $P^{Ph}{}_2N^{ArCF3}{}_2$-Pd-MAH, **4.2**, (entry 2) did not afford significant quantities of **4.7 lin**. In contrast, $P^{tBu}{}_2N^{ArCF3}{}_2$ Pd G3, **4.3**, was a highly effective and selective precatalyst for **4.7-br** at 5 mol% loading (entry 3). $P^{Ph}{}_2N^{ArCF3}{}_2$ Pd G3, **4.4**, showed similar catalytic activity and selectivity for **4.7-lin** (entry 4). It should be noted that for complex **4.4**, increasing the temperature from 85 °C to 100 °C was beneficial to the catalytic activity – this will be discussed further in Section 4.5.4.

Table 4.1 Catalytic reactions with the P_2N_2 Pd complexes at 1 mol% loading

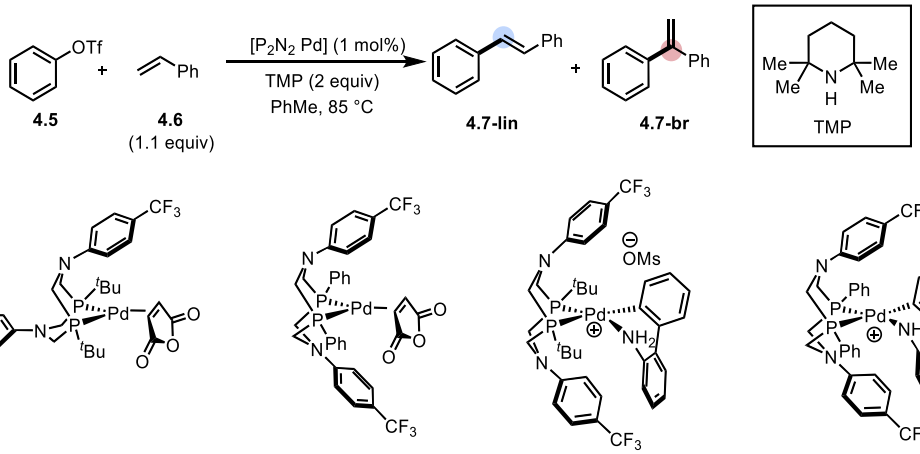

$P^{tBu}{}_2N^{ArCF3}{}_2$-Pd-MAH (**4.1**) | $P^{Ph}{}_2N^{ArCF3}{}_2$ Pd G3 (**4.2**) | $P^{tBu}{}_2N^{ArCF3}{}_2$ Pd G3 (**4.3**) | $P^{Ph}{}_2N^{ArCF3}{}_2$ Pd G3 (**4.4**)

Entry	Precatalyst	**4.7-br** (% yield)	**4.7-lin** (% yield)
1	$P^{tBu}{}_2N^{ArCF3}{}_2$-Pd-MAH (**4.1**)	4%	<1%
2	$P^{Ph}{}_2N^{ArCF3}{}_2$-Pd-MAH (**4.2**)	<1%	9%
3	$P^{tBu}{}_2N^{ArCF3}{}_2$ Pd G3 (**4.3**)	22%	<1%
4	$P^{Ph}{}_2N^{ArCF3}{}_2$ Pd G3 (**4.4**)	<1%	20%

Linear conditions: phenyl triflate (0.20 mmol), styrene (0.22 mmol), TMP (0.40 mmol), $P^{Ph}{}_2N^{ArCF3}{}_2$ Pd complex (1 mol%), toluene (0.2 M), 85 °C for 16 h. **Branched conditions**: phenyl triflate (0.20 mmol), styrene (0.22 mmol), TMP (0.40 mmol), $P^{tBu}{}_2N^{ArCF3}{}_2$ Pd complex (1 mol%), toluene (0.1 M), 85 °C for 16 h. Crude ratio are given as assessed by GC-FID.

Based on the combined results from Table 4.1 and Table 4.2, the P_2N_2 Pd G3 complexes (**4.3** and **4.4**) are effective precatalysts for coupling phenyl triflate with styrene. Both the linear (**4.7-lin**; stilbene) and branched (**4.7-br**; 1,1'-diphenylethylene) products could be obtained with synthetically relevant selectivity by simply changing the P-substituent on the P_2N_2 ligand. The P_2N_2-Pd-MAH complexes (**4.1** and **4.2**) indicated that trace formation of the expected regioisomer can be observed, however, these Pd(0) species are not effective precatalysts. Maleic anhydride (MAH) could be a stronger coordinating ligand than styrene and could competitively bind to Pd,

thus inhibiting productive catalysis. This poisoning could be further studied through spiking small amounts of MAH to see if catalytic activity of a working system is inhibited.

Table 4.2 Catalytic reactions with the P_2N_2 Pd complexes at 5 mol% loading

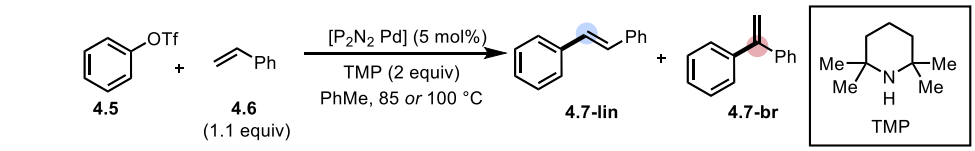

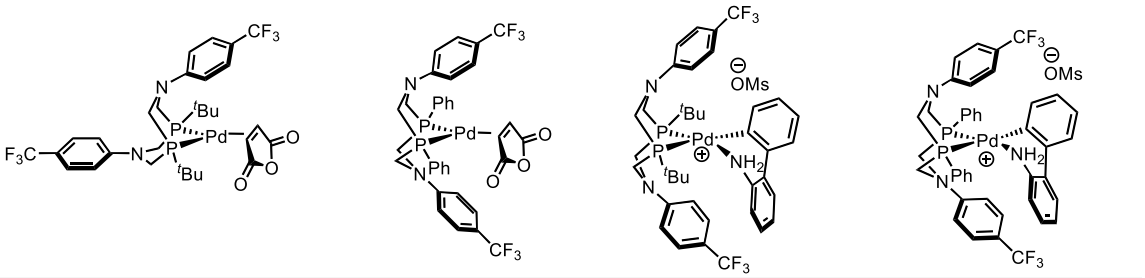

$P^{tBu}{}_2N^{ArCF3}{}_2$-Pd-MAH (**4.1**) | $P^{Ph}{}_2N^{ArCF3}{}_2$ Pd G3 (**4.2**) | $P^{tBu}{}_2N^{ArCF3}{}_2$ Pd G3 (**4.3**) | $P^{Ph}{}_2N^{ArCF3}{}_2$ Pd G3 (**4.4**)

Entry	Precatalyst	Temperature (° C)	**4.7-br** (% yield)	**4.7-lin** (% yield)
1	$P^{tBu}{}_2N^{ArCF3}{}_2$-Pd-MAH (**4.1**)	85	Trace	-
2	$P^{Ph}{}_2N^{ArCF3}{}_2$-Pd-MAH (**4.2**)	100	-	Trace
3	$P^{tBu}{}_2N^{ArCF3}{}_2$ Pd G3 (**4.3**)	85	88%	5%
4	$P^{Ph}{}_2N^{ArCF3}{}_2$ Pd G3 (**4.4**)	100	5%	83%

Linear conditions: phenyl triflate (0.10 mmol), styrene (0.11 mmol), TMP (0.20 mmol), $P^{Ph}{}_2N^{ArCF3}{}_2$ Pd complex (5 mol%), toluene (0.1 M), 100 °C for 16 h. **Branched conditions**: phenyl triflate (0.10 mmol), styrene (0.11 mmol), TMP (0.20 mmol), $P^{tBu}{}_2N^{ArCF3}{}_2$ Pd complex (5 mol%), toluene (0.1 M), 85 °C for 16 h. Crude ratio are given as assessed by GC-FID. For entry 3, crude GC-FID ratio of **4.7-br**:**4.7-lin** was 16.5:1. For entry 4, crude GC-FID ratio of **4.7-lin:4.7-br** was 16:1.

4.5.4 Optimization of the selective Mizoroki-Heck couplings of aryl triflates with styrenes

In Section 4.5.1, we showed that the ligand $P^{tBu}{}_2N^{ArCF3}{}_2$ allowed for the synthesis of 1,1'-diphenylethylene from a Mizoroki-Heck coupling with styrene. This has been further supported in Sections 4.7.6 and 4.7.7. Our initial HTE result was reproduced on a 0.2 mmol scale (Scheme 4.2 C1). Additional experimental details for this reproduction are provided in Section 4.7.8. We further optimized this coupling which used the HTE conditions as a starting point (Scheme 4.4), as branched selective couplings of styrenes are not common and selective control of the product by modifying the first coordination sphere of a P_2N_2 ligand is unprecedented.

Scheme 4.4 HTE conditions which served as a starting point for further optimization

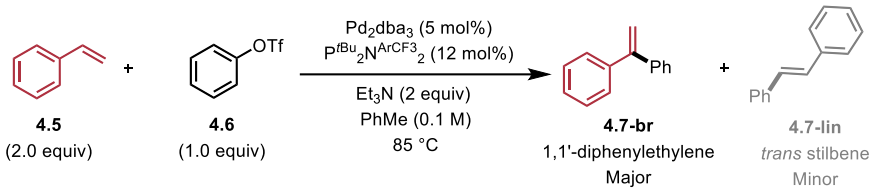

Table 4.3 shows a small selection of the optimization. A more detailed optimization is presented in Section 4.7.12 along with Table 4.14. In the optimal conditions for obtaining **4-7-br**, the $P^{tBu}{}_2N^{ArCF3}{}_2$ Pd G3 precatalyst (**4.3**) was highly effective in combination with 2,2,6,6-tetramethylpiperidine as a base (entry 1). Pd_2dba_3 could be effectively combined with free ligand, $P^{tBu}{}_2N^{ArCF3}{}_2$, to obtain product **4.7-br** in similar yield (entry 2), however, reproducibility issues were observed between different commercial sources of Pd_2dba_3.[35] As a result, we selected $P^{tBu}{}_2N^{ArCF3}{}_2$ Pd G3 as the optimal precatalyst since it had consistent results between batches. Under the conditions optimized for the branched selective coupling, $P^{Ph}{}_2N^{ArCF3}{}_2$ Pd G3 (**4.4**), the phenyl analogue was selective for the linear product **4.7-lin** at 85 °C; however moderate yield was obtained (entry 3). The yield for **4.7-lin** could be simply improved by increasing the temperature

of the reaction to 100 °C (entry 4). With these optimized conditions in hand, a formal scope could be evaluated. This minimal modification is in contrast to other methodologies which require larger changes to the reaction system to alter selectivity (Scheme 4.1).

Table 4.3 Optimization of the site-selective coupling

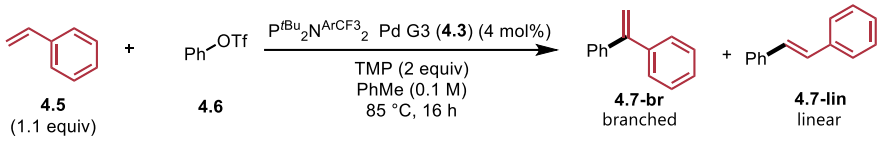

4.5 (1.1 equiv) + **4.6** → **4.7-br** branched + **4.7-lin** linear

Entry	Modification	Major product	Yield of major product (%)
1	None	**4.7-br**	83
2	Pd_2dba_3 /P$^{tBu}_2$ N$^{ArCF3}_2$ [a]	**4.7-br**	76
3	P$^{Ph}_2$N$^{ArCF3}_2$ Pd G3 (**4.4**) at 85 °C	**4.7-lin**	59
4	P$^{Ph}_2$N$^{ArCF3}_2$ Pd G3 (**4.4**) at 100 °C	**4.7-lin**	89

General reaction conditions: Aryl triflate (0.05 mmol), styrene (0.055 mmol), 2,2,6,6-tetramethylpiperidine (0.10 mmol), P^{tBu}N$^{ArCF3}_2$ Pd G3 (**4.3**) (4 mol%, 0.002 mmol), toluene (0.50 mL), 85°C for 16 h. 0.05 mmol of 1,3,5 – trimethoxybenzene was added as internal standard (1 mL of a 0.05 M stock solution in PhMe). Yields are given as assessed by GC-FID calibration curve (see Section 4.7.15 GC-FID calibration curves. [a]2 mol% Pd dimer and 4 mol% P_2N_2 were used.

4.5.6 Scope of the P_2N_2 ligand controlled regiodivergent arylation of styrenes

While initial HTE hits indicated that both Pd and Ni were viable in regioselective Mizoroki-Heck couplings using P_2N_2 ligands, the P_2N_2 Pd G3 catalysts were an appealing entry point to selective Mizoroki-Heck chemistry owing to their bench stability, ease of preparation, and consistency. Reaction optimization (Table 4.3) with 4 mol% of the P$^{Ph}_2$N$^{ArCF3}_2$ Pd G3 precatalyst (Scheme 4.3; **4.4**) revealed general, high-yielding, and regioselective conditions featuring TMP as a base in toluene at 85 °C with 1.1 equiv of the alkene coupling partner. With these conditions, a selection of styrenes and aryl triflates were coupled to provide (*E*)-stilbenes **4.7-lin** to **4.12-lin** in

54-93% yield with regioselectivities ranging from 8:1 to 19:1 (Scheme 4.5). Unprotected indole was tolerated but gave a lower 5:1 regioselectivity (**4.13-lin**), while tyrosine derivative **4.14-lin** and Lewis basic heterocyclics **4.15-lin**, **4.16-lin**, and **4.17-lin** were prepared with high linear selectivity.

With the $P^{tBu}{}_2N^{ArCF3}{}_2$ Pd G3 precatalyst (**4.3**), 1,1'-diarylethylenes **4.7-br** to **4.12-br** could be prepared from simple aryl triflates with regioselectivities ranging from 8:1 to >20:1 and yields between 36-95% (Scheme 4.5). Unprotected indole **4.13-br** and a tyrosine derivative **4.14-br** could again be coupled.

While in most cases, the two different catalysts enabled highly selective access to both regioisomers, some exceptions were observed. $P^{tBu}{}_2{}^{NArCF3}{}_2$ Pd G3 (Scheme 4.3; **4.3**) was not selective for the branched product **4.15-br**, while products **4.16-br**, and **4.17-br** were not accessible in high yields (see Section 4.5.7.2). In contrast, vinyl-substituted pyridine **4.18-br** and thiazole **4.19-br** were prepared with $P^{tBu}{}_2{}^{NArCF3}{}_2$ Pd G3 (**4.3**) but these substrates did not react with $P^{Ph}{}_2{}^{NArCF3}{}_2$ Pd G3 (Scheme 4.3; **4.4**) (see Section 4.5.7.1). Furthermore, to highlight the broad applicability of $P^{tBu}{}_2{}^{NArCF3}{}_2$ Pd G3 (Scheme 4.3; **4.3**), N-vinyl pyrrolidone was arylated with high branched selectivity to give **4.20-br**), while $P^{Ph}{}_2N^{ArCF3}{}_2$ Pd G3 (Scheme 4.3; **4.4**) did not react with this substrate. Further scope limitations are discussed in Section 4.5.7.

Lastly, a small selection of bioactive scaffolds and derivatives were also prepared. $P^{Ph}{}_2N^{ArCF3}{}_2$ Pd G3 (Scheme 4.3; **4.4**) enabled coupling of vinyl loratidine derivative to afford **4.21-lin**, and $P^{tBu}{}_2N^{ArCF3}{}_2$ Pd G3 (Scheme 4.3; **4.3**) provided access to **4.22-br**, the methyl ester analogue of the leukemia drug bexarotene.[36] *Trans* combretastatin A4 (**4.23-lin**), a natural product metabolite, was prepared with good yield and linear selectivity with $P^{Ph}{}_2{}^{NArCF3}{}_2$ Pd G3 (Scheme

4.3; **4.4**),[37] while $P^{tBu}{}_2N^{ArCF3}{}_2$ Pd G3 (Scheme 4.3; **4.3**) could be used to prepare the regioisomer, isocombretastatin A4 (**4.23-br**), a potent bioactive non-natural analogue of combretastatin A4.[38]

Scheme 4.5 Scope of ligand-controlled site selectivity in the coupling of aryl triflates with alkenes

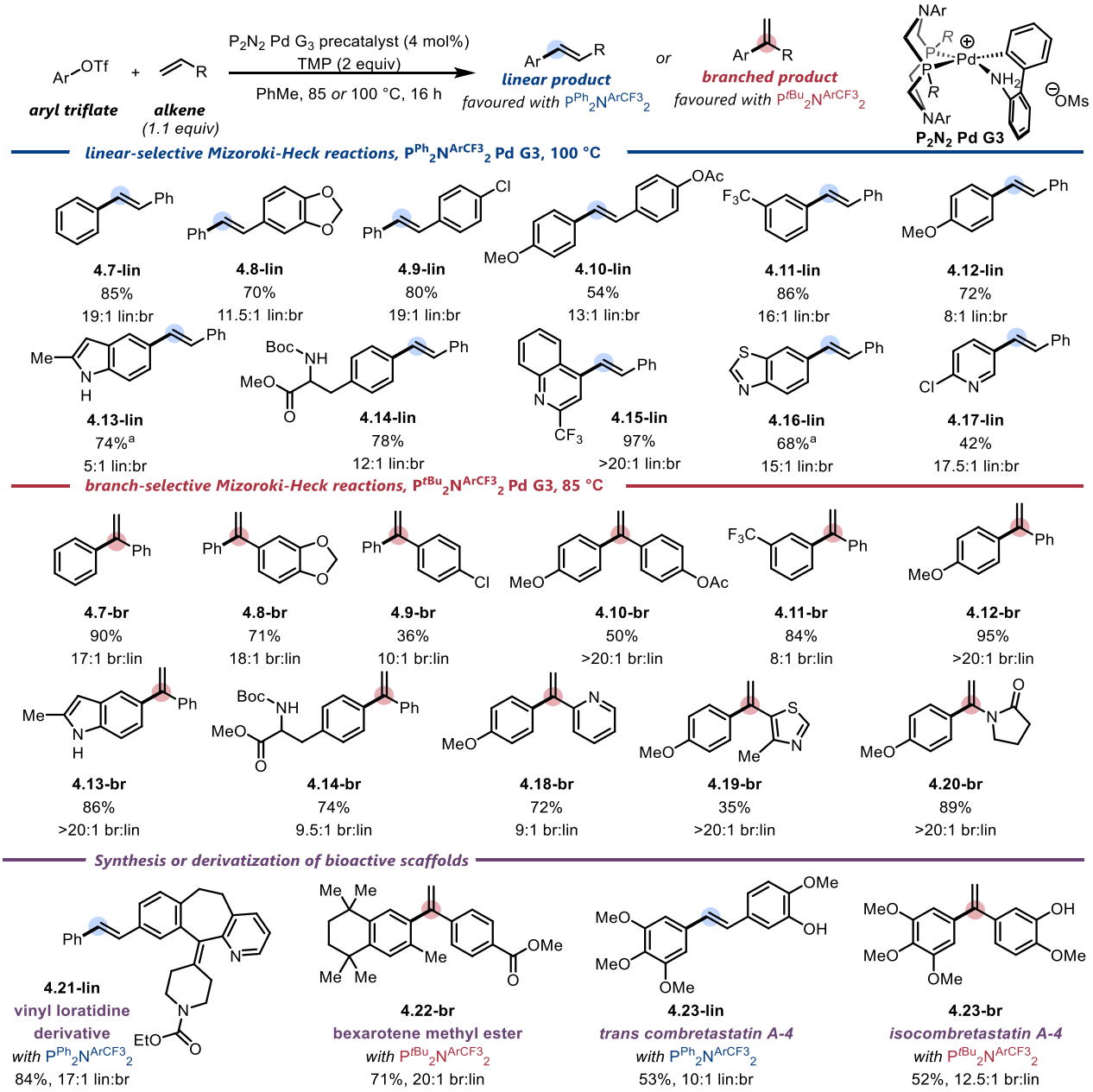

Linear-selective conditions: aryl triflate (0.20 mmol), alkene (0.22 mmol), TMP (0.40 mmol), $P^{Ph}{}_2N^{ArCF3}{}_2$ Pd G3 (4 mol%), toluene (0.1 M), 100 °C for 16 h. **Branched-selective conditions**: aryl triflate (0.20 mmol), alkene (0.22 mmol), TMP (0.40 mmol), $P^{tBu}{}_2N^{ArCF3}{}_2$ Pd G3 (4 mol%), toluene (0.1 M), 85 °C for 16 h. Regioisomeric ratios (*rr*) are measured on the crude reaction mixtures using GC analysis, or in the case of products >400 Da, by crude ^{1}H NMR. Isolated yields are reported as single regioisomers (*rr* ≥19:1). [a]With 8 mol% P_2N_2 Pd G3 precatalyst

4.5.7 Limitations of the P_2N_2 ligand-controlled regiodivergent arylation of styrenes

While evaluating the scope of this transformation, several products were not obtained in synthetically useful yield and/or regioselectivity. A selection of such substrates are displayed below with some general notes or observations (Scheme 4.6-Scheme 4.8).

4.5.7.1 Limitations of the $P^{Ph}{}_2N^{ArCF3}{}_2$ Pd G3 precatalyst (4.4)

Scheme 4.6 highlights specific scope limitations with the linear coupling. Limitations include poor reactivity or regioselectivity. All examples presented were included as part of the branched selective scope and had high regioselectivity for the branched product (Scheme 4.5). Of particular note, examples with sterically hindered alkenes (**4.19-lin**) or hindered aryl triflates (**4.22-lin**) tended to afford poor linear selectivity.

Scheme 4.6 Limitations of linear coupling. Reactions that were successful with $P^{tBu}{}_2N^{ArCF3}{}_2$ Pd G3 (4.3) precatalyst but unsuccessful with $P^{Ph}{}_2N^{ArCF3}{}_2$ Pd G3 (4.4) precatalyst

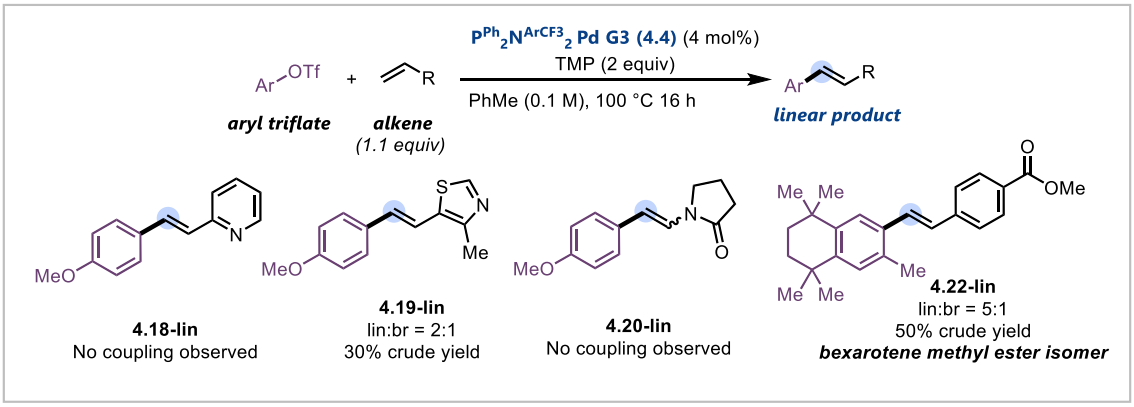

$P^{Ph}{}_2N^{ArCF3}{}_2$ Pd G3 (4.4) conditions: aryl triflate (0.20 mmol), alkene (0.22 mmol), TMP (0.40 mmol), $P^{Ph}{}_2N^{ArCF3}{}_2$ Pd G3 (4.**4**) (4 mol%), toluene (0.1 M), 100 °C for 16 h. Crude ratios are given as assessed by GC-FID.

4.5.7.2 Limitations of the $P^{tBu}{}_2N^{ArCF3}{}_2$ Pd G3 precatalyst (4.3)

Scheme 4.7 highlights specific scope limitations with the branched coupling. Limitations include poor reactivity or regioselectivity. All examples presented were included as part of the linear selective scope and had high regioselectivity for the linear product (Scheme 4.5). Of particular interest, the coupling of 2-(trifluoromethyl)quinolin-4-yl triflate using the branch-selective conditions resulted in *inverted selectivity* (**4.15-br**). In other words, the linear regioisomer was obtained as the major product (**4.15-lin**), albeit with low selectivity. Throughout the evaluation of our scope, this represents the only example that deviated from the absolute selectivity trends. We hypothesize that this unanticipated result is due to the highly electron deficient nature of 2-(trifluoromethyl)quinolin-4-yl triflate. Heterocyclic products (**4.16-br**) and (**4.17-br**) were obtained in low yield but high selectivity, indicating that targeted optimization for these products may be possible. Vinyl loratidine derivative **4.21-br** was synthesized in high yield but had moderate selectivity. However, separation of leftover alkene from the desired regioisomer was problematic. We anticipate that using the aryl triflate in excess or using equimolar stoichiometry between coupling partners would allow for isolation of **4.21-br**.

Scheme 4.7 Limitations of branched coupling. Reactions that were successful with $P^{Ph}{}_2N^{ArCF3}{}_2$ Pd G3 (4.4) precatalyst but unsuccessful with $P^{tBu}{}_2N^{ArCF3}{}_2$ Pd G3 precatalyst (4.3)

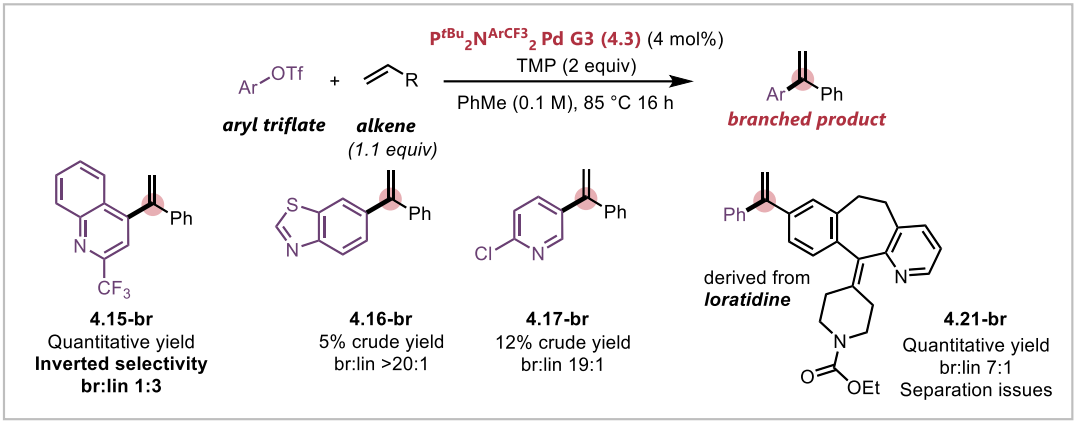

$P^{tBu}{}_2N^{ArCF3}{}_2$ Pd G3 (4.3) conditions: aryl triflate (0.20 mmol), alkene (0.22 mmol), TMP (0.40 mmol), $P^{tBu}{}_2N^{ArCF3}{}_2$ Pd G3 (**4.3**)(4 mol%), toluene (0.1 M), 85 °C for 16 h. Crude ratios are given as assessed by GC-FID, or in the case of 4.21-br crude NMR spectroscopy.

4.5.7.3 Limitations of both $P^{Ph}{}_2N^{ArCF3}{}_2$ Pd G3 (4.4) and $P^{tBu}{}_2N^{ArCF3}{}_2$ Pd G3 precatalysts (4.4)

Scheme 4.8 highlights challenging examples across both linear and branched couplings. 4-(imidazol-1-yl)phenyl triflate (**4.24-lin** and **4.24-br**) had limited reactivity with both precatalysts. No reactivity was observed with $P^{tBu}{}_2N^{ArCF3}{}_2$ Pd G3. 2-pyridine triflate (**4.25-lin** and **4.25-br**) was within scope with both catalyst systems; however, desired products were obtained in moderate yield. Additionally, **4.25-br** was obtained with poor regioselectivity, indicating low synthetic utility. Analogously, cyclohexenyl triflate reacted with both catalyst systems (**4.26-lin** and **4.26-br**); however, a large amount of isomerization of the products was observed by GC-FID (*regiomeric ratios* << 5:1).It should be noted that general selectivity trends were conserved – with linear conditions leading to more linear product and branched conditions leading to more branched products. It is possible that electronically-biased vinyl triflates may suppress or decrease isomerization pathways, however, this class of substrates was not studied. 4-vinyl benzoic acid did not result in the formation of either linear (**4.27-lin**) or branched (**4.27-br**)

products with both catalyst system. This suggests that certain Brønsted acids are not tolerated under the reaction conditions. Attempts to increase the equivalency of base or change the solvent system to DMF did not enable coupling with 4-vinyl benzoic acid.

Scheme 4.8 Challenging or poorly selective substrates with both $P^{tBu}{}_2N^{ArCF3}{}_2$ Pd G3 (4.3) and $P^{Ph}{}_2N^{ArCF3}{}_2$ Pd G3 (4.4) precatalysts

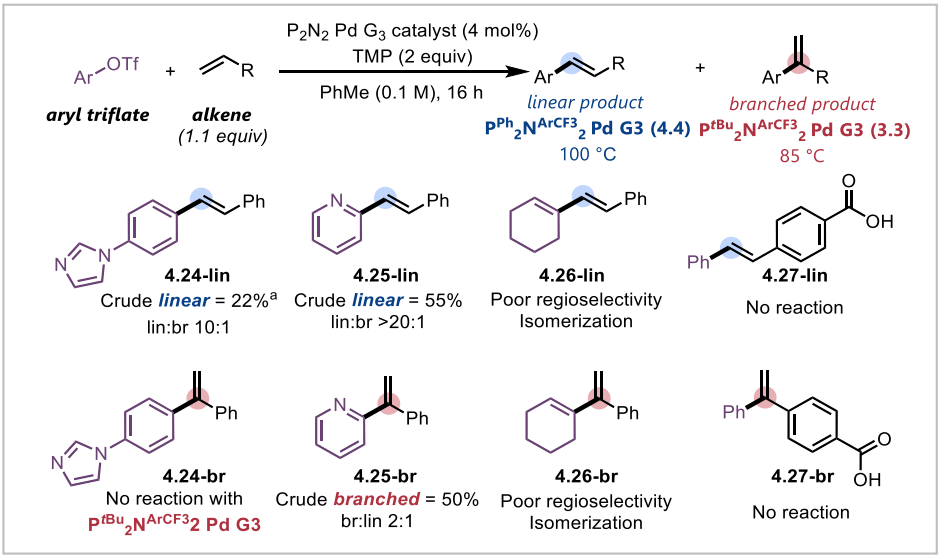

$P^{tBu}{}_2N^{ArCF3}{}_2$ Pd G3 (4.3) conditions: aryl triflate (0.20 mmol), alkene (0.22 mmol), TMP (0.40 mmol), $P^{tBu}{}_2N^{ArCF3}{}_2$ Pd G3 (**4.3**) (4 mol%), toluene (0.1 M), 85 °C for 16 h. **$P^{Ph}{}_2N^{ArCF3}{}_2$ Pd G3 (4.4) conditions**: aryl triflate (0.20 mmol), alkene (0.22 mmol), TMP (0.40 mmol), $P^{Ph}{}_2N^{ArCF3}{}_2$ Pd G3 (**4.4**) (4 mol%), toluene (0.1 M), 100 °C for 16 h. Crude ratios are given as assessed by GC-FID. [a] Double precatalyst loading was used (8 mol%).

From the results of Scheme 4.7 and Scheme 4.8, we can note that the two most electron-deficient triflates which were screened resulted in poor or inverted selectivity for the branched selective coupling (**4.15-br** and **4.25-br**). This suggests that the electronic nature of the aryl triflate has a strong impact on the reaction outcome and that highly electron-deficient triflates are not selective coupling partners for the synthesis of branched 1,1'-diarylethylenes.

4.5.8 DFT studies

Since all Pd(0) and Pd(II) complexes isolated suggest both the $P^{Ph}{}_2N^{ArCF3}{}_2$ and $P^{tBu}{}_2N^{ArCF3}{}_2$ ligands exhibit similar binding modes and nuclearity (Scheme 4.3), we surmised that the divergent selectivity must originate from subtle steric and/or electronic effects in the transition state of the alkene insertion. Accordingly, we sought to model the mechanism of the reaction between styrene and the cationic P_2N_2 Pd(II) complexes using density functional theory (DFT) (Scheme 4.9). It was found that the styrene substrate forms a π-complex with the Pd(II) center where the C=C bond axis is perpendicular to the Pd–C_{Ar} bond. Rotation of the substrate and its migratory insertion (TS insertion) can proceed through two different pathways. The transition state where the styrene Ph group is in close proximity with the phosphine R group will lead to the linear product (TS insertion-linear) while the transition state where the styrene Ph substituent is rotated 180 degrees will lead to the branched product (TS insertion-branched). The subsequent insertion and beta-hydride elimination were found to be lower-energy, so TS-insertion is rate limiting and regiodetermining (see Figure 4.1). To better understand the origin for the ligand-controlled differences in transition state barriers for branched and linear selectivity, we analyzed the key transition state by DFT analysis. While ligands containing P^{t}Bu and PPh substituents are known to have substantial electronic differences, the origin of the regioselective insertion step appears to derive primarily from steric effects. The rigid cyclic backbone of the P_2N_2 ligands imposes a conformation on the P substituent where it will have contact with the incoming styrene particularly just in the transition state leading to the linear product (TS insertion linear). This interaction appears critical in dictating the regioselectivity. The styrene aryl ring can interact with $P^{Ph}{}_2N^{ArCF3}{}_2$ in a geometry with limited steric repulsion

(destabilizing) and significant compensatory dispersion and electrostatic interactions (stabilizing).

Scheme 4.9 DFT calculations indicating relative energy barriers (in kcal/mol) for the π-bond insertion with P_2N_2 Pd complexes

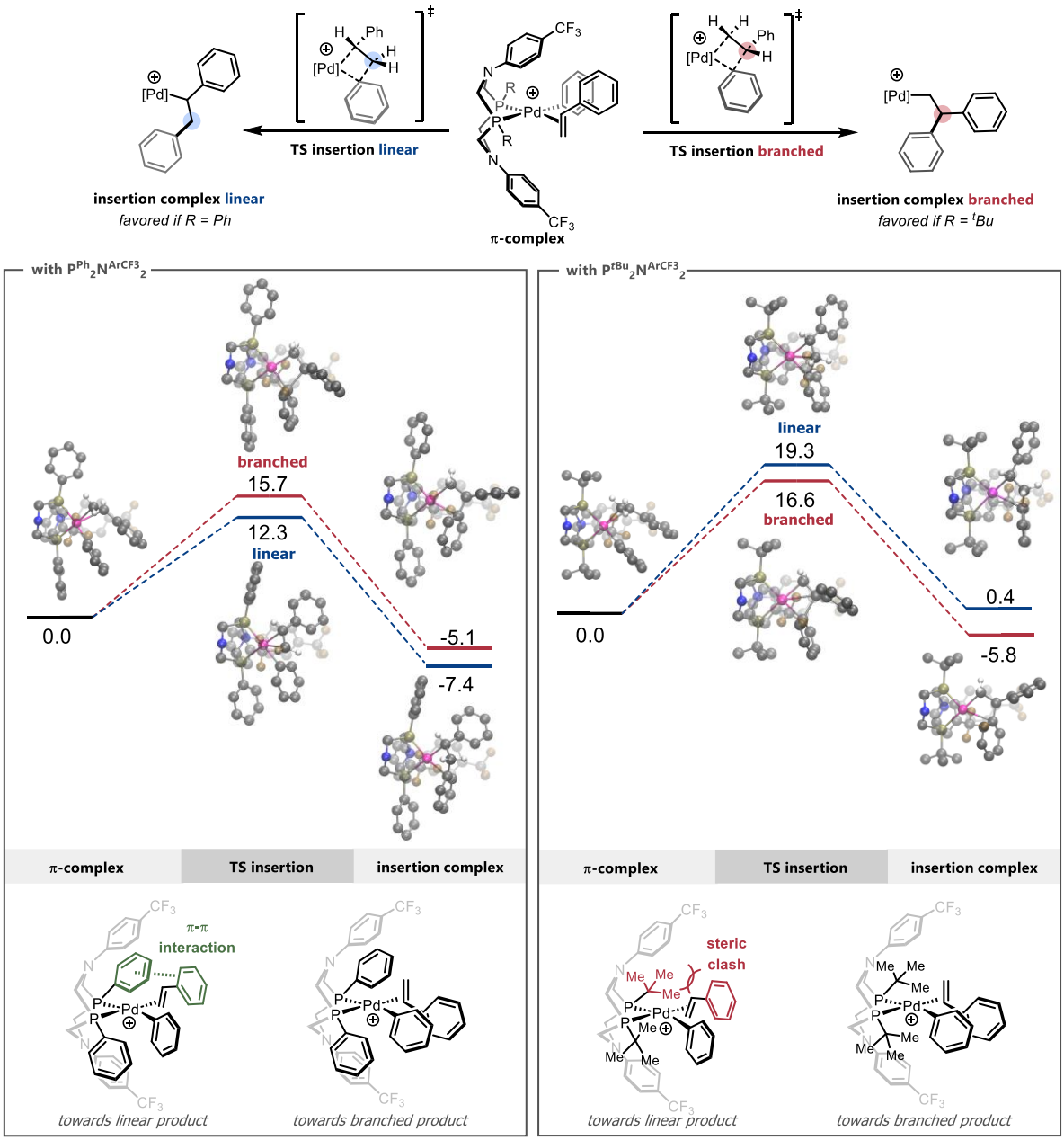

DFT method used for calculations: B3LYP-D3BJ/def2-TZVP-CPCM(toluene)// B3LYP-D3BJ/def2-SVP-CPCM(toluene)

Figure 4.1 Complete DFT-calculated Gibbs energy reaction profile for comparing the relative regiodivergency of the $[Pd(P^{R}{}_2N^{ArCF3}{}_2)(Ph)(C_6H_5CH{=}CH_2)]^+$ complexes.[a]

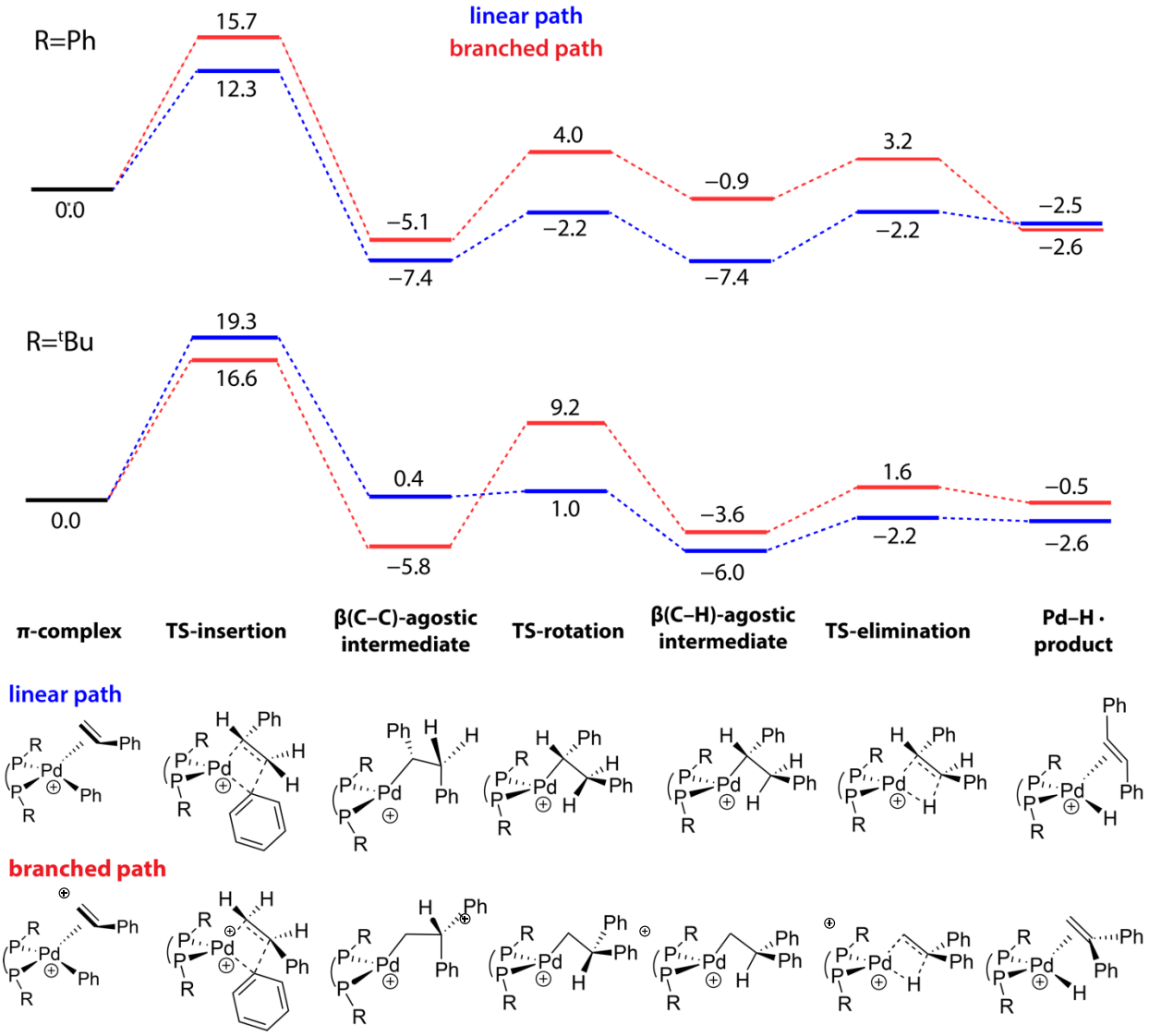

[a]Values reported in kcal/mol. Complete DFT-calculated Gibbs energy reaction profile for the insertion of styrene into the Pd–Ph bond of the $[Pd(P^{R}{}_2N^{ArCF3}{}_2)(Ph)(C_6H_5CH{=}CH_2)]^+$ complex, where R=Ph (top) or R=^{t}Bu (bottom). The branched pathway (red) generates 1,1-diphenylethylene while the linear path generates (*E*)-stilbene. All values are calculated using B3LYP-D3BJ/def2-TZVP-CPCM(toluene)// B3LYP-D3BJ /def2-SVP-CPCM(toluene). The D3BJ dispersion correction and CPCM model were used in both the optimization and single point energies.

This π-π interaction between the ligand P-Ph group and the styrene arene ring results in the linear pathway being lower in energy than the branched pathway (linear: $\Delta G^{‡}$=12.3 kcal/mol, branched: $\Delta G^{‡}$=15.7 kcal/mol). This trend is reversed for the $P^{tBu}{}_2N^{ArCF3}{}_2$ transition states (branched: $\Delta G^{‡}$=16.6 kcal/mol, linear: $\Delta G^{‡}$=19.3 kcal/mol). A decomposition of the interactions

between these groups shows that this difference in energy is primarily due to a higher steric (exchange) energy term between the ^{t}Bu groups and the styrene phenyl ring in the transition state (TS insertion branched) than those seen in the $P^{Ph}{}_2N^{ArCF3}{}_2$ ligand (Scheme 4.9). This is consistent with the steric repulsion between the ligand *tert*-butyl groups and the styrene aromatic group destabilizing the path to the linear product, resulting in selectivity for the branched product. The DFT calculations were performed using ORCA 5.0.4.[39] Structures were optimized using the B3LYP exchange-correlation functional[40] with the def2-SVP basis set/core potential.[41] Single point energies were calculated at the optimized structure using the def2-TZVP basis set/core potential. The D3BJ dispersion correction was used.[42] A conductor-like polarizable continuum model (CPCM) was used to model the toluene solvent.[43] The origin of the difference in the barriers for the linear and branched paths for the R=^{t}Bu and R=Ph ($P^{R}{}_2N^{ArCF3}{}_2$) ligands were calculated using the sSAPT0 variant of symmetry adapted perturbation theory (SAPT)[44] using Psi4 1.5.[45]

4.6 Conclusions, advancement in the field, and future work

A high-throughput study comparing the utility of P_2N_2 ligands compared to typical ligands used for Ni- and Pd-catalyzed Mizoroki-Heck couplings was performed. $P^{tBu}N^{ArCF3}{}_2$ demonstrated high regioselectivity for the branched (α-arylated) product for all four olefins studied, in contrast to all other ligands screened (Scheme 4.2). Conversely, $P^{Ph}N^{ArCF3}{}_2$ was identified as a ligand which enabled high regioselectivity for the (*E*)-linear (β-arylated) product for the coupling with styrene. While a range of promising Ni and Pd systems featuring P_2N_2 were identified, we chose to study the site-selective arylation of styrene as the ability to control the site of arylation could be controlled by the first-coordination sphere including the P_2N_2 ligand. While modifications of the second or outer coordination sphere are known to influence reactivity (see Section 1.5.4), this represents the first example of a family of P_2N_2 ligands controlling site-selectivity for C-C bond formation. By simply changing a *tert*-butyl substituent on a P_2N_2 ligand to a phenyl group, a complete change in absolute regiochemistry was observed.

Well-defined and conveniently accessible Pd-(P_2N_2)-MAH and (P_2N_2) Pd G3 complexes were prepared with both $P^{Ph}N^{ArCF3}{}_2$ and $P^{tBu}N^{ArCF3}{}_2$ to investigate difference in ligand binding (Scheme 4.3). To the best of our knowledge, this represents the first time a Pd(0) P_2N_2 complex has been prepared.[46] Similarly, this is the first report of a P_2N_2 Buchwald-type precatalyst. No significant difference in binding was observed between the $P^{Ph}N^{ArCF3}{}_2$ and $P^{tBu}N^{ArCF3}{}_2$ complexes which could account for the observed change in selectivity.

The scope of the Mizoroki-Heck coupling of aryl triflates with styrenes was broad and both catalyst systems were high-yielding for their respective products (Scheme 4.5). While some

exceptions were observed (Section 4.5.7), in general, $P^{tBu}N^{ArCF3}{}_2$ is selective for the branched product (1,1'-diarylethylenes), whereas, $P^{Ph}N^{ArCF3}{}_2$ is selective for the linear product (stilbenes).

DFT studies (Section 4.5.8) uncovered that an unexpected edge-to-face π-π interaction between the P-Ph group and styrene in the π-bond insertion (regiodetermining) step could account for the observed linear selectivity (Scheme 4.9). Conversely, the steric bulk and lack of π-π interaction afforded by the *tert* butyl group disfavours the linear pathway. The transition state leading to the branched product positions the styrene phenyl group further away from the P-substituent of the P_2N_2 ligand.

4.6.1 Advancements in the field

After submission of this work to a peer-reviewed journal, a similar methodology was reported by the Leitner group (Scheme 4.10). Leitner and coworkers report the site-selective decarboxylative Mizoroki-Heck coupling of carboxylic acids with alkenes.[47] In this work, a small change of the ligand structure was able to alter selectivity for the linear or branched products. It should be noted, however, that only one example of linear selectivity was reported and the focus of this work was instead on the branched products. This method was predominantly limited to the use of 2,6-dimethoxybenzoic acid as the coupling partner. All other reported starting materials, such as 2-methoxybenzoic acid gave poor yields ($\leq$ 20%). The DFT study of Leitner's work indicated that a π-π interaction between a phenyl group on the ligand and the aryl group on the styrene was responsible for linear selectivity. Conversely, altering the ligand structure with a bulkier 2,6-diisopropyl phenyl group disfavors the linear pathway. This study is highly reflective of the conclusions of our DFT study (Section 4.5.8)

The findings of Leitner et al. are consistent with our work and represent another unique way to control selectivity of the Mizoroki-Heck coupling with small alterations of the ligand framework. However, our methodology is broader in scope and does not require directing groups or aggressive reaction conditions to proceed.

Scheme 4.10 Advancements in the field after submission

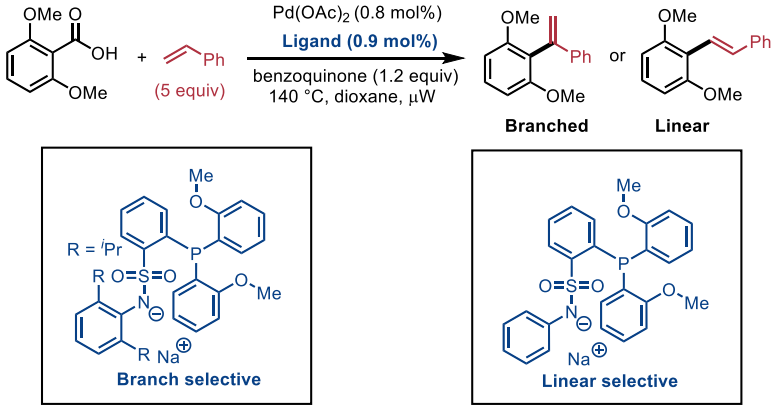

4.6.2 Future directions of this research

Our experimental and computational findings led to us to consider further mechanistic questions which could lead us to the rational design of new P_2N_2 ligands. The study of the edge-to-face π-π interaction could provide further insight into the site-selectivity of the transformation disclosed in Section 4.5.6. To the best of our knowledge, notable non-covalent interactions in the first-coordination sphere have not been reported with P_2N_2 metal complexes and this offers a new way for this class of ligands to be used, distinct from all other known applications.

We anticipate that the existence of the edge-to-face π-π interaction can be experimentally probed with a series of P_2N_2 ligands, featuring electronically and sterically distinct aryl groups on phosphorus (Scheme 4.11). The effect of these substitution patterns could be studied computationally, in parallel with experiments, to model relative trends. One could expect

that the magnitude of the π-π interaction changes as the aryl group is made more electron-rich (e.g. with a *para* methoxy group) or rendered more electron-deficient (e.g. with a *para* trifluoromethyl group). As a result, we hypothesize that selectivity could be altered by changing the electronics of the aromatic ring bound to phosphorus. Ideally, a clear trend would be observed; for example, an electron-deficient arene improves the selectivity whereas an electron-rich arene worsens the selectivity (or vice versa). If this is the case, the non-covalent interaction could be further tuned through rational ligand design to improve the linear selectivity of the transformation (see Section 4.5.7.1 for challenging examples). While taking the work of Leitner and coworkers into account (Scheme 4.10), it is highly possible that a P_2N_2 ligand made from a sterically-encumbered primary phosphine could disrupt the π-π interaction and result in formation of the branched product. Macrocyclic P_2N_2 dimers, made from bulky primary phosphines, have been prepared in the primary literature.[48] This indicates that sterically bulky substituents on phosphorus should be tolerated when preparing P_2N_2 ligands.

Scheme 4.11 Probing the π-π interaction with new P_2N_2 ligands

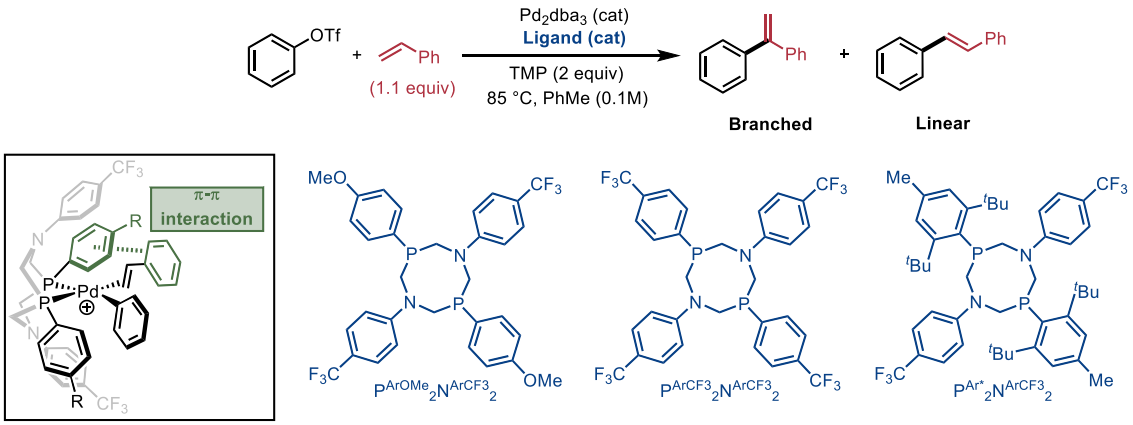

We also hypothesize that the high branched selectivity of $P^{tBu}{}_2N^{ArCF3}{}_2$ ligand can be further extended beyond the alkenes that were studied in Sections 4.5.1 and 4.5.6. $P^{tBu}{}_2N^{ArCF3}{}_2$ Pd G3

(**4.3**) could be a broadly applicable precatalyst for the branched selective coupling of aryl triflates with alkenes. This work could also be extended to the general coupling of aryl halides with alkenes featuring a stoichiometric triflate salt, similar to the work of Jamison and coworkers.[4b] General, unified conditions are uncommon in Mizoroki-Heck coupling and our precatalyst could be highly effective for a range of Heck-type couplings.

4.6.3 Final conclusions

Despite the prominence of the Mizoroki-Heck reaction as a powerful catalytic method to form C–C bonds, its implementation in synthetic methodologies has remained limited compared to other Pd-catalyzed couplings. In this work, a high-throughput screen identified 1,5-diaza-3,7-diphosphacyclooctane ligands as being broadly effective towards a range of alkene substrates with comparable or superior reactivity to more well-established ligand systems. For the palladium-catalyzed coupling of aryl triflates with styrenes – a challenging transformation despite its simplicity – two P_2N_2 ligands were found to enable regiodivergent outcomes, with a P-Ph ligand providing high linear selectivity and a P^{tBu} ligand providing access to the branched regioisomer. Several novel P_2N_2 Pd complexes were prepared and characterized, indicating that differences in speciation or coordination of the pendant N-arene were not contributing factors in regioselectivity. DFT calculations uncovered a favorable π-π interaction between the styrene group and the $P^{Ph}{}_2N^{ArCF3}{}_2$ ligand which could explain its preference for the linear pathway. Conversely, the bulky $P^{tBu}{}_2N^{ArCF3}{}_2$ ligand destabilizes the linear transition state due to steric hindrance and an inability to provide stabilizing π-π interactions, inverting the regiochemical outcome. P_2N_2s are well known to be powerful ligands, particularly due to the flexible, basic nitrogen atoms in the ligand's second coordination sphere, enabling H_2 splitting and related

transformations.[11a] This work demonstrates both a new application and proposes a new unique feature that differentiates P_2N_2s from more commonly used ligand classes. The rigid positioning of the P-substituent results in close contact with incoming reactants, enabling high regiocontrol in this Pd-catalyzed cross-coupling. We suspect that further study of these P_2N_2s may continue to reveal new applications and demonstrate that these are an underappreciated, readily accessible ligand class for organic synthesis.

4.7 Experimental

Unless otherwise indicated, reactions were conducted in a nitrogen-filled glovebox. Column chromatography was performed manually using Silicycle F60 40−63 μm silica gel. Analytical thin layer chromatography (TLC) was conducted with aluminum-backed EMD Millipore Silica Gel 60 F_{254} pre-coated plates. Visualization of developed plates was performed under UV light (254 nm). For certain purifications, cerium ammonium molybdate (CAM) or potassium permanganate ($KMnO_4$) stains were used to better visualize the compounds on the TLC plates.

4.7.1 Instrumentation

^{1}H NMR and ^{13}C NMR were recorded on a Bruker AVANCEII 300 MHz, a Bruker AVANCEII 400 MHz, Bruker 400 MHz, Bruker AVANCEIII 500 MHz Bruker. ^{1}H NMR spectra were internally referenced to the residual solvent signal (e.g., $CDCl_3$ = 7.26 ppm). ^{13}C NMR spectra were internally referenced to the residual solvent signal (e.g., $CDCl_3$ = 77.00 ppm). Data for ^{1}H NMR are reported as follows: chemical shift (δ ppm), multiplicity (s = singlet, d = doublet, t = triplet, q = quartet, m = multiplet), coupling constant (Hz), integration. Crude yields for optimization studies were obtained by GC-FID or ^{1}H NMR analysis of the crude reaction mixture. Calibration curves were

prepared from pure commercial samples with 1,3,5-trimethoxybenzene as an internal standard. Melting point ranges were determined on a Canlab Gallen Kamp Melting Point Apparatus. Accurate mass data (EI) was obtained from an Agilent 5977A GC/MSD using MassWorks 4.0 from CERNO Bioscience.[49] HRMS data (ESI) was obtained from a Micromass Q-TOF 2 quadrupole time-of-flight mass spectrometer with an ESI source. Infrared spectra were collected on solid samples using a Cary 630 FTIR (Agilent Technologies) and are reported in terms of frequency of absorption (cm^{-1}).

4.7.2 Materials

Organic solvents were purified by rigorous degassing with nitrogen before passing through a PureSolv solvent purification system. Low water content was confirmed by Karl Fischer titration (<25 ppm for all solvents). Unless otherwise noted, reagents were used as received. Pd_2dba_3 (97%) was purchased from Sigma Aldrich and used without further purification. Phenylphosphine was obtained as a 10% wt. solution in hexanes from Sigma Aldrich. Cyclohexylphosphine and *tert*-butylphosphine were generously donated from Cytec-Solvay as neat liquids. Primary phosphines were used in the glovebox to avoid any reaction with oxygen. Commercial ligands were purchased from Sigma Aldrich, Combi-Blocks, Fisher Scientific, or Strem Chemicals. 2,2,6,6-Tetramethylpiperidine (TMP) (99%) was obtained from Combi-Blocks. Unless otherwise noted, all other commercially available starting materials were obtained from Sigma-Aldrich, TCI America, Fisher Scientific, Acros Organics, Alfa Aesar, Combi-Blocks, or Oakwood Chemicals and used as received. Aryl triflates were synthesized following a general procedure (Section 4.7.16.1). All P_2N_2 ligands were synthesized following a general procedure (Chapter 5).

4.7.3 High-throughput general procedure

Scheme 4.12 Overview of the HTE reaction conditions

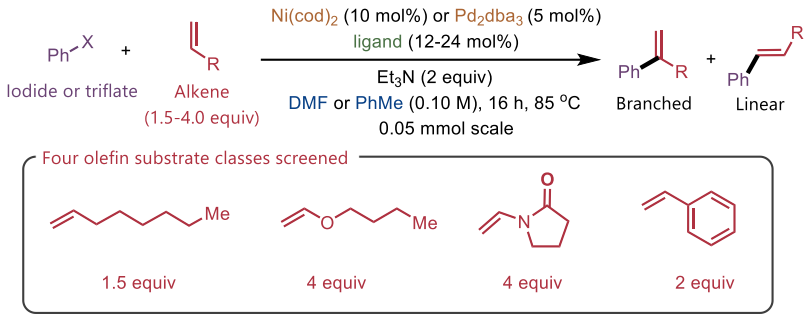

General considerations: All manipulations were performed in a glovebox under a nitrogen atmosphere. All liquids were vigorously degassed with inert gas before shipping inside. All reactions were run at on a 0.05 mmol scale at a 0.1 M concentration. Glassware and consumables were used as received from the original packaging – i.e. Vials and stirbars were *not* oven dried before use.

General procedure: Ligand (0.006 mmol if bidentate or 0.012 mmol if monodentate) and metals (0.005 mmol Ni or 0.0025 mmol Pd dimer) were mixed in the appropriate solvent (0.50 mL of PhMe or DMF). Et_3N was added (0.10 mmol), followed by alkene (0.075 mmol-0.20 mmol), and aryl (pseudo)halide (0.05 mmol). Plate was sealed and the reactions were stirred at 85 °C with a moderate stir rate (~ 200-500 rpm) for 16 hours. 0.025 mmol of internal standard (1,3,5-trimethoxybenzene) was added to each vial and an aliquot from each reaction well was separately filtered through a plug of silica with a mixture of MeCN/EtOAc. The crude results were analyzed by GC-FID and, if unknown peaks were observed, subsequently analyzed by GC-MS to identify side-products.

96 well-plate preparation: All 96 well-plates were run in an aluminum block assembly (Analytical Sales and Services, cat. no. 96973). Glass inserts (8 × 40-mm, 1.2-mL vials; Chemglass Life Sciences, cat. no. CV-2103-0840) were loaded into the wells with a pair of clean tweezers. Micro stir bars (Parylene-coated micro stir bars, VP Scientific, cat. no. VP 712-1) were dispensed into the 96-well plates using a stir bar dispenser (VP Scientific, cat. no. VP-711A-1S/D).

Ligand dispensing: Ligands were dispensed as stock solutions in the appropriate reaction solvent (DMF or PhMe) when possible. Monodentate ligands were prepared as 0.048 M stock solutions. Bidentate ligands were prepared as 0.024 M stock solutions. The following ligands were insoluble at the specified concentration in PhMe and were individually weighed as solids: $P^{Ph}{}_2N^{ArCF3}{}_2$, $P^{Cy}{}_2N^{ArCF3}{}_2$, $P^{tBu}{}_2N^{ArCF3}{}_2$, $P^tBu_3{\bullet}HBF_4$, IMes•HCl, Xantphos and 1,10-phenanthroline. The following ligands were insoluble at the specified concentration in DMF and were individually weighed as solids: $P^{Cy}{}_2N^{ArCF3}{}_2$, $P^{tBu}{}_2N^{ArCF3}{}_2$, dppf, and Xantphos. 250 µL of each stock solutions (0.012 mmol of monodentate or 0.006 mmol of bidentate) or neat solvent (for wells which had ligands weighed by hand) were dispensed to the appropriate locations using an automated Freeslate CM3 via positive displacement micropipette tips.

Precatalyst dispensing: Precatalysts were dispensed as stock solutions in DMF or PhMe when possible. 0.01 M stock solutions of Pd_2dba_3 in PhMe and DMF were prepared. Rigorous agitation was required to render the solutions homogeneous and, once homogeneous, the solutions were quickly dispensed by multichannel micropipettes. A 0.02 M stock solution of $Ni(cod)_2$ in PhMe was prepared. $Ni(cod)_2$ was insoluble in DMF at the desired concentration, so 1 scoop of $Ni(cod)_2$ was added to the appropriate vials using a plastic scoop (TWD TradeWinds, ASPS-01, Disposable

Antistatic Polypropylene Sample Transfer Scoop, 1-3 mg capacity) by hand in the glovebox. 250 µL of the stock solutions (0.005 mmol of Ni or 0.0025 mmol of Pd) or neat DMF (for reactions with Ni) were rapidly dispensed by hand using a multichannel micropipette to the required vials. **Note**: Pd_2dba_3 was dispensed as a slurry. It was crucial to agitate the solution and dispense immediately. After standing for a few minutes, heterogeneous dark purple solids were found to precipitate out of the Pd stock solutions – therefore, the slurry was shaken and dispensed quickly.

Dispensing of base: Triethylamine (7.0 µL, 0.10 mmol, 2.0 equiv) was dispensed by hand neat into each vial using a multichannel micropipette.

Deprotonation of NHC precursor: To ensure quantitative deprotonation of the IMes•HCl under reaction conditions, 1 scoop (approximately 2 mg) of NaO^tBu was added to all vials with the NHC by hand using a plastic scoop (TWD TradeWinds, ASPS-01, Disposable Antistatic Polypropylene Sample Transfer Scoop, 1-3 mg capacity).

Dispensing of alkenes: Olefins were dispensed by hand neat using a multichannel micropipette. 1-octene (11.8 µL, 0.075 mmol, 1.5 equiv); *n*-butyl vinyl ether (25.9 µL, 0.20 mmol, 4 equiv); *N*-vinyl pyrrolidone (21.4 µL, 0.20 mmol, 4 equiv); styrene (11.4 µL, 0.1 mmol, 2 equiv) were dispensed to appropriate wells.

Dispensing of (pseudo)halides: PhI (5.6 µL, 0.05 mmol, 1 equiv,) or PhOTf (8.1 µL, 0.05 mmol, 1 equiv) were dispensed, by hand, neat using a multichannel micropipette to the appropriate vials.

Heating the plates: Plates were sealed by placing a PFA sheet (Analytical Sales and Services, cat. no. 96967) and two rubber gaskets (Analytical Sales and Services, cat. no. 96965) on top of the

aluminum block followed by screwing in the plate lid with 1.5” stainless steel screws. The sealed HTE plate was removed from the glovebox and placed in a heated tumble stirrer at 85 °C equipped with a mica deck insert (V&P Scientific, cat. no. VP 710C5-7A-CC, VP741D, VP710C5-7-2) and stirred for 16 hours.

4.7.4 Work-up of high-throughput experiments

Addition of internal standard: After 16 hours, the aluminum plate was removed from the tumble stirrer, left to cool, and the plate lids removed. A Symyx S12209 Core Module Discovery Tools Synthesis Workstation was used to add an internal standard and dilute the mixture. With this tool, 125 µL of a 0.20 M solution of 1,3,5-trimethoxybenzene in PhMe was added to each vial, followed by 250 µL MeCN. The plate was then re-sealed and stirred on the tumbler stirrer at room temperature for at least 20 minutes to ensure homogeneity.

Preparation of filter plate: A 96-well filter plate (Pall Laboratory, cat. no. 8684) was loaded with ~0.5 cm of silica gel and placed on top of a second 96-well-plate (Analytical Sales and Services, cat. no. 96973) charged with empty glass inserts (8 × 30-mm, 0.75-mL vials; Chemglass Life Sciences, cat. no. CV-2100-0830).

Preparation of GC-FID samples: The aluminum plate was removed from the tumbler stirrer. The plate lid was removed and 10 µL from each well was dispensed onto the filter plate, followed by 500 µL of MeCN using a Symyx S12209 Core Module Discovery Tools Synthesis Workstation. Compressed air was applied using CEREX 96 II Multi Channel SPE System to facilitate filtration. Each well of the filter plate was rinsed with EtOAc and filtered with compressed air such that the filtered vials were nearly full with solvent. The filtered 96-well plate was then sealed and analyzed

using a GC-FID (GC/MSD; Agilent, model no. 5977A and 7890B) equipped with an autosampling arm (*xyz* autosampler, CTC Analytics, model no. Pal LSI 85). The crude GC-FID data was subsequently manually processed.

4.7.5 High-throughput plate layout and ligand structures

Figure 4.2 Overview of plate layout used for high-throughput experimentation

	L1	L2	L3	L4	L5	L6	L7	L8	L9	L10	L11	L12	
A	**PhOTf**	**PhOTf**	**PhOTf**	**PhOTf**	**PhOTf**	**PhOTf**	**PhOTf**	**PhOTf**	**PhOTf**	**PhOTf**	**PhOTf**	**PhOTf**	$Ni(cod)_2$
B	PhI	PhI	PhI	PhI	PhI	PhI	PhI	PhI	PhI	PhI	PhI	PhI	$Ni(cod)_2$
C	**PhOTf**	**PhOTf**	**PhOTf**	**PhOTf**	**PhOTf**	**PhOTf**	**PhOTf**	**PhOTf**	**PhOTf**	**PhOTf**	**PhOTf**	**PhOTf**	Pd_2dba_3
D	PhI	PhI	PhI	PhI	PhI	PhI	PhI	PhI	PhI	PhI	PhI	PhI	Pd_2dba_3
E	**PhOTf**	**PhOTf**	**PhOTf**	**PhOTf**	**PhOTf**	**PhOTf**	**PhOTf**	**PhOTf**	**PhOTf**	**PhOTf**	**PhOTf**	**PhOTf**	$Ni(cod)_2$
F	PhI	PhI	PhI	PhI	PhI	PhI	PhI	PhI	PhI	PhI	PhI	PhI	$Ni(cod)_2$
G	**PhOTf**	**PhOTf**	**PhOTf**	**PhOTf**	**PhOTf**	**PhOTf**	**PhOTf**	**PhOTf**	**PhOTf**	**PhOTf**	**PhOTf**	**PhOTf**	Pd_2dba_3
H	PhI	PhI	PhI	PhI	PhI	PhI	PhI	PhI	PhI	PhI	PhI	PhI	Pd_2dba_3
	L1	**L2**	**L3**	**L4**	**L5**	**L6**	**L7**	**L8**	**L9**	**L10**	**L11**	**L12**	

PhMe	DMF

Figure 4.3 Structures of all ligands used in the HTE screen

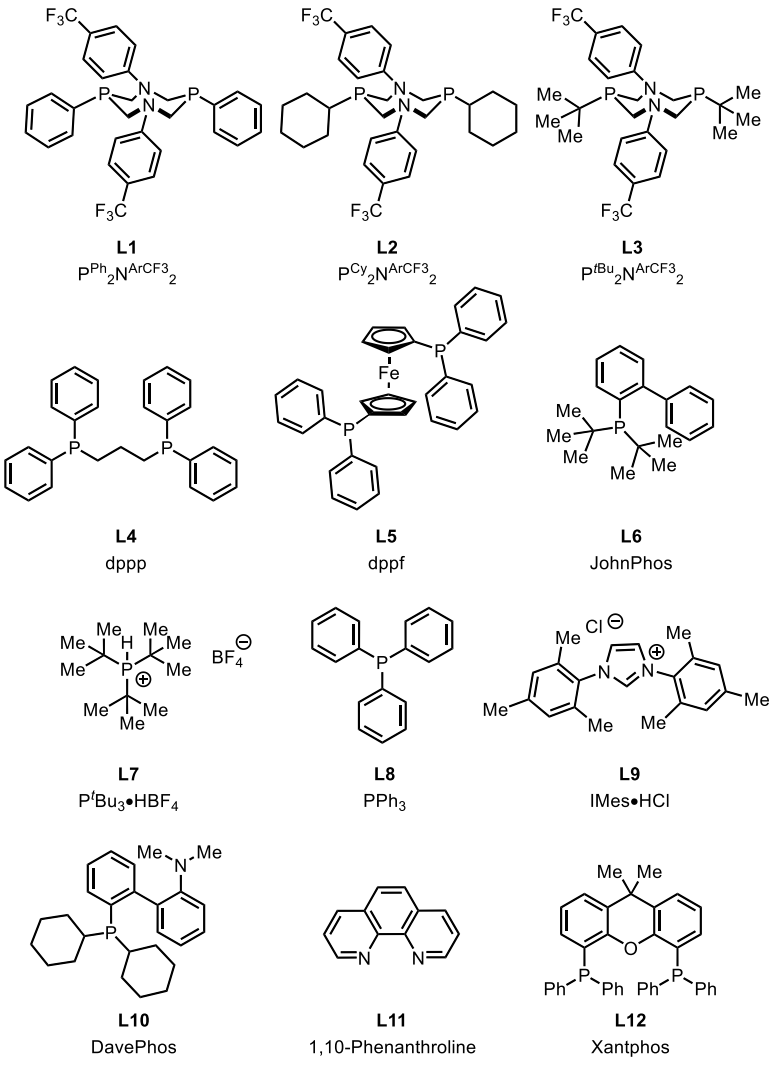

4.7.6 Styrene: Abridged results

Table 4.4 Normalized yields of the Mizoroki-Heck reaction with styrene.a Figure 4.2 shows a general plate overview including the reaction conditions for each row A-H. Figure 4.3 details the identities of L1-L12.

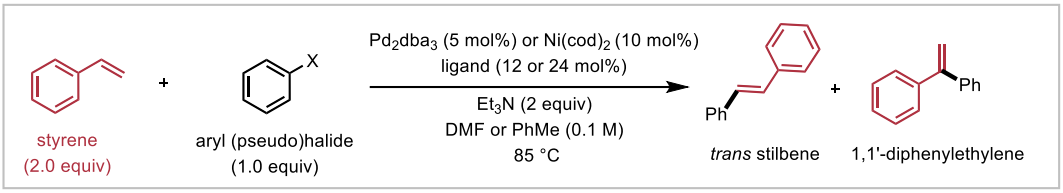

	L1	L2	L3	L4	L5	L6	L7	L8	L9	L10	L11	L12
A	0.87	0.74	0.07	0.43	0.35	0	0	0.11	0.02	0	0.1	0.07
B	0.89	0.15	0.07	0.2	0.07	0	0.02	0.1	0	0	0.03	0.07
C	0	0.02	0.58	0.91	0.63	0.01	0	0	0.03	0.02	0	0.03
D	0	0	0	0	0	0.07	0.13	0	0.02	0.01	0	0
E	0.09	0.22	0.13	0.1	0.07	0.02	0	0.05	0.03	0.05	0	0.04
F	0.15	0.12	0.09	0.24	0.07	0	0.01	0.01	0	0.06	0	0
G	0.04	0	0.31	0.74	0.46	0.23	0	0.34	0.18	0.03	0.17	0.01
H	0	0	0.01	0.48	0.42	0.96	0.98	0.27	1	0.34	0.1	0.06

[a]All integrals were obtained through crude GC-FID analysis of the 96 well-plate. The crude ratio of product to internal standard (I.S.) was determined by adding the integrals of all product regioisomers and dividing the resulting sum by the integral of the internal standard (1,3,5-trimethoxybenzene). To normalize the crude ratio of product to internal standard, each data entry was divided by the highest ratio of product to internal standard. For Table 4.4, the highest product/I.S. was 4.29. The crude product/I.S. of each well was divided by 4.29 to get normalized yields. It should be noted that Table 4.4 simply indicates conversion and makes no interpretation of regioselectivity.

Figure 4.4 Normalized yields of the Mizoroki-Heck reaction with styrene represented as bar graphs. Figure 4.2 shows a general plate overview including the reaction conditions for each row A-H. Figure 4.3 details the identities of L1-L12.

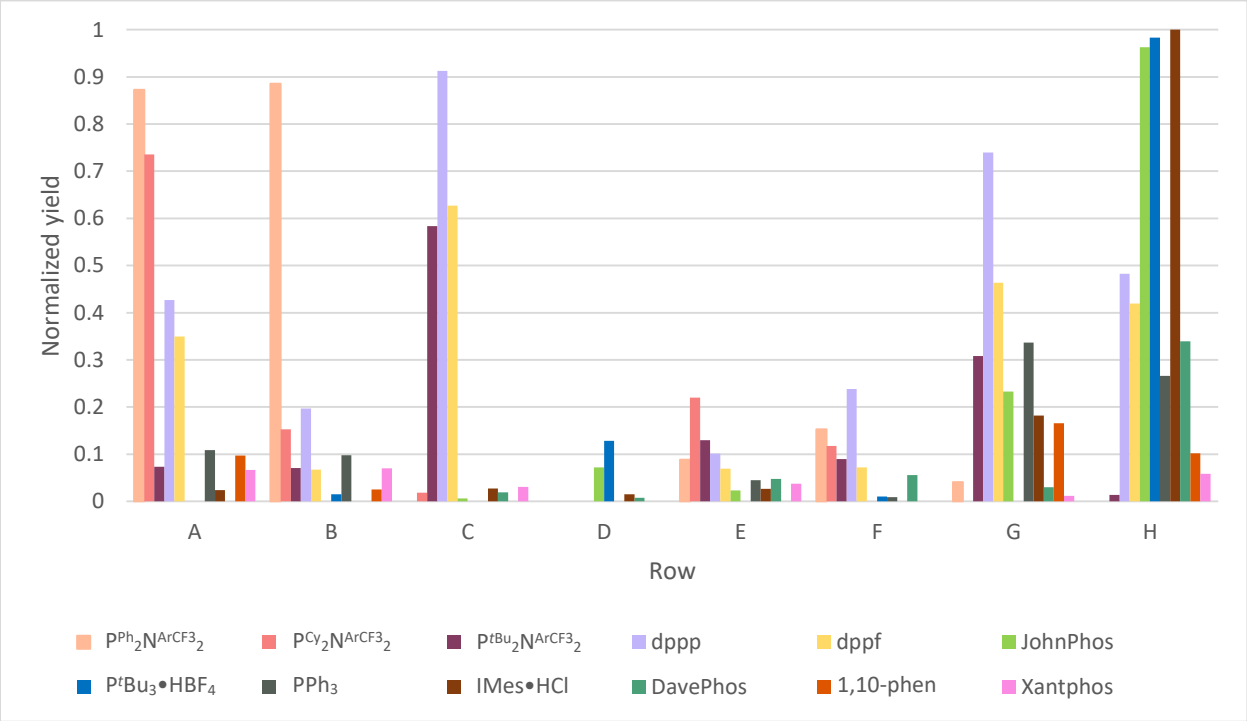

Figure 4.4 represents an alternate way of presenting the data of Table 4.4. All integrals were obtained through crude GC-FID analysis of the 96 well-plate. The crude ratio of product to internal standard (I.S.) was determined by adding the integrals of all product regioisomers and dividing the resulting sum by the integral of the internal standard (1,3,5-trimethoxybenzene). To normalize the crude ratio of product to internal standard, each data entry was divided by the highest ratio of product to internal standard. For Figure 4.4, the highest product/I.S. was 4.29. The crude product/I.S. of each well was divided by 4.29 to get normalized yields. It should be noted that Figure 4.4 simply indicates conversion and makes no interpretation of regioselectivity.

4.7.7 Styrene selectivity

Table 4.5 Selectivity for the Mizoroki-Heck reaction with styrene. Results are presented as a selectivity ratio.[a] Figure 4.2 shows a general plate overview including the reaction conditions for each row A-H. Figure 4.3 details the identities of L1-L12**.**

	L1	L2	L3	L4	L5	L6	L7	L8	L9	L10	L11	L12
A	0.85	0.43		0.2	-0.05							
B	0.97	1		0.82								
C			-1	0.62	-0.48							
D												
E		0.33										
F	0.92			-0.01								
G			-1	0.06	-0.43	0.96		0.92	0.41		0.9	
H				0.77	0.79	0.77	0.78	0.78	0.87	0.72		

[a] Only data points which had a normalized yield of >0.15 are presented on Table 4.6. Selectivity ratio is a measure of regioisomeric selectivity between two possible products. $\text{Selectivity ratio} = \frac{\text{integral of linear selectivity} - \text{integral of branch selectivity}}{\text{integral of linear selectivity} + \text{integral of branch selectivity}}$ .In this case, a selectivity ratio of -1 would indicate complete selectivity for the branched regioisomer, whereas a selectivity ratio of 1 would indicate complete linear selectivity. Conversely, a selectivity ratio around zero is indicative of low regioselectivity. Linear selective reactions (forming *trans* stilbene) are indicated in pale red and branched selective reactions (forming 1,1'-diphenylethylene) are indicated in pale blue. Reactions in pale purple had virtually no selectivity for either product.

Figure 4.5 Graph showing all styrene reactions which had greater than >10:1 regioselectivity for one regioisomer and a normalized yield > 0.15. Figure 4.2 shows a general plate overview including the reaction conditions for each row A-H. $P^{Ph}{}_2N^{ArCF3}{}_2$, PPh_3, and IMES•HCl were selective for *trans* stilbene (linear product). $P^{tBu}{}_2N^{ArCF3}{}_2$ was selective for 1,1'-diphenylethylene (branched product).

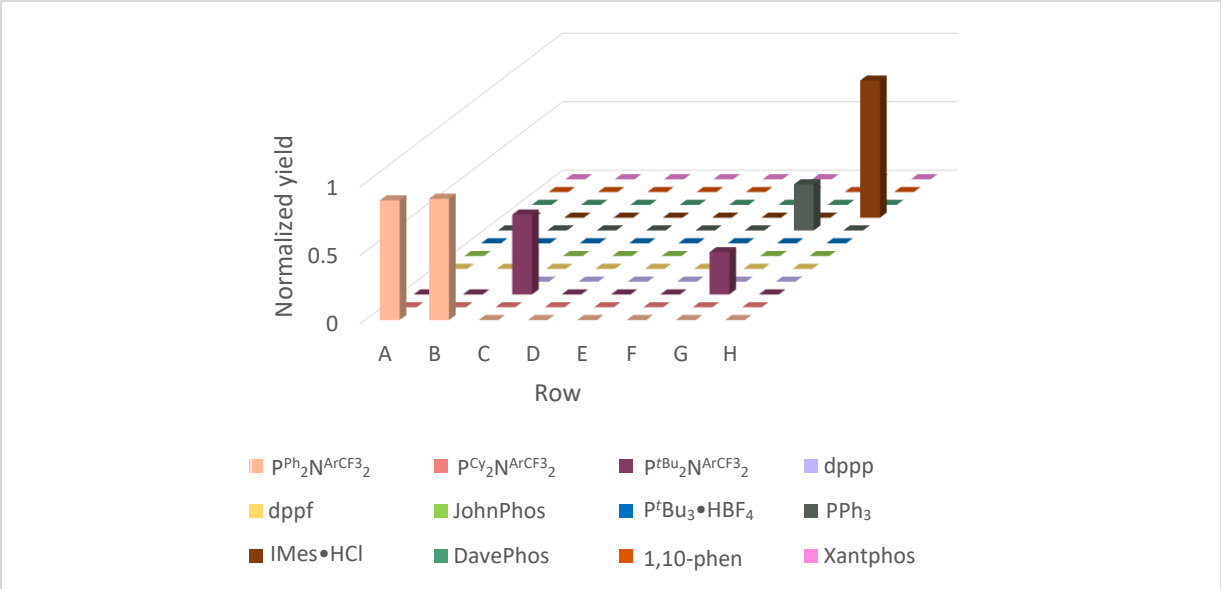

4.7.8 Reproduction and isolation of key HTE findings

After carrying out and analyzing the 384 Mizoroki-Heck experiments on 0.05 mmol scale, select hits were identified and reproduced on 0.20 mmol scale (Scheme 4.13). Procedures are listed below.

Scheme 4.13 Reaction conditions for the experiments reported in Scheme 4.2C

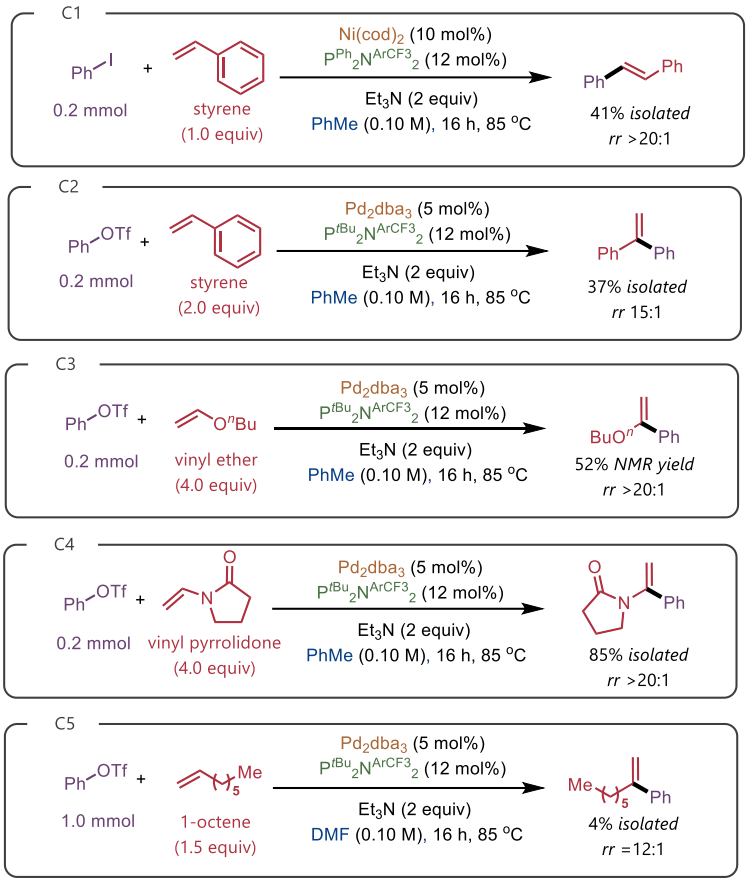

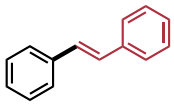

***Trans*-stilbene (Scheme 4.2C box 1)** was prepared inside the glovebox. To a dry 8 mL screw-capped reaction vial equipped with a magnetic stir bar, $Ni(cod)_2$ (5.5mg, 0.10 equiv, 0.02 mmol) and $P^{Ph}{}_2N^{ArCF3}{}_2$ (14.2 mg, 0.12 equiv, 0.024 mmol) were added and dissolved in PhMe (2.0 mL). Et_3N (55.8 µL, 2 equiv, 0.40 mmol), styrene (22.9 µL,1 equiv, 0.2 mmol) and PhI (22.3 µL, 1 equiv, 0.2 mmol) were added to the stirring solution. The vial was capped, removed from the glovebox, and placed in a stirring (350 rpm) pre-heated mineral oil bath at 85 °C. After stirring for 16 hours, the reaction vial was removed from the oil bath and cooled down to room temperature. The reaction mixture was diluted with DCM. An aliquot was filtered through silica and analyzed by GC-FID to assess crude linear:branch ratio (> 20:1). Solvent was removed in vacuo. The product was purified by column chromatography with hexanes to afford ***trans*-stilbene** as a white solid (14.8 mg, 41% yield). **^{1}H NMR** ($CDCl_3$, 300 MHz) δ (ppm) 7.55-7.50 (m, 4H), 7.40-7.34 (m, 4H), 7.30-7.24 (m, 2H), 7.12 (s, 2H). **^{13}C{^{1}H} NMR** ($CDCl_3$, 75 MHz) δ (ppm) 137.3, 128.6, 127.6, 126.5. Spectral data is in accordance with a previous report.[50] Note: An excess of styrene was found to promote the formation of styrene dimers/oligomers when using $Ni(cod)_2$ at the 0.2 mmol scale. These species were challenging to separate from the stilbene product. The equivalency of styrene was decreased from 2 equiv to 1 equiv to remove the formation of these side-products.

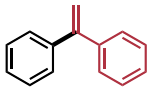

1,1'diphenylethylene (Scheme 4.2C box 2) was prepared in the glovebox. To a dry 8 mL screw-capped reaction vial equipped with a magnetic stir bar, Pd_2dba_3 (9.1 mg, 0.05 equiv, 0.01 mmol) and $P^{tBu}{}_2N^{ArCF3}{}_2$ (13.2 mg, 0.12 equiv, 0.024 mmol) were added and dissolved in PhMe (2.0 mL). Et_3N (55.8 µL, 2 equiv, 0.40 mmol), styrene (45.8 µL, 2 equiv, 0.4 mmol) and PhOTf (32.4 µL, 1 equiv, 0.2 mmol) were added to the stirring solution. The vial was capped, removed from the glovebox, and placed in a stirring (350 rpm) pre-heated mineral oil bath at 85 °C. After stirring for 16 hours, the reaction vial was removed from the oil bath and cooled down to room temperature. The reaction mixture was diluted with DCM. An aliquot was filtered through silica and analyzed by GC-FID to assess crude branch:linear ratio (15:1). Solvent was removed in vacuo. The product was purified by column chromatography with hexanes to afford **Scheme 4.2C box 2** as a colourless oil (13.3 mg, 37% yield). **^{1}H NMR** ($CDCl_3$, 300 MHz) δ

(ppm) 7.40-7.30 (m, 10H), 5.48 (s, 2H). **$^{13}C\{^{1}H\}$ NMR** ($CDCl_3$, 75 MHz) δ (ppm) 150.0, 141.4, 128.2, 128.1, 127.7, 114.3. Spectral data is in accordance with a previous report.[51]

(1-butoxyethenyl)benzene (Scheme 4.2C box 3) was prepared in the glovebox. To a dry 8 mL screw-capped reaction vial equipped with a magnetic stir bar, Pd_2dba_3 (9.1 mg, 0.05 equiv, 0.01 mmol) and $P^{tBu}{}_2N^{ArCF3}{}_2$ (13.2 mg, 0.12 equiv, 0.024 mmol) were added and dissolved in PhMe (2.0 mL). Et_3N (55.8 µL, 2 equiv, 0.40 mmol), *n*-butyl vinyl ether (103.5 µL, 4 equiv, 0.8 mmol) and PhOTf (32.4 µL, 1 equiv, 0.2 mmol) were added to the stirring solution. The vial was capped, removed from the glovebox, and placed in a stirring (350 rpm) pre-heated mineral oil bath at 85 °C. After stirring for 16 hours, the reaction vial was removed from the oil bath and cooled down to room temperature. An aliquot was filtered through silica and analyzed by GC-FID to assess crude branch:linear ratio. The reaction was diluted with DCM, 0.05 mmol 1,3,5-trimethoxybenzene was added to the reaction mixture as internal standard (1 mL of a 0.05 M stock solution).The reaction was quenched with 0.5 mL of 2M $HCl_{(aq)}$ and stirred at room temperature for 60 minutes. The organic phase was separated using a Pasteur pipette and was filtered through a plug of silica. The silica was then rinsed with EtOAc to ensure transfer and the solvent was removed in vacuo. Acetophenone, the hydrolysis product of **(1-butoxyethenyl)benzene**, was obtained in 52% yield (crude ^{1}H NMR in $CDCl_3$).

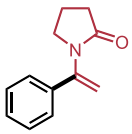

1-(1-phenylvinyl)-pyrrolidin-2-one (Scheme 4.2C box 4) was prepared inside the glovebox. To a dry 8 mL screw-capped reaction vial equipped with a magnetic stir bar, Pd_2dba_3 (9.1 mg, 0.05 equiv, 0.01 mmol) and $P^{tBu}{}_2N^{ArCF3}{}_2$ (13.2 mg, 0.12 equiv, 0.024 mmol) were added and dissolved in PhMe (2.0 mL). Et_3N (55.8 µL, 2 equiv, 0.40 mmol), N-vinyl pyrrolidone (85.5 µL, 4 equiv, 0.8 mmol) and PhOTf (32.4 µL, 1 equiv, 0.2 mmol) were added to the stirring solution. The vial was capped, removed from the glovebox, and placed in a stirring (350 rpm) pre-heated mineral oil bath at 85 °C. After stirring for 16 hours, the reaction vial was removed from the oil bath and cooled down to room temperature. The reaction mixture was diluted with DCM. An aliquot was filtered through silica and analyzed by GC-FID to assess crude linear: branch ratio (> 20:1). Solvent was removed in vacuo. The product was purified by column chromatography with 30% to 50% EtOAc in hexanes to afford **1-(1-phenylvinyl)-pyrrolidin-2-one** as a colourless oil (31.6 mg, 84% yield). **^{1}H NMR** (C_6D_6, 300 MHz) δ (ppm) 7.26-7.20 (m, 2H), 7.16-

7.06 (m, 3H), 5.32 (s, 1H), 5.14 (s, 1H), 2.86 (t, *J* = 6.9 Hz, 2H), 2.03 (t, *J* = 8.0 Hz, 2H), 1.23 (quint, *J* = 7.5 Hz, 2H). **^{13}C{^{1}H} NMR** (C_6D_6, 75 MHz) *δ* (ppm) 173.0, 144.5, 137.6, 128.4, 127.0, 107.5, 48.8, 31.8, 18.3. Spectral data is in accordance with a previous report.[52]

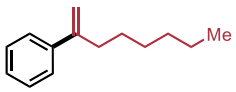

Oct-1-en-2-ylbenzene (Scheme 4.2C box 5) was prepared in the glovebox. To a dry 8 mL screw-capped reaction vial equipped with a magnetic stir bar, Pd_2dba_3 (9.1 mg, 0.05 equiv, 0.01 mmol) and $P^{tBu}{}_2N^{ArCF3}{}_2$ (13.2 mg, 0.12 equiv, 0.024 mmol) were added and dissolved in PhMe (2.0 mL). Et_3N (55.8 µL, 2 equiv, 0.40 mmol), 1-octene (47.1 µL, 1.5 equiv, 0.30 mmol), and PhOTf (32.4 µL, 1 equiv, 0.2 mmol) were added to the stirring solution. The vial was capped, removed from the glovebox, and placed in a stirring (350 rpm) pre-heated mineral oil bath at 85 °C. After stirring for 16 hours, the reaction vial was removed from the oil bath and cooled down to room temperature. The reaction was diluted with DCM (~5 mL) and 0.05 mmol 1,3,5-trimethoxybenzene was added to the reaction mixture as internal standard (1 mL of a 0.05 M stock solution).An aliquot was filtered through silica and analyzed by GC-FID to assess crude branch:linear ratio (12:1). A liquid-liquid extraction was performed three times with 10 mL of water. The organic extract was dried with sodium sulfate, filtered, and solvent was removed in vacuo. **Oct-1-en-2-ylbenzene** was obtained in 15% yield (crude ^{1}H NMR in $CDCl_3$).This procedure was repeated on a 1 mmol scale and the product was purified by column chromatography with hexanes to afford **oct-1-en-2-ylbenzene** as a colourless oil (7.5 mg, 4% yield). **^{1}H NMR** ($CDCl_3$, 400 MHz) *δ* (ppm) 7.43-7.37 (m, 2H), 7.35-7.29 (m, 2H), 7.28-7.23 (m, 1H), 5.25 (d, *J* = 1.2 Hz, 1H), 5.05 (d, *J* = 1.2 Hz, 1H), 2.50 (t, *J* = 7.5 Hz, 2H), 1.48-1.39 (m, 2H), 1.36-1.22 (m, 6H), 0.86 (t, *J* = 6.8Hz, 3H). **^{13}C {^{1}H} NMR** ($CDCl_3$, 100 MHz) *δ* (ppm) 148.8, 141.5, 128.2, 127.2, 126.1, 112.0, 35.3, 31.7, 29.0, 28.2, 22.6, 14.1. Spectral data is in accordance with a previous report.[4b]

4.7.9 NMR spectra for isolated HTE reproductions

***Trans* stilbene (Scheme 4.2C box 1),** ^{1}H, $CDCl_3$, 300 MHz

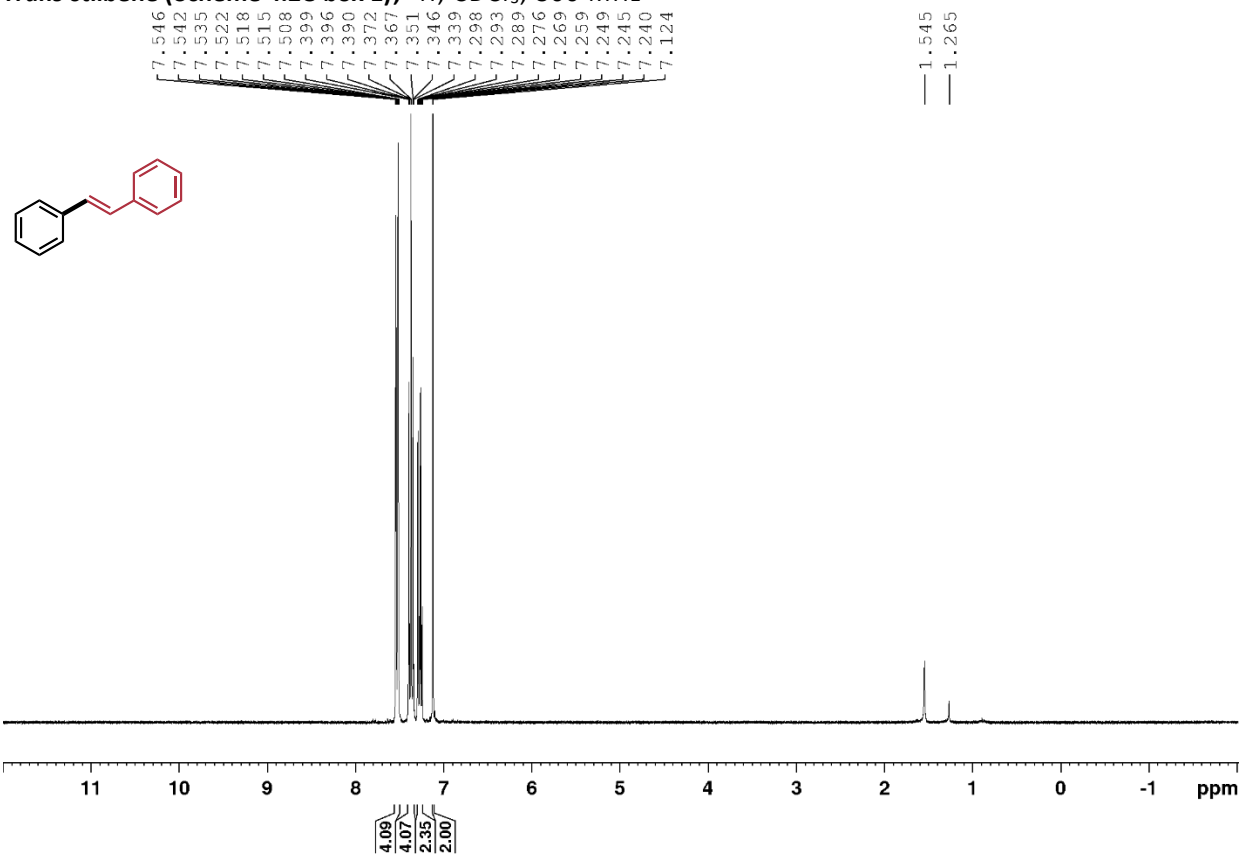

***Trans* stilbene (Scheme 4.2C box 1),** $^{13}C\{^{1}H\}$, $CDCl_3$, 75 MHz

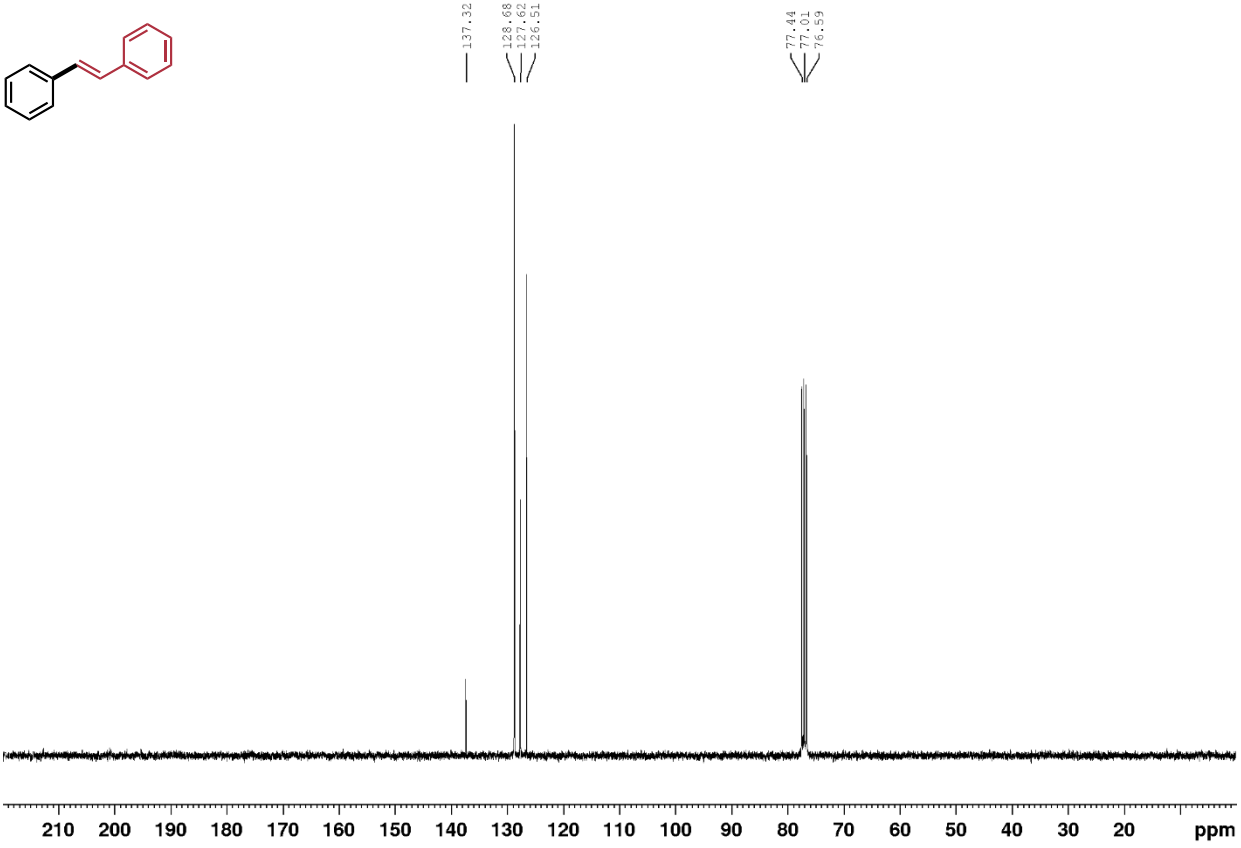

1,1'-diphenylethylene (Scheme 4.2C box 2), ^{1}H, $CDCl_3$, 300 MHz

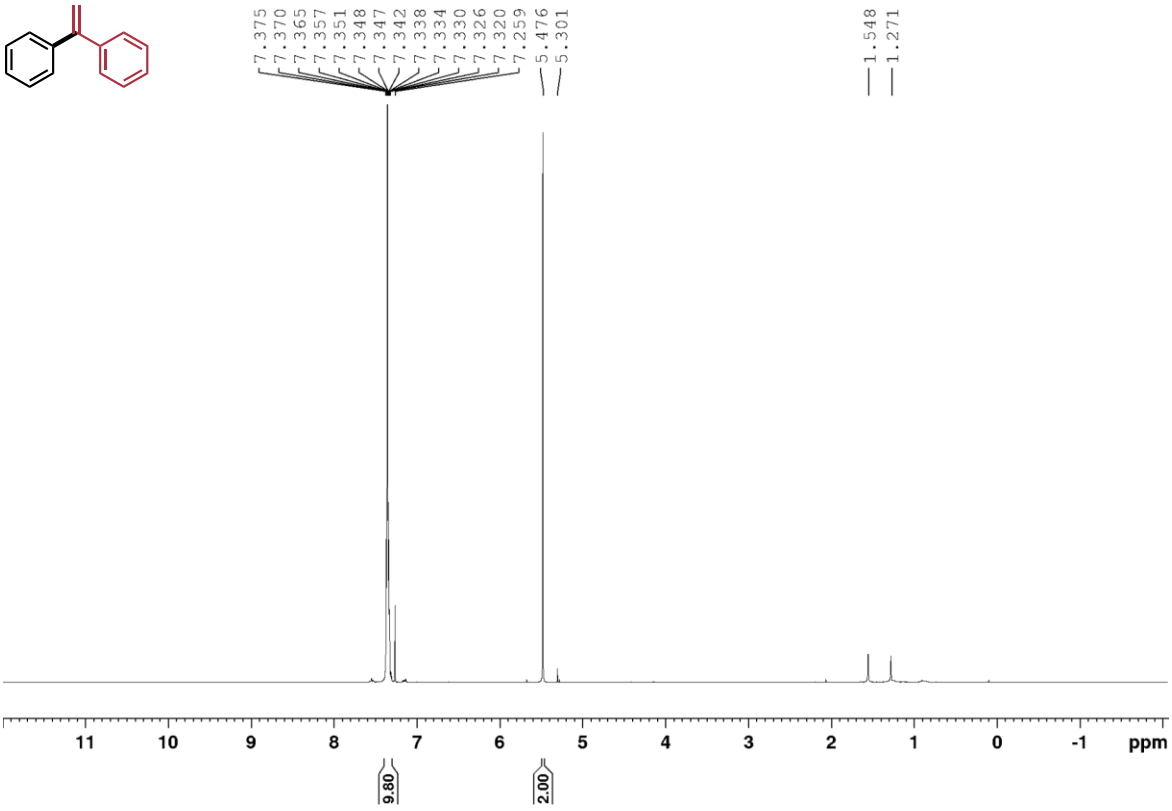

1,1'-diphenylethylene (Scheme 4.2C box 2), $^{13}C\{^{1}H\}$, $CDCl_3$, 100 MHz

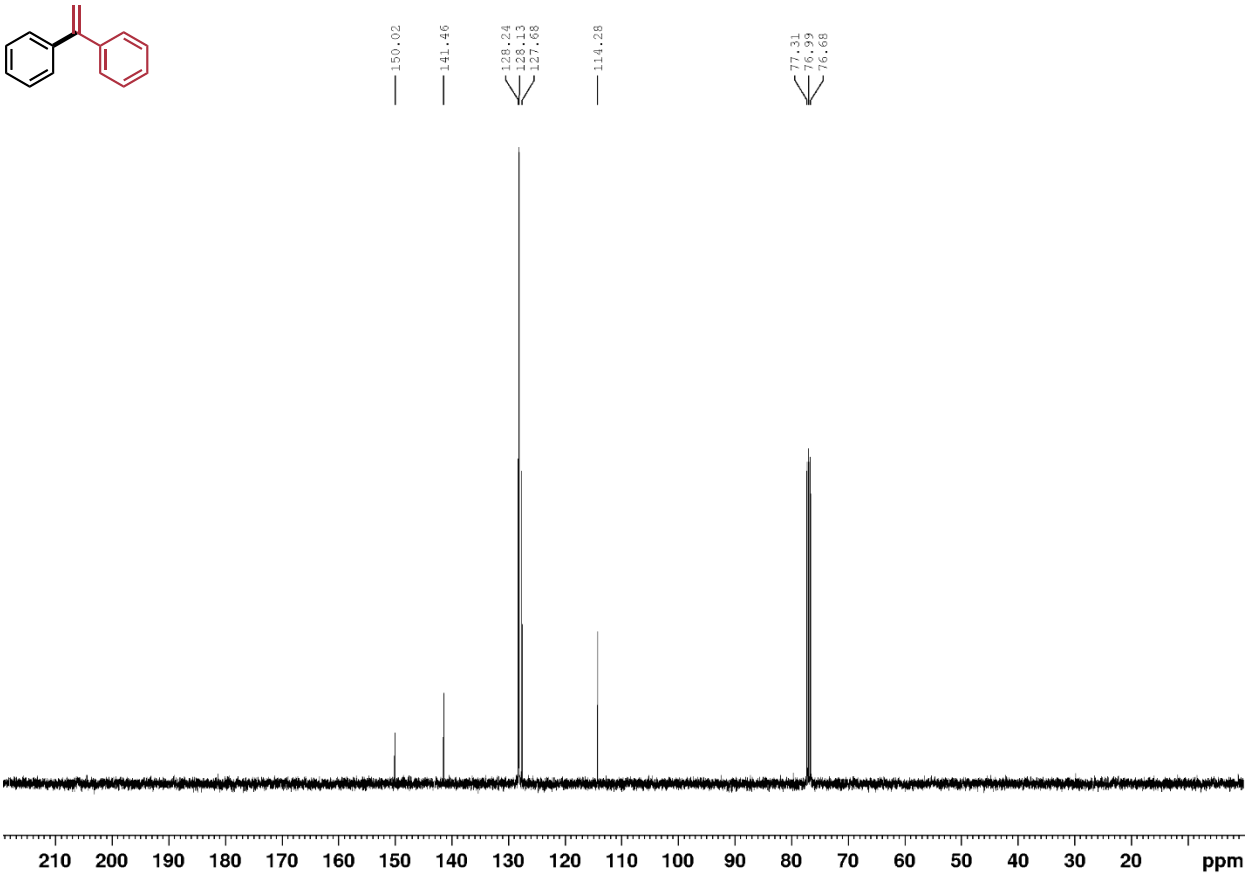

1-(1-phenylvinyl)-pyrrolidin-2-one (Scheme 4.2C box 4), ^{1}H, C_6D_6, 300 MHz

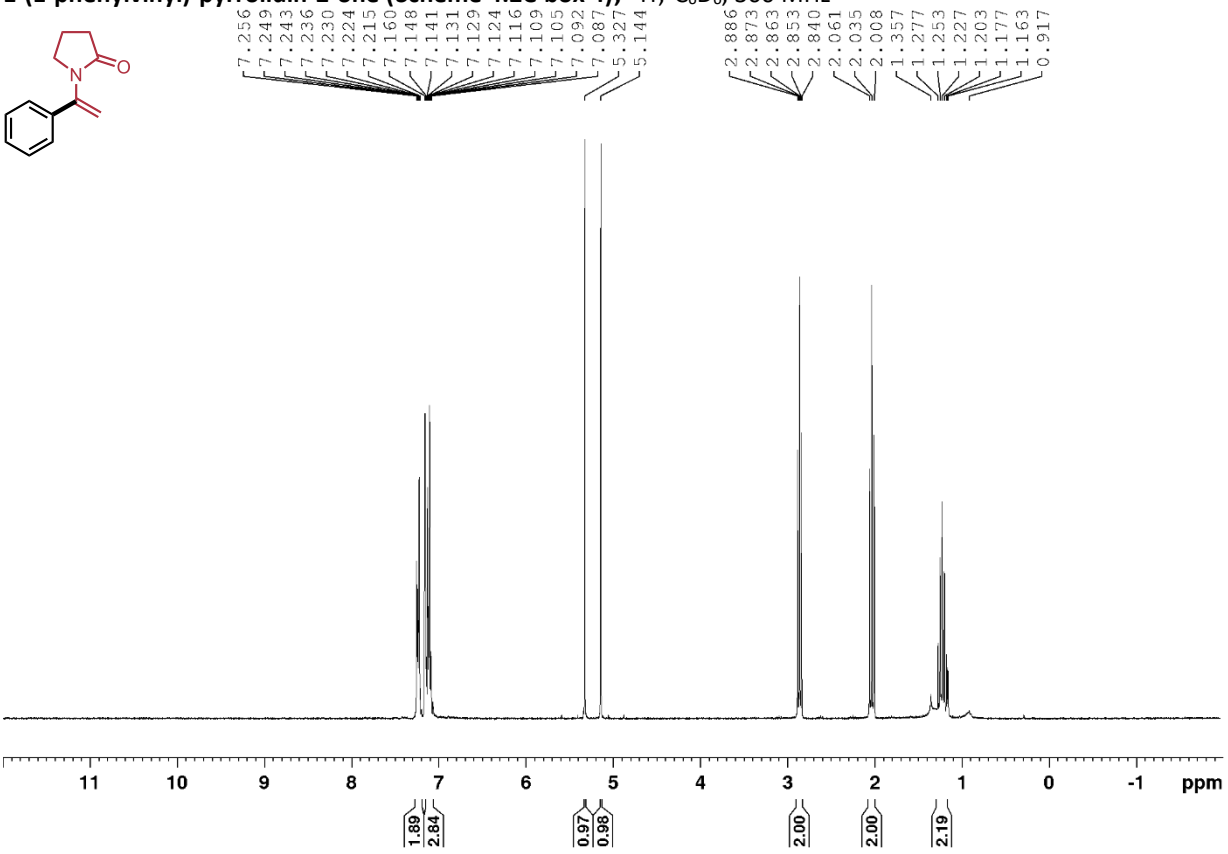

1-(1-phenylvinyl)-pyrrolidin-2-one (Scheme 4.2C box 4), $^{13}C\{^{1}H\}$, C_6D_6, 75 MHz

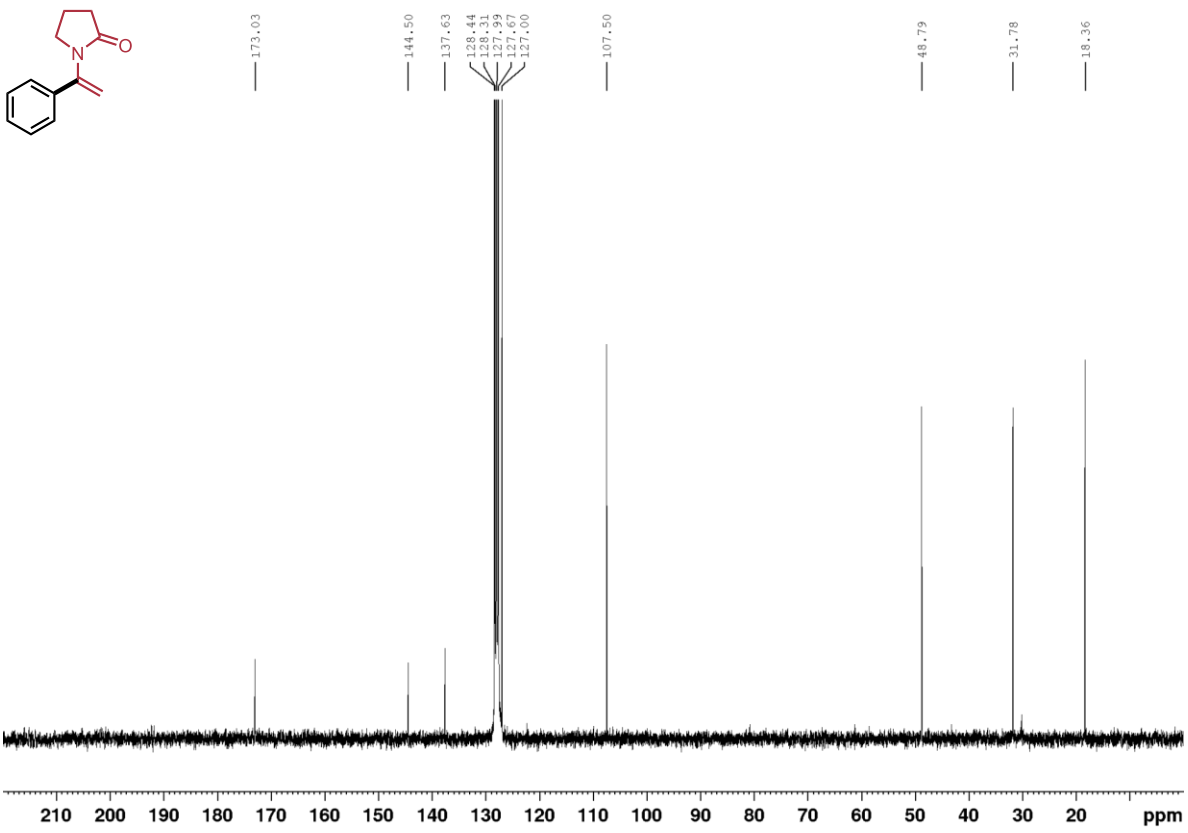

Oct-1-en-2-ylbenzene (Scheme 4.2C box 5), ^{1}H, $CDCl_3$, 400 MHz

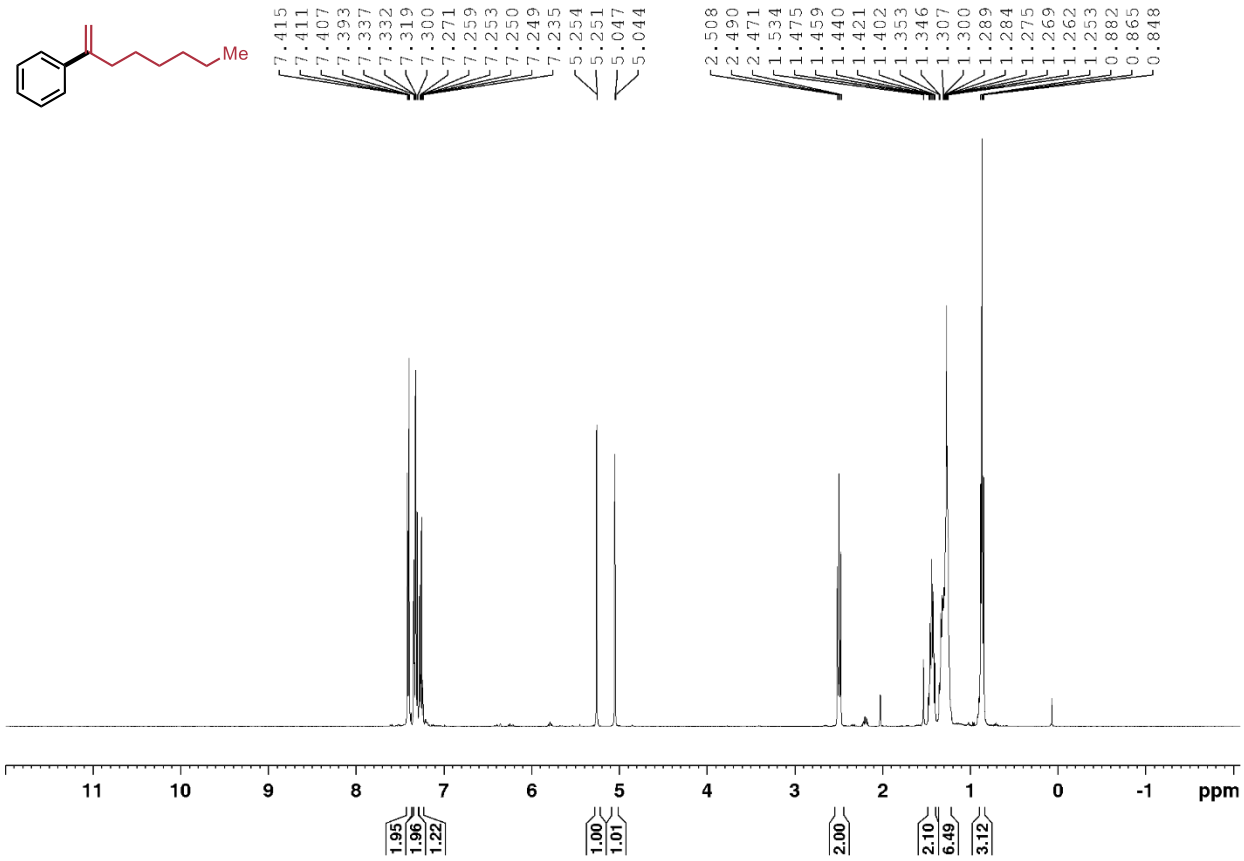

Oct-1-en-2-ylbenzene (Scheme 4.2C box 5), $^{13}C\{^{1}H\}$, $CDCl_3$, 100 MHz

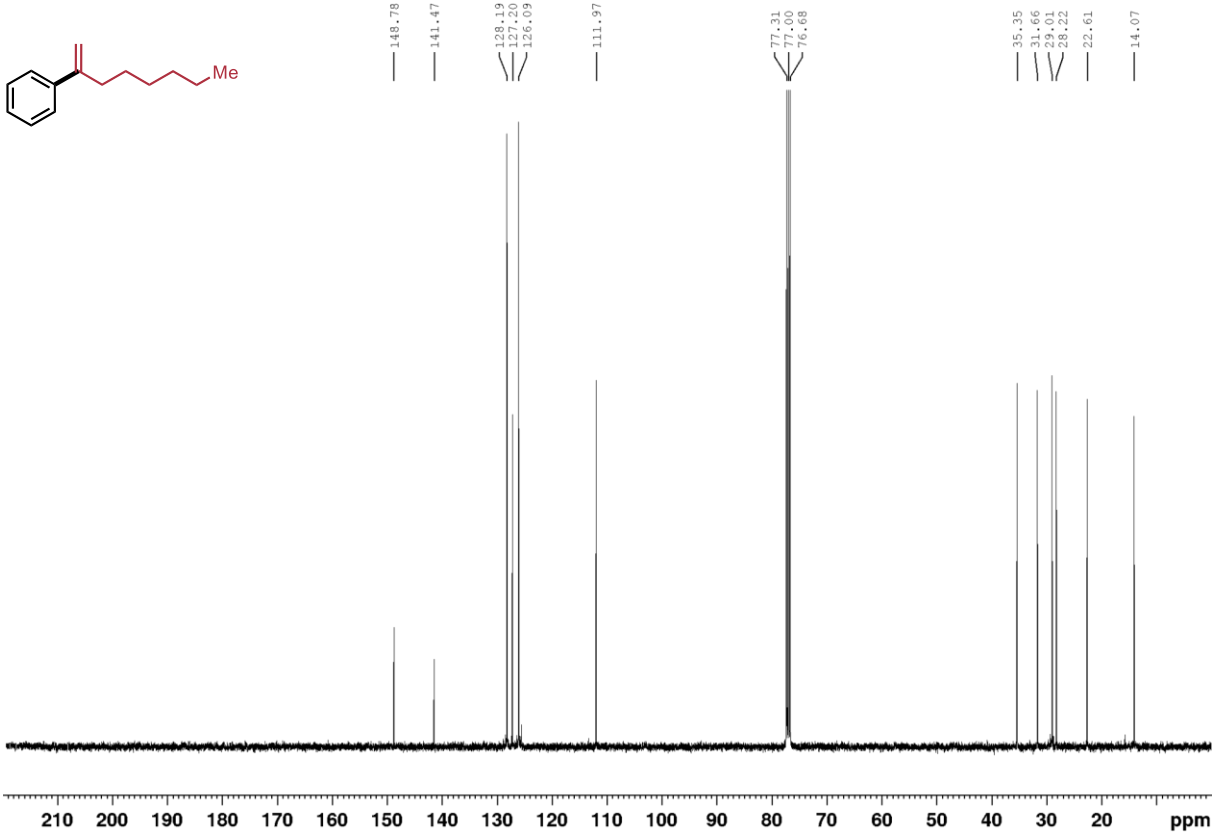

4.7.10 Averaged data from styrene plate

Table 4.7 Normalized average conversion of the Mizoroki-Heck reaction with styrene sorted by ligand identity. The normalized yields from Table 4.4 and Figure 4.4 are sorted by ligand identity and have been averaged.

Entry	Column	Ligand	Average normalized yield	Total number of reactions
1	L1	$P^{Ph}{}_2N^{ArCF3}{}_2$	0.25	8
2	L2	$P^{Cy}{}_2N^{ArCF3}{}_2$	0.16	8
3	L3	$P^{tBu}{}_2N^{ArCF3}{}_2$	0.16	8
4	L4	dppp	0.39	8
5	L5	dppf	0.26	8
6	L6	JohnPhos	0.16	8
7	L7	$P^tBu_3 \bullet HBF_4$	0.14	8
8	L8	PPh_3	0.11	8
9	L9	IMes•HCl	0.16	8
10	L10	DavePhos	0.06	8
11	L11	1,10-phenanthroline	0.05	8
12	L12	XantPhos	0.03	8

Table 4.8 Normalized average conversion of the Mizoroki-Heck reaction with styrene by ligand and precatalyst identity. The normalized yields Table 4.4 and Figure 4.4 are sorted by ligand identity and further divided based on the metal precatalyst used.

Column	Ligand	Average normalized yield $Ni(cod)_2$	Average normalized yield $Pd_2(dba)_3$	Total number of reactions
L1	$P^{Ph}{}_2N^{ArCF3}{}_2$	0.50	0.01	8 (4 Ni + 4 Pd)
L2	$P^{Cy}{}_2N^{ArCF3}{}_2$	0.31	0.01	8 (4 Ni + 4 Pd)
L3	$P^{tBu}{}_2N^{ArCF3}{}_2$	0.09	0.23	8 (4 Ni + 4 Pd)
L4	dppp	0.24	0.53	8 (4 Ni + 4 Pd)
L5	dppf	0.14	0.38	8 (4 Ni + 4 Pd)
L6	JohnPhos	0.01	0.32	8 (4 Ni + 4 Pd)
L7	$P^tBu_3 \bullet HBF_4$	0.01	0.28	8 (4 Ni + 4 Pd)
L8	PPh_3	0.07	0.15	8 (4 Ni + 4 Pd)
L9	IMes•HCl	0.01	0.31	8 (4 Ni + 4 Pd)
L10	DavePhos	0.03	0.10	8 (4 Ni + 4 Pd)
L11	1,10-phenanthroline	0.03	0.07	8 (4 Ni + 4 Pd)
L12	XantPhos	0.04	0.03	8 (4 Ni + 4 Pd)

Table 4.9 Normalized average conversion of the Mizoroki-Heck reaction with styrene by ligand and solvent identity. The normalized yields from Table 4.4 and Figure 4.4 are sorted by ligand identity and further divided based on the solvent used

Column	Ligand	Average normalized yield PhMe	Average normalized yield DMF	Total number of reactions
L1	$P^{Ph}{}_2N^{ArCF3}{}_2$	0.44	0.07	8 (4 PhMe + 4 DMF)
L2	$P^{Cy}{}_2N^{ArCF3}{}_2$	0.23	0.08	8 (4 PhMe + 4 DMF)
L3	$P^{tBu}{}_2N^{ArCF3}{}_2$	0.18	0.14	8 (4 PhMe + 4 DMF)
L4	dppp	0.38	0.39	8 (4 PhMe + 4 DMF)
L5	dppf	0.26	0.26	8 (4 PhMe + 4 DMF)
L6	JohnPhos	0.02	0.30	8 (4 PhMe + 4 DMF)
L7	P^tBu_3•HBF_4	0.04	0.25	8 (4 PhMe + 4 DMF)
L8	PPh_3	0.05	0.16	8 (4 PhMe + 4 DMF)
L9	IMes•HCl	0.02	0.30	8 (4 PhMe + 4 DMF)
L10	DavePhos	0.01	0.12	8 (4 PhMe + 4 DMF)
L11	1,10-phenanthroline	0.03	0.07	8 (4 PhMe + 4 DMF)
L12	XantPhos	0.04	0.03	8 (4 PhMe + 4 DMF)

Table 4.10 Normalized average conversion of the Mizoroki-Heck reaction with styrene by ligand and aryl pseudohalide identity. The normalized averaged yields from Table 4.4 and Figure 4.4 are sorted by ligand identity and further divided based on the (pseudo)halide used.

Column	Ligand	Average normalized yield PhOTf	Average normalized yield PhI	Total number of reactions
L1	$P^{Ph}{}_2N^{ArCF3}{}_2$	0.25	0.26	8 (4 PhOTf + 4 PhI)
L2	$P^{Cy}{}_2N^{ArCF3}{}_2$	0.24	0.07	8 (4 PhOTf + 4 PhI)
L3	$P^{tBu}{}_2N^{ArCF3}{}_2$	0.27	0.04	8 (4 PhOTf + 4 PhI)
L4	dppp	0.55	0.23	8 (4 PhOTf + 4 PhI)
L5	dppf	0.38	0.14	8 (4 PhOTf + 4 PhI)
L6	JohnPhos	0.07	0.26	8 (4 PhOTf + 4 PhI)
L7	$P^tBu_3 \bullet HBF_4$	0	0.28	8 (4 PhOTf + 4 PhI)
L8	PPh_3	0.12	0.09	8 (4 PhOTf + 4 PhI)
L9	IMes•HCl	0.07	0.25	8 (4 PhOTf + 4 PhI)
L10	DavePhos	0.02	0.10	8 (4 PhOTf + 4 PhI)
L11	1,10-phenanthroline	0.07	0.03	8 (4 PhOTf + 4 PhI)
L12	XantPhos	0.04	0.03	8 (4 PhOTf + 4 PhI)

Table 4.11 Normalized average conversion of the Mizoroki-Heck reaction with styrene by solvent identity. The normalized averaged yields from Table 4.4 and Figure 4.4 are sorted by solvent identity.

Solvent	Average normalized ligand	Total number of reactions
PhMe	0.14	48
DMF	0.18	48

Table 4.12 Normalized average conversion of the Mizoroki-Heck reaction with styrene by metal precatalyst and solvent identity. The normalized averaged yields from Table 4.4 and Figure 4.4 are sorted by metal precatalyst identity and further divided based on the solvent used.

Metal	Solvent	Average normalized yield	Total number of reactions
$Ni(cod)_2$	PhMe	0.18	24
$Ni(cod)_2$	DMF	0.06	24
$Ni(cod)_2$	Both	0.12	48
Pd_2dba_3	PhMe	0.10	24
Pd_2dba_3	DMF	0.30	24
Pd_2dba_3	Both	0.20	48

Table 4.13 Normalized average conversion of the Mizoroki-Heck reaction with styrene by aryl (pseudo)halide and metal identity. The normalized averaged yields from Table 4.4 and Figure 4.4 are sorted by aryl (pseudo)halide identity and further divided based on the solvent used.

(Pseudo)halide	Solvent	Average normalized yield	Total number of reactions
PhOTf	PhMe	0.21	24
PhOTf	DMF	0.14	24
PhOTf	Both	0.17	48
PhI	PhMe	0.08	24
PhI	DMF	0.22	24
PhI	Both	0.15	48

Table 4.14 Normalized average conversion of the Mizoroki-Heck reaction with styrene by aryl (pseudo)halide and metal identity. The normalized averaged yields from Table 4.4 and Figure 4.4 are sorted by aryl (pseudo)halide identity and further divided based on the metal precatalyst used.

(Pseudo)halide	Metal	Average normalized yield	Total number of reactions
PhOTf	$Ni(cod)_2$	0.15	24
PhOTf	$Pd_2(dba)_3$	0.20	24
PhOTf	Both	0.17	48
PhI	$Ni(cod)_2$	0.10	24
PhI	$Pd_2(dba)_3$	0.20	24
PhI	Both	0.15	48

4.7.11 Combined data from all 4 main plates (styrene, *n*-butyl vinyl ether, N-vinyl pyrrolidone, 1-octene)

Figure 4.6 Graph showing all normalized yields (conversion) HTE results together. There are no interpretations on this graph about regioselectivity

.

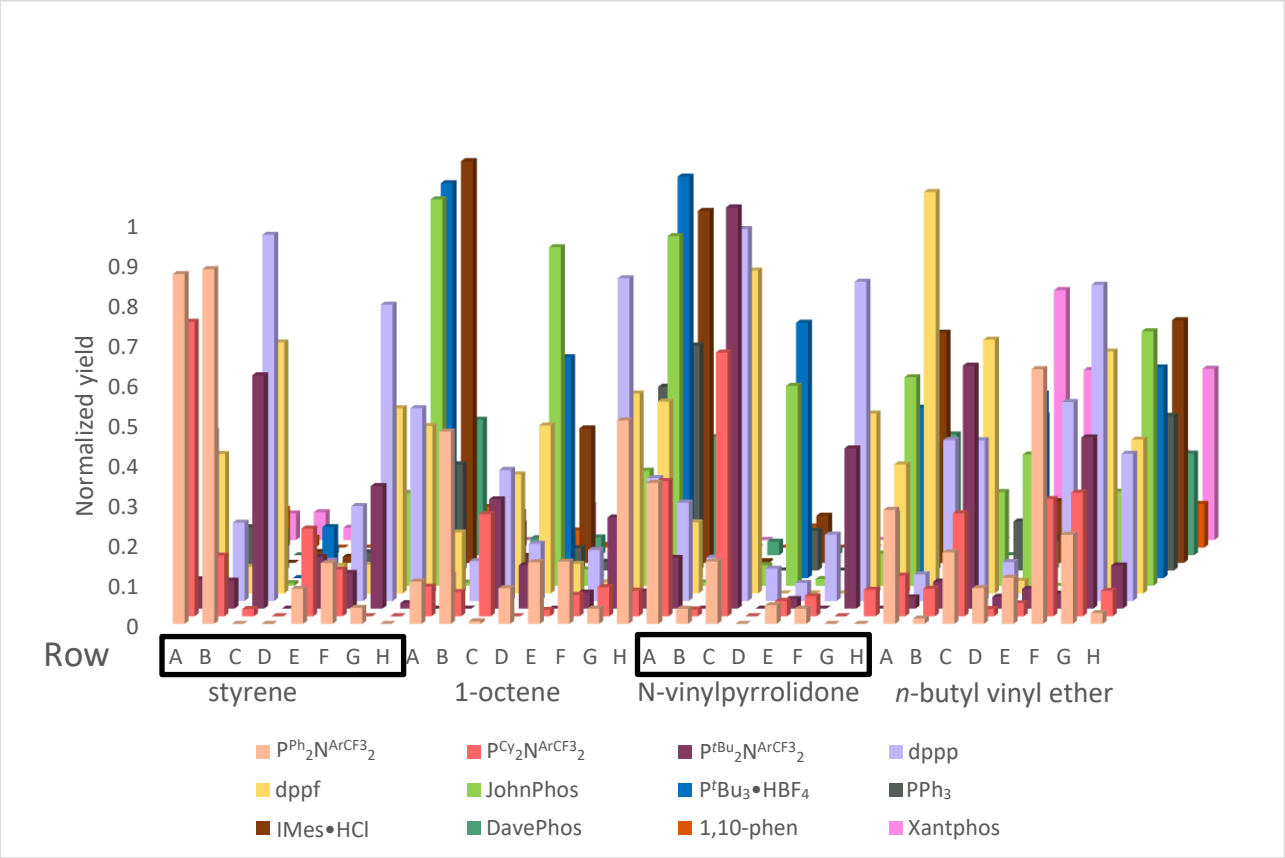

Figure 4.7 Graph showing all data points that had regioisomeric ratios of >10:1 for a single regioisomer and a normalized yield > 0.15.

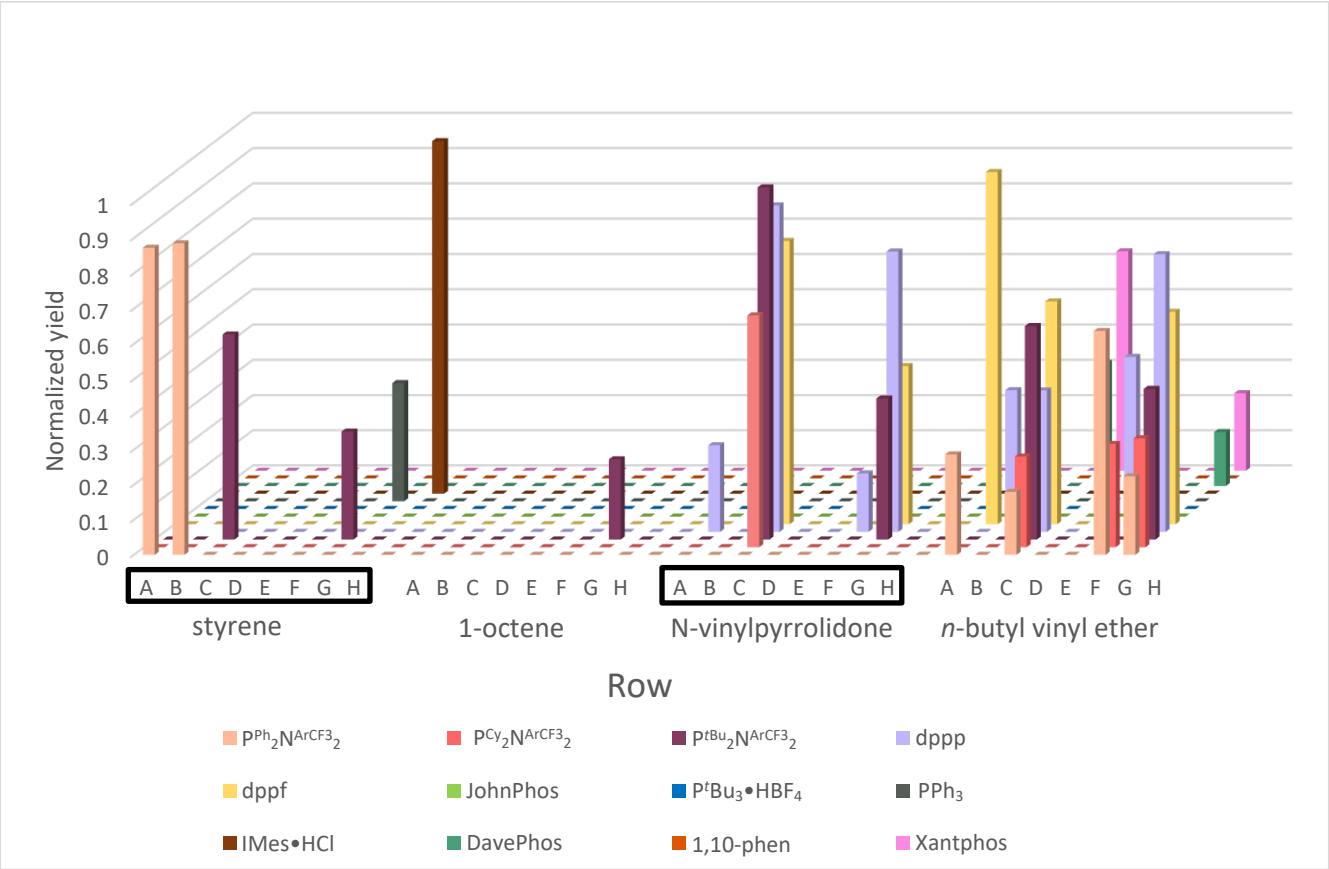

4.7.12 Additional optimization results

Table 4.14 shows one variable-at-a-time optimization of the coupling reaction. Crude ratios between the branched product (**4.7-br**) and linear (**4.7-lin**) were assessed using GC-FID. The areas of respective products was normalized to the area of the internal standard (0.05 mmol of 1,3,5-trimethoxybenzene). Calibration curves can be used to convert the observed ratios product-to-internal standard into crude yields. Further information about the calibrations curves and how to use them are detailed in Section 4.7.15.

Table 4.15 Data for the optimization of the HTE result

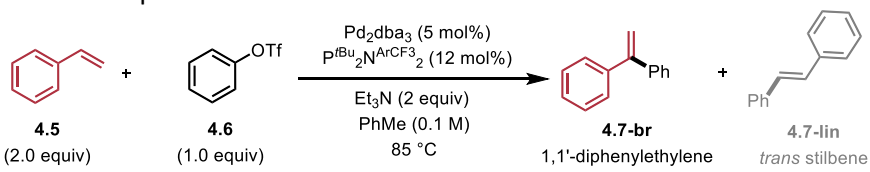

4.5 (2.0 equiv) + **4.6** (1.0 equiv) → **4.7-br** 1,1'-diphenylethylene + **4.7-lin** *trans* stilbene

Entry	Modification	**4.7-br** /I.S.[a]	**4.7-lin**/I.S.[a]	Branch-to-linear (GC-FID)
1	None	3.18	0.15	21:1
2	HTE result[b]	1.69	0.08	21:1
3	Pd(Cp)(cinnamyl) (5 mol%) as precatalyst and TMP as base	1.74	0.03	>40:1
4	Pd_2dba_3•$CHCl_3$ (2.5 mol%) as precatalyst and TMP as base	3.70	0.18	21:1
5	$P^{tBu}{}_2N^{ArCF3}{}_2$ Pd G3 (**4.3**) (5 mol%) as precatalyst	2.38	0.08	30:1
6	$PdCl_2(PhCN)_2$ (5 mol%) as precatalyst	0	0	0
7	$P^{tBu}{}_2N^{Bn}{}_2$ (3 mol%) as ligand	0	0	0
8	20 hours	3.38	0.12	28:1
9	70 °C	1.89	0.09	21:1
10	100 °C	2.65	0.14	19:1
11	NEt_3 (3 equiv)	2.29	0.10	23:1
12	Hunig's base (DIPEA) as base	3.93	0.15	26:1

General reaction conditions: Aryl triflate (0.10 mmol), styrene (0.20 mmol), base (0.20 mmol), $P^{tBu}{}_2N^{ArCF3}{}_2$ (3 mol%), Pd_2dba_3 (2.5 mol%) in PhMe (0.1 M) at 85°C for 16 h. 0.05 mmol of 1,3,5 –trimethoxybenzene added as internal standard. Crude branch-to-linear ratios are given as assessed by GC-FID analysis. [a]Ratio of the area of product divided by the area of internal standard. [b]See Scheme 4.4 for reaction conditions.

Table 4.12 Data for the optimization of the HTE result (continued)

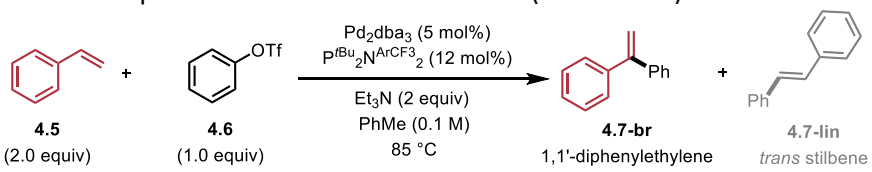

Entry	Modification	**4.7-br** /I.S.[a]	**4.7-lin**/I.S.[a]	Branch-to-linear (GC-FID)
13	2,2,6,6-tetramethylpiperidine (TMP) as base	4.64	0.20	23:1
14	K_3PO_4 as base	1.18	0.10	12:1
15	THF as solvent	1.53	0.04	38:1
16	Dioxane as solvent	2.49	0.15	17:1
17	1.5 equiv. styrene	2.64	0.15	18:1

General reaction conditions: Aryl triflate (0.10 mmol), styrene (0.20 mmol), base (0.20 mmol), $P^{tBu}{}_2N^{ArCF3}{}_2$ (3 mol%), Pd_2dba_3 (2.5 mol%) in PhMe (0.1 M) at 85°C for 16 h. 0.05 mmol of 1,3,5 –trimethoxybenzene added as internal standard. Crude branch-to-linear ratios are given as assessed by GC-FID analysis. [a]Ratio of the area of product divided by the area of internal standard. [b]See Scheme 4.4 for reaction conditions.

4.7.12.1 Extended precatalyst study for linear selective coupling

Table 4.16 Preliminary optimization studies for palladium catalyst and metal to ligand ratio

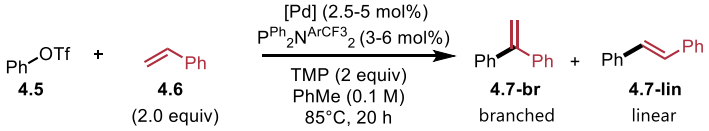

Entry	Precatalyst	$P^{Ph}{}_2N^{ArCF3}{}_2$ loading	**4.7-br** (% yield)	**4.7-lin** (% yield)
1	Pd_2dba_3 (2.5 mol%)	3 mol%	4%	88%
2	Pd_2dba_3 (2.5 mol%)	6 mol%	not observed	trace
3	Pd(Cp)(cinnamyl) (5 mol%)	3 mol%	4%	67%
4	Pd(Cp)(cinnamyl) (5 mol%)	6 mol%	5%	94%
5	$[Pd(allyl)Cl]_2$(2.5 mol%)	3 mol%	trace	7%
6	$[Pd(allyl)Cl]_2$(2.5 mol%)	6 mol%	trace	7%
7	$[Pd(cinnamyl)Cl]_2$ (2.5 mol%)	3 mol%	trace	13%
8	$[Pd(cinnamyl)Cl]_2$ (2.5 mol%)	6 mol%	trace	12%

General reaction conditions: Aryl triflate (0.10 mmol), styrene (0.20 mmol), 2,2,6,6-tetramethylpiperidine (0.20 mmol), Pd (2.5 mol%) if dimeric source or (5 mol%) if monomeric source, $P^{Ph}{}_2N^{ArCF3}{}_2$ in PhMe (0.1 M) at 85 °C for 20 h. 0.05 mmol of 1,3,5-trimethoxybenzene added as internal standard. Crude yields are given as assessed by GC-FID calibration.

4.7.13 P_2N_2 Pd G3 precatalyst synthesis and characterization

Scheme 4.14 Synthesis of P_2N_2 Pd G3 complexes

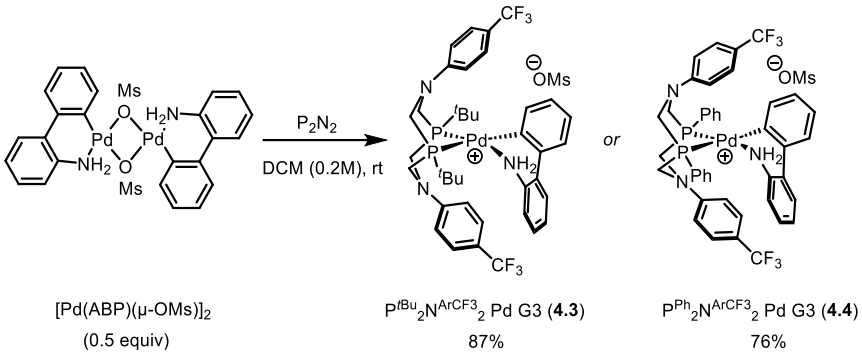

[Pd(ABP)(μ-OMs)]$_2$ (0.5 equiv)

$P^{tBu}{}_2N^{ArCF3}{}_2$ Pd G3 (**4.3**) 87%

$P^{Ph}{}_2N^{ArCF3}{}_2$ Pd G3 (**4.4**) 76%

General procedure for Pd G3 catalyst synthesis: Adapted from the literature,[31] [Pd(ABP)(μ-OMs)]$_2$(0.50 equiv) (obtained according to the literature)[53] and the appropriate P_2N_2 (1.00 equiv) were combined in a dry 2 dram vial, charged with a stir bar, and purged with argon. Anhydrous dichloromethane was added to the vial under argon so that the reaction concentration was 0.20 M. After, the reaction mixture was stirred at room temperature for 60 minutes.

$P^{tBu}{}_2N^{ArCF3}{}_2$ Pd G3 (4.3): Prepared from general procedure outlined above. The solids quickly dissolved in DCM to make a homogeneous solution. After 60 minutes, the solution was concentrated to ~0.30 mL using a rotary evaporator (water bath kept at room temperature), triturated from pentanes and subsequently filtered through a fine porosity fritted funnel under ambient atmosphere. The precipitate was washed with pentanes. The beige solid was dried in vacuo and used without further purification (0.05 mmol scale, 53.9 mg, 59%). The synthesis could be scaled up to a 1.35 mmol scale with an increase in yield (1.08 g, 87%).**^{1}H NMR** ($CDCl_3$, 500 MHz) δ (ppm) 7.65 (d, *J* = 8.6 Hz, 2H), 7.34 (d, *J* = 7.5 Hz, 1H), 7.16-7.06 (m, 5H), 7.01 (d, *J* = 7.9 Hz, 1H), 6.98 (d, *J* = 7.8 Hz, 1H), 6.77-6.71 (*br m*, 2H), 6.67 (d, *J* = 7.7 Hz, 1H), 6.50 (d, *J* = 8.3 Hz, 2H), 5.92 (*br* s, 1H), 5.86-5.76 (m, 1H), 5.20 (*br* s, 1H), 4.50 (d, *J* = 15.7 Hz, 1H), 4.40 (d, *J* = 15.4 Hz, 1H), 4.27-4.17 (m, 3H), 4.09 (d, *J* = 16.4 Hz, 1H), 3.95 (d, *J* = 15.1 Hz, 1H), 3.77 (d, *J* = 15.0 Hz, 1H), 2.52 (s, 3H), 1.38 (d, *J* = 14.4 Hz, 9H), 0.94 (d, *J* = 14.7 Hz, 9H). **^{13}C{^{1}H} NMR** ($CDCl_3$, 125 MHz) δ (ppm) 150.93, 150.87, 150.83, 150.04, 150.0, 138.7, 138.6, 138.53, 138.51, 138.46, 138.45,

135.63, 135.61, 128.6, 127.2-127.1 (m, peaks at 127.17, 127.14 with broad shoulders), 127.0-126.88 (m, peaks at 126.99,126.95, 126.93, 126.90), 126.80-126.7 (m, peaks at 126.78, 126.76 with broad shoulders), 125.8, 125.3, 124.30 (q, *J* = 271.1 Hz), 124.29 (q, *J* = 271.1 Hz), 122.7 (q, *J* = 33.0 Hz), 120.7(q, *J* = 33.0 Hz), 119.5, 116.7, 114.8, 49.7 (d, *J* = 6.1 Hz), 49.6 (d, *J* = 6.9 Hz), 49.1 (d, *J* = 4.6 Hz), 49.0 (d, *J* = 5.5 Hz), 47.3-46.0 (m, overlapped peaks at 47.2, 47.12, 47.10, 47.04, 47.00), 39.7, 33.6 (d, *J* = 13.2 Hz), 30.5 (d, *J* = 7.5 Hz), 27.7(d, *J* = 4.4 Hz), 27.0. **^{19}F{^{1}H} NMR** ($CDCl_3$, 470 MHz) *δ* (ppm) -61.3 and -61.4. **^{31}P{^{1}H} NMR** ($CDCl_3$, 202 MHz) *δ* (ppm) 20.2 (d, *J* = 36 Hz) and 11.3 (d, *J* = 36 Hz). Trace amounts of free ligand (<5%) present in spectra. **Note:** Due to complexity of the ^{13}C{^{1}H} due to overlapping aromatic regions, owing to ^{31}P-coupled peaks and ^{19}F coupled peaks, it was not always possible to assign multiplicity. As result, ambiguous peaks are reported literally as observed without further interpretation. **Accurate mass (ESI+):** m/z calculated for [$C_{38}H_{44}N_3F_6P_2Pd$] Theoretical: 822.1955. Found: 822.1947. **ATR-FTIR** (neat) ν(cm^{-1}): 2951, 1609, 1520, 1464, 1371, 1324, 1191, 1164, 1104, 1069, 1037, 983, 937, 809, 752, 737. **X-ray quality crystals** were obtained by layering in an NMR tube of hexanes (ca. 1.5-2 mL) over a solution of the compound in $CHCl_3$ (200-300 µL).

$P^{Ph}_2N^{ArCF3}_2$ Pd G3 (4.4): Prepared from general procedure outlined above. The solids were found to quickly dissolve in DCM to make a homogeneous solution and a white slurry was generally observed to form within a few minutes of stirring. After 60 minutes, the reaction was filtered with a fine porosity fritted funnel under ambient atmosphere and the precipitate was washed with pentanes. The white solid was dried in vacuo and used without further purification on a 0.05 mmol scale (73.4 mg, 76%). The reaction could be scaled up to a 0.4 mmol scale without a change in yield or purity (293.4 mg, 76%). **Note:** In the case of no slurry formation, the reaction mixture was concentrated to ~0.3 mL with a rotary evaporator (water bath kept at room temperature) and triturated from pentane. The white solid was subsequently filtered, washed with pentanes, and dried in vacuo.**^{1}H NMR** ($(D_3C)_2SO$, 500 MHz) *δ* (ppm) 7.93-7.81 (m, 4H), 7.80-7.74 (m, 1H), 7.58 (d, *J* = 7.6 Hz, 2H), 7.51-7.45 (m, 1H), .7.43-7.31 (m, 7H), 7.20 (d, *J* = 7.7 Hz, 2H), 7.17 (d, *J* = 6.3 Hz, 1H), 7.03 (quin, *J* = 6.7 Hz, 2H), 6.88-6.81 m, 3H), 6.66 (d, *J* = 6.9 Hz, 1H), 6.36 (t, *J* = 7.0 Hz, 1H), 5.48 (d, *J* = 15.7 Hz, 1H), 4.82 (d, *J* = 15.7 Hz, 1H), 4.70 (d, *J* = 14.3 Hz, 1H), 4.64 (d, *J* = 15.3 Hz, 1H), 4.57 (d, *J* = 14.8 Hz, 1H), 4.49 (d, *J* = 15.2 Hz, 1H), 4.28 (d, *J* = 15.1 Hz,

1H), 2.32 (s, 3H). **$^{13}C\{^{1}H\}$ NMR** ($(D_3C)_2SO$, 125 MHz) δ (ppm) 156.95, 156.90, 156.1, 156.0, 150.7, 149.2, 139.7, 139.6, 138.5, 137.0, 136.9, 135.80, 135.79, 131.8, 131.7, 131.49, 131.48, 131.05, 131.04, 130.4, 130.3, 128.9, 128.7, 128.6, 128.2, 127.9, 127.7, 127.4, 127.1, 126.9, 126.8, 126.7 (*br*), 126.3 (*br*), 126.2, 125.9, 125.7, 125.6, 125.6, 125.5, 125.4, 125.3, 124.9, 124.8, 123.6, 123.4, 121.4, 121.3, 120.5, 120.3, 120.0, 119.8, 119.7, 119.4, 119.2, 116.2, 115.7, 54.0, 53.9, 51.7, 51.4, 49.3, 49.2, 49.0, 48.9, 39.8. **$^{19}F\{^{1}H\}$ NMR** ($(D_3C)_2SO$, 470 MHz) δ (ppm) -59.5 and -59.6. **$^{31}P\{^{1}H\}$ NMR** ($(D_3C)_2SO$, 202 MHz) δ (ppm) 12.3 (d, J = 44 Hz) and -5.4 (d, J = 44 Hz). **Note** Due to complexity of the $^{13}C\{^{1}H\}$ due to overlapping aromatic regions, owing to ^{31}P-coupled peaks and ^{19}F coupled peaks, it was not possible to assign multiplicity. As result, all peaks are reported literally as observed without further interpretation. **Accurate mass (ESI+):** m/z calculated for [$C_{42}H_{36}N_3F_6P_2Pd$] Theoretical: 864.1323. Found: 864.1335. **ATR-FTIR** (neat) ν (cm^{-1}): 3059, 1611, 1576, 1520, 1496, 1436, 1377, 1327, 1246, 1191, 1108, 1072, 1039, 1000, 981, 835, 813, 767, 753, 734, 692. **X-ray quality crystals** were obtained by layering in an NMR tube of hexanes (ca. 1.5-2 mL) over a solution of the compound in CH_2Cl_2 (200-300 µL).

$P^{tBu}{}_2N^{ArCF3}{}_2$ Pd G3 (4.3), ^1H, $CDCl_3$, 500MHz

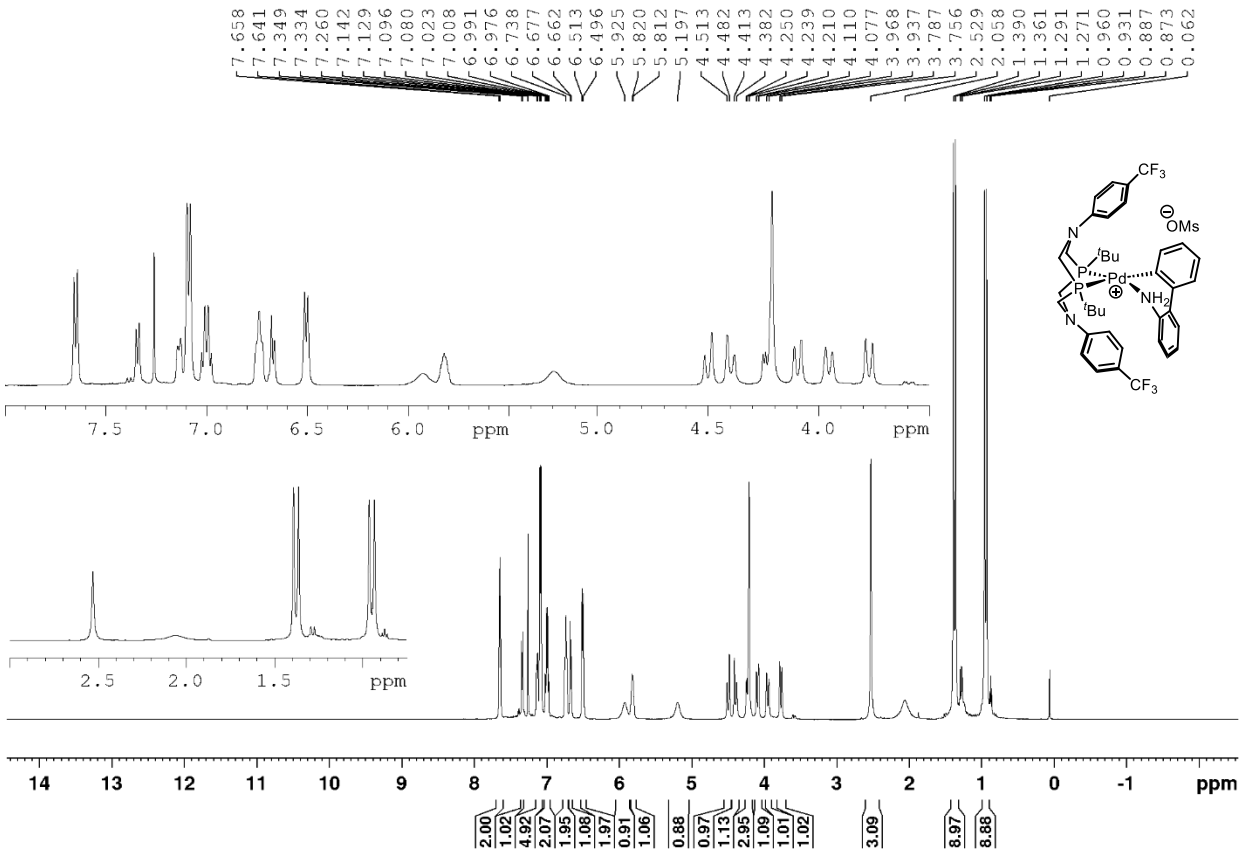

$P^{tBu}{}_2N^{ArCF3}{}_2$ Pd G3 (4.3), $^{13}C\{^1H\}$, $CDCl_3$, 125 MHz

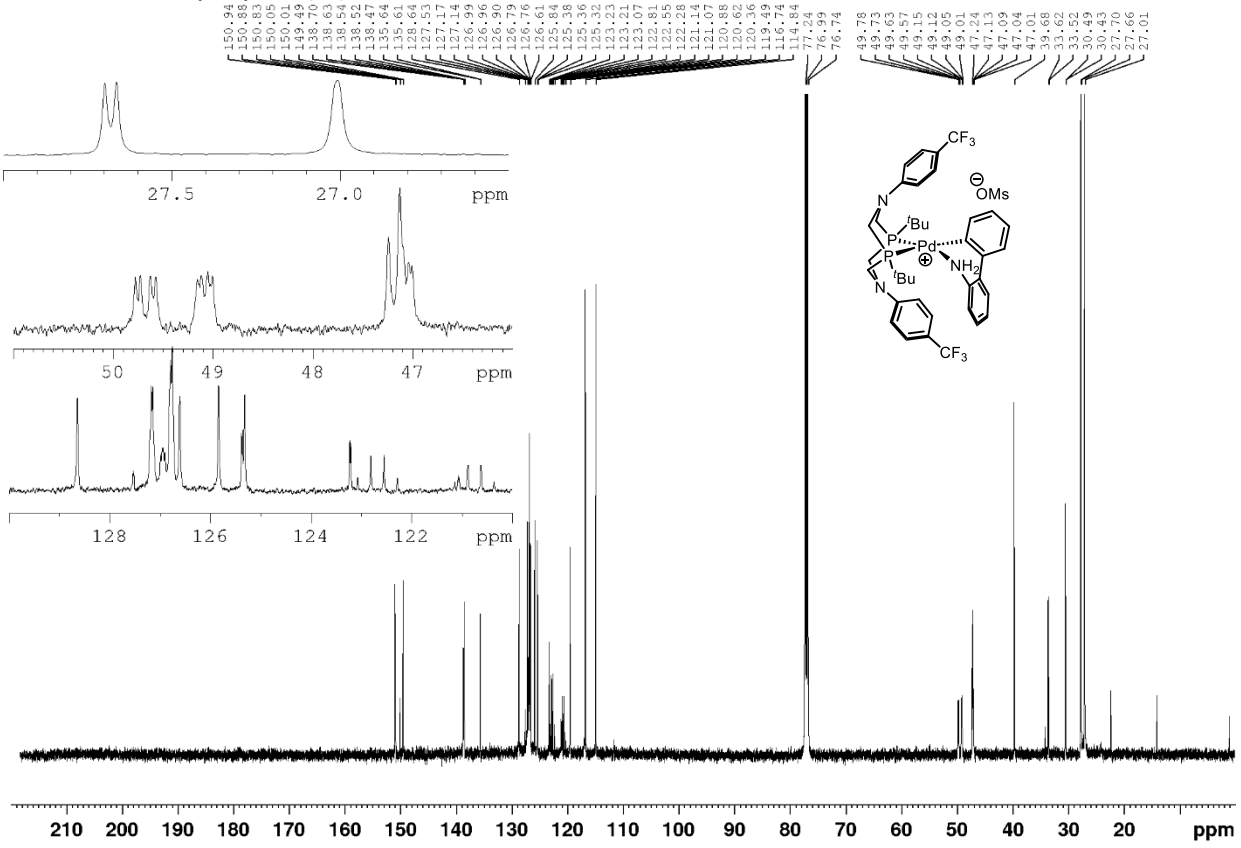

$P^{tBu}{}_2N^{ArCF3}{}_2$ Pd G3 (4.3), ^{1}H-$^{13}C\{^{1}H\}$ HSQC, $CDCl_3$

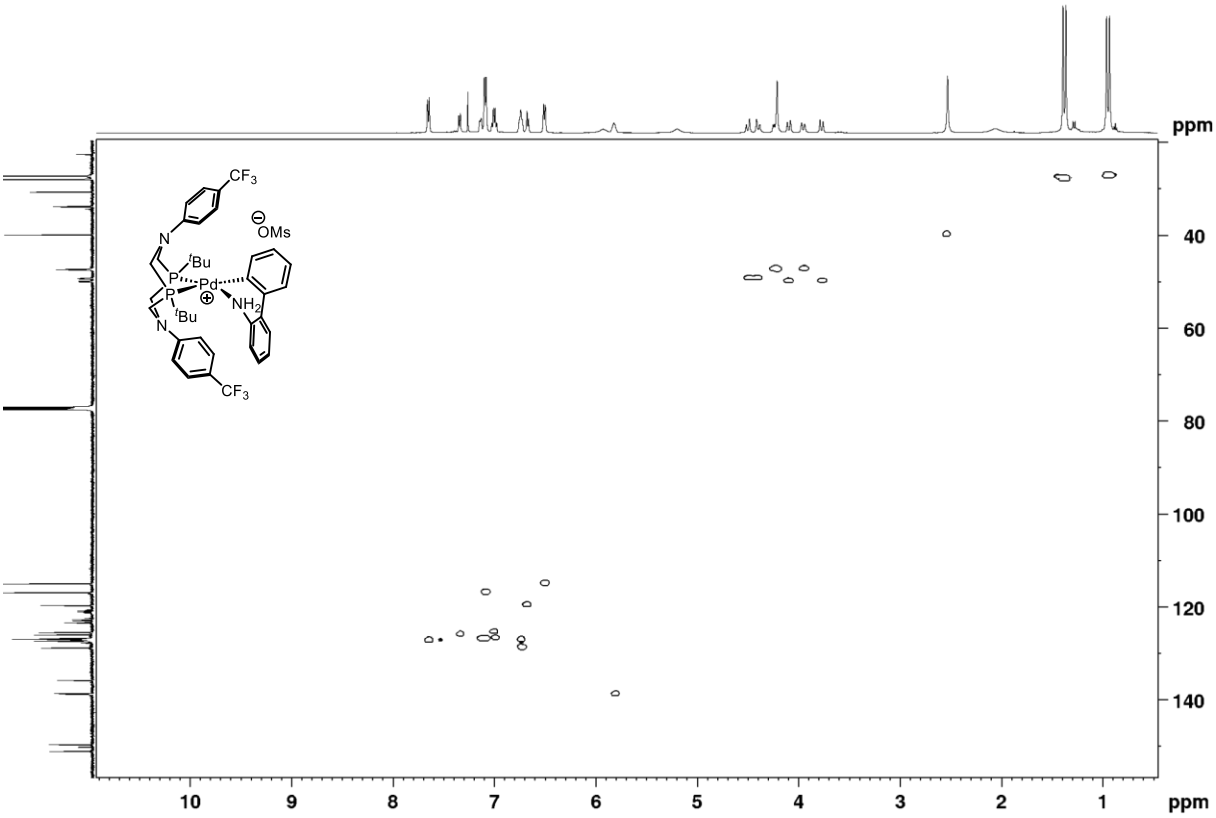

$P^{tBu}{}_2N^{ArCF3}{}_2$ Pd G3 (4.3), ^{1}H-$^{13}C\{^{1}H\}$ HSQC, $CDCl_3$ zoomed in

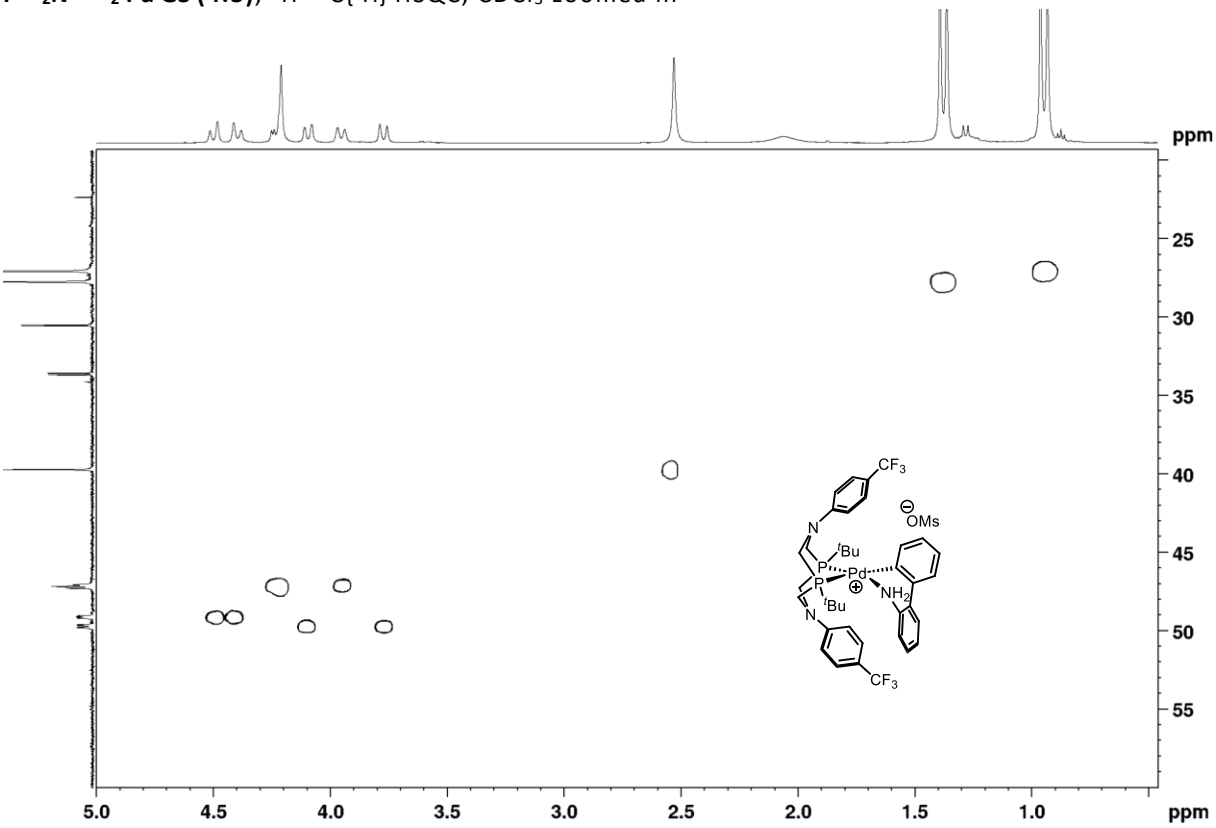

$P^{tBu}{}_2N^{ArCF3}{}_2$ Pd G3 (4.3), ^{1}H-$^{13}C\{^{1}H\}$ HSQC, $CDCl_3$ zoomed in

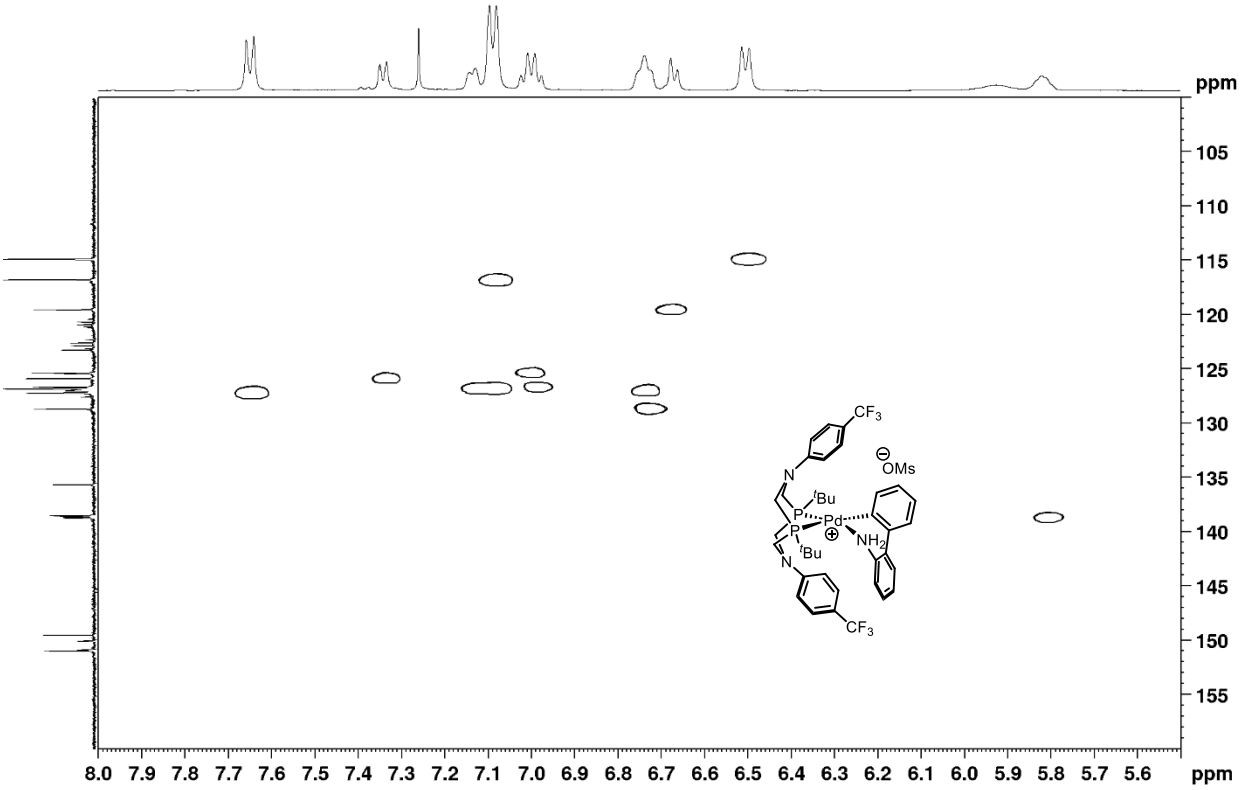

$P^{tBu}{}_2N^{ArCF3}{}_2$ Pd G3 (4.3), $^{19}F\{^1H\}$, $CDCl_3$, 470 MHz

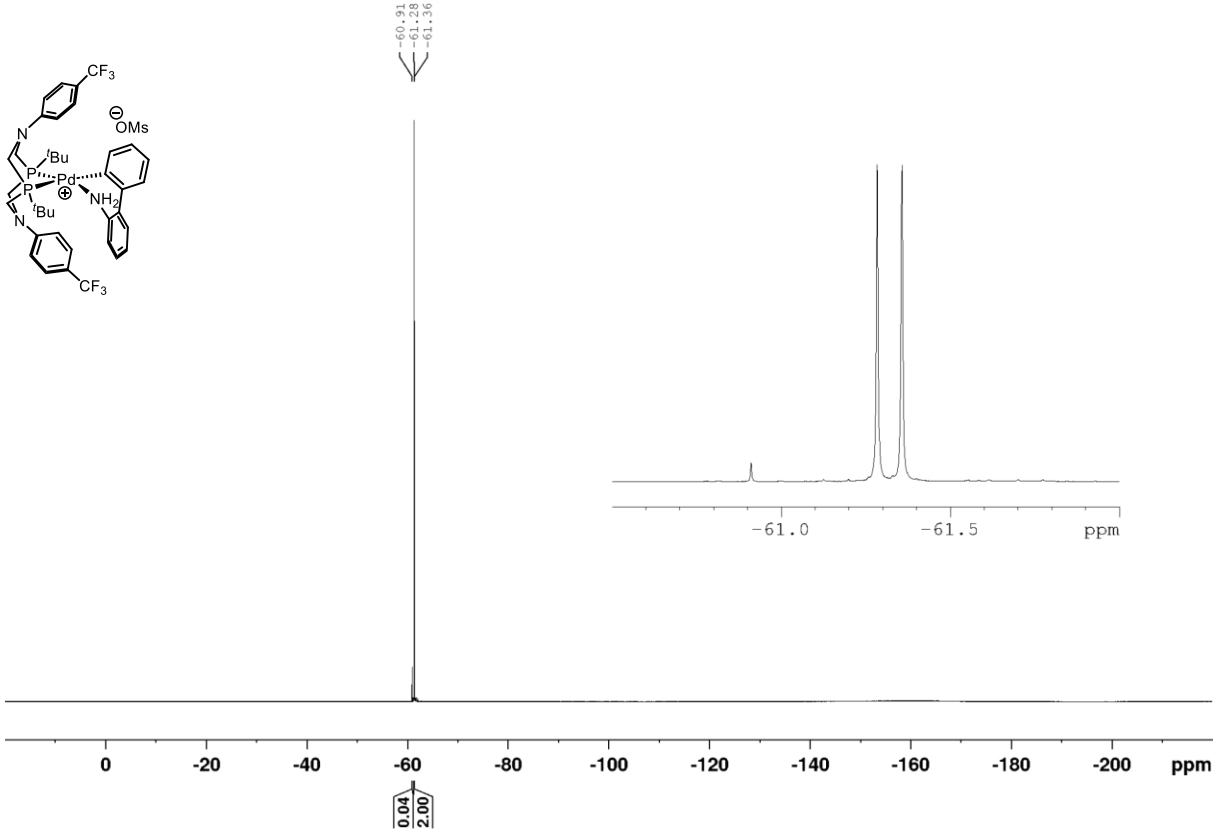

$P^{tBu}{}_2N^{ArCF3}{}_2$ Pd G3 (4.3), $^{31}P\{^1H\}$, $CDCl_3$, 202 MHz

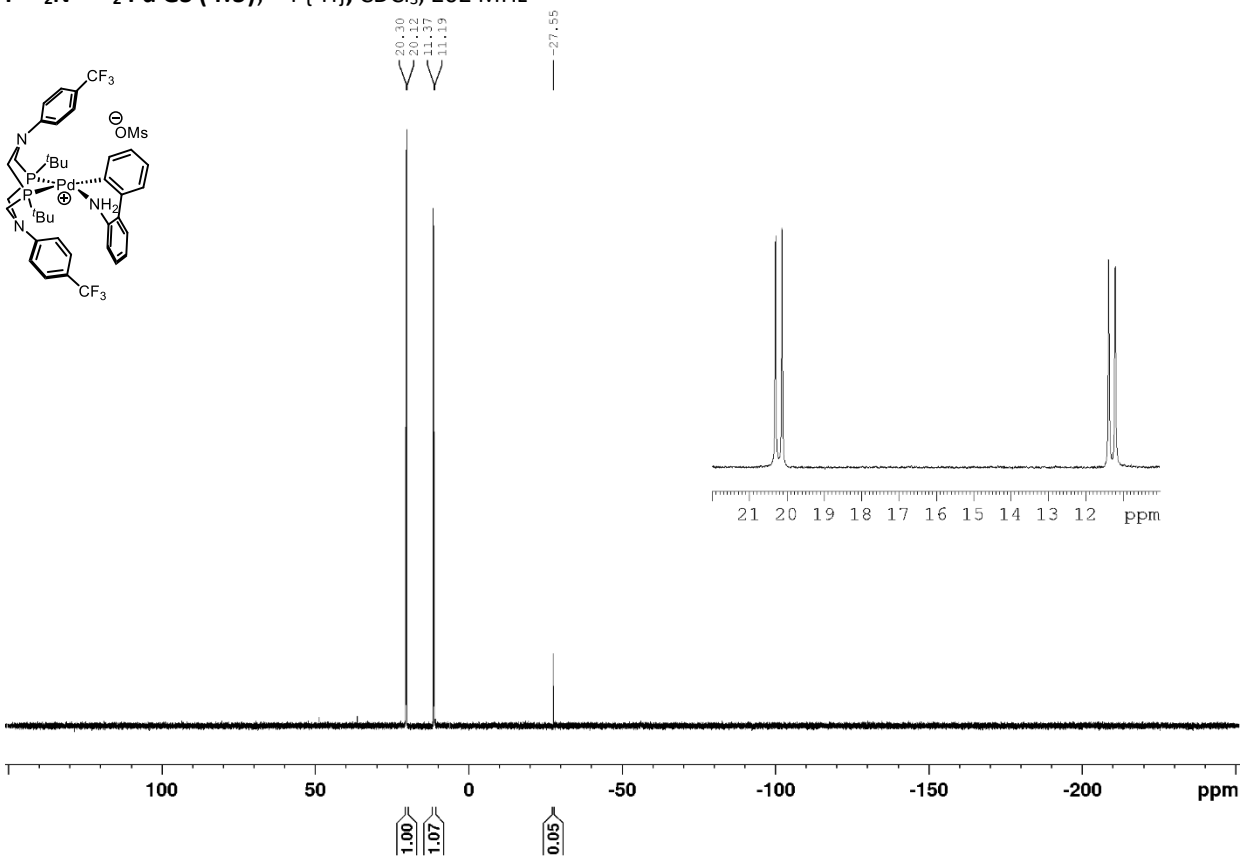

Figure 4.8 ATR-FTIR of solid $P^{tBu}{}_2N^{ArCF3}{}_2$ Pd G3 (4.3)

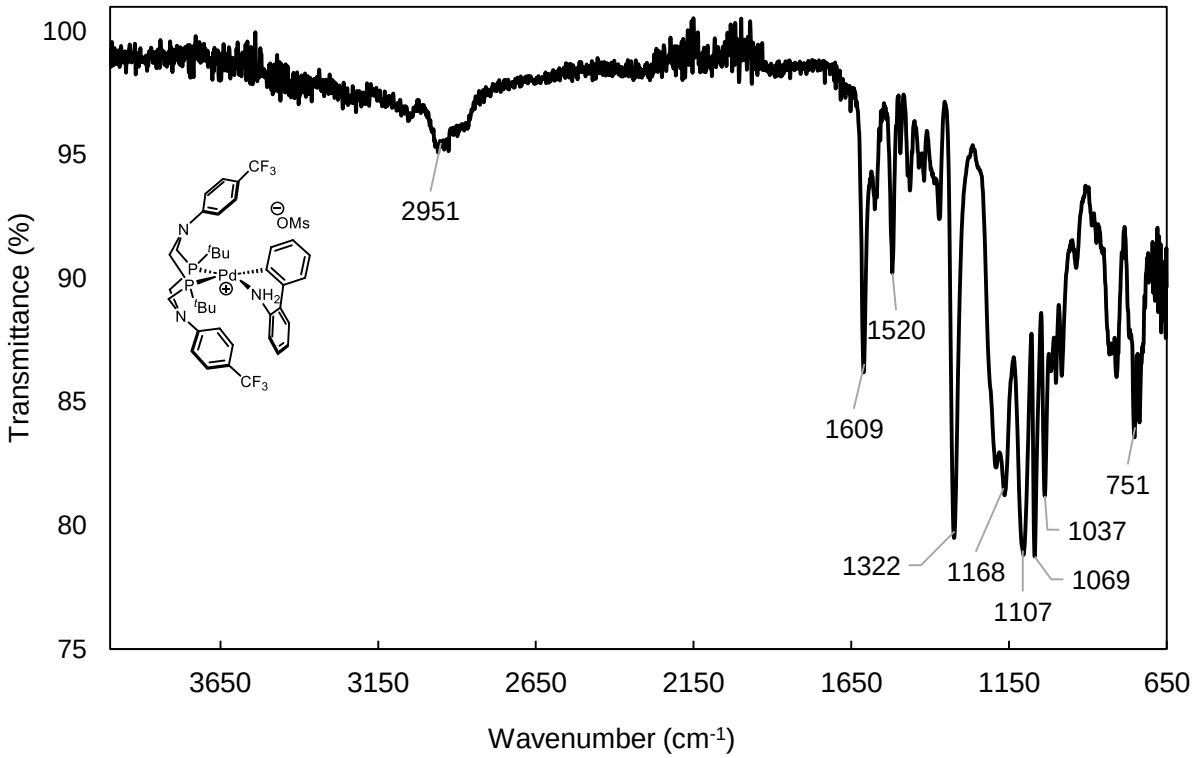

$P^{Ph}_2N^{ArCF3}_2$ Pd G3 (4.4), ^1H, $(D_3C)_2SO$, 500MHz

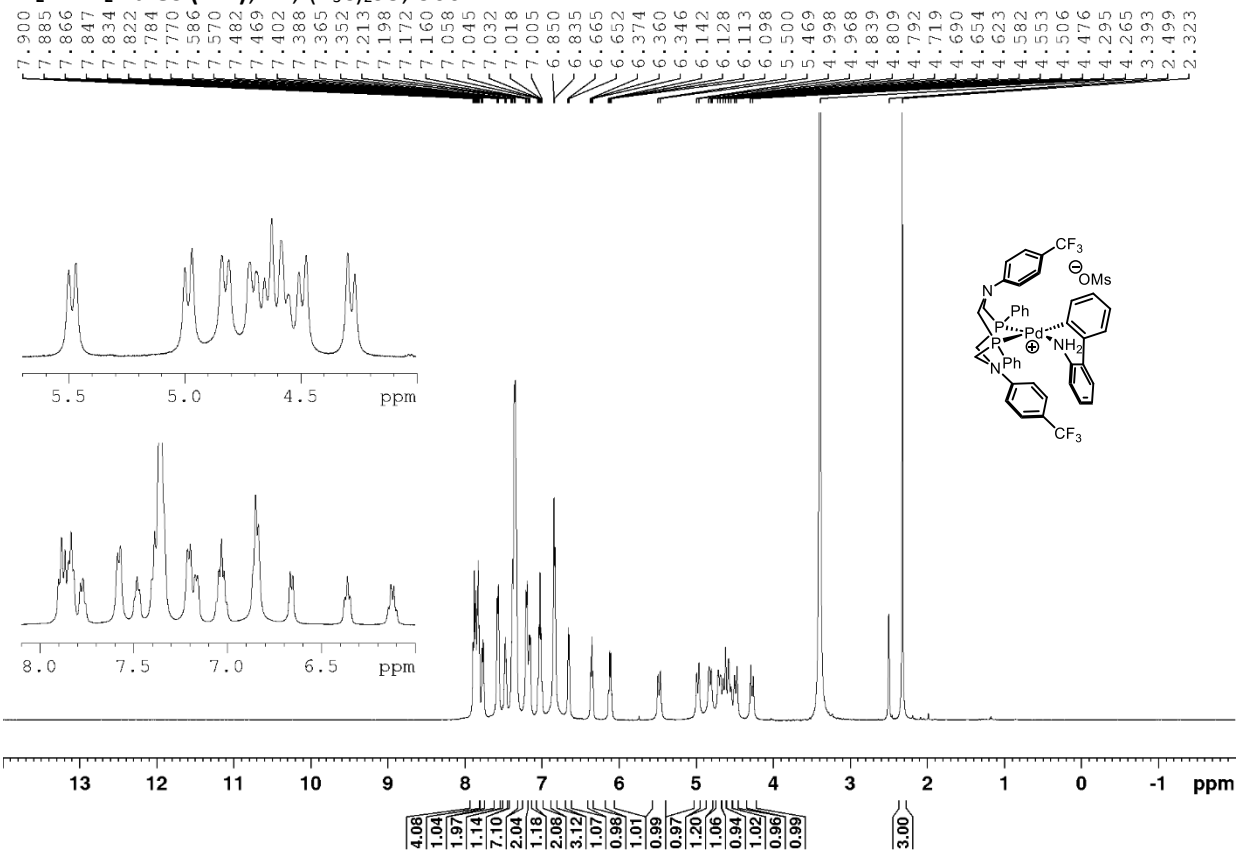

$P^{Ph}_2N^{ArCF3}_2$ Pd G3 (4.4), $^{13}C\{^1H\}$, $(D_3C)_2SO$, 125MHz

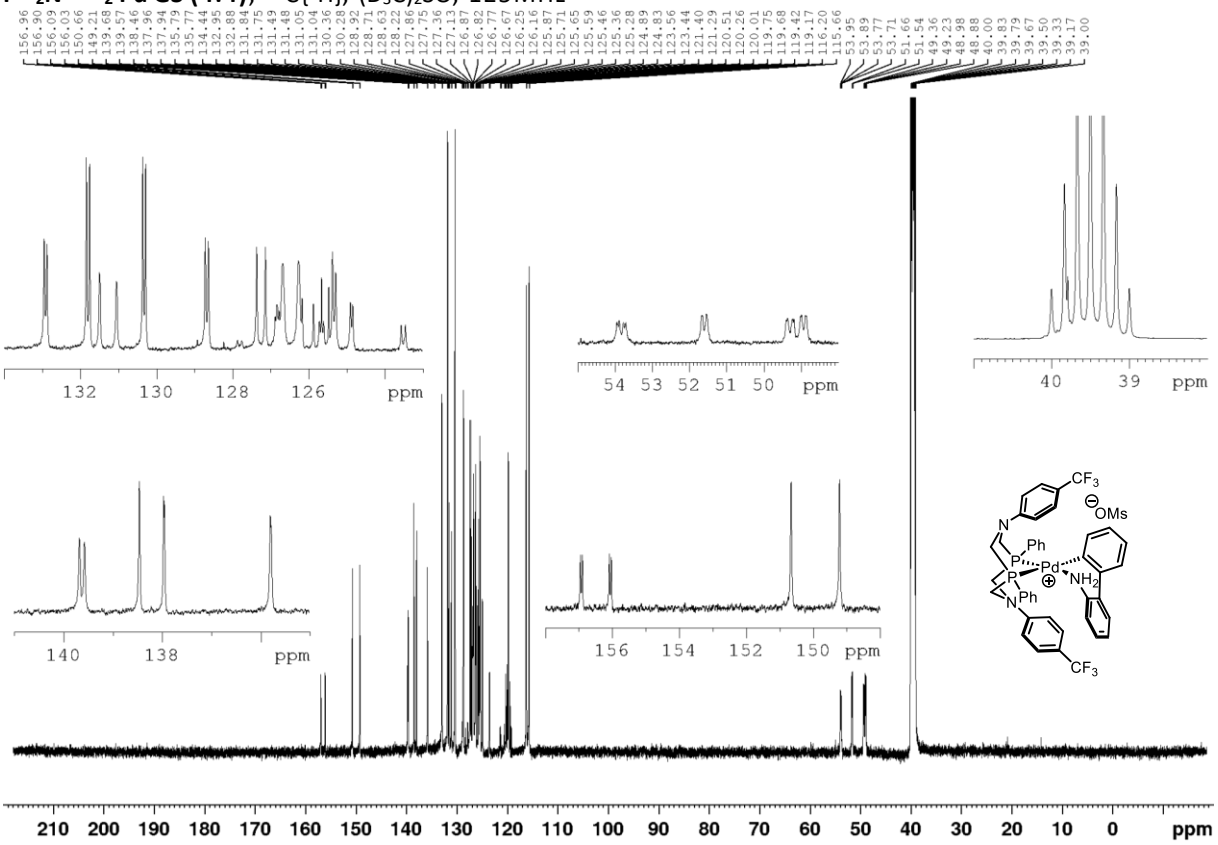

$P^{Ph}_2N^{ArCF3}_2$ Pd G3 (4.4), Dept-135, $(D_3C)_2SO$, 125MHz

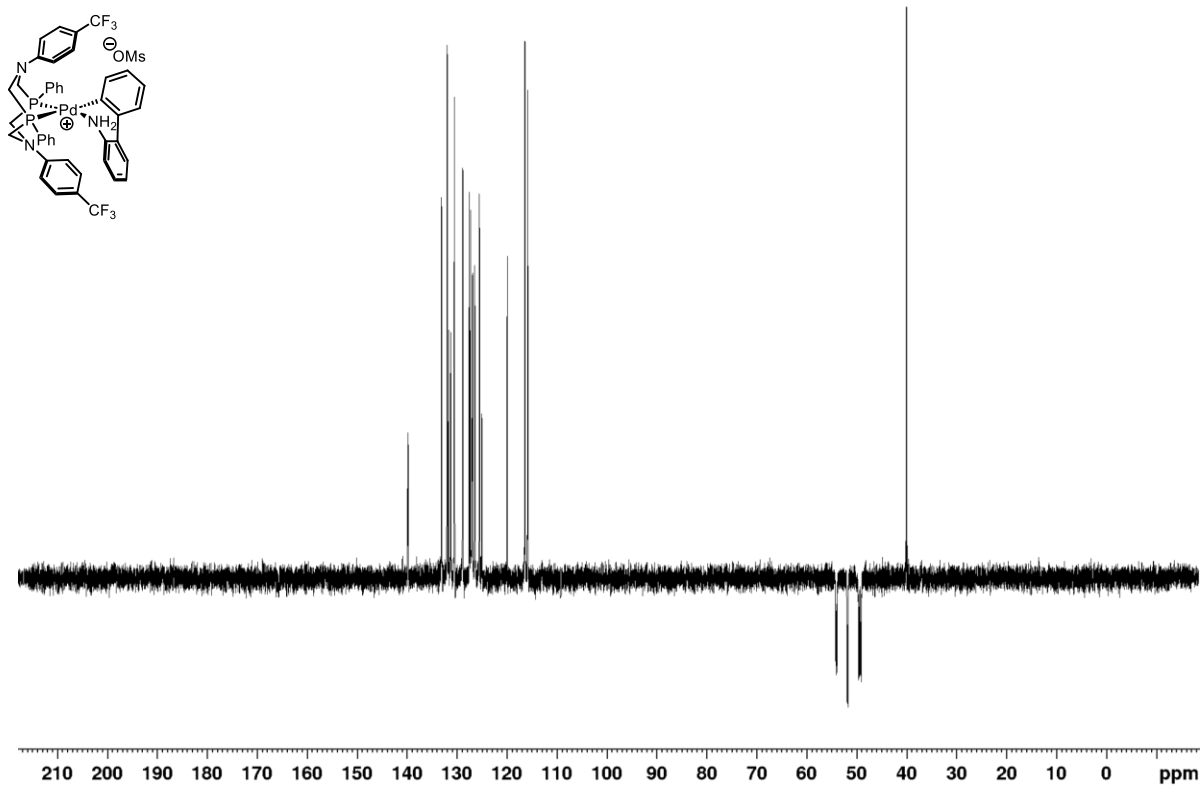

$P^{Ph}{}_2N^{ArCF3}{}_2$ Pd G3 (4.4), ^{1}H-$^{13}C\{^{1}H\}$ HSQC, $(D_3C)_2SO$, 125MHz

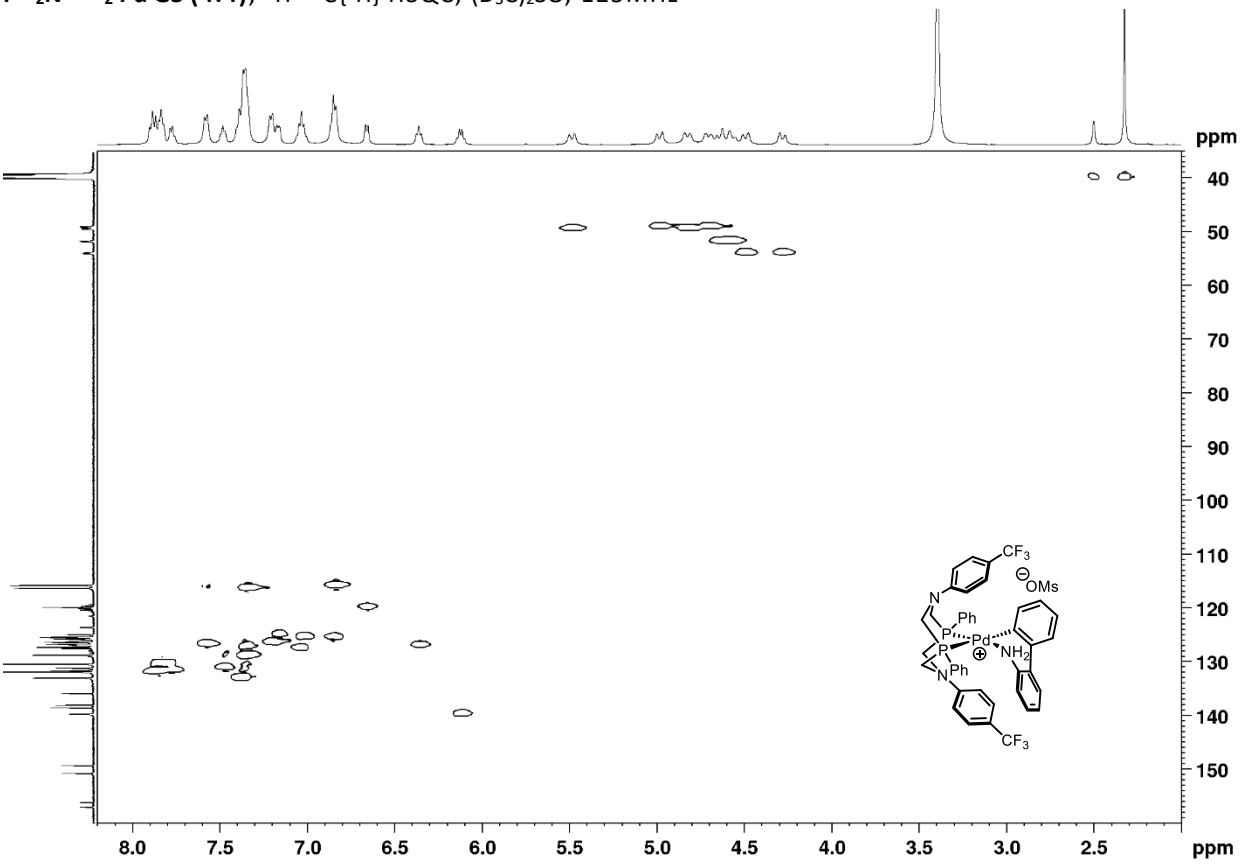

$P^{Ph}{}_2N^{ArCF3}{}_2$ Pd G3 (4.4), ^{1}H-$^{13}C\{^{1}H\}$ HSQC, $(D_3C)_2SO$, 125MHz (zoomed-in)

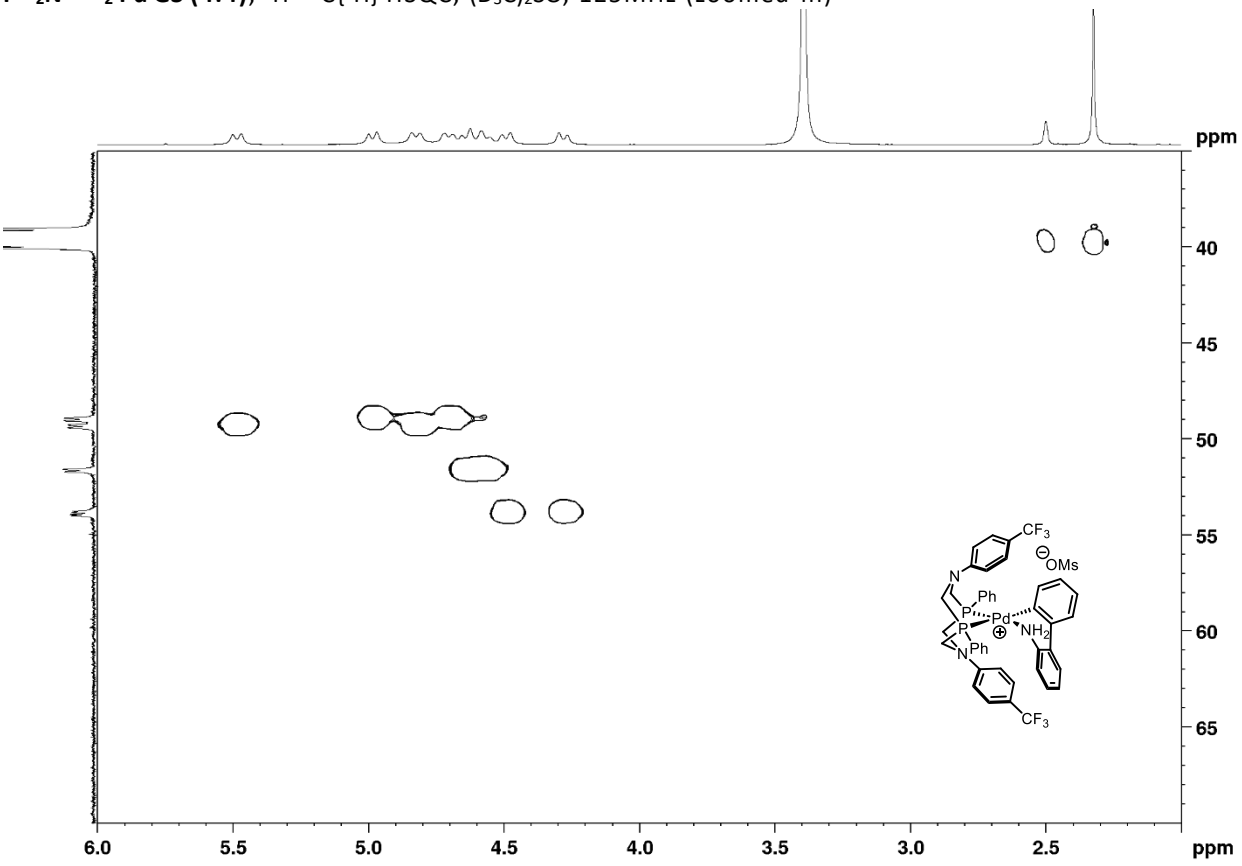

$P^{Ph}{}_2N^{ArCF3}{}_2$ Pd G3 (4.4), ^{1}H-$^{13}C\{^{1}H\}$ HSQC, $(D_3C)_2SO$, 125MHz (zoomed-in)

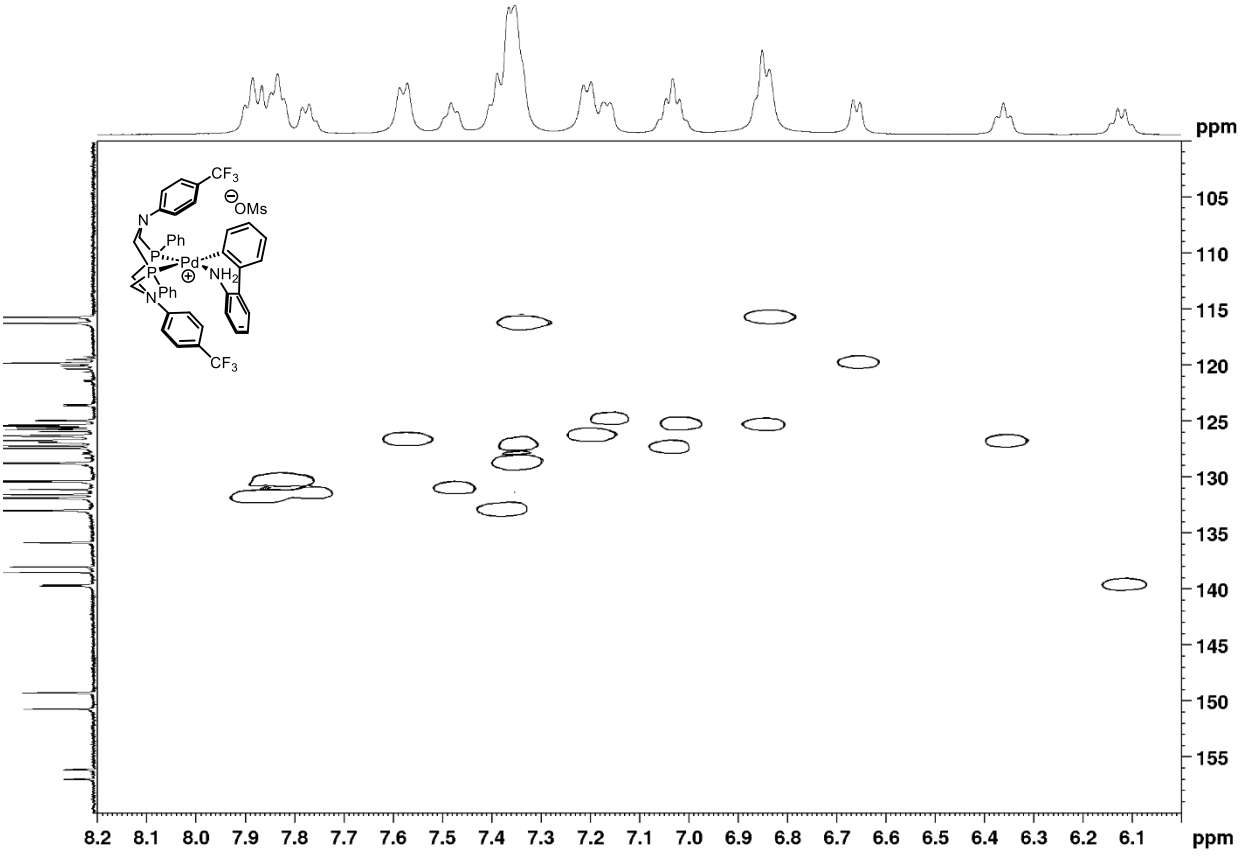

$P^{Ph}_2N^{ArCF3}_2$ Pd G3 (4.4), $^{19}F\{^1H\}$, $(D_3C)_2SO$, 470MHz

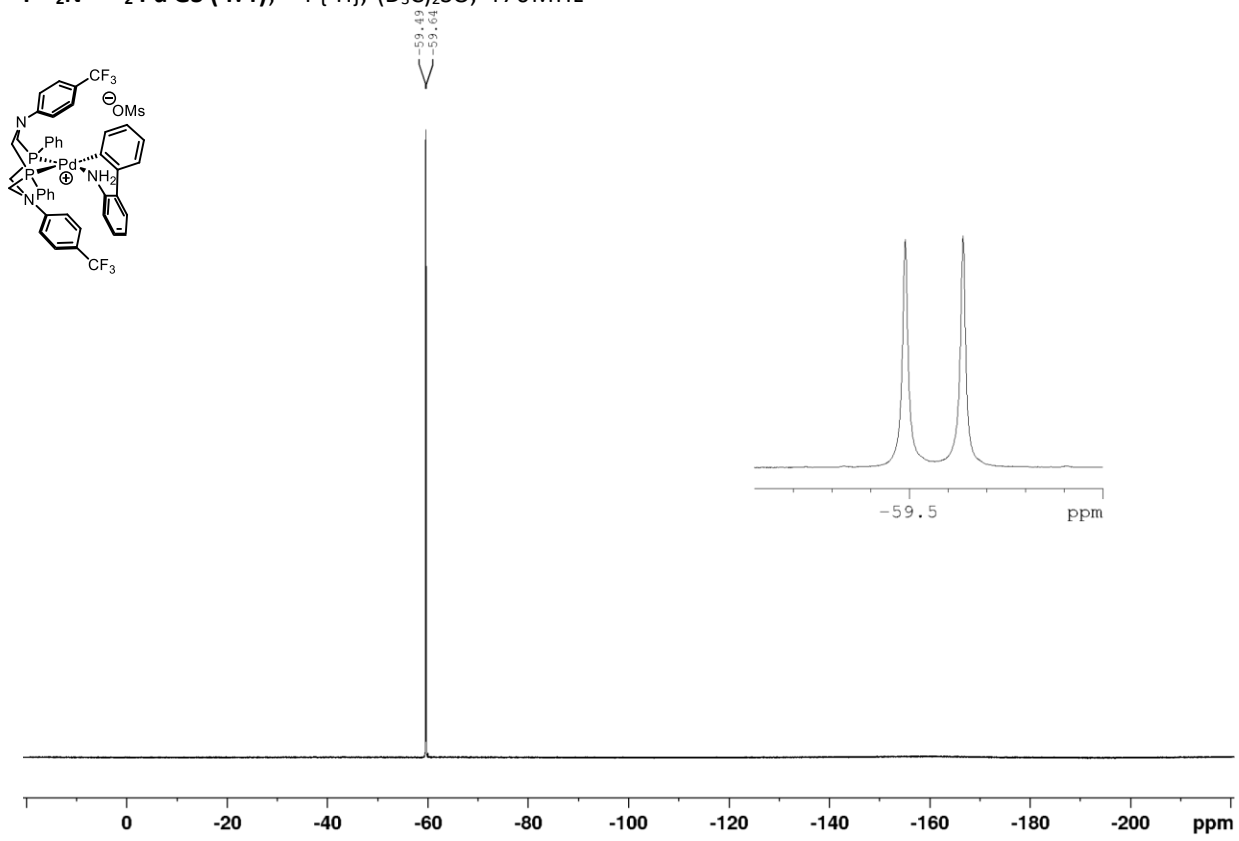

$P^{Ph}{}_2N^{ArCF3}{}_2$ Pd G3 (4.4), $^{31}P\{^1H\}$, $(D_3C)_2SO$, 202MHz

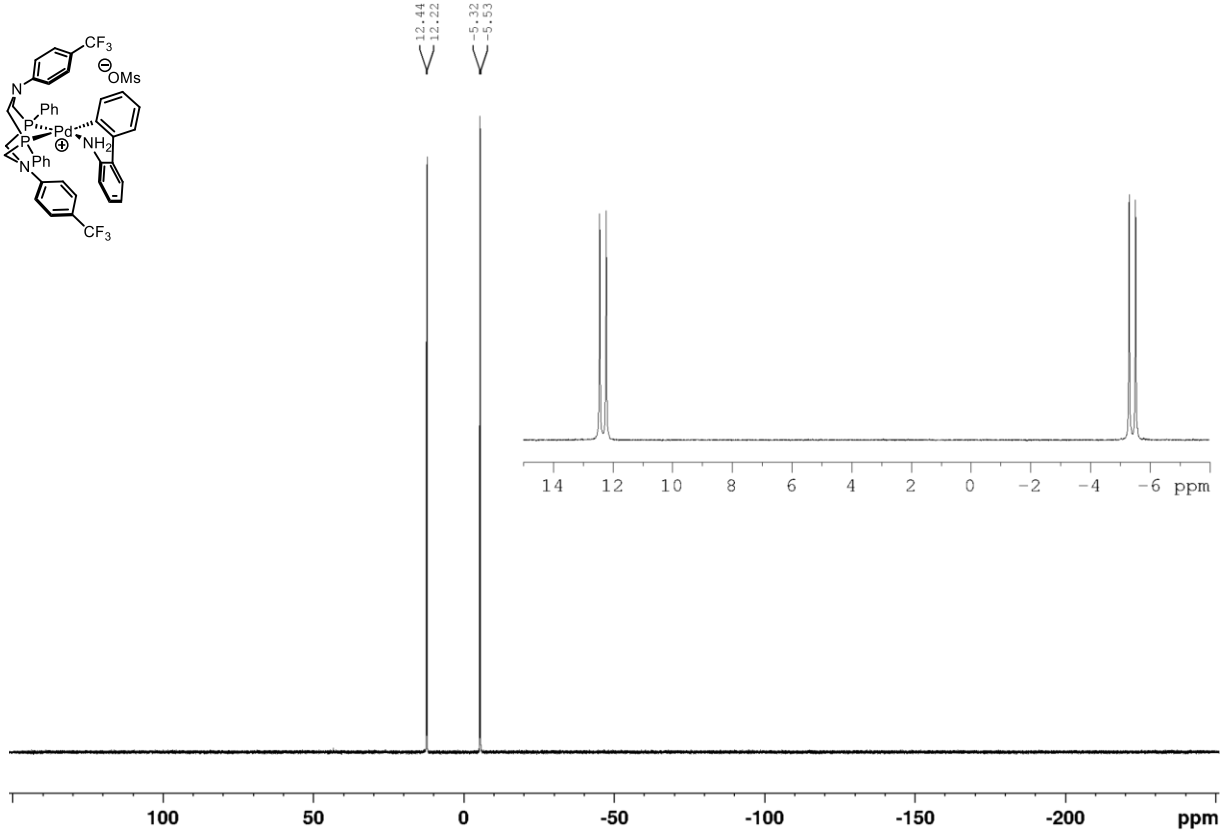

Figure 4.9 ATR-FTIR of $P^{Ph}{}_2N^{ArCF3}{}_2$ Pd G3

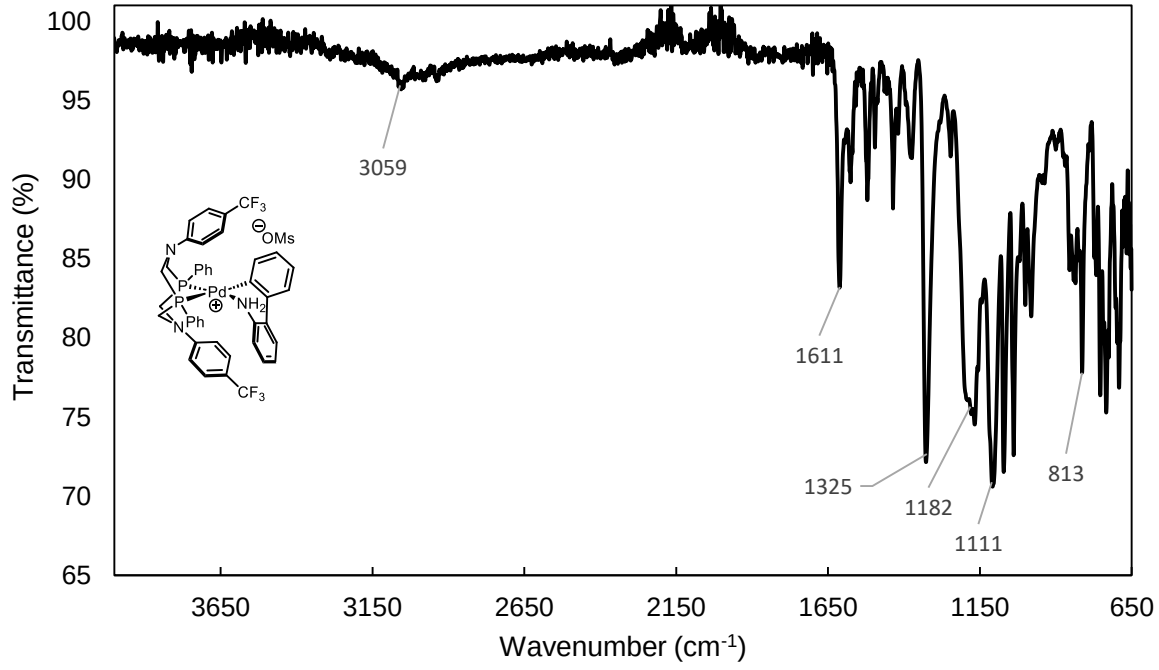

4.7.14 Crystallographic details

***Data Collection and Processing*.** Samples of **$P^{tBu}{}_2N^{ArCF3}{}_2$-Pd-MAH (4.1)**, **$P^{Ph}{}_2N^{ArCF3}{}_2$-Pd-MAH (4.2)**, **$P^{tBu}{}_2N^{ArCF3}{}_2$ Pd G3 (4.3)**, and **$P^{Ph}{}_2N^{ArCF3}{}_2$ Pd G3 (4.4)** were mounted on a Mitegen polyimide micromount with a small amount of Paratone N oil. All X-ray measurements were made on a Bruker Kappa Axis Apex2 diffractometer at a temperature of 110 K. The data collection strategy was a number of ω and ϕ scans which collected data up to $2\theta_{max}$ as listed in Table 4.17. The frame integration was performed using SAINT.[54] The resulting raw data was scaled and absorption corrected using a multi-scan averaging of symmetry equivalent data using SADABS.[55]

***Structure Solution and Refinement*.** The structure of **$P^{tBu}{}_2N^{ArCF3}{}_2$-Pd-MAH (4.1)** was solved by using a dual space methodology using the SHELXT program.[56] Most non-hydrogen atoms were obtained from the initial solution. The remaining atomic positions were obtained from subsequent difference Fourier maps. The hydrogen atoms were introduced at idealized positions and were allowed to ride on the parent atom. The CF_3-aryl group bound to atom N2 was disordered over two positions. The disorder could be described as a small rotation about an axis passing through N2 and running perpendicular to the C6-C8-C16 plane. The angle subtended from N2 to the *para* carbon positions (C19 and C19') was 6.75º. The occupancy factor for the major component refined to a value of 0.501(8). The asymmetric unit also included a 0.5 of CH_2Cl_2 molecule which resided on a crystallographic glide plane. In addition, another CH_2Cl_2 molecule was fractionally occupied and disordered across a glide as well. The occupancy for this second CH_2Cl_2 molecule refined to a value of 0.175(3). The structural model was fit to the data using full matrix least-squares based on F^2. The calculated structure factors included corrections for anomalous dispersion from the usual tabulation. The structure was refined using the SHELXL

program from the SHELX suite of crystallographic software.[57] Graphic plots were produced using the Mercury program.[58]

Figure 4.10 ORTEP drawing of $P^{tBu}{}_2N^{ArCF3}{}_2$-Pd-MAH (4.1) showing naming and numbering scheme. Ellipsoids are at the 50% probability level and hydrogen atoms were omitted for clarity. The minor component of the disordered CF_3-aryl group was also omitted for clarity.

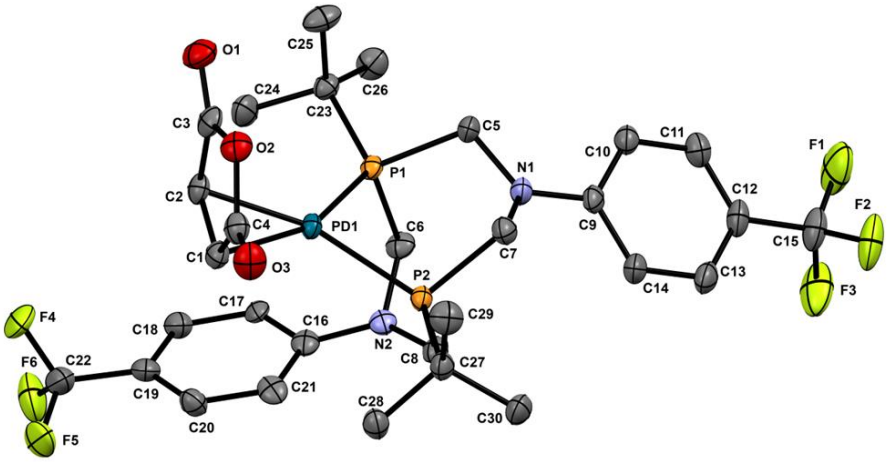

***Structure Solution and Refinement*.** The structure for **$P^{Ph}_2N^{ArCF3}_2$-Pd-MAH (4.2)** was solved by using a dual space methodology using the SHELXT program.[56] Most non-hydrogen atoms were obtained from the initial solution. The remaining atomic positions were obtained from difference Fourier maps. The hydrogen atoms were introduced at idealized positions and were allowed to ride on the parent atom. Both CF_3 groups were disordered. The occupations for the predominant rotamers refined to values 0.759(10) and 0.72(2) for the CF_3 groups contains atoms C21{F1,F2,F3} and C34{F4,F5,F6} respectively. The CH_2Cl_2 of solvation was also disordered by rotation about the C35-Cl1 bond to give two distinct positions for the Cl2 atom. The occupancy for the predominant orientation refined to a value of 0.512(8). The structural model was fit to the data using full matrix least-squares based on F^2. The calculated structure factors included corrections for anomalous dispersion from the usual tabulation. The structure was refined using the SHELXL program from the SHELX suite of crystallographic software.[57] Graphic plots were produced using the Mercury program.[58]

Figure 4.11 ORTEP drawing of $P^{Ph}{}_2N^{ArCF3}{}_2$-Pd-MAH (4.2) showing naming and numbering scheme. Ellipsoids are at the 50% probability level and hydrogen atoms and disordered fluorine atoms were omitted for clarity.

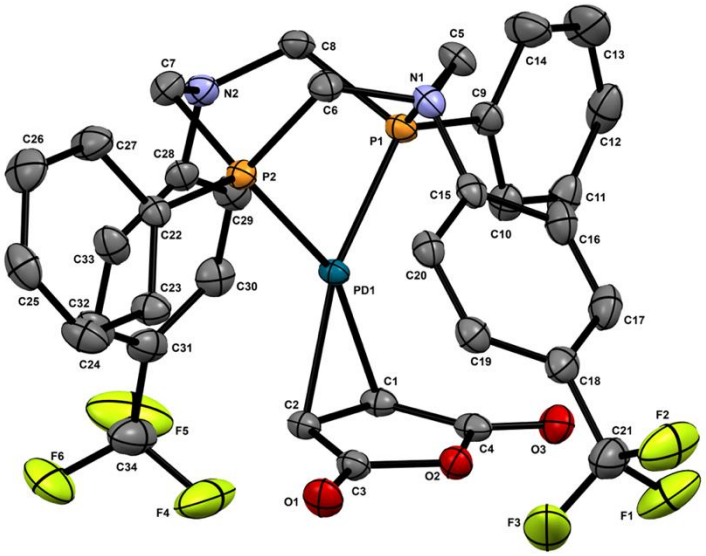

***Structure Solution and Refinement*.** The structure of **$P^{tBu}{}_2N^{ArCF3}{}_2$ Pd G3 (4.3)** was solved by using a dual space methodology using the SHELXT program.[56] All non-hydrogen atoms were obtained from the initial solution. The asymmetric unit contained the cation/anion pair, two $CHCl_3$ molecules an *n*-hexane molecule laying across a crystallographic 2-fold axis. The hydrogen atoms were introduced at idealized positions and were allowed to ride on the parent atom. The occupancy of the hexane molecule was allowed to refine and converged to a value of 0.636(15). The CF_3 group containing atom C30 was disordered over two orientations, rotated by approximately 44º about the C27 – C30 bond vector. The occupancy of the primary orientation refined to a value of 0.844(8). The $CHCl_3$ molecule containing atom C40 was disordered over two orientations. The occupancy factor for the primary orientation refined to a value of 0.0905(5). The structural model was fit to the data using full matrix least-squares based on F^2. The calculated structure factors included corrections for anomalous dispersion from the usual tabulation. The structure was refined using the SHELXL program from the SHELX suite of crystallographic software.[57] Graphic plots were produced using the Mercury program.[58]

Figure 4.12 ORTEP drawing of $P^{tBu}{}_2N^{ArCF3}{}_2$ Pd G3 (4.3) representative cation showing naming and numbering scheme. Ellipsoids are at the 50% probability level and hydrogen atoms were omitted for clarity.

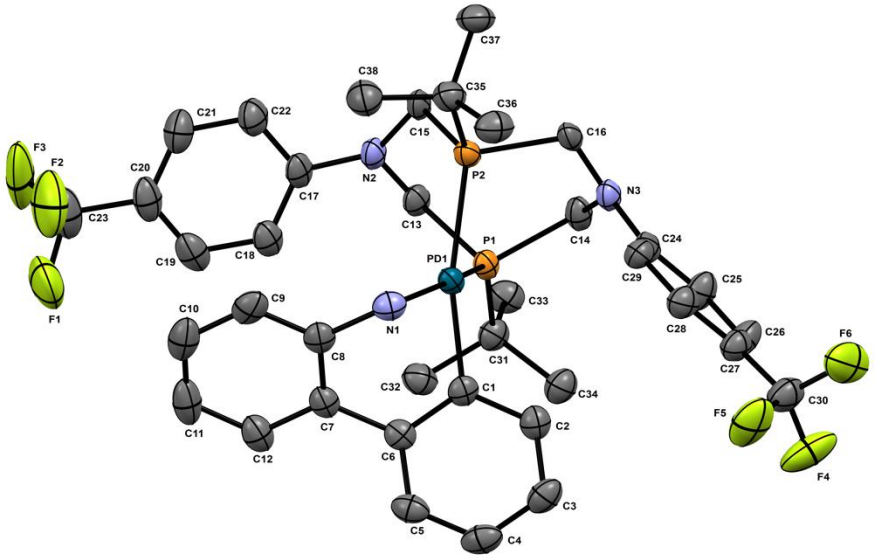

***Structure Solution and Refinement*.** The structure of **$P^{Ph}_2N^{ArCF3}_2$ Pd G3 (4.4)** was solved by using a dual space methodology using the SHELXT program.[56] All non-hydrogen atoms were obtained from the initial solution. The asymmetric unit contained four symmetry independent complexes and their corresponding anions as well as several CH_2Cl_2 molecules of solvation. Some of the solvent molecules were disordered over several sites. For this reason, the solvent contributions to the X-ray scattering subjected to a solvent masking procedure as implemented by the SQUEEZE routine included in the PLATON program.[59] The hydrogen atoms were introduced at idealized positions and were allowed to ride on the parent atom. The structural model was fit to the data using full matrix least-squares based on F^2. The calculated structure factors included corrections for anomalous dispersion from the usual tabulation. The structure was refined using the SHELXL program from the SHELX suite of crystallographic software.[57] Graphic plots were produced using the Mercury program.[58]

Figure 4.13. ORTEP drawing of $P^{Ph}_2N^{ArCF3}_2$ Pd G3 (4.4) representative cation showing naming and numbering scheme. Ellipsoids are at the 50% probability level and hydrogen atoms were omitted for clarity.

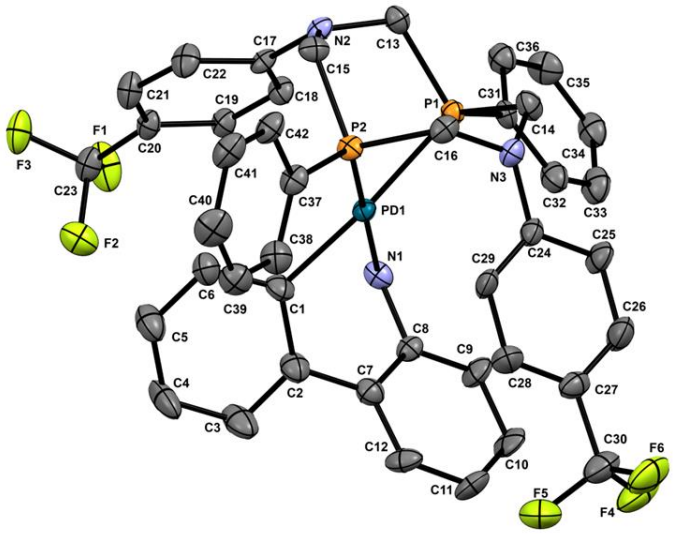

Table 4.17. Selected structural parameters for $P^{R}{}_{2}N^{R'}{}_{2}$ Pd complexes.

Structural Parameter	**$P^{Ph}{}_{2}N^{ArCF3}{}_{2}$- Pd-MAH (4.1)**	**$P^{tBu}{}_{2}N^{ArCF3}{}_{2}$- Pd-MAH (4.2)**	**$P^{Ph}{}_{2}N^{ArCF3}{}_{2}$ Pd G3 (4.3)**	**$P^{tBu}{}_{2}N^{ArCF3}{}_{2}$ Pd G3 (4.4)**
Bond Lengths (Å)				
Pd(1)-P(1)	2.2913(9)	2.2854(9)	2.336(3)	2.2603(15)
Pd(1)-P(2)	2.2935(8)	2.3031(12)	2.246(2)	2.3724(15)
$Pd(1)\text{-}C(1)_{MAH}$	2.120(2)	2.113(3)		
$Pd(1)\text{-}C(2)_{MAH}$	2.125(2)	2.124(3)		
$Pd(1)\text{-}C(1)_{ABP}$			2.028(9)	2.051(5)
$Pd(1)\text{-}N(1)_{ABP}$			2.124(7)	2.131(5)
Bond Angle (˚)				
P(1)-Pd(1)-P(2)	85.34(2)	85.68(3)	82.63(9)	83.31(6)
Geometry Index[60]				
τ_4			0.06	0.21

Table 4.18 Summary of crystal data for $P^{R}{}_2N^{R'}{}_2$ Pd complexes.

Compound (CCDC #)	**$P^{Ph}{}_2N^{ArCF3}{}_2$- Pd-MAH** **(4.1)** (2263168)	**$P^{tBu}{}_2N^{ArCF3}{}_2$- Pd-MAH** **(4.2)** (2262706)	**$P^{Ph}{}_2N^{ArCF3}{}_2$ Pd G3** **(4.3)** (2262704)	**$P^{tBu}{}_2N^{ArCF3}{}_2$ Pd G3** **(4.4)** (2262705)
Formula	$C_{35}H_{30}Cl_2F_6N_2O_3P_2Pd$	$C_{30.67}H_{37.35}Cl_{1.35}F_6N_2O_3P_2Pd$	$C_{43}H_{39}F_6N_3O_3P_2PdS$	$C_{42.91}H_{54.45}Cl_6F_6N_3O_3P_2PdS$
Formula Weight (*g/mol*)	879.85	812.27	960.17	1187.33
Crystal Dimensions (*mm*)	0.216 × 0.196 × 0.086	0.297 × 0.282 × 0.074	0.427 × 0.160 × 0.061	0.416 × 0.147 × 0.036
Crystal Colour and Habit	gold prism	colourless prism	colourless prism	colourless sword
Crystal System	orthorhombic	orthorhombic	monoclinic	monoclinic
Space Group	P b c a	A b a 2	P 2_1	C 2/c
Temp, K	110	110	110	110
a, Å	16.698(5)	15.726(6)	17.517(11)	27.389(9)
b, Å	18.013(5)	24.110(10)	25.515(13)	18.720(7)
c, Å	23.117(8)	18.032(7)	20.026(9)	23.757(9)
α,°	90	90	90	90
β,°	90	90	90.619(13)	120.335(9)
γ,°	90	90	90	90
V, $Å^3$	6953(4)	6837(5)	8950(8)	10513(6)
Number of reflections to determine	9988	9766	9267	9912

final unit cell				
Min and Max theta for cell determination, °	4.52, 52.48	5.18, 59.56	4.7, 52.76	4.78, 47.74
Z	8	8	8	8
F(000)	3536	3299	3904	4839
r (*g/cm*)	1.681	1.578	1.425	1.500
l, Å, (MoKa)	0.71073	0.71073	0.71073	0.71073
μ, (cm^{-1})	0.852	0.809	0.599	0.820
Diffractometer Type	Bruker Kappa Axis Apex2	Bruker Kappa Axis Apex2	Bruker Kappa Axis Apex2	Bruker Kappa Axis Apex2
Scan Type(s)	j and w scans	j and w scans	j and w scans	j and w scans
Max theta for data collection, °	59.262	64.174	53.544	50.154
Measured fraction of data	0.999	0.998	0.999	0.998
Number of reflections measured	343830	182173	356858	159202
Unique reflections measured	9788	11956	38053	9323
R_{merge}	0.0930	0.0547	0.0917	0.1136
Number of reflections	9788	11956	38053	9323

included in refinement				
Cut off Threshold Expression	I > 2s(I)	I > 2s(I)	I > 2s(I)	I > 2s(I)
Structure refined using	full matrix least-squares using F^2	full matrix least-squares using F^2	full matrix least-squares using F^2	full matrix least-squares using F^2
Weighting Scheme	$w=1/[s^2(Fo^2)+(0.0294P)^2+12.3341P]$ where $P=(Fo^2+2Fc^2)/3$	$w=1/[s^2(Fo^2)+(0.0331P)^2+9.6025P]$ where $P=(Fo^2+2Fc^2)/3$	$w=1/[s^2(Fo^2)+(0.0458P)^2+40.6095P]$ where $P=(Fo^2+2Fc^2)/3$	$w=1/[s^2(Fo^2)+(0.0458P)^2+40.6095P]$ where $P=(Fo^2+2Fc^2)/3$
Number of parameters in least-squares	526	527	2130	623
R_1	0.0330	0.0300	0.0538	0.0626
wR_2	0.0754	0.0709	0.1306	0.1753
R_1 (all data)	0.0479	0.0347	0.0643	0.0819
wR_2 (all data)	0.0843	0.0734	0.1363	0.1940
GOF	1.016	1.050	1.065	1.050
Maximum shift/error	0.002	0.004	0.001	0.000
Min & Max peak heights on final DF Map (e^-/Å)	-1.376, 0.777	-1.158, 1.016	-1.025, 1.286	-1.560, 1.202

Where:

$R_1 = \Sigma(|F_o| - |F_c|) / \Sigma F_o$

$wR_2 = [\ \Sigma (w(F_o^2 - F_c^2)^2) / \Sigma (w F_o^4)\ ]^{½}$

GOF = $[\ \Sigma (w(F_o^2 - F_c^2)^2) / (\text{No. of reflns.} - \text{No. of params.})$

4.7.15 GC-FID calibration curves

4.7.15.1 GC-FID calibration curve for *trans*-stilbene (as major product)

1.25 mmol (225.3 mg) of *trans*-stilbene was added to a 25 mL volumetric flask and diluted with DCM (0.05 M stock solution). Six vials were prepared with differing amounts of *trans*-stilbene stock – 0.50 mL, 1.00 mL, 1.50 mL, 2.00 mL, 3.00 mL, 4.00 mL. 1 mL of a 0.05 M 1,3,5-trimethoxybenzene stock solution in PhMe was added to each vial as internal standard (0.05 mmol). Samples were diluted with EtOAC for GC-FID analysis.

Table 4.19 GC-FID calibration curve for *trans*-stilbene (as major product**)**

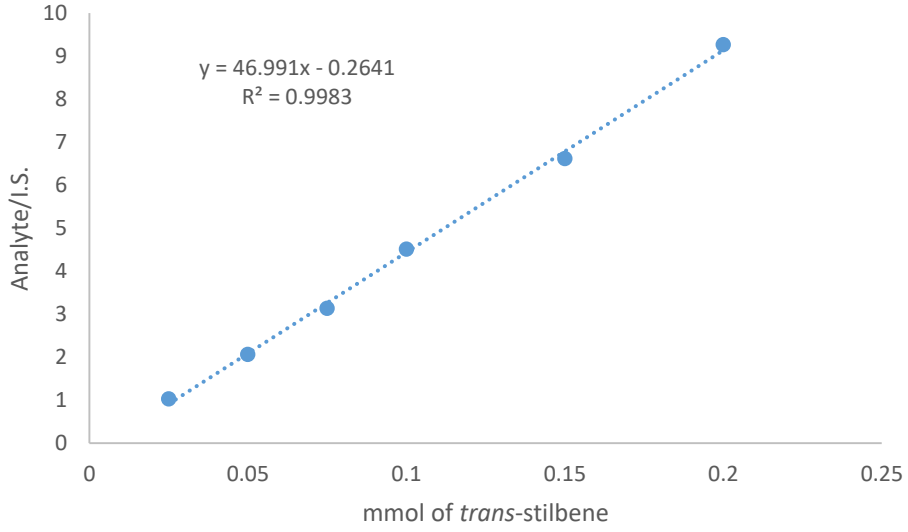

4.5.15.2 GC-FID calibration curve for 1,1-diphenylethylene (as minor product)

0.125 mmol (22.5 mg) of 1,1-diphenylethylene was added to a 25 mL volumetric flask and diluted with PhMe (0.005 M). Six vials were prepared with differing amounts of 1,1-diphenylethylene – 0.40 mL, 0.80 mL, 1.20 mL, 1.60 mL, 2.00 mL. 1 mL of a 0.05M 1,3,5-trimethoxybenzene stock solution in PhMe was added to each vial as internal standard (0.05 mmol). Samples were diluted with EtOAC for GC-FID analysis.

Table 4.20. GC-FID calibration curve for 1,1-diphenylethylene (as minor product)

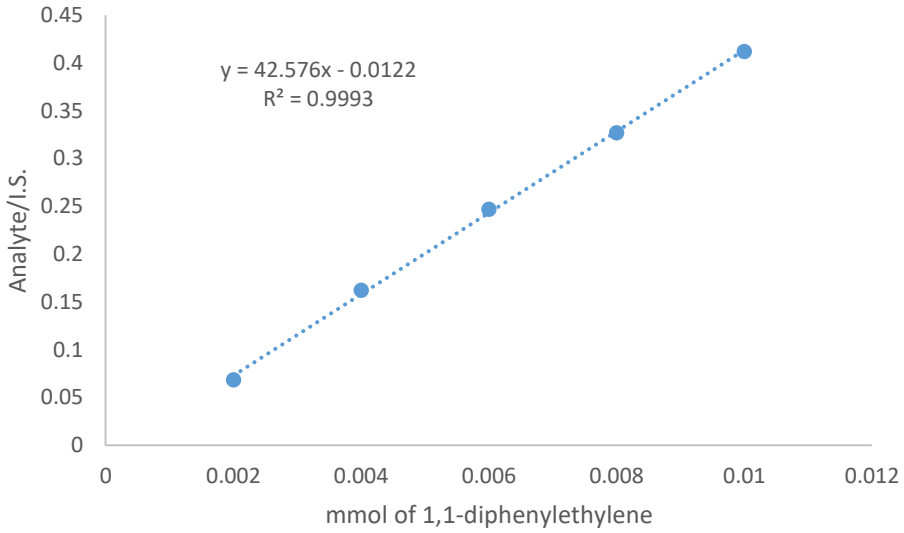

4.5.15.3 GC-FID calibration curve for 1,1-diphenylethylene (as major product)

A 0.05 M solution of 1,1-diphenylethylene in PhMe was prepared. 1.25 mmol (225.3 mg) of 1,1-diphenylethylene was added to a 25 mL volumetric flask and diluted with PhMe. Six vials were prepared with differing amounts of 1,1-diphenylethylene – 0.50 mL, 1.00 mL, 1.50 mL, 2.00 mL, 3.00 mL, 4.00 mL. 1 mL of a 0.05M 1,3,5-trimethoxybenzene stock solution in PhMe was added to each vial as internal standard (0.05 mmol). Samples were diluted with EtOAC for GC-FID analysis.

Table 4.21. GC-FID calibration curve for 1,1-diphenylethylene (as major product)

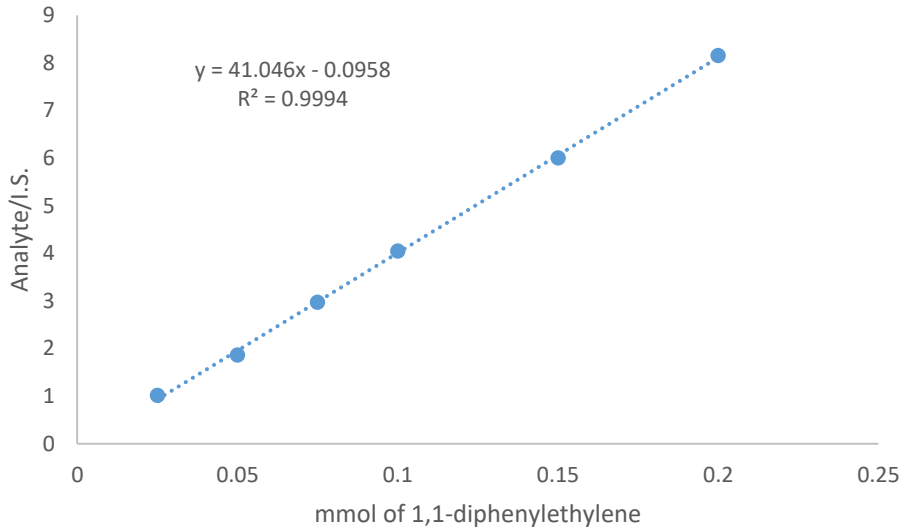

4.5.15.4 GC-FID calibration curve for *trans*-stilbene (as minor product)

A 0.005 M solution of *trans*-stilbene in DCM was prepared. 0.125 mmol (22.5 mg) of the analyte was added to a 25 mL volumetric flask and diluted with the DCM. Six vials were prepared with differing amounts of *trans*-stilbene stock – 0.40 mL, 0.80 mL, 1.20 mL, 1.60 mL, 2.00 mL. 1 mL of a 0.05 M 1,3,5-trimethoxybenzene stock solution in PhMe was added to each aliquot as internal standard (0.05 mmol). Samples were diluted with EtOAC for GC-FID analysis.

Table 4.22. GC-FID calibration curve for *trans*-stilbene (as minor product)

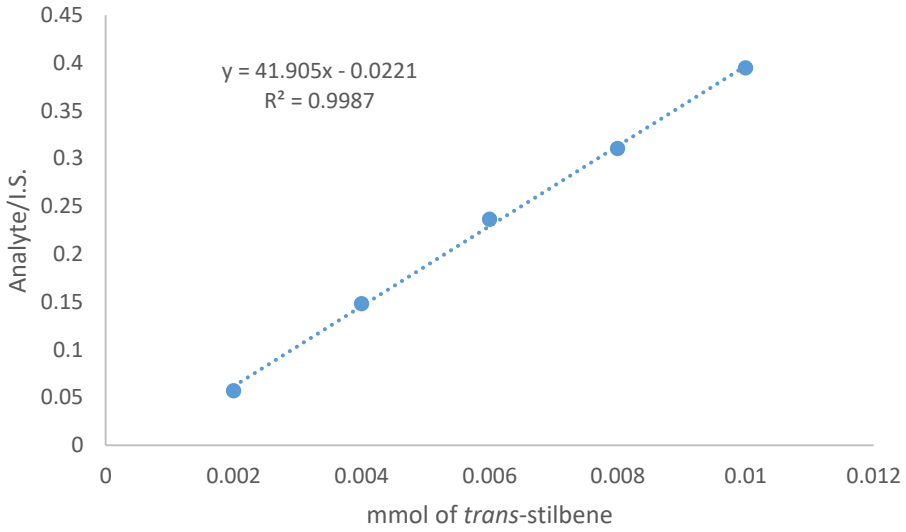

4.7.15.5 Use of calibration curves to determine crude yield

The crude GC-FID ratios could be converted to percent yield by using the correct calibration curves in Sections 4.7.15.1-4.5.15.4. For example, if **4.7-br** is the major product and **4.7-lin** is the minor product– then the curves found in Section 4.5.15.3 and Section 4.5.15.4 could be used to convert the GC-FID ratio to a percent yield. An example is shown below:

For entry 1 on Table 4.14, a ratio of 3.18 was obtained when dividing the area of **4.7-br** by the area of internal standard. The respective curve would be found in Section 4.5.15.3. The line of

best fit has a formula of $y = 41.046x - 0.0958$, where y is the ratio of **4.7-br** and x is the mmol of **4.7-br.** Therefore, for entry 1, $3.18 = 41.046x - 0.0958$. Solving for x gives a value of 0.08 mmol. Since the reaction was set up on a 0.10 mmol scale, this would correspond to a 80% yield of **4.7-br**.

4.7.16 Synthesis of starting materials

4.7.16.1 Synthesis of aryl triflates

Unless otherwise noted, all aryl triflates were synthesized according to the procedure of Goossen et al.[61] The spectral data of all triflates known in the primary literature matched previous reported syntheses. Figure 4.14 modified procedures were used for indole (**4.28**)[62] and quinoline (**4.29**).[63] Scheme 4.15 shows the synthesis of **4.31**, the only novel aryl triflate prepared using the standard procedure.[61]

Figure 4.14 Structure of aryl triflates 4.28 and 4.29.

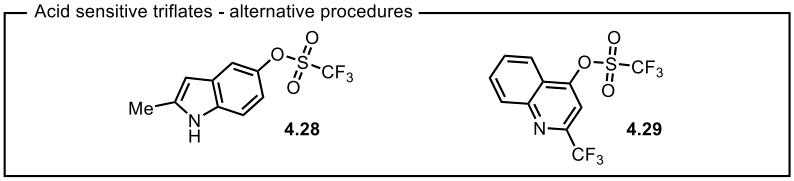

Scheme 4.15 Procedure for the synthesis of aryl triflate 4.31

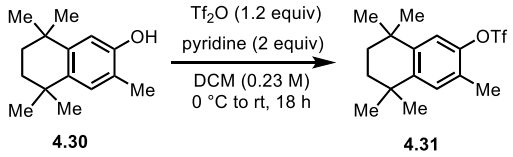

Triflate **4.31** was prepared by a procedure adapted from Goosen et al. [61] A 50 mL round bottom flask equipped with an appropriately sized stir bar was dried in the oven (120 °C) for an hour and cooled to room temperature in a desiccator. 3,5,5,8,8-Pentamethyl-5,6,7,8-tetrahydronaphthalen-2-ol (500 mg, 2.29 mmol, 1 equiv)[64] was weighed into the flask under ambient atmosphere and subsequently dissolved in anhydrous dichloromethane (10 mL).

Pyridine was added (0.37 mL, 4.58 mmol, 2 equiv) to the stirring solution. The flask was then cooled to 0 °C and Tf_2O was added to the stirring solution dropwise via syringe (0.45 mL, 2.75 mmol, 1.2 equiv). The solution slowly warmed to room temperature and was stirred for 18 h (total) or until deemed complete by TLC. The reaction was quenched with 15 mL of 2 M $HCl_{(aq)}$, extracted with DCM (3 x 15 mL) in a separatory funnel, and the organic layers were recombined. The crude mixture was dried with Na_2SO_4 and filtered through a coarse porosity fritted filter. Solvent was evaporated from the filtrate in vacuo. The resulting residue was dry-loaded with SiO_2 and purified by column chromatography with 0% to 5% Et_2O in Hexanes to afford **4.31** as a white solid (748.0 mg, 93%).**^{1}H NMR** ($CDCl_3$, 300 MHz) δ (ppm) 7.18 (s, 1H), 7.10 (s, 1H), 2.31 (s, 3H), 1.68 (s, 4H), 1.27 (s, 6H), 1.26 (s, 6H). **^{13}C{^{1}H} NMR** ($CDCl_3$, 75 MHz) δ (ppm) 146.6, 145.1, 130.1, 127.3, 118.8, 118.7 (q, J = 320.2 Hz), 34.8, 34.6, 34.3, 34.0, 31.7, 31.6, 16.0. **^{19}F{^{1}H} NMR** ($CDCl_3$, 282 MHz) δ (ppm) -73.8. **Accurate Mass (EI)** $C_{16}H_{21}F_3O_3S$ Theoretical: 350.1158. Found: 350.1144. Spectral Accuracy: 98.2%. **Melting point** 50-55 °C.

3,5,5,8,8-pentamethyl-5,6,7,8-tetrahydronaphthalen-2-yl triflate (4.31) ,^{1}H, $CDCl_3$, 300MHz

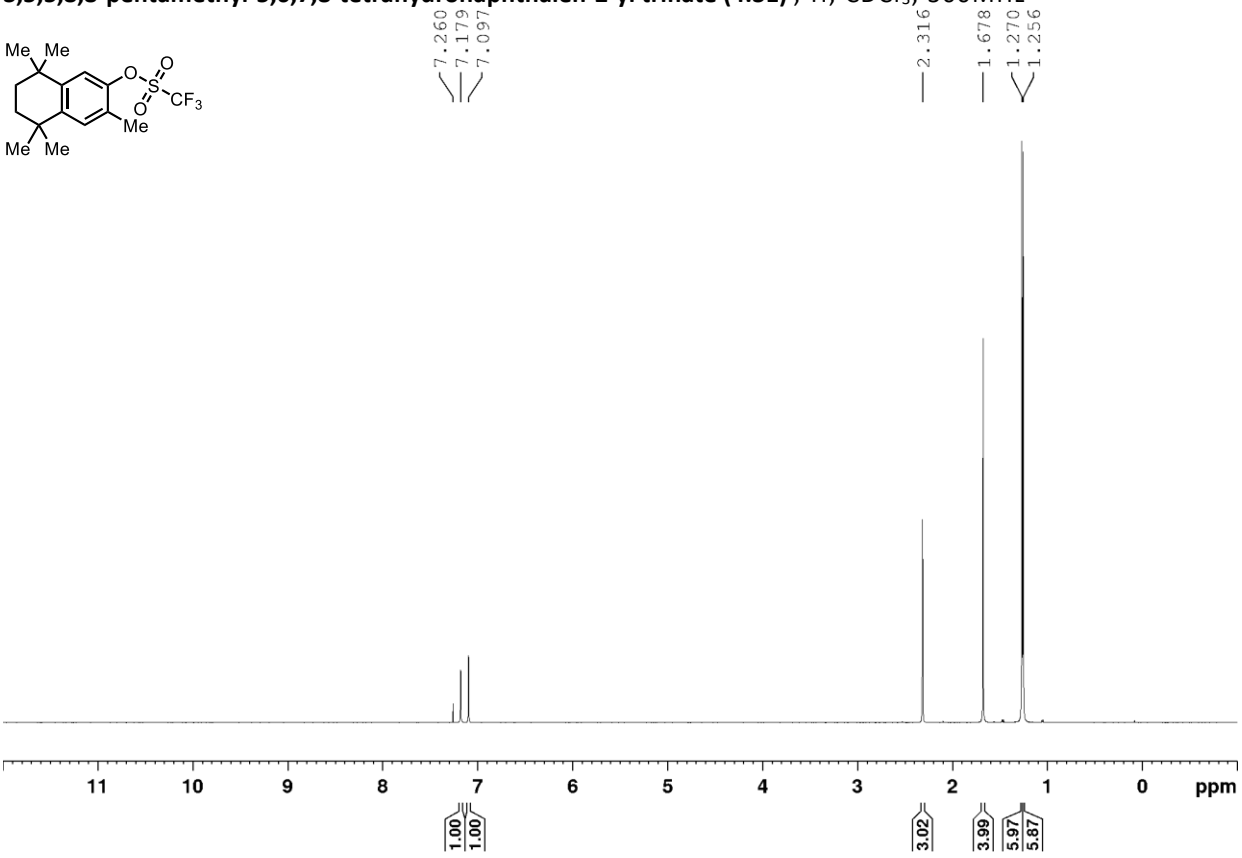

3,5,5,8,8-pentamethyl-5,6,7,8-tetrahydronaphthalen-2-yl triflate (4.31) ,$^{13}C\{^{1}H\}$, $CDCl_3$, 75 MHz

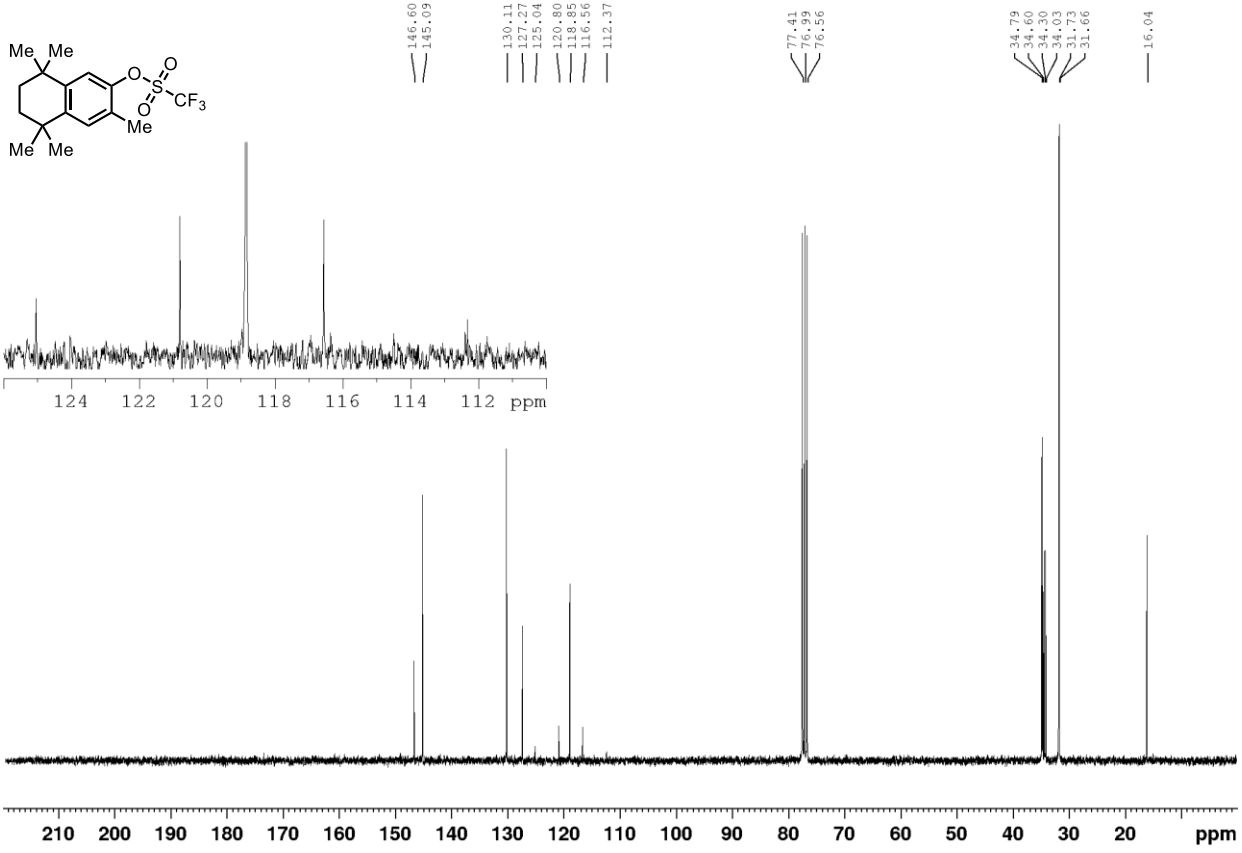

3,5,5,8,8-pentamethyl-5,6,7,8-tetrahydronaphthalen-2-yl triflate (4.31) ,$^{19}F\{^{1}H\}$, $CDCl_3$, 282 MHz

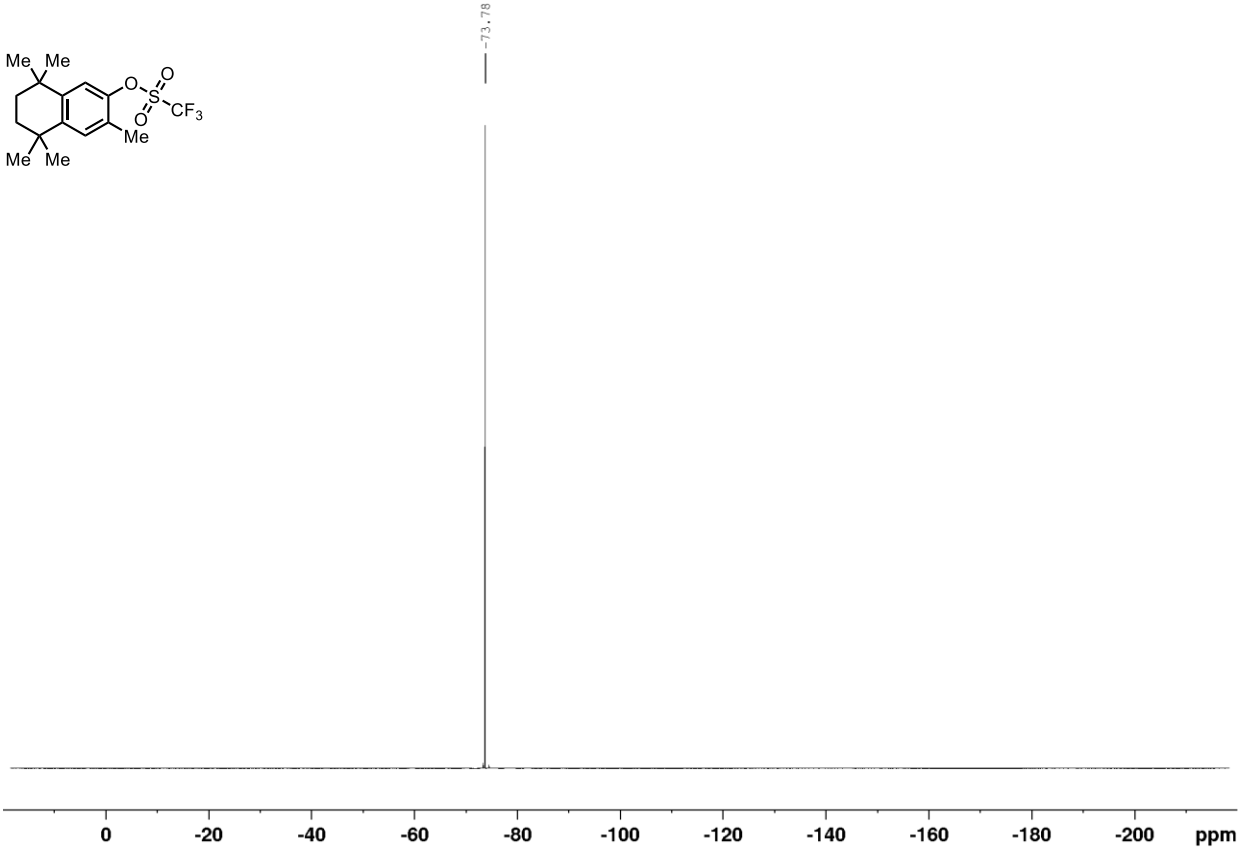

4.5.16.2 Synthesis of styrenes

Benzo[5,6]cyclohepta[1,2-b]pyridin-11-ylidene)piperidine-1-carboxylate (**4.32**) was synthesized following a known literature protocol (Figure 4.15).[65]

Figure 4.15 Structure of 4.32

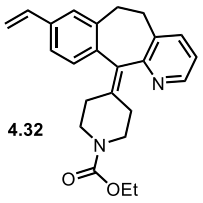

4.7.17 General Procedures A & B: Regioselective Mizoroki-Heck couplings with styrene

Scheme 4.16 Optimized conditions for the Mizoroki-Heck couplings

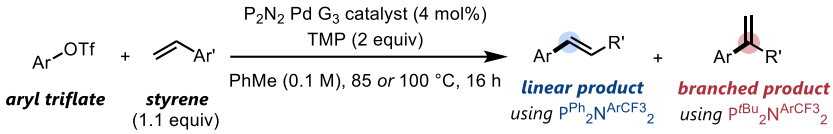

For linear selective coupling, General Procedure A: $P^{Ph}{}_2N^{ArCF3}{}_2$ Pd G3 (4.4) was used and reactions were run at 100 °C.

For branch selective coupling, General Procedure B: $P^{tBu}{}_2N^{ArCF3}{}_2$ Pd G3 (4.3) was used and reactions were run at 85 °C.

P_2N_2 Pd G3 (0.04 equiv, 0.008 mmol) was added to a dry 8 mL screw-capped reaction vial equipped with a magnetic stir bar outside the glovebox along with any solid starting materials. The vial was shipped inside the glovebox and PhMe was added (2.00 mL) via syringe. TMP (2 equiv, 0.40 mmol), aryl triflate (0.20 mmol), and alkene (1.1 equiv, 0.22 mmol) were added using a weight-calibrated micropipette if liquid. The vial was capped, removed from the glovebox, and placed in a stirring (350 rpm) pre-heated mineral oil bath at the indicated reaction temperature. After stirring for 16 hours, the reaction vial was removed from the oil bath and cooled to room

temperature. The reaction mixture was diluted with ethyl acetate and a small aliquot was filtered through a silica plug for crude GC-FID analysis to determine ratio of regioisomers. The reaction mixture was purified by flash column chromatography with SiO_2 to obtain pure compound in ≥19:1 *rr* (regiomeric ratio).

Note: While reactions were set up in the glovebox, P_2N_2 Pd G3 complexes were stored in a moisture-free desiccator and weighed outside the glovebox.

4.7.18 Characterization data for reactions with $P^{Ph}{}_2N^{ArCF3}{}_2$ Pd G3 (4.4) (linear products)

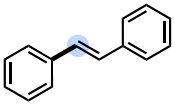

***Trans*-stilbene (4.7-lin)** was prepared according to **general procedure A**. Crude lin:br as assessed by GC-FID was 19:1.The product was purified by column chromatography with 0% to 3% Et_2O in hexanes to afford **4.10-lin** as a white solid (30.6 mg, 85% yield). **^{1}H NMR** ($CDCl_3$, 300 MHz) δ (ppm) 7.55-7.50 (m, 4H), 7.40-7.34 (m, 4H), 7.30-7.24 (m, 2H), 7.12 (s, 2H). **^{13}C{^{1}H} NMR** ($CDCl_3$, 75 MHz) δ (ppm) 137.3, 128.7, 127.6, 126.5. Spectral data is in accordance with a previous report.[50]

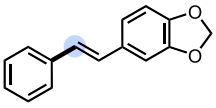

***(E)*-5-styrylbenzo[d][1,3]dioxole (4.8-lin)** was prepared according to **general procedure A**. Crude lin:br as assessed by GC-FID was 11.5:1.The product was purified by column chromatography with 0% to 3% Et_2O in hexanes to afford **4.7-lin** as a white solid (31.5 mg, 70% yield). **^{1}H NMR** ($CDCl_3$, 400 MHz) δ (ppm) 7.51-7.47 (m, 2H), 7.35 (t, *J* = 7.6 Hz, 2H), 7.27-7.22 (m, 1H), 7.08 (d, *J* = 1.7 Hz, 1H), 7.04 (d, *J* = 16.3 Hz, 1H), 6.97-6.92 (m, 2H), 6.81 (d, *J* = 8.0 Hz, 1H), 5.98 (s, 2H). **^{13}C{^{1}H} NMR** ($CDCl_3$, 100 MHz) δ (ppm) 148.1, 147.3, 137.4, 131.8, 128.6, 128.3, 127.3, 127.0, 126.3, 121.4, 108.4, 105.5, 101.9. Spectral data is in accordance with a previous report.[66]

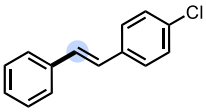

***(E)*-1-Chloro-4-styrylbenzene (4.9-lin)** was prepared according to **general procedure A**. Crude lin:br as assessed by GC-FID was 19:1. The product was purified by column chromatography with hexanes to afford **4.8-lin** as a white solid (34.2 mg, 80% yield). **^{1}H NMR** ($CDCl_3$, 400 MHz) δ (ppm) 7.53-7.49 (m, 2H), 7.44 (d, *J* = 8.6 Hz, 2H), 7.40-

7.26 (m, 5H), 7.11-7.03 (m, 2H). **$^{13}C\{^{1}H\}$ NMR** ($CDCl_3$, 100 MHz) δ (ppm) 136.9, 135.8, 133.1, 129.3, 128.8, 128.7, 127.8, 127.6, 127.3, 126.5. Spectral data is in accordance with previous reports.[67]

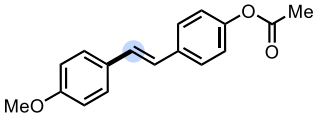

***(E)*-1-(4'-methoxyphenyl)-2-(4-acetoxyphenyl)ethene (4.10-lin)** was prepared according to **general procedure A**. Crude lin:br as assessed by GC-FID was 13:1.The product was purified by column chromatography with 0% to 10% Et_2O in hexanes to afford **4.9-lin** as a white solid (28.9 mg, 54% yield). **^{1}H NMR** ($CDCl_3$, 400 MHz) δ (ppm) 7.49 (m, 2H), 7.45 (m, 2H), 7.10 (m, 2H), 7.02 (d, *J* = 16.3 Hz, 1H), 6.95 (d, *J* = 16.3 Hz, 1H), 6.90 (m, 2H), 3.83 (s, 3H), 2.31 (s, 3H). **$^{13}C\{^{1}H\}$ NMR** ($CDCl_3$, 100 MHz) δ (ppm) 169.5, 159.3, 149.7, 135.4, 129.9, 128.4, 127.7, 127.1, 125.5, 121.7, 114.1, 55.3, 21.1. Spectral data is in accordance with a previous report.[68]

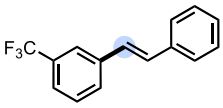

***(E)*-3-trifluoromethylstilbene (4.11-br)** was prepared according to **general procedure A**. Crude lin:br as assessed by GC-FID was 16:1. The product was purified by column chromatography with hexanes to afford **4.11-lin** as a white solid (42.7 mg, 86% yield). **^{1}H NMR** ($CDCl_3$, 400 MHz) δ (ppm) 7.77 (*br* s, 1H), 7.68 (d, *J* = 7.5 Hz, 1H), 7.57-7.45 (m, 4H), 7.40 (t, *J* = 7.5 Hz, 2H), 7.33-7.29 (m, 1H), 7.19 (d, *J* = 16.4 Hz, 1H), 7.12 (d, *J* = 16.3 Hz, 1H). **$^{13}C\{^{1}H\}$ NMR** ($CDCl_3$, 100 MHz) δ (ppm) 138.1, 136.6, 131.1 (q, *J* = 32.1 Hz), 130.5, 129.5, 129.1, 128.7, 128.1, 127.1, 126.7, 124.1 (q, *J* = 272.4 Hz), 124.0 (q, *J* = 3.80 Hz), 123.0 (q, *J* = 3.80 Hz). **$^{19}F\{^{1}H\}$ NMR** ($CDCl_3$, 376 MHz) δ (ppm) -62.7. Spectral data is in accordance with previous reports.[69]

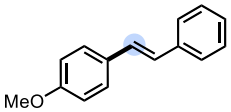

(*E*)-1-(phenyl)-2-(4'-methoxyphenyl)ethene (4.12-lin) was prepared according to **general procedure A**. Crude lin:br as assessed by GC-FID was 8:1. The product was first purified by column chromatography with 0% to 7.5% Et_2O in hexanes. A second column on the mixed fractions was run with 2% Et_2O in hexanes and all product was recombined to afford **4.12-lin** as a white solid (30.4 mg, 72% yield). **^{1}H NMR** ($CDCl_3$, 500 MHz) δ (ppm) 7.51-7.48 (m, 2H), 7.46 (d, *J* = 8.5 Hz, 2H), 7.34 (t, *J* = 7.7 Hz, 2H), 7.25-7.21 (m, 1H), 7.07 (d, *J* = 16.3 Hz, 1H), 6.98 (d, *J* = 16.3 Hz, 1H), 6.90 (d, *J* = 8.8 Hz, 2H), 3.83 (s, 3H). **$^{13}C\{^{1}H\}$ NMR** ($CDCl_3$, 125 MHz) δ (ppm) 159.3, 137.6, 130.1, 128.6, 128.2, 127.7, 127.2, 126.6, 126.2, 114.1, 55.3. Spectral data is in accordance with previous reports.[70]

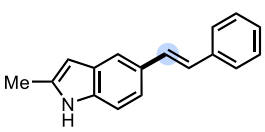

(*E*)-2-methyl-5-styryl-1*H*-indole (4.13-lin) was prepared according to **general procedure A**, however, the catalyst loading was doubled from 4 mol% to 8 mol%. Crude lin:br as assessed by GC-FID was 5:1. The product was purified by column chromatography with 5% to 15% EtOAc in hexanes to afford **4.13-lin** as a light beige solid (34.5 mg, 74% yield). **^{1}H NMR** ($CDCl_3$, 300 MHz) δ (ppm) 7.85 (*br* s, 1H), 7.64 (s, 1H), 7.55-7.51 (m, 2H), 7.39-7.33 (m, 3H), 7.28-7.20 (m, 3H), 7.07 (d, *J* = 16.2 Hz, 1H), 6.23 (s, 1H), 2.45 (s, 3H). **^{13}C{^{1}H} NMR** ($CDCl_3$, 100 MHz) δ (ppm) 138.1, 135.9, 135.7, 130.2, 129.4, 129.3, 128.6, 126.8, 126.1, 125.7, 119.7, 118.3, 110.4, 100.7, 13.7. **Accurate Mass (EI)** $C_{17}H_{15}N$ Theoretical: 233.1199. Found: 233.1228. Spectral Accuracy: 98.9%. **Melting point** 134-138 °C.

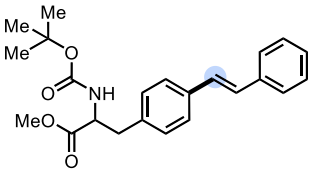

Methyl (*E*)-2-((*tert*-butoxycarbonyl)amino)-3-(4-styrylphenyl)propanoate (4.14-lin) was prepared according to **general procedure A**. Crude lin:br as assessed by ^{1}H NMR was 12:1.The product was purified by column chromatography with 10% to 20% EtOAc in hexanes to afford **4.14-lin** as a white solid (59.5mg, 78% yield). Mixture of rotamers, consistent with starting triflate.[71] **^{1}H NMR** ($CDCl_3$, 400 MHz) δ (ppm) 7.51 (d, *J* = 7.4 Hz, 2H), 7.45 (d, *J* = 8.1 Hz, 2H), 7.36 (t, *J* = 7.6 Hz, 2H), 7.28-7.23 (m, 1H), 7.14-7.10 (m, 2H), 7.08 (s, 2H), 5.04 (d, *J* = 8.0 Hz, 0.85H), 4.78 (*br* s, 0.15H), 4.60 (q, *J* = 6.6 Hz, 0.85H), 4.41 (*br* s, 0.15H), 3.72 (s, 3H), 3.13 (dd, *J* = 13.8 Hz, 5.7 Hz, 1H), 3.06 (dd, *J* = 13.8 Hz, 6.0 Hz, 1H),1.43 (s, 9H). **^{13}C{^{1}H} NMR** ($CDCl_3$, 100 MHz) δ (ppm) 172.3, 155.0, 137.2, 136.1, 135.4, 129.6, 128.6, 128.5, 128.2, 127.6, 126.6, 126.4, 79.9, 54.3, 52.2, 38.0, 28.2. **Accurate mass (ESI+):** m/z calculated for [$C_{23}H_{27}NO_4Na$] Theoretical: 404.1838. Found: 404.1803. **Melting point** 115-120 °C.

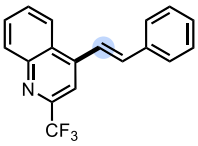

(*E*)-4-styryl-2-(triluoromethyl)quinoline (4.15-lin) was prepared according to **general procedure A**. Crude lin:br as assessed by GC-FID was >20:1.The product was purified by column chromatography with 25% to 70% PhMe in hexanes to afford **4.15-lin** as a white solid (58.3 mg, 97% yield). **^{1}H NMR** ($CDCl_3$, 300 MHz) δ (ppm) 8.32-8.22 (m, 2H), 7.93 (s, 1H), 7.88-7.79 (m, 2H), 7.74-7.64 (m, 3H), 7.50-7.36 (m, 4H). **^{13}C{^{1}H} NMR** ($CDCl_3$, 125 MHz) δ (ppm) 147.81 (q, *J* = 34.2 Hz), 147.78, 145.3, 136.7, 136.0, 130.7, 130.5, 129.3, 129.0, 128.4, 127.3, 126.9, 123.4, 121.9, 121.6 (q, *J* = 266.4 Hz), 112.6 (q, *J* =

2.2 Hz). **^{19}F{^{1}H} NMR** ($CDCl_3$, 282 MHz) δ (ppm) -67.5. **Accurate Mass (EI)** $C_{12}H_{12}NF_3$ Theoretical: 299.0916. Found: 299.1023. Spectral Accuracy: 98.9%. **Melting point** Decomposition

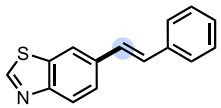

(*E*)-6-styryl-benzothiazole (4.16-lin) was prepared according to **general procedure A** with the catalyst loading doubled from 4 mol% to 8 mol%. Crude lin:br as assessed by GC-FID was 15:1. The product was purified by column chromatography with 1% to 10% EtOAc in hexanes to afford **4.16-lin** as a white solid (32.4 mg, 68% yield). **^{1}H NMR** ($CDCl_3$, 400 MHz) δ (ppm) 8.98 (*br* s, 1H), 8.11 (d, *J* = 8.5 Hz, 1H), 8.06 (d, *J* = 1.4 Hz, 1H), 7.72 (dd, *J* = 8.5 Hz, 1.6 Hz, 1H), 7.58-7.52 (m, 2H), 7.39 (t, *J* = 8.6 Hz, 2H), 7.32-7.27 (m, 1H), 7.26-7.21 (m, 1H), 7.19 (d, *J* = 16.4 Hz, 1H). **^{13}C{^{1}H} NMR** ($CDCl_3$, 100 MHz) δ (ppm) 154.0, 152.8, 137.0, 135.2, 134.7, 129.7, 128.7, 127.9, 127.8, 126.6, 124.7, 123.6, 119.7. **Accurate Mass (EI)** $C_{15}H_{11}NS$ Theoretical: 237.0607. Found: 237.0566. Spectral Accuracy: 98.0%. **Melting point** 128-134 °C

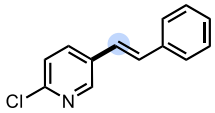

***(E)*-2-Chloro-5-styryl-pyridine (4.17-lin)** was prepared according to **general procedure A**. Crude lin:br as assessed by GC-FID was 17.5:1. The product was purified by column chromatography with 0% to 6% EtOAc in hexanes to afford **4.17-lin** as a white solid (18.3 mg, 42% yield). **^{1}H NMR** ($CDCl_3$, 400 MHz) δ (ppm) 8.48 (d, *J* = 2.6 Hz, 1H), 7.81 (dd, *J* = 8.3 Hz, 2.5 Hz, 1H), 7.54-7.50 (m, 2H), 7.41-7.36 (m, 2H), 7.34-7.29 (m, 2H), 7.15 (d, *J* = 16.4 Hz, 1H), 7.03 (d, *J* = 16.4 Hz, 1H). **^{13}C{^{1}H} NMR** ($CDCl_3$, 100 MHz) δ (ppm) 149.9, 148.1, 136.3, 135.3, 132.1, 131.5, 128.8, 128.5, 126.7, 124.2, 123.4. Spectral data is in accordance with previous reports.[72]

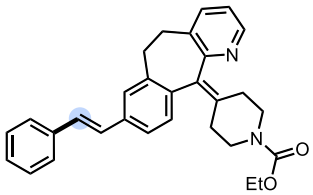

Ethyl (*E*)-4-(8-styryl-5,6-dihydro-11*H*-benzo[5,6]cyclohepta[1,2-*b*]pyridin-11-ylidene)piperidine-1-carboxylate (4.21-lin) was prepared according to **general procedure A**. Crude lin:br as assessed by crude ^{1}H was 17:1. The product was purified by column chromatography with 15% to 35% acetone in hexanes to afford **4.21-lin** as a white semi-solid (75.3 mg, 84% yield). **^{1}H NMR** ($CDCl_3$, 300 MHz) δ (ppm) 8.44 (dd, *J* = 4.7, 1.2 Hz, 1H), 7.56-7.50 (m, 2H), 7.50-7.46 (m, 1H), 7.43-7.34 (m, 4H), 7.32-7.27 (m, 1H), 7.26-7.21 (m, 1H), 7.16-7.08 (m, 3H), 4.18 (q, *J* = 7.1 Hz, 2H), 3.87 (*br* s, 2H), 3.56-3.36 (m, 2H), 3.26-3.11 (m, 2H), 2.98-2.85 (m,

2H), 2.60-2.30 (m, 4H), 1.29 (t, *J* = 7.1 Hz, 3H). **$^{13}C\{^{1}H\}$ NMR** ($CDCl_3$, 75 MHz) δ (ppm) 157.4, 155.4, 146.5, 138.5, 137.8, 137.3, 137.2, 136.8, 136.4, 135.0, 133.5, 129.6, 128.6, 128.5, 128.1, 127.5, 127.2, 126.3, 124.0, 122.0, 61.2, 44.8, 44.7, 31.9, 31.6, 30.7, 30.5, 14.6. **Accurate mass (ESI+):** m/z calculated for [$C_{30}H_{30}N_2O_2Na$] Theoretical: 473.2205. Found: 473.2226.

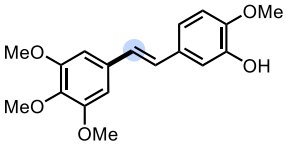

***Trans* combretastatin A-4 (4.23-lin)** was prepared according to **general procedure A**. Crude lin:br as assessed by GC-FID was 10:1. The product was purified by column chromatography with 20% to 50% EtOAc in hexanes to afford **4.23-lin** as a white solid (33.4 mg, 53% yield). **^{1}H NMR** ($CDCl_3$, 300 MHz) δ (ppm) 7.14 (d, *J* = 2.1 Hz, 1H), 6.97 (dd, *J* = 8.3 Hz, 2.1 Hz, 1H), 6.90 (d, *J* = 3.2 Hz, 2H), 6.84 (d, *J* = 8.3 Hz, 1H), 6.71 (s, 2H), 5.66 (*br* s, 1H), 3.91 (s, 6H), 3.90 (s, 3H), 3.86 (s, 3H). **$^{13}C\{^{1}H\}$ NMR** ($CDCl_3$, 100 MHz) δ (ppm) 153.3, 146.4, 145.7. 137.6, 133.3, 130.9, 127.7, 127.0, 119.2, 111.7, 110.6, 103.3, 60.9, 56.0, 55.9. Spectral data is in accordance with a previous report.[73]

4.7.19 NMR spectra for reactions with $P^{Ph}{}_2N^{ArCF3}{}_2$ Pd G3 (4.4) (linear products)

Stilbene (4.7-lin), ^1H, $CDCl_3$, 400 MHz

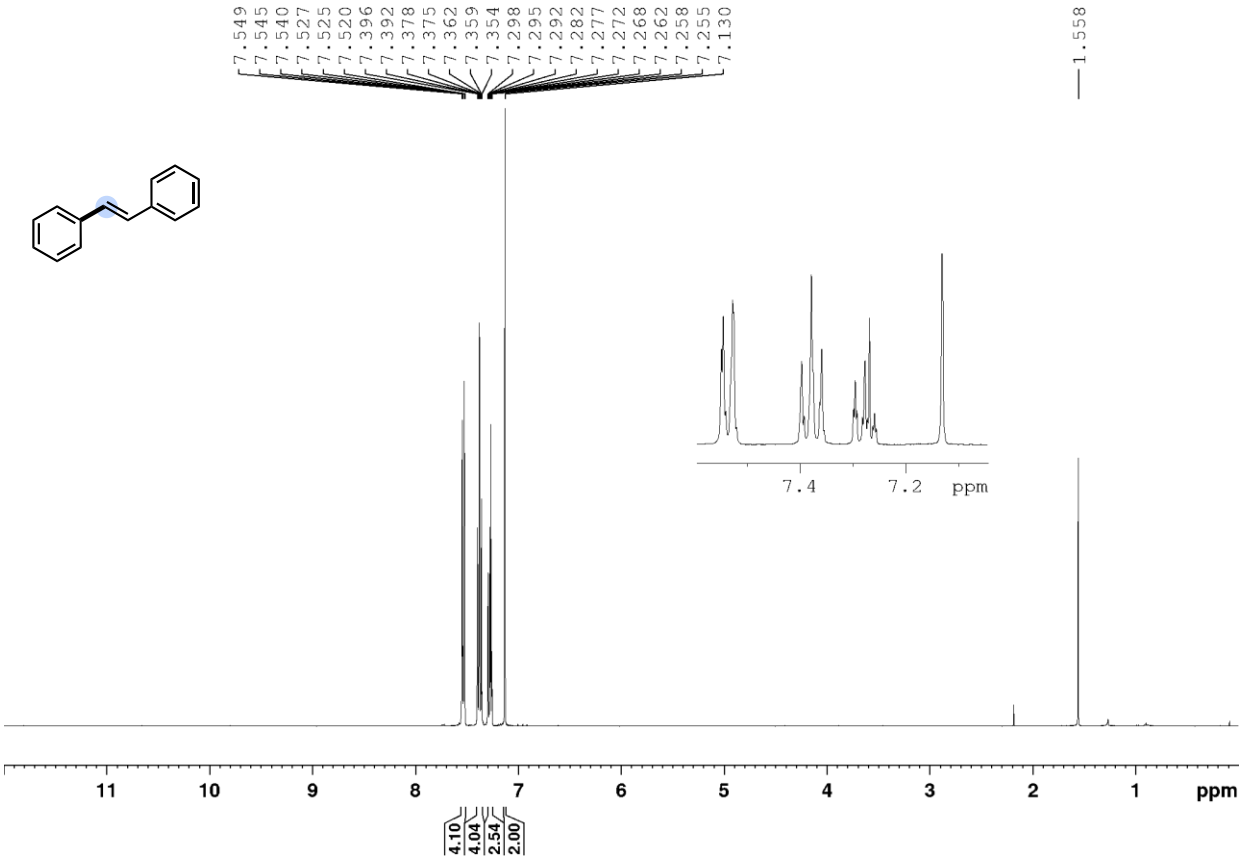

Stilbene (4.7-lin), $^{13}C\{^{1}H\}$, $CDCl_3$, 100 MHz

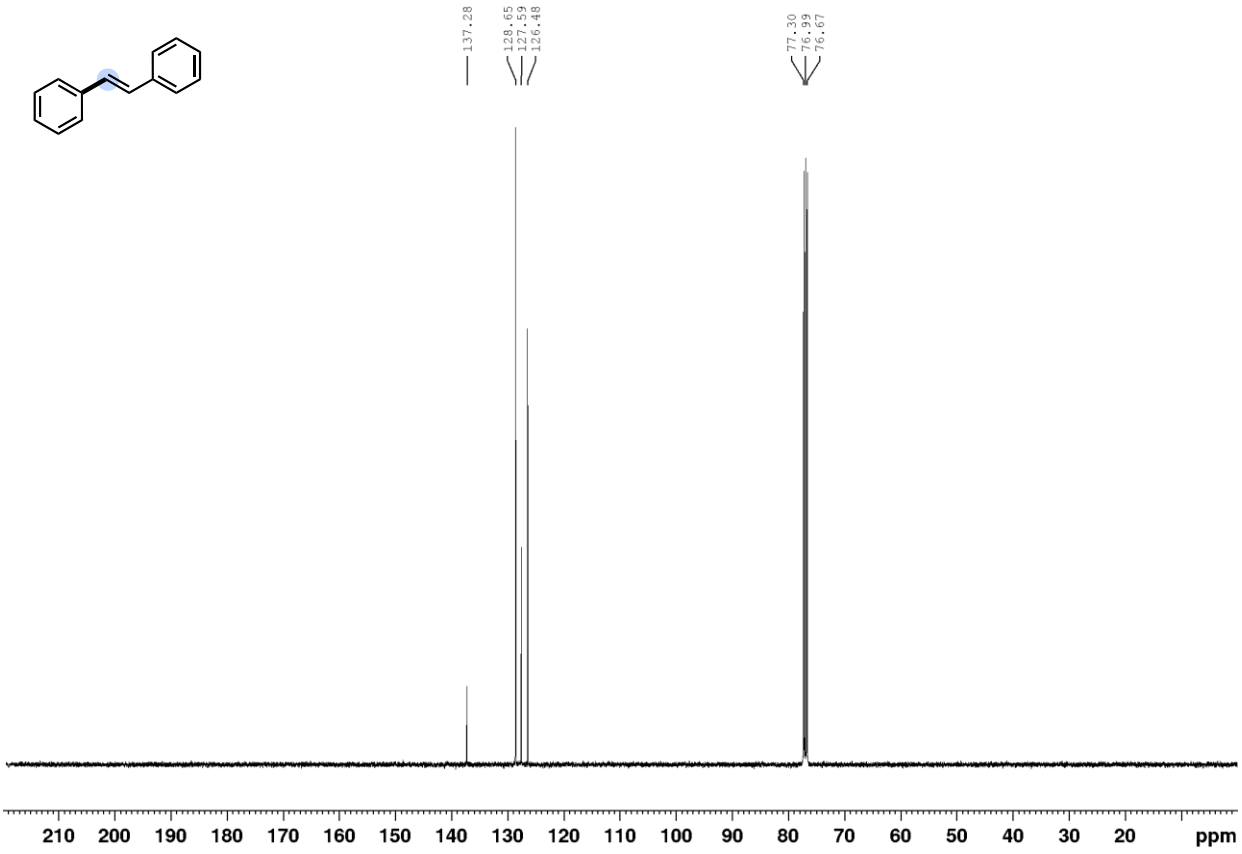

***(E)*-5-styrylbenzo[d][1,3]dioxole (4.8-lin)**, ^{1}H, $CDCl_3$, 400 MHz

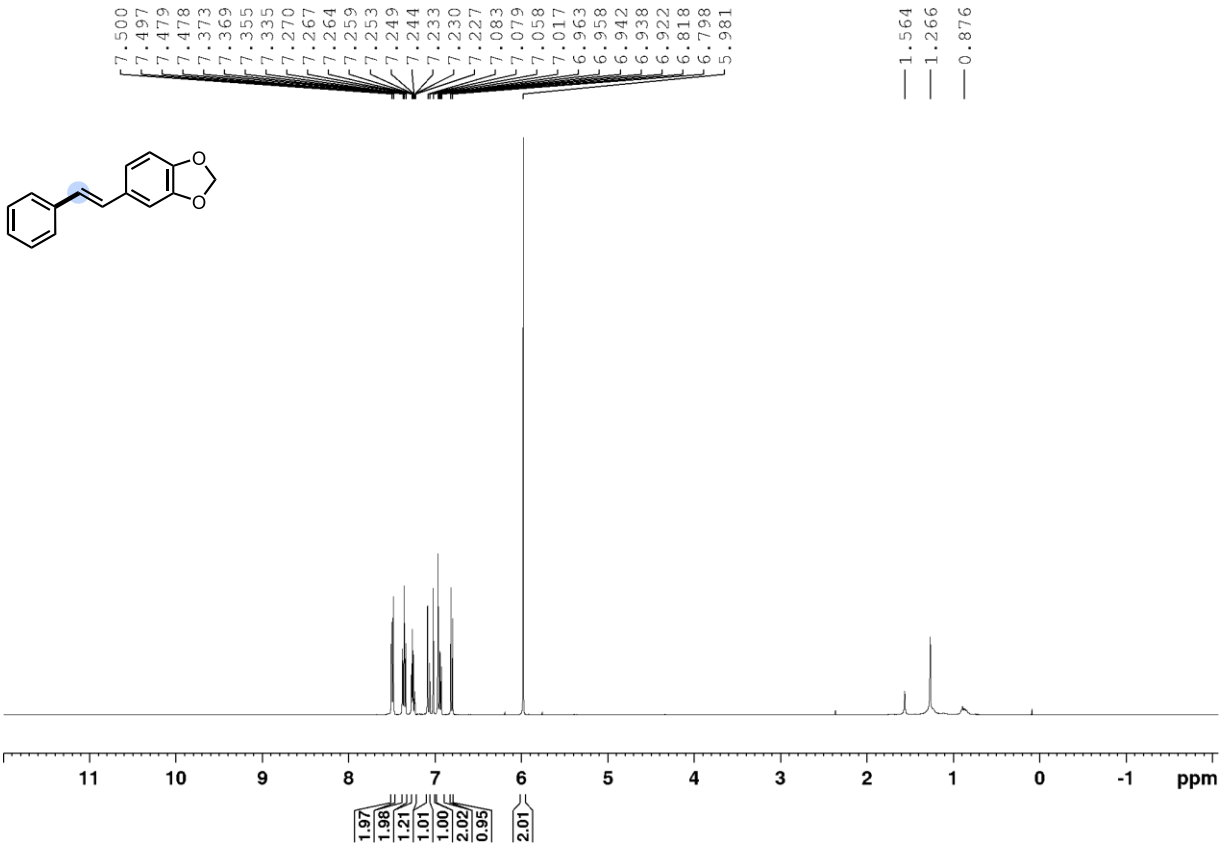

***(E)*-5-styrylbenzo[d][1,3]dioxole (4.8-lin)**, $^{13}C\{^{1}H\}$, $CDCl_3$, 100 MHz

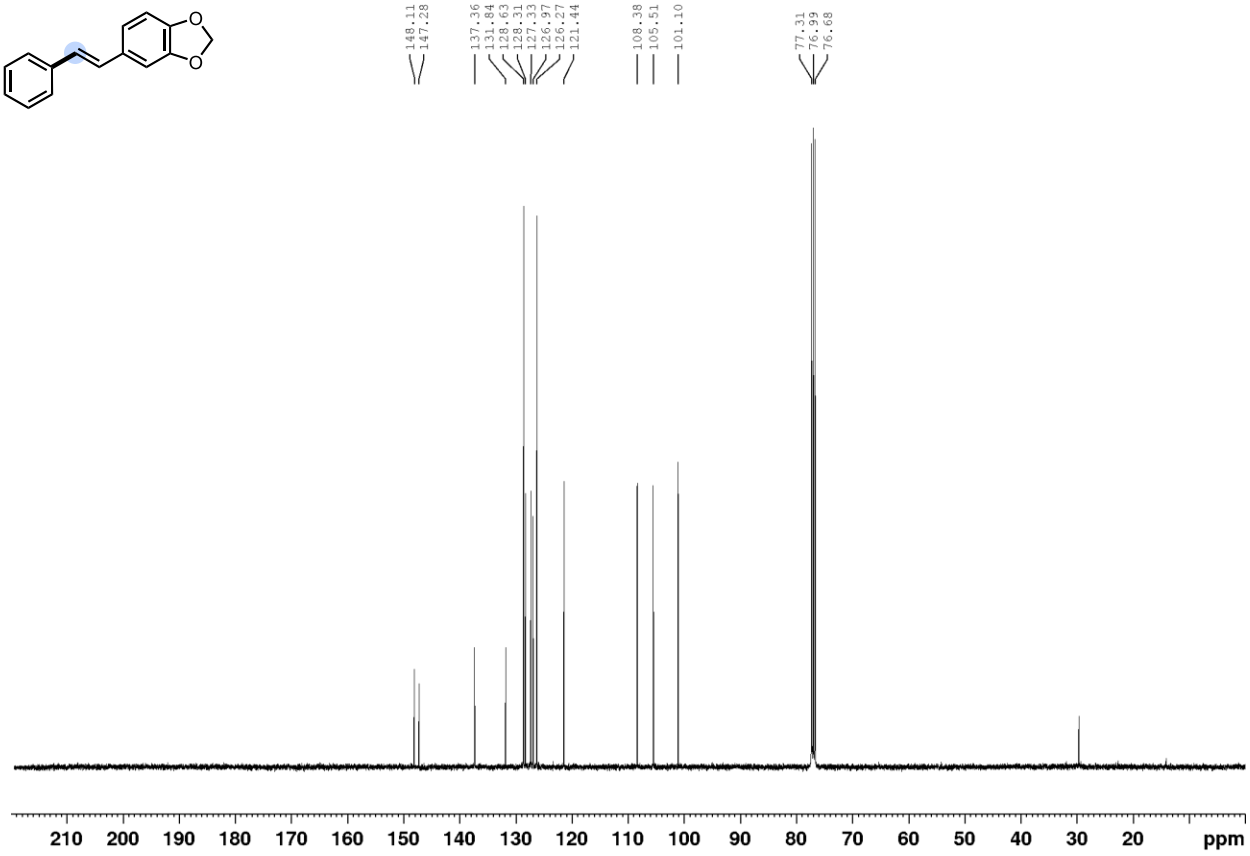

***(E)*-1-Chloro-4-styrylbenzene (4.9-lin)**, ^{1}H, $CDCl_3$, 400 MHz

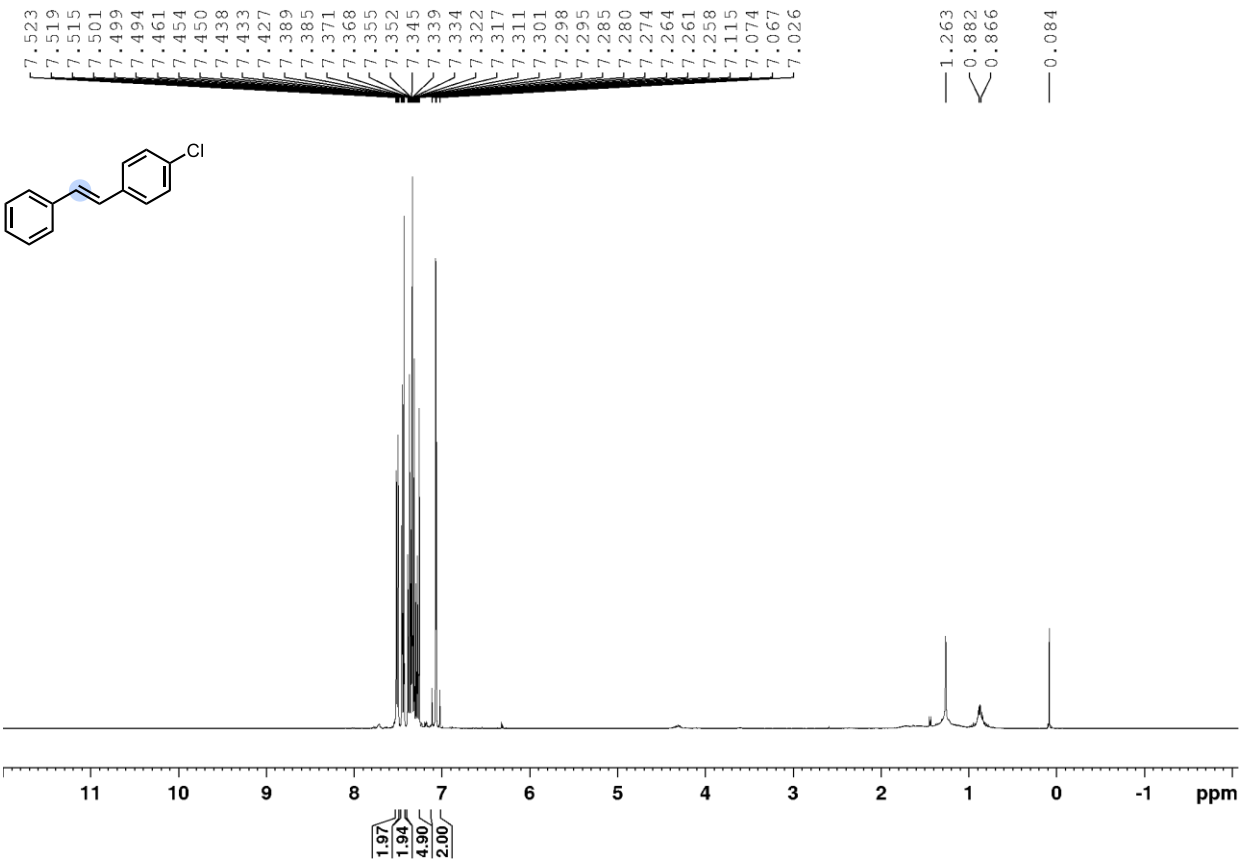

***(E)*-1-Chloro-4-styrylbenzene (4.9-Iin)**, $^{13}C\{^{1}H\}$, $CDCl_3$, 100 MHz

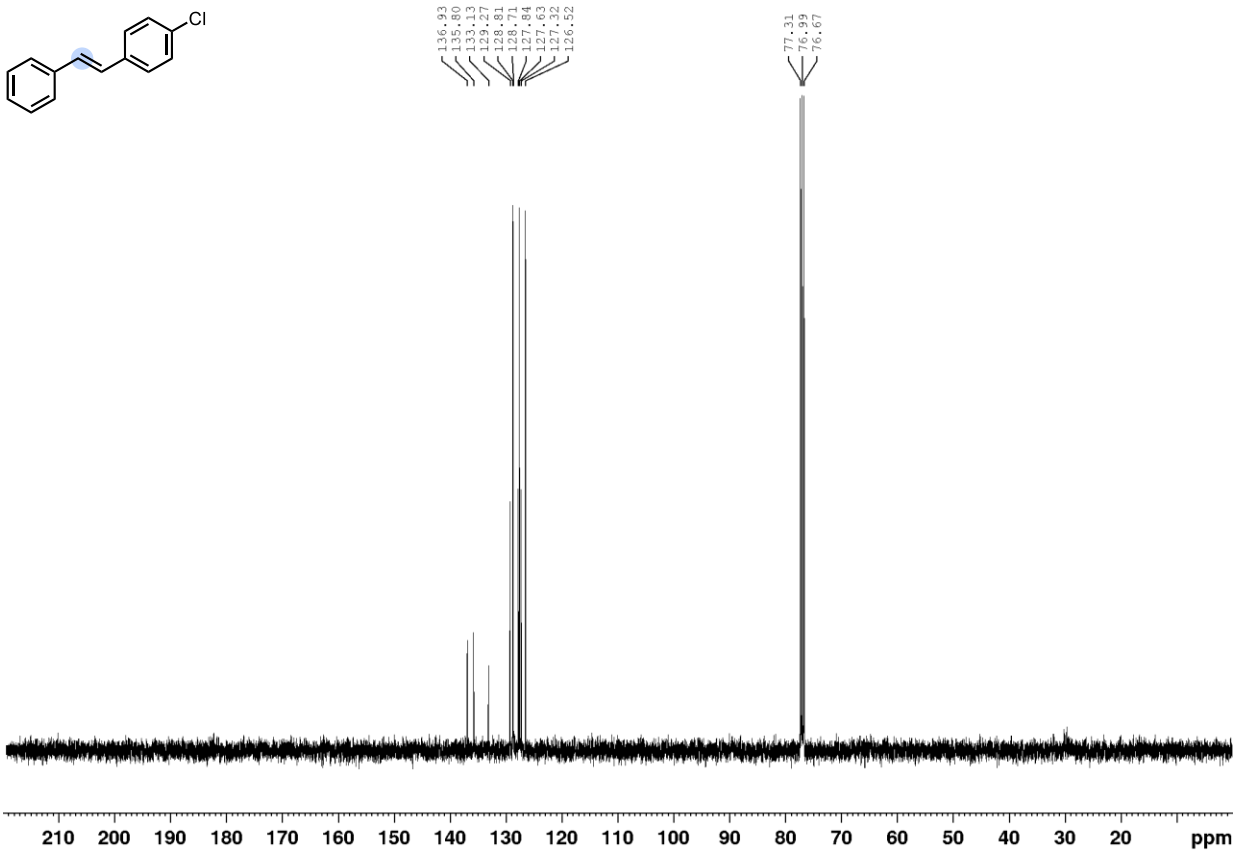

***(E)*-1-(4'-methoxyphenyl)-2-(4-acetoxyphenyl)ethene (4.10-lin)**, ^{1}H, $CDCl_3$, 400 MHz

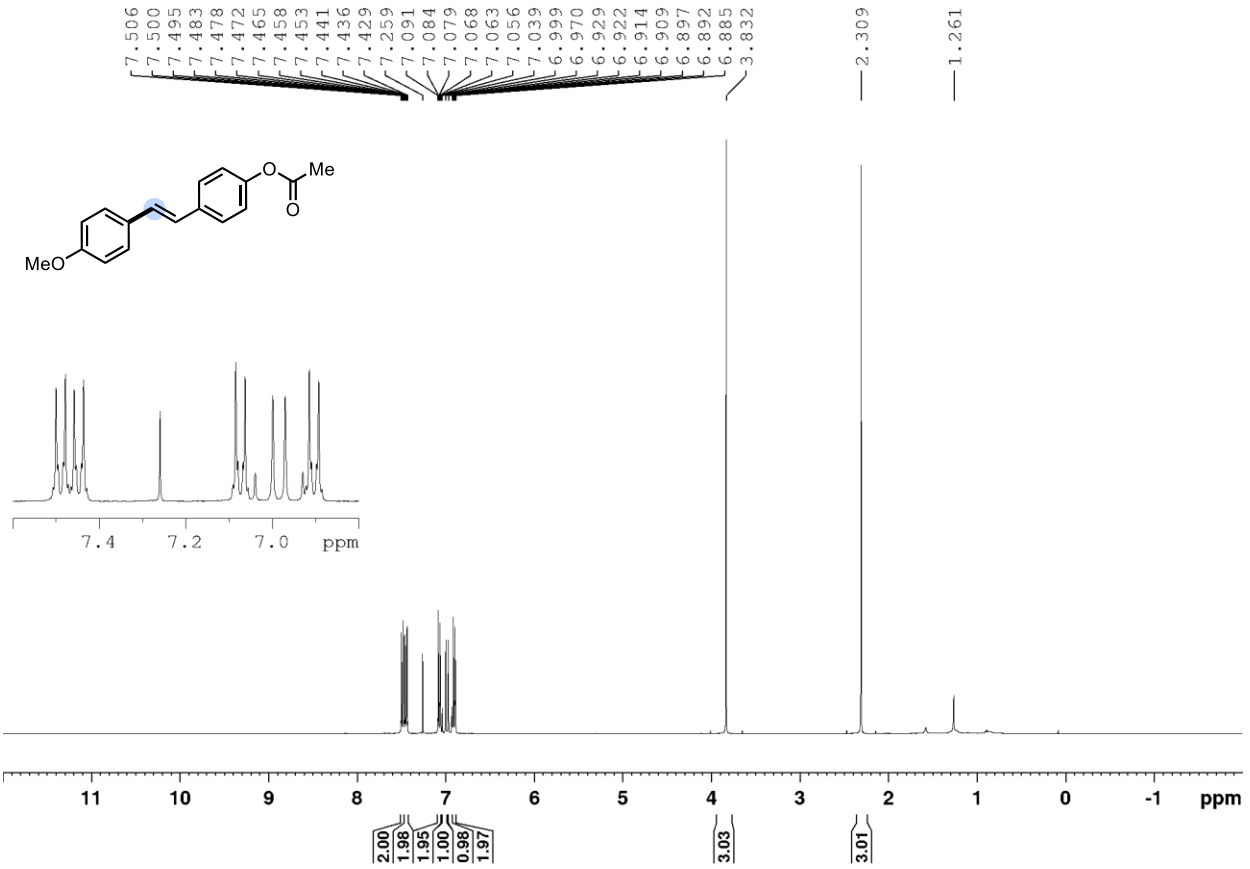

***(E)*-1-(4'-methoxyphenyl)-2-(4-acetoxyphenyl)ethene (4.10-lin)**, $^{13}C\{^{1}H\}$, $CDCl_3$, 100 MHz

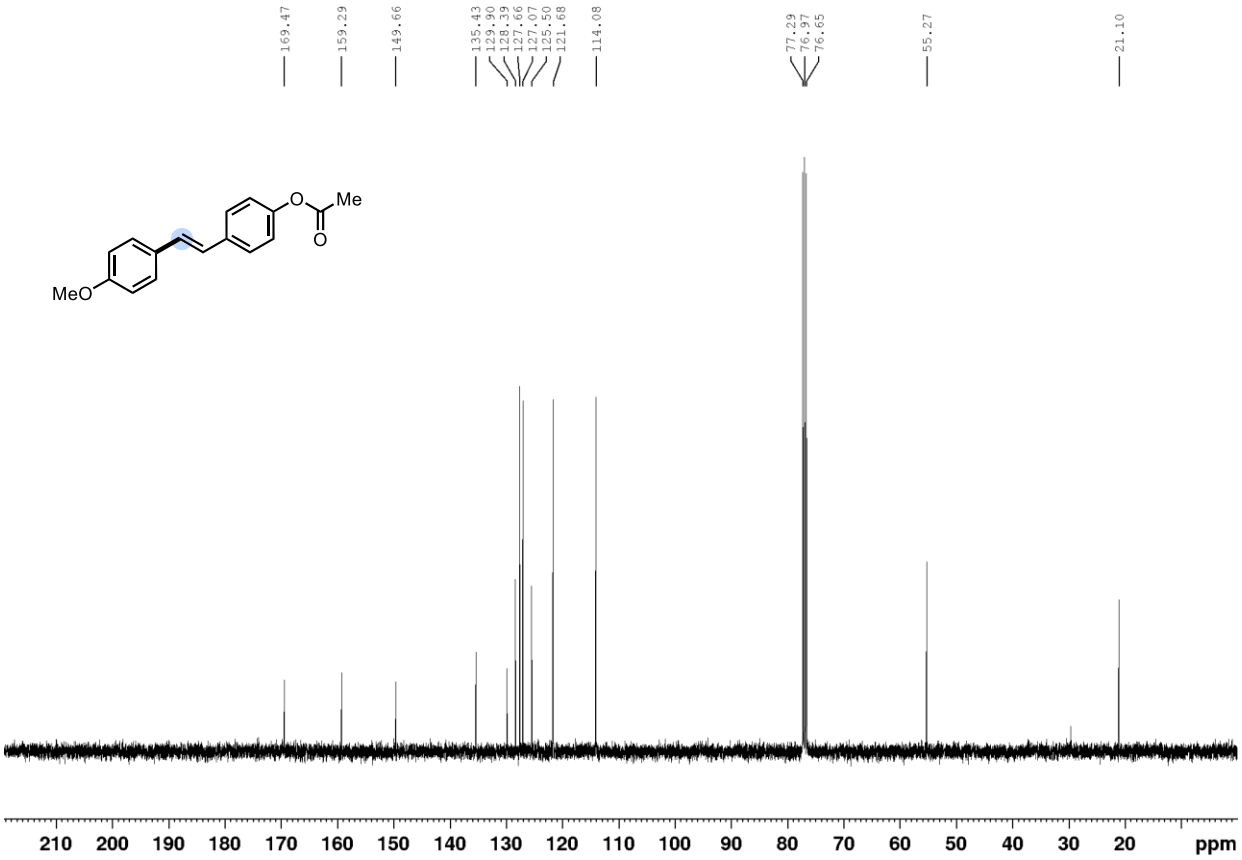

***(E)*-3-trifluoromethylstilbene (4.11-lin)**, ^{1}H, $CDCl_3$, 400 MHz

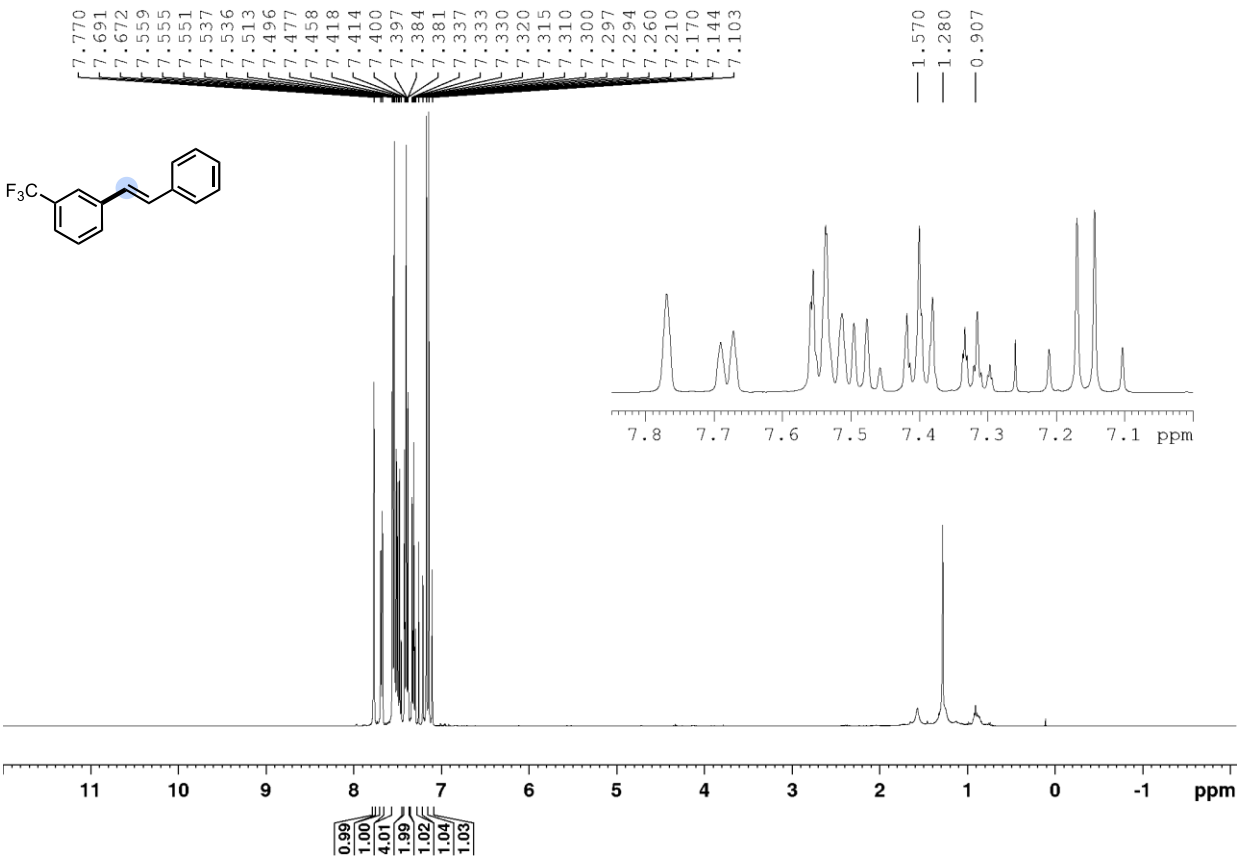

***(E)*-3-trifluoromethylstilbene (4.11-lin)**, $^{13}C\{^{1}H\}$, $CDCl_3$, 100 MHz

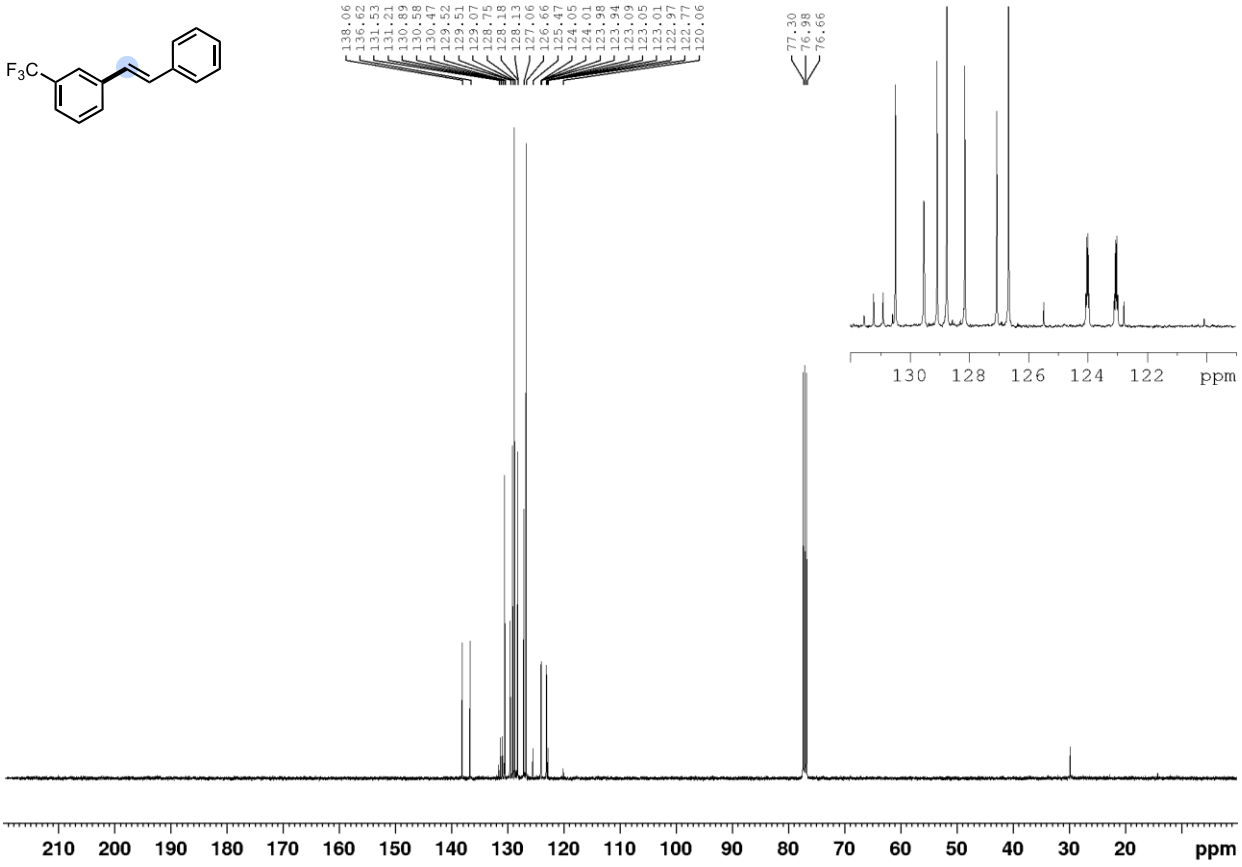

***(E)*-3-trifluoromethylstilbene (4.11-lin)**, $^{19}F\{^{1}H\}$, $CDCl_3$, 376 MHz

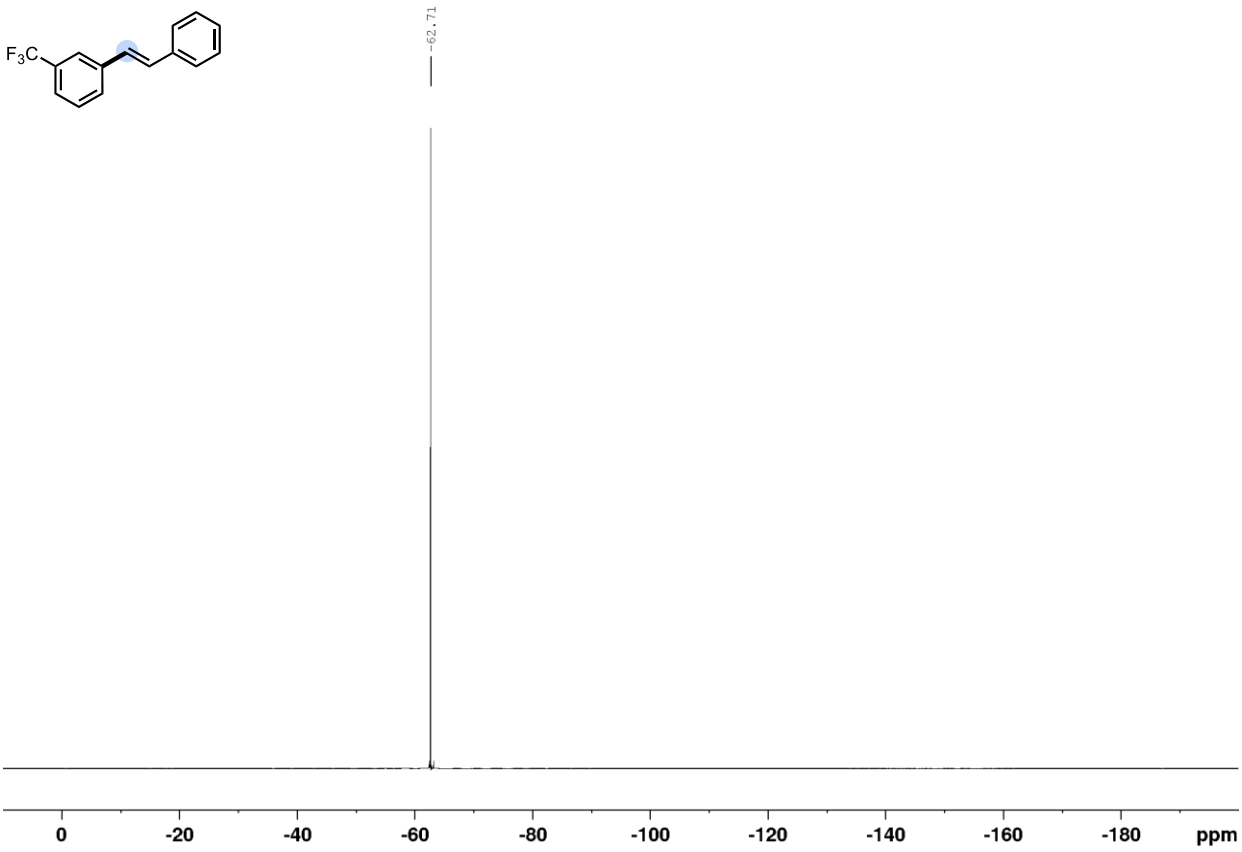

(*E*)-1-(phenyl)-2-(4'-methoxyphenyl)ethene (4.12-lin), ^{1}H, $CDCl_3$, 500 MHz

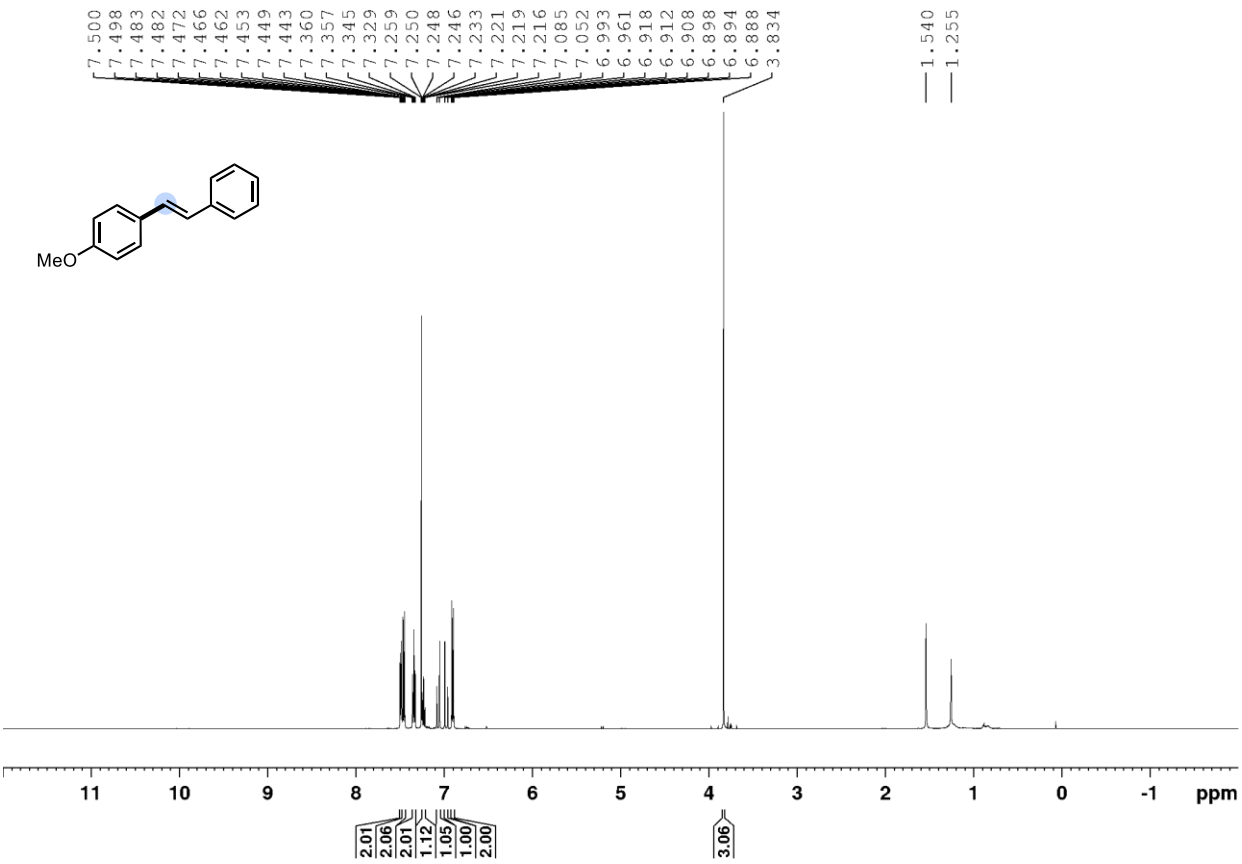

(*E*)-1-(phenyl)-2-(4'-methoxyphenyl)ethene (4.12-lin), $^{13}C\{^{1}H\}$, $CDCl_3$, 125 MHz

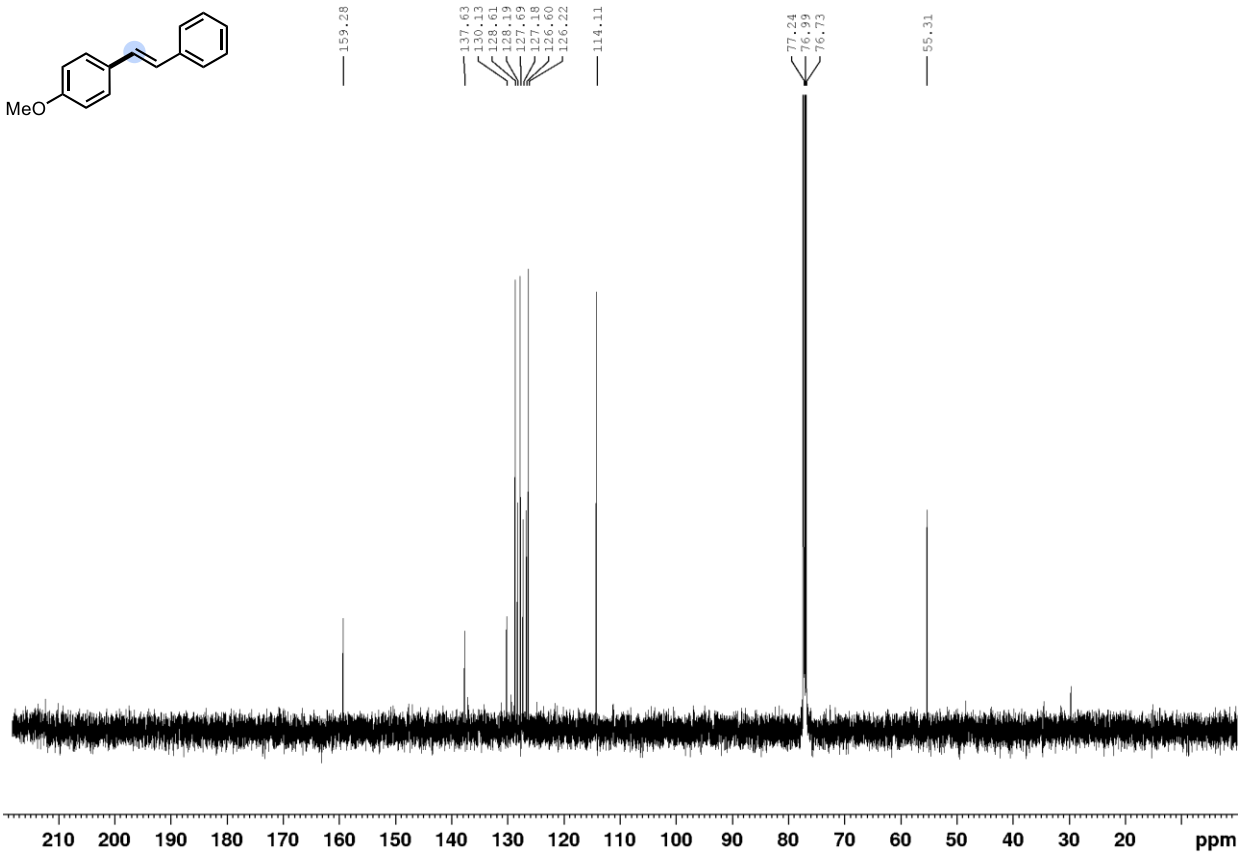

(*E*)-2-methyl-5-styryl-1*H*-indole (4.13-lin), ^{1}H, $CDCl_3$, 400 MHz

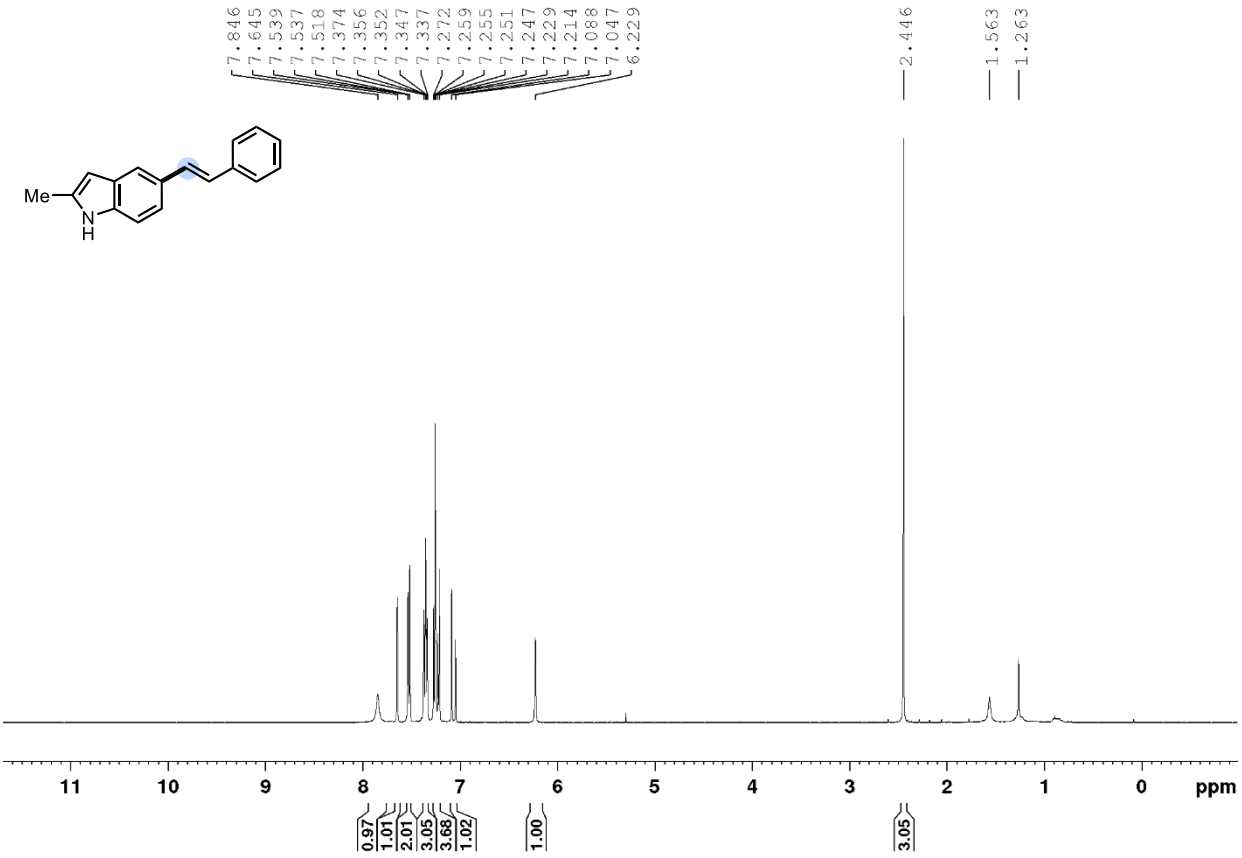

(*E*)-2-methyl-5-styryl-1*H*-indole (4.13-lin), $^{13}C\{^{1}H\}$, $CDCl_3$, 100 MHz

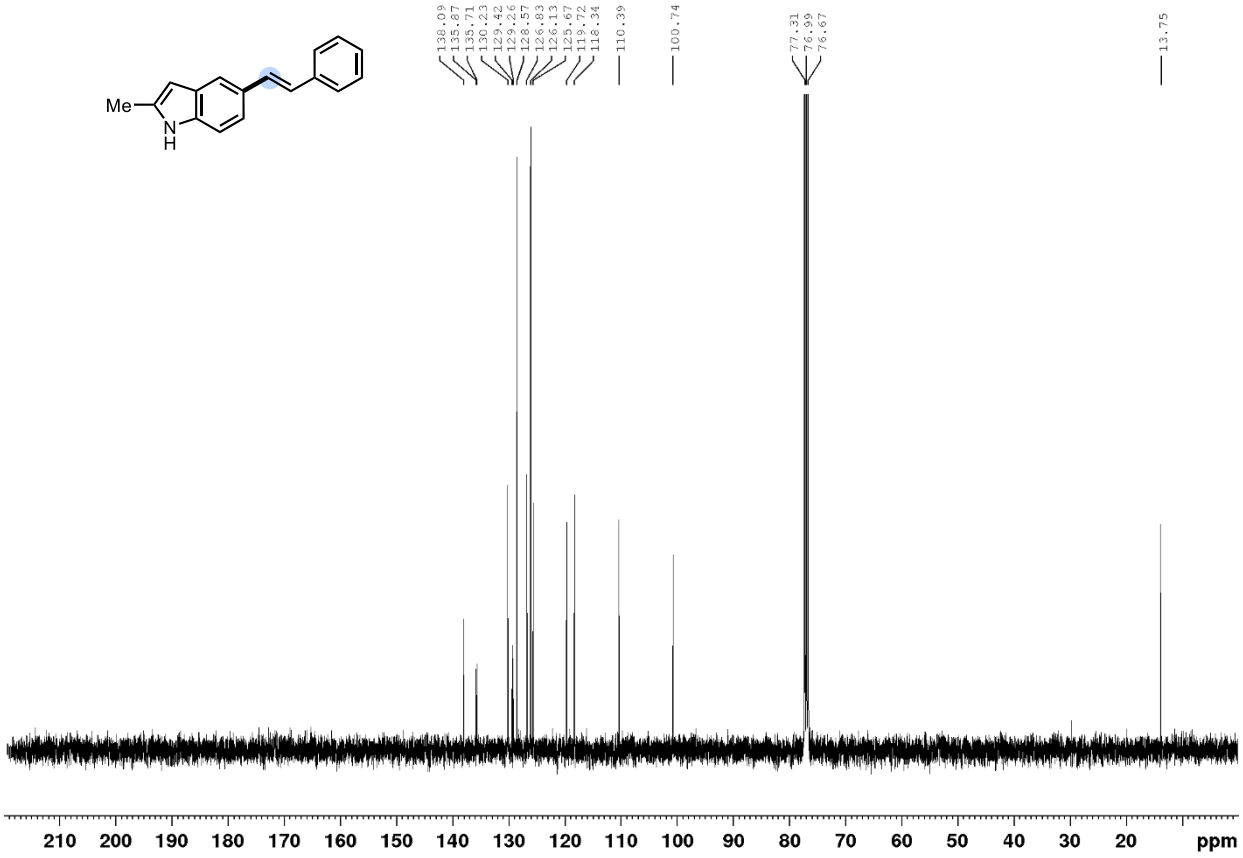

Methyl (*E*)-2-((*tert*-butoxycarbonyl)amino)-3-(4-styrylphenyl)propanoate (4.13-lin), ^{1}H, $CDCl_3$, 400 MHz

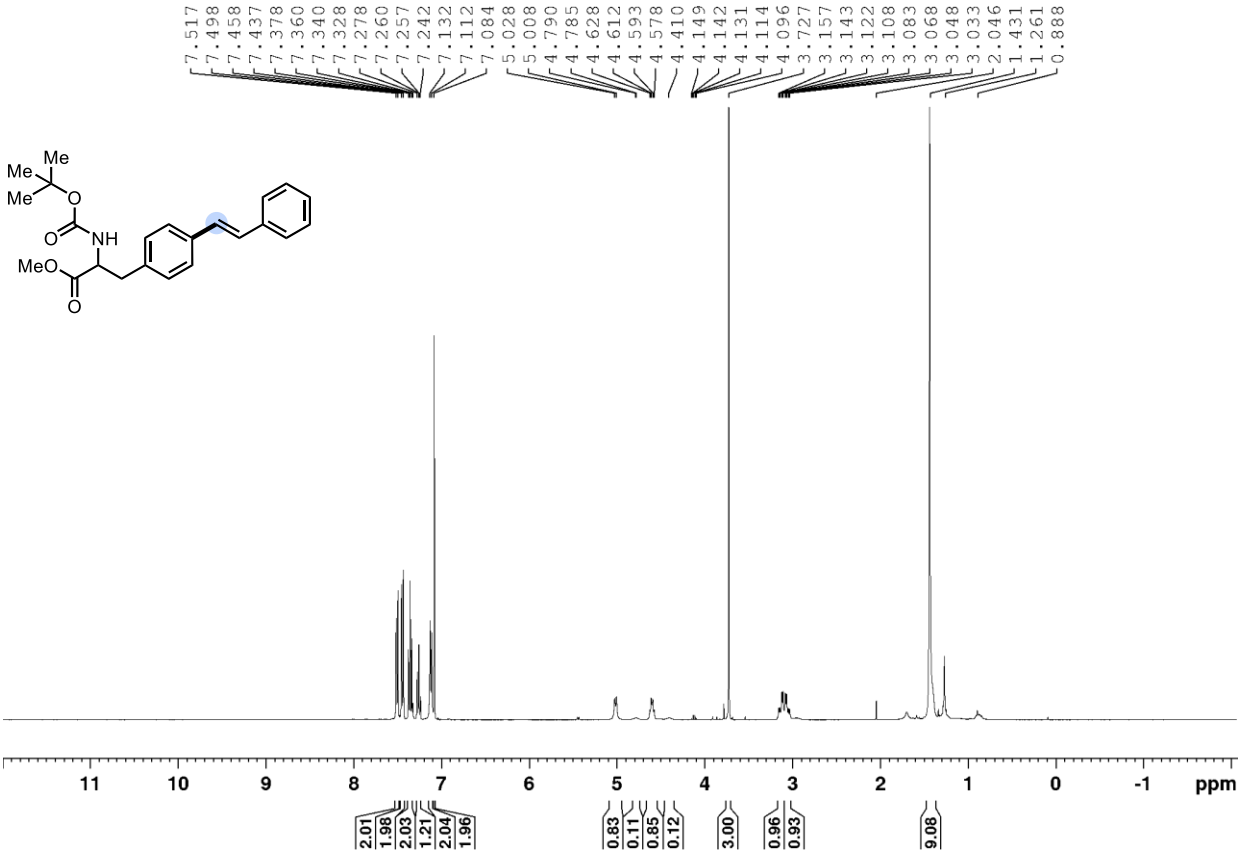

Methyl (*E*)-2-((*tert*-butoxycarbonyl)amino)-3-(4-styrylphenyl)propanoate (4.13-lin), $^{13}C\{^{1}H\}$, $CDCl_3$, 100 MHz

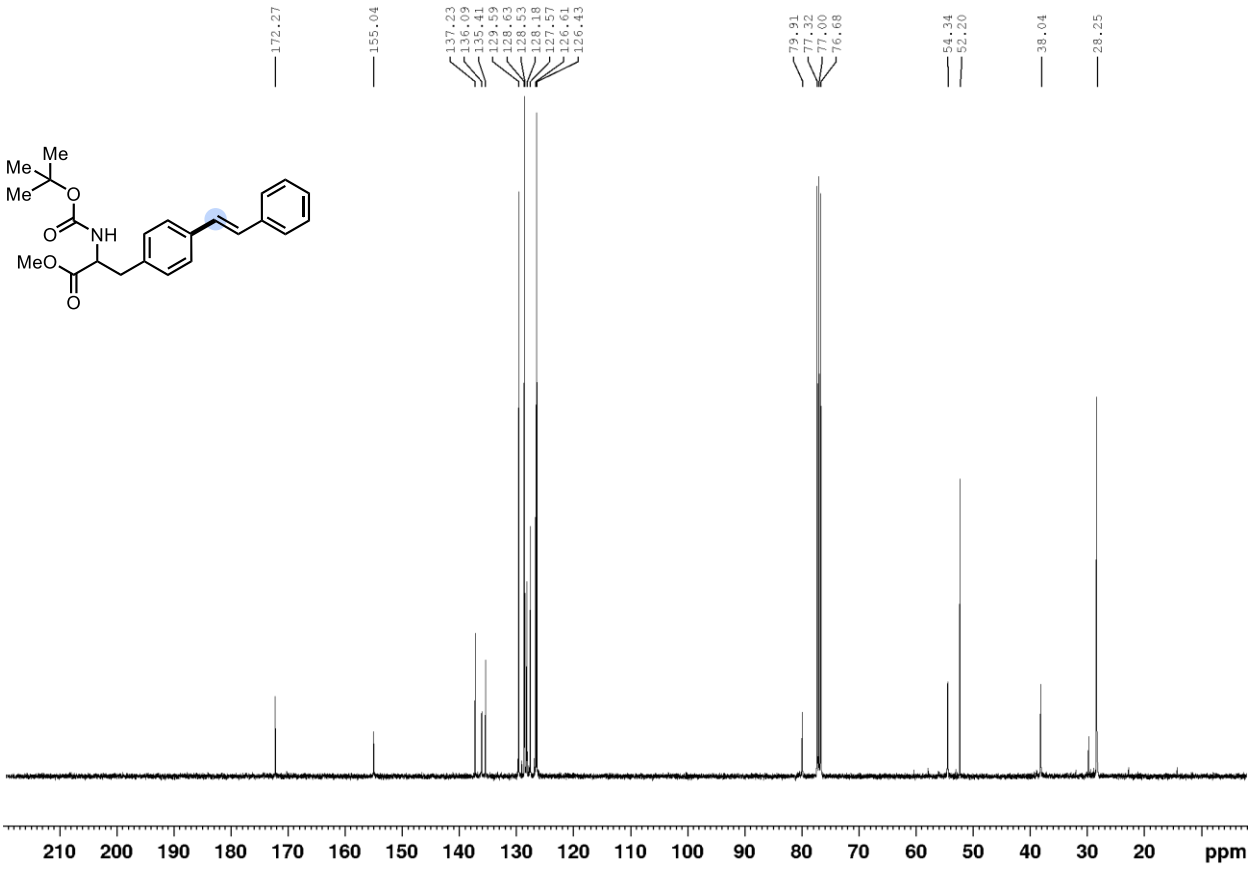

(*E*)-4-styryl-2-(triluoromethyl)quinoline (4.15-lin), ^{1}H, $CDCl_3$, 300 MHz

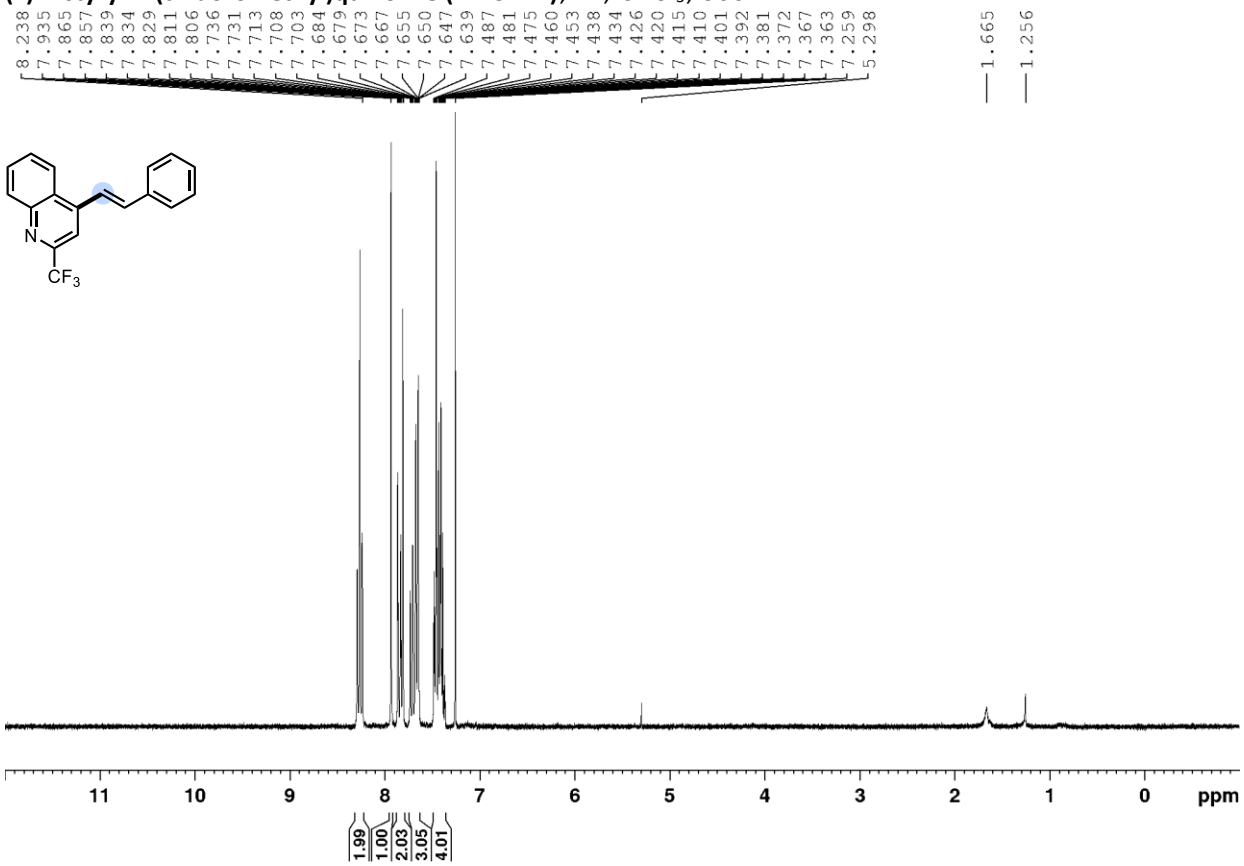

(*E*)-4-styryl-2-(triluoromethyl)quinoline (4.15-lin), $^{13}C\{^{1}H\}$, $CDCl_3$, 125 MHz

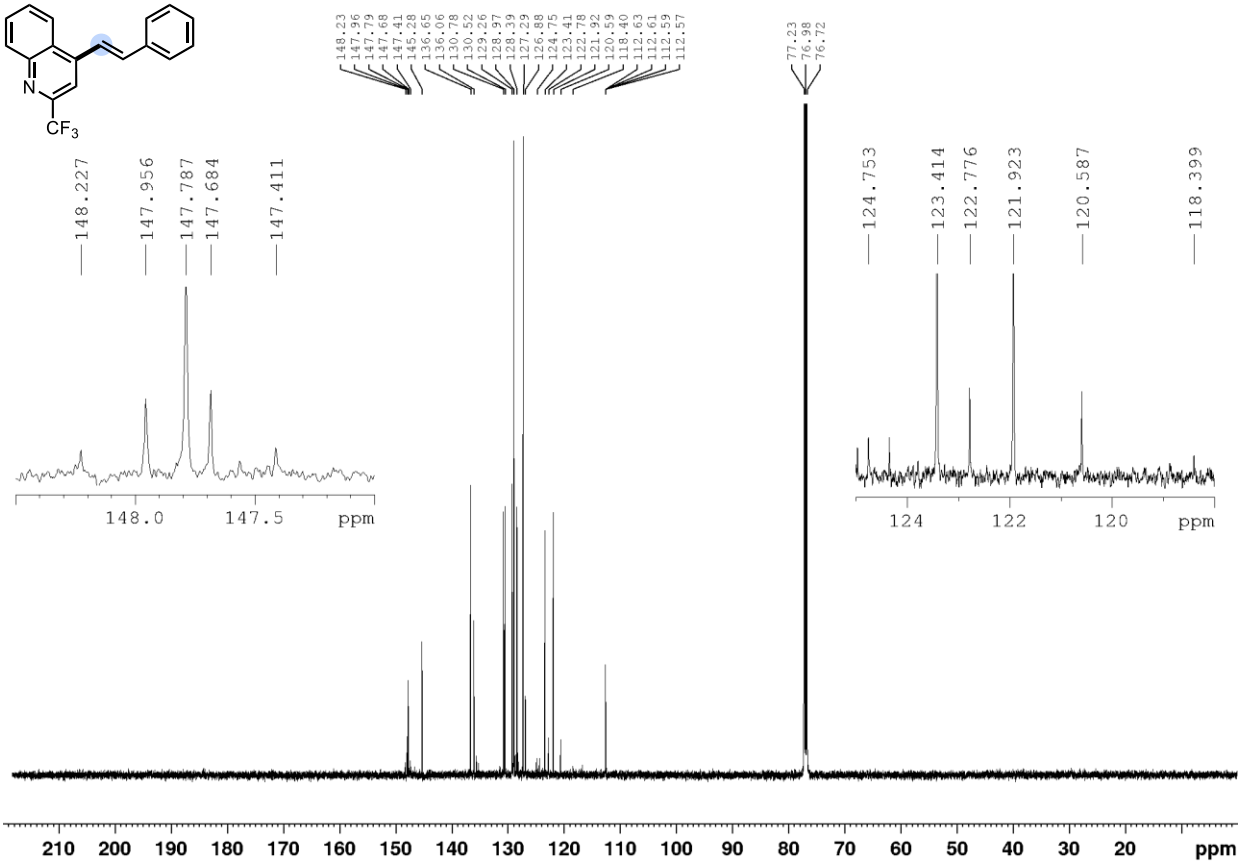

(*E*)-4-styryl-2-(triluoromethyl)quinoline (4.15-lin), $^{19}F\{^{1}H\}$, $CDCl_3$, 282 MHz

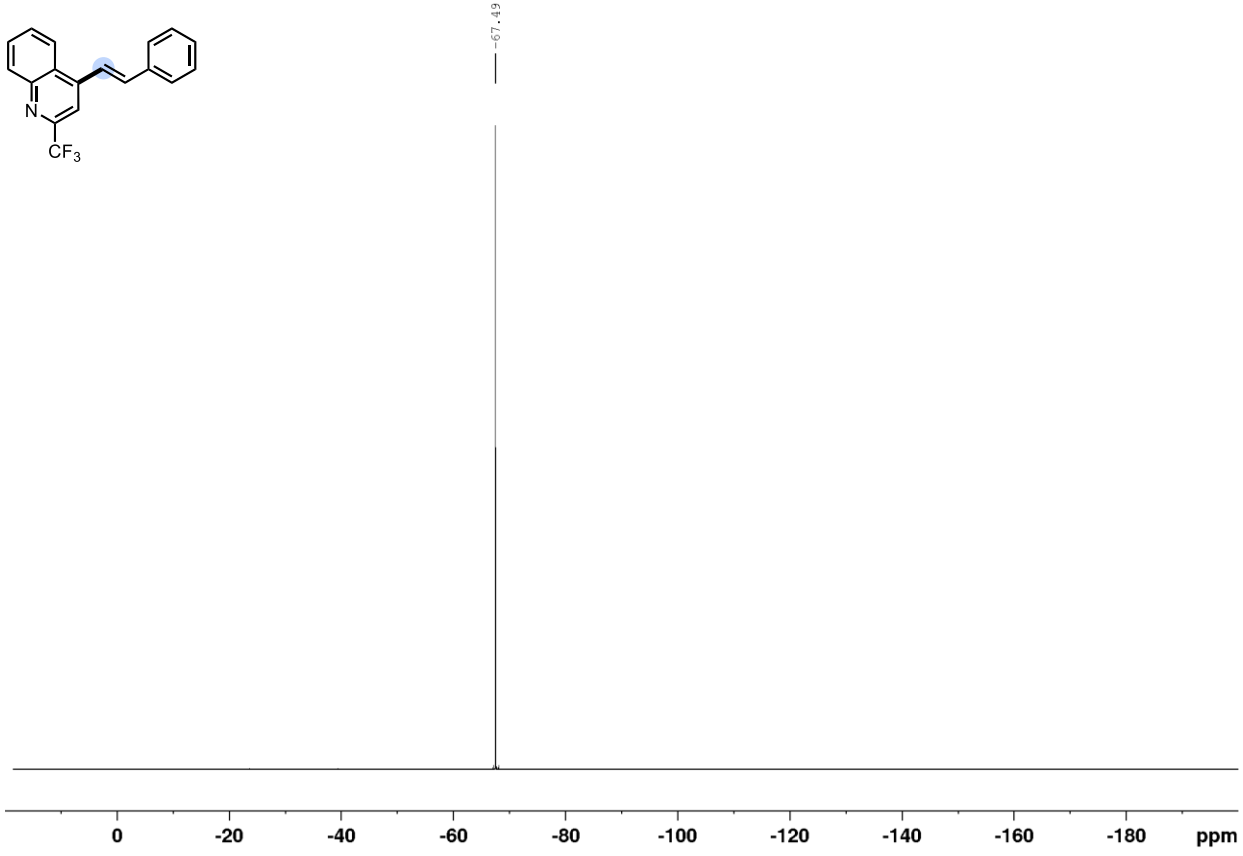

(*E*)-6-styryl-benzothiazole (4.16-lin), ^{1}H, $CDCl_3$, 400 MHz

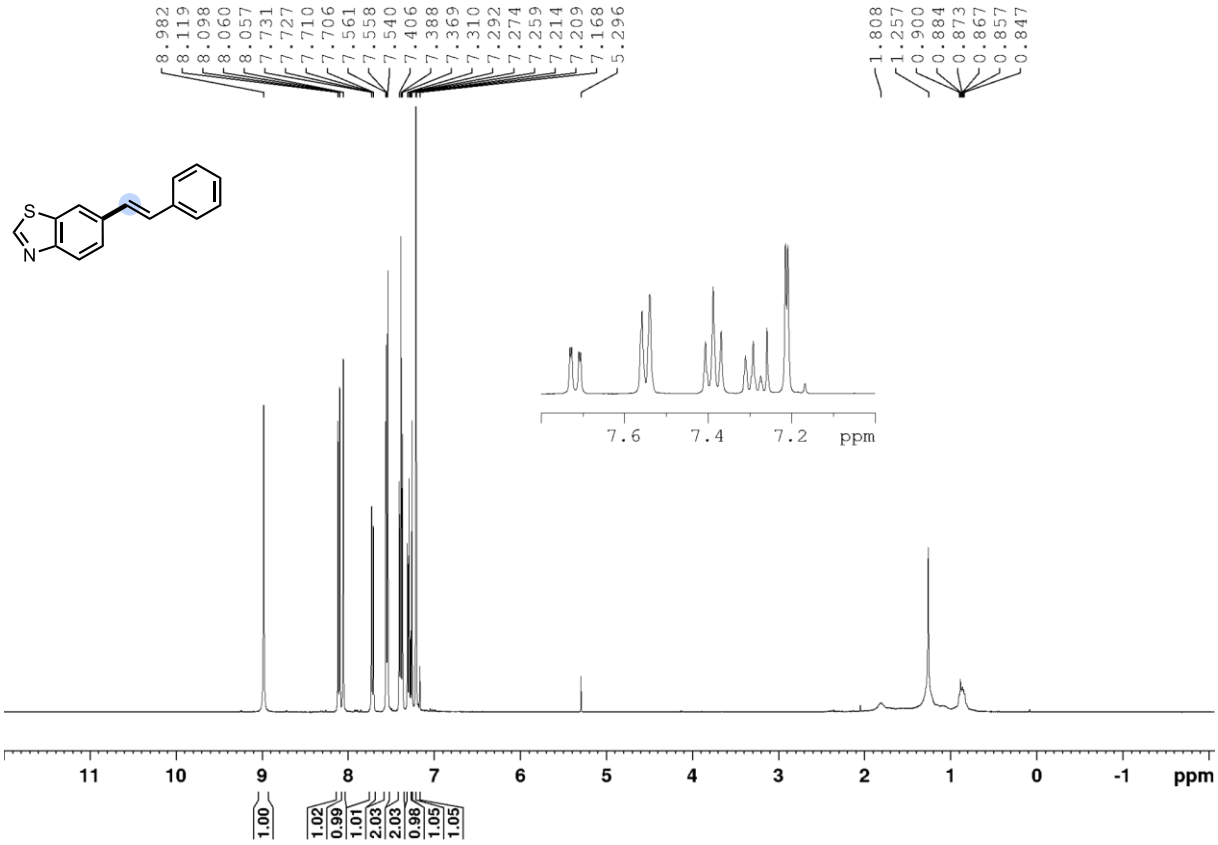

(*E*)-6-styryl-benzothiazole (4.16-lin), $^{13}C\{^{1}H\}$, $CDCl_3$, 100 MHz

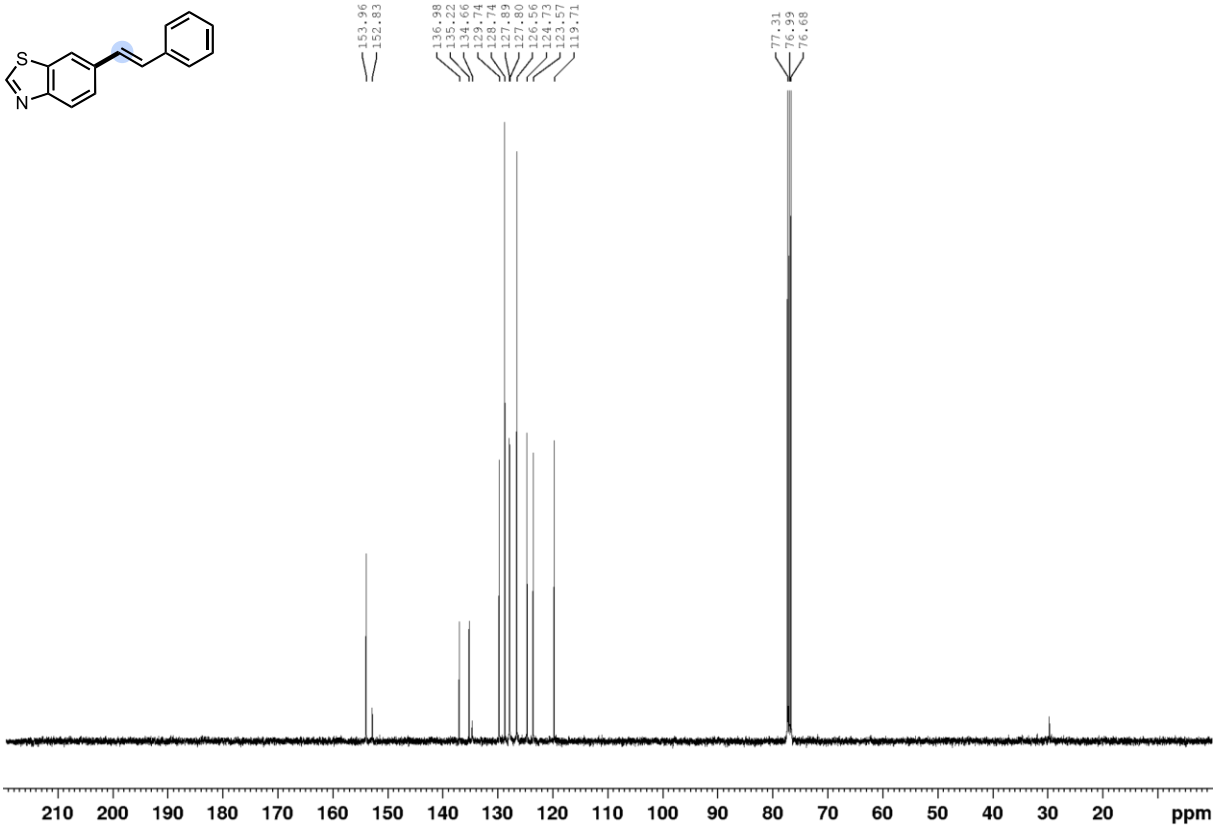

***(E)*-2-Chloro-5-styryl-pyridine (4.17-lin)**, ^{1}H, $CDCl_3$, 400 MHz

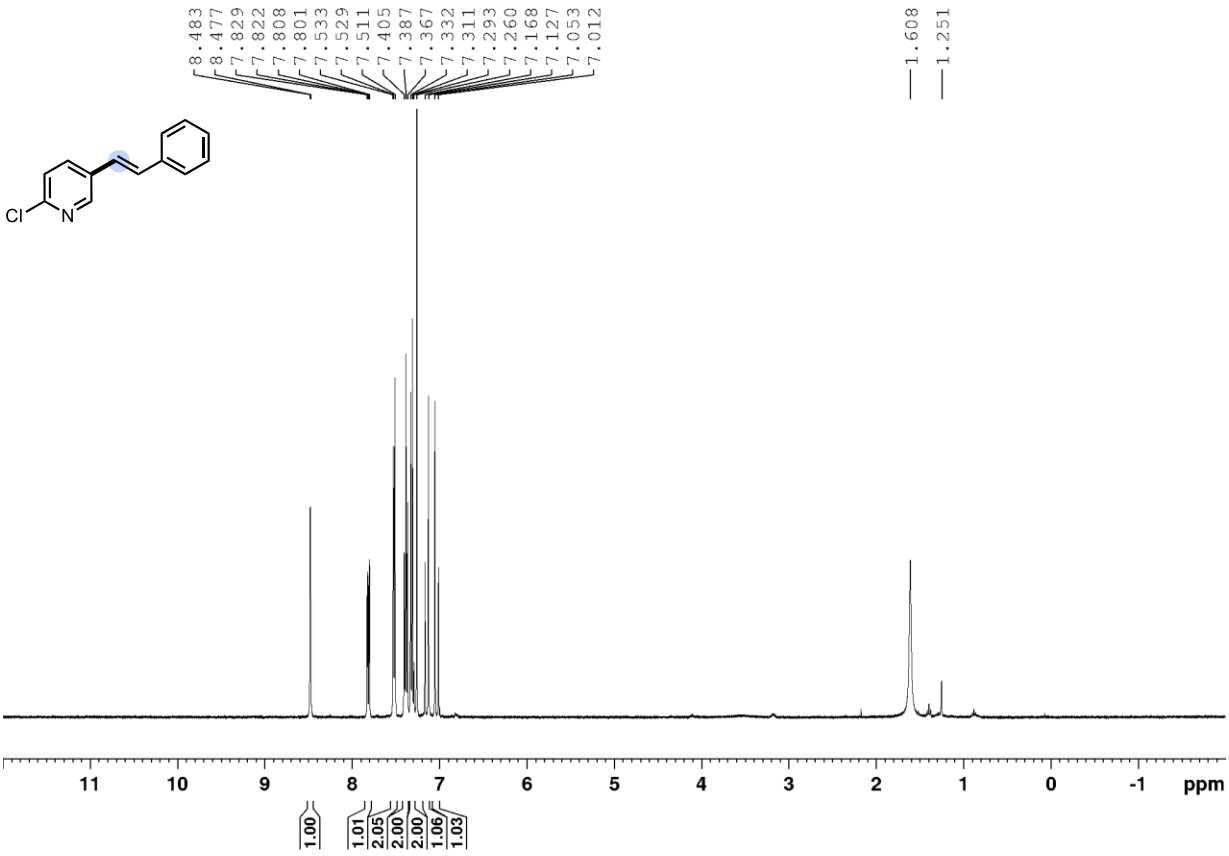

***(E)*-2-Chloro-5-styryl-pyridine (4.17-lin)**, $^{13}C\{^{1}H\}$, $CDCl_3$, 100 MHz

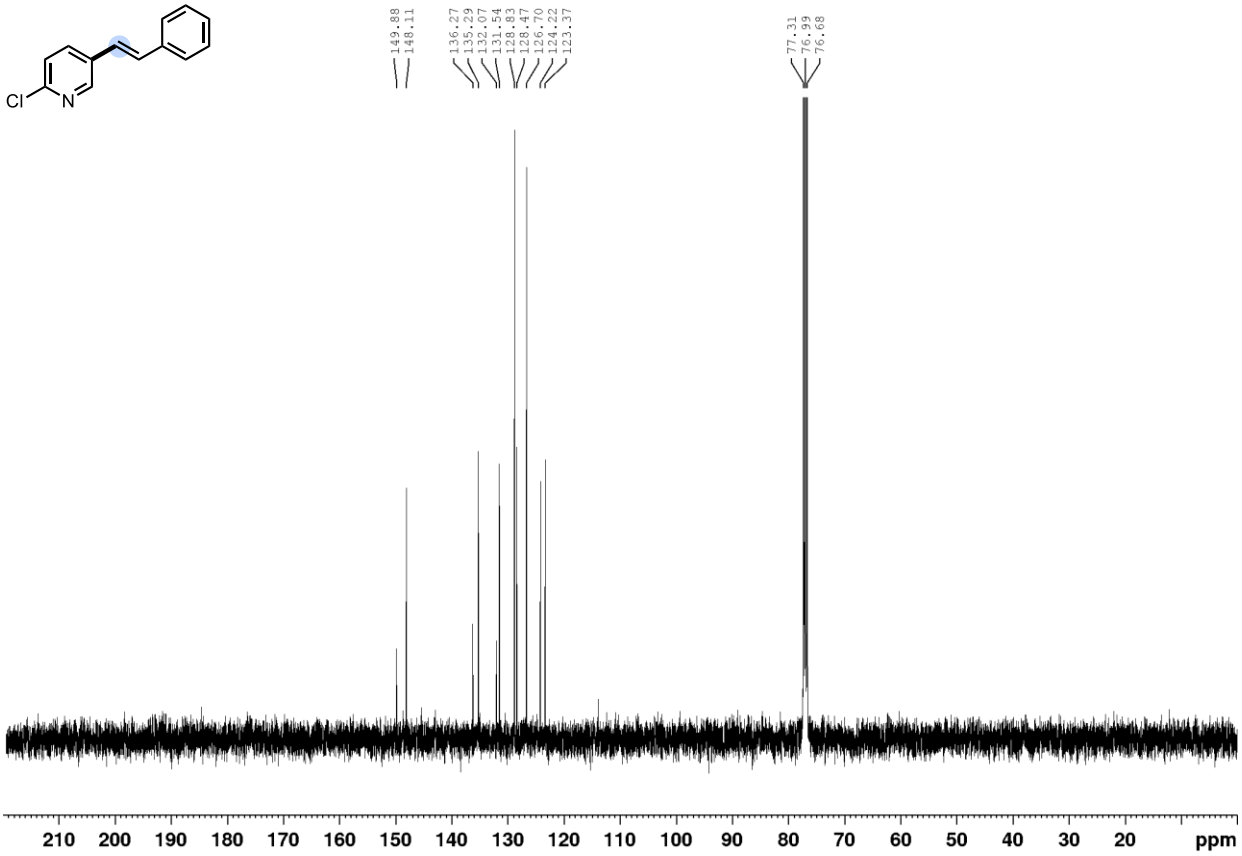

Ethyl (*E*)-4-(8-styryl-5,6-dihydro-11*H*-benzo[5,6]cyclohepta[1,2-*b*]pyridin-11-ylidene)piperidine-1-carboxylate (4.21-lin), ^{1}H, $CDCl_3$, 300 MHz

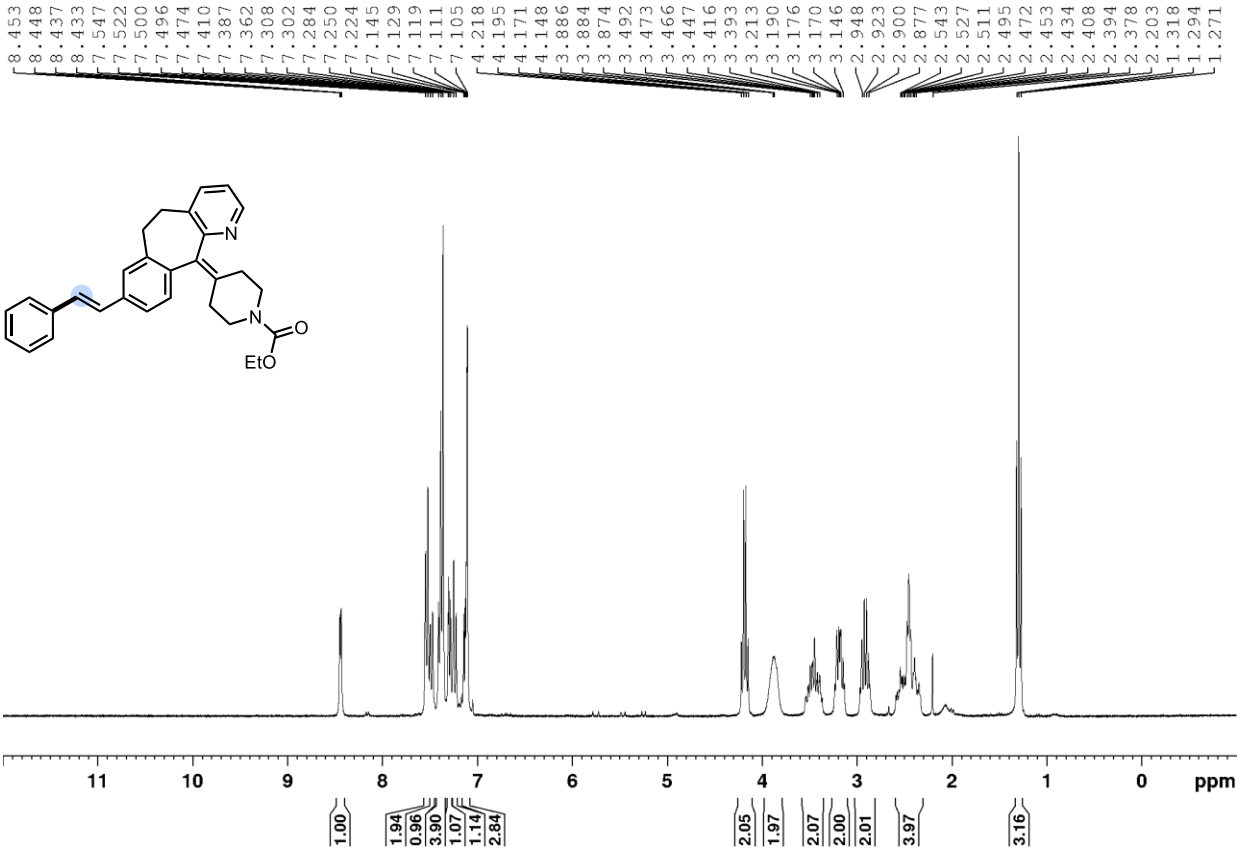

Ethyl (*E*)-4-(8-styryl-5,6-dihydro-11*H*-benzo[5,6]cyclohepta[1,2-*b*]pyridin-11-ylidene)piperidine-1-carboxylate (4.21-lin), $^{13}C\{^{1}H\}$, $CDCl_3$, 75 MHz

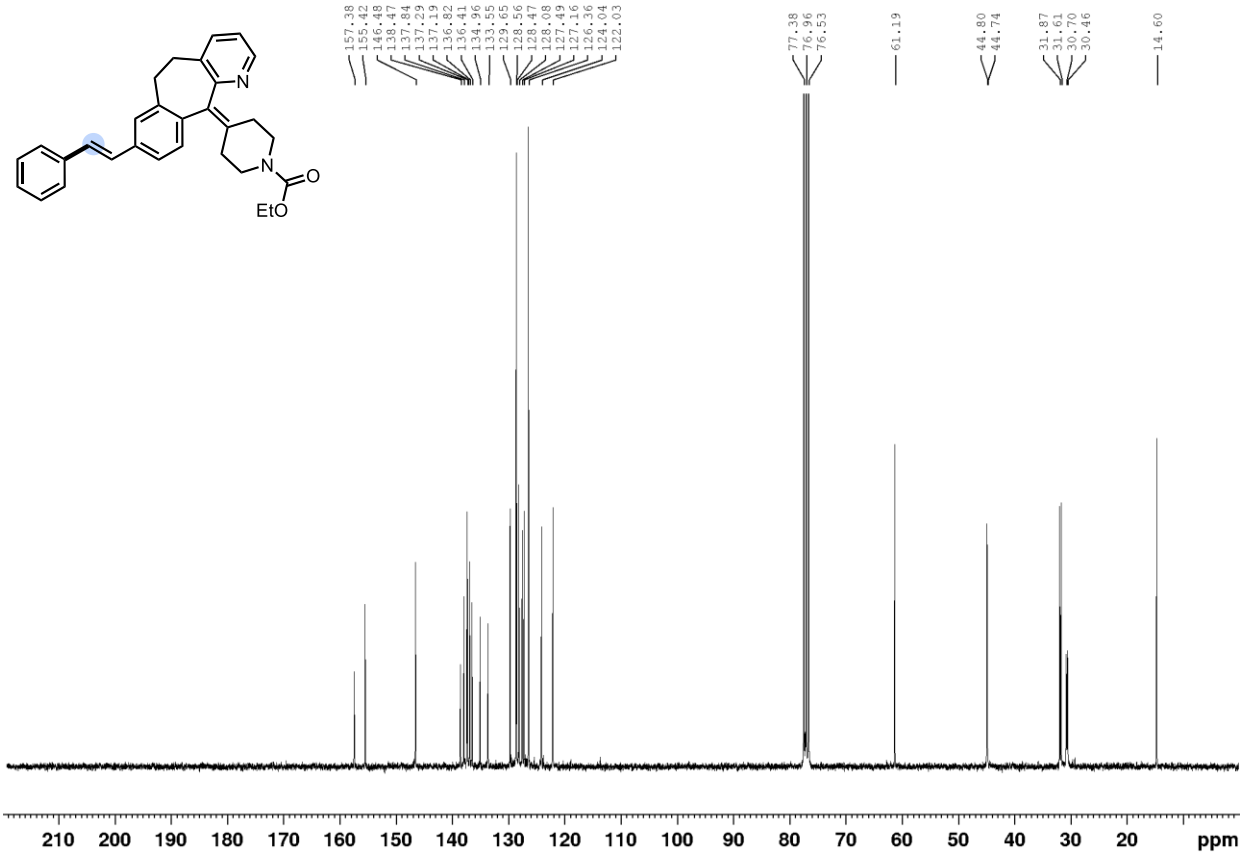

***Trans* combretastatin A-4 (4.23-lin)**, ^{1}H, $CDCl_3$, 400 MHz

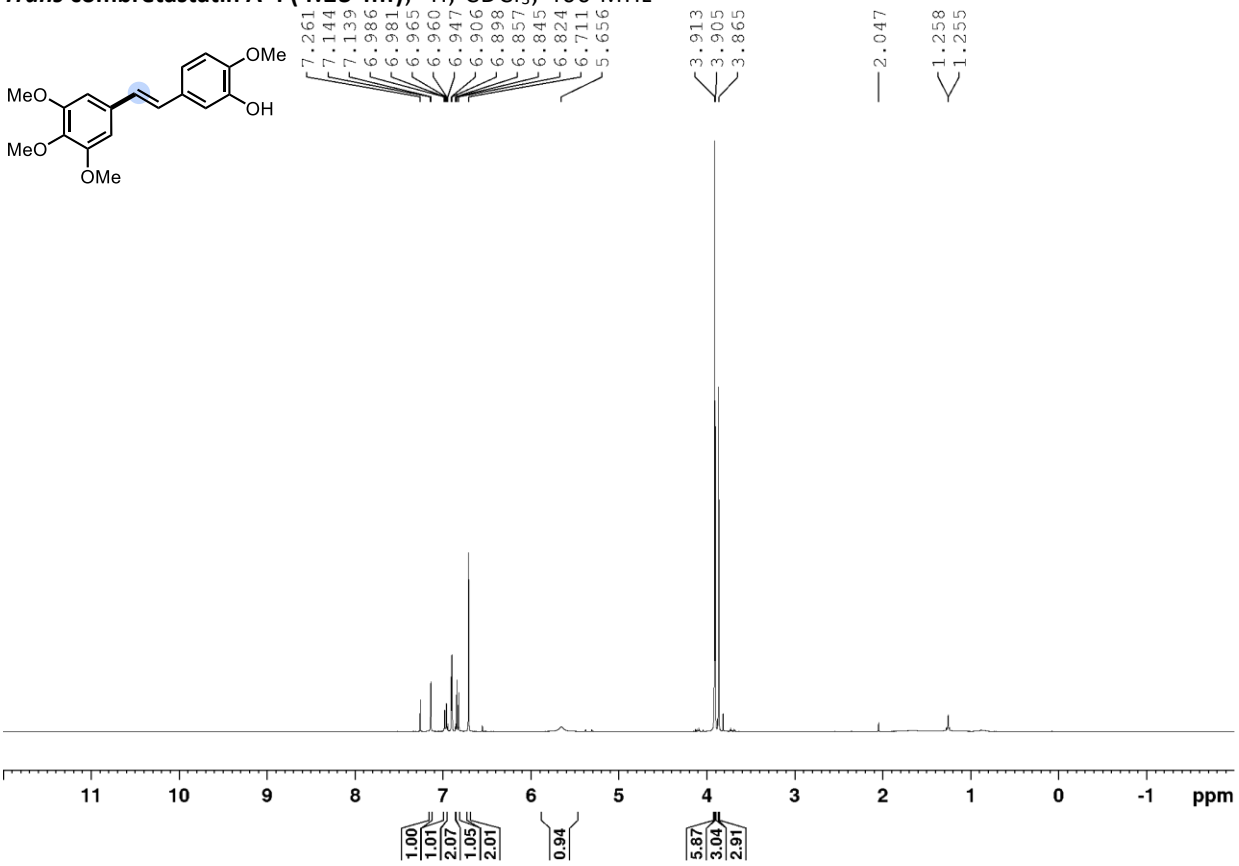

***Trans* combretastatin A4 (4.23-lin)**, $^{13}C\{^{1}H\}$, $CDCl_3$, 100 MHz

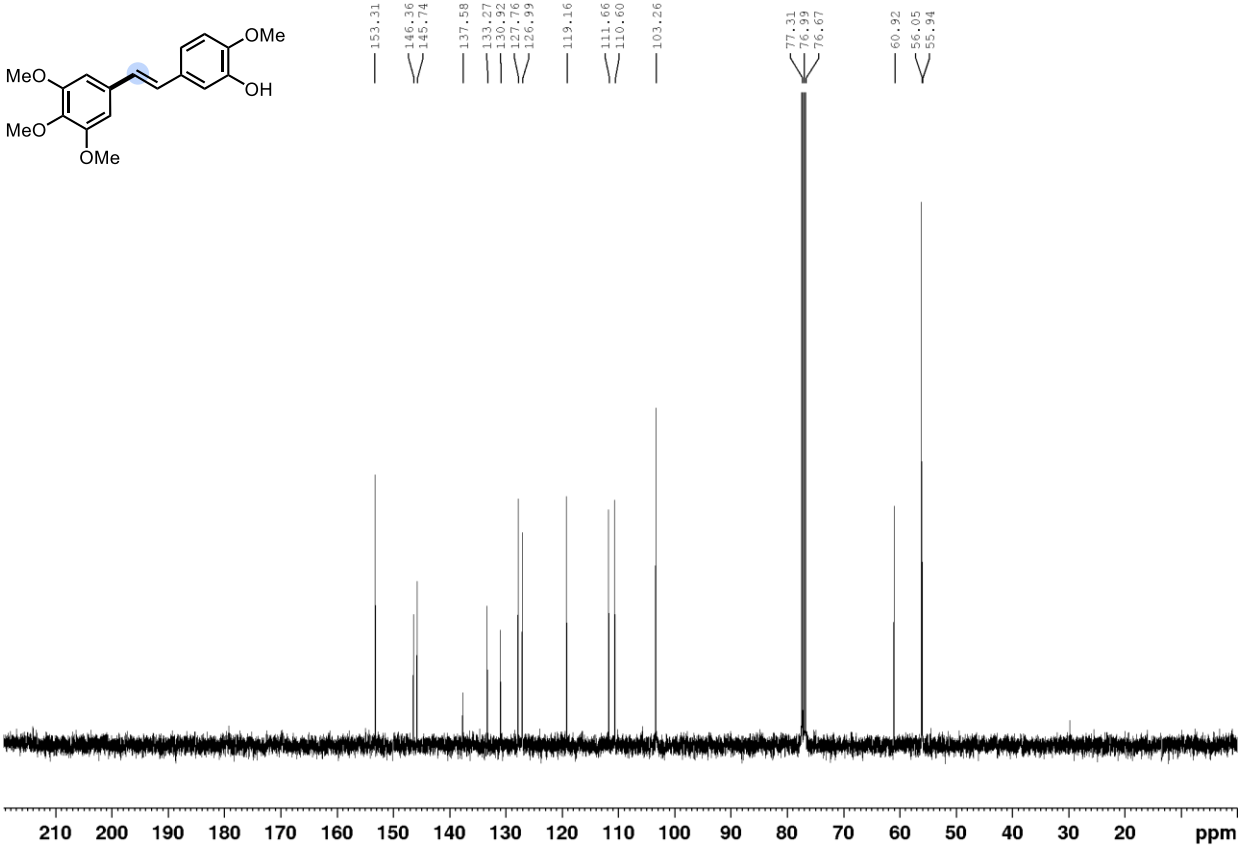

4.7.20 Characterization data for reactions with $P^{tBu}{}_2N^{ArCF3}{}_2$ Pd G3 (4.3) (branched products)

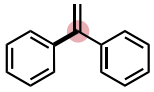

1,1'diphenylethylene (4.7-br) was prepared according to **general procedure B**. Crude br:lin as assessed by GC-FID was 17:1.The product was purified by column chromatography with PhMe to afford **4.7-br** as a colourless oil (32.4 mg, 90% yield). **^{1}H NMR** ($CDCl_3$, 300 MHz) δ (ppm) 7.40-7.30 (m, 10H), 5.48 (s, 2H). **^{13}C{^{1}H} NMR** ($CDCl_3$, 75 MHz) δ (ppm) 150.0, 141.4, 128.2, 128.1, 127.7, 114.3. Spectral data is in accordance with a previous report.[51]

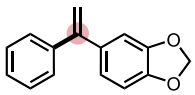

5-(1-Styryl)benzo[1,3]dioxole (4.8-br) was prepared according to **general procedure B**. Crude br:lin as assessed by GC-FID was 18:1. The product was purified by column chromatography with 0% to 4% Et_2O in hexanes. A second column was run in 0% to 20% PhMe in hexanes to afford **4.8-br** as a low melting solid (31.8 mg, 71% yield). **^{1}H NMR** ($CDCl_3$, 300 MHz) δ (ppm) 7.37-7.29 (m, 5H), 6.84-6.80 (m, 2H), 6.79-6.75 (m, 1H), 5.79 (s, 2H), 5.39 (d, J = 1.3 Hz, 1H), 5.36 (d, J = 1.2 Hz, 1H). **^{13}C{^{1}H} NMR** ($CDCl_3$, 75 MHz) δ (ppm) 149.6, 147.4, 147.2, 141.6, 135.7, 128.3, 128.1, 127.7, 122.0, 113.3, 108.6, 107.9, 101.0. Spectral data is in accordance with a previous report.[74]

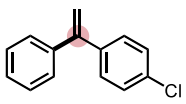

1-(4-chlorophenyl)-1-phenylethene (4.9 -br) was prepared according to **general procedure B**. Crude br:lin as assessed by GC-FID was 10:1.The product was purified by column chromatography with hexanes to afford **4.9-br** as a colourless oil (15.6 mg, 36 % yield). **^{1}H NMR** ($CDCl_3$, 400 MHz) δ (ppm) 7.37-7.26 (m, 9H), 5.47 (d, J = 1.0 Hz, 1H), 5.45 (d, J = 1.0 Hz, 1H). **^{13}C{^{1}H} NMR** ($CDCl_3$, 100 MHz) δ (ppm) 148.9, 141.0, 139.9, 133.6, 129.5, 128.3, 128.25, 128.16, 127.9, 114.7. Spectral data is in accordance with a previous report. [75]

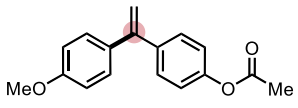

1-(4-Acetoxy-phenyl)-1-(4-methoxy-phenyl)-ethylene (4.10-br) was prepared according to **general procedure B**. Crude br:lin as assessed by GC-FID was >20:1. The product was purified by column chromatography with 2% to 8% Et_2O in hexanes to afford **4.10-br** as a white solid (27.0 mg, 50% yield). **^{1}H NMR** ($CDCl_3$, 300 MHz) δ (ppm) 7.38-7.32 (m, 2H), 7.31-7.24 (d, 2H), 7.08-7.02 (d, 2H), 6.90-6.84 (m, 2H), 5.40-5.38 (m, 1H), 5.35-5.33 (m, 1H), 3.83 (d, J = 1.2 Hz, 3H), 2.31 (d, J = 1.2 Hz, 3H). **^{13}C{^{1}H} NMR** ($CDCl_3$, 100 MHz) δ (ppm) 169.6, 159.5, 150.3, 148.7, 139.6, 133.8, 129.5, 129.4, 121.3, 113.7, 113.3, 55.4, 21.3. **Accurate Mass (EI)** $C_{17}H_{16}O_6$ Theoretical: 268.1094. Found: 268.1146. Spectral Accuracy: 99.4%. **Melting point** 66-70 °C.

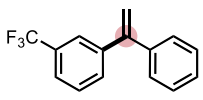

1-(1-phenylvinyl)-3-(trifluoromethyl)benzene (4.11-br) was prepared according to **general procedure B**. Crude br:lin as assessed by GC-FID was 8:1.The product was purified by column chromatography with hexanes to afford **4.11-br** as a colourless oil (41.9 mg, 84% yield). **^{1}H NMR** ($CDCl_3$, 400 MHz) δ (ppm) 7.64 (*br* s, 1H), 7.59 (d, J = 7.6 Hz, 1H), 7.52 (d, J = 7.9 Hz, 1H), 7.46 (t, J = 7.7 Hz, 1H), 7.39-7.31 (m, 5H), 5.57 (d, J = 0.8 Hz, 1H), 5.52 (d, J = 0.8 Hz, 1H). **^{13}C{^{1}H} NMR** ($CDCl_3$, 100 MHz) δ (ppm) 148.9, 142.3,

140.6, 131.6, 130.6 (q, *J* = 32.1 Hz), 128.6, 128.4, 128.10, 128.09, 124.9 (q, *J* = 3.8 Hz), 124.4 (q, *J* = 3.8 Hz), 124.1 (q, *J* = 274.9 Hz), 115.6. **^{19}F{^{1}H} NMR** ($CDCl_3$, 376 MHz) *δ* (ppm) -62.5. Spectral data is in accordance with a previous report.[75]

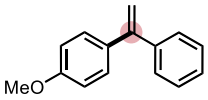

1-(4-methoxyphenyl)-1-phenylethene (4.12-br) was prepared according to **general procedure B**. Crude br:lin as assessed by GC-FID was >20:1. The product was purified by column chromatography with 0% to 4% Et_2O in hexanes to afford **4.12-br** as a white solid (39.9 mg, 95% yield). **^{1}H NMR** ($CDCl_3$, 300 MHz) *δ* (ppm) 7.40-7.26 (m, 7H), 6.91-6.85 (m, 2H), 5.42 (d, *J* = 1.3 Hz, 1H), 5.37 (d, *J* = 1.3 Hz, 1H), 3.84 (s, 3H). **^{13}C{^{1}H} NMR** ($CDCl_3$, 100 MHz) *δ* (ppm) 159.3, 149.5, 141.8, 133.9, 129.4, 128.3, 128.1, 127.6, 113.5, 112.9, 55.3. Spectral data is in accordance with a previous report.[76]

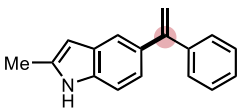

2-methyl-5-(1-phenylvinyl)-1*H*-indole (4.13-br) was prepared according to **general procedure B**. Crude br:lin as assessed by GC-FID was >20:1. The product was purified by column chromatography (SiO_2 was neutralized with trimethylamine prior to starting) with 0% to 20% EtOAc in hexanes to afford **4.13-br** as a colourless oil (40.2 mg, 86% yield). **^{1}H NMR** (C_6D_6, 400 MHz) *δ* (ppm) 7.74 (t, *J* = 0.7 Hz, 1H), 7.53-7.49 (m, 2H), 7.36 (dd, *J* = 8.4 Hz, 1.7 Hz, 1H), 7.19-7.09 (m, 4H), 6.97 (d, *J* = 8.4 Hz, 1H), 6.43 (*br* s, 1H), 6.09 (t, *J* = 1.0 Hz, 1H), 5.57 (d, *J* = 1.6 Hz, 1H), 5.46 (d, *J* = 1.6 Hz, 1H), 1.87 (d, *J* = 0.7 Hz, 1H). **^{13}C{^{1}H} NMR** (C_6D_6, 125 MHz) *δ* (ppm) 152.0, 143.3, 136.3, 135.0, 133.8, 129.7, 128.9, 128.3, 127.7, 122.1, 120.2, 112.7, 110.1, 101.0, 13.3. **Accurate Mass (EI)** $C_{17}H_{15}N$ Theoretical: 233.1199. Found: 233.1226. Spectral Accuracy: 97.6% **Note:** Title compound decomposes through hydrolysis over time in acidic media such as $CDCl_3$.

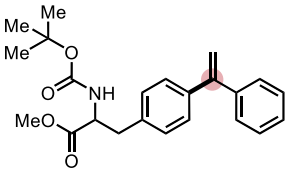

Methyl 2-((tert-butoxycarbonyl)amino)-3-(4-(1-phenylvinyl)phenyl)propanoate (4.14-br) was prepared according to **general procedure B**. Crude br:lin as assessed by ^{1}H NMR was 9.5:1.The product was purified by column chromatography with 10% to 20% EtOAc in hexanes, followed by a second column with 5% to 12% EtOAc in hexanes to afford **4.14-br** as a colourless oil (56.4 mg, 74% yield). Mixture of rotamers, consistent with starting triflate.[72] **^{1}H NMR** ($CDCl_3$, 300 MHz); *δ* (ppm) 7.35-7.30 (m, 5H), 7.29-7.25 (m, 2H), 7.12-7.07 (m, 2H), 5.45 (d, *J* = 1.2 Hz, 1H), 5.43 (d, *J* = 1.2 Hz, 1H), 5.02 (d, *J* = 8.1 Hz, 0.85H), 4.75 (*br* s, 0.15H), 4.61 (q, *J* = 6.5 Hz, 0.85H), 4.42 (*br* s, 0.15H), 3.73 (s, 3H), 3.15 (dd, *J* = 13.8 Hz, 5.4 Hz 1H), 3.05 (dd, *J* = 14.0 Hz, 6.4 Hz 1H), 1.42 (s, 9H). **^{13}C{^{1}H} NMR** ($CDCl_3$, 75 MHz) *δ* (ppm) 172.3, 155.0, 149.6, 141.4, 140.1, 135.5, 129.1, 128.3, 128.2, 128.1, 127.7, 114.2, 79.9, 54.3, 52.2, 38.0, 28.2. **Accurate mass (ESI+):** m/z calculated for [$C_{23}H_{27}NO_4Na$] Theoretical: 404.1838. Found: 404.1818.

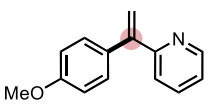

2-(1-(4-methoxyphenyl)vinyl)pyridine (4.18-br) was prepared according to **general procedure B**. Crude br:lin as assessed by GC-FID was 9:1. The product was purified by column chromatography with 25% to 35% Et_2O in hexanes to afford **4.18-br** as a colourless oil (30.6 mg, 72% yield). **^{1}H NMR** ($CDCl_3$, 300 MHz) *δ* (ppm) 8.64 (ddd, *J* = 4.8, 1.8, 0.9 Hz, 1H), 7.64 (m, 1H), 7.31 - 7.27 (m, 3H), 7.21 (ddd, *J* = 7.5, 4.8, 1.2 Hz, 1H), 6.91 - 6.87 (m, 2H), 5.86 (d, *J* = 1.5 Hz, 1H), 5.56 (d, *J* = 1.5 Hz, 1H), 3.83

(s, 3H). **$^{13}C\{^{1}H\}$ NMR** ($CDCl_3$, 100 MHz) δ (ppm) 159.3, 158.9, 149.3, 148.6, 136.2, 132.8, 129.5, 122.8, 122.3, 116.5, 113.6, 55.3. Spectral data is in accordance with a previous report.[77]

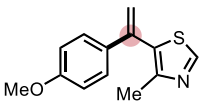

5-(1-(4-methoxyphenyl)vinyl)-4-methylthiazole (4.19-br) was prepared according to **general procedure B**. Crude br:lin as assessed by GC-FID was >20:1. The product was purified by column chromatography with 10% to 20% EtOAc in hexanes to afford **4.19-br** as a colourless oil (16.3 mg, 35% yield). **^{1}H NMR** ($CDCl_3$, 500 MHz) δ (ppm) 8.68 (br s, 1H), 7.27-7.24 (m, 2H), 6.88-6.85 (m, 2H), 5.66 (d, J = 0.88 Hz, 1H), 5.32 (d, J = 0.80 Hz, 1H), 3.82 (s, 3H), 2.28 (s, 3H). **$^{13}C\{^{1}H\}$ NMR** ($CDCl_3$, 125 MHz) δ (ppm) 159.7, 150.5, 150.4, 139.2, 132.7, 131.8, 128.3, 116.9, 113.7, 55.3, 16.2. **Accurate Mass (EI)** $C_{13}H_{13}NOS$ Theoretical: 231.0712. Found: 231.0746. Spectral Accuracy: 98.8%.

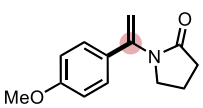

N-(1-[4-methoxyphenyl]ethenyl)-2-pyrrolidinone (4.20-br) was prepared according to **general procedure B**. Crude α:β as assessed by GC-FID was >20:1.The product was purified by column chromatography with 50% to 70% EtOAc in hexanes to afford **4.20-br** as a light yellow oil (38.6 mg, 89% yield). **^{1}H NMR** ($CDCl_3$, 500 MHz) δ (ppm) 7.26 (d, J = 8.8 Hz, 2H), 6.86 (d, J = 8.8 Hz, 2H), 5.31 (s, 1H), 5.18 (s, 1H), 3.80 (s, 3H), 3.53 (*apparen*t t, J = 7.0 Hz, 2H), 2.54 (m, 2H), 2.09 (quint, J = 6.0 Hz, 2H). **$^{13}C\{^{1}H\}$ NMR** ($CDCl_3$, 125 MHz) δ (ppm) 174.5, 159.8, 143.1, 130.5, 128.6, 127.5, 113.7, 107.8, 55.2, 49.6, 31.9, 18.5. Spectral data is in accordance with a previous report.[78]

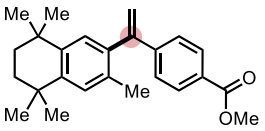

Methyl-4-[1-(5,6,7,8-Tetrahydro-3,5,5,8,8-pentamethyl-2-naphthalenyl)ethenyl]-benzoate (4.22-br) was prepared according to **general procedure B**. Crude br:lin as assessed by GC-FID was 20:1. The product was purified by column chromatography with 1% to 2% Et_2O in hexanes to afford **4.22-br** as a white solid (52.3 mg, 71% yield). **^{1}H NMR** ($CDCl_3$, 300 MHz) δ (ppm) 7.96 (d, J = 8.6 Hz, 2H), 7.35 (d, J = 8.6 Hz, 2H), 7.14 (s, 1H), 7.08 (s, 1H), 5.81 (d, J = 1.3 Hz, 1H), 5.33 (d, J = 1.3 Hz, 1H), 3.91 (s, 3H), 1.95 (s, 3H), 1.71 (s, 4H), 1.31 (s, 6H), 1.28 (s, 6H). **$^{13}C\{^{1}H\}$ NMR** ($CDCl_3$, 75 MHz) δ (ppm) 166.9, 149.1, 145.5, 144.3, 142.3, 138.0, 132.7, 129.6, 128.9, 128.03, 128.00, 126.5, 116.8, 52.0, 35.1, 34.0, 33.8, 31.9, 31.8, 19.9. Spectral data is in accordance with a previous report.[79]

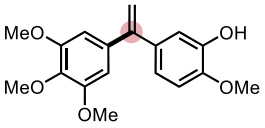

Isocombretastatin A4 (4.23-br) was prepared according to **general procedure B**. Crude br:lin as assessed by GC-FID was 12.5:1.The product was purified by column chromatography with 20% to 35% EtOAc in hexanes to afford **4.23-br** as an off-white solid (32.8 mg, 52% yield). **^{1}H NMR** ($CDCl_3$, 400 MHz) δ (ppm) 6.97 (d, J = 2.0 Hz, 1H), 6.85 (dd, J = 8.3 Hz, 2.0 Hz, 1H), 6.81 (d, J = 8.4 Hz, 1H), 6.55 (s, 2H), 5.60 (*br* s, 1H), 5.38 (d, J = 1.2 Hz, 1H), 5.31 (d, J = 1.2 Hz, 1H), 3.91 (s, 3H), 3.87 (s, 3H), 3.82 (s, 6H). **$^{13}C\{^{1}H\}$ NMR** ($CDCl_3$, 100 MHz) δ (ppm)152.7, 149.5, 146.3, 145.1, 137.4, 134.6, 120.1, 114.4, 112.8, 110.1, 105.6, 60.9, 56.1, 55.9. Spectral data is in accordance with a previous report.[80]

4.7.21 NMR spectra for reactions with $P^{tBu}{}_2N^{ArCF3}{}_2$ Pd G3 (4.3) (branched products)

1,1'-diphenylethylene (4.7-br), ^1H, $CDCl_3$, 400 MHz

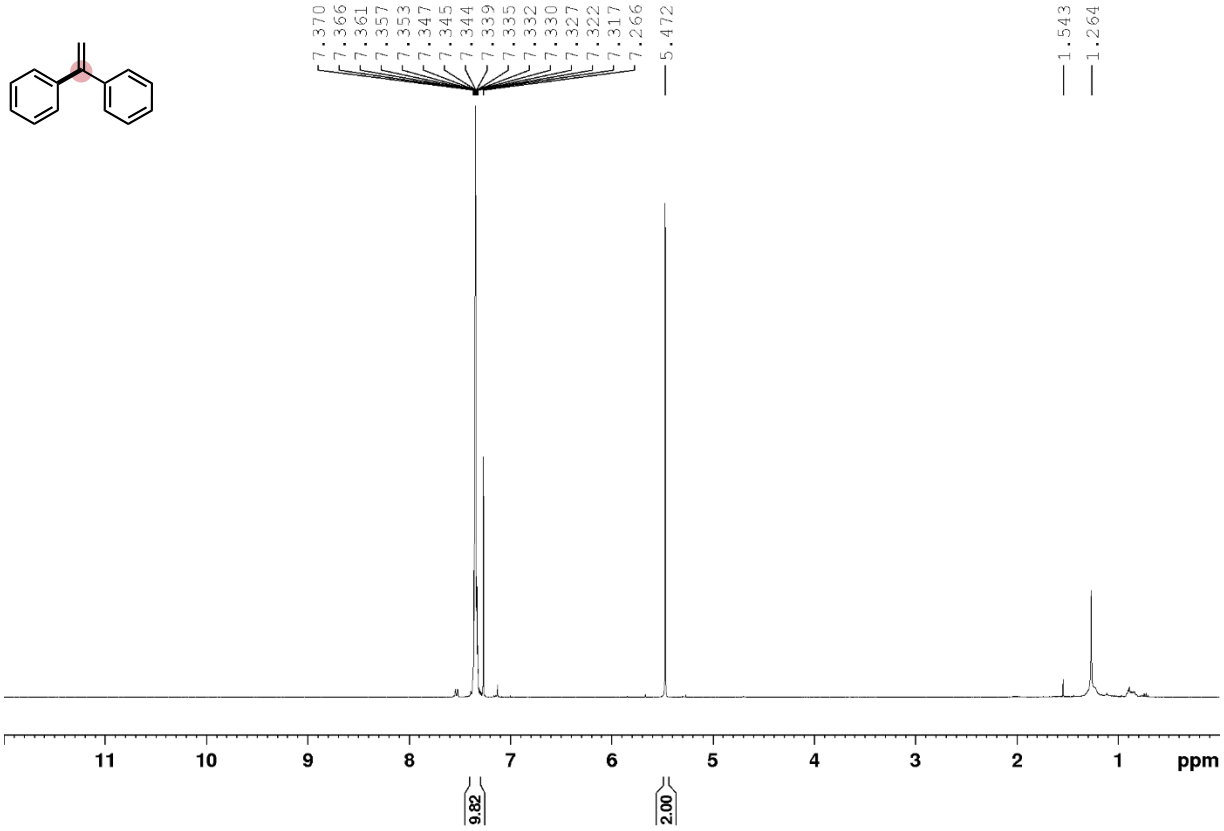

1,1'-diphenylethylene (4.7-br), ^{13}C, $CDCl_3$, 100 MHz

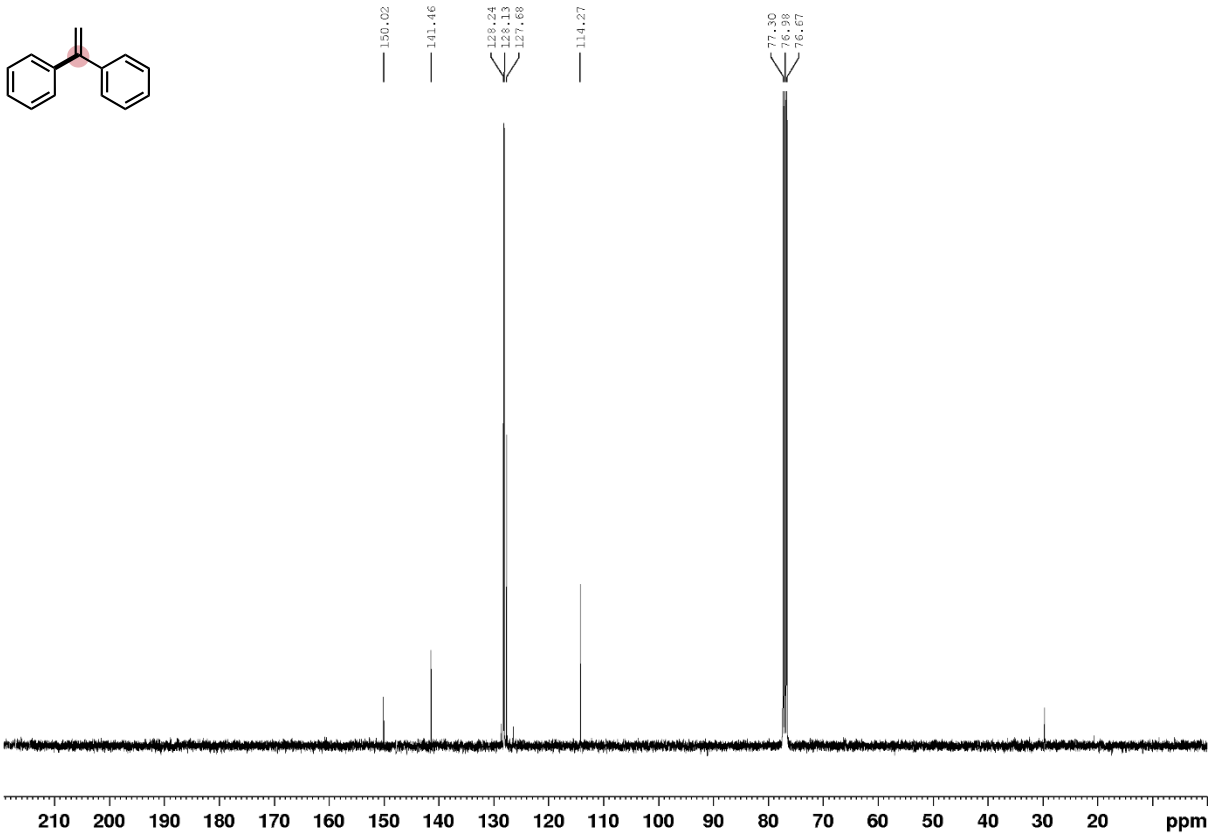

5-(1-Styryl)benzo[1,3]dioxole (4.8-br), ^{1}H, $CDCl_3$, 300 MHz

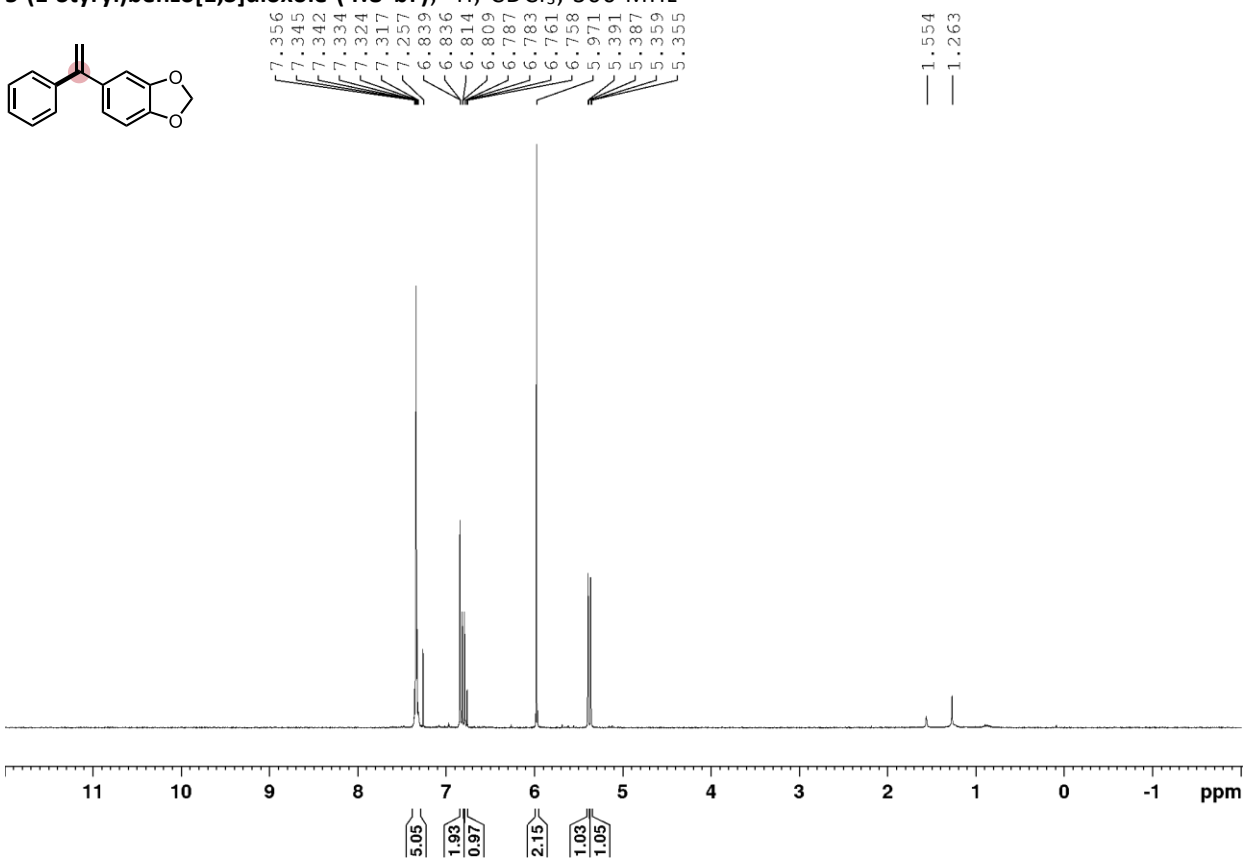

5-(1-Styryl)benzo[1,3]dioxole (4.8-br), $^{13}C\{^{1}H\}$, $CDCl_3$, 75 MHz

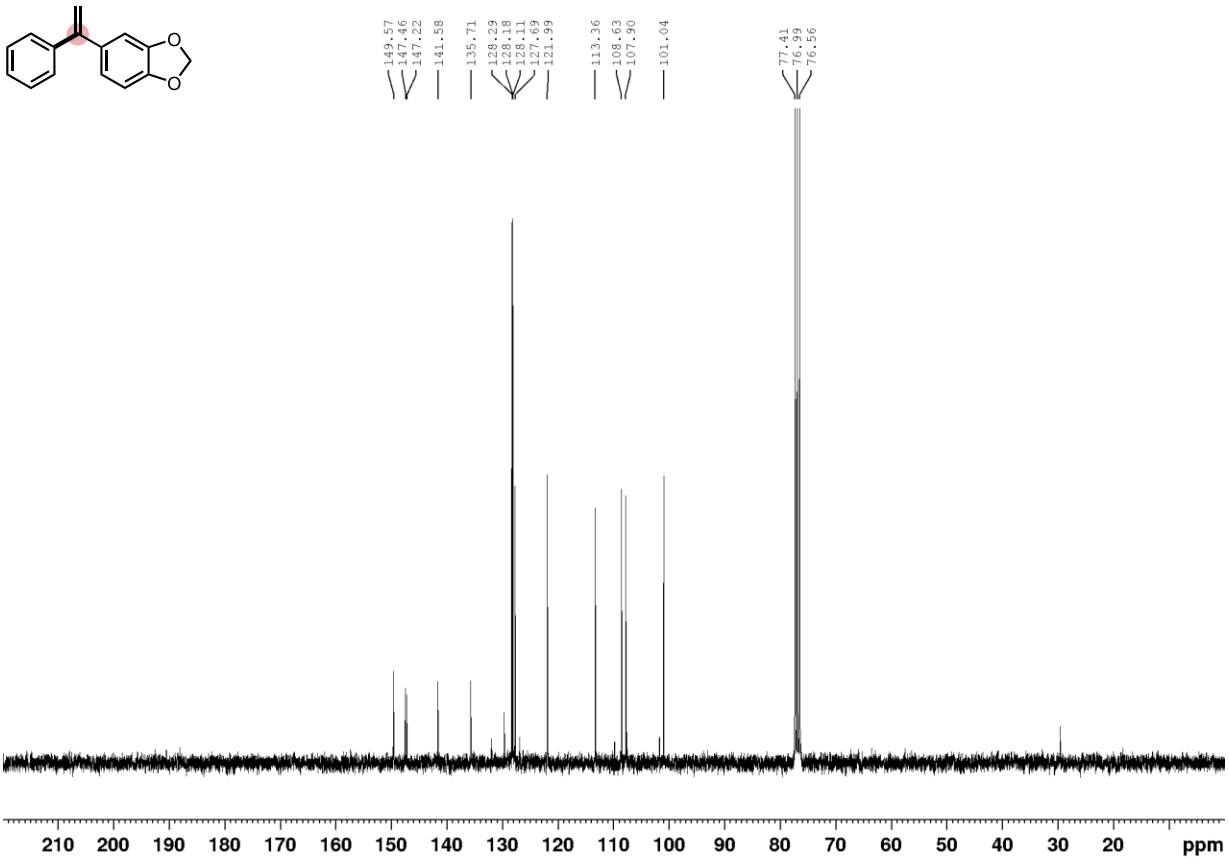

1-(4-chlorophenyl)-1-phenylethene (4.9-br), ^{1}H, $CDCl_3$, 400 MHz

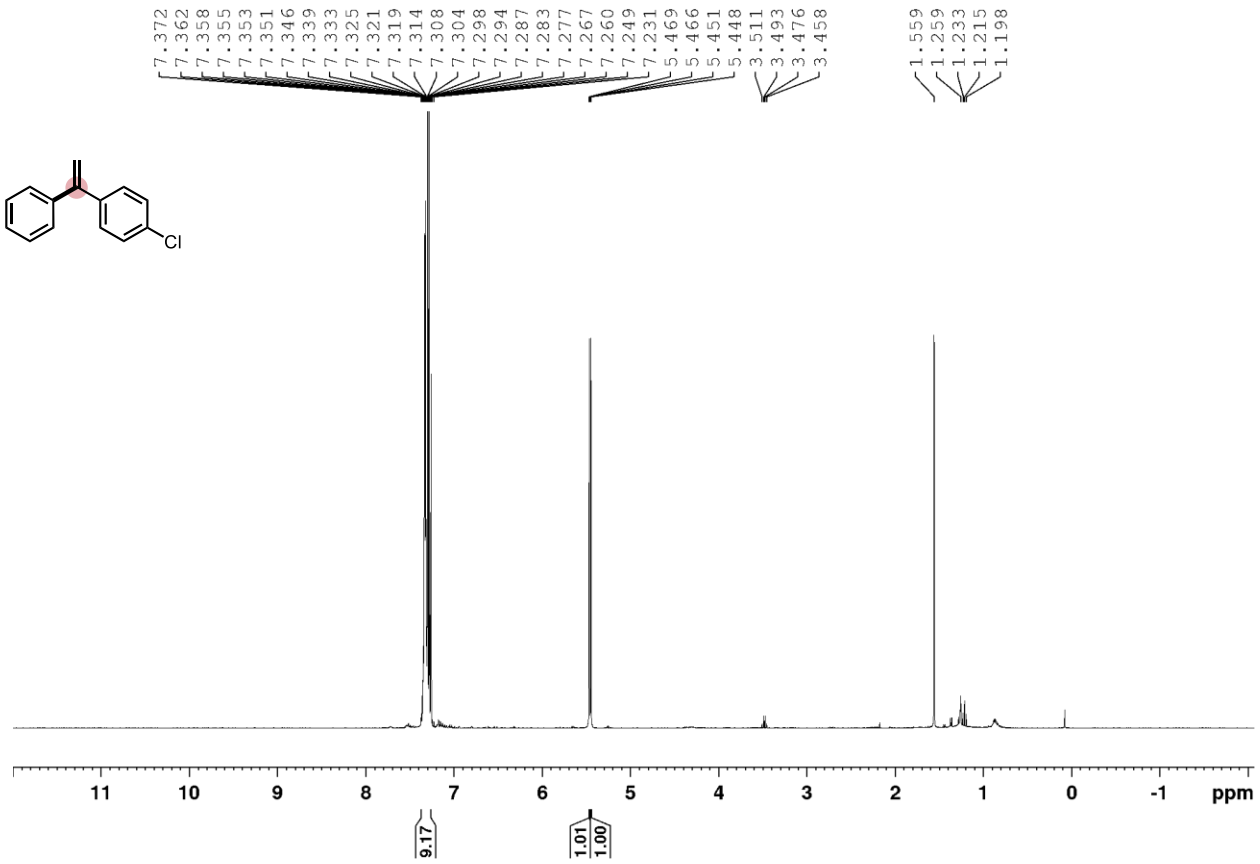

1-(4-chlorophenyl)-1-phenylethene (4.9-br), $^{13}C\{^{1}H\}$, $CDCl_3$, 100 MHz

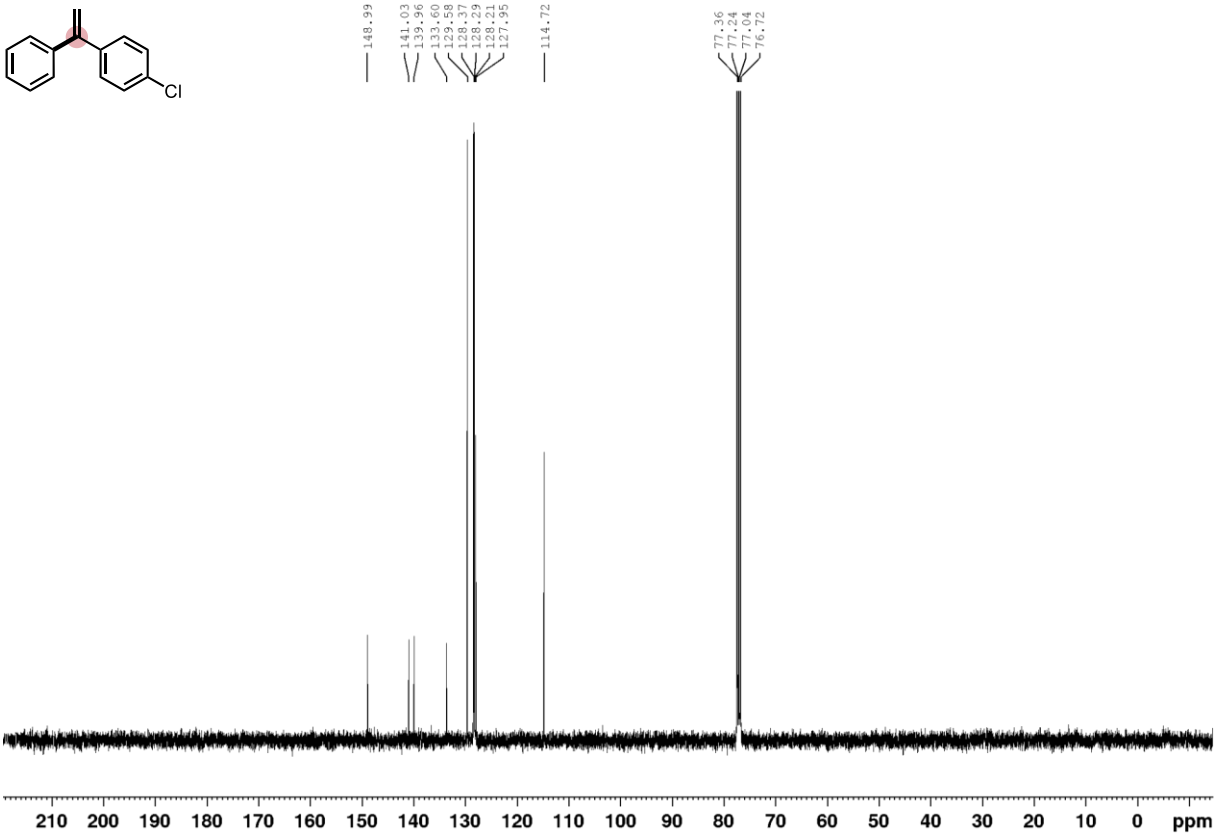

1-(4-Acetoxy-phenyl)-1-(4-methoxy-phenyl)-ethylene (4.10-br), ^{1}H, $CDCl_3$, 300 MHz

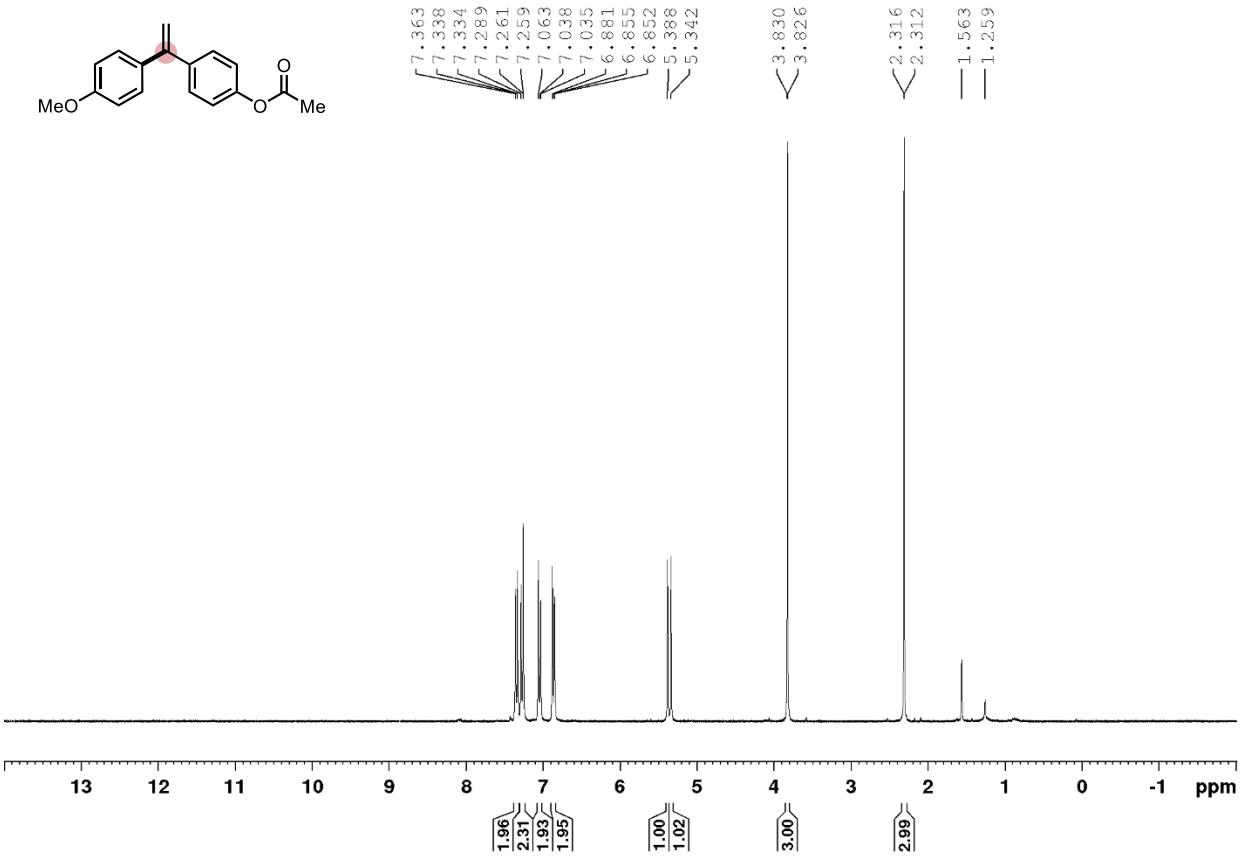

1-(4-Acetoxy-phenyl)-1-(4-methoxy-phenyl)-ethylene (4.9-br), $^{13}C\{^{1}H\}$, $CDCl_3$, 75 MHz

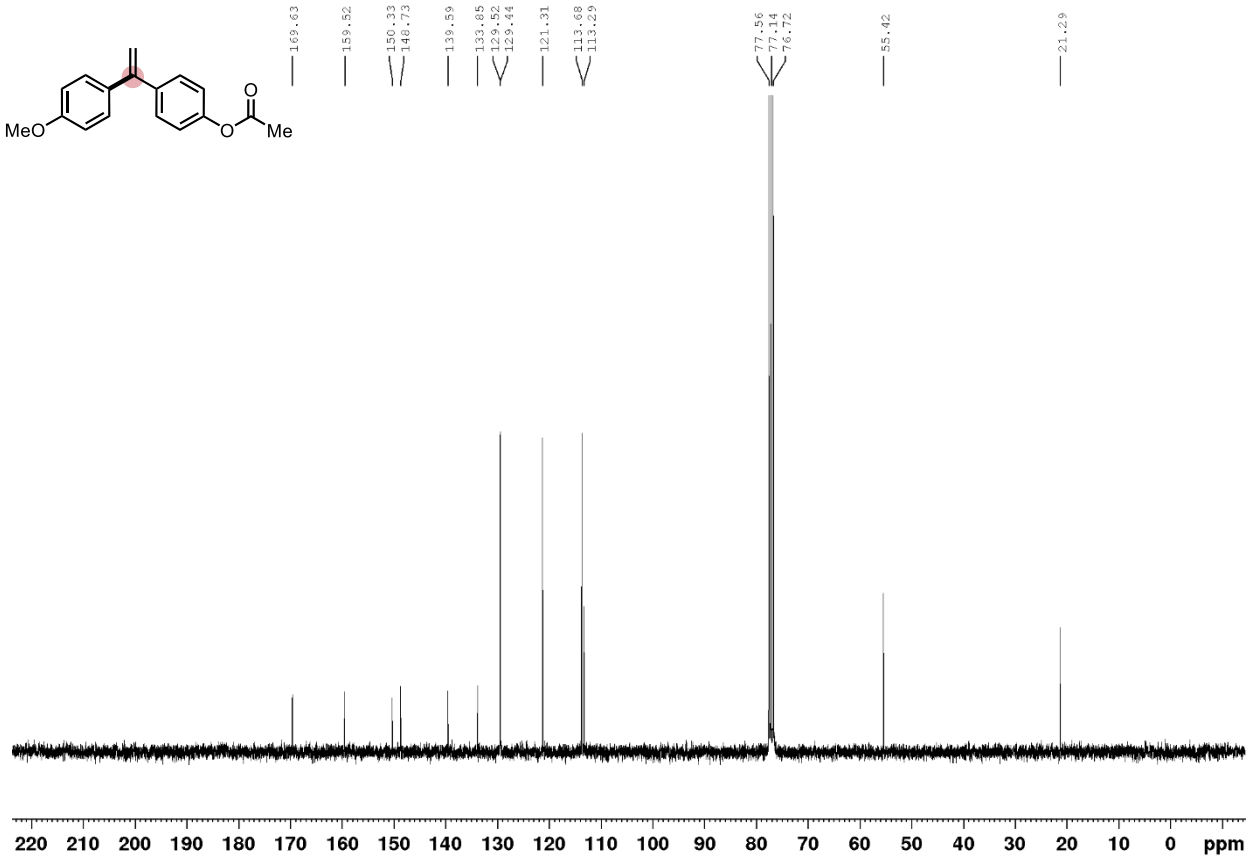

1-(1-phenylvinyl)-3-(trifluoromethyl)benzene (4.11-br), ^{1}H, $CDCl_3$, 400 MHz

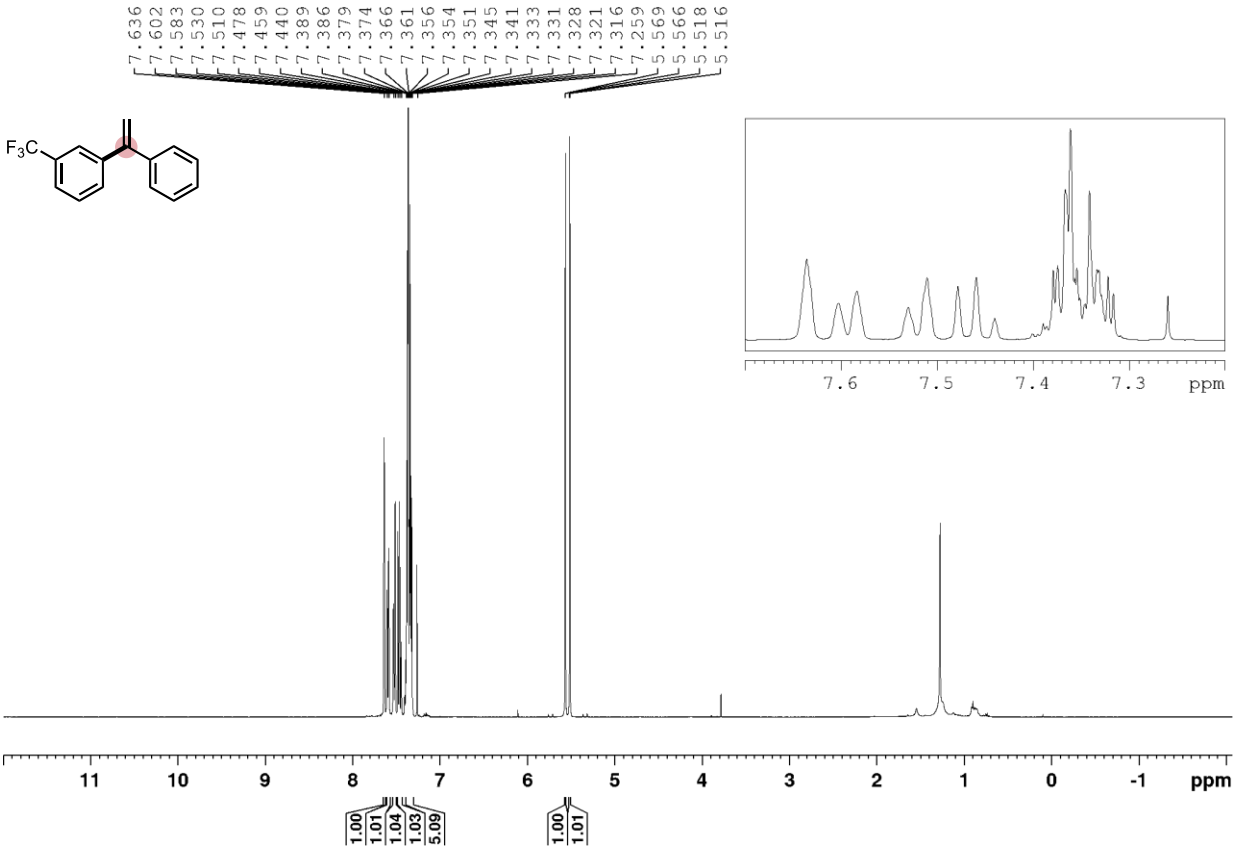

1-(1-phenylvinyl)-3-(trifluoromethyl)benzene (4.11-br), $^{13}C\{^{1}H\}$, $CDCl_3$, 100 MHz

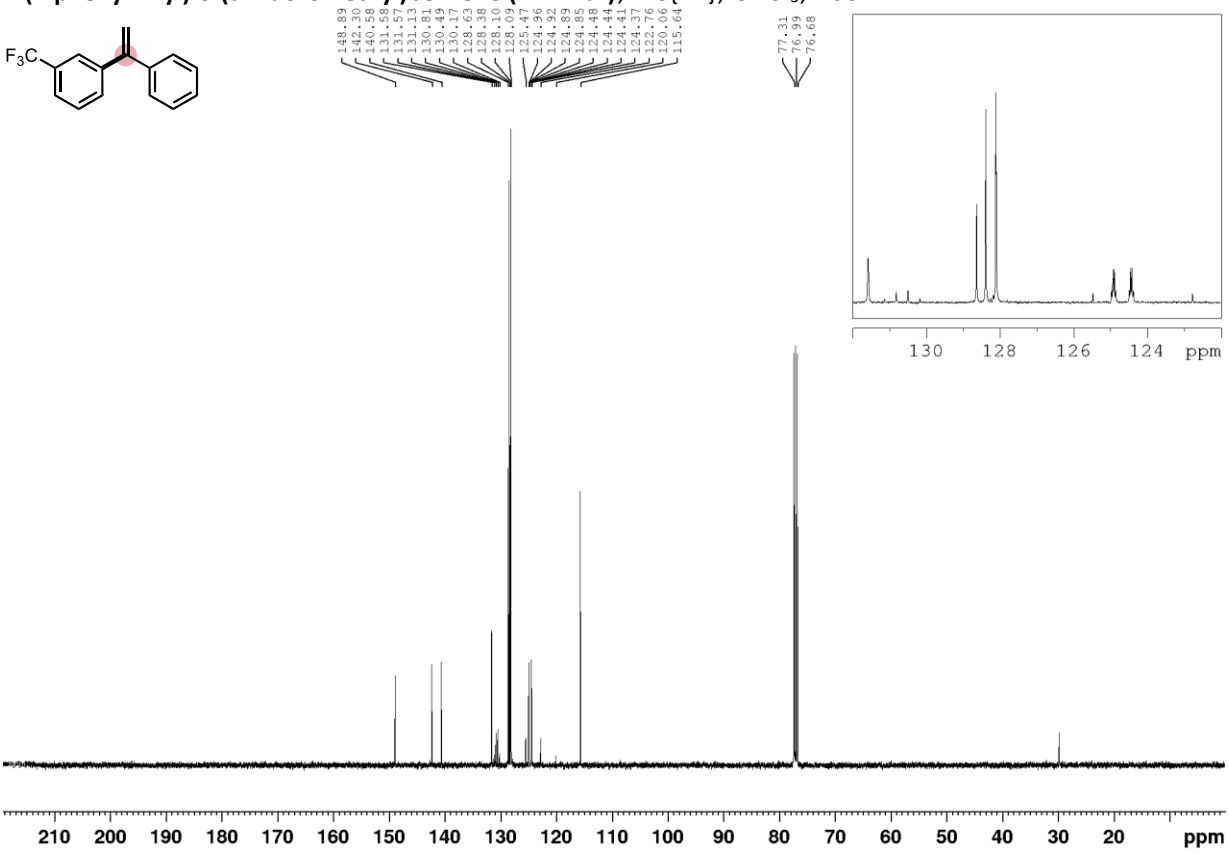

1-(1-phenylvinyl)-3-(trifluoromethyl)benzene (4.11-br), $^{19}F\{^{1}H\}$, $CDCl_3$, 376 MHz

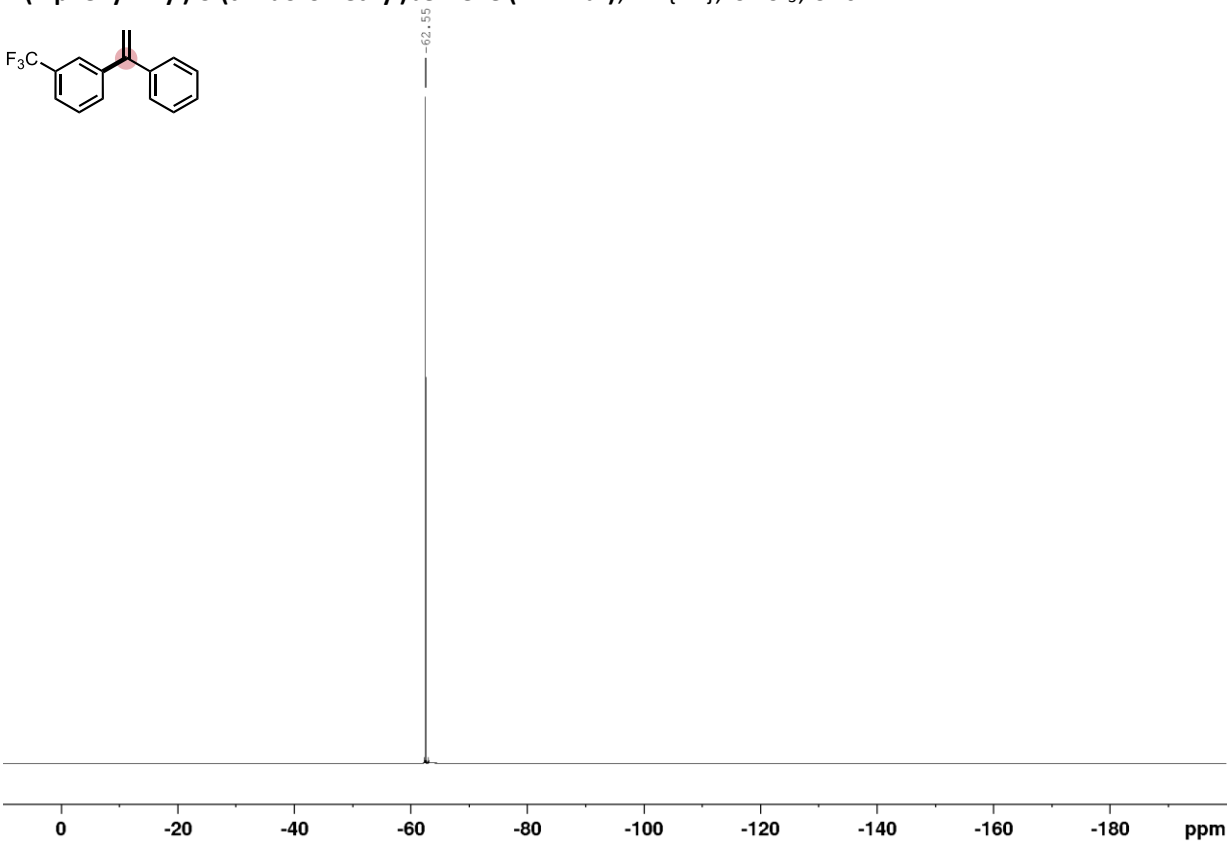

1-(4-methoxyphenyl)-1-phenylethene (4.12-br), ^{1}H, $CDCl_3$, 300 MHz

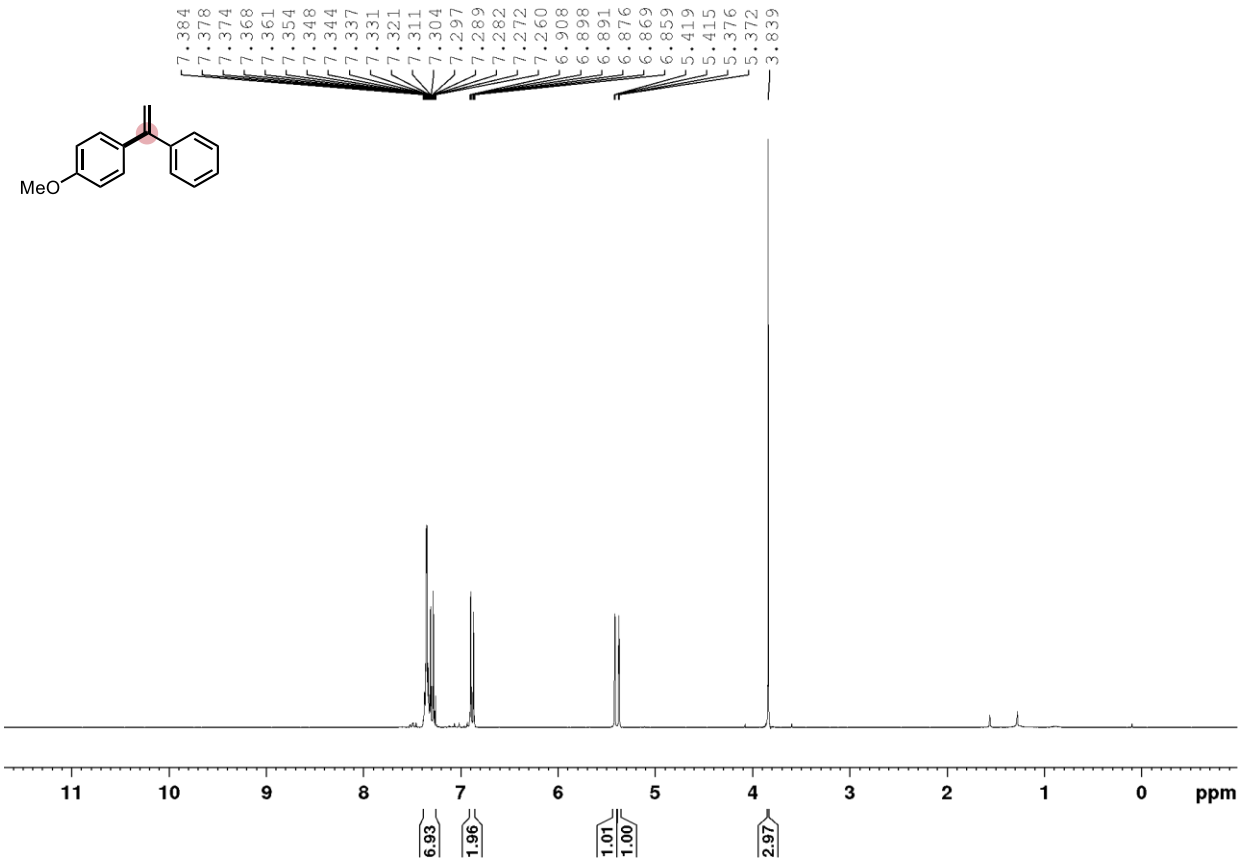

1-(4-methoxyphenyl)-1-phenylethene (4.12-br), $^{13}C\{^{1}H\}$, $CDCl_3$, 75 MHz

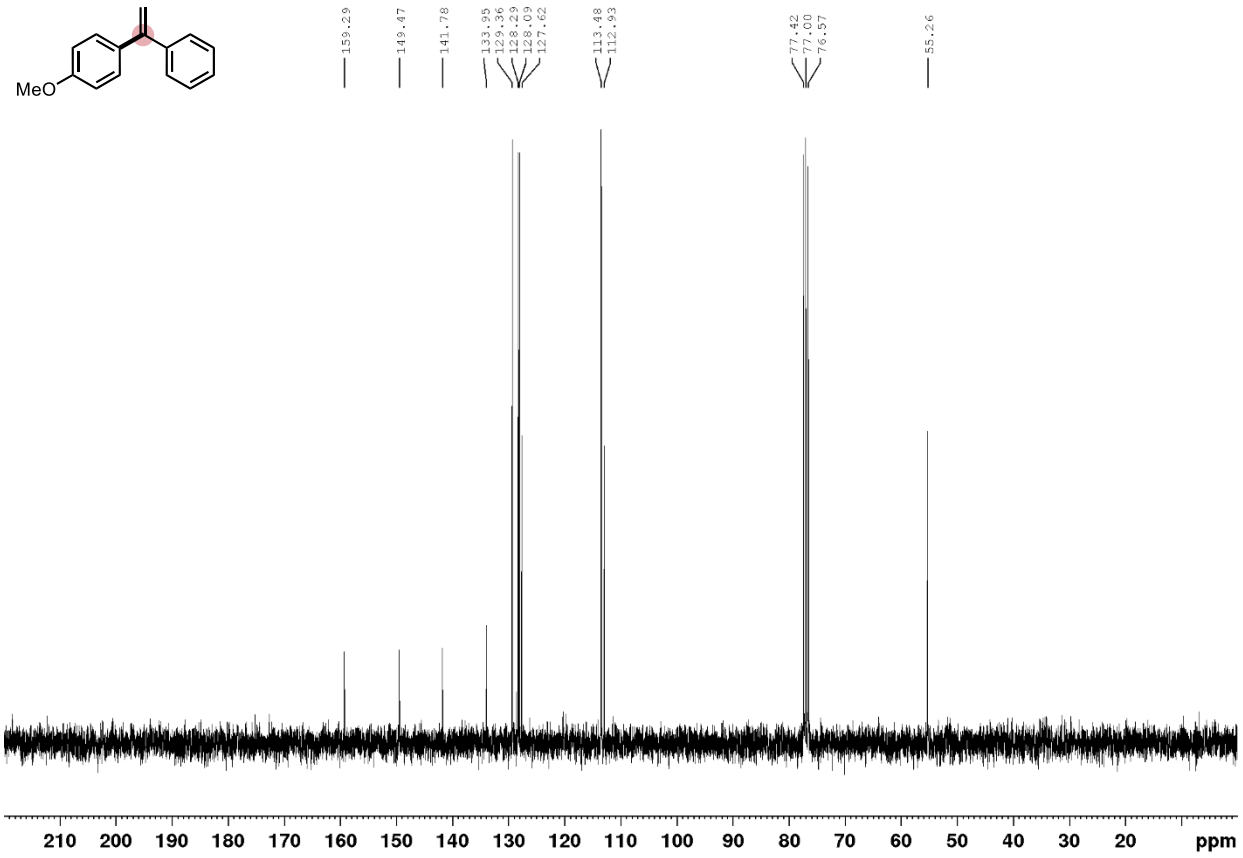

2-methyl-5-(1-phenylvinyl)-1*H*-indole (4.13-br), ^{1}H, C_6D_6, 400 MHz

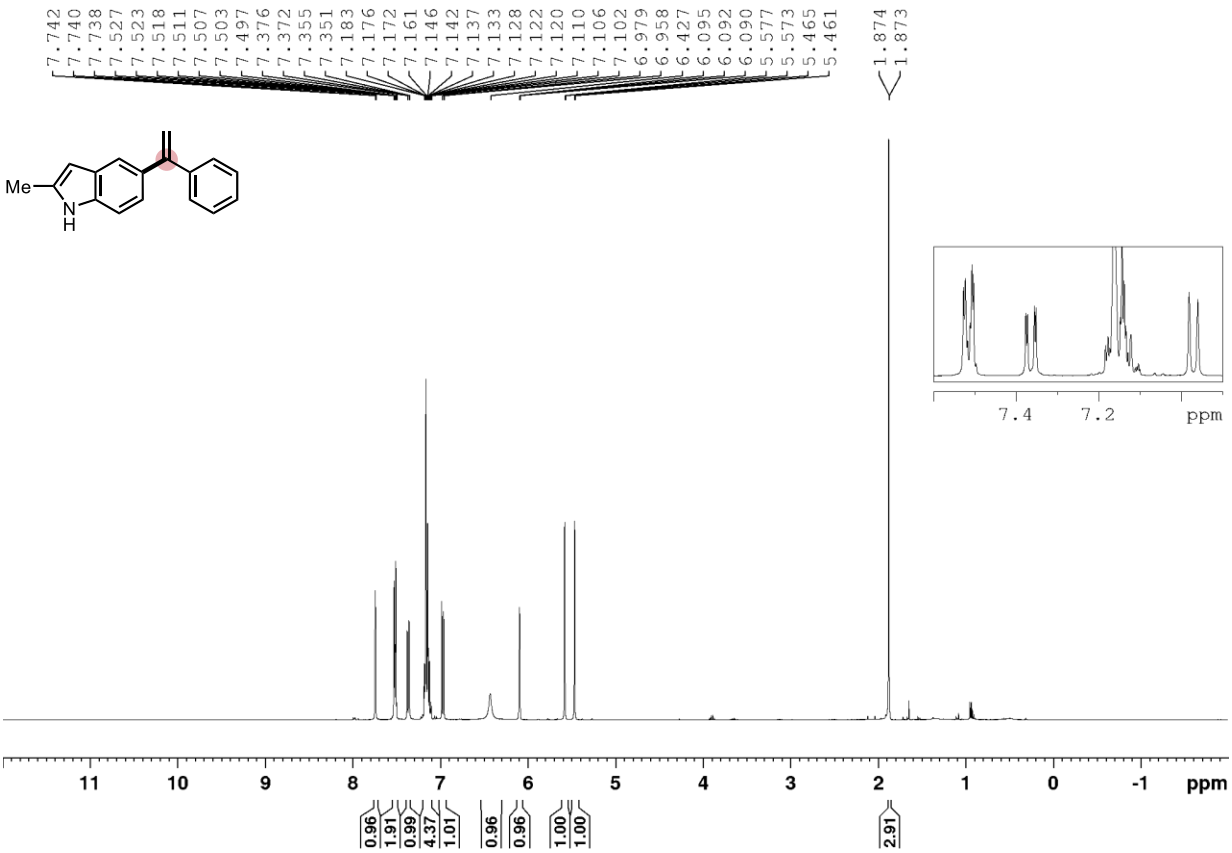

2-methyl-5-(1-phenylvinyl)-1*H*-indole (4.13-br), $^{13}C\{^{1}H\}$ C_6D_6, 125 MHz

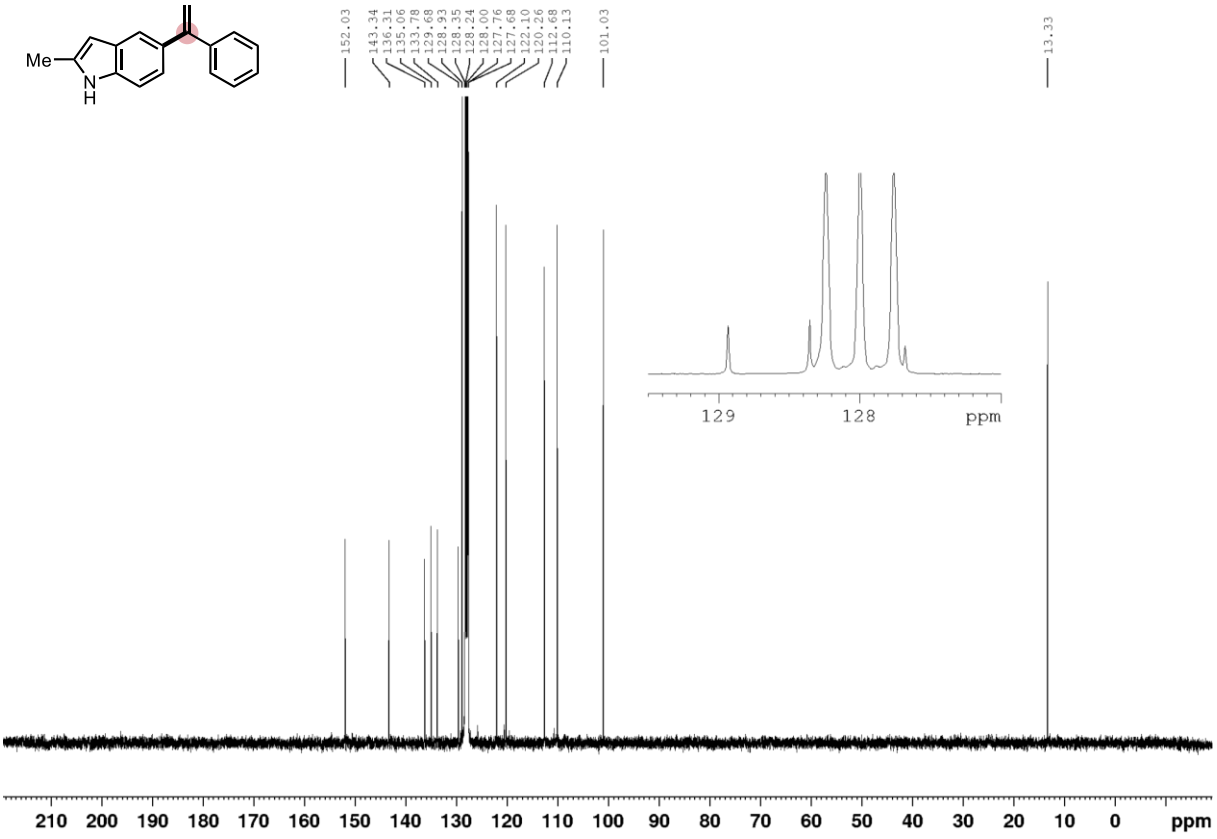

Methyl 2-((tert-butoxycarbonyl)amino)-3-(4-(1-phenylvinyl)phenyl)propanoate (4.14-br), ^{1}H, $CDCl_3$, 300 MHz

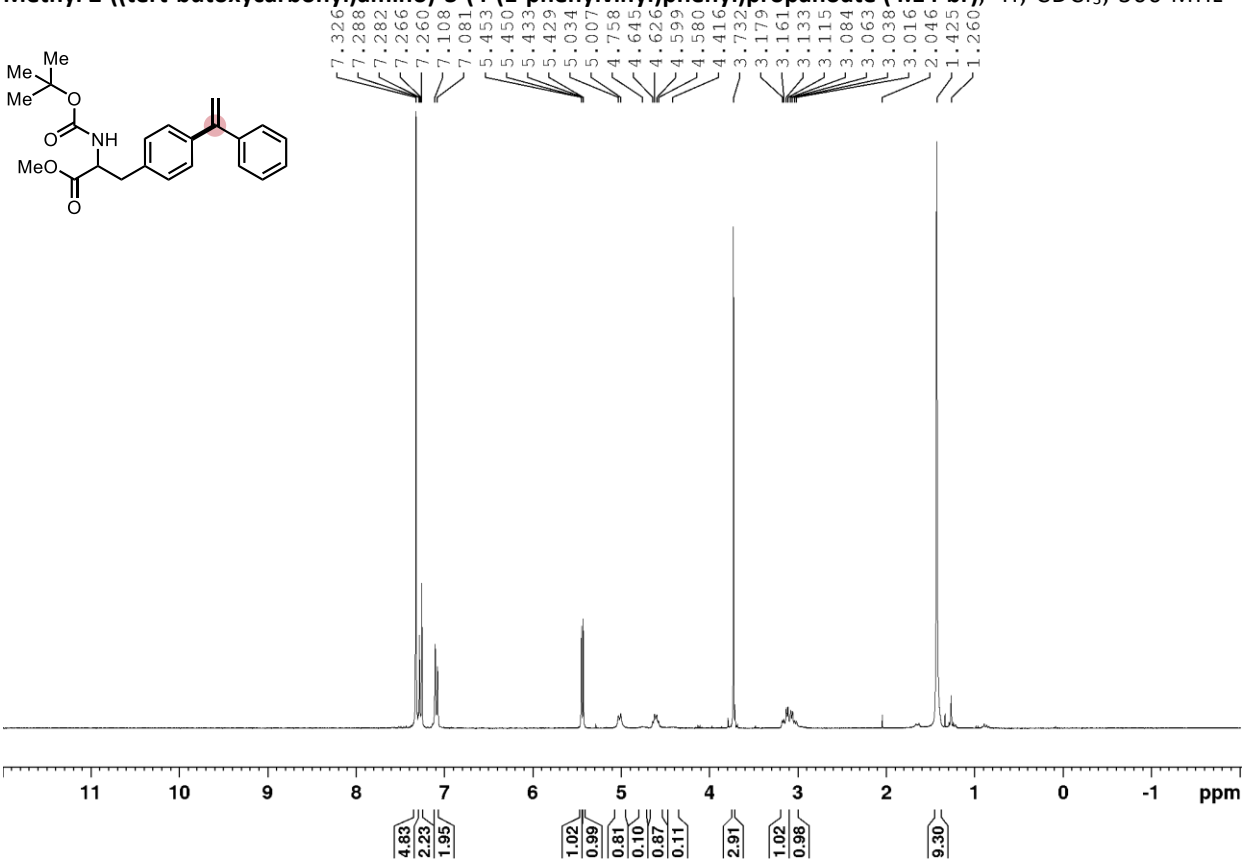

Methyl 2-((tert-butoxycarbonyl)amino)-3-(4-(1-phenylvinyl)phenyl)propanoate (4.14-br), $^{13}C\{^{1}H\}$, $CDCl_3$, 75 MHz

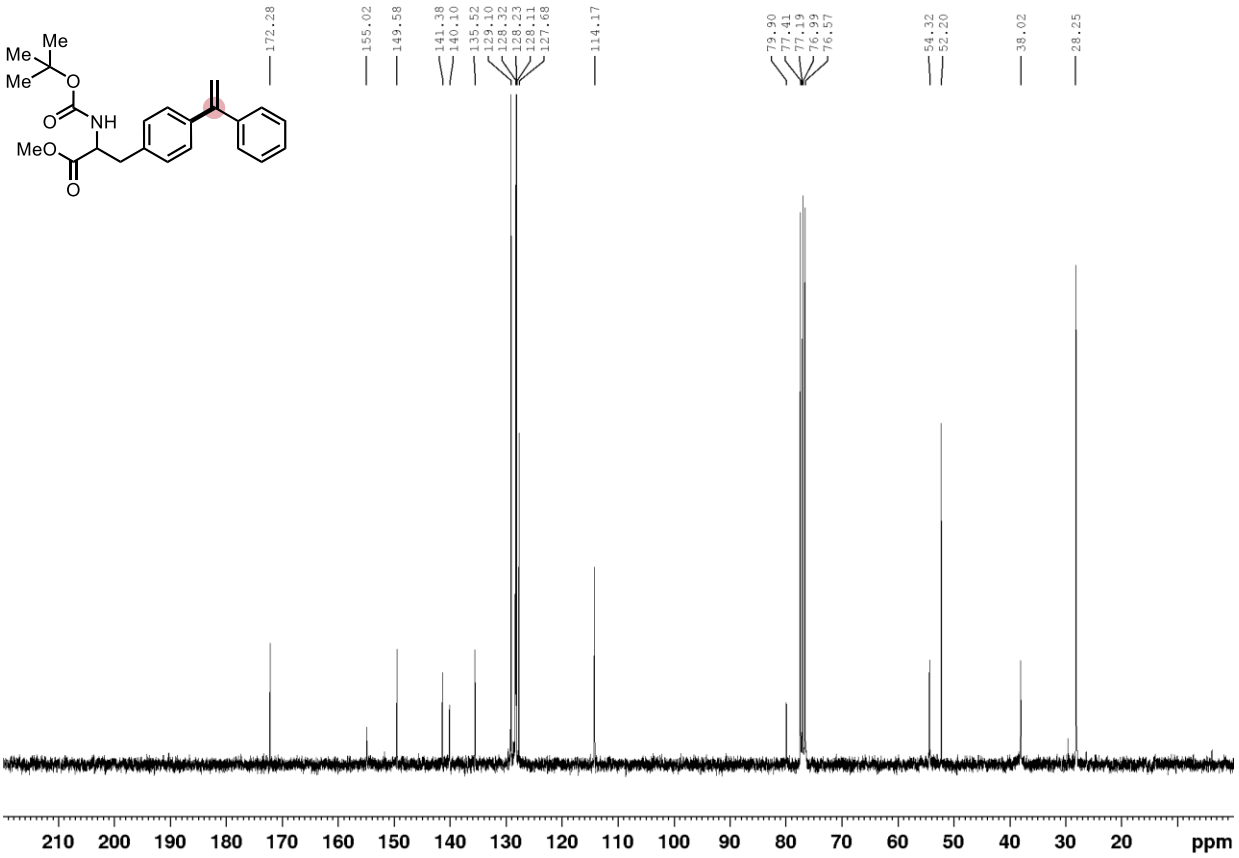

2-(1-(4-methoxyphenyl)vinyl)pyridine (4.18-br), ^{1}H, $CDCl_3$, 300 MHz

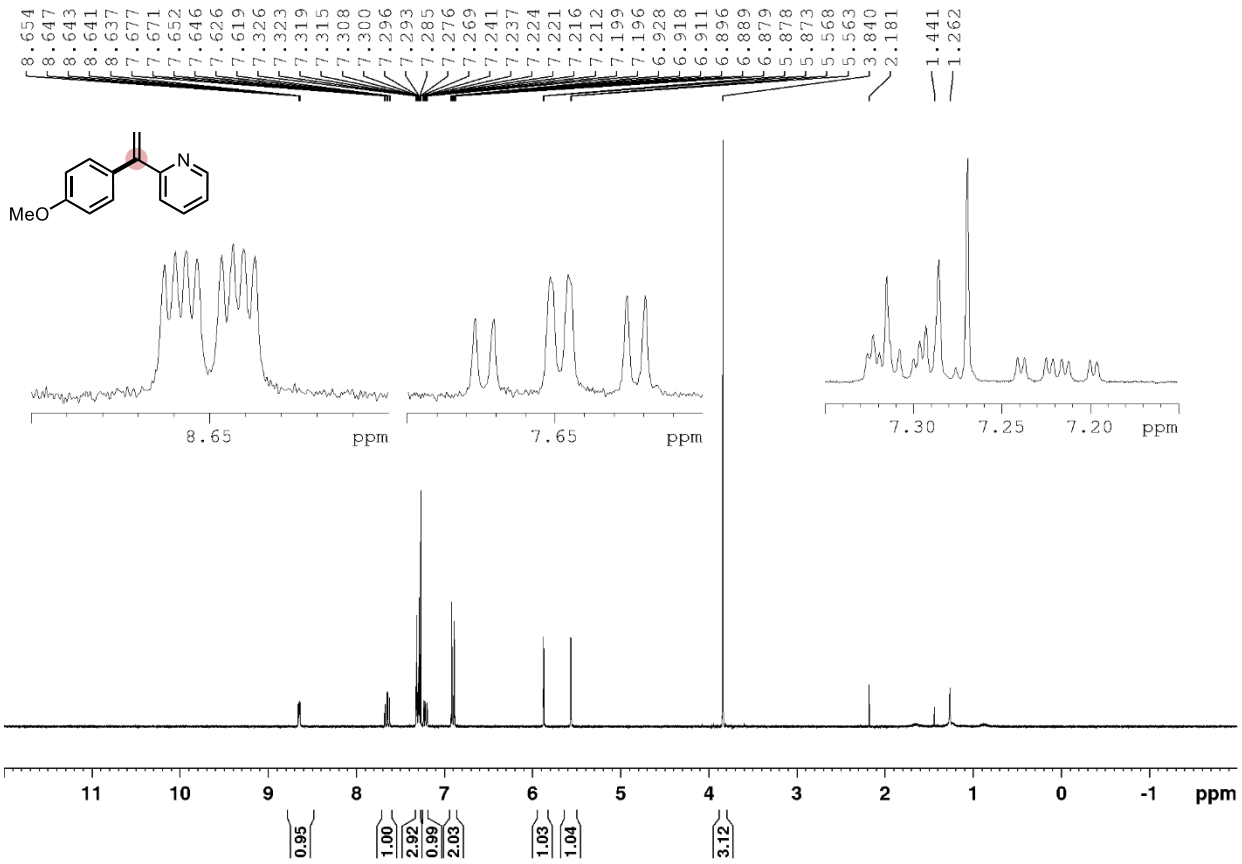

2-(1-(4-methoxyphenyl)vinyl)pyridine (4.18-br), $^{13}C\{^{1}H\}$, $CDCl_3$, 100 MHz

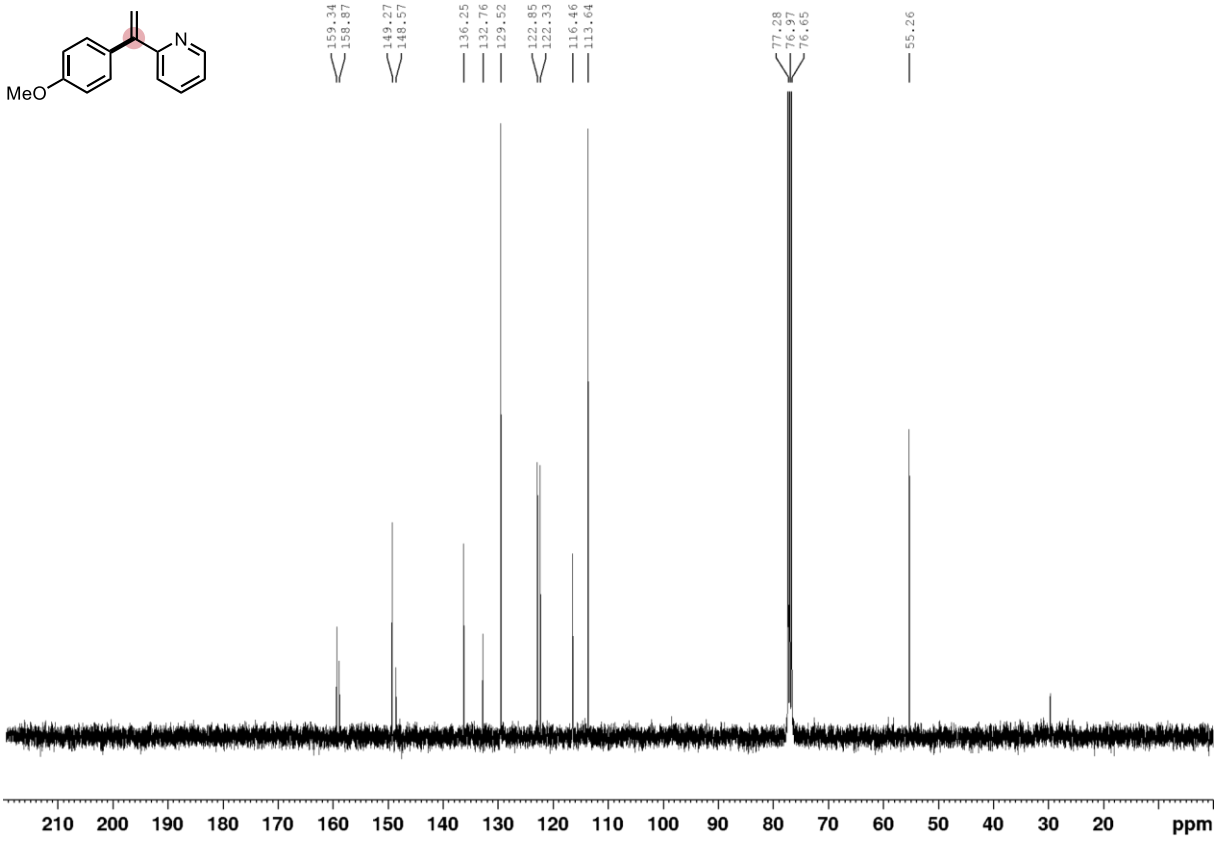

5-(1-(4-methoxyphenyl)vinyl)-4-methylthiazole (4.19-br), ^{1}H, $CDCl_3$, 500 MHz

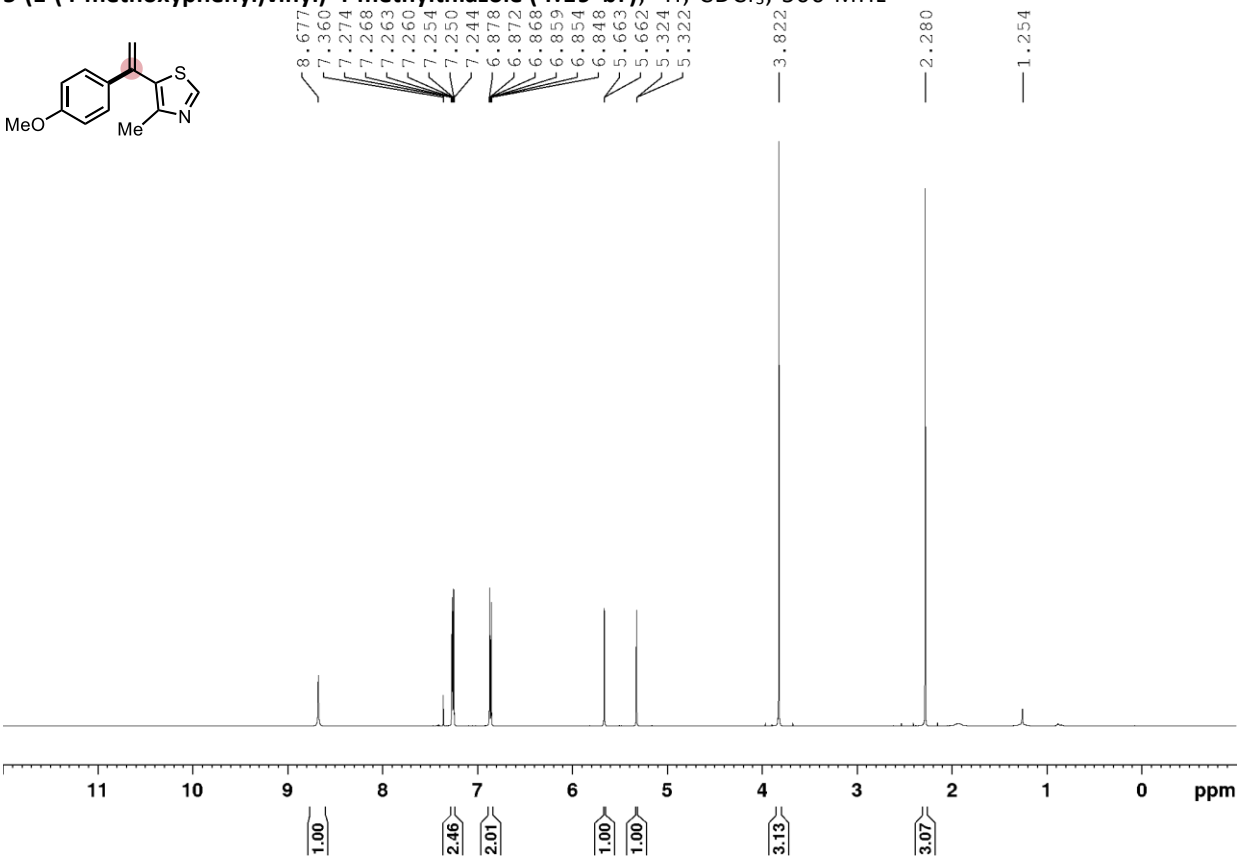

5-(1-(4-methoxyphenyl)vinyl)-4-methylthiazole (4.19-br), $^{13}C\{^{1}H\}$, $CDCl_3$, 125 MHz

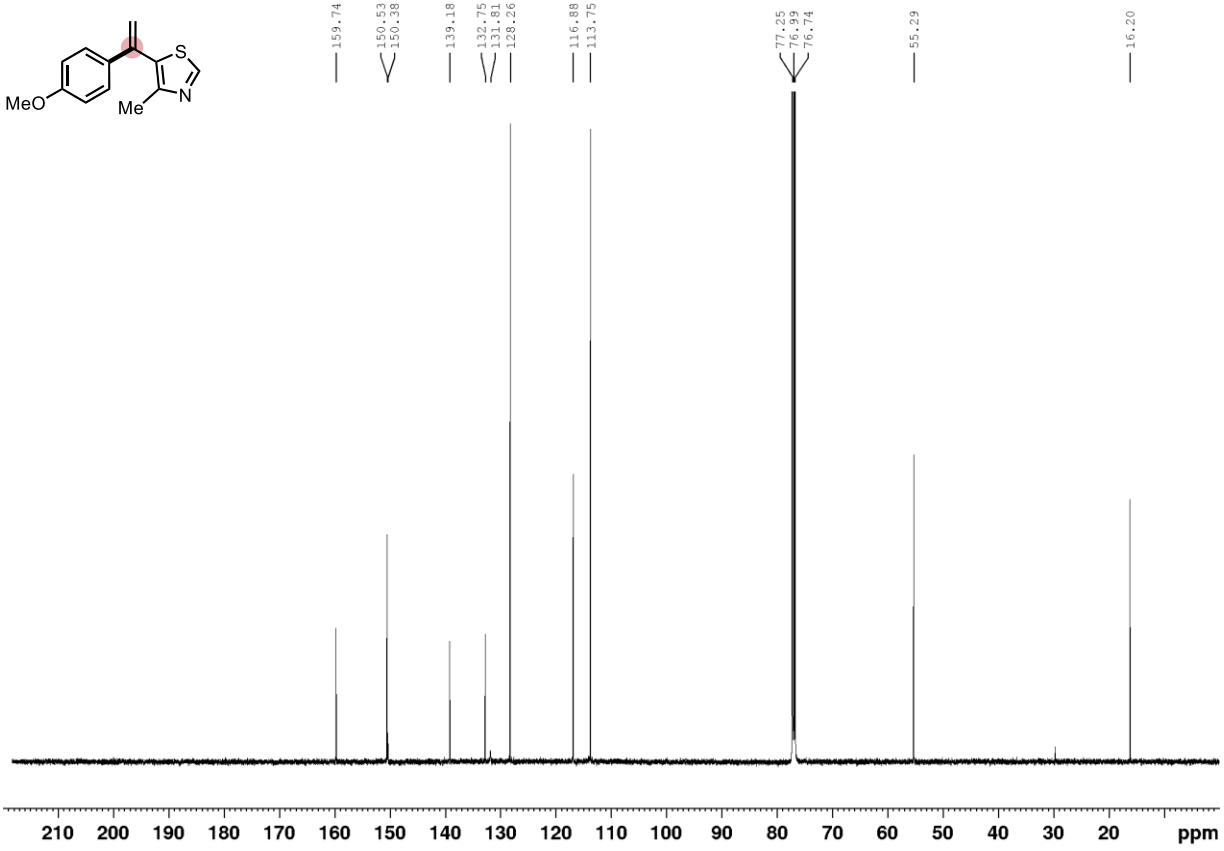

N-(1-[4-methoxyphenyl]ethenyl)-2-pyrrolidinone (4.20-br), ^{1}H, $CDCl_3$, 500 MHz

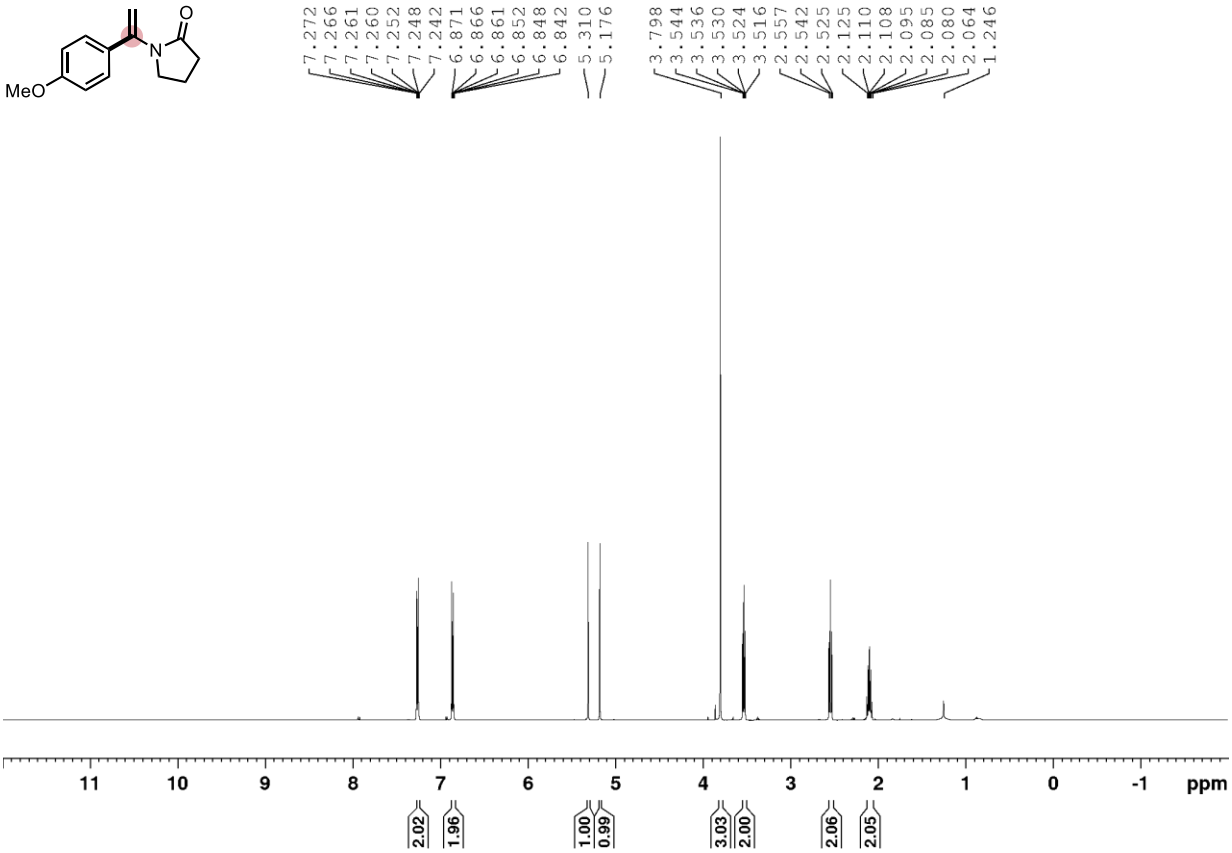

N-(1-[4-methoxyphenyl]ethenyl)-2-pyrrolidinone (4.20-br), $^{13}C\{^{1}H\}$, $CDCl_3$, 125 MHz

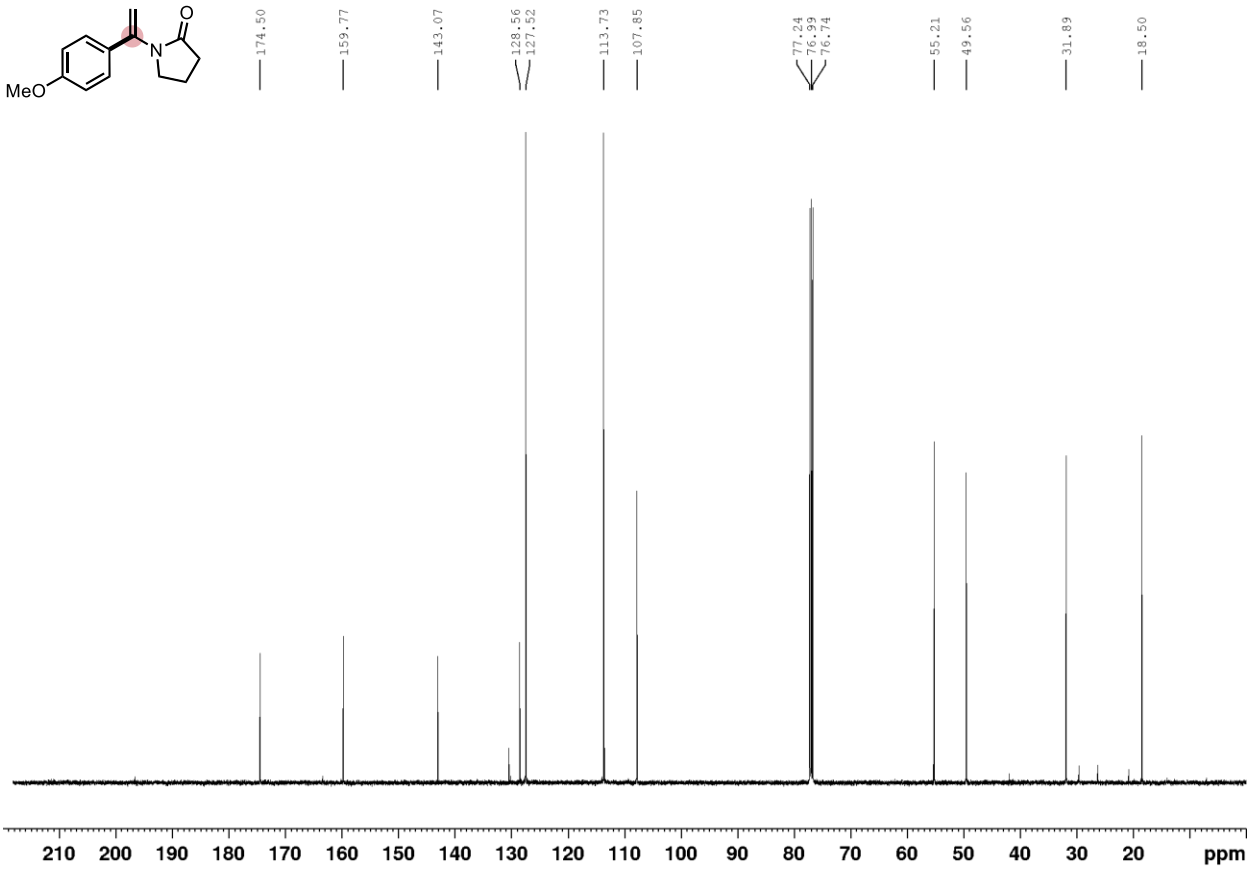

Methyl-4-[1-(5,6,7,8-Tetrahydro-3,5,5,8,8-pentamethyl-2-naphthalenyl)ethenyl]-benzoate (4.22-br) ^{1}H, $CDCl_3$, 300 MHz

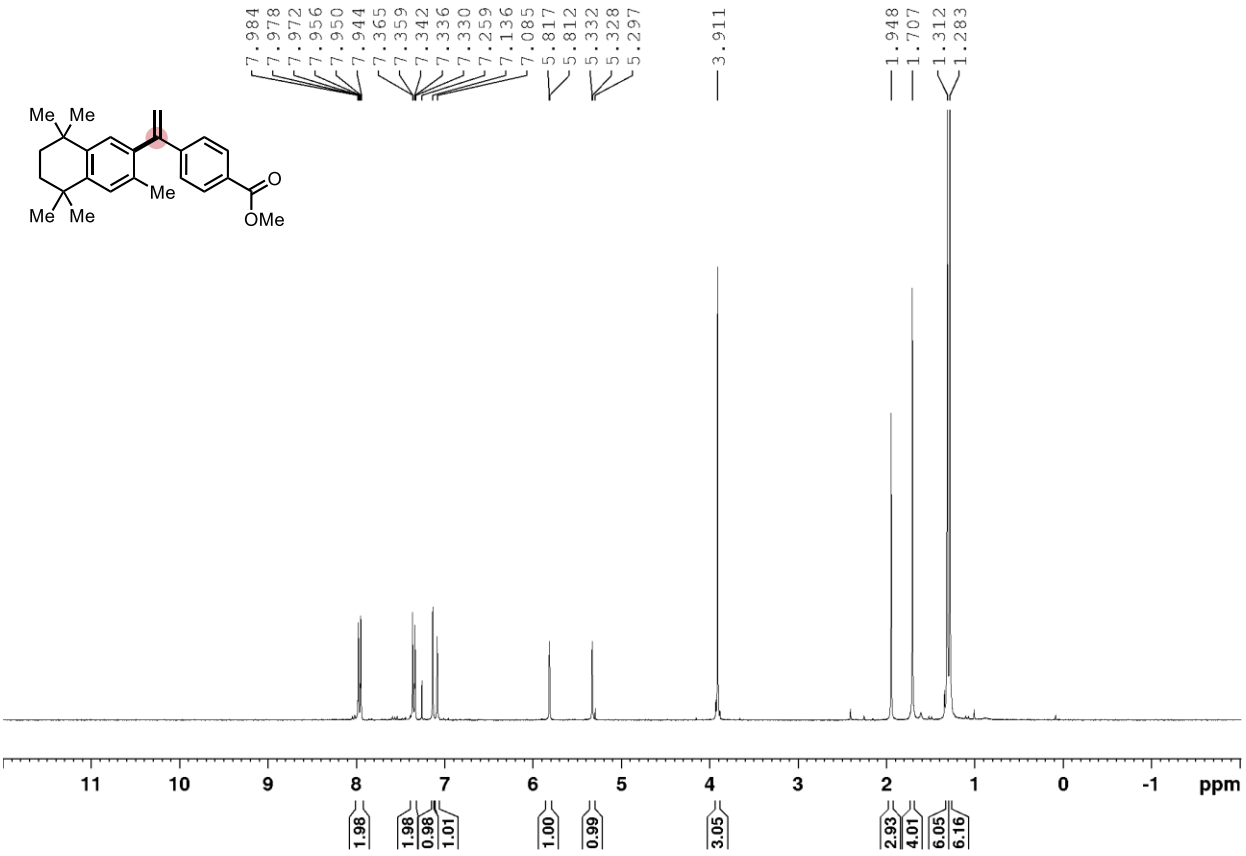

Methyl-4-[1-(5,6,7,8-Tetrahydro-3,5,5,8,8-pentamethyl-2-naphthalenyl)ethenyl]-benzoate (4.22-br), $^{13}C\{^{1}H\}$, $CDCl_3$, 75 MHz

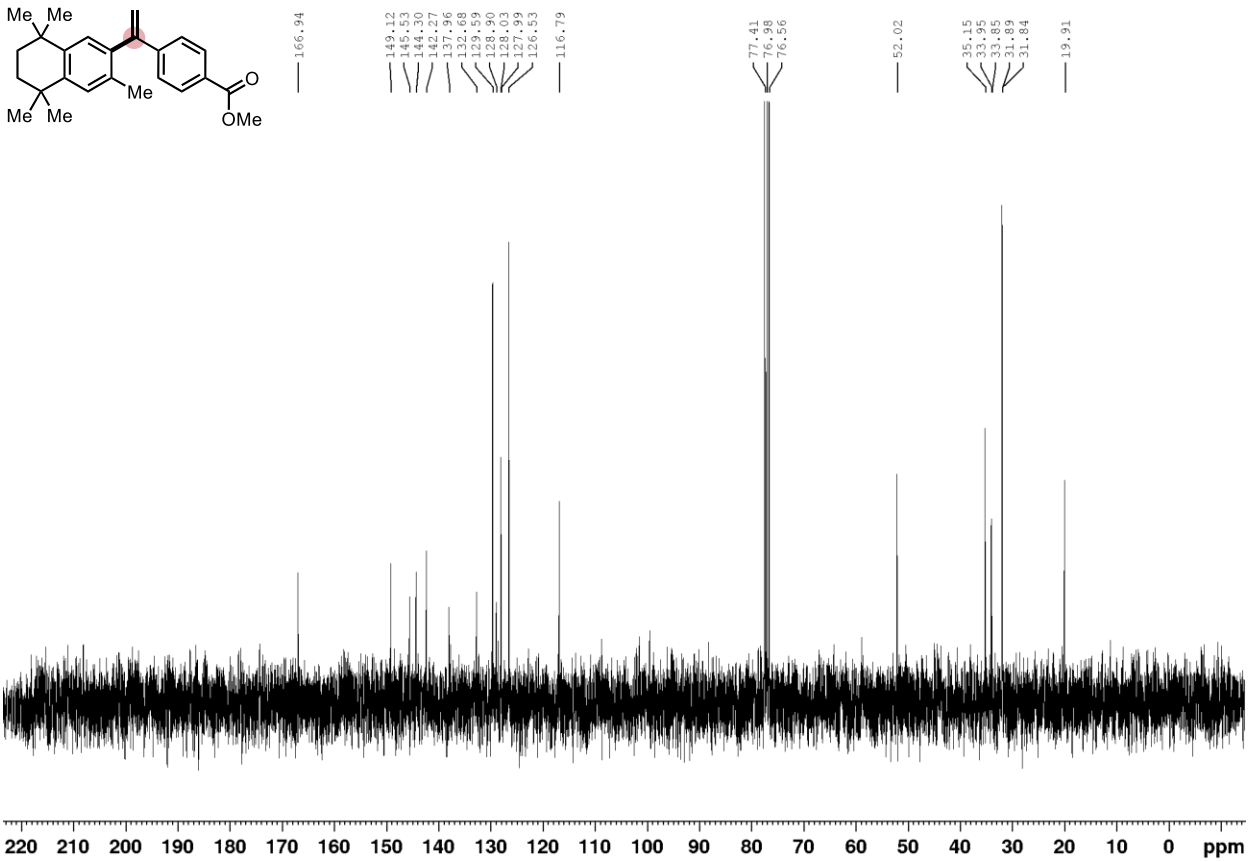

Isocombretastatin A4 (4.23-br), ^{1}H, $CDCl_3$, 400 MHz

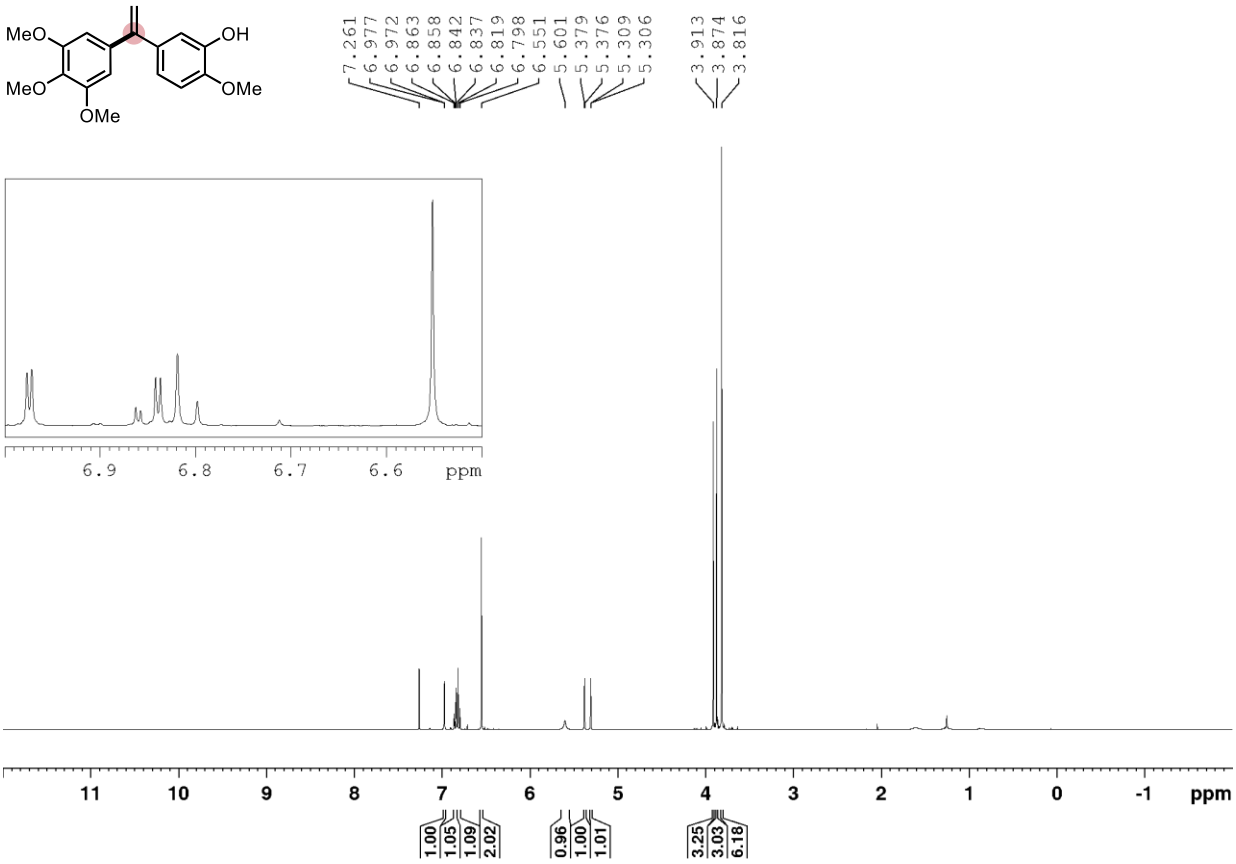

Isocombretastatin A-4 (4.23-br), $^{13}C\{^{1}H\}$, $CDCl_3$, 100 MHz

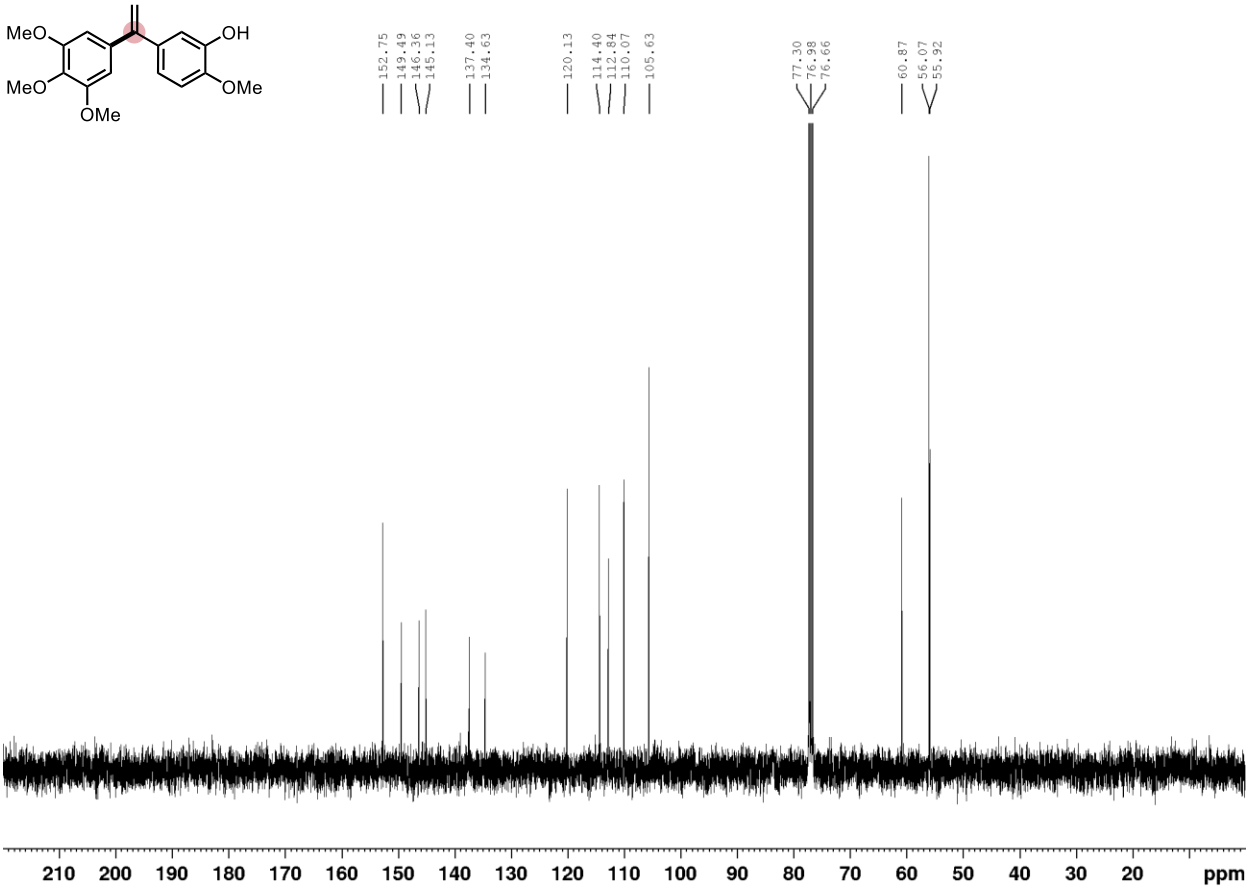

4.8 References

[1] For early contributions to the Mizoroki-Heck reaction see: (a) Moritani, I. and Fujiwara, Y. Aromatic substitution of styrene-palladium chloride complex. *Tetrahedron Lett.* **1967**, 1119-1122. (b) Heck, R. F. Acylation, methylation, and carboxyalkylation of olefins by Group VIII metal derivatives. *J. Am. Chem. Soc.* **1968**, *90*, 5518-5526. (c) Heck, R. F. The palladium-catalyzed arylation of enol esters, ethers, and halides. A new synthesis of 2-aryl aldehydes and ketones. *J Am. Chem. Soc.* **1968**, *90*, 5535-5538. (d) Fujiwara, Y.; Moritani, I.; Danno, S.; Asano, R.; Teranishi, S. Aromatic substitution of olefins. VI. Arylation of olefins with palladium (II) acetate. *J. Am. Chem. Soc.* **1969**, *91*, 7166-7169. (e) Mizoroki, T.; Mori, K.; Ozaki, A. Arylation of olefin with aryl iodide catalyzed by palladium. *Bull. Chem. Soc. Jpn.* **1971**, *44*, 581-581. (f) Heck, R. F. and Nolley, J. P. Palladium-catalyzed vinylic hydrogen substitution reactions with aryl, benzyl, and styryl halides. *J. Org. Chem.* **1972**, *37*, 2320-2322. (g) Dieck, H. A. and Heck, R. F. Organophosphinepalladium complexes as catalysts for vinylic hydrogen substitution reactions. *J. Am. Chem. Soc.* **1974**, *96*, 1133-1136.

[2] For an overview of the Mizoroki-Heck reaction including historical context and applications see: (a) Heck, R. F. Palladium-catalysed vinylation of organic halides. *Org React*. **1982**, *27*, 345-390. (b) Davies, G. D.; Hallberg, A. 1,2-Additions to heteroatom-substituted olefins by organopalladium reagents. *Chem. Rev.* **1989**, *89*, 1433-1445. (c) de Meijere, A. and Meyer, F. E. Fine feathers make fine birds: The Heck reaction in modern garb. *Angew. Chem. Int. Ed.* **1995**, *33*, 2379-2411. (d) Beletskaya, I. P.; Cheprakov, A. V. The Heck reaction as a sharpening stone of palladium catalysis. *Chem Rev.* **2000**, *100*, 3009-3066. (e) Oestreich, M. *The Mizoroki-Heck Reaction*; John Wiley & Sons, Ltd. **2009**.

[3] Roughley, S. D.; Jordan, A. M. The medicinal chemist's toolbox: An analysis of reactions used in the pursuit of drug candidates. *J. Med. Chem.* **2011**, *54*, 3451-3479. .

[4] For regioselective reactions with terminal alkyl alkenes see (a) Werner, E. W.; Sigman, M. S. Operationally simple and highly (*E*)-styrenyl-selective Heck reactions of electronically nonbiased olefins. *J. Am. Chem. Soc*. **2011**, *133*, 9692–9695. (b) Tasker, S. Z.; Gutierrez, A. C.; Jamison, T. F. Nickel-catalyzed Mizoroki–Heck reaction of aryl sulfonates and chlorides with electronically unbiased terminal olefins: High selectivity for branched products. *Angew. Chem. Int. Ed.* **2014**, *53*, 1858-1861. (c) Matsubara, R.; Gutierrez, A. C.; Jamison, T. F. Nickel-catalyzed Heck-type reactions of benzyl chlorides and simple olefins. *J. Am. Chem. Soc.* **2011**, *133*, 19020-19023. (d) Qin, L.; Ren, X.; Lu, Y.; Li, Y.; Zhou, J. Intermolecular Mizoroki–Heck reaction of aliphatic olefins with high selectivity for substitution at the internal position. *Angew. Chem. Int. Ed.* **2012**, *51*, 5915-5919 (e) Qin, L.; Hirao, H.; Zhou, J. Regioselective Heck reaction of aliphatic olefins and aryl halides *Chem. Commun.* **2013**, *49*, 10236-10238. (f) Zhou, J.; Huang, X.; Teng, S.; Chi, Y. R. Nickel-catalyzed Heck reaction of cycloalkenes using aryl sulfonates and pivalates. *Chem Commun.* **2021**, *57*, 3933-3936.

[5] For specific examples of vinyl ethers in Mizoroki-Heck couplings see: (a) Domzalska-Piecyzykolan, A.; Funes-Ardoiz, I.; Furman, B.; Bolm, C. Selective approaches to α- and β-arylated vinyl ethers. *Angew. Chem. Int. Ed.* **2021**, *61*, e202109801. (b) Cabri, W.; Candiani, I.; Bedeschi, A. Ligand-controlled -regioselectivity in palladium-catalyzed arylation of butyl vinyl ether. *J. Org. Chem.* **1990**, *55*, 3654-3655. (c) Andersson, C.-M.; Hallberg, A. Palladium-catalyzed vinylation of alkyl vinyl ethers with enol triflates. A convenient synthesis of 2-alkoxy 1,3-dienes. *J. Org. Chem*. **1989**, *54*, 1502-1505. (d) Larhed, M.; Andersson, C.-M.; Hallberg, A. Chelation-controlled, palladium-catalyzed arylation of enol ethers with aryl triflates. Ligand control of selection for α-or β-arylation of [2-(dimethylamino)ethoxy]ethene. *Tetrahedron* **1994**, *50*, 285-304. (e) Jeffrey, T.; David, M. [Pd/Base/QX] catalyst systems for directing Heck-type reactions. *Tetrahedron Lett.* **1998**, *39*, 5751-5754. (f) Littke, A. F.; Fu, G. A versatile catalyst for Heck reactions of aryl chlorides and aryl bromides under mild conditions. *J. Am. Chem. Soc.* **2001**, *123*, 6989-7000. (g) Bengston, A.; Larhed, M.; Hallberg, A. Protected indanones by a Heck–aldol annulation reaction. *J. Org. Chem.* **2002**, *67*, 5854-5856. (h) Mo, J.; Xiao, J. The Heck reaction of electron-rich olefins with regiocontrol by hydrogen-bond donors. *Angew. Chem. Int. Ed.* **2006**, *45*, 4152-4157. (i) Liu, S.; Berry, N.; Thomson, N.; Pettman, A.; Hyder, Z.; Mo ,J.; Xiao, J. Pd–mBDPP-catalyzed regioselective internal arylation of electron-rich olefins by aryl halides. *J. Org. Chem.* **2006**, *71*, 7467–7470. (j) Machado, A. H. L.; de Sousa, M. A., Patto, D. C. S.; Azevedo, L. F. S.; Bombonato, F. I.; Correia, C. R. D. The scope of the Heck arylation of enol ethers with arenediazonium salts: a new approach to the synthesis of flavonoids. *Tetrahedron Lett*. **2009**, *50*, 1222-1225. (k) McConville, M.; Saidi, O.; Blacker, J.; Xiao, J. Regioselective Heck vinylation of electron-rich olefins with vinyl halides: Is the neutral pathway in operation? *J. Org.*

Chem. **2009**, *74*, 2692-2698. (l) Hartman, R. L.; Naber, J. R.; Buchwald, S. L; Jensen, K. F. Multistep microchemical synthesis enabled by microfluidic distillation. *Angew. Chem. Int. Ed.* **2010**, *49*, 899-903. (m) Ruan, J.; Iggo, J. A.; Berry, N. G., Xiao, J. Hydrogen-bonding-promoted oxidative addition and regioselective arylation of olefins with aryl chlorides. *J. Am. Chem. Soc.* **2010**, *132*, 16689-16699. (n) Gøgsig, W. M.; Kleimark, J.; Lill S. O. N.; Korsager, S.; Lindhardt, A. T.; Norrby, P.-O.; Skrydstrup, T. Mild and efficient nickel-catalyzed Heck reactions with electron-rich olefins. *J. Am. Chem. Soc.* **2012**, *134*, 443-452. (o) Becica, J.; Glaze, O. D.; Hruszkewycz, D. P.; Dobereiner, G. E.; Leitch, D. C. The influence of additives on orthogonal reaction pathways in the Mizoroki–Heck arylation of vinyl ethers. *React. Chem. Eng.*, **2021**, *6*, 1212-1219.

[6] (a) Ehle, A. R.; Zhou, Q.; Watson, M. P. Nickel(0)-catalyzed Heck cross-coupling via activation of Aryl C–OPiv bonds. *Org. Lett.* **2012**, *14*, 1202-1205. (b) Zou, Y.; Qin, L.; Ren, X.; Lu, Y.; Li, Y.; Zhou, J. Selective arylation and vinylation at the α position of vinylarenes. *Chem. Eur. J.* **2013**, *19*, 3504-3511. For specific examples of linear selective coupling with styrenes see: (c) Boldrini, G. P.; Savoia, D.; Tagliavini, E.; Trombini, C.; Umani Ronchi, A. Nickel-catalyzed coupling of activated alkenes with organic halides. *J. Organomet. Chem*. **1986**, *301*, C62−C64. (d) Lebedev, S. A.; Lopatina, V. S.; Petrov, E. S.; Beletskaya, I. P. Condensation of organic bromides with vinyl compounds catalysed by nickel complexes in the presence of zinc. *J. Organomet. Chem.* **1988**, *344*, 253−259. (e) Bhanage, B. M.; Zhao, F.; Shirai, M.; Arai, M. Heck reaction using nickel/TPPTS catalyst and inorganic base on supported ethylene glycol phase. *Catal. Lett.* **1998**, *54*, 195-198. (f) Walker, B. R. and Sevov, C. S. An electrochemically promoted, nickel-catalyzed Mizoroki–Heck reaction. *ACS Catal.* **2019**, *9*, 7197-7203. For regioirregular (branched) reactions with styrenes see (g) Garnes-Portolés, F.; Greco, R.; Olivier-Meseguer, J.; Castellanos-Soriano, J.; Jiménez, M. C.; López-Haro; M.; Hernández-Garrido, J. C.; Boronat, M.; Pérez-Ruiz, R.; Levya-Pérez, A. Regioirregular and catalytic Mizoroki–Heck reactions. *Nat. Catal.* **2021**, *4*, 293-303. (j) Lui, K.; Leifert, D.; Studer, A. cooperative triple catalysis enables regioirregular formal Mizoroki–Heck reactions. *Nat. Synth*. **2022**, 565-575.

[7] For general examples of electron rich-olefins in Mizoroki-Heck couplings: (a) Cabri, W. and Candiani, I. Recent developments and new perspectives in the Heck reaction. *Acc. Chem. Res.* **1995**, *28*, 2-7. (b) Vallin, K .S. A.; Zhang, Q.; Larhed, M.; Curran, D. P.; Hallberg, A. A new regioselective Heck vinylation with enamides. Synthesis and investigation of fluorous-tagged bidentate ligands for fast separation. *J. Org. Chem.* **2003**, *68*, 6639-6645. (c) Tu, T.; Hou, X.-L.; Dai, L.-X. Highly regio- and enantioselective Heck reaction of *N*-methoxycarbonyl-2-pyrroline with planar chiral diphosphine-oxazoline ferrocenyl ligands. *Org. Lett.* **2003**, *5*, 3651-3653. (d) Hansen, A. L.; Skrydstrup, T. Regioselective Heck couplings of α,β-unsaturated tosylates and mesylates with electron-rich olefins. *Org Lett.* **2005**, *7*, 5585-5587. (e) Hansen, A. L.; Skrydstrup, T. Fast and regioselective Heck couplings with *N*-acyl-*N*-vinylamine derivatives. *J. Org. Chem.* **2005**, *70*, 5997-6003. (f) Hyder, Z.; Ruan, J.; Xiao, J. Hydrogen-bond-directed catalysis: Faster, regioselective and cleaner Heck arylation of electron-rich olefins in alcohols. *Chem. Eur. J.* **2008**, *14*, 5555-5566. (g) Liu, Z.; Xu, D.; Tang, W.; Xu, L.; Mo, J.; Xiao, J. A general method for regioselective Heck arylation of electron-rich *N*-acyl-*N*-vinylamine with aryl halides. *Tetrahedron Lett*. **2008**, *49*, 2756-2760. (h) Pelletier, G.; Larivée, A.; Charette, A. B. Highly regioselective intermolecular arylation of 1,2,3,4-tetrahydropyridines. *Org. Lett.* **2008**, *10*, 4791-4794. (i) Gøgsig, W. M.; Lindhardt, A. T.; Dekhane, M.; Grouleff, J.; Skrydstrup, T. Heteroaromatic tosylates as electrophiles in regioselective Mizoroki–Heck-coupling reactions with electron-rich olefins *Chem. Eur. J.* **2009**, *15*, 5950-5955. (j) Guo, Q.; Deng, B.; Zhang, H.; Qin, J. Arylations of substituted enamides by aryl iodides: Regio- and stereoselective synthesis of (Z)-β-amido-β-arylacrylates. *Org. Lett*. **2013**, *15*, 4604–4607.

[8] For general examples of electron-deficient olefins in Mizoroki-Heck couplings see: (a) Feuerstein, M.; Doucet, H.; Santelli, M. Efficient Heck vinylation of aryl halides catalyzed by a new air-stable palladium−tetraphosphine complex. *J. Org. Chem*. **2001**, *66*, 5923–5925. (b) Fall, Y.; Doucet, H.; Santelli, M. Selective Heck reaction of aryl bromides with cyclopent-2-en-1-one or cyclohex-2-en-1-one. *Tetrahedron* **2009**, *65*, 489-495. (c) Gottumukkala, A. L.; de Vries, J. G.; Minnaard, A. J. Pd–NHC catalyzed conjugate addition versus the Mizoroki–Heck reaction. *Chem. Eur. J.* **2011**, *17*, 3091-3095. (d) Wucher, P.; Caporaso, L.; Roesle, P.; Ragone, F.; Cavallo, L.; Mecking, S.; Göttker-Schnetmann. Breaking the regioselectivity rule for acrylate insertion in the Mizoroki–Heck reaction. *Proc. Natl. Acad. Sci. U.S.A.* **2011**, *108*, 8955-8959. (e) Gowla, T. N.; Pabba, J. Selective Heck reaction of electron-rich aryl bromides with cyclic alkenones. *Tetrahedron Lett.* **2015**, *56*, 1801-1804.(f) Canterbury, D. P.; Hesp, K. D.; Polivkova, J. Palladium-catalyzed β-(hetero)arylation of α,β-unsaturated valerolactams. *Org. Biomol. Chem.*, **2016**, *14*, 7731-7734. (g) Islam, M. S.; Nahra, F.; Tzouras, N. V.; Barakat, A.; Cazin, C. S. J.; Nolan, S. P.; Al-Majid, A. M. Mizoroki–Heck cross-coupling of acrylate derivatives with aryl halides catalyzed by palladate pre-catalysts. *Eur. J. Inorg. Chem.***2019**, *2019*, 4695-4699.

[9] For a general review on regioselective couplings of electronically-unbiased alkenes see: Deb A.; Maiti, D. Emergence of unactivated olefins for the synthesis of olefinated arenes. *Eur. J. Chem.* **2017**, *2017*, 1239-1252.

[10] Zhang, W. S.; Ji, D.-W.; Li, Y.; Zhang, X.-X.; Mei, Y.-K.; Chen, B.-Z.; Chen, Q.-A. Nickel-catalyzed divergent Mizoroki–Heck reaction of 1,3-dienes. *Nat. Commun.* **2023**, *14*, 651

[11] (a) Wiedner, E. S.; Appel, A. M.; Raugei, S.; Shaw, W. J.; Bullock, R. M. Molecular catalysts with diphosphine ligands containing pendant amines. *Chem. Rev.* **2022**, *122*, 12427–12474.(b) Moiseev, D. V. and James, B. R. Phospha-Mannich reactions of RPH_2, R_2PH, and R_3P. *Phosphorus. Sulfur. Silicon Relat. Elem*. **2022**, *197*, 327−391.

[12] (a) Firhi, A.; Luart, D.; Len, C.; Solhy, A.; Chevrin, C.; Polshettiwar, V. Suzuki–Miyaura cross-coupling coupling reactions with low catalyst loading: a green and sustainable protocol in pure water. *Dalton Trans.* **2011**, *40*, 3116-3121. (b) Bow, J.-P. P.; Boyle, P. D.; Blacquiere, J. M. Substrate-mediated deactivation of a Ru($P^{tBu}_2N^{Bn}_2$) cooperative complex. *Eur. J. Inorg. Chem.* **2015**, *2015*, 4162-4166. (c) Stubbs, J. M.; Bow, J.-P. J.; Hazlehurst, R. J.; Blacquiere, J. M. Catalytic cyclization and competitive deactivation with Ru($P^{R}_2N^{R'}_2$)complexes. *Dalton Trans.***2016**, *45*, 17100-17103. (d) Stubbs, J. M.; Chapple, D. E.; Boyle, P. D.; Blacquiere, J. M. Catalyst pendent-base effects on cyclization of alkynyl amines. *ChemCatChem* **2018**, 1*0*, 4001-4009. (e) Stubbs, J. M.; Bridge, B. J.; Blacquiere, J. M. Optimizing ligand structure for low-loading and fast catalysis for alkynyl-alcohol and amine cyclization. *DaltonTrans*. **2019**, *48,* 7928-7937. (f) Bridge, B. J.; Boyle, P. D.; Blacquiere, J. M. endo-Selective iron catalysts for intramolecular alkyne hydrofunctionalization. *Organometallics* **2020**, *39*, 2570–2574. (g) Chapple, D. E.; Boyle, P. D.; Blacquiere, J. M. Origin of stability and inhibition of cooperative alkyne hydrofunctionalization catalysts, *ChemCatChem*, **2021**, *13*, 3789-3800. (h) Isbrandt, E. S.; Nasim, A.; Zhao, K.; Newman S. G. Catalytic aldehyde and alcohol arylation reactions facilitated by a 1,5-diaza-3,7-diphosphacyclooctane ligand *J. Am. Chem. Soc.* **2021**, *143*, 14646-14656. (i) Chapple; D. E.; Hoffer, M. A.; P.D. Boyle, P. D.; Blacquiere J. M. Alkyne hydrofunctionalization mechanism including an off-cycle alkoxycarbene deactivation complex, *Organometallics* **2022**, *41*, 1532-1542 (j) Nasim, A.; Thomas, G. T.; Ovens, J. S.; Newman, S. G. Reductive 1,2-arylation of isatins. *Org. Lett*. **2022**, *24*, 7232-7236

[13] For a report of a Mizoroki-Heck reaction featuring a P,N-acetal ligand, see: Uruş, S.; Keleş, M.; Köşker, S. Synthesis and characterization of Pd(II) and Ru(II) tetradentate *N,N,N,N*-(diphosphinomethyl)amine ligands: Catalytic properties in transfer hydrogenation and Heck coupling reactions. *Heterocycles* **2020**, *100*, 1019-1034.

[14] (a) Krska, S. W.; DiRocco, D. A.; Dreher, S. D.; Shevlin, M. The evolution of chemical high-throughput experimentation to address challenging problems in pharmaceutical synthesis. *Acc. Chem. Res*. **2017**, *50*, 2976–2985. (b) Allen, C. L.; Leitch, D. C.; Anson, M. S.; Zajac, M .A. The power and accessibility of high-throughput methods for catalysis research. *Nat. Catal.* **2019**, *2*, 2-4. (c) Isbrandt, E. S.; Sullivan, R. J.; Newman, S. G. High throughput strategies for the discovery and optimization of catalytic reactions. *Angew. Chem. Int. Ed.* **2019**, *58*, 7180-7191. (b) Cook, A.; Clément, R.; Newman, S. G. Reaction screening in multiwell plates: high-throughput optimization of a Buchwald–Hartwig amination. *Nature Prot*. **2021**, *16*, 1152-1169.

[15] For discussions on the comparison of Pd and Ni in Mizoroki-Heck reactions see: (a) Liu, L. L.; Fu, Y.; Luo, S. W.; Chen, Q.; Guo, Q.-X. Comparing nickel- and palladium-catalyzed Heck reactions. *Organometallics* **2004**, *23*, 2114–2123. (b) Menezes da Silva, V. H.; Braga, A. A. C.; Cundari, T. R. N-Heterocyclic carbene based nickel and palladium complexes: A DFT comparison of the Mizoroki–Heck catalytic Ccycles. *Organometallics* **2016**, *35*, 3170–3181. (c) Bhakta, S.; Ghosh, T. Emerging Nickel catalysis in Heck reactions: Recent developments. *Adv. Syn. Catal.* **2020**, *362*, 5257-5274. (d) Alisha, M.; Philip, R. M.; Anilkumar, G. Low-cost transition metal-catalyzed Heck-type reactions: An overview. *Eur. J. Org. Chem*. **2022**, *2022*, e202101384.

[16] For discussions on the comparison of neutral and cationic Mizoroki-Heck reactions see: Bäcktorp, C. and Norrby, P.-O. A DFT comparison of the neutral and cationic Heck pathways. *Dalton Trans.,* **2011**, *40*, 11308-11314.

[17] Section 2.5.1 of: Sherwood, J.; Clark, J. H.; Fairlamb, I. J. S.; Slattery, J. M. Solvent effects in palladium catalysed cross-coupling reactions. *Green Chem.* **2019**, *21*, 2164-2213.

[18] Cabri, W.; Candiani, I.; Bedeshi, A.; Santi, R. Palladium-catalyzed arylation of unsymmetrical olefins. Bidentate phosphine ligand controlled regioselectivity. *J. Org. Chem*. **1992**, *57*, 3558 – 3563.

[19] Zhang, L.; Jiang, Z., Dong, C.; Xue, X.; Qui, R.; Tang, W.; Li, H.; Xiao, J.; Xu, L. Palladium-catalyzed highly regioselective Mizoroki–Heck arylation of allylamines with aryl chlorides. *ChemCatChem* **2014**, *6*, 311-318.

[20] (a) Neumann, H.; Sergeev, A. G.; Spannenberg, A.; Beller, M. Efficient palladium-catalyzed synthesis of 2-aryl propionic acids. *Molecules* **2020**, *25*, 3421. (b) Johnphos is marketed as a ligand for Mizoroki-Heck cross coupling by retailers (eg. Sigma Aldrich: PN 638439).

[21] (a) Yang, C. and Nolan, S. P. A highly efficient palladium/imidazolium salt system for catalytic Heck reactions. *Synlett* **2001**, 1539-1542. (b) Inamoto, K.; Kuroda, J.; Danjo, T.; Sakamoto, T. Highly efficient Nickel-catalyzed Heck reaction using Ni(acac)2/N-heterocyclic carbene catalyst. *Synlett* **2005**, 1624-1626.

[22] Xu, H.-J.; Zhao, Y.-Q.; Zhou, X.-F. Palladium-catalyzed Heck reaction of aryl chlorides under mild conditions promoted by organic ionic bases. *J. Org. Chem*. **2011**, *76*, 8036–8041.

[23] (a) Cabri, W.; Candiani, I.; Bedeschi, A.; Santi, R. Bidentate nitrogen ligands in Heck type reactions. *Synlett* **1992**, 871-872. (b) Cabri, W.; Candiani, I.; Bedeschi, A.; Santi, R. 1,10-Phenanthroline derivatives: a new ligand class in the Heck reaction. Mechanistic aspects. *J. Org. Chem.* **1993**, *58*, 7421–7426.

[24] Kashani, S. K.; Jessiman, J. E.; Newman, S. G. Exploring homogeneous conditions for mild Buchwald–Hartwig amination in batch and flow. *Org. Process Res. Dev*. **2020**, *24*, 1948–1954.

[25] Open Reaction database is found at: **https://open-reaction-database.org.** Data set IDs are listed below:
Styrene plate: ord_dataset-0316886541d9435489859c2ad7edc863
1-octene plate: ord_dataset-1d3a1a6fb70d46c084602d0688967afc
n-butyl vinyl ether plate: ord_dataset-52bd3b0ec72c443aab113bcea09bf3f4
N-Vinylpyrrolidone plate: ord_dataset-ce5045aceb214cfc8bfd0ef3031e2737

[26] For selected examples of ligand controlled regiodivergency see: (a) Ke, Y.; Li, W.; Liu, W.; Kong, W. Ni-catalyzed ligand-controlled divergent and selective synthesis. *Sci. China Chem*. **2023**, *66*, 1-26. (b) Irifune, K.; Yamazaki, K.; Nakamuro, T.; Murakami, M.; Miura, T. Ligand-controlled regiodivergence in nickel-catalyzed vinylcyclopropane rearrangement. *Angew. Chem. Int. Ed.* **2023**, ASAP, e202307826.

[27] (a) Strelnik, I. D..; Musina, E. I.; Grachova, E.; Karasik, A. A.; Sinyashin, O. Luminescent copper(I) and gold(I) complexes of 1,5-diaza-3,7-diphosphacyclooctanes. *Phosphorus Sulfur Silicon Relat. Elem.* **2016**, *191*, 1518-1519. (b) Strelnik, I. D.; Musina, E. I.; Ignatieva, S. N.; Balueva, A. S.; Gerasimova, T. P.; Katsyuba, S. A.; Krivolapov, D. B.; Dobrynin, A. B.; Bannwarth, C.; Grimme, S.; Kolesnikov, I. E.; Karasik, A. A.; Sinayashin, O. G. Pyridyl containing 1,5-diaza-3,7-diphosphacyclooctanes as bridging ligands for dinuclear copper(I) complexes. *Z. Anorg. Allg. Chem.* **2017**, *643*, 895-902. (c) Strelnik, I. D.; Dayanova, I. R.; Krivolapov, D. B.; Litvinov, I. A.; Musina, E. I.; Karasik, A. A.; Sinyashin, O. G. Unpredicted concurrency between P,P-chelate and P,P-bridge coordination modes of 1,5-diR-3,7-di(pyridine-2-yl)-1,5-diaza-3,7-diphosphacyclooctane ligands in copper(I) complexes. *Polyhedron*, **2018**, *139,* 1-6.

[28] (a) Mock, M. T.; Chen, S.; Rousseau, R.; O'Hagen, M. J.; Dougherty, W. G.; Kassel, W. S.; DuBois, D. L.; Bullock, R. M. A rare terminal dinitrogen complex of chromium. *Chem. Commun*., **2011**, *47*, 12212-12214. (b) Hulley, E. B.; Helm, M. L.; Bullock, R. M. Heterolytic cleavage of H_2 by bifunctional manganese(i) complexes: impact of ligand dynamics, electrophilicity, and base positioning. *Chem. Sci.,* **2014**, *5*, 4729-4741. (c) Hulley, E. B.; Kumar, N.; Raugei, S.; Bullock, R. M. Manganese-based molecular electrocatalysts for oxidation of hydrogen. *ACS Catal.* **2015**, *5*, 6838-6847. (d) Zhang, S.; Appel, A. M.; Bullock, R. M. Reversible heterolytic cleavage of the H–H Bond by molybdenum complexes: Controlling the dynamics of exchange between proton and hydride. *J. Am. Chem. Soc*. **2017**, *139*, 7376–7387. (e) Bhattacharya, P.; Heiden, Z. M.; Chambers, G. M.; Johnson, S. I.; Bullock, R. M.; Mock, M. T. Catalytic ammonia oxidation to dinitrogen by hydrogen atom abstraction. *Angew. Chem. Int. Ed*. **2019**, *58*, 11618-11624.

[29] Klug, C. M.; O'Hagan, M.; Bullock, M. R.; Appel, A. M.; Wiedner, E. S. Impact of weak agostic interactions in nickel electrocatalysts for hydrogen oxidation. *Organometallics* **2017**, *36*, 2275–2284.

[30] Huang, J.; Isaac, M.; Watt, R.; Becica, J.; Dennis, E.; Saidaminov, M. I.; Sabbers, W. A.; Leitch, D. C. ^{DMP}DAB–Pd–MAH: A versatile Pd(0) source for precatalyst formation, reaction screening, and preparative-scale synthesis. *ACS Catal.* **2021**, *11,* 5636–5646.

[31] Bruno, N. C.; Tudge, M. T.; Buchwald, S. L. Design and preparation of new palladium precatalysts for C–C and C–N cross-coupling reactions. *Chem. Sci*. **2013**, *4,* 916-920.

[32] Yang, L.; Powell, D. R.; Houser, R. P. Structural variation in copper (I) complexes with pyridylmethylamide ligands: structural analysis with a new four-coordinate geometry index, τ4. *Dalton Trans.,* **2007**, 955-964.

[33] Barder, T. E.; Biscoe, M. R.; Buchwald, S. L. Structural insights into active catalyst structures and oxidative addition to (biaryl)phosphine−palladium complexes via density functional theory and experimental studies. *Organometallics* **2007**, *26*, 2183–2192

[34] Franz, J. A.; O'Hagan, M.; Ho, M.-H.; Liu, T.; Helm, M. L.; Lense, S.; DuBois, D. L.; Shaw, W. J.; Appel, A. M.; Raugei, S.; Bullock, R. M. Conformational dynamics and proton relay positioning in nickel catalysts for hydrogen production and oxidation. *Organometallics* **2013**, *32*, 7034–7042.

[35] Chernyshev, V. M.; Ananikov, V. P. Nickel and palladium catalysis: Stronger demand than ever. *ACS Catal.* **2022**, *12*, 1180–1200.
[36] (a) Boehm, M. F.; Zhang, L.; Badea, B. A.; White, S. K.; Mais, D. E.; Berger, E.; Suto, C. M.; Goldman, M. E.; Heyman, R. A. Synthesis and structure-activity relationships of novel retinoid X receptor-selective retinoids. *J. Med. Chem.* **1994**, *37*, 2930–2941. (b) Farol, L. T. and Hymes, K. B. Bexarotene: a clinical review. *Expert Rev. Anticancer Ther*. **2004**, *4*, 180-188.
[37] Song, M.-Y.; He, Q.-R.; Wang, Y.-L.; Wang, H.-R.; Jiang, T.-C.; Tang, J.-J.; Gao, J.-M. Exploring diverse-ring analogues on Combretastatin A4 (CA-4) olefin as microtubule-targeting agents. *Int. J. Mol. Sci.* **2020**, *21*, 1817.
[38] (a) Messaoudi, S.; Trégier, B.; Hamaze, A.; Provot, O.; Peyrat, J. -F.; De Losada, J. R.; Liu, J.-M.; Bignon, J.; Wdzieczak-Bakala, J.; Thoret, S.; Dubois, J.; Brion, J.-D.; Alami, M. Isocombretastatins A versus Combretastatins A: The forgotten isoCA-4 isomer as a highly promising cytotoxic and antitubulin agent. *J. Med. Chem*. **2009**, *52*, 4538–4542. (b) Hamze A.; Alami, M.; Provot, O. Developments of isoCombretastatin A-4 derivatives as highly cytotoxic agents. *Eur. J. Med. Chem.* **2020**, *190,* 112110
[39] Neese, F.; Wennmohs, F.; Becker, U.; Riplinger, C. The ORCA quantum chemistry program package. *J. Chem. Phys.* **2020**, *152*, 224108.
[40] (a) Becke, A. D. Density-functional thermochemistry. III. The role of exact exchange. *J. Chem. Phys.* **1993**, *98*, 5648-5652. (b) Lee, C.; Yang, W.; Parr, R. G. Development of the Colle-Salvetti correlation-energy formula into a functional of the electron density. *Phys. Rev. B* **1988**, *37*, 785–789.
[41] Weigend, F.; Ahlrichs, R. Balanced basis sets of split valence, triple zeta valence and quadruple zeta valence quality for H to Rn: Design and assessment of accuracy. *Phys. Chem. Chem. Phys*. **2005**, *7*, 3297–3305.
[42] Grimme, S.; Antony, J.; Ehrlich, S.; Krieg, H. A consistent and accurate ab initio parametrization of density functional dispersion correction (DFT-D) for the 94 elements H-Pu. *J. Chem. Phys.* **2010**, *132*, 154104.
[43] Cossi, M.; Rega, N.; Scalmani, G.; Barone, V. Energies, structures, and electronic properties of molecules in solution with the C-PCM solvation model. *J. Comput. Chem.* **2003**, *24*, 669–681.
[44] Parker, T. M.; Burns, L. A.; Parrish, R. M.; Ryno, A. G.; Sherrill, C. D. Levels of symmetry adapted perturbation theory (SAPT). I. Efficiency and performance for interaction energies. *J. Chem. Phys.* **2014**, *140*, 094106.
[45] Smith, D. G. A.; Burns, L. A.; Simmonett, A. C.; Parrish, R. M.; Schieber, M. C.; Galvelis, R.; Kraus, P.; Kruse, H.; Di Remigio, R.; Alenaizan, A.; James, A. M.; Lehtola, S.; Misiewicz, J. P.; Scheurer, M.; Shaw, R. A.; Schriber, J. B.; Xie, Y.; Glick, Z. L.; Sirianni, D. A.; O'Brien, J. S.; Waldrop, J. M.; Kumar, A.; Hohenstein, E. G.; Pritchard, B. P.; Brooks, B. R.; Schaefer, H. F., III; Sokolov, A. Y.; Patkowski, K.; DePrince, A. E., III; Bozkaya, U.; King, R. A.; Evangelista, F. A.; Turney, J. M.; Crawford, T. D.; Sherrill, C. D. PSI4 1.4: Open-source software for high-throughput quantum chemistry. *J. Chem. Phys.* **2020**, *152*, 184108.
[46] For representative examples of known Pd(II) P_2N_2 complexes see: (a) Kane, J. C.; Wong, E. H.; Yap, G. P.; Rheingold, A. L. Synthesis and structural studies of molybdenum and palladium complexes of 1, 5-diaza-3, 7-diphosphacyclooctane ligands. *Polyhedron*, **1999**, *18*, 1183-1188. (b) Ignatieva, S. N.; Balueva, A. S.; Karasik, A. A.; Latypov, S. K.; Nikonova, A. G.; Naumova, O. E.; Lönnecke, P.; Hey-Hawkins, E.; Sinyashin, O. G. First representative of optically active *P*-L-menthyl-substituted (aminomethyl)phosphine and its borane and metal complexes. *Inorg. Chem*. **2010**, *49*, 5407–5412. (c) Fihri, A.; Luart, D.; Len, C.; Solhy, A.; Chevrin, C.; Polshettiwar, V. Suzuki–Miyaura cross-coupling coupling reactions with low catalyst loading: A green and sustainable protocol in pure water. *Dalton Trans*. **2011**, *40*, 3116-3121. (d) Karasik, A. A.; Heinicke, J. W.; Balueva, A. S.; Thede, G.; Jones, P. G.; Sinyashin, O. G. Pt- and Pd-complexes with acyclic and heterocyclic *P*-hydroxyaryl-substituted *N*-phosphanylmethyl amino acids $RP(CH_2NHR')_2$ and $(RPCH_2NR'CH_2)_2$– Evaluation of (P^O)M chelate formation. *Eur. J. Inorg. Chem.* **2020**, *2020*, 3682–3691.
[47] Jenthra, S.; Mondal, T.; Kemper, G.; Lantzius-Beninga, M.; Hölscher, M.; Leitner, W. Ligand-controlled palladium-catalyzed decarboxylative Heck coupling for regioselective access to branched olefins. *ACS Catal.* **2023**, *13*, 10085–10093.
[48] Kulikov, D. V.; Balueva, A. S.; Karasik, A. A.; Kozlov, A. V.; Latypov, S. K.; Kataeva, O. N.; Lönnecke, P.; Hey-Hawkins, E.; Sinyashin, O. G. Novel 36- and 38-membered P,N-containing cyclophanes with large hydrophobic cavities. *Phosphorus, Sulfur, and Silicon Relat. Elem.* **2008**, *183*, 667–668.

[49] Wang, Y. & Gu, M. The concept of spectral accuracy for MS. *Anal. Chem*. **2010**, *82*, 7055–7062.

[50] Lerch, S.; Fritsch, S.; Strassner, T. The Mizoroki-Heck reaction in tunable aryl alkyl ionic liquids. *Eur. J. Org. Chem.* **2022**, *2022*, e202200008.
[51] Liu, R.; Zhang, T.; Huang, B.; Cai, M. Recyclable and reusable $PdCl_2(PPh_3)_2$/PEG-400/H_2O system for the hydrophenylation of alkynes with sodium tetraphenylborate. *J. Chem. Res.* **2021**, *45*, 172–178.
[52] Hsu, C.-M.; Li, C.-B.; Sun, C.-H. Bipyridine-modulated palladium-catalyzed oxidative Heck-type reactions of arylboronic acids with olefins. *J. Chin. Chem. Soc.* **2009**, *56*, 873–880.
[53]Ingoglia, B. T.; Buchwald, S. L. Oxidative addition complexes as precatalysts for cross-coupling reactions requiring extremely bulky biarylphosphine ligands. *Org. Lett.* **2017**, *19*, 2853–2856.
[54] Bruker-AXS, SAINT version 2013.8, **2013**, Bruker-AXS, Madison, WI 53711, USA.
[55] Bruker-AXS, SADABS version 2012.1, **2012**, Bruker-AXS, Madison, WI 53711, USA.
[56] Sheldrick, G. M. SHELXT-integrated space-group and crystal-structure determination. *Acta Cryst*. **2015**, *A71*, 3–8.
[57] Sheldrick, G. M. Crystal structure refinement with SHELXL. *Acta Cryst*. **2015**, *C71*, 3–8.
[58] Macrae, C. F.; Bruno, I. J.; Chisholm, J. A.; Edington, P. R.; McCabe, P.; Pidcock, E.; Rodriguez-Monge, L.; Taylor, R.; van de Streek, J.; Wood, P. A. Crystal forms of the antibiotic 4-aminosalicylic acid: Solvates and molecular salts with doxane, morpholine, and piperazine. *J. Appl. Cryst.,* **2008**, *41*, 466–470.
[59] Spek, A. L. PLATON SQUEEZE: a tool for the calculation of the disordered solvent contribution to the calculated structure factors. *Acta Cryst.* **2015**, *C71*, 9–18.
[60] Yang, L.; Powell, D. R.; Houser, R. P. Structural variation in copper(I) complexes with pyridylmethylamide ligands: structural analysis with a new four-coordinate geometry index, τ_4. *Dalton Trans*., **2007**, 955–964.
[61] Goossen, L. J.; Rodriguez, N.; Linder, C. Decarboxylative biaryl synthesis from aromatic carboxylates and aryl triflates. *J. Am. Chem. Soc.* **2008**, *130*, 15248–15249.
[62] Mattsson, C.; Svensson, P.; Boettcher, H.; Sonesson, C. Structure–activity relationship of 5-chloro-2-methyl-3-(1,2,3,6-tetrahydropyridin-4-yl)-1*H*-indole analogues as 5-HT_6 receptor agonists. *Eur. J. Med. Chem.* **2013**, *63*, 578–588.
[63] St. Onge, P.; Khan, S. I.; Cook, A.; Newman, S. G. Reductive cleavage of $C(sp^2)$–CF_3 bonds in trifluoromethylpyridines. *Org. Lett.* **2023**, *25*, 1030–1034.
[64] Sun, E. T.; Anderson, M. B.; Anderes, K. L.; Christie, L. C.; Do , Q.-Q. T.; Feng, J.; Goetzen, T.; Hong, Y.; Iatsimirskaia, E. A.; Li, H.; Luthin, D. R.; Paderes, G. D.; Pathak, V. P.; Rajapakse, R. J.; Shackelford, S.; Tompkins, E. V.; Truesdale, L. K.; Vazir, H. Non-peptide GnRH agents, pharmaceutical compositions and methods for their uses, and processes for preparing them. WO2002098363A2.
[65] Niu, D.; Buchwald, S. L. Design of modified amine transfer reagents allows the synthesis of α-chiral secondary amines via CuH-catalyzed hydroamination. *J. Am. Chem. Soc.* **2015**, *137*, 9716–9721.
[66] Siddiki, S. M.; Touchy, A. S.; Kon, K.; Shimizu, K. Direct olefination of alcohols with sulfones by using heterogeneous platinum catalysts. *Chem. Eur. J.* **2016**, *22*, 6111–6119.
[67] Xia, S.; Cao, D.; Zeng, H.; He, L.-N.; Li, C.-J. Nickel-catalyzed stereoselective alkenylation of ketones mediated by hydrazine. *JACS Au* **2022**, *2*, 1929–1934.
[68] Aukland, M. H.; Talbot, F. J. T.; Fernández-Salas, J. A.; Ball, M.; Pulis, A. P.; Procter, D. J. An interrupted Pummerer/nickel-catalysed cross-coupling sequence. *Angew. Chem. Int. Ed.* **2018**, *57*, 9785–9789.
[69] Zhang, Z.; Zhang, D.; Zhu, L.; Zeng, D.; Kambe, N.; Qiu, R. Pd-catalyzed cross-coupling of organostibines with styrenes to give unsymmetric (*E*)-stilbenes and (1*E*,3*E*)-1,4-diarylbuta-1,3-dienes and fluorescence properties of the products. *Org. Lett.* **2021**, *23*, 5317–5322.
[70] Meng, G.; Szostak, M. General olefin synthesis by the palladium-catalyzed Heck reaction of amides: Sterically controlled chemoselective N-C activation. *Angew. Chem. Int. Ed.* **2015**, *54*, 14518–14522.
[71] Zhao, M. M.; Zhang, H.; Iimura, S.; Bednarz, M. S.; Kanamarlapudi, R. C.; Yan, J.; Lim, N.-K.; Wu, W. Process development of tryptophan hydroxylase inhibitor LX1031, a drug candidate for the treatment of irritable bowel syndrome. *Org. Process Res. Dev.* **2020**, *24*, 261–273.
[72] Arterburn, J. B.; Corona, C.; Rao, K. V.; Carlson, K. E.; Katzenellenbogen, J. A. Synthesis of 17-α-substituted estradiol-pyridin-2-yl hydrazine conjugates as effective ligands for labeling with Alberto's complex *fac*-$[Re(OH_2)_3(CO)_3]^+$ in water. *J. Org. Chem.* **2003**, *68*, 7063–7070.
[73] Belger, C.; Plietker, B. Aryl–aryl interactions as directing motifs in the stereodivergent iron-catalyzed hydrosilylation of internal alkynes. *Chem. Commun.* **2012**, *48*, 5419–5421.
[74] Lei, C.; Yip, Y. J.; Zhou, J. S. Nickel-catalyzed direct synthesis of aryl olefins from ketones and organoboron reagents under neutral conditions. *J. Am. Chem. Soc.* **2017**, *139*, 6086–6089.

[75] Zou, Y.; Qin, L.; Ren, X.; Lu, Y.; Li, Y.; Zhou, J. Selective arylation and vinylation at the α position of vinylarenes. *Chem. Eur. J.* **2013**, *19*, 3504–3511.
[76] Bess, E. N.; Sigman, M. S. Distinctive meta-directing group effect for iridium-catalyzed 1,1-diarylalkene enantioselective hydrogenation. *Org. Lett.* **2013**, *15*, 646–649.
[77] Nakano, Y.; Black, M. J.; Meichan, A. J.; Sandoval, B. A.; Chung, M. M.; Biegasiewicz, K. F.; Zhu, T.; Hyster, T. K. Photoenzymatic hydrogenation of heteroaromatic olefins using 'Ene'-reductases with photoredox catalysts. *Angew. Chem. Int. Ed.* **2020**, *59*, 10484–10488.
[78] Colbon, P.; Ruan, J.; Purdie, M.; Xiao, J. Direct acylation of aryl chlorides with aldehydes by palladium−pyrrolidine Co-catalysis. *Org. Lett.* **2010**, *12*, 3670–3673.
[79] Faul, M. M.; Ratz, A. M.; Sullivan, K. A.; Trankle, W. G.; Winneroski, L. L. Synthesis of novel retinoid X receptor-selective retinoids. *J. Org. Chem.* **2001**, *66*, 5772–5782.
[80] Ganapathy, D.; Sekar, G. Efficient synthesis of polysubstituted olefins using stable palladium nanocatalyst: Applications in synthesis of Tamoxifen and Isocombretastatin A4. *Org. Lett.* **2014**, *16*, 3856–3859.

Chapter 5 : Synthesis and Characterization of 1,5-Diaza-3,7-diphosphacyclooctanes (P_2N_2) Ligands

5.1 Introduction

As described in Section 1.5.1, there are multiple ways to synthesize P_2N_2 ligands. However, the most common method is a two-step one pot procedure starting from paraformaldehyde and a primary phosphine. Our methodology was slightly adapted from previous literature reports[1] and with it we prepared a library of P_2N_2 ligands to study in catalytic reactions. This mini-chapter contains our general procedure, characterization data for new ligands, and troubleshooting.

5.2 Reuse permissions

The general procedure was directly derived from the Supporting Information of the manuscript "Controlling Reactivity and Selectivity in the Mizoroki-Heck Reaction: High Throughput Evaluation of 1,5-Diaza-3,7-diphosphacyclooctane Ligands", by Eric S. Isbrandt, Devon E. Chapple, Phuc Tu, Victoria Dimakos, Anne Marie M. Beardall, Paul D. Boyle, Christopher N. Rowley, Johanna M. Blacquiere, and Stephen G. Newman, currently in submission.

Characterization data for $\mathbf{P^{Cy}_2N^{ArCF3}_2}$, $\mathbf{P^{Cy}_2N^{ArOMe}_2}$, and $\mathbf{P^{Ph}_2N^{ArCF3}_2}$ were directly adapted from the Supporting Information of Catalytic Aldehyde and Alcohol Arylation Reactions Facilitated by a 1,5-Diaza-3,7-diphosphacyclooctane Ligand", by Eric S. Isbrandt, Amrah Nasim, Karen A. Zhao, and Stephen G. Newman, published in *J. Am. Chem. Soc.* **2021**, 143, 14646-14656. The dissertation author is the primary author of this manuscript. Additionally, the ligand troubleshooting section form this manuscript was rewritten to remove any ambiguity and to add additional details discovered after the original publication (eg. light sensitivity).

Characterization data for $\mathbf{P^{tBu}_2N^{ArCF3}_2}$ was directly adapted from the Supporting Information of "Controlling Reactivity and Selectivity in the Mizoroki-Heck Reaction: High Throughput Evaluation of 1,5-Diaza-3,7-diphosphacyclooctane Ligands"

All other ligands have not been incorporated as part of a manuscript. Where applicable, the characterization data is referenced to a previous literature report. However, $\mathbf{P^{iBu}_2N^{ArCF3}_2}$ is novel and this dissertation is the first synthetic report.

5.3 Contributions

All work in this chapter was performed by the dissertation author.

5.4 Experimental

Unless otherwise indicated, reactions were conducted under an atmosphere of nitrogen in glass pressure tubes (e.g. CG-1880-R) that were oven-dried (120 °C) or flame-dried, charged with a dry stirbar, and shipped into a glovebox. All reagents and solvents were used as received with no further purification. Reagent alcohol (PN 277649), aniline, *p*-anisidine, and paraformaldehyde (PN 158127) were purchased from Sigma Aldrich. 4-aminobenzotrifluoride (MFCD00064396) was purchased from Combi-Blocks. Phenyl phosphine (PN 674389) was purchased as a 10% weight solution in hexanes from Sigma Aldrich. Phosphinoferrocene (MFCD20922899) was purchased as a solid from Strem. Cyclohexylphosphine, *tert*-butylphosphine, and *iso*-butylphosphine were generously donated as neat liquids by Cytec-Solvay.

5.4.1 Instrumentation

All spectra were recorded on a Bruker AVANCE 300 MHz spectrometer, Bruker AVANCEII 300 MHz spectrometer, or a Bruker AVANCEIII 500 MHz spectrometer. All NMR experiments were performed in a J-Young tube or a screw cap NMR tube under inert atmosphere. ^{1}H NMR spectra were internally referenced to the residual solvent signal (e.g., $CDCl_3$ = 7.26 ppm). ^{13}C NMR spectra were internally referenced to the residual solvent signal (e.g., $CDCl_3$ = 77.00 ppm). Data for ^{1}H NMR are reported as follows: chemical shift (δ ppm), multiplicity (s = singlet, d = doublet, t = triplet, q = quartet, m = multiplet), coupling constant (Hz), integration.

5.5 General procedure for synthesis of P_2N_2 ligands

Scheme 5.1 One-pot synthesis of 1,5-diaza-,3,7-diphosphacyclooctane (P_2N_2) ligands.

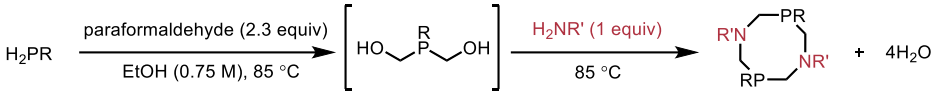

General procedure for the synthesis of P_2N_2 ligands with $P^{tBu}{}_2N^{ArCF3}{}_2$ as a representative example: A 100 mL Chemglass heavy wall round bottom pressure vessel (CG-1880-R) and stir bar were oven-dried (120 °C) and immediately shipped into a glovebox. Inside, paraformaldehyde (powder, 95%, Sigma Aldrich; 1.73 g, 57.6 mmol, 2.3 equiv) was added to the flask followed by *tert*-butylphosphine (4.13 mL, 25 mmol, 1 equiv) as a neat liquid. The reaction slurry was diluted with 35 mL of anhydrous reagent alcohol (Sigma Aldrich, PN 277649), sealed, and shipped out of the glovebox. The reaction was heated at 85 °C, during which the viscous slurry turned into a clear, homogeneous liquid. After 16 hours, the reaction flask was allowed to cool and then shipped back into the glovebox. 4-Aminobenzotrifluoride (3.15 mL, 25 mmol, 1 equiv) was added to the solution portionwise (~1 mL per portion). The reaction was again sealed, removed from the glovebox, covered in aluminum foil (4-aminobenzotrifluoride-derived side-products were identified when exposed to light), and heated at 85 °C for 16 hours, during which an off-white solid precipitated out of the solution. The flask was transferred back into the glovebox, and acetonitrile (40 mL) was added. The resulting mixture was stored overnight in the glovebox freezer (-20 °C) to induce further crystallization. After 24 hours, the mixture was filtered using a fritted funnel in the glovebox. The crude solid was washed with HPLC-grade hexanes (15 mL) followed by portions of acetonitrile (total volume ~100 mL). The remaining white solid was removed from the glovebox and residual solvent was removed in vacuo with a Schlenk line. The

purity of the resulting powder was assessed by NMR spectroscopy for all relevant nuclei (e.g. ^{1}H, $^{13}C\{^{1}H\}$, $^{19}F\{^{1}H\}$, $^{31}P\{^{1}H\}$) by dissolving the sample in $CDCl_3$ under inert atmosphere. Sample was transferred to a screw-cap NMR tube. 4.87 g of white solid was obtained (71% isolated yield based on theoretical yield of 12.5 mmol).

Safety note: Primary phosphines are highly flammable, pyrophoric, pungent, and toxic compounds that are readily oxidized. They should *always* be handled under inert atmosphere. All glassware and equipment that comes in contact with the phosphine should be sealed in an air-tight container and subsequently quenched with an aqueous bleach bath. This mixture is transferred to a labelled bleach waste container for disposal. After sitting overnight, the glassware is rinsed with water a few times to remove any residual bleach. Afterwards, organic solvent can be used to finish the cleaning process. Primary phosphines also tend to have a powerful lasting stench – any spills should be quickly cleaned up and disposed of safely. If the glassware is properly quenched and cleaned, there should be no stench.

5.6 Ligand synthesis troubleshooting

- The quality of reagents was important when preparing P_2N_2 ligands. For example, in the synthesis of $\mathbf{P^{Cy}_2N^{ArCF3}_2}$, older bottles of 4-(trifluoromethyl)aniline, which were kept in an organic cabinet, were found to give substantially lower yields than newer, high purity bottles. We have found that storing 4-(trifluoromethyl)aniline in a glovebox freezer at -20°C slows decomposition of the compound.
- Ligand synthesis is thought to be sensitive to water. Care should be taken to exclude moisture and use strictly anhydrous solvent.
- The synthesis of $\mathbf{P^{Cy}_2N^{ArCF3}_2}$ gave the best yields when done at relatively high concentration (> 0.5 M) and scale (> 25 mmol). This synthesis has been fully reproduced by multiple group members.
- These ligands, as solid powders, are stable under aerobic atmospheres for variable durations. $\mathbf{P^{tBu}_2N^{ArCF3}_2}$ and $\mathbf{P^{Ph}_2N^{ArCF3}_2}$ could be stored in a normal desiccator (in other words; not inert atmosphere storage) for months without noticeable decomposition. $\mathbf{P^{Cy}_2N^{ArCF3}_2}$ does not seem to be as stable and could be stored outside the glovebox for approximately two weeks before yellow discolouration is observed.
- When in solution, P_2N_2 ligands have been observed to oxidize rapidly, as assessed by $^{31}P\{^1H\}$ NMR. This is consistent with the study of Dubois and coworkers performing electrocataysis under an oxygen atmosphere.[2] Similarly, oily P_2N_2 derivatives are unstable in aerobic atmosphere and must be stored in the glovebox.
- Protonating the ligands with anhydrous $HBF_4 \bullet Et_2O$ to create a phosphonium salt was not successful and resulted in a poorly defined messy mixture.

- The primary phosphines used were all volatile and foul-smelling. The glovebox should be thoroughly purged after their use. All phosphine waste was sealed in an air-tight container prior to shipping out, opened in a fumehood and immediately quenched with an aqueous solution of bleach (~50% v/v) in a fumehood.
- 4-(trifluoromethyl)aniline is unstable to light and it is important to shield reaction vessels with aluminum foil after addition of this reactant. When the synthesis of $\mathbf{P^{Cy}_2N^{ArCF3}_2}$ was performed in a well-lit fumehood, a yellow powder was obtained rather than the normal white powder. GC-MS analysis of the powder (dissolved in acetone) revealed a 4-(trifluoromethyl)aniline-derived side-product (Figure 5.1). Decomposition of anilines are known in the literature. This side-product has not been observed since modification of the procedure to avoid light.

Scheme 5.2 Side-product observed when the synthesis of $\mathbf{P^{Cy}_2N^{ArCF3}_2}$ was exposed to light

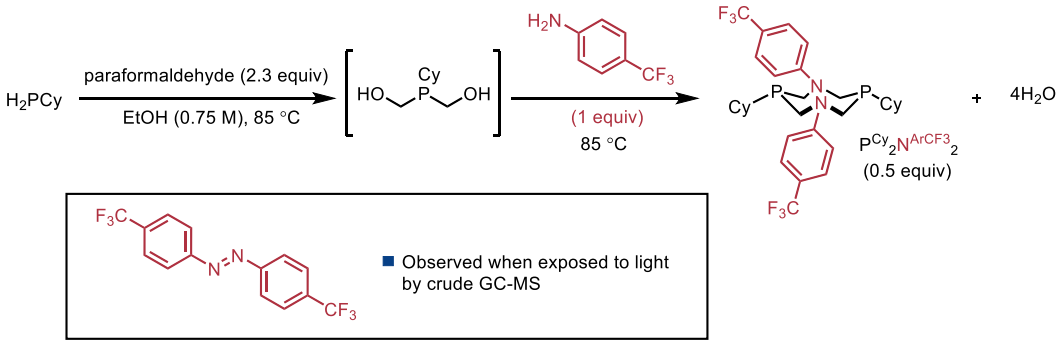

5.7 Conclusions

P_2N_2 ligands have been thoroughly studied over the past 40 years, with a variety of methods for their synthesis known. To achieve the work reported in Chapters 2-4, a thorough understanding of these methods was necessary. Furthermore, we reported a slightly modified synthetic procedure to prepare a diverse library of P_2N_2 ligands for use in cross-coupling chemistry. Screening of this library uncovered unique reactivity; these results are further described in Chapters 2-4. This chapter demonstrates the ease of which P_2N_2 ligands can be accessible to synthetic organic chemists.

5.8 Characterization of P_2N_2 ligands

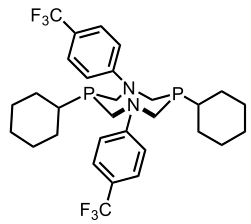

1,5-bis(*p*-benzotrifluoride)-3,7-bis(cyclohexyl)-1,5,3,7-diazadiphosphacyclooctane ($P^{Cy}_2N^{ArCF3}_2$) was prepared according to the general procedure on a 33 mmol scale (66 mmol of starting materials). $P^{Cy}_2N^{ArCF3}_2$ was isolated as a creamy off-white solid (18.8 g, 94% yield). **^{1}H NMR** ($CDCl_3$, 500 MHz) δ (ppm) 7.45 (d, J = 8.7 Hz, 2.95H), 7.41 (d, J = 8.7 Hz, 3.84H), 6.91 (d, J = 8.7 Hz, 2.98H), 6.67 (d, J = 8.8 Hz, 3.99H), 4.35 (t, J = 13.9 Hz, 4.11H), 3.99 (dq, J = 14.4 Hz, 1.68Hz, 3.01H), 3.74 (t, J = 14.4 Hz, 3.04H), 3.60 (dd, J = 15.1 Hz, 4.85Hz, 4H), 2.02-1.68 (m, 20.17H), 1.67-1.60 (m, 2.14H), 1.52-1.27 (m, 18.67H). **^{13}C{^{1}H} NMR** ($CDCl_3$, 126 MHz) δ (ppm) 151.4, 147.8, 126.3-126.2 (m), 125.1 (q, J = 270.3 Hz), 124.9 (q, J = 270.3 Hz), 118.8 (q, J = 32.7 Hz), 117.9(q, J = 32.7 Hz), 112.7 (t, J = 2.2 Hz), 111.7 (t, J = 3.1 Hz), 55.4, 55.2, 49.2 (d, J = 6.7 Hz), 49.1 (d, J = 6.7 Hz), 29.8 (d, J = 12.2 Hz), 29.2 (d, J = 10.5 Hz), 27.0 (d, J = 8.6 Hz), 26.7 (d, J = 9.7 Hz), 26.3-26.2 (m). **^{19}F{^{1}H} NMR** ($CDCl_3$, 470 MHz) δ (ppm) -60.9, -61.1. **^{31}P{^{1}H} NMR** ($CDCl_3$, 202 MHz) δ (ppm) –27.9, -39.3. **Note**: $P^{Cy}_2N^{ArCF3}_2$ was previously reported in the primary literature as two conformers in the ^{31}P spectra but one conformer in the ^{1}H.[3] Our NMR sample displayed two conformers (major previously reported and minor unreported) in approximately 3:2 ratio with some overlapping peaks in the aliphatic region of the ^{1}H spectrum.

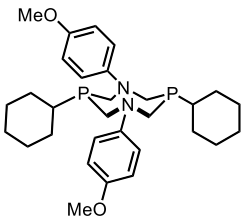

1,5-bis(4-methoxybenzene)-3,7-bis(cyclohexyl)-1,5,3,7-diazadiphosphacyclooctane ($P^{Cy}_2N^{ArOMe}_2$), was prepared according to the general procedure on a 25 mmol scale (50 mmol of starting materials). $P^{Cy}_2N^{ArOMe}_2$ was isolated as an off-white chunky solid (8.0 g, 61% yield). Characterization of the compound matched a previous reported synthesis.[4] **^{1}H NMR** ($CDCl_3$, 300 MHz) δ (ppm) 7.06-6.99 (m, 2.0H), 6.88-6.77 (m, 6.17H), 6.70-6.63 (m, 4.18H), 4.67-4.61 (m, 0.39H), 4.44-4.37 (m, 0.43H), 4.26-4.12 (t, J = 14.3 Hz, 3.94H), 3.78 (s, 2.65H), 3.71 (s, 5.96H), 3.64-3.51 (m, 5.78H), 1.97-0.98 (m, 29.7H). **^{31}P{^{1}H} NMR** ($CDCl_3$, 121MHz) δ (ppm) -42.9, -38.4, 27 (trace impurity). **Note: $P^{Cy}_2N^{ArOMe}_2$**was previously reported in the primary literature as one conformer.[1] Our NMR sample displayed two conformers (major previously reported and minor unreported) in approximately 3:2 ratio with overlapping peaks. The reported major conformer had two chemical shifts for the –OMe groups (singlet at δ = 3.78 for 3H and singlet at δ = 3.71 for 3H). We suspect the minor conformer has the two –OMe groups chemically equivalent and overlapping at δ = 3.71, whereas, for this structure, the two phosphorus atoms are chemically inequivalent (one phosphorus signal overlaps with the major peak at δ -42.9 and displaying a second peak at -38.4).

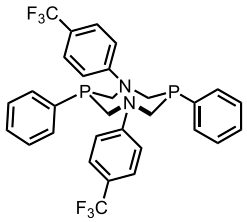

1,5-bis(*p*-benzotrifluoride)-3,7-bis(phenyl)-1,5,3,7-diazadiphosphacyclooctane ($P^{Ph}_2N^{ArCF3}_2$)was prepared according to the general procedure on a 2.5 mmol scale (5 mmol of starting materials). Crude solid was filtered and subsequently purified by rinsing impurities away with hexanes and MeCN. $P^{Ph}_2N^{ArCF3}_2$ was isolated as a white solid (0.594 g, 40% yield). **^{1}H NMR** ($CDCl_3$, 300 MHz) δ (ppm) 7.59-7.66 (m, 4H), 7.49-7.55(m, 6H), 7.44 (d,

J = 8.8 Hz, 4H), 6.75 (d, *J* = 8.8 Hz, 4H), 4.48 (t, *J* =, 13.9 Hz, 5.5 Hz, 4H), 4.06 (dd, *J* = 14.9 Hz, 4.8 Hz, 4H). **^{19}F{^{1}H} NMR** ($CDCl_3$, 282 MHz) *δ* (ppm) -61.1. **^{31}P{^{1}H} NMR** ($CDCl_3$, 121 MHz) *δ* (ppm) -51.4. Spectral data matches previous reported characterization of **$P^{Ph}_2N^{ArCF3}_2$**.[4]

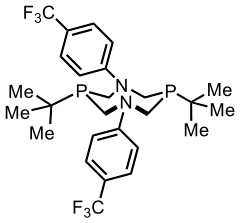

1,5-bis(*p*-benzotrifluoride)-3,7-bis(*tert*-butyl)-1,5,3,7-diazadiphosphacyclooctane ($P^{tBu}_2N^{ArCF3}_2$**)** was prepared according to the general procedure on a 12.5 mmol scale (25 mmol of starting materials). The crude solid was filtered and subsequently rinsed with hexanes and MeCN to remove impurities. **$P^{tBu}_2N^{ArCF3}_2$** was isolated as a white powder (4.87 g, 71% yield).**^{1}H NMR** ($CDCl_3$, 500 MHz) *δ* (ppm) 7.40 (d, *J* =, 8.7 Hz, 4.34H, major+minor), 6.89 (d, *J* = 8.7 Hz, 0.31H, minor), 6.69 (d, *J* = 8.8 Hz, 4.00H, major), 4.41 (t, *J* = 13.9 Hz, 4.02H, major), 4.13-4.05 (m, 0.32H, minor), 3.66 (t, *J* = 14.6 Hz, 0.63H, minor), 3.59 (dd, *J* = 14.8, 4.6 Hz, 4.03H, major), 1.29 (d, *J* = 10.4 Hz, 18.4H, major), 1.24 (d, *J* = 11.4 Hz, 1.90H, minor). **^{13}C{^{1}H} NMR** ($CDCl_3$, 125 MHz) *δ* (ppm) 147.8, 126.2 (q, *J* = 3.7 Hz), 125.1 (q, *J* = 270.3 Hz), 117.8 (q, *J* = 32.7 Hz),112.5 (t, *J* = 2.4 Hz, minor), 111.6 (t, *J* = 3.2 Hz, major), 54.96 (d, *J* = 23.6 Hz, major), 54.96 (d, *J* = 15.4 Hz, minor), 29.4-29.2 (m), 27.4-27.2 (m). **^{19}F{^{1}H} NMR** ($CDCl_3$, 470 MHz) *δ* (ppm) -61.0 (major), -61.1 (minor). **^{31}P{^{1}H} NMR** ($CDCl_3$, 202 MHz) *δ* (ppm) -21.1 (minor), -27.7 (major). **Note** P_2N_2 ligands are flexible and can exist as conformers in solution. Two conformers were observed in a ~10:1 ratio in the ^{1}H.

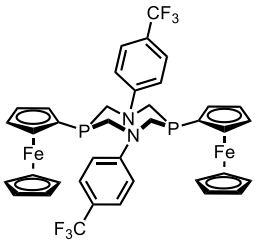

1,5-bis(4-benzotrifluoride)-3,7-bis(ferrocenyl)-1,5,3,7-diazadiphosphacyclooctane ($P^{Fc}_2N^{ArCF3}_2$**)** was prepared according to the general procedure on a 0.35 mmol scale (0.70 mmol of starting materials). **$P^{Fc}_2N^{ArCF3}_2$** was isolated as a yellow solid (72.0 mg, 24% yield). **^{1}H NMR** ($CDCl_3$, 500 MHz) *δ* (ppm) 7.49 (d, *J* = 7.7 Hz, 4H), 6.86 (d, *J* = 7.9 Hz, 4H), 4.51-4.21 (m, 24H), 3.76 (d, *J* = 13.4 Hz, 4H). **^{19}F{^{1}H} NMR** ($CDCl_3$, 470 MHz) *δ* (ppm) -61.0, -61.1, -61.3. **^{31}P{^{1}H} NMR** ($CDCl_3$, 202 MHz) *δ* (ppm) –43.6, -56.3. Conformers observed

Note: Some aliphatic impurities were observed. This is most likely the result of running the synthesis on a significantly smaller than normal scale. H_2PFc can be prepared on a large scale through a recent procedure.[5] If **$P^{Fc}_2N^{ArCF3}_2$** was prepared on a larger scale and impurities were still observed, we could purify by recrystallization.

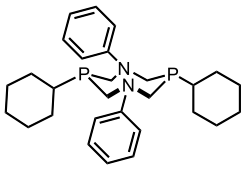

1,5-bis(*p*-benzotrifluoride)-3,7-bis(*iso*-butyl)-1,5,3,7-diazadiphosphacyclooctane ($P^{Cy}_2N^{Ph}_2$**)** was prepared according to the general procedure on a 16.5 mmol scale (33 mmol of starting materials). **$P^{Cy}_2N^{Ph}_2$** was isolated as a white solid which was poorly soluble in organic solvent (7.20 g, 94% yield). **^{1}H NMR** ($(CD_3)_2CO$, 300 MHz) *δ* (ppm) 7.20-7.12 (m, 4H), 6.98-6.92 (m, 4H), 6.68-6.63(m, 2H), 4.06-3.94 (m, 4H), 3.83-3.69 (m, 4H), 2.00-1.91 (m, 4H), 1.83-1.76 (m,4H), 1.72-1.66 (m, 2H), 1.37-1.26 (m, 12H). **^{31}P{^{1}H} NMR** ($(CD_3)_2CO$, 121 MHz) *δ* (ppm) –27.1, -42.5.Conformers observed. Spectral data is in general accordance with a previous literature report in $CDCl_3$.[6]

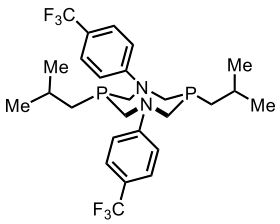

1,5-bis(*p*-benzotrifluoride)-3,7-bis(*iso*-butyl)-1,5,3,7-diazadiphosphacyclooctane ($P^{iBu}_2N^{ArCF3}_2$) was prepared according to the general procedure on a 12.5 mmol scale (25 mmol of starting materials). $P^{iBu}_2N^{ArCF3}_2$ was isolated as a creamy off-white solid (2.90 g, 42% yield). **^{1}H NMR** ($CDCl_3$, 500 MHz) δ (ppm) 7.47 (d, J = 8.7 Hz, 0.26H), 7.43 (d, J = 8.8 Hz, 3.85H), 6.92 (d, J = 8.8 Hz, 0.25H), 6.68 (d, J = 8.8 Hz, 4.00H), 4.18 (t, J = 14.7 Hz, 3.99H), 3.91 (d, J = 14.6 Hz, 0.24H), 3.68 (t, J = 14.3 Hz, 0.26H), 3.49 (dd, J = 15.1 Hz, 4.6 Hz, 3.92H), 1.96-1.86 (m, 2.08H), 1.85-1.77 (m, 0.19H), 1.43 (dd, J = 7.2 Hz, 1.2 Hz, 0.24H), 1.33 (d, J = 7.1 Hz, 3.94H), 1.14 (d, J = 6.6 Hz, 11.94H), 1.08 (d, J = 6.6 Hz, 0.80H). **^{13}C{^{1}H} NMR** ($CDCl_3$, 202 MHz) δ (ppm) 150.1 (minor), 147.9, 126.3 (q, J = 3.7 Hz), 125.0 (q, J = 270.3 Hz), 118.1 (q, J = 32.7 Hz), 111.7 (t, J = 3.3 Hz), 112.6 (minor), 58.1 (d, J = 17.8 Hz), 52.3 (dd, J = 16.6 Hz, 6.1 Hz), 34.3 (d, J = 14.1 Hz), 26.53 (d, J = 14.0 Hz) (minor), 26.47 (d, J = 14.0 Hz), 24.4 (d, J = 8.5 Hz), 24.2 (d, J = 8.5 Hz) (minor).**^{19}F{^{1}H} NMR** ($CDCl_3$, 470 MHz) δ (ppm) -60.9 (major), -61.1 (minor) **^{31}P{^{1}H} NMR** ($CDCl_3$, 202 MHz) δ (ppm) -39.4 (minor), -54.5 (major). **Note:** Conformers were observed, integrations are reported literally. $^{13}C\{^1H\}$ only shows some of the minor conformer peaks.

5.9 Spectra of P_2N_2 ligands

$P^{Cy}_2N^{ArCF3}_2$, ^1H, $CDCl_3$, 500 MHz, mixture of conformers

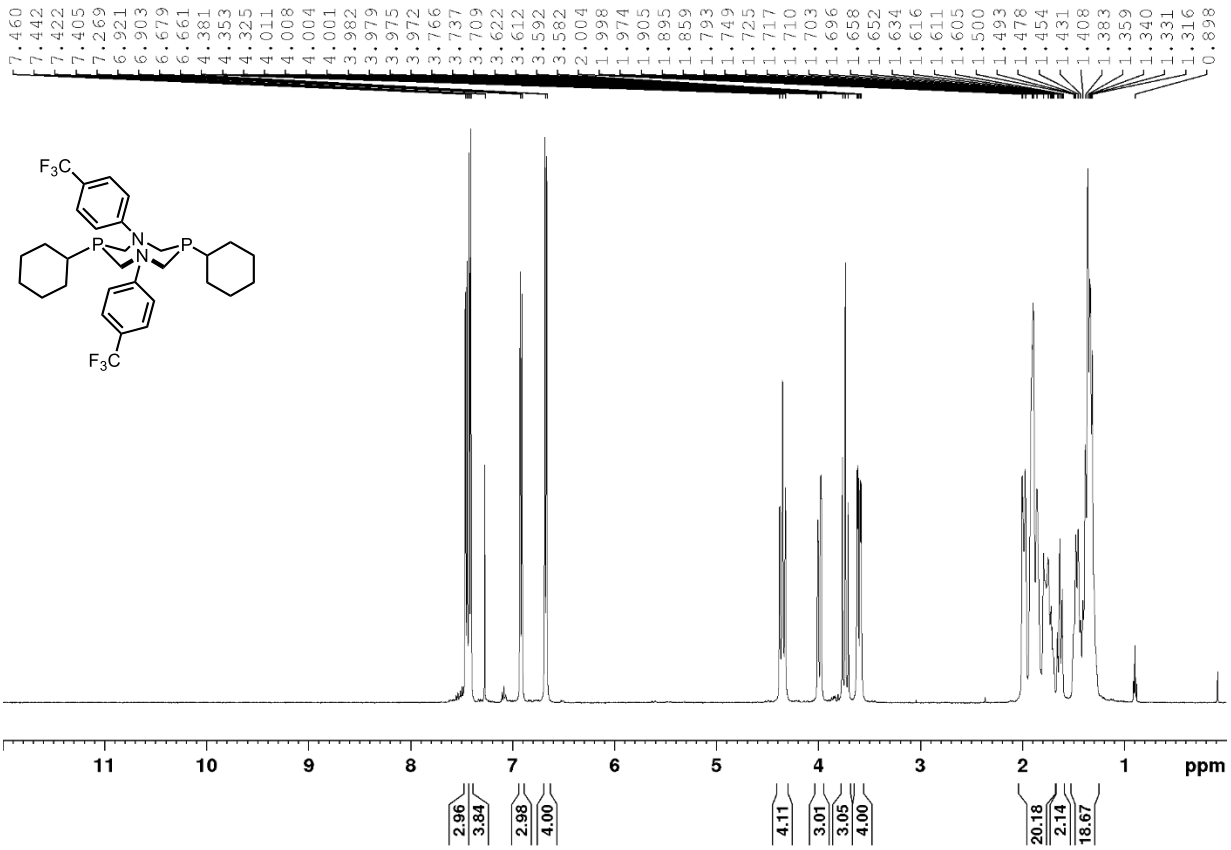

$P^{Cy}_2N^{ArCF3}_2$, $^{13}C\{^1H\}$, $CDCl_3$, 126 MHz, mixture of conformers

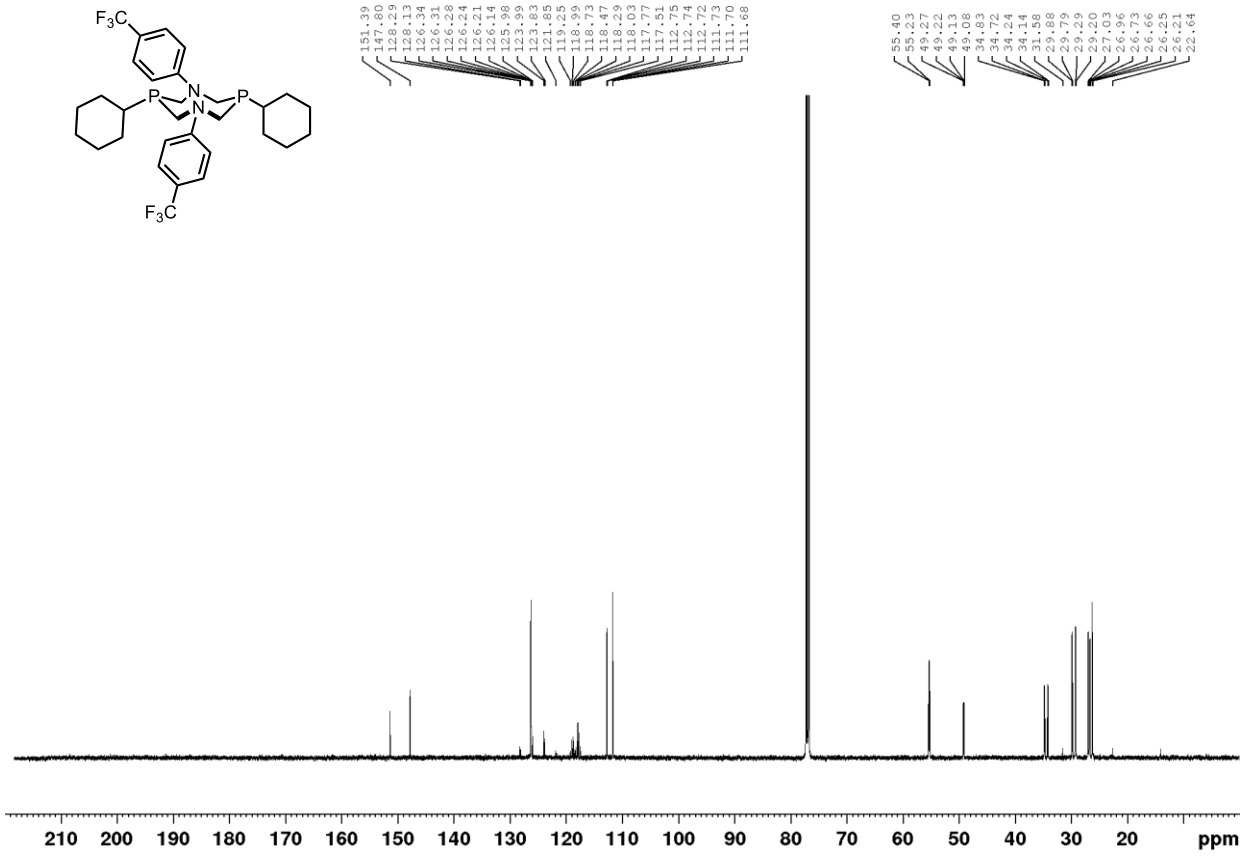

$P^{Cy}N^{ArCF3}{}_2$, $^{19}F\{^1H\}$, $CDCl_3$, 470 MHz, mixture of rotomers

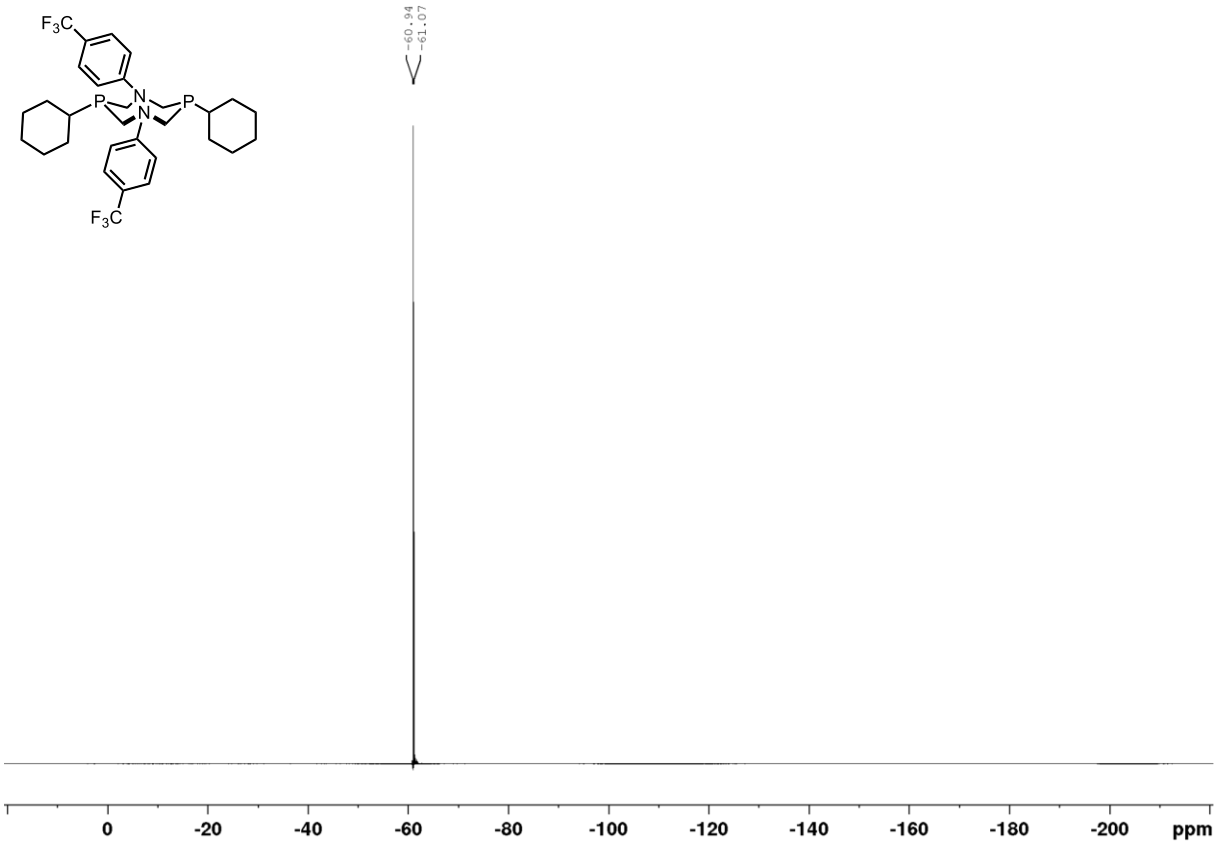

$P^{Cy}_2N^{ArCF3}_2$, $^{31}P\{^1H\}$, $CDCl_3$, 202 MHz, mixture of rotomers

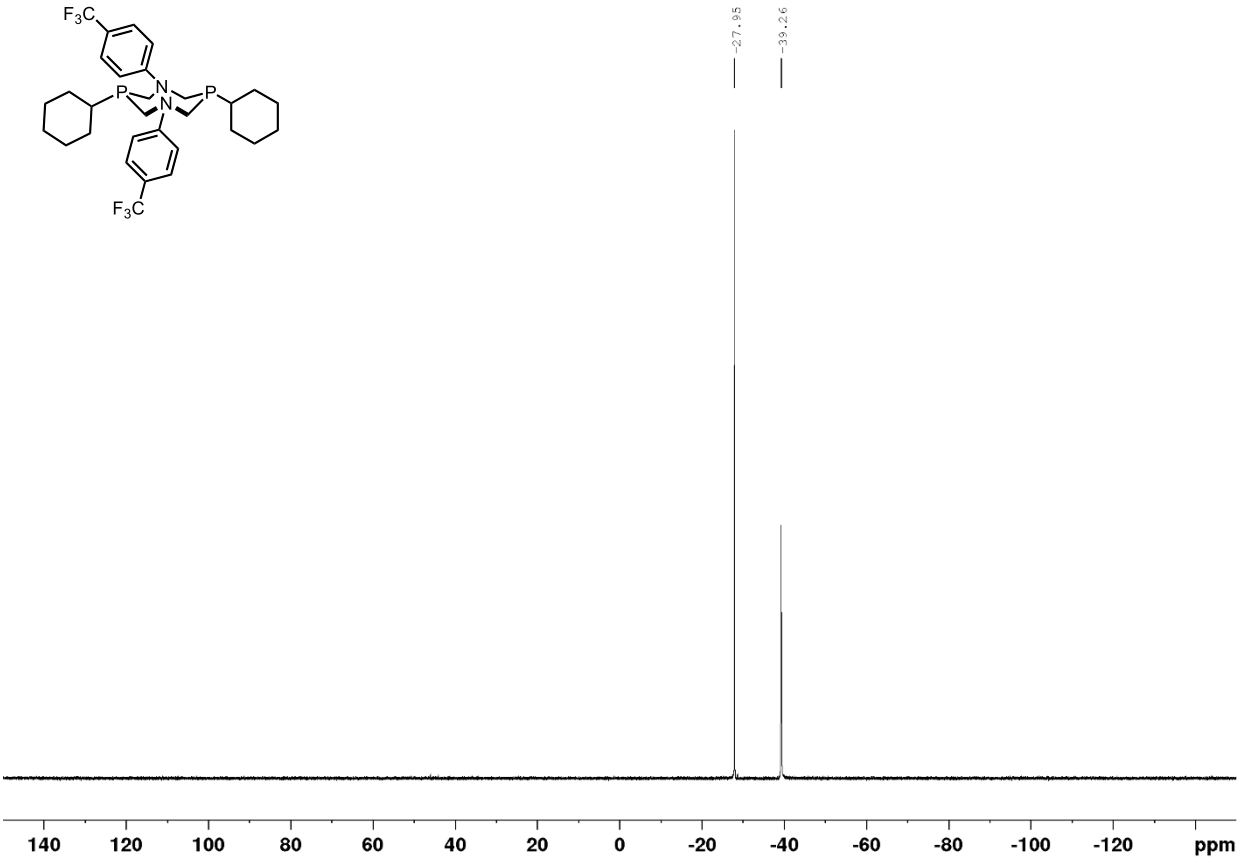

$P^{Cy}_2N^{ArOMe}_2$, ^1H, $CDCl_3$, 300 MHz, mixture of rotomers

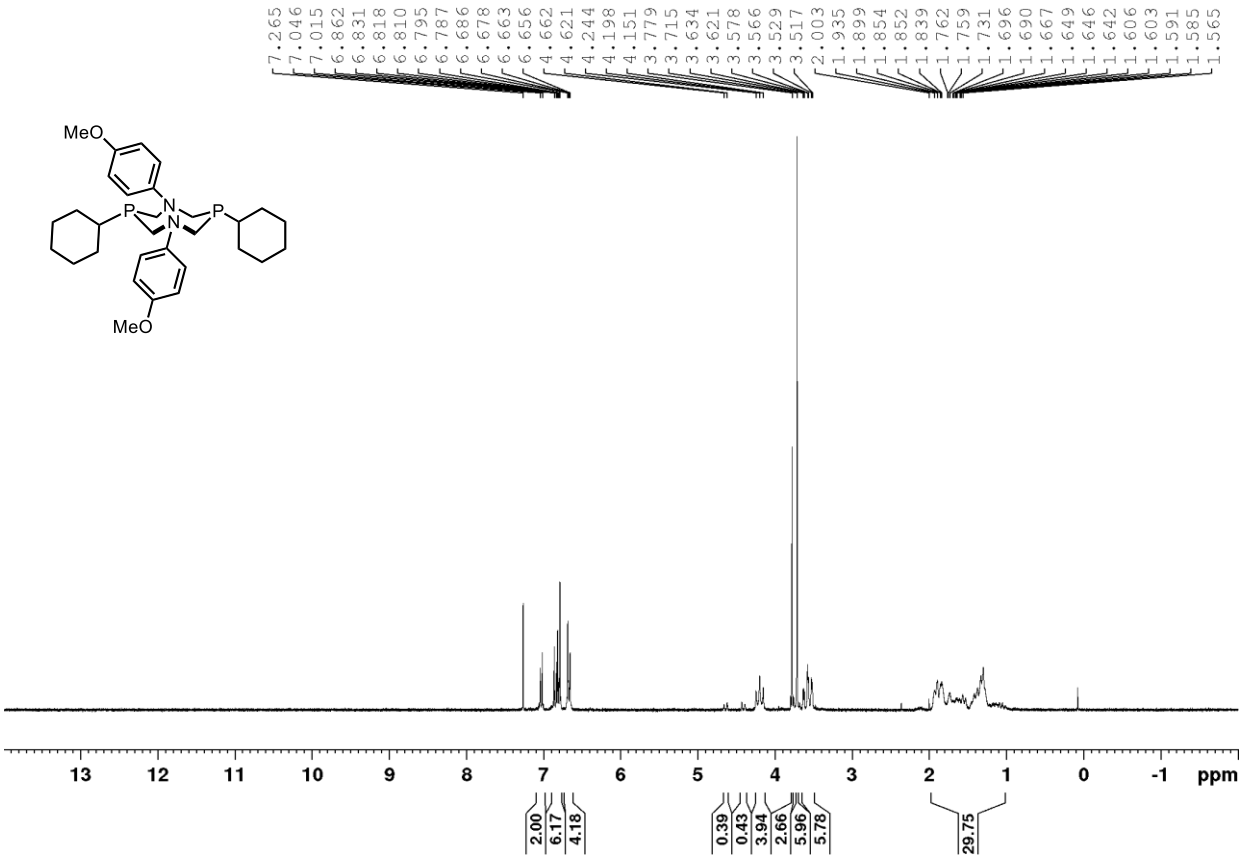

$P^{Cy}_2N^{ArOMe}_2$, $^{31}P\{^1H\}$, $CDCl_3$, 121 MHz, mixture of rotomers

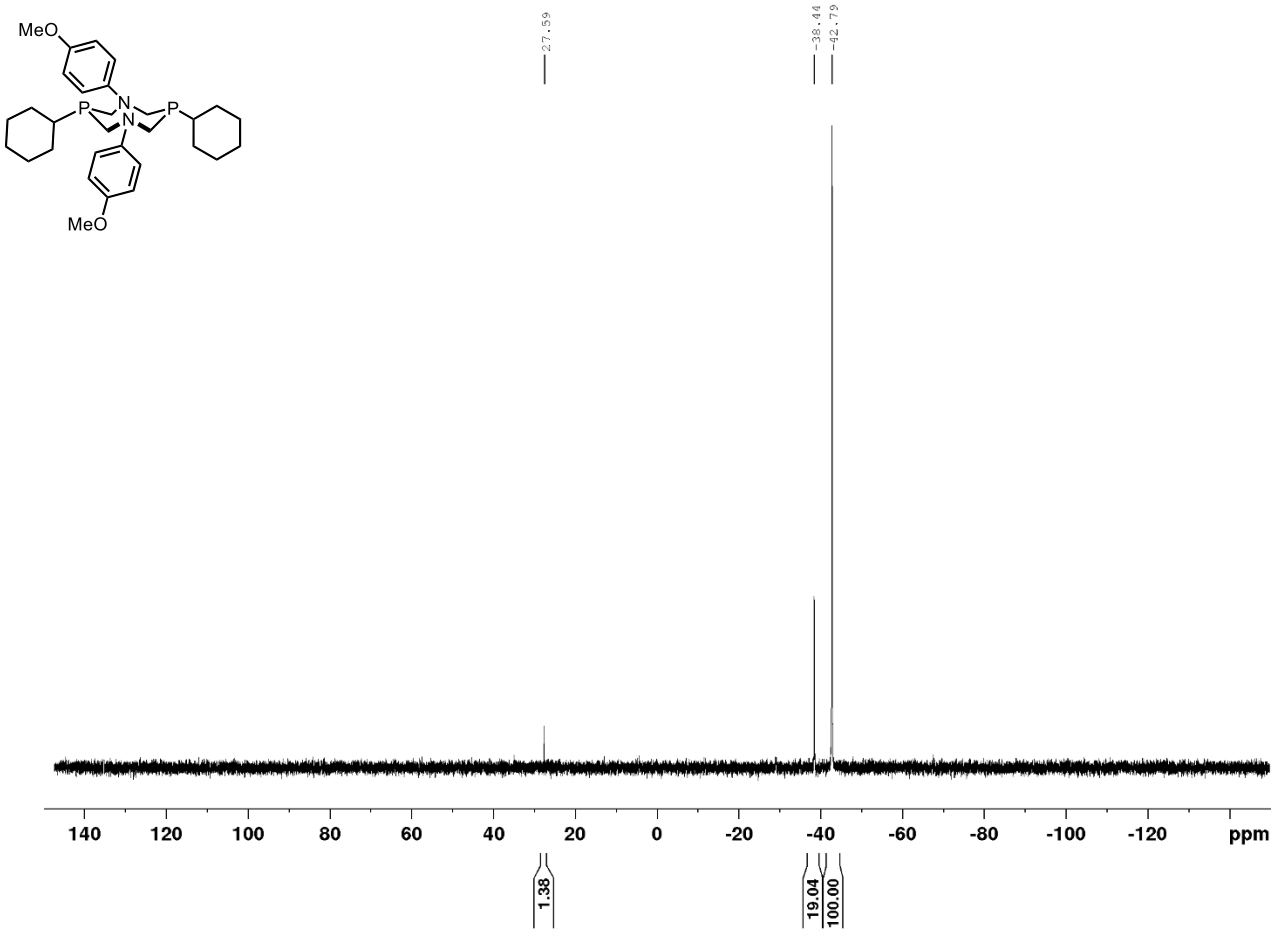

$P^{Ph}_2N^{ArCF3}_2$, ^1H, $CDCl_3$, 300 MHz

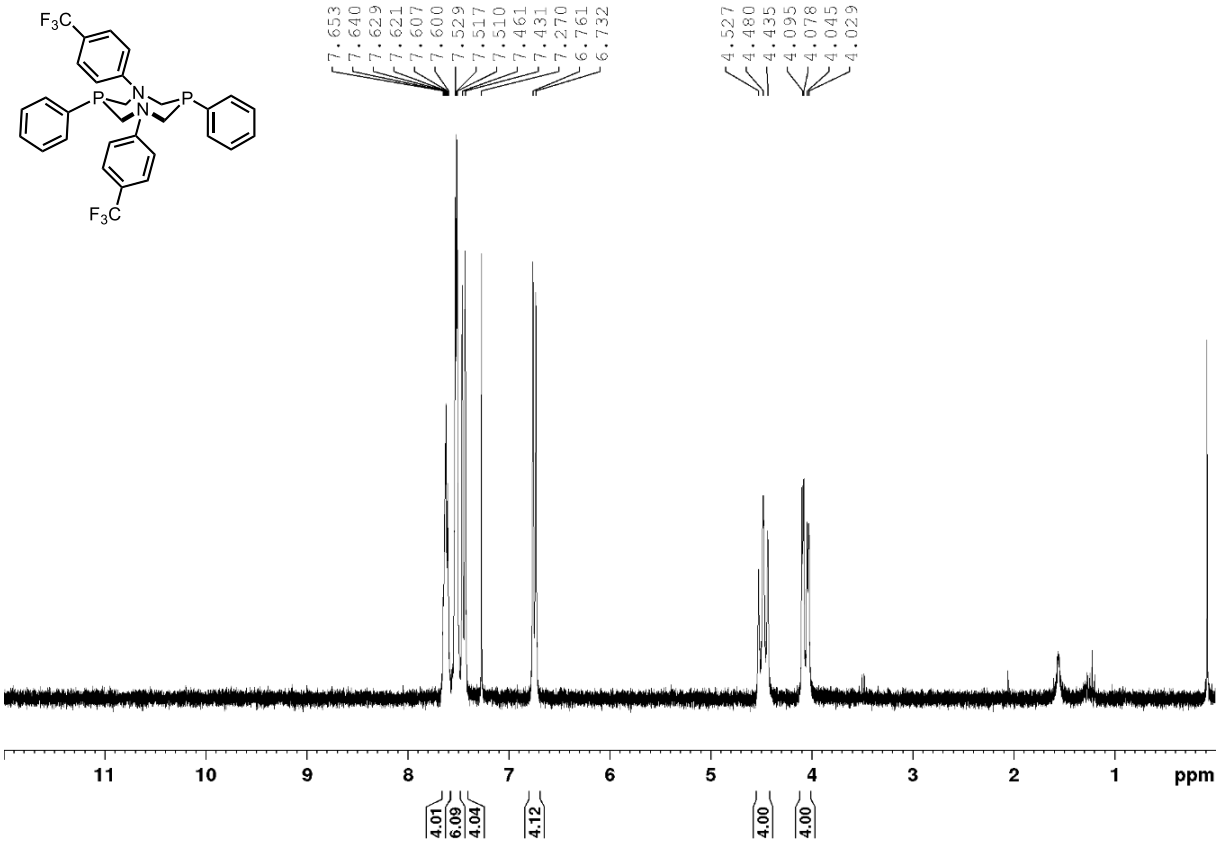

$P^{Ph}_2N^{ArCF3}_2$, $^{19}F\{^1H\}$, $CDCl_3$, 282 MHz

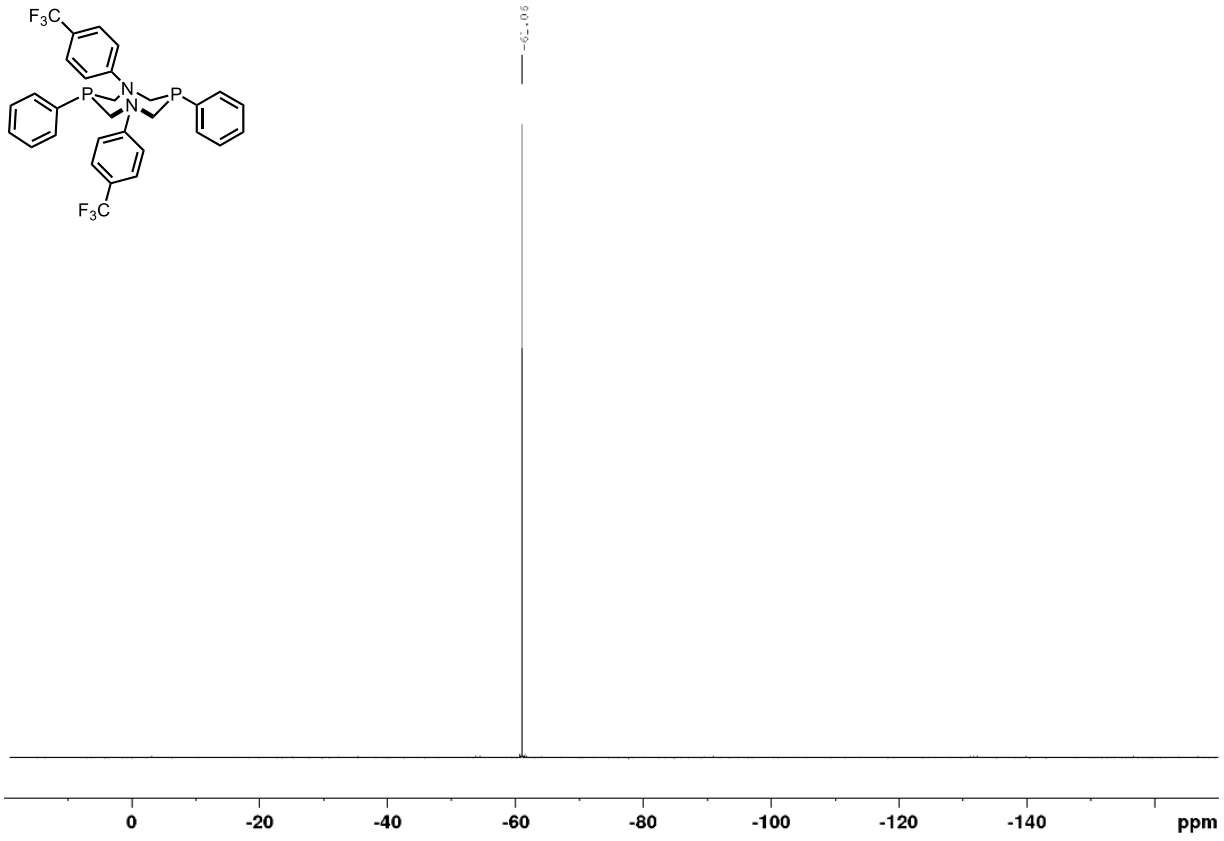

$P^{Ph}_2N^{ArCF3}_2$, $^{31}P\{^1H\}$, $CDCl_3$, 121.5 MHz

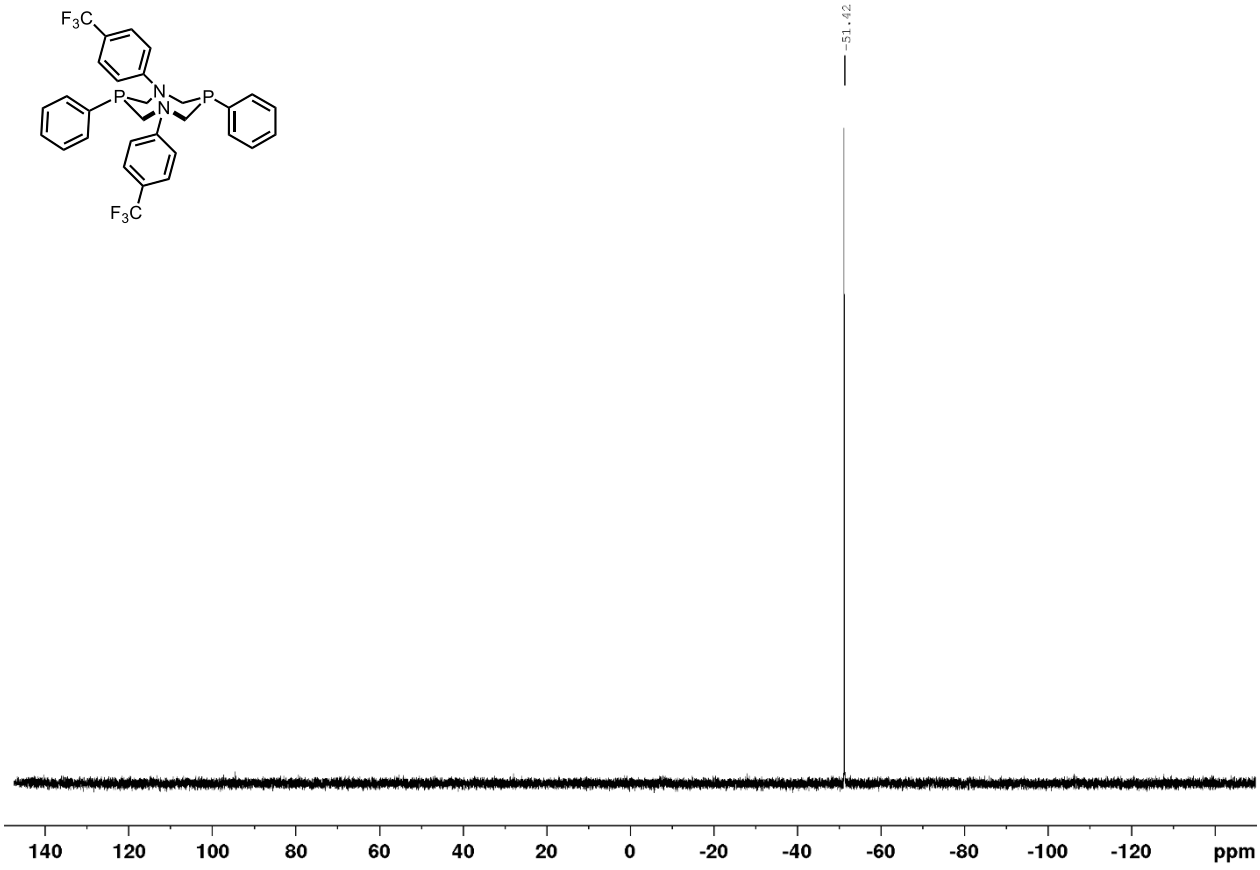

$P^{tBu}{}_2N^{ArCF3}{}_2$, ^1H, $CDCl_3$, 500MHz

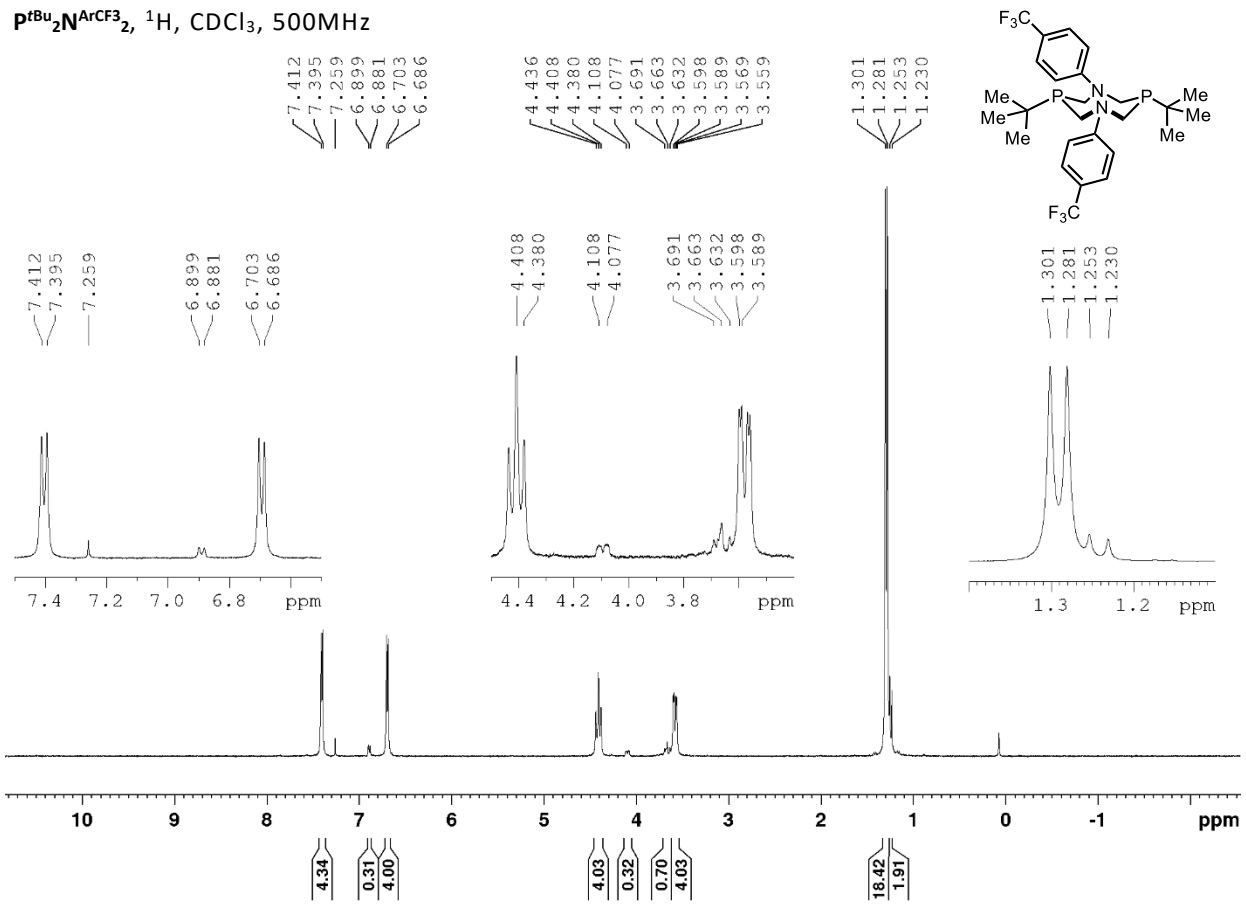

$P^{tBu}{}_2N^{ArCF3}{}_2$, $^{13}C\{^1H\}$, $CDCl_3$, 125MHz

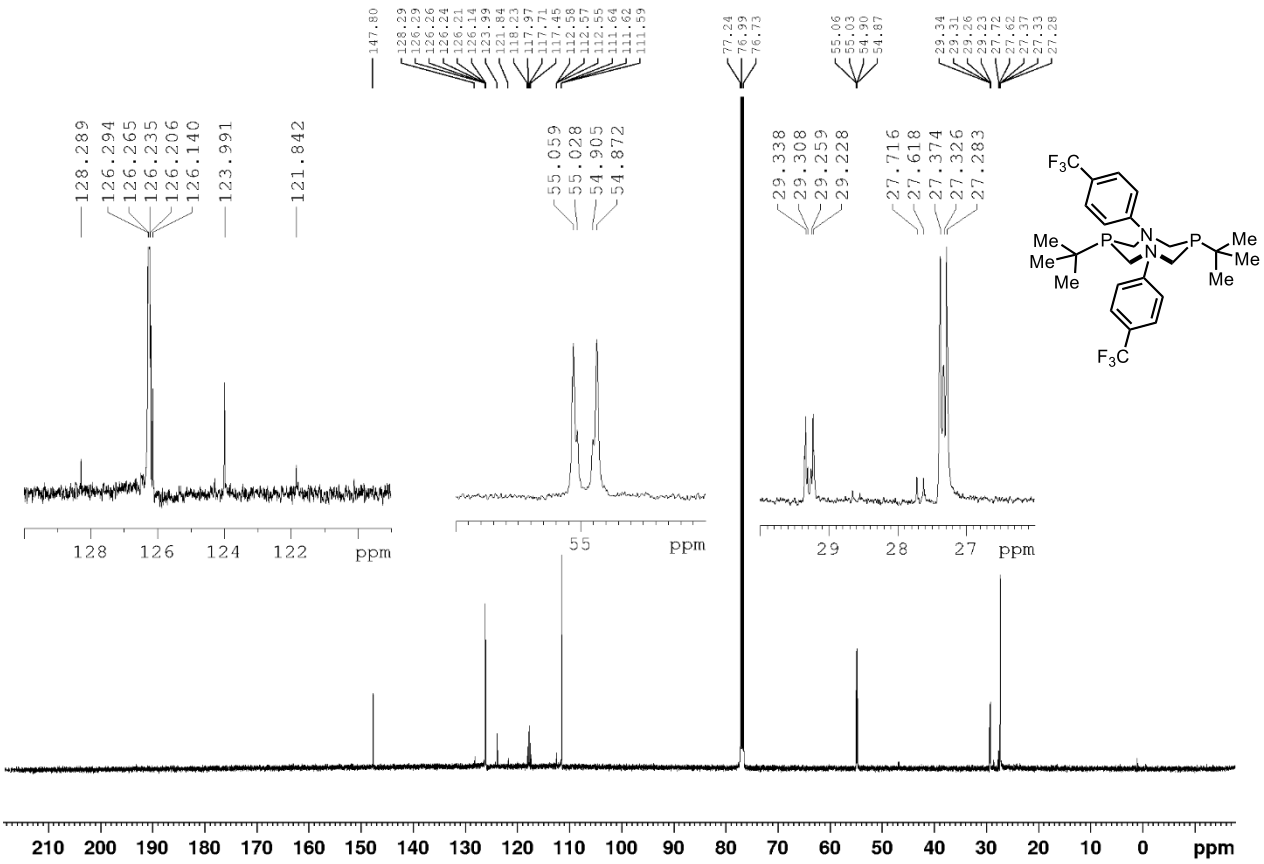

$P^{tBu}{}_2N^{ArCF3}{}_2$, ^{1}H-^{13}C HSQC, $CDCl_3$

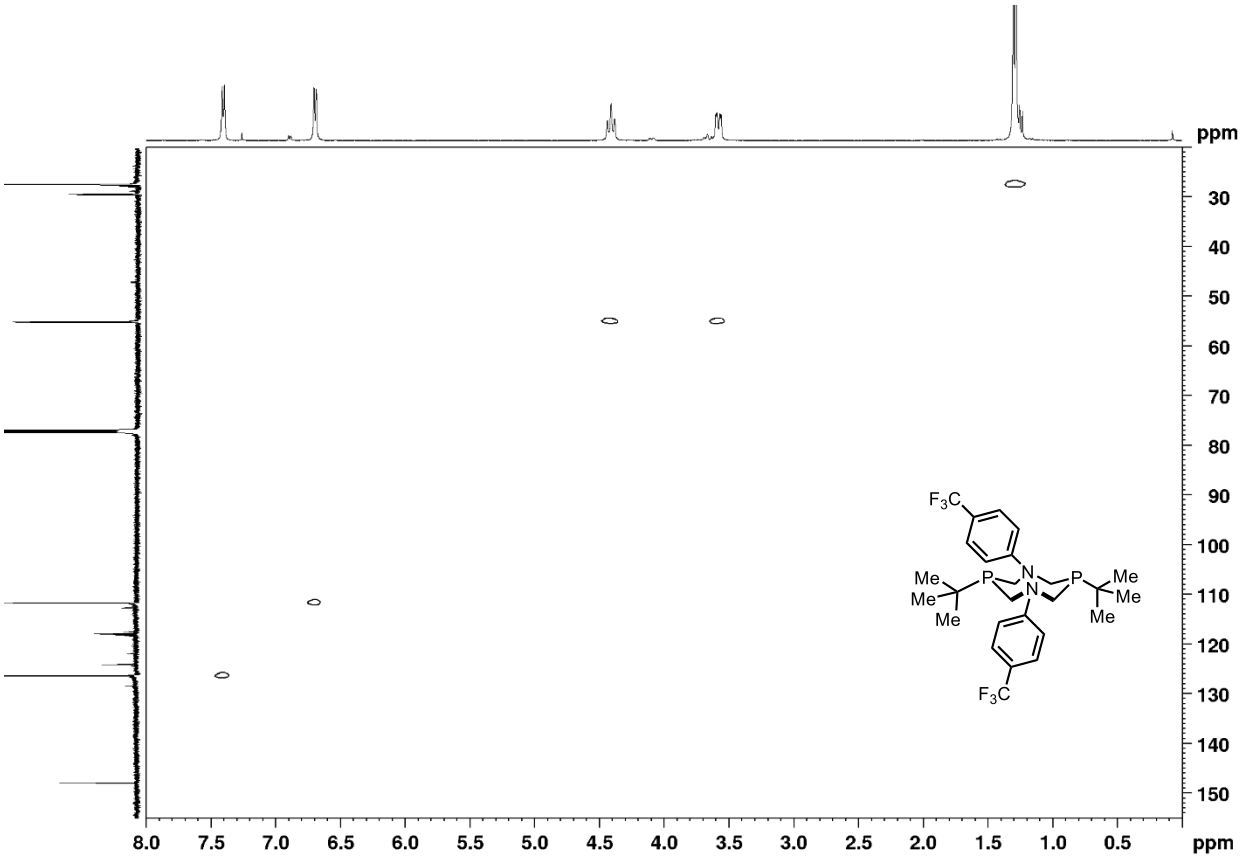

$P^{tBu}{}_2N^{ArCF3}{}_2$, ^{1}H-^{13}C HMBC, $CDCl_3$

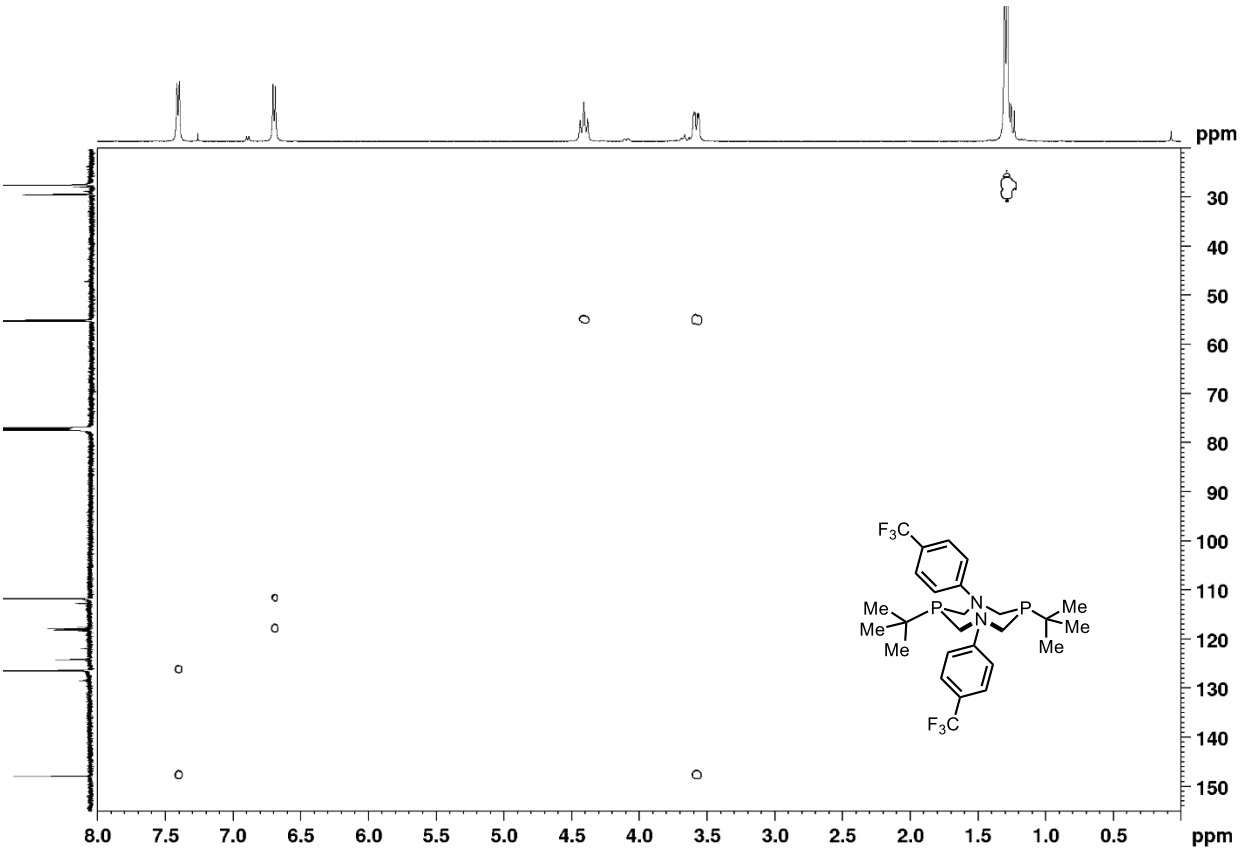

$P^{tBu}{}_2N^{ArCF3}{}_2$, $^{19}F\{^1H\}$, $CDCl_3$, 470 MHz

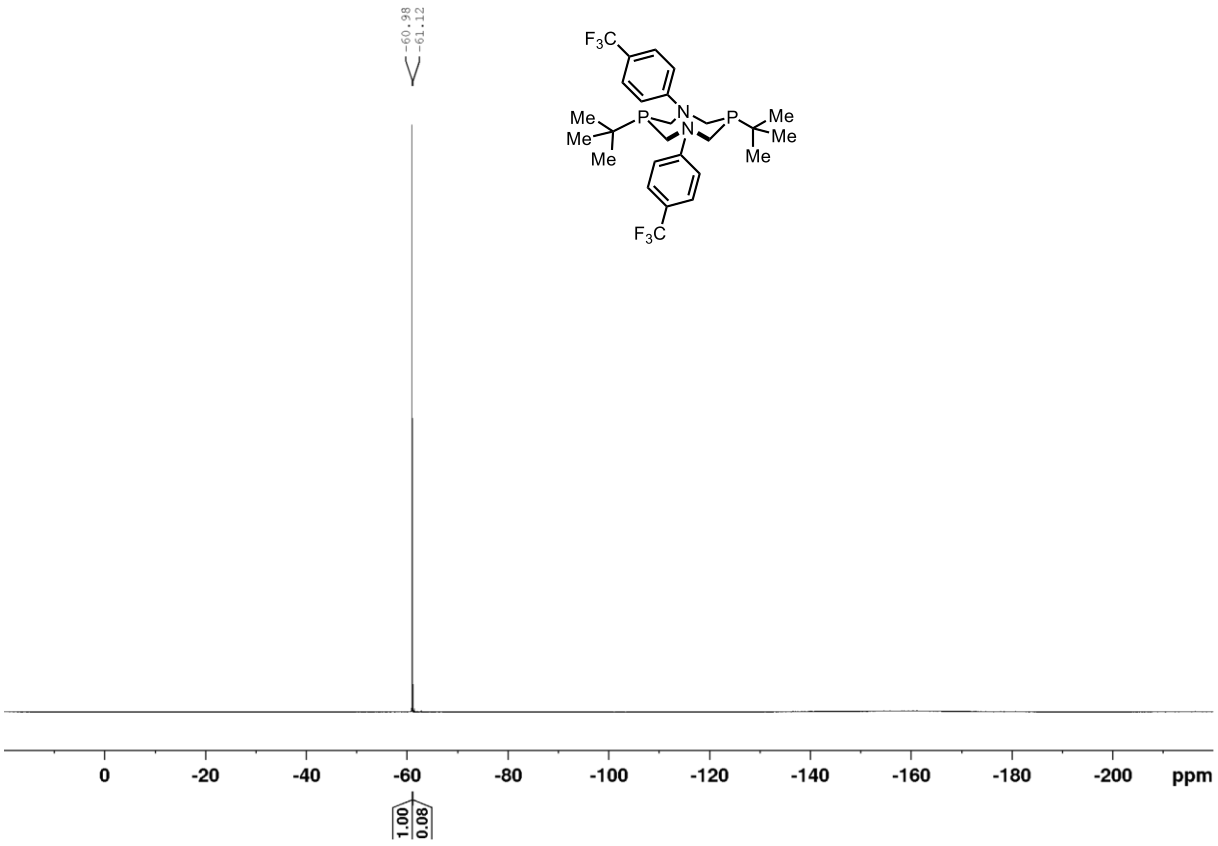

$P^{tBu}{}_2N^{ArCF3}{}_2$, $^{31}P\{^1H\}$, $CDCl_3$, 202 MHz

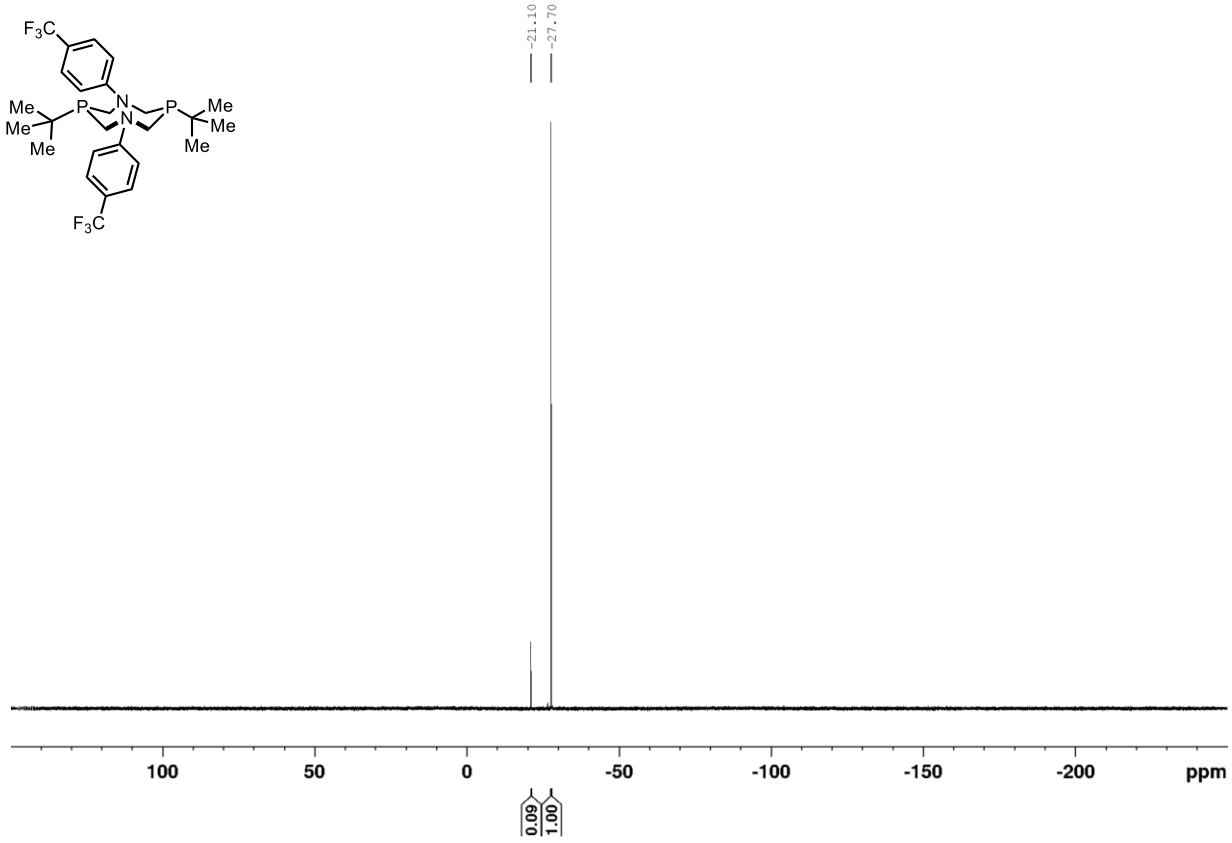

1,5-bis(4-benzotrifluoride)-3,7-bis(ferrocenyl)-1,5,3,7-diazadiphosphacy clooctane ($P^{Fc}_2N^{ArCF3}_2$), ^1H, $CDCl_3$, 500MHz

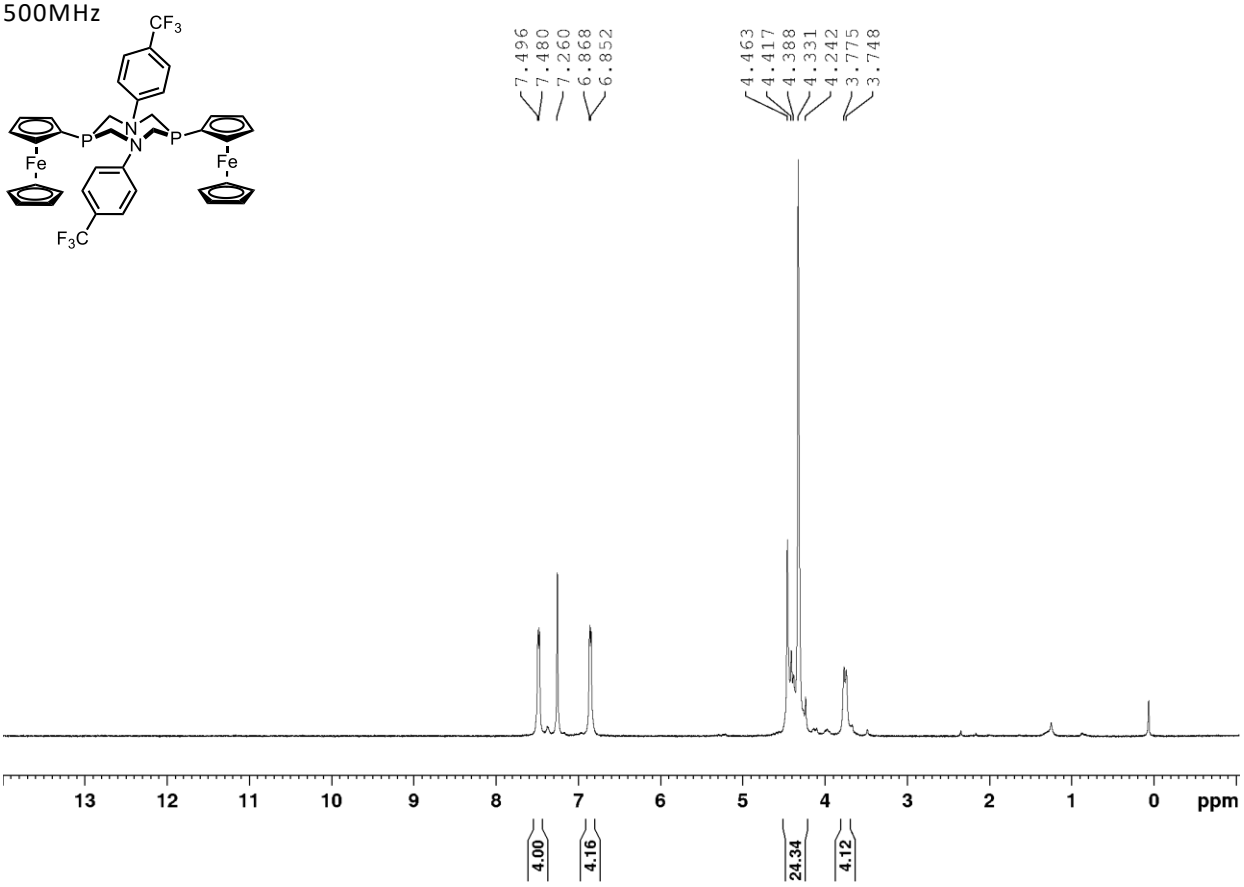

1,5-bis(4-benzotrifluoride)-3,7-bis(ferrocenyl)-1,5,3,7-diazadiphosphacyclooctane ($P^{Fc}_2N^{ArCF3}_2$), $^{19}F\{^1H\}$, $CDCl_3$, 470 MHz

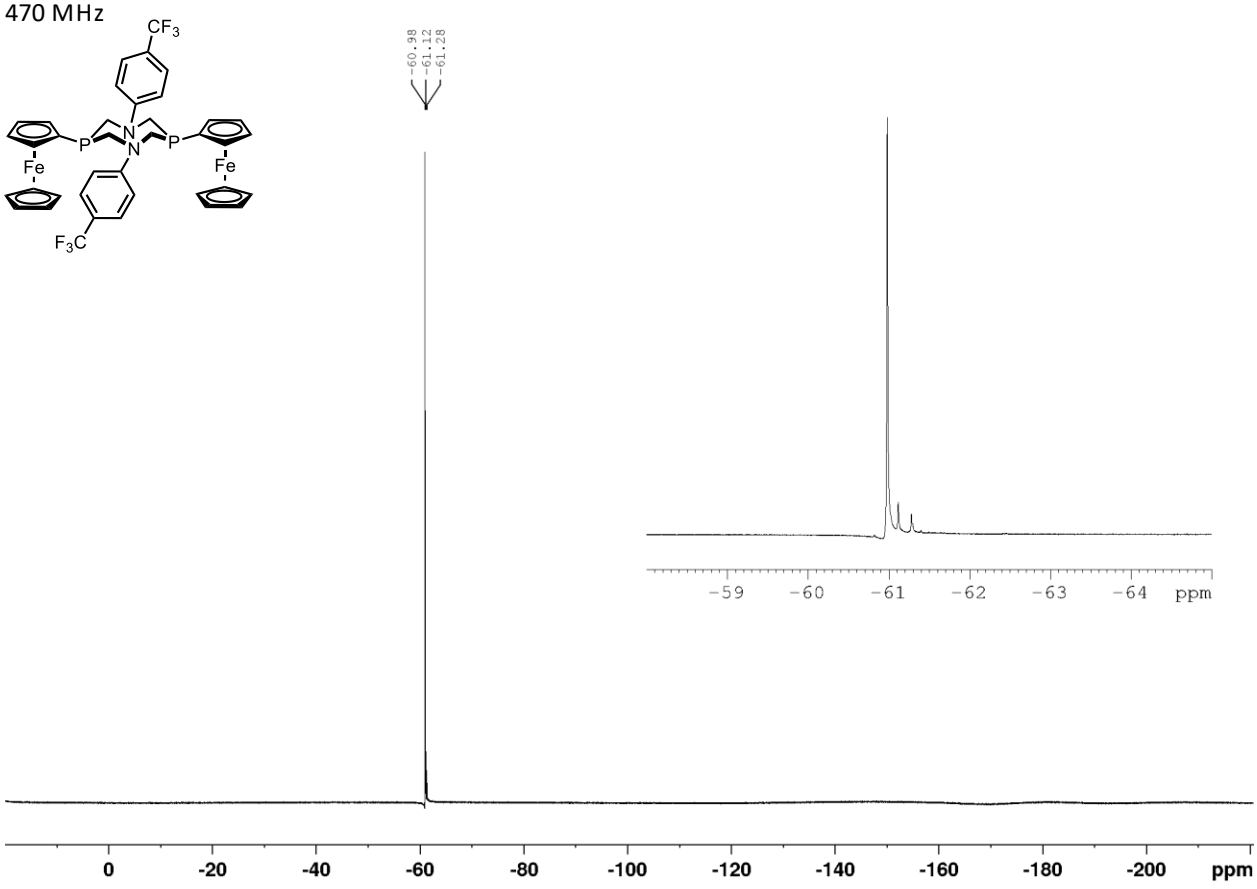

1,5-bis(4-benzotrifluoride)-3,7-bis(ferrocenyl)-1,5,3,7-diazadiphosphacyclooctane ($P^{Fc}_2N^{ArCF3}_2$), $^{31}P\{^1H\}$, $CDCl_3$, 202MHz

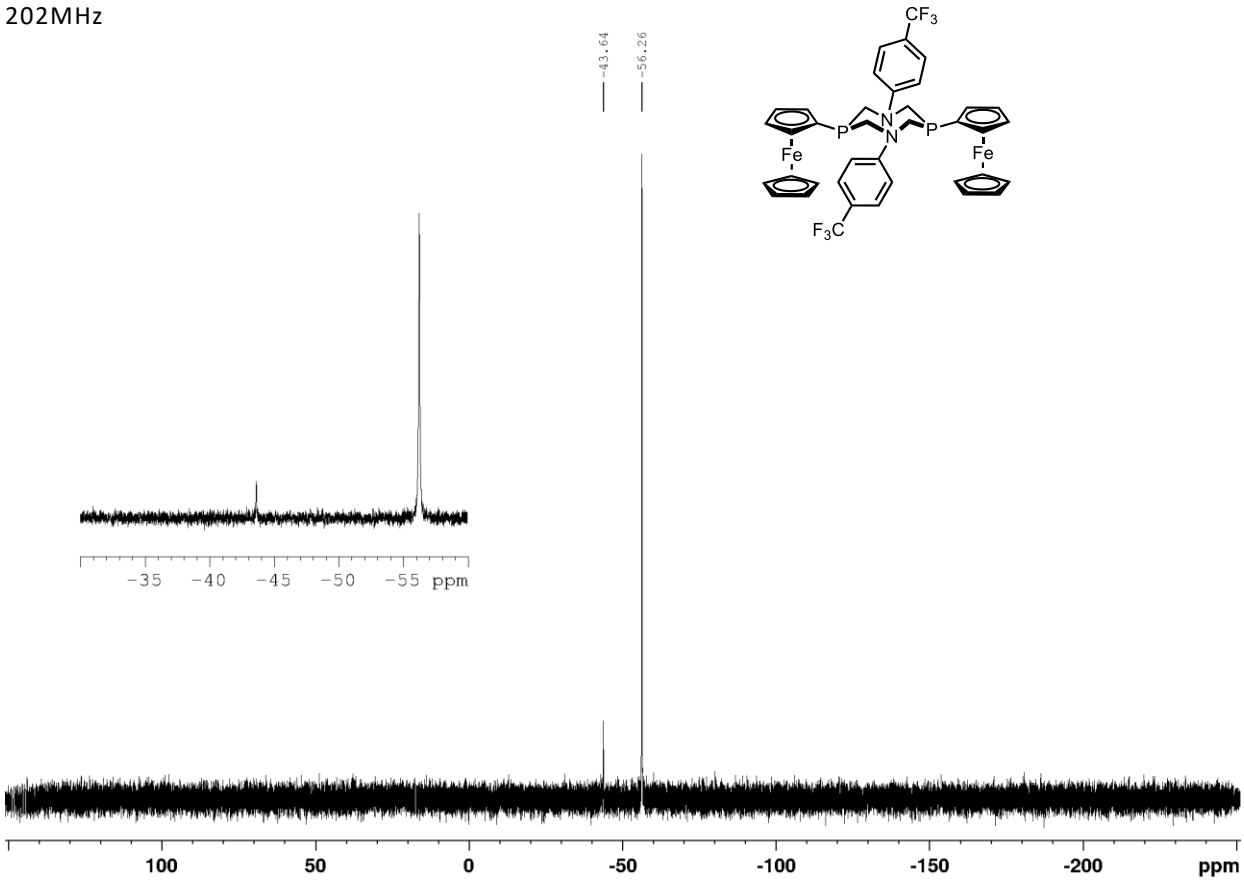

1,5-bis(*p*-benzotrifluoride)-3,7-bis(cyclohexyl)-1,5,3,7-diazadiphosphacyclooctane ($P^{Cy}_2N^{Ph}_2$), ^1H, $(CD_3)_2CO$, 300MHz

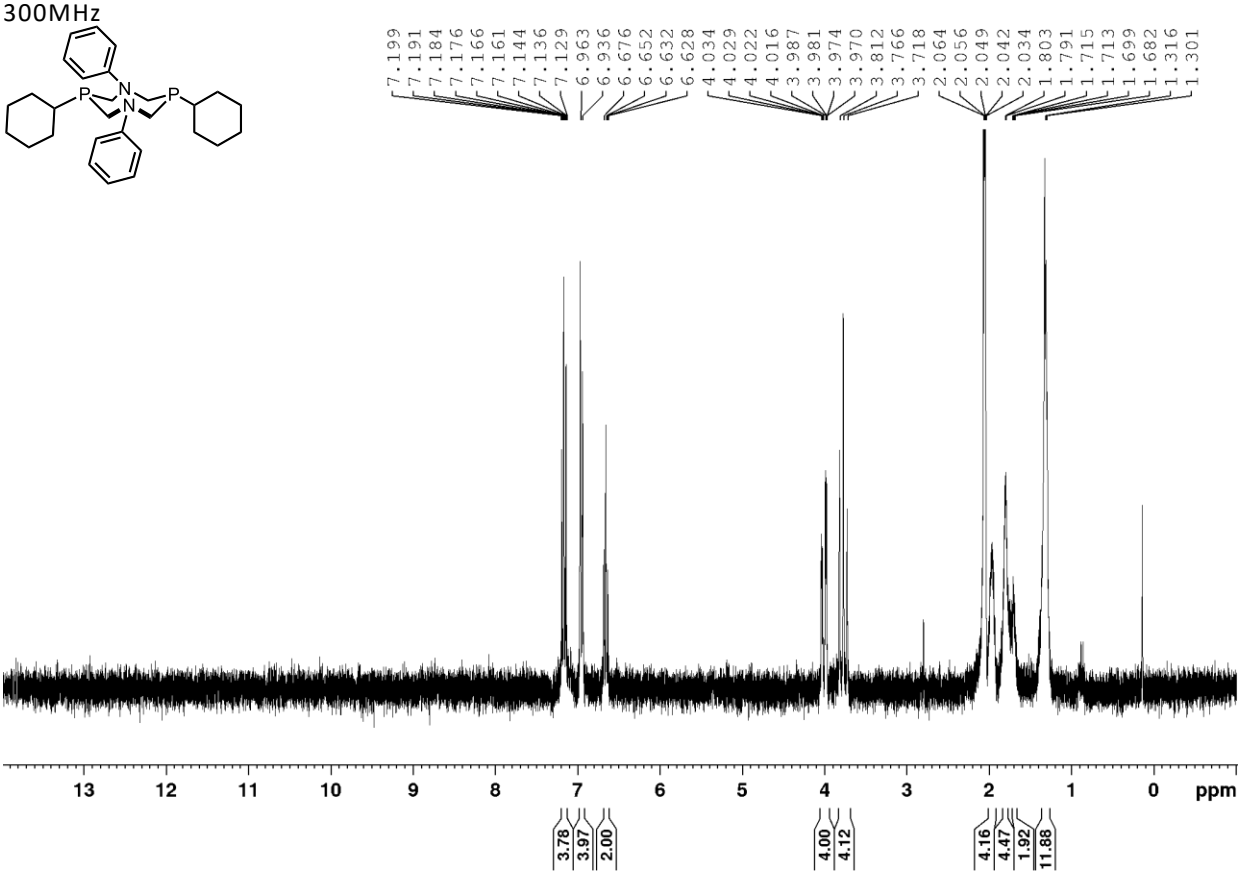

1,5-bis(*p*-benzotrifluoride)-3,7-bis(cyclohexyl)-1,5,3,7-diazadiphosphacyclooctane ($P^{Cy}_2N^{Ph}_2$), $^{31}P\{^1H\}$, $(CD_3)_2CO$, 121 MHz

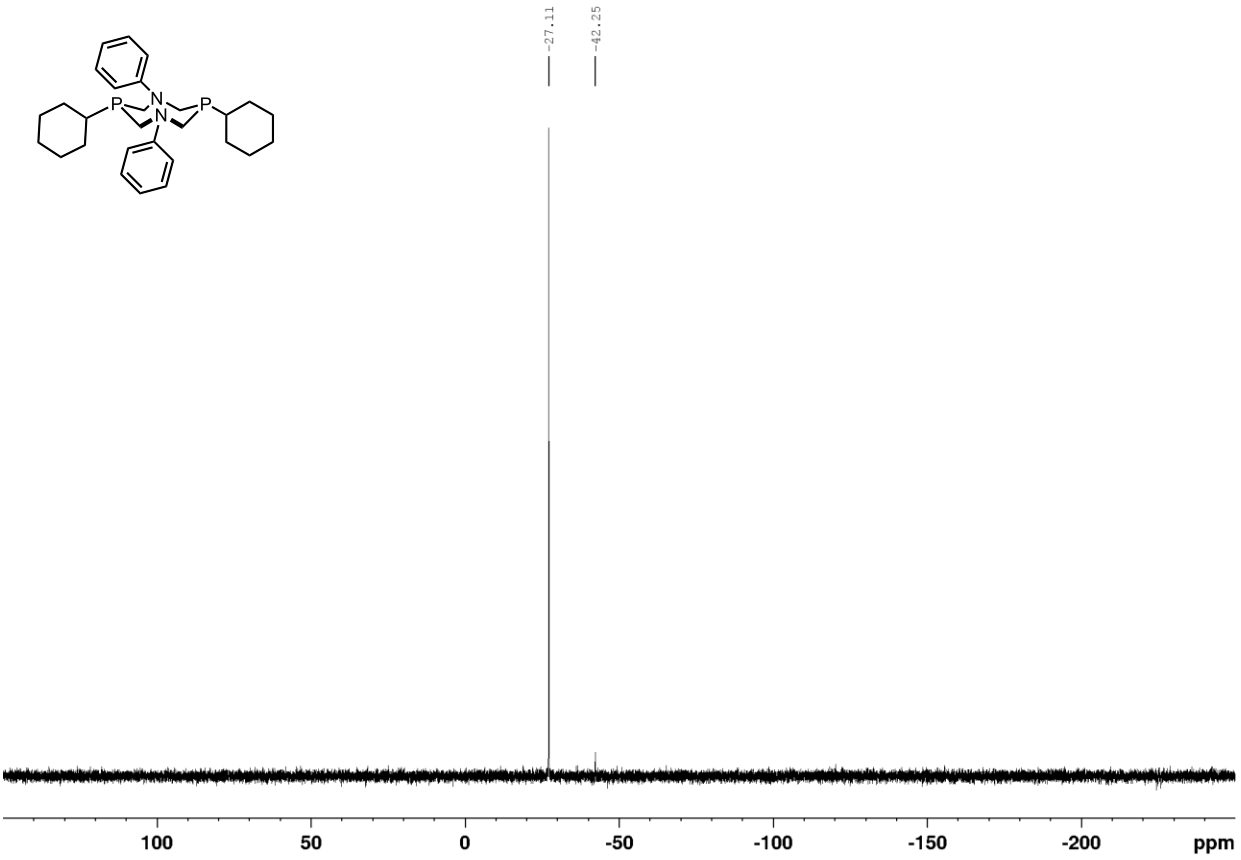

1,5-bis(*p*-benzotrifluoride)-3,7-bis(isobutyl)-1,5,3,7-diazadiphosphacyclooctane ($P^{iBu}_2N^{Ph}_2$),^{1}H, $CDCl_3$, 500 MHz

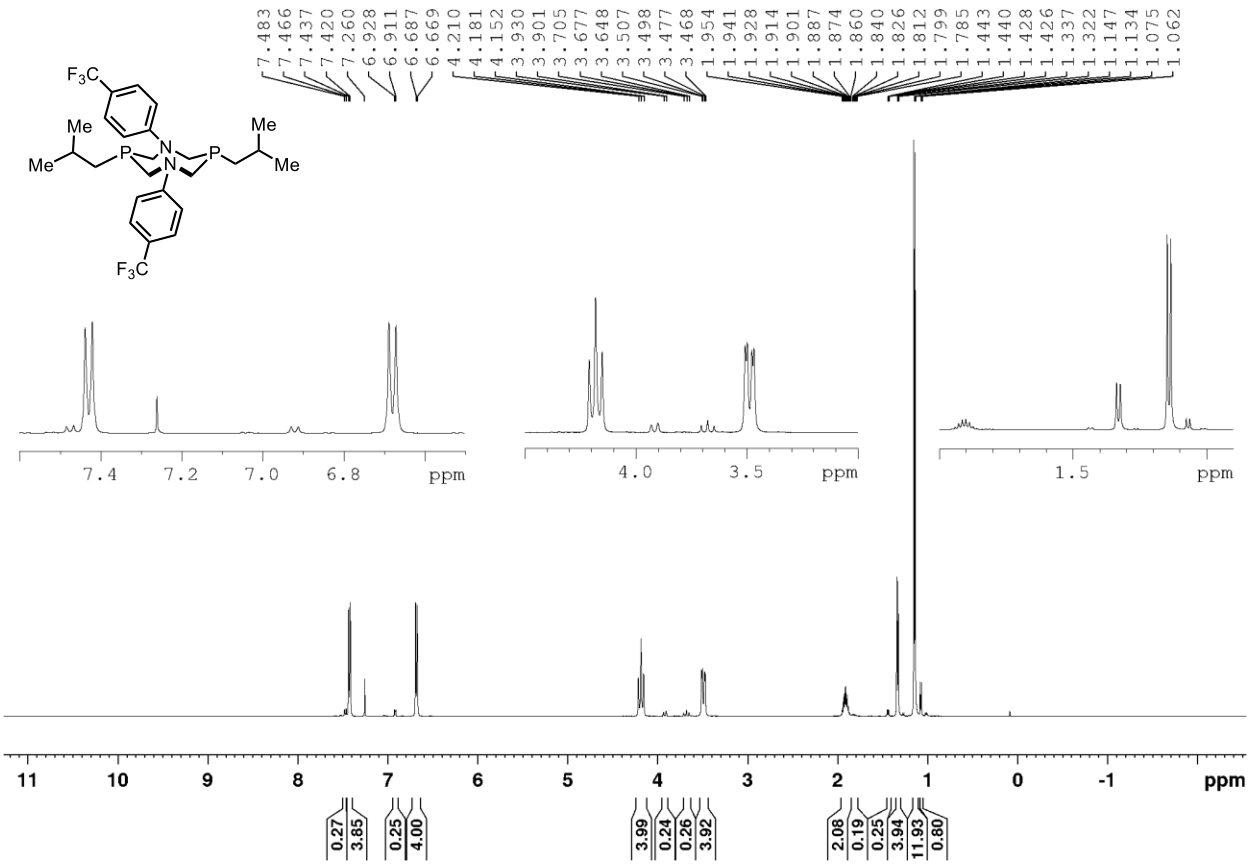

1,5-bis(*p*-benzotrifluoride)-3,7-bis(isobutyl)-1,5,3,7-diazadiphosphacyclooctane ($P^{iBu}_2N^{Ph}_2$),$^{13}C\{^1H\}$, $CDCl_3$, 125 MHz

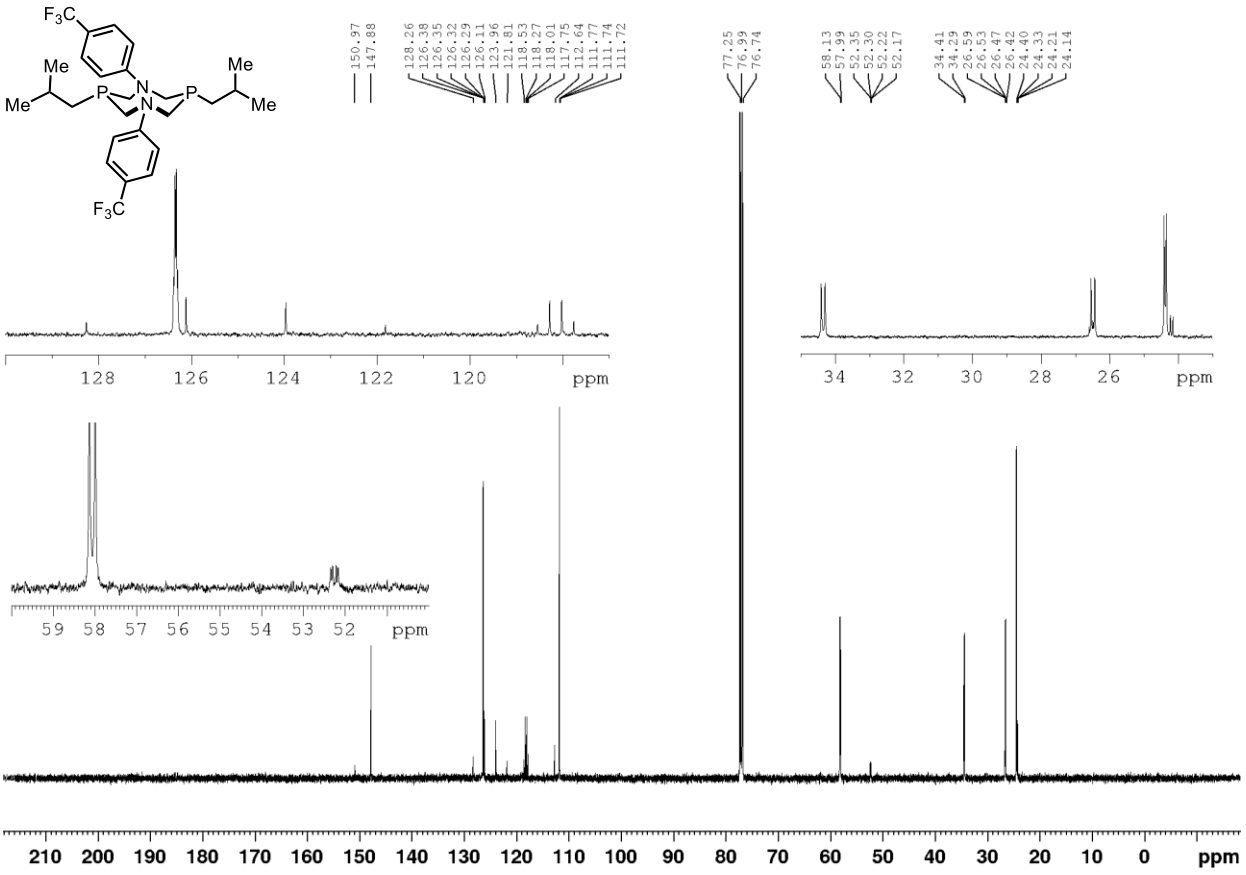

1,5-bis(*p*-benzotrifluoride)-3,7-bis(isobutyl)-1,5,3,7-diazadiphosphacyclooctane ($P^{iBu}_2N^{Ph}_2$), HSQC, $CDCl_3$

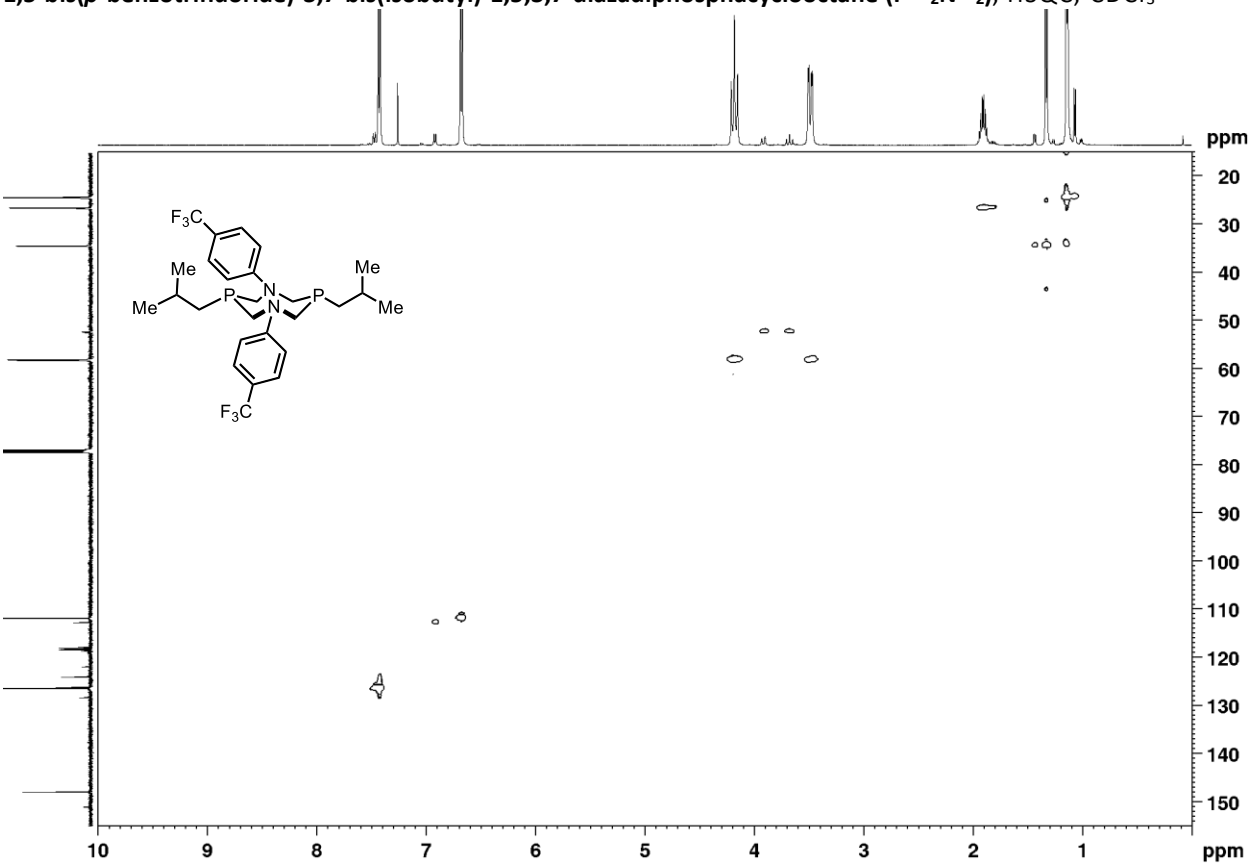

,

1,5-bis(*p*-benzotrifluoride)-3,7-bis(isobutyl)-1,5,3,7-diazadiphosphacyclooctane ($P^{iBu}_2N^{Ph}_2$), HSQC, $CDCl_3$, Zoomed-in

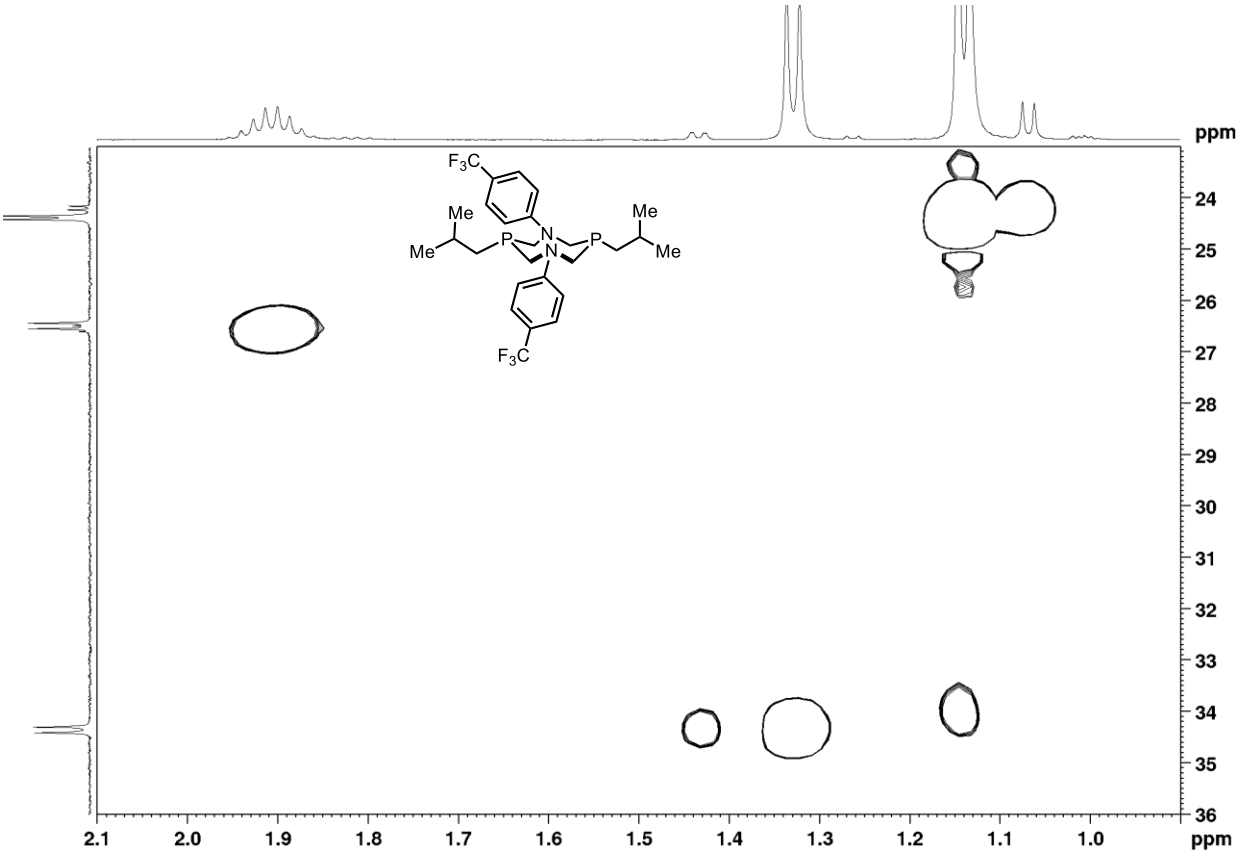

1,5-bis(*p*-benzotrifluoride)-3,7-bis(isobutyl)-1,5,3,7-diazadiphosphacyclooctane ($P^{iBu}_2N^{Ph}_2$), HSQC, $CDCl_3$, Zoomed in

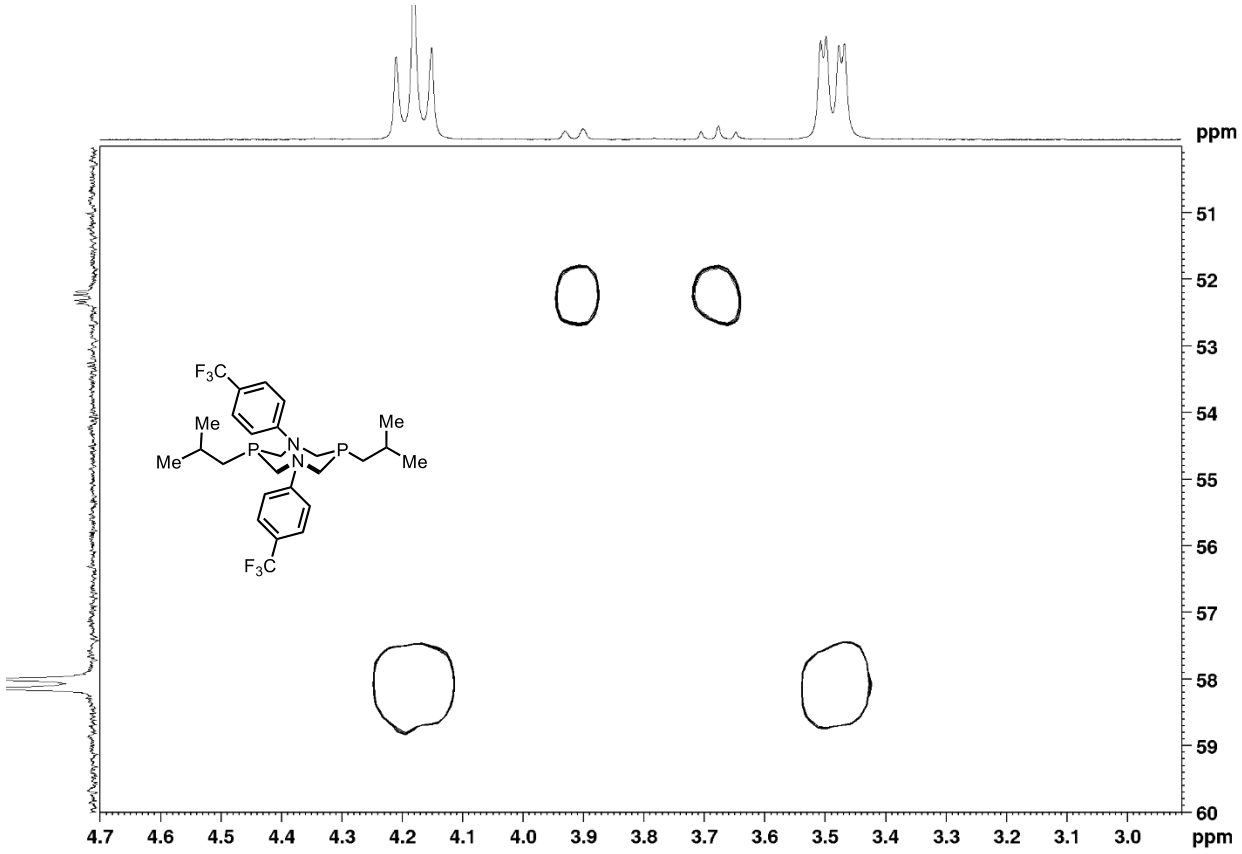

1,5-bis(*p*-benzotrifluoride)-3,7-bis(isobutyl)-1,5,3,7-diazadiphosphacyclooctane ($P^{iBu}_2N^{Ph}_2$), HSQC, $CDCl_3$, Zoomed in

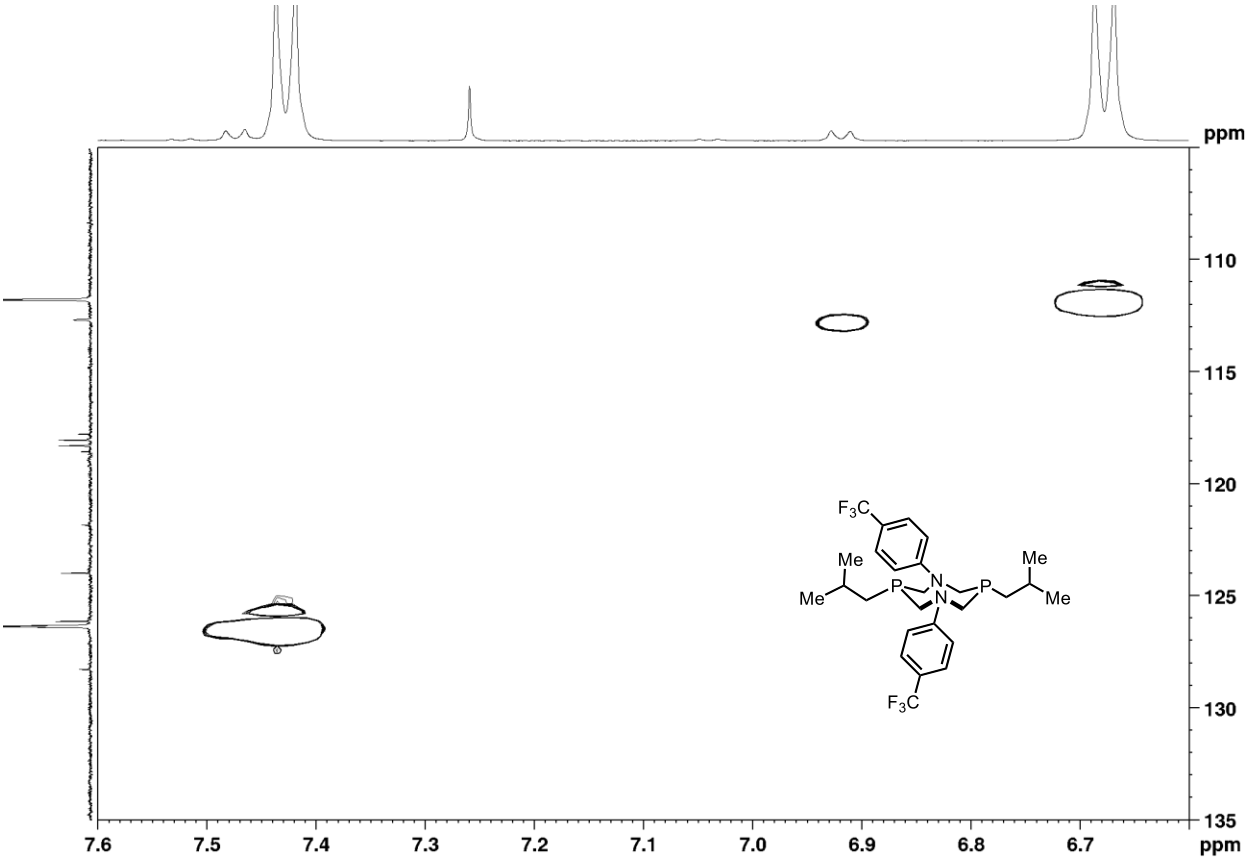

1,5-bis(*p*-benzotrifluoride)-3,7-bis(isobutyl)-1,5,3,7-diazadiphosphacyclooctane ($P^{iBu}_2N^{Ph}_2$), $^{19}F\{^1H\}$, $CDCl_3$, 470 MHz

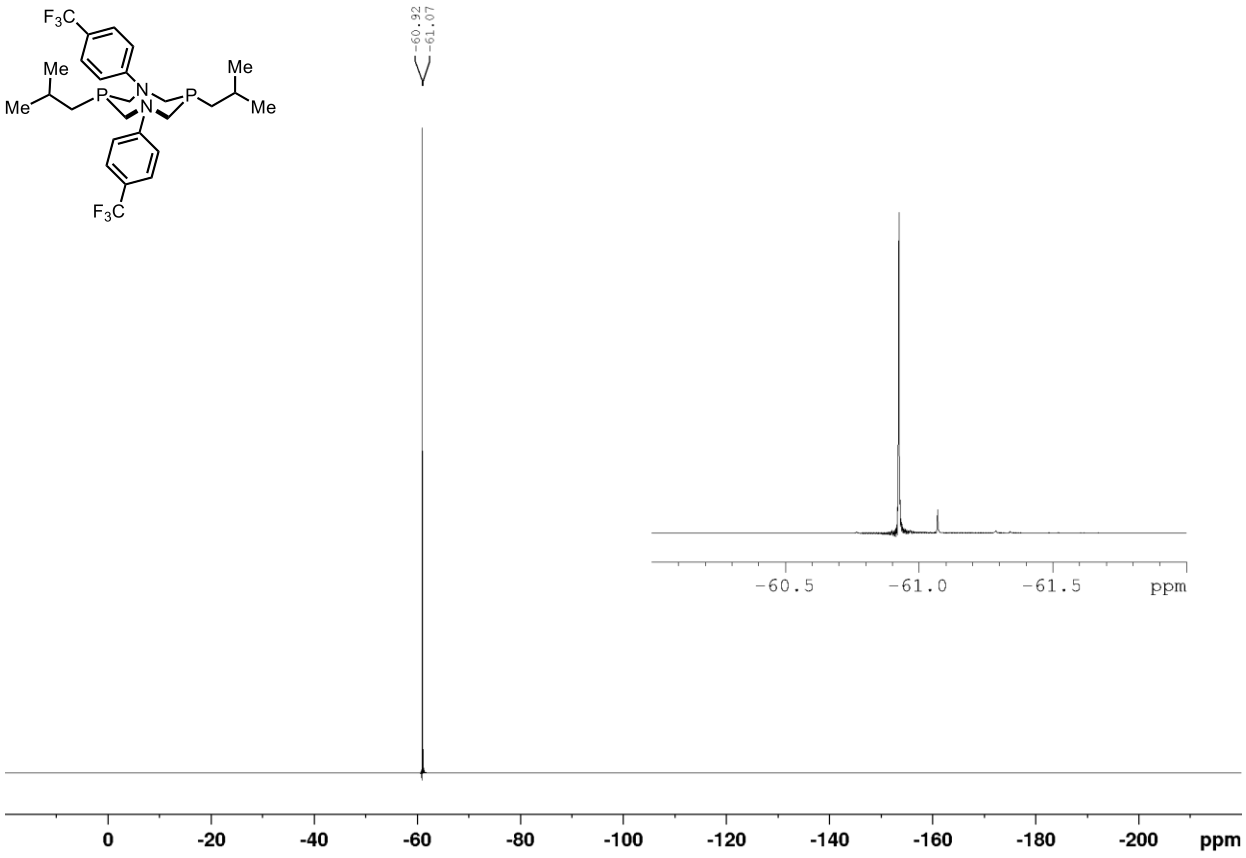

1,5-bis(*p*-benzotrifluoride)-3,7-bis(isobutyl)-1,5,3,7-diazadiphosphacyclooctane ($P^{iBu}_2N^{Ph}_2$), $^{31}P\{^1H\}$, $CDCl_3$, 202 MHz

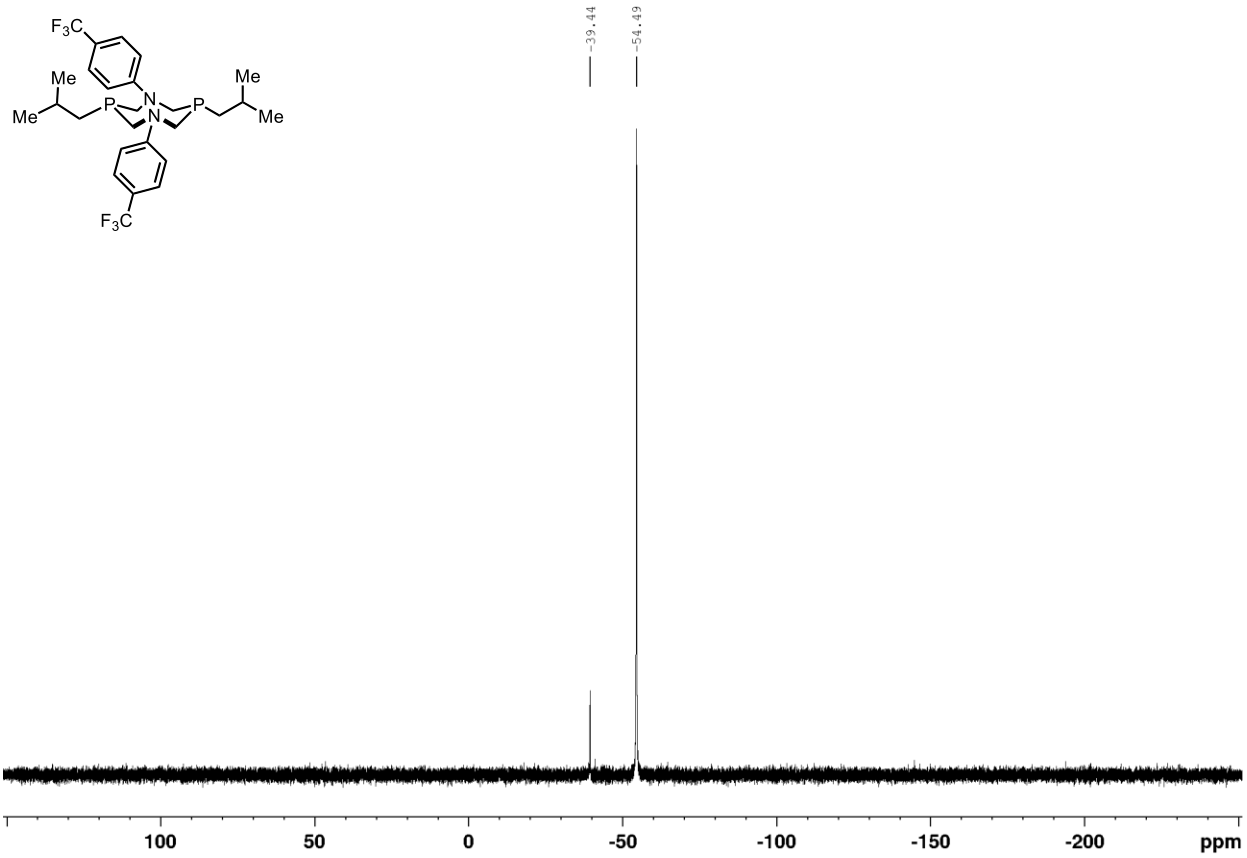

5.10 References

[1] For examples of representative procedures see: (a) Stubbs, J. M.; Chapple, D. E.; Boyle, P. D.; Blacquiere, J. M. Catalyst Pendent-Base Effects on Cyclization of Alkynyl Amines. *ChemCatChem* **2018**, *10*, 4001-4009. (b) Kilgore, U. J.; Stewart, M. P.; Helm, M. L.; Dougherty, W. G.; Kassel, W. S.; Dubois, M. R.; Dubois, D. L.; Bullock, R. M. Studies of a series of $[Ni(P^{R}_2N^{Ph}_2)_2(CH_3CN)]^{2+}$ complexes as electrocatalysts for H_2 production: Substituent variation at the phosphorus atom of the P_2N_2 ligand. *Inorg. Chem.* **2011**, *50*, 10908–10918.

[2] Yang, J. Y.; Bullock, R. M.; Dougherty, W. G.; Kassel, W. S.; Twamley, B.; Dubois, D. L.; Rakowski Dubois, M. Reduction of oxygen catalyzed by nickel diphosphine complexes with positioned pendant amines. *Dalton Trans.* **2010**, *39*, 3001-3010.

[3] Seu, C. S.; Appel, A. M.; Doud, M. D.; DuBois, D. L.; Kubiak, C. P. Formate oxidation via β-deprotonation in $[Ni(P^{R}_2N^{R'}_2)_2(CH_3CN)]^{2+}$ complexes. *Energy Environ. Sci.* **2012**, *5*, 6480-6490.

[4] Kilgore, U.J.; Roberts, J. A. S.; Pool, D. H.; Appel, A. M.; Stewart, M. P.; DuBois, M. R.; Dougherty, W. G.; Kassel, W. S.; Bullock, R. M.; DuBois, D. L. $[Ni(P^{Ph}_2N^{C6H4X}_2)_2]^{2+}$ Complexes as electrocatalysts for H_2 production: Effect of substituents, acids, and water on catalytic rates. *J. Am. Chem. Soc.* **2011**, *133*, 5861-5872.

[5] Surgenor, B. A.; Taylor, L. J.; Nordheider, A.; Slawin, A. M. Z.; Athukorala Arachchige, K. S.; Woollins, J. D.; Kilian, P. An efficient, scalable synthesis of ferrocenylphosphine and dichloroferrocenylphosphine. *RSC Adv.* **2016**, *6*, 5973–5976.

[6] Fihri, A.; Luart, D.; Len, C.; Solhy, A.; Chevrin, C.; Polshettiwar, V. Suzuki–Miyaura cross-coupling coupling reactions with low catalyst loading: A green and sustainable protocol in pure water. *Dalton Trans.* **2011**, *40*, 3116-3121.

Chapter 6 : Final Conclusions and Future Directions of the Work

As evidenced by Chapters 2-4, 1,5-Diaza-3,7-diphosphacyclooctanes (P_2N_2) ligands are underappreciated cross-coupling ligands. We anticipate that there are many directions; including development of new methodologies along with possible extensions of the current applications. While each respective chapter concludes with specific conclusions, a more general outlook is provided within this chapter to provide a bigger picture.

6.1 Discovery of new reactions: High-throughput experimention

Despite the prevalence of transition metal P_2N_2 complexes (Section 1.5.3), particularly for first-row transition metals, cross-couplings have only been reported with Pd and Ni.[1] Well-defined precatalysts bound to P_2N_2's were recently reported with nickel[1c] and palladium[1d] (Section 4.5.3). High-throughput experimentation enables rapid and broad screening of chemical space and could serve to uncover new areas of interest.Campeau and Hazari note that industrial synthetic chemists are searching for large data sets, detailed understanding about scope limitations, and applications of methodologies to highly-functionalized scaffolds.[2] We believe that high-throughput screenings can serve to uncover broader pictures and, owing to the low abundance of published cross-couplings with P_2N_2 ligands, that this chemical space has not been even remotely covered.

6.1.1 Diverse metal screenings

A range of commercially-available transition metal precatalysts commonly featured in cross-coupling chemistry can be screened in parallel to discover reactivity. An example of a possible target could be new methods to forge sp^3-sp^3 C–C bonds as general broad coupling conditions remain largely elusive.[2, 3] A hypothetical plan for 864 (9x96 well-plates) experiments is

represented in Scheme 6.1, derived from a combination of literature precedence[4] and the desire to solve challenging reactions. It should be noted that Karen Zhao (B.Sc. Hon.), an undergraduate who was directly mentored, performed some preliminary research in this general area. However, further optimization and broader screenings are required to fully determine whether P_2N_2 ligands can solve challenges in this field.

Scheme 6.1 A proposed high-throughput campaign

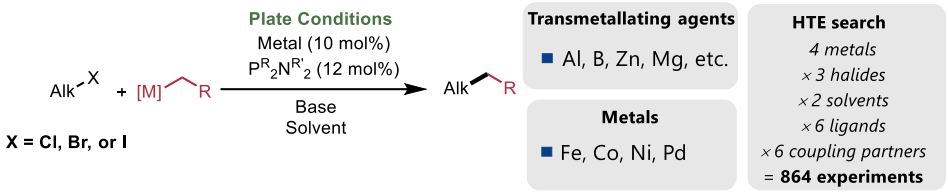

6.1.2 Benchmarking P_2N_2 ligands as highly efficient ligands in Ni- or Pd-couplings

Similar to the work done with the Mizoroki-Heck coupling (Chapter 4), high-throughput benchmarking studies could be done with other common cross-coupling partners. For example, detailed plates could be run targeting Suzuki-Miyaura or Buchwald-Hartwig cross-couplings and comparing the performance of P_2N_2 ligands to gold standard ligands. HTE plates could be run to see if P_2N_2 ligands have better performance or enable challenging couplings not generally afforded by the best ligands in the literature. Nickel and palladium systems would be the focus of this branch of research. Karen Zhao (Hon. B.Sc.) and Filiz Sevinc (Hon. B.Sc.), two undergraduate students who were directly mentored, performed research in this general area. As was the case for sp^3–sp^3 C–C coupling, while promising initial results were obtained, larger data sets are required to properly assess the performance of the P_2N_2 ligands with established ligands.

6.2 Mechanistic probes: Synthesis of P_2N_2 analogues

While high reactivity and selectivity has been afforded by P_2N_2 ligands in cross-coupling (Chapters 2-4), the exact mechanistic reasons remain ambiguous. The synthesis of $P^{Ar}{}_2N^R{}_2$ variants was discussed in Section 4.6.2 to probe effects on the postulated π-π edge-to-face interaction, the preparation of related bidentate phosphines could, more broadly, test the importance of structural features of the ligands.

$(R_2PCH_2)_2NR'$ ligands are readily prepared from slight modification of the P_2N_2 synthesis Chapter 5; the biggest difference is the use of a secondary phosphine instead of a primary phosphine (Scheme 6.2A).[5] These acyclic N-bridged bis(phosphine) ligands could serve to answer relevant questions about whether the cyclic 8-membered core of a P_2N_2 ligand is required for catalytic activity. Ni complexes of $(R_2PCH_2)_2NR'$ ligands are known and, like P_2N_2 ligands, it is proposed that the amine arm is able to act as an internal pendant base.[6]

Cyclic derivatives of the P_2N_2 scaffold have also been studied in the primary literature. For example, Helm and coworkers reported an $8P_2N$ ligand (Scheme 6.2B), which formally replaces one nitrogen atom of the P_2N_2 scaffold with a methylene group ($-CH_2-$).[7] The related electrochemical studies indicated that similar rates of hydrogen production were observed between a $Ni(P_2N_2)_2$ complex and the corresponding $Ni(8P_2N)_2$ species. Preparation of the analogous 7-membered $7P_2N$ ligand (1,3,6-Azadiphosphacycloheptane) has also been reported (Scheme 6.2C).[8] Helm and colleagues found that $Ni(7P_2N)_2$ precatalyst had significantly higher rates of hydrogen production than either $Ni(P_2N_2)_2$ or $Ni(8P_2N)_2$ complexes.[7] Helm et al. proposed that by contracting the ring size, the equilibrium distribution of conformers was affected. By favoring catalytically active conformers, the rate of hydrogen production increased.

Preparation of $8P_2N$ and $7P_2N$ variants of our optimized P_2N_2 ligands would be highly desirable to probe whether a second pendant nitrogen arm is required for cross-couplings. One barrier to making a large library of $8P_2N$ or $7P_2N$ ligands is that, due to the loss of structural symmetry, these compounds are diastereomeric and less accessible than the corresponding P_2N_2 ligand. The *meso* diastereomer is typically purified from a mixture of diastereomers through selective crystallization,[7,8] although slow interconversion of the diastereomers has also been reported.[9] Despite an abundance of $7P^{Ph}{}_2N^R$ derivatives in the primary literature,[10] alkyl substituents on phosphorus are unreported. $7P^{Alk}{}_2N^R$ derivatives can, most likely, be accessed through similar synthesis of a known $8P^{Cy}{}_2N$ ligand.[11] $8P_2N$ or $7P_2N$ ligands would serve to answer the general question: how important is the second pendant amine arm for catalysis?

Scheme 6.2 "P_2N_1"Analogues of P_2N_2 ligands

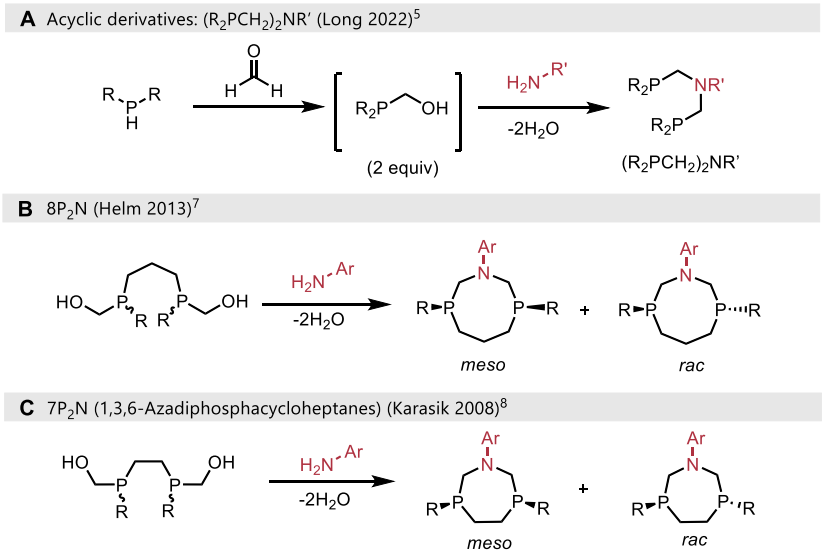

P_4N_2 ligands have also been developed for electrocatalytic applications.[12] P_4N_2 ligands feature the 1,5-diaza-3,7-diphosphacyclooctane backbone but have pendant phosphino groups attached to the cyclic diphosphacyclooctane atoms through an alkyl linker (Scheme 6.3A).[13] The resulting metal complexes are typically bound tetradentate κ^4-P,P,P,P. Cobalt-hydride P_4N_2

complexes are strong reductants[12] and recently, have been applied to the catalytic reduction of organic functionalities with H_2 by the Zhang and Wen groups.[14] Examples demonstrate selective 1,2-reduction of α,β-unsaturated carbonyls along with the reduction of heteroaromatics (Scheme 6.3B).[14] In our nickel-catalyzed transformations (Chapter 2 and Chapter 3), we noted that at least two equivalents of P_2N_2 ligand were optimal relative to our metal centre. Therefore, a catalytic reaction using P_4N_2 in a 1:1 stoichiometry to Ni would be interesting to try. If a P_4N_2 ligand is comparable to the corresponding P_2N_2 ligand, the reaction could be monitored by $^{31}P\{^1H\}$ NMR to determine if the pendant arms are hemi-labile during catalysis. This could serve to provide additional mechanistic insight into the catalytically active species. It is also possible that a P_4N_2 ligand would simply coordinatively saturate a nickel centre and suppress any catalytic activity. In such a case, this would suggest that a $[Ni(P_2N_2)_2]$ species is not an active catalyst. We don't believe that a $[Ni(P_2N_2)_2]$ is catalytically competent for our reaction and could serve to be a resting state of the catalyst.

A conformationally locked P_2N_2 variant, 1,5-diaza-3,7-diphosphabicyclo[3.3.1]nonane, has been prepared and used in iron catalysis (Scheme 6.4A).[15] By tethering the amino groups together through a methylene linker, the P_2N_2 ligand is fixed in a chair-chair conformation when bound to a metal. This ligand could be used to assess whether catalytic activity is observed with this particular conformer. However, this experiment is not perfect as the electronic properties of the nitrogen substituent are not reflective of working catalytic systems, which are derived from anilines. 1,2-diaminobenzene can be used to prepare a similarly rigid P_2N_2 ligand more reflective of our ligands (Scheme 6.4B).[16]

Scheme 6.3 P_4N_2 ligands and their application in reductive catalysis

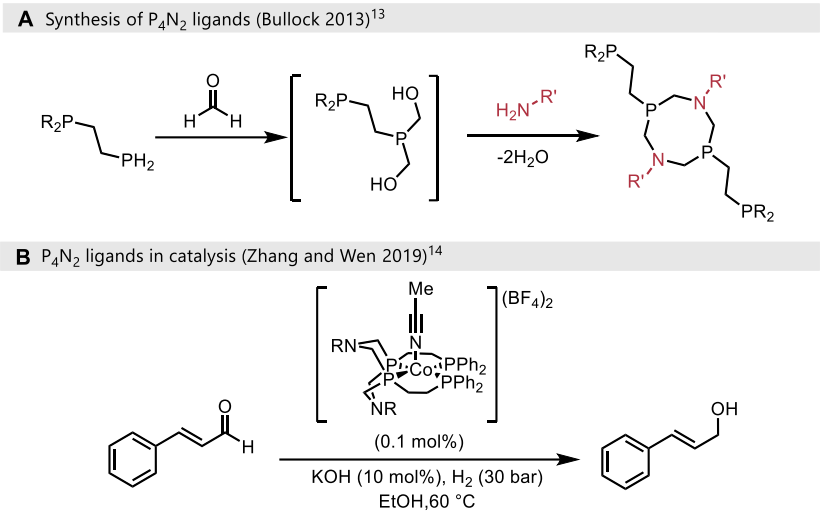

One hypothesis to account for the observed site-selectivity presented in Chapter 4, is that one of the P_2N_2 ligands acts as a hemi-labile monodentate ligand through part of the catalytic cycle. $P^{tBu}{}_2N^{ArCF3}{}_2$ was observed to be a bulky ligand (Section 4.5.2), with distortion from ideal square planar geometry in the solid crystalline state. A "P_1N_3" ligand could be prepared, which would formally replace one of the phosphorus atoms of the P_2N_2 core with an amine, to see whether catalytic activity is retained. This general scaffold has been applied to rhodium catalysis (Scheme 6.4C),[17] however, a less rigid analogue would be desirable to be closer in structure to working ligands for transition metal-catalyzed cross-couplings (Scheme 6.4D).

Scheme 6.4 Rigid P_2N_2 derivatives (and beyond)

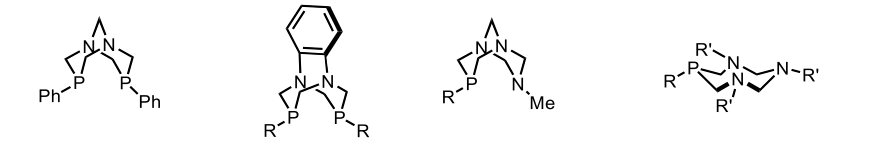

A Whittlesey (2009)[15] **B** Arbuzov (1982)[16] **C** Gonsalvi (2006)[17] **D** Proposed "P_1N_3" backbone

6.3 Characterization of organometallic complexes

Another way to probe the difference between P_2N_2 ligands and the catalytic activity of their metal complexes would be to directly study the chemical properties of well-defined organometallic complexes. For example, metal carbonyl complexes featuring a series of P_2N_2 ligands could be prepared and studied by infrared spectroscopy. The carbonyl stretch, as recorded using IR spectroscopy, can be used to measure how electron-rich a ligand is.[18] A strongly σ-donating ligand allows for more metal back-bonding which decrease the triple bond character of the C—O bond and consequently the frequency of the C—O stretch. If no variation in CO-stretch is observed between complexes derived from structurally-related P_2N_2 ligands (eg. $P^{Cy}{}_2N^{ArCF3}{}_2$ vs $P^{Cy}{}_2N^{Ph}{}_2$), one may propose that distal functionalities do not have a large influence on the σ-donation properties of the phosphorus atoms. Conversely, significant differences in the carbonyl stretching frequencies between a series of related P_2N_2 ligands could indicate that inductive effects of the nitrogen substituent significantly alter the electronics of phosphorus' lone pairs.

It is also plausible that the observed differences in catalytic activity, such as in Table 2.3, could be a result of complex conformational dynamics of the P_2N_2 ligands. As discussed in Section 1.5.4 and Section 6.2, the equilibrium distribution of accessible conformers for a given system can vary profoundly based on seemingly subtle changes to the ligand structure. Alternatively, the observed difference in reactivity between ligands could simply be a consequence of the solubility of associated metal complexes.

6.4 The future of P_2N_2 ligands in cross-coupling

Chapters 2-4 showcase the synthetic utility of P_2N_2 ligands in organic cross-coupling reactions. We firmly believe that this is not simply the extent of their use but, instead, it is the start of their application in metal-catalyzed cross-couplings. While some mechanistic work has been performed, additional studies are required to pinpoint why this class of ligands is highly effective in 1,2-carbonyl insertion or site-selective Mizoroki-Heck chemistry. Further studies into the mechanistic aspects of P_2N_2 ligands and extension of the applications of P_2N_2 ligands in organic synthesis are currently on-going.

6.5 References

[1] (a) Fihri, A.; Luart, D.; Len, C.; Solhy, A.; Chevrin, C.; Polshettiwar, V. Suzuki–Miyaura cross-coupling coupling reactions with low catalyst loading: a green and sustainable protocol in pure water. *Dalton Trans*. **2011**, *40*, 3116-3121. (b) Isbrandt, E. S.; Nasim, A.; Zhao, K.; Newman, S. G. Catalytic aldehyde and alcohol arylation reactions facilitated by a 1,5-diaza-3,7-diphosphacyclooctane ligand. *J. Am. Chem. Soc.* **2021**, *143*, 14646–14656. (c) Nasim, A.; Thomas, G. T.; Ovens, J. S.; Newman, S. G. Reductive 1,2-arylation of isatins. *Org. Lett.* **2022**, *24*, 7232–7236. (d) Isbrandt, E. S.; Chapple, D. E.; Tu, N. P. T.; Dimakos, V.; Beardall, A. M. M.; Boyle, P. D.; Rowley, C.; Blacquiere, J. M.; Newman, S. G. Controlling reactivity and selectivity in the Mizoroki-Heck reaction: High throughput evaluation of 1,5-diaza-3,7-diphosphacyclooctane ligands*. J. Am. Chem. Soc.* **2024**, *in press*. Preprint available at: *ChemRxiv* **2023**. DOI: 10.26434/chemrxiv-2023-t9p7j

[2] Campeau, L.-C.; Hazari, N. Cross-coupling and related reactions: Connecting past success to the development of new reactions for the future. *Organometallics* **2019**, *38*, 3–35.

[3] Yuan, W.; Zheng, S.; Hu, Y. Recent advances in C(sp^3)–c(sp^3) cross-coupling via metallaphotoredox strategies. *Synthesis* **2021**, *53*, 1719–1733.

[4] For representative literature precedence for metal catalyzed C(sp^3)–C(sp^3) couplings see: (a) Netherton, M. R.; Dai, C.; Neuschütz, K.; Fu, G. C. Room-temperature alkyl−alkyl Suzuki cross-coupling of alkyl bromides that possess β-hydrogens. *J. Am. Chem. Soc.* **2001**, *123*, 10099–10100. (b) Jana, R.; Pathak, T. P.; Sigman, M. S. Advances in transition metal (Pd,Ni,Fe)-catalyzed cross-coupling reactions using alkyl-organometallics as reaction partners. *Chem. Rev.* **2011**, *111*, 1417–1492. (b) Komeyama, K.; Michiyuki, T.; Osaka, I. Nickel/cobalt-catalyzed C(sp^3)–C(sp^3) cross-coupling of alkyl halides with alkyl tosylates. *ACS Catal.* **2019**, *9*, 9285–9291.

[5] For a representative synthesis see: Cooper, S. M.; Siakalli, C.; White, A. J. P.; Frei, A.; Miller, P. W.; Long, N. J. Synthesis and anti-microbial activity of a new series of bis(diphosphine) rhenium(v) dioxo Complexes. *Dalton Trans.* **2022**, *51*, 12791–12795.

[6] Duan, L.; Wang, M.; Li, P.; Wang, N.; Wang, F.; Sun, L. Synthesis, protonation and electrochemical properties of trinuclear $NiFe_2$ complexes $Fe_2(CO)_6(\mu_3\text{-}S)_2[Ni(Ph_2PCH_2)_2NR]$ (R = *n*-Bu, Ph) with an internal pendant nitrogen base as a proton relay. *Inorg. Chim. Acta* **2009**, 362, 372-376.

[7] Wiese, S.; Kilgore, U. J.; Ho, M.-H.; Raugei, S.; Dubois, D. L.; Bullock, R. M.; Helm, M. L. Hydrogen production using nickel electrocatalysts with pendant amines: Ligand effects on rates and overpotentials. *ACS Catal*. **2013**, *3*, 2527–2535.

[8] Karasik, A. A.; Balueva, A. S.; Moussina, E. I.; Naumov, R. N.; Dobrynin, A. B.; Krivolapov, D. B.; Litvinov, I. A.; Sinyashin, O. G.. 1,3,6-Azadiphosphacycloheptanes: A novel type of heterocyclic diphosphines. *Heteroat. Chem.* **2008**, *19*, 125–132.

[9] Musina, E. I.; Wittmann, T. I.; Strelnik, I. D.; Naumova, O. E.;Karasik, A. A.; Krivolapov, D. B.; Islamov, D. R.; Kataeva,O. N.; Sinyashin, O. G.; Lönnecke, P.; Hey-Hawkins, E. Influence of the *rac–meso* isomerization of seven-membered cyclicbisphosphines on the predominant formation of chelate complexes.*Polyhedron* **2015**,*100*, 344–350.

[10] For additional examples of $7P_2N$ ligands see: (a) Musina, E. I.; Karasik, A. A.; Balueva, A. S.; Strelnik, I. D.; Fesenko, T. I.; Dobrynin, A. B.; Gerasimova, T. P.; Katsyuba, S. A.; Kataeva, O. N.; Lönnecke, P.; Hey-Hawkins, E.; Sinyashin, O. G. Synthesis and stereoselective interconversion of chiral 1-aza-3,6-diphosphacycloheptanes. *Eur. J. Inorg. Chem.* **2012**, *2012*, 1857–1866. (b) Fesenko, T. I.; Strelnik, I. D.; Musina, E. I.; Karasik, A. A.; Sinyashin, O. G. Synthesis of 1-(pyridylalkyl)-1-aza-3,6-diphosphacycloheptanes. *Russ. Chem. Bull.* **2012**, *61*, 1792–1797.

[11] Stolley, R. M.; Darmon, J. M.; Das, P.; Helm, M. L. Nickel bis-diphosphine complexes: Controlling the binding and heterolysis of H_2. *Organometallics* **2016**, *35*, 2965–2974.

[12] Wiedner, E. S.; Appel, A. M.; Dubois, D. L.; Bullock, R. M. Thermochemical and mechanistic studies of electrocatalytic hydrogen production by cobalt complexes containing pendant amines. *Inorg. Chem.* **2013**, *52*, 14391–14403.

[13] Wiedner, E. S.; Roberts, J. A. S.; Dougherty, W. G.; Kassel, W. S.; Dubois, D. L.; Bullock, R. M. Synthesis and electrochemical studies of cobalt(III) monohydride complexes containing pendant amines. *Inorg. Chem*. **2013**, *52*, 9975–9988.

[14] (a) Duan, Y.-N.; Du, X.; Cui, Z.; Zeng, Y.; Liu, Y.; Yang, T.; Wen, J.; Zhang, X. Homogeneous hydrogenation with a cobalt/tetraphosphine catalyst: A superior hydride donor for polar double bonds and *N*-heteroarenes. *J. Am. Chem.*

Soc. **2019**, *141*, 20424–20433. (b) Zhang, S.; Zhou, R.; Duan, Y.; Zhou, Y.; Zhang, X.; Wen, J. Homogeneous dearomative hydrogenation with a Co/P_4N_2 catalyst: A nucleophilic approach. *Chem. Eur. J.* **2023**, *29*, e202203189.
[15] Burrows, A. D.; Harrington, R. W.; Kirk, A. S.; Mahon, M. F.; Marken, F.; Warren, J. E.; Whittlesey, M. K. Synthesis, characterization, and electrochemistry of a series of iron(II) complexes containing self-assembled 1,5-diaza-3,7-diphosphabicyclo[3.3.1]nonane Ligands. *Inorg. Chem*. **2009**, *48*, 9924–9935.
[16] Arbuzov, B. A.; Erastov, O. A.; Romanova, I. P.; Efremov, Y. Y.; Musin, R. Z. Reaction of dihydroxymethylphenylphosphine with *o*-phenylenediamine. *Russ. Chem. Bull*. **1982**, *31*, 399–401.
[17] Phillips, A. D.; Bolaño, S.; Bosquain, S. S.; Daran, J.-C.; Malacea, R.; Peruzzini, M.; Poli, R.; Gonsalvi, L. A new class of rhodium(I) κ^1-P and κ^2-P,N complexes with rigid PTN(R) ligands (PTN = 7-phospha-3-methyl-1,3,5-triazabicyclo[3.3.1]nonane). *Organometallics* **2006**, *25*, 2189–2200.
[18] Kühl, O. Predicting the net donating ability of phosphines—do we need sophisticated theoretical methods? *J. Coord. Chem.* **2005**, *249*, 693-704.